Université de Liège

Faculté des Sciences
Département de Géologie
Pétrologie sédimentaire

Université de Liège

Sedimentary development and correlation of long-term off-reef to shallow-water Devonian carbonate records in Europe

Ph.D. dissertation to obtain the degree of Doctor of Sciences
from the Université de Liège by

Damien Pas

Promotor: Prof. Dr. Frédéric Boulvain
Co-promotor: Dr. Anne-Christine Da Silva

June 2015

Département de Géologie
Université de Liège

Members of the dissertation committee:

Prof. Dr. Emmanuelle Javaux
Liège University (ULg), Belgium

Prof. Dr. Johan Yans
Namur University (UNamur), Belgium

Prof. Dr. Xavier Devleeschouwer
Institut Royal des Sciences naturelles de Belgique (IRSNB)

Dr. Thomas Suttner
Geological Survey of Austria (GSA)

Acknowledgements

I should like to express my sincere gratitude to Prof. dr. Frédéric Boulvain who has given me the opportunity to be his assistant and to start a PhD under his supervision. I am grateful for his untiring support and guidance through all the stages of this project. I also want to thank him for all the stimulating discussions we had and for always answering my constant requests despite his very busy timetable.

I am also deeply indebted to dr. Anne-Christine Da Silva, my co-supervisor, for the repeated scientific supports, for her availability, for her numerous suggestions in the structuration of my research and the meticulous reading of my manuscripts (which were always full of red when they were returned to me). I also want to thank Anne-Christine for all the delicious chocolate/tea times we have shared and her permanent positive energy.

To the members of my PhD committee, Emmanuelle Javaux and Johan Yans thank you for your support, discussions and feedback, year after year on my scientific results

A special thanks also goes to Jean-Paul Cullus, the thin-section assistant, who is often behind the scene of our research in sedimentology but who is more than essential for our extensive petrographic work; and to Nicolas Delmelle, who has prepared and analyzed a large amount of samples for elemental geochemistry.

My sincere thanks go to Pierre Cornet, Pierre Bultynck, Peter Königshof, Thomas Suttner, Erika Kido, David De Vleeschouwer, Xavier Devleeschouwer, Simo Spassov, Monica Pondrelli, Marie Coen-Aubert and Carlo Corradini for collaborating in past and future projects.

I would like to extend my gratitude to the all of the faculty and staff of the B20 at the University of Liège who provided assistance during measurements, agreeable working atmosphere and delicious sweets for our Friday lunches: Jaqueline Vander Auwera, Olivier Bolle, Salvatrice Montalbano, Sylvain Dechamps, Hocine Djouber, Hanene Belghithi, Olivier Namur, Jean-Clair Duchêne, Pierre Cornet, Bernard Charlier, Eddy Custine, Oscar Laurent. Many thanks to my colleagues from B19 and B18, Maxime Baijot, Frédéric Hatert, Hans-Balder Havenith, Philippe Cerfontaine, Edouard Poty, Nathalie Fagel, Joël Laval, Joël Otten, Julien Denayer, Valentin Fischer and many others.

Very special thanks go to Mariella Guadagnano and Joëlle Schmetz for all the logistic support and the very warm and welcoming atmosphere of their offices.

Even if he left the B20 two years ago, a special thank goes to Jonathan Michel for all the very educative (or not) and scientific (or not) discussions and the valuable advice and numerous coffee breaks we shared around this unforgettable and wonderful "SENSEO". After the difficult departure of "Jonny", the coffee maker stayed behind and is still frequently used as we are perpetuating the tradition with Mehrdad Sardar Abadi, a wonderful PhD from Iran and the new tenant of "Jonny"'s office. Hopefully, it will continue to brew coffee for several generations of postgraduate students.

My deep appreciation goes to Megh Raj Dhital and Prabin Kayasta who drove me around and helped me find my way through Kathmandu and the surrounding areas during my first field work in Nepal.

As an Assistant in the Department of Geology, I have had the chance to teach and supervise many students and I want to thank them all for their fresh ideas and the all fun we shared in the lab or at their parties. Though some were occasionally absentminded and/or noisy, their general positive attitude has helped me to recover the strength needed for my research. In this respect my best memories go to Nicolas Demaude, Corentin Labaye, Hélène Jadot and Gilles Neufcourt who were all sitting and writing their master theses in my office.

I want to thank Chantal Vandendungen for her precious help in reading and revising the English of this manuscript.

I would like to give special thanks to all those people that surrounded me and supported me during the completion of this project. My dearest parents my deepest thanks go to you for your unconditional and untiring support and care. Many friends, even if they don't know about that, have contributed by their words or mood to change my mind and recover a positive attitude in those moments were progress was very slow or when my health was not very good (François-Phill, Palmito, Adri, Laurent, Antoine, Geof, Arthur, PX, Ngu) and many others who should recognize themselves from my multiple activities (Capoeira, GAC, Ganesh-himal). I may still write several pages on all the fascinating and helpful people I met during my PhD and who have contributed in their own way to the completion of this project.

Finally, I would like to thank my love, Eugenia, for her unquestionable support, but mostly for her courage and patience to cope with my highly changing moods during this relatively long project. Благодарю вас от всего сердца Евгения.

Abstract

The Devonian Period was characterized by extensive shallow-marine regions, with the largest carbonate platform development of the Phanerozoic Eon. The research carried out in this thesis integrates field work, petrographic analysis, conodont biostratigraphy, elemental and carbon isotope geochemistry, magnetic susceptibility and magnetic hysteresis measurement. The aim, to better understand and characterize the environmental conditions that led to the development of three of the largest European Devonian carbonate platforms. This multi-disciplinary study also proposes to validate the use of magnetic susceptibility as a reliable tool for palaeoenvironmental reconstruction and long-distance correlation in marine carbonate.

Fieldwork was conducted on four key sections of the European Pre-Mesozoic massifs: the Ardennes (La Thure and Fromelennes-Flohimont), the Rheinisches Schiefergebirge (Burgberg) and the Carnic Alps (Freikofel). The large quantity and in-depth analysis of rock samples and thin-sections has demonstrated the fascinating environmental diversity that shaped the carbonate platforms in the Rhenohecynian and Paleotethys oceans towards the mid-late Devonian times.

The aforementioned analysis has enabled the development of reconstructed sedimentary models and large-scale shallowing-deepening histories for each section. New and published biostratigraphic data provided reliable age constraints for the foremost environmental changes evident in each of the sections. $\delta^{13}C$ results from the Frasnian – Famennian boundary in the Burgberg and Freikofel sections have revealed Kellwasser events in limestone lithologies.

Based on the analysis of ±1800 samples, a high-resolution magnetic susceptibility (χ_{in}) curve for each section has been developed, highlighting the strong link between the χ_{in} signatures and the syn-sedimentary parameters, such as carbonate productivity/sedimentation rate, water agitation and siliciclastic input. The comparison between χ_{in} and elemental geochemistry datasets has demonstrated the inherent-parallel link existing between the siliciclastic input proxies and the variation in χ_{in} signature in each of the sections. Magnetic hysteresis measurements have shown that ferromagnetic minerals such as magnetite control the χ_{in} signal. By comparing our data sets with published data we could confirm that our χ_{in} signal is remagnetized. However links between siliciclastic input proxies and χ_{in}, and between χ_{in} and environmental parameters have proven a relatively good preservation of the primary depositionally-induced χ_{in} signal.

Finally, by integrating complete data and establishing a correlation chart including the four long-term χ_{in} curves, it is apparent that on a regional scale long-term χ_{in} trends can be correlated, as long as the evolution of the main depositional setting in the sections studied remains comparable. The significant

impact of syn-sedimentary parameters on the final χ_{in} signature seems to obscure the imprint of parameters driving variations in continental erosion (e.g., climate, sea-level and tectonic variations) and therefore limiting the inter-regional correlations. This collaborative project on time-series analysis of long-term high-resolution χ_{in} records in the Dinant Syncline has revealed the imprint of astronomical parameters, giving rise to a more accurate estimate of the Givetian Stage's duration.

Résumé

Le Dévonien est caractérisé par de larges zones marines peu profondes et le développement le plus spectaculaire des plates-formes carbonatées de l'ère Phanérozoïque. Le travail de recherche réalisé durant cette thèse de doctorat intègre de nombreuses données issues de l'analyse pétrographique, de la biostratigraphie des conodontes, des isotopes stables du carbone, de la géochimie des éléments en traces et majeurs, de la susceptibilité magnétique et de l'analyse du magnétisme d'hystérésis pour mieux comprendre et caractériser le développement surprenant des environnements de plates-formes carbonatées dans trois des plus grandes plates-formes du Dévonien d'Europe. Cette étude multidisciplinaire vise également à la meilleure compréhension et la validation de la susceptibilité magnétique comme outil pour les corrélations longue-distance de longues séquences sédimentaires et la reconstruction des paléo-environnements carbonatés.

Le travail de terrain a été réalisé sur quatre coupes remarquables appartenant aux massifs pré-mésozoiques Ardennais (La Thure et Fromelennes-Flohimont), Rhéno-hercynien et des Alpes Carniques. L'ensemble des analyses sur les échantillons rocheux et les lames minces ont permis de mettre en évidence et d'illustrer la diversité fascinante des environnements de plates-formes carbonatées durant le Dévonien Moyen et Supérieur dans les océans Paléotéthys et « Rhénohercynien ».

A partir des analyses de roche et de lame mince, les modèles sédimentaires et les courbes de microfacies ont pu être construites pour chacune des coupes sélectionnées. Ces résultats ont permis d'établir une histoire des variations du niveau marin relatif pour toutes nos zones d'étude. L'utilisation combinée de nos nouvelles données biostratigraphiques et de celles déjà publiées nous ont également permis de mettre sur pied un timing pour les grands changements environnementaux caractérisant les longs intervalles temporels sélectionnés pour ce travail. L'analyse du $\delta^{13}C$ proche de la limite Frasnien – Famennien dans les coupes de Burgberg et de Freikofel a mis en évidence les événements Kellwasser dans des lithologies inhabituelles (cf. calcaire).

Sur base de l'analyse de ±1800 échantillons nous avons pu établir les courbes de susceptibilité magnétique (χ_{in}) pour chacune des coupes sélectionnées et nous avons mis en évidence un lien signifiant entre le signal de χ_{in} et les paramètres syn-sédimentaires tels que la production carbonatée/le taux de sédimentation, l'énergie du milieu et les apports silicoclastiques. La comparaison entre χ_{in} et la géochimie élémentaire a montré le lien inhérent existant entre les éléments marqueurs du détritisme et la variation du signal de χ_{in}.

Les analyses du magnétisme d'hystérésis ont permis de démontrer que les minéraux ferromagnétiques contrôlent le signal de susceptibilité magnétique. De plus, en comparant nos

données d'hystérésis avec les données publiées nous avons pu confirmer que notre signal de χ_{in} était un signal remagnétisé. Néanmoins le lien existant entre les marqueurs du détritisme et la χ_{in}, ainsi que celui entre les paramètres environnementaux et la χ_{in}, prouvent une relativement bonne préservation du signal de χ_{in} enregistré durant le dépôt du sédiment.

Finalement, l'intégration complète des données et la construction d'une charte de corrélation entre les différentes coupes, incluant les quatre courbes de χ_{in}, nous ont permis d'établir qu'à une échelle régionale, les variations à long terme dans les tendances de la χ_{in} peuvent être corrélées aussi longtemps que les évolutions au cours du temps des environnements de dépôt à corréler restent comparables. En revanche, les paramètres syn-sédimentaires semblent dominer le signal final de χ_{in}, et empêcher les corrélations entre les environnements de plates-formes séparés par de longues distances (cf. inter-régionales). Notre collaboration sur l'analyse des séries temporelles réalisée sur les données de χ_{in} des coupes du Synclinorium de Dinant, nous a permis de montrer l'influence des paramètres astronomiques durant la sédimentation et par la suite d'estimer de manière plus précise la durée de l'étage Givetien. Ceci est une application importante des mesures de susceptibilité magnétique comme marqueur climatique et pour améliorer la qualité des données temporelles dans les sédiments anciens.

Table of contents


Present day shallow-marine reef near Safaga, Red Sea, Egypt

Chapter 1

General introduction

1. The problematics of research

Understanding the complex relation between sea-level, climate, and biotic events in the geologic past is one of the most important goals for future geological research because our knowledge of ancient climatic and environmental variations that affected the geological past over long-time scales has remained very limited (Brett et al., 2011).

Throughout Earth history the Devonian Period (418.8 ±2.9 to 359.1 ±0.4 Ma; De Vleeschouwer and Parnell (2014) revealed itself to be one of the most fascinating intervals in the geological time scales because of intense but episodic biotic changes, variable greenhouse and icehouse climates, and sea-level fluctuations. The Middle Devonian onward is characterized by the massive appearance of land plants. It culminated in the development of huge swamps and rain forests during the Carboniferous which are preserved as large coal seams. Furthermore, the Devonian was characterized by extensive shallow-marine areas which, in combination with adequate environmental conditions had led to the largest tract of reef system through the Phanerozoic. During the Devonian time, carbonate platforms were large and widespread in equatorial North America and Eurasia, some of them covered 2000 km in length (Copper, 2002). The astonishing extension of carbonate platforms during the Middle Devonian is well-represented by the light-blue colour above 60°S and below 60°N (Fig. 1).

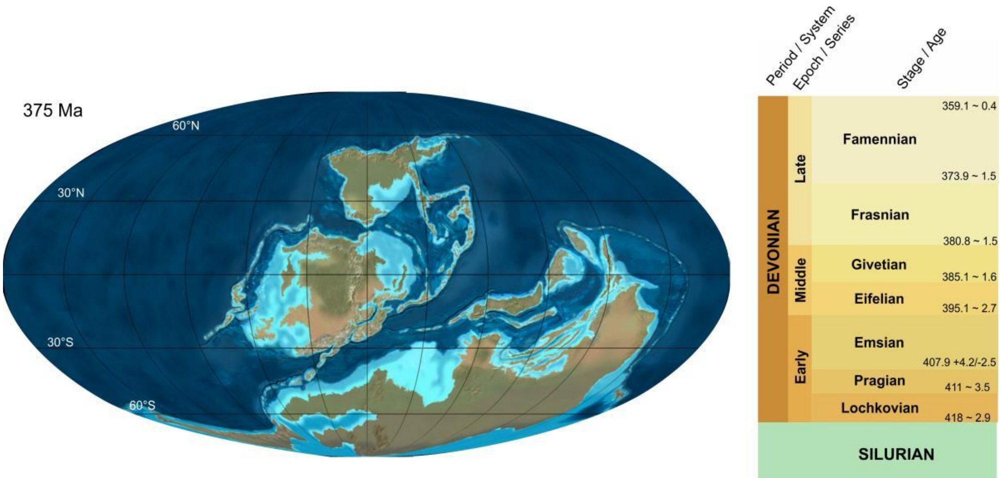

Fig. 1 *Middle Devonian palaeogeography (reconstruction by Dr. Ron Blakey) and time scale after De Vleeschouwer and Parnell (2014)*

Devonian reef-related sedimentary records are important archives of past life, climate and environment. These records are clearly visible and well-preserved in pre-Mesozoic massifs of Europe. Devonian carbonate complexes from Belgium/France (Ardennes), Germany (Rheinisches Schiefergebirge and Hartz Mountain) and Austrian/Italian border (Carnic Alps) are among the largest in Europe and have been the focus of many researches dealing with taxonomy, stratigrahy, sedimentology and geochemistry (see Pas et al., 2013; Pas et al., 2014a; Pas et al., 2014b for an overview of the references). Despite our need to get a better knowledge on the long-term environmental and climatic changes that affected geological times, most current sedimentological studies dedicated to Devonian carbonate platform only focus on short time scale or on a single location. Moreover, owing to the local geometrical complexity resulting from the Variscan and Alpine orogenies, the lack of a precise biostratigraphic control (mostly in shallow-water setting) and locally hardly accessible outcrops, these researches are often based on limited stratigraphic interval and often relate to a specific depositional setting. Therefore, detailed insight into the sedimentological characterization and reconstruction of European Devonian carbonate platforms over a long period of time are fairly rare.

These last decades, magnetic susceptibility (χ_{in}) has been broadly used as correlation tool as well as an indicator of changes in environmental and depositional setting for past sedimentary records. In the studies of ancient limestones, variation in χ_{in} has proven to be relatively independent of facies changes and to be similar over relatively long distances (e.g., intra- to extra-basinal) (Ellwood et al., 2001; Hladil et al., 2006; Mabille et al., 2008; Whalen and Day, 2008; Bábek et al., 2010; Boulvain et al., 2010; Riquier et al., 2010; Da Silva and Boulvain, 2012). These studies established that primary χ_{in} signal in ancient marine carbonate is possibly ruled by the amount of magnetic components inherited from condition that prevailed during deposition, such as climate, sea-level or tectonic variations. Indeed, these large-scaled fluctuations are the primary causes of changes in siliciclastic supply basinward, which is itself the strongest χ_{in} primary-controlling factor (Vanderaveroet et al., 1999; Ellwood et al., 2000; Tribovillard et al., 2006; Devleeschouwer et al., 2010; Śliwinski et al., 2010; Śliwiński et al., 2012). For instance, chemical weathering – its intensity and compositional trends – depends on terrestrial climate, and this allows us to use χ_{in} of marine sediments as a recorder of climate and sea-level changes over geological time. It is also important to note that a number of authors (Hladil, 2002; Ellwood et al., 2006; Hladil et al., 2006; Hladil et al., 2010) stated that magnetic minerals in carbonate sediments can also be supplied from eolian suspension and atmospheric dust. Recently, Boulvain et al. (2010) compared the long-term trends in magnetic susceptibility between two km-thick Eifelian-Frasnian sections from Belgium and the Czeck Republic. Regardless the very different background of palaeogeography, sedimentary rate, facies and the history of local sea-level changes, a remarkable similarity in the χ_{in} trends was observed between these two sections (Fig. 2). Such correlation has brought up many questions on the nature of the long-term forcing parameters that were active at the inter-regional scale and the link between χ_{in} and environmental parameters. According to Boulvain et al. (2010), similarities between long-term trends in χ_{in} must be the result of some “latent, global or latitudinal climatic eustatic regime”. These authors, based their hypotheses on the fact that the really high sea levels during some significant Givetian and Frasnian intervals correspond to large segments of the record where the χ_{in} signal is the lowest. During these times, epeiric seas, microcontinents, islands as well as coastal lowlands, changed to carbonate platforms or carbonate seas. The climates may have been “less dusty”, or less affected by continentally derived winds and corresponding dust.

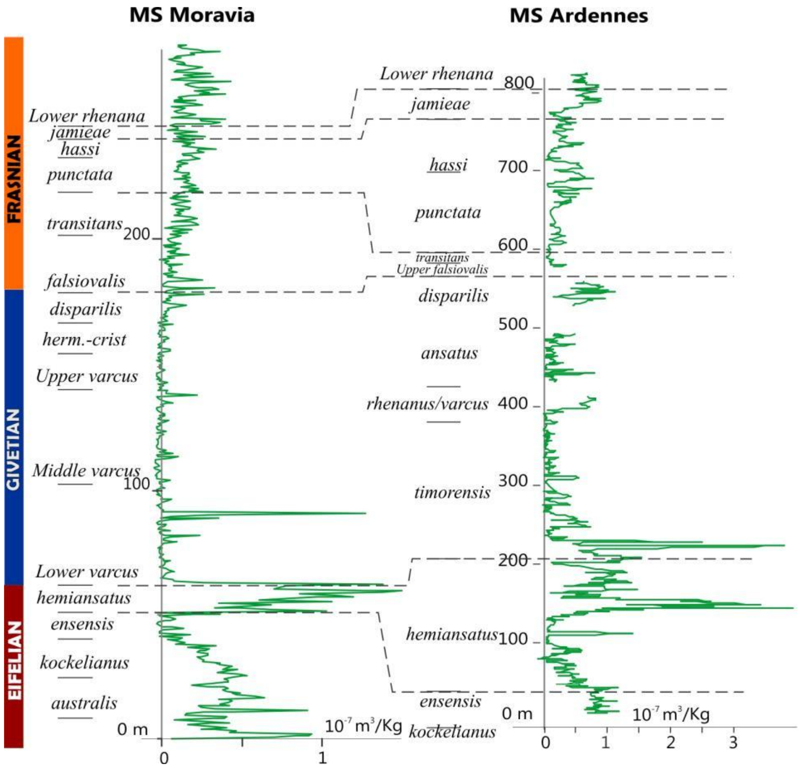

Fig. 2 *km-thick Eifelian – Frasnian χ_{in} correlation pattern between Ardennes and Czech Republic (redraw after Boulvain et al., 2010).*

These hypotheses are challenging and show that χ_{in} could really be used for tracking climate and environmental changes over long-time scale in carbonate records. Over the last few years numerous cyclostratigraphic studies focusing on the Devonian highlighted the potential of χ_{in} signal as a recorder of Milankovitch cycles and thus contributed to the reconstruction of past climate. (Ellwood et al., 2011; De Vleeschouwer et al., 2012a; De Vleeschouwer et al., 2012b; García-Alcalde et al., 2012; Da Silva et al., 2013; De Vleeschouwer et al., 2013; De Vleeschouwer et al., 2014; Ellwood et al., 2014). The link between the magnetic susceptibility signal and the Milankovitch cycles established in these studies advocate a χ_{in} records triggered by climatically driven processes. Moreover, these cyclostratigraphic studies have allowed to significantly improve the Devonian time scale (De Vleeschouwer et al., 2012b; De Vleeschouwer et al., 2014), which remains the less precise Period of the Phanerozoic era (Gradstein et al., 2012). However, those who pretend to use χ_{in} as a recorder of the past environmental and climatic evolution must demonstrate that the primary inherited signal has been is preserved. Indeed, ancient sedimentary sequences (e.g., Palaeozoic) can be affected by multiple post-depositional transformations such as diagenesis and metamorphism which often leads to the obliteration or distortion of the primary depositionally-induced χ_{in} signal (Schneider et al., 2004; Devleeschouwer et al., 2010; Riquier et al., 2010; Da Silva et al., 2012; Da Silva et al., 2013). In such cases, the recorded magnetic susceptibility signal can be the combined manifestation of a primary detrital, bacteria-related and/or pedogenesis signature and the precipitation of secondary mineralogical phases during early or late diagenesis. Such results have clearly established that a consistent palaeoenvironmental and climatic reconstruction requires a good control of both primary-induced depositional setting and secondary diagenetic signature. In their work, Boulvain et al. (2010) did not give any support or indication concerning the preservation of their recorded magnetic susceptibility signal and it is therefore necessary to validate and complement their results to acquire and provide new data on robust palaeoenvironmental and magnetic studies over the similar time interval.

2. Objectives

What does the long-term sedimentary records from major Devonian carbonate successions teach us on the regional and global palaeoenvironmental development of European carbonate platforms over a long timescale? What are the fundamental criteria to provide a meaningful analysis of past environmental changes and their correlation based on magnetic susceptibility records? Are the long-term correlations of χ_{in} records reliable on a large timescale? What is the link between χ_{in} and environmental parameters on this timescale?

In order to address these questions we have conducted a reliable multi-disciplinary study of the following selected regions: 1) Ardennes (Belgium and France), 2) Rheinisches Schiefergebirge (Germany) and 3) Carnic Alps (Italy/Austria) (Fig. 3) because they expose stratigraphically extended and well-preserved carbonate successions in three of the largest European carbonate complexes.

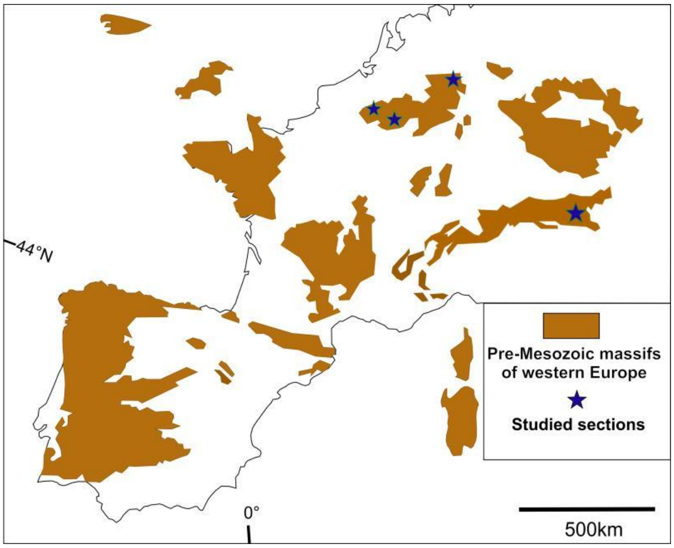

Fig. 3 *Pre-Mesozoic massifs of western Europe with location of the four sections investigated in this PhD (redraw after Eguíluz et al., 2000).*

First, we want to provide a detailed sedimentological and biostratigraphical characterization and illustration of the four selected sections and to accurately reconstruct the depositional contexts that allowed sedimentary archives to be deposited and preserved. Beyond this, we want to establish a precise timing of the major environmental changes that affected these contexts over the specific periods of time characterizing the sections. By integrating published regional and global geological literature with our sedimentological and biostratigraphic results we aim to deliver answers to specific and more general questions on carbonate platform evolutions within Western Europe.

Secondly, we intend to collect the largest possible amount of magnetic susceptibility, major/trace elements and hysteresis measurement to provide (a) a relevant geochemical and geophysical database for each section under investigation in this PhD. By comparing geophysical, sedimentological and geochemical data sets we want to explain and discriminate if the recorded magnetic susceptibility signal in each location corresponds to a primary signal or to a more complex combination of a primary and secondary diagenetic overprinting. In other words, do our magnetic susceptibility data sets reflect the original depositional information or do they correspond to a composite signal.

Thirdly we aim to build a comprehensive scheme and test the magnetic susceptibility techniques as proxy for environmental reconstruction and intra- to extra basinal correlation. In parallel to this we expect to improve our knowledge on the main triggers responsible of the correlation between long-term χ_{in} trends.

3. Structure of the thesis

This thesis gathers both published chapters presenting specific sedimentological investigations conducted on our selected Mid-Late Devonian sections (Chapters 2, 3 and 4), and unpublished (or not yet published) chapters which complement the magnetic susceptibility and geochemical data sets (Chapters 2 and 5) and offer a summary and conclusion on the major issues of this thesis (Chapters 6 and 7).

In Chapter 2 (Pas et al., 2013) we present the sedimentology and biostratigraphy of the continuous Middle Devonian to Mississippian Burgberg section located in the Eastern part of the Rhenish Massif. We illustrate, characterize and reconstruct the evolution of depositional settings that occured in the fore-reef fringe of one of the largest atoll reef described in Europe, i.e., the Brilon Reef Complex, which belongs to the Rhenohercynian basin. In addition, we emphasize the needs to study fore-reef setting in order to provide a precise timing of the major changes that occurred in shallow-water context over a long period of time. In addition to the published data, a complementary geochemical and magnetic susceptibility dataset for the Burgberg section is added and discussed in the second part of this Chapter.

In Chapter 3 we present a dataset including sedimentology, geochemistry and magnetic susceptibility for two outstanding Belgian and French sections (respectively the La Thure and Fromelennes-Flohimont sections) belonging respectively to the northwestern and southern margin of the Dinant Syncline, which belongs to the Rhenohercynian basin. Part 1 of this Chapter is dedicated to the illustration and characterization of the fascinating shallow-water Givetian sediments observed in both sections and the reconstruction of respective palaeoenvironmental models. Then, we aim to reconstruct the large-scale palaeoenvironmental changes and compare them in both sections in order to underline major vertical and lateral facies changes that shaped the Givetian platform in the Dinant Basin. The second part of this Chapter (Pas et al., 2014a) proposes a detailed sedimentological study of the outstanding and continuous Frasnian section recorded in the La Thure quarry and provides a sedimentological model covering the entire sequence of facies in the northwestern margin of the Dinant Syncline. Lithostratigraphic and biostratigraphic published datasets have been combined with new sedimentological and geochemical analyses in order to gain a better understanding of the depositional and environmental changes occurring within the Lower and Middle Frasnian interval in the north-western fringe of the Frasnian platform..

In Chapter 4 (Pas et al., 2014b) we document a detailed sedimentological study of the continuous latest Givetian – early Famennian succession (Freikofel Limestone and Pal Limestone) observed in the upper part of the Freikofel section in order to provide a detailed analysis and illustration of the Upper Devonian “transitional” and pelagic facies within the Carnic Alps. We present a new dataset including conodont biostratigraphy, geochemistry (major and trace element analysis and $\delta^{13}C$ stable isotopes) and magnetic susceptibility analyses in order to gain a better understanding of the depositional and environmental changes in a fore-reef setting within the Carnic Alps. Moreover, the biostratigraphic control of the succession offers the first opportunity to establish a reliable timing for the reworking and demise/drowning of the reefal structure within the Cellon-Kellerwand Nappe. This should improve our knowledge of global changes over a long timescale in Palaeozoic.

Chapter 5 aims to improve our understanding of the origin of the χ_{in} variations recorded in all our sections (and broadly in Palaeozoic limestone succession) and as a corollary, to establish the restriction and applicability of the χ_{in} measurements as palaeoenvironmental/palaeoclimatic proxy and correlative tool in marine limestone. To this end, we have analyzed magnetic hysteresis measurements collected in all the sections, the magnetic susceptibility and well-known detrital input proxies (Al_2O_3, SiO_2, TiO_2, K_2O, Zr, etc.) in order to assess the impact of the detrital primary signature on the χ_{in} signal. Furthermore we have compared our data sets with those of published literature.

Chapter 6 firstly aims to summarize major results on time ranges, depositional settings and long-term palaeoenvironmental changes, magnetic susceptibility and major and trace elements geochemistry and hysteresis magnetic measurements. Based on all previously summarized results, the second part of this Chapter address the reliability of the χ_{in} signal for the long-term correlation over long-distance.

Then, we conclude the Chapter by presenting a key application of the magnetic susceptibility signal for in the recognition of astronomical parameters in Paleozoic sediments.

Chapter 7 presents the major results of this thesis.

4. Methodology

One of the major assets of this PhD thesis is the large number of techniques that have been applied to all the selected sections. These techniques include: 1) bed by bed sampling, facies and microfacies analysis, 2) conodont biostratigraphy, 3) magnetic susceptibility, 4) magnetic hysteresis measurement, 5) major and trace element geochemistry and 6) $\delta^{13}C$ stable isotope measurement.

4.1 Bed by bed description and sampling

Selecting sections and sampling

Selecting of sections, field analysis, sampling and facies description constitute the base of this PhD thesis and have been handled with particular care. A critical aspect was to select suitable sections covering the longest possible stratigraphic interval throughout Mid-Late Devonian while being located in different European carbonate platform settings. For the identification of these sections, numerous reported data have been analyzed and international collaborations were initiated. The fieldwork for this study was undertaken in five distinct field seasons: February 2010, August 2011, October 2011 to March 2012 and August 2014. Initial help in September 2010 was provided by Peter Konigshof from the Senckenberg Institute, who introduced the Devonian stratigraphy of the eastern Rheinisches Schiefergebirge and helped us to find the most suitable outcrop for this study. A two-week fieldwork in August 2011 was then spent in the Carnic Alps and Thomas Suttner from the University of Graz suggested a suitable section at the Italian/Austrian border, which had been preliminary investigated by Schnellbächer (2010). Two major field seasons were completed in Belgium and France, based on the preliminary results of two master thesis (Poulain, 2006; Labaye, 2012).

In each of the four sections, a similar sampling procedure was undertaken, which consisted in collecting at least one sample every 25 cm. But outcrop conditions were variable; therefore, different sampling regimes were performed. In the case of condensed level, where beds are very thin, we collected samples in each bed (~5 cm). In the case of thick and massive beds where the sampling was really hard and sometime unsafe (e.g., Freikofel section), one sample every meter was locally the best sampling rate we could perform. We have taken great care to collect well-preserved samples (e.g., low weathering, dolomitization) as well as a sufficient amount for thin-sections confection, geochemical analyses, magnetic susceptibility measurements and in some case conodont biostratigrphy (e.g., Burgberg and Freikofel sections). Sampling procedure for each section is further detailed in Chapters 3, 4 and 5.

In the early step of this PhD, a first field work was undertaken in Nepal with the help of Megh Raj Dhital from the Thribuvan University (Kathmandu, Nepal) who assisted the organization of a field campaign in the Mustang area. The Devonian section we had planned to samples was expected to be suitable (Marpha section, Garzanti, 1999) but once on site we discovered rocks that were too metamorphosed for our objectives. According to this we decided to samples a section near Kathmandu expected to be Devonian. However, our new datation results yielded an Mid-Late Ordovician age (see Annexes; Pas et al., 2011). Even if results from this investigation contributed substantially to the Palaeozoic sedimentology of Nepal they are not used in this dissertation.

Description of sections and samples

For each section, a thorough description was carried out including bed thickness, fauna (including identification, size, shape and orientation of the fossils), sedimentary structures and relative clay content of each bed. Facies were methodically described on the field or on polished slap while microfacies description are based on thin-section analyses and follow the textural classification from Dunham (1962) and Embry and Klovan (1972). Estimation of sorting is based on the visual charts of Pettijohn et al. (1972) and visual percentage estimation is based on Baccelle and Bosellini (1965). In respect to the preliminary facies analysis, thin-sections were sometime stained using Dickson solution to differentiate calcite, dolomite, ferroan calcite and ferroan dolomite (Dickson, 1965). Furthermore, microfacies were classified from the most distal to the most proximal setting and microfacies curves were constructed for all the sections. As some microfacies represent event-like features they were not limited to a specific depositional setting. For example, limestone with a concentration of shell material can be formed in different shallow-marine and deep-marine facies zones (e.g., Flügel, 2004; p. 799). Therefore, our classification of microfacies in a distal – proximal transect considers 1) the stratigraphic position, 2) the lateral extension and 3) the taphonomy of fossils that characterize the shell beds within the sedimentary sequence (e.g., Kidwell and Bosence, 1991; Fürsich and Oschmann, 1993). Tables summarizing the main microfacies features are provided in Supplementary Material. A total of ~1400 samples were collected for thin-section analysis (La Thure section: ~300 samples; Fromelennes-Flohimont section: ~550 samples; Burgberg section: ~340 samples; Freikofel section: ~200 samples).

4.2. Conodont biostratigraphy

According to the poor biostratigraphic constraint or the necessity to control reported conodont data for the Freikofel and Burgberg sections, we collected a total of 32 samples for conodont biostratigraphy (Freikofel section: 18 samples; Burgberg section: 14 samples). Conodont samples mass was +/- 400 gr and they were totally dissolved with ~ 12 % HCOOH formic acid. Conodonts picked out from dissolution residue were carefully classified and photographed in collaboration with Pierre Bultynck from the Royal Belgian Institute of Natural Sciences. These determinations have provided a precise biostratigraphic framework for our research. Biostratigraphic framework for the Fromelennes-Flohimont and La Thure sections is based on the literature.

4.3. Magnetic susceptibility

Magnetic susceptibility measures the degree of magnetization of a material in response to an applied magnetic field (Dunlop, 1995). The magnetic susceptibility (K) is defined as K = M/H. In other words, the magnetic susceptibility is the ratio between the magnetic field induced in a material (magnetization per unit volume = M) by an external uniform field (H). M and H are both magnetic field and are both expressed in ampere per meter (A/m). K is thus a dimensionless parameter but it can be normalized by volume or by mass.

In this work we referred to the mass-calibrated magnetic susceptibility. It corresponds to the ratio between the volumetric susceptibility (K) and mass and it is expressed in m^3/kg. Different abbreviations have been used in this PhD to describe the mass-calibrated magnetic susceptibility: in published Chapters 2, 3 and 4 we used MS while abbreviation χ_{in} is used for other chapters.

On the whole we have measured the magnetic susceptibility of a representative set of ~1900 samples in the four sections under investigation (La Thure section: 750 samples; Burgberg section: 340 samples; Fromelennes-Flohimont section: 800 samples; Freikofel section: 340 samples). Each sample was measured three times with KLY-3 (Kappabridge from AGICO sited at the University of Liège) and weighted with a precision of 0.01g. This allows the definition of the low-field mass-calibrated magnetic susceptibility for each sample and the establishment of the magnetic susceptibility curve. Magnetic susceptibility curves are presented in Chapters 2, 3, 4 and 7.

4.4. Magnetic hysteresis measurement

Hysteresis measurements for this research were conducted on a representative set of 72 samples in the four sections studied for this PhD (Burgberg section: 18 samples; Freikofel section: 14 samples; La Thure section: 20 samples; Fromelennes-Flohimont section: 20 samples).

Magnetic hysteresis is the relationship between the strength of a variable applied field (H) and the intensity of magnetization (M) induced in a selected substance by this field. Hysteresis behavior of a sample varies in relation with the amount of dia-, para, and ferromagnetic components constituting the sample.

Magnetic hysteresis measurements for this research were acquired, in collaboration with Simo Spassov, using a J-Coercivity "rotation" magnetometer that was developed by the Kazan University (Burov et al., 1986) and sited at the Geophysical center of the Royal Meteorological Institute.

J-Coercivity “rotation” magnetometer allows us to construct isothermal magnetisation curves, more commonly called hysteresis loops. For these measurements, cuboid rock is weighted with a precision of 0.001 gr and the average mass of sample is 2.5 gr. Once the samples is fixed inside of the device, the rotation starts and the magnetizing field increases every 0.5 mT from 0 to +500 mT, then decreases to zero and further decreased to –500 mT. Induced remanent magnetization was measured at each field increment/decrement. Finally, the decay of the IRM_{500mT} was monitored for about 100 s. Additional information on the hysteresis loop and remanence decay curves are provided in Chapter 6. Parameters that can be extracted from hysteresis loops, remanance decay curve and initial magnetic susceptibility (χ_{in}) are M_s, M_{rs}, H_c, H_{cr}, χ_{HF}, χ_{ferro}, χ_{in}, M_{rs}/M_s, H_{cr}/H_c and S_d (Synthetic tables for each section are available in Supplementary material). Definitions and use of all these parameters are described in Chapter 6, dedicated to the results of magnetic measurements.

4.5. Majors and trace elements geochemistry

Major and trace elements were measured on 145 samples in the four sections studied for this PhD (Burgberg section: 34 samples; Freikofel section: 15 samples; La Thure section: 54 samples; Fromelennes-Flohimont section: 42 samples). The 72 hysteresis magnetic measurements were done on samples for which we have geochemical analysis. For the Burgberg, Freikofel and Fromelennes-Flohimont sections, major and trace elements were measured using X-ray Fluorescence (ARL 9400 XP XRF instrument, University of Liège) on regularly spaced samples throughout the sections. The analysed rock samples were carefully cleaned prior to treatment: weathered surfaces were removed. The major elements (SiO_2, TiO_2, K_2O and Al_2O_3) were analysed on lithium tetra- and meta-borate fused glass discs, with matrix corrections following the Traill-Lachance algorithm and were expressed in elemental oxide concentration. Trace elements (Zr, Cu, Ni and Sr) were measured on pressed powder pellets and data were corrected for matrix effects by Compton peak monitoring and expressed in elemental concentration. Precision and accuracy were both shown to be better than 1% for major elements and 5% for trace elements as proven by international standards and analyses of replicate samples, respectively. All these measurement were carried out in collaboration with Nicolas Delmelle and Jacqueline Vander Auwera from the University of Liège.

Concerning the La Thure section, major and trace element concentrations were measured at Activation Laboratories Ltd (Ancaster, Ontario, Canada) in collaboration with Xavier Devleeschouwer from the Royal Belgian Institute of Natural Sciences. Analyses were performed by ICP-MS (major, minor and trace elements). The samples were prepared by fusion with sodium peroxide Na_2O_2 which totally solubilized all the minerals analyzed in an aqueous solution after treatment. Synthetic tables with all important elements measured for each section are provided in Supplementary material.

4.6. $\delta^{13}C_{carb}$ stable isotopes

Analyses of $\delta^{13}C_{carb}$ were done on 63 samples collected around the proposed Frasnian – Famennian boundary interval in the Burgberg and Freikofel sections using bulk mudstone-wackestone. Powdered samples reacted with phosphoric acid in an online carbonate preparation (Kiel III carbonate device) connected to a Thermo-Delta plus XL mass spectrometry instrument at the Vrij Universiteit Brussel, Belgium. Samples were calibrated to the NBS19 standard ($\delta^{13}C$ =1.95 promille VPDB). These measures were done in collaboration with Philipe Claeys and David De Vleeschouwer from the Vrij Universiteit Brussel.

5. General geological overview

This section aims to provide a general overview to the geological context for the sections selected in our PhD. Detailed geological context for each section is provided in Chapters 2, 3 and 4.

During the Middle Devonian, the Burgberg, the La Thure and the Fromelennes-Flohimont sections were located on the southern margin of the Old Red Continent (e.g., Laurussia) within the Rhenohercynian Basin in a tropical position around 20°S (Fig. 4. During the Givetian, this area was part of a wide carbonate platform in the northern passive margin of the Rhenohercynian Ocean (Fig. 2a). At the present time, the Middle Devonian carbonate platform extends from the Avesnois Basin (northern France) to Aachen (western Germany) in the east. In addition, isolated carbonate complexes grew in the east and the southwest (Rheinisches Schiefergebirge and Torbay Reef Complex in southern England respectively e.g., Garland et al. (1996)). The Burgberg section currently belongs to the northeastern part of the Rhenohercynian Massif while the La Thure and Fromelennes-Flohimont sections are located in the east (Fig. 2b; Rhenohercynian Massif extend east to west from the Ardennes to the Rheinisches Schiefergebirge and the Hartz Mountains in Germany).

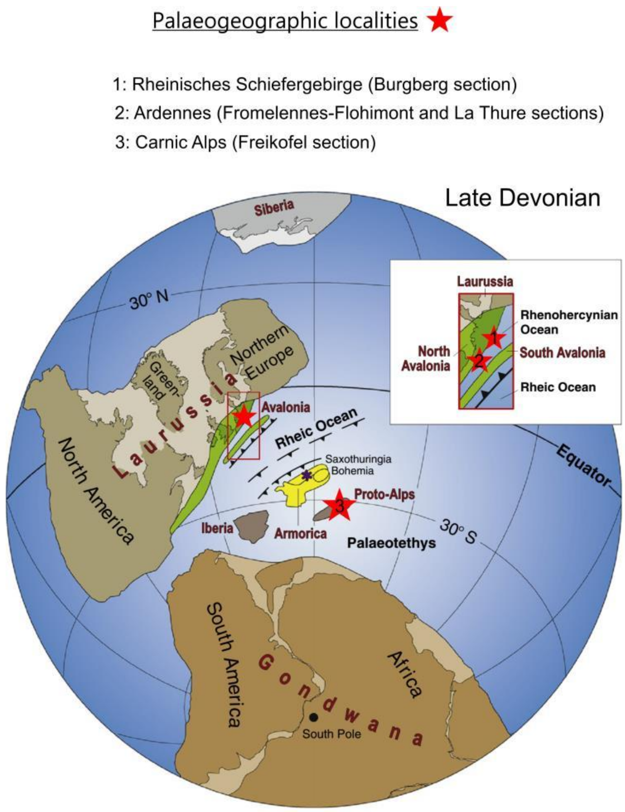

Fig. 4 *Location of Ardennes, Rheinisches Schiefergebirge and Carnic Alps in a palaeogeographic reconstruction for the Late Devonian (modified from Eckelmann et al., 2014).*

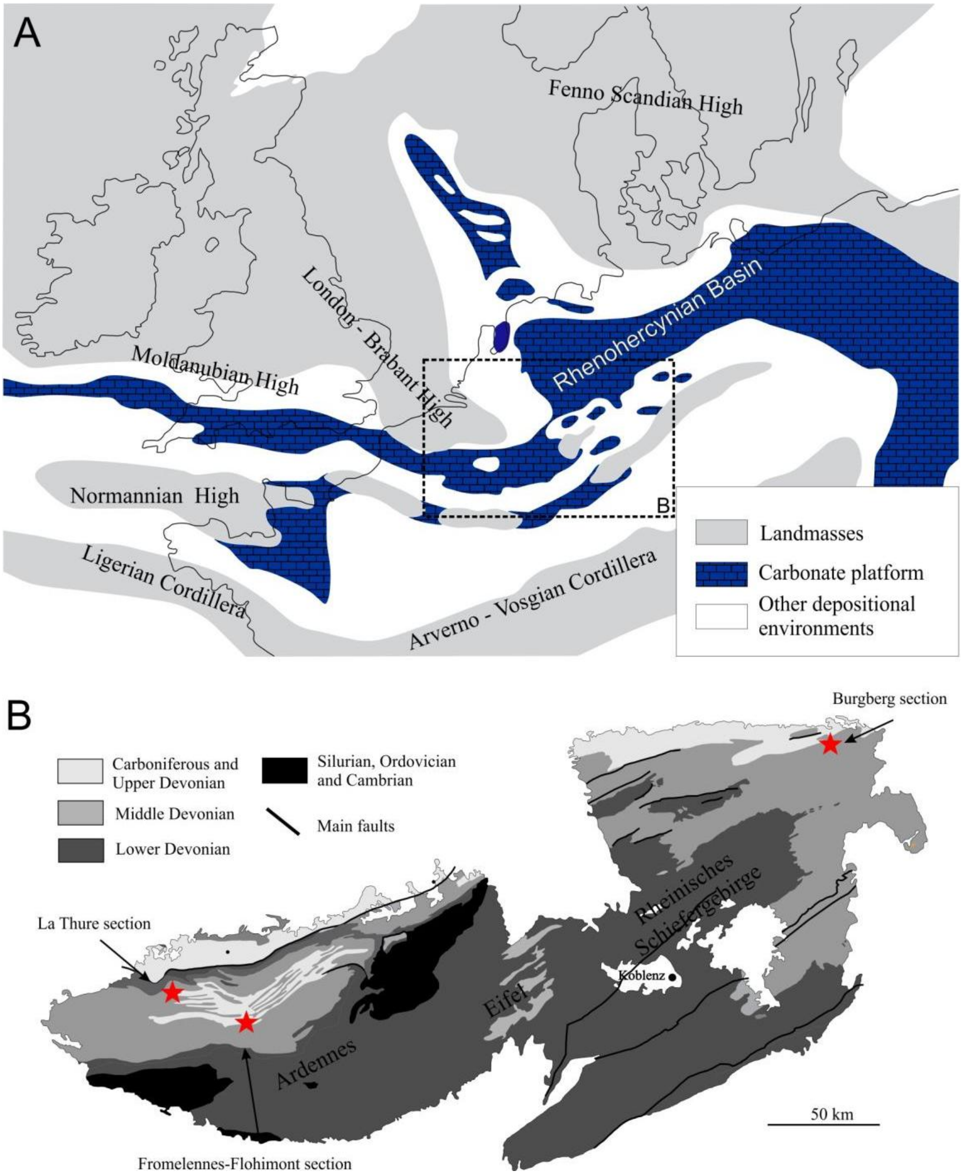

Fig. 5 a *Palaeogeographic reconstruction showing the extension of the carbonate platform developed on the northern Europe during the Middle Devonian before the Variscan orogeny (modified from Ziegler, 1982; McKerrow and Scotese, 1990). The enlargement of the dotted line area is illustrated in the* **Fig. 5b. b** *Geological map of the Rhenohercynian Massif modified after Wehrmann et al. (2005) locating the Burgberg, Fromelennes-Flohimont and La Thure sections.*

During the Middle Devonian the Freikofel section was located 30°S in the Paleotethys Ocean within the Proto-Alps Basin, north of Gondwana (Schönlaub and Histon, 2000) (Fig. 1). At the present time, the Freikofel section is situated in the Carnic Alps, which corresponds to the southern margin of the European Variscides and belongs to an east–west striking South Alpine domain of the Alps, extending across the Italian–Austrian border (Fig. 3).

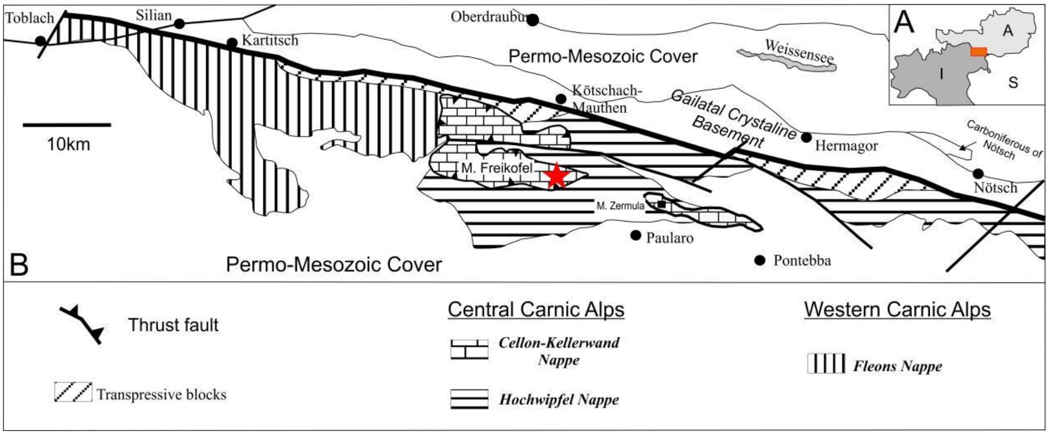

Fig. 3 a *Location of the Carnic Alps at the Austrian-Italian border.* **b** *Location of the Mont Freikofel in the carnic chains (redrawn from Läufer et al., 2001).*

6. References

Bábek, O., Kalvoda, J., Aretz, M., Cossey, P.J., Devuyst, F.X., Herbig, H.G. and Sevastopulo, G. (2010) The correlation potential of magnetic susceptibility and outcrop gamma-ray logs at Tournaisian-Viséan boundary sections in Western Europe. *Geologica Belgica*, **13,** 291-308.

Baccelle, L. and Bosellini, A. (1965) Diagrammi per la stima visiva della composizione percentuale nelle rocce sedimentarie. *Annali della Università di Ferrara, Sezione IX, Science Geologiche e Paleontologiche*, **1,** 59-62.

Boulvain, F., Da Silva, A.C., Mabille, C., Hladil, J., Gersl, M., Koptikova, L. and Schnabl, P. (2010) Magnetic Susceptibility Correlation of Km-Thick Eifelian-Frasnian Sections (Ardennes and Moravia). *Geologica Belgica*, **13,** 309-318.

Brett, C.E., Schindler, E. and Königshof, P. (2011) Sea-level cyclicity, climate change, and bioevents in Middle Devonian marine and terrestrial environments: An overview. *Palaeogeography, Palaeoclimatology, Palaeoecology*, **304,** 1-2.

Burov, B., Nurgaliev, D.K. and Jasonov, P.G. (1986) *Paleomagnetic Analysis* Kazan University Press, Kazan, 176 pp.

Copper, P. (2002) Silurian and Devonian reefs: 80 million years of global greenhouse between two ice ages. In: *Phanerozoic Reef Patterns. SEPM, Special Publication* (Eds w. Kiessling, E. Flügel and J. Golonka), **72**, pp. 181-238.

Da Silva, A.C. and Boulvain, F. (2012) Analysis of the Devonian (Frasnian) platform from Belgium: A multi-faceted approach for basin evolution reconstruction. *Basin Research*, **24,** 338-356.

Da Silva, A.C., De Vleeschouwer, D., Boulvain, F., Claeys, P., Fagel, N., Humblet, M., Mabille, C., Michel, J., Sardar Abadi, M., Pas, D. and Dekkers, M.J. (2013) Magnetic susceptibility as a high-resolution correlation tool and as a climatic proxy in Paleozoic rocks - Merits and pitfalls: Examples from the Devonian in Belgium. *Marine and Petroleum Geology*, **46,** 173-189.

Da Silva, A.C., Dekkers, M.J., Mabille, C. and Boulvain, F. (2012) Magnetic susceptibility and its relationship with paleoenvironments, diagenesis and remagnetization: Examples from the Devonian carbonates of Belgium. *Studia Geophysica et Geodaetica*, **56,** 677-704.

De Vleeschouwer, D., Boulvain, F., Da Silva, A.-C., Pas, D., Labaye, C. and Claeys, P. (2014) The astronomical calibration of the Givetian (Middle Devonian) timescale (Dinant Synclinorium, Belgium). *Geological Society, London, Special Publications*, **414**.

De Vleeschouwer, D., Da Silva, A.C., Boulvain, F., Crucifix, M. and Claeys, P. (2012a) Precessional and half-precessional climate forcing of Mid-Devonian monsoon-like dynamics. *Climate of the Past*, **7,** 1427-1455.

De Vleeschouwer, D. and Parnell, A.C. (2014) Reducing time-scale uncertainty for the devonian by integrating astrochronology and bayesian statistics. *Geology*, **42,** 491-494.

De Vleeschouwer, D., Rakociński, M., Racki, G., Bond, D.P.G., Sobień, K. and Claeys, P. (2013) The astronomical rhythm of Late-Devonian climate change (Kowala section, Holy Cross Mountains, Poland). *Earth and Planetary Science Letters*, **365,** 25-37.

De Vleeschouwer, D., Whalen, M.T., Day, J.E. and Claeys, P. (2012b) Cyclostratigraphic calibration of the Frasnian (Late Devonian) time scale (Western Alberta, Canada). *Bulletin of the Geological Society of America*, **124,** 928-942.

Devleeschouwer, X., Petitclerc, E., Spassov, S. and Préat, A. (2010) The Givetian-Frasnian boundary at nismes parastratotype (Belgium): The magnetic susceptibility signal controlled by ferromagnetic minerals. *Geologica Belgica*, **13,** 351-366.

Dickson, J.A.D. (1965) A Modified staining technique for carbonates in thin section. *Nature*, **205,** 587.

Dunham, R.J. (1962) Classification of carbonate rocks according to depositional texture. In: *Classification of carbonate rocks* (Ed W.E. Ham), pp. 108-121. American Association of Petroleum Geologists Memoir.

Dunlop, D.J. (1995) Magnetism in rocks. *Journal of Geophysical Research*, **100,** 2161-2174.

Eckelmann, K., Nesbor, H.D., Königshof, P., Linnemann, U., Hofmann, M., Lange, J.M. and Sagawe, A. (2014) Plate interactions of Laurussia and Gondwana during the formation of Pangaea - Constraints from U-Pb LA-SF-ICP-MS detrital zircon ages of Devonian and Early Carboniferous siliciclastics of the Rhenohercynian zone, Central European Variscides. *Gondwana Research*, **25,** 1484-1500.

Eguíluz, L., Gil Ibarguchi, J.I., Ábalos, B. and Apraiz, A. (2000) Superposed Hercynian and Cadomian orogenic cycles in the Ossa-Morena zone and related areas of the Iberian Massif. *Bulletin of the Geological Society of America*, **112,** 1398-1413.

Ellwood, B., Crick, R.E., Garcia-Alcalde Fernandez, J.L., Soto, F.M., Truyols-Massoni, M., El Hassani, A. and Kovas, E.J. (2001) Global correlation using magnetic susceptibility data from Lower Devonian rocks. *Geology*, **29,** 583–586.

Ellwood, B.B., Algeo, T.J., El Hassani, A., Tomkin, J.H. and Rowe, H.D. (2011) Defining the timing and duration of the Kačák Interval within the Eifelian/Givetian boundary GSSP, Mech Irdane, Morocco, using geochemical and magnetic susceptibility patterns. *Palaeogeography, Palaeoclimatology, Palaeoecology*, **304,** 74-84.

Ellwood, B.B., Balsam, W.L. and Roberts, H.H. (2006) Gulf of Mexico sediment sources and sediment transport trends from magnetic susceptibility measurements of surface samples. *Marine Geology*, **230,** 237-248.

Ellwood, B.B., Crick, R.E., Hassani, A.E., Benoist, S.L. and Young, R.H. (2000) Magnetosusceptibility event and cyclostratigraphy method applied to marine rocks: Detrital input versus carbonate productivity. *Geology*, **28,** 1135-1138.

Ellwood, B.B., El Hassani, A., Tomkin, J.H. and Bultynck, P. (2014) A climate-driven model using time-series analysis of magnetic susceptibility (χ) datasets to represent a floating-point high-resolution geological timescale for the Middle Devonian Eifelian stage. *Geological Society, London, Special Publications*, **414**.

Embry, A.F. and Klovan, J.E. (1972) Absolute water depth limits of Late Devonian paleoecological zones. *Geologische Rundschau*, **61,** 672-686.

Flügel, E. (2004) *Microfacies analysis of carbonate rocks. Analysis, Interpretation and Application*. Springer-Verlag, Berlin, 976 pp.

Fürsich, F.T. and Oschmann, W. (1993) Shell beds as tools in basin analysis: the Jurassic of Kachchh, western India. *Journal of the Geological Society (London)*, **150,** 169-185.

García-Alcalde, J.L., Ellwood, B.B., Soto, F., Truyóls-Massoni, M. and Tomkin, J.H. (2012) Precise timing of the Upper Taghanic Biocrisis, Geneseo Bioevent, in the Middle-Upper Givetian (Middle Devonian) boundary in Northern Spain using biostratigraphic and magnetic susceptibility data sets. *Palaeogeography, Palaeoclimatology, Palaeoecology*, **313-314,** 26-40.

Garland, J., Tucker, M.E. and Scrutton, C.T. (1996) Microfacies analysis and metre-scale cyclicity in the Givetian back-reef sediments of southeast Devon. *Proceedings - Ussher Society*, **9,** 31-36.

Garzanti, E. (1999) Stratigraphy and sedimentary history of the Nepal Tethys Himalaya passive margin. *Journal of Asian Earth Sciences*, **17,** 805-827.

Gradstein, F.M., Ogg, J.G., Schmitz, M.D. and Ogg, G.M. (2012) Preface. *The Geologic Time Scale 2012*, **1-2,** xv-xvi.

Hladil, J. (2002) Geophysical records of dispersed weathering products on the Frasnian carbonate platform and early Famennian ramps in Moravia, Czech Republic: Proxies for eustasy and palaeoclimate. *Palaeogeography, Palaeoclimatology, Palaeoecology*, **181,** 213-250.

Hladil, J., Cejchan, P., Babek, O., Koptikova, L., Navratil, T. and Kubinova, P. (2010) Dust - A geology-orientated attempt to reappraise the natural components, amounts, inputs to sediment, and importance for correlation purposes. *Geologica Belgica*, **13,** 367-384.

Hladil, J., Gersl, M., Strnad, L., Frana, J., Langrova, A. and Spisiak, J. (2006) Stratigraphic variation of complex impurities in platform limestones and possible significance of atmospheric dust: a study with emphasis on gamma-ray spectrometry and magnetic susceptibility outcrop logging (Eifelian-Frasnian, Moravia, Czech Republic). *International Journal of Earth Sciences*, **95,** 703-723.

Kidwell, S.M. and Bosence, D.W. (1991) Taphonomy and time-averaging of marine shelly faunas. *Taphonomy: releasing the data locked in the fossil record. Plenum, New York***,** 115-209.

Labaye, C. (2012) *Sédimentologie du Givetien et du Frasnien de la carrière de La Thure*, Université de Liège, unpublished master thesis, 58 pp.

Läufer, A.L., Hubich, D.H. and Loeschke, J.L. (2001) Variscan geodynamic evolution of the Carnic Alps (Austria/Italy). *International Journal of Earth Sciences*, **90,** 855-870.

Mabille, C., Pas, D., Aretz, M., Boulvain, F., Schröder, S. and Silva, A.C. (2008) Deposition within the vicinity of the Mid-Eifelian High: Detailed sedimentological study and magnetic susceptibility of a mixed ramp-related system from the Eifelian Lauch and Nohn formations (Devonian; Ohlesberg, Eifel, Germany). *Facies*, **54,** 597-612.

McKerrow, W.S. and Scotese, C.R. (1990) *Paleozoic Palaeogeography and biogeography*. Geological Society of London, Memoir, 433 pp.

Pas, D., Da Silva, A.C., Cornet, P., Bultynck, P., Königshof, P. and Boulvain, F. (2013) Sedimentary development of a continuous Middle Devonian to Mississippian section from the fore-reef fringe of the Brilon Reef Complex (Rheinisches Schiefergebirge, Germany). *Facies*, **59,** 969-990.

Pas, D., Da Silva, A.C., Devleeschouwer, X., De Vleeschouwer, D., Labaye, C., Cornet, P., Michel, J. and Boulvain, F. (2014a) Sedimentary development and magnetic susceptibility evolution of the Frasnian in Western Belgium (Dinant Synclinorium, La Thure section). *Geological Society, London, Special Publications*, **414**.

Pas, D., Da Silva, A.C., Suttner, T., Kido, E., Bultynck, P., Pondrelli, M., Corradini, C., De Vleeschouwer, D., Dojen, C. and Boulvain, F. (2014b) Insight into the development of a carbonate platform through a multi-disciplinary approach: A case study from the Upper Devonian slope deposits of Mount Freikofel (Carnic Alps, Austria/Italy). *International Journal of Earth Sciences*, **103,** 519-538.

Pas, D., Silva, A.C.D., Dhital, M.R. and Boulvain, F. (2011) Sedimentology of a Mid-Late Ordovician carbonate mud-mound complex from the Katmandu nappe in Central Nepal. *Journal of Asian Earth Sciences*, **42,** 452-467.

Pettijohn, F.J., Potter, P.N. and Siever, R. (1972) *Sand and sandstone*. Springer, Berlin.

Poulain, G. (2006) *Etude sédimentologique du Groupe de Givet à Givet*, Université de Liège, unpublished master thesis, 49 pp.

Riquier, L., Averbuch, O., Devleeschouwer, X. and Tribovillard, N. (2010) Diagenetic versus detrital origin of the magnetic susceptibility variations in some carbonate Frasnian-Famennian boundary sections from Northern Africa and Western Europe: Implications for paleoenvironmental reconstructions. *International Journal of Earth Sciences*, **99,** 57-73.

Schneider, J., de Wall, H., Kontny, A. and Bechstadt, T. (2004) Magnetic susceptibility variations in carbonates of the La Vid Group (Cantabrian Zone, NW-Spain) related to burial diagenesis. *Sedimentary Geology*, **166,** 73-88.

Schnellbächer, P. (2010) *Stratigraphy, transport mechanisms and provenience of Devonian carbonate slope deposits (Freikofel, Carnic Alps)*, Universität Greifswald, unpublish master thesis, 124 pp.

Schönlaub, H.P. and Histon, K. (2000) The Palaeozoic evolution of the southern Alps. *Mitteilungen der Österreichischen Geologischen Gesellschaft*, **92,** 15-34.

Śliwinski, M.G., Whalen, M.T. and Day, J. (2010) Comparison of magnetic susceptibility (MS) and other geochemical proxies from the Middle-Late Frasnian of the Canadian Rocky Mountains: Implications for paleoenvironmental and paleoclimatic analyses and interpretations of the punctata Event. *Przeglad Geologiczny*, **58,** 1152-1160.

Śliwiński, M.G., Whalen, M.T., Meyer, F.J. and Majs, F. (2012) Constraining clastic input controls on magnetic susceptibility and trace element anomalies during the Late Devonian punctata Event in the Western Canada Sedimentary Basin. *Terra Nova*, **24,** 301-309.

Tribovillard, N., Algeo, T.J., Lyons, T. and Riboulleau, A. (2006) Trace metals as paleoredox and paleoproductivity proxies: An update. *Chemical Geology*, **232,** 12-32.

Vanderaveroet, P., Averbuch, O., Deconinck, J.F. and Chamley, H. (1999) A record of glacial/interglacial alternations in Pleistocene sediments off New Jersey expressed by clay mineral, grain-size and magnetic susceptibility data. *Marine Geology*, **159,** 79-92.

Wehrmann, A., Hertweck, G., Brocke, R., Jansen, U., Königshof, P., Plodowski, G., Schindler, E., Wilde, V., Blieck, A. and Schultka, S. (2005) Paleoenvironment of an Early Devonian land-sea transition: A case study from the southern margin of the old red continent (Mosel Valley, Germany). *Palaios*, **20,** 101-120.

Whalen, M.T. and Day, J.E. (2008) Magnetic susceptibility, biostratigraphy, and sequence stratigraphy: Insights into Devonian carbonate platform development and basin infilling, western Alberta, Canada. *Society for Sedimentary Geology*, **89,** 291-314.

Ziegler, A.P. (1982) *Geological Atlas of Western and Central Europe*. Shell Internationale Petroleum Maatschappij, 130 pp.

Geopetal structures in tabulate coral, Givetian limestone, Burgberg, Germany

Chapter 2

The Burgberg section (Rheinisches Schiefergebirge, Germany)

First part

Sedimentary development of a continuous Middle Givetian to Lower Carboniferous section from the fore-reef fringe of the Brilon reef-complex (Rheinisches Schiefergebirge, Germany)

Based on: Pas, D., Da Silva, A.C., Cornet, P., Bultynck, P., Königshof, P., Boulvain, F. (2013) : Sedimentary development of a continuous Middle Givetian to Lower Carboniferous section from the fore-reef fringe of the Brilon reef-complex (Rheinisches Schiefergebirge, Germany). *Facies,* 59, 969-990.

Sedimentary development of a continuous Middle Devonian to Mississippian section from the fore-reef fringe of the Brilon Reef Complex (Rheinisches Schiefergebirge, Germany)

Damien Pas · Anne-Christine Da Silva · Pierre Cornet · Pierre Bultynck · Peter Königshof · Frédéric Boulvain

Received: 4 June 2012 / Accepted: 19 November 2012 / Published online: 22 December 2012

Abstract The Brilon-reef complex is one of the biggest Devonian carbonate buildups ($\sim 80\ km^2$) of the Rheinisches Schiefergebirge. The Burgberg section is located in the southeastern fore-reef area of the Brilon Reef Complex and exposes a succession of strata (117 m thick), which extends from the Middle Givetian (middle *varcus* conodont Zone) to the Viséan (*bilineatus* conodont Zone). Field and microfacies observations led to the definition of nine microfacies that are integrated into a sedimentary model divided into off-reef, intermediate fore-reef, and proximal fore-reef sedimentary domains (SD). The off-reef domain (SD1) is the most distal setting observed and is characterized by fine-grained sediments, dominated by pelagic biota and the local occurrence of gravity-flow deposits. The intermediate fore-reef (SD2) is characterized by a mixture of biota and sediments coming from both deeper-water and shallow-water sources and is influenced by storm and gravity-flow currents. In this domain, *Renalcis* mound-like structures developed locally. Finally, the proximal fore-reef (SD3) corresponds to the most proximal setting that is strongly influenced by gravity-flow currents derived from the Brilon Reef Complex. The temporal evolution of microfacies in the fore-reef setting of the Burgberg section show five main paleoenvironmental trends influenced by the onset, general development, and demise/drowning of the Brilon Reef Complex. Fore-reef to off-reef lithologies and their temporal changes are from the base to the top of the section: (U1)—fine-grained sediments with large reef debris, corresponding to the initial development of the reef building upon submarine volcaniclastic deposits during the Middle Givetian (middle *varcus* Zone) and first export of reef debris in the fore-reef setting; (U2)—high increase of reef-derived material in the fore-reef area, corresponding to a significant progradation of the reef from the Middle Givetian to the Early Frasnian (maximum extension of the Brilon Reef Complex to the south, *disparilis* to the *falsiovalis* conodont biozones); (U3)—progressive decrease of shallow-water derived material and increase of fine-grained sediments and deep-water biota into the fore-reef setting, corresponding to the stepwise withdrawal of the reef influence; from the Middle to the Late Frasnian (*jamieae* conodont Zone); (U4)—development of a submarine rise characterized by nodular and cephalopod-bearing limestones extending from the Late Frasnian to the Late Famennian corresponding to the demise and drowning of the Brilon Reef Complex as a result of the Late Frasnian Kellwasser events (upper *rhenana* and *triangularis* conodont biozones); (U5)—significant deepening of the Burgberg area starting in the Late Famennian, directly followed by an aggrading trend marked by pelagic shales overlying the nodular limestone deposits.

Keywords Microfacies · Brilon fore-reef · Rheinisches Schiefergebirge · Mid-Late Devonian · Carboniferous · Sedimentology · Kellwasser events

D. Pas (✉) · A.-C. Da Silva · P. Cornet · F. Boulvain
Sedimentary Petrology, B20, University of Liège (ULg), Sart-Tilman, 4000 Liège, Belgium
e-mail: dpas@ulg.ac.be

P. Bultynck
Department of Paleontology, Royal Belgian Institute of Natural Sciences, rue Vautier 29, 1000 Brussels, Belgium

P. Königshof
Senckenberg, Research Institute and Natural History Museum Frankfurt, Senckenberganlage 25, 60325 Frankfurt, Germany

Introduction

During Middle Devonian time, the Brilon Reef Complex, western Germany, belonged to a large carbonate platform belt developed at the southern margin of the Old Red Continent. This reef complex is considered to be one of the largest Middle Devonian carbonate buildups ($\sim$80 km^2) identified within the eastern Rheinisches Schiefergebirge (RS). Among the various Middle Devonian reef complexes recognized throughout the world (Copper 2002), the Brilon Reef Complex is one of the first studied and most investigated. The mapping, stratigraphic, and facies studies of the 1930s and 1960s provided a first summary on the dimension of the reef complex and an overview on the main lithologies and their distribution pattern in the area (Paeckelmann 1936; Jux 1960; Bär 1968). Aiming to characterize the Devonian reefs of Central Europe, Krebs (1967, 1971, 1974) interpreted the Brilon reef as an "isolated carbonate complex (atoll) at the outer shelf margin." Using new data from the federal drilling project, Brinckmann (1981) identified two steps of reef growth: an early phase at the northern margin of the complex, beginning in the Middle Devonian (possibly as early as Eifelian), and a later phase at the southern margin beginning in the Late Givetian. However, the reef growth might have started earlier in the southern margin, as Malmsheimer et al. (1990) identified the first reef-related debris during the lower *varcus* Zone (early Givetian).

Reef growth at the northern and southern margin during Late Givetian and Early Frasnian resulted in the formation of an atoll-like reef (Brinckmann 1981). Based on drill core from the south of the Brilon Reef Complex, Machel (1990) developed a model for the Middle Devonian and Early Frasnian facies including back-reef, reef-core, and fore-reef setting. Using this model, Machel (1990) recognized three main stages of carbonate sedimentation in the Brilon Reef Complex: (1) Initiation of carbonate sedimentation starting with the final phase of Middle Devonian volcanism, (2) major accumulation of "reefal sediment", and (3) deposition of sediment in which reef influence is not clearly defined. Conodont biostratigraphy indicates that carbonate sedimentation commenced in the Late Givetian and lasted until at least the beginning of the Frasnian but the Givetian-Frasnian boundary was not clearly identified (Machel 1990). Machel (1990) and Städter and Koch (1987) recognized that through the Upper Givetian, the reef-core shifted gradually towards the basin located in the southeast. In the same period, Stritzke (1990) performed a general facies study of the southeastern margin of the Brilon Reef Complex on the basis of 15 sections (including the Burgberg section). This study resulted in the definition of three main facies corresponding to reef-core, fore- and off-reef setting, and their evolution from the Middle Givetian to the Upper Famennian (middle v*arcus* to lower *bisphatodus* zones).

In summary, the Brilon Reef Complex was the subject of various studies providing a good overview on the major facies belts and their general evolution through time. However, a comprehensive study integrating the entire development of the reef (onset, expansion, and drowning) built on a detailed facies description of a long and continuous interval was still lacking. In this paper, we document a detailed sedimentological study of the continuous Middle Givetian to Viséan interval ($\sim$40 Ma) recorded in the Burgberg section in order to provide a detailed sedimentological model covering the entire sequence of facies in the southeastern area of the Brilon Reef Complex. We combined paleontological and sedimentological datasets from the literature and new geochemical data (δ^{13}C analysis around the Frasnian-Famennian boundary) in order to gain a better understanding of the depositional and environmental changes in a fore-reef setting within the Rheinisches Schiefergebirge. Moreover, the good biostratigraphic control of most of the succession offers the first opportunity to provide a well-constrained timing of the onset, main development, and demise/drowning of the reefal structure in its southeastern part and to improve our knowledge of global changes over a long time scale. This outstanding succession in a fore-reef setting is also an opportunity to evaluate the potential of a single section in the recognition of major paleoenvironmental changes occurring in shallow-water reefal habitats.

Location and geological background

The Rhenohercynian Massif (RM) is composed of Paleozoic (Ordovician to Carboniferous) sedimentary and volcanic rocks that were accumulated in the southern part of the Old Red Continent. The RM extends east to west from the Ardennes area in Belgium to the Rheinisches Schiefergebirge and the Harz Mountains in Germany. The rocks of the RM were deformed and folded during the Variscan orogeny; deformation and very low to low-grade metamorphism prograded from the SE to NW during the Late Carboniferous Period (e.g., Ahrendt et al. 1983). During the Middle Devonian, the Burgberg section was located on the southern margin of the Old Red Continent within the Rhenohercynian Basin (Fig. 1), close to the Brilon Reef Complex. In the late Early and Middle Devonian, eustatic sea level rise, leading to a shoreline shifts to the north (e.g., Johnson 1970; Johnson et al. 1985; House 1985), deeply changed the sedimentary setting of the southern margin of the Old Red Continent. The onset of these significant sea-level changes is marked by the change from siliciclastic, deltaic shallow-marine environments ("Rhenish" facies) in the Lower Devonian, to an open-marine argillaceous shale and pure limestone-dominated facies ("Hercynian" facies) in the Middle Devonian (Erben 1962). This transgression resulted in the development of Middle Devonian large-scale reef structures in the RS, such as the Brilon Reef Complex.

During the Middle Devonian, extensional tectonics in the southern and eastern part of the RS lead to submarine volcanism (summary and further references in Nesbor 2004; Kroner et al. 2007; Königshof et al. 2010; Salamon and Königshof 2010). This volcanism produced submarine rises that enabled reef growth in a basinal facies setting, and the southern fringe area of the Brilon Reef Complex is thought to have developed simultaneous to the placement of these volcanic rocks ("Hauptgrünsteinzug") in a basinal setting (Sunkel 1990). At the southeastern margin of Brilon, accumulation of reef debris started in the Middle Givetian (lower v*arcus* Zone) (Malmsheimer et al. 1990), while in the northern part it started in the Lower Devonian (possibly as early as Eifelian) (Brinckmann 1981). Flourishing reef growth at the northern and southern margin from the Late Givetian to the Early Frasnian led to the establishment of an atoll-like reef (Brinckmann 1981). During the Upper Devonian, the drowning of the Brilon Reef Complex is confirmed by Upper Devonian and Lower Carboniferous condensed cephalopod limestones overlying the Brilon Reef Complex (Malmsheimer et al. 1990). In terms of regional geology, the Burgberg section belongs to the northern flank of the Messinghausen anticline (Fig. 2), southeast of the Brilon anticline. In the eastern RS, the Middle Devonian reefal limestone is referred to as "Massenkalk" (von Dechen 1858). According to Krebs (1967, 1974), the "Massenkalk" can be divided into three lithologic units: (1) an initial biostromal "bank-type Massenkalk" ("Schwelm" facies of Paeckelmann 1922); (2) a subsequent biohermal "reef-type Massenkalk" ("Dorp" facies of Krebs 1967); (3) a "cap-type Massenkalk" ("Iberg" facies of Krebs 1967). The time-equivalent of the "Massenkalk" in the off-reef and back-reef setting is called the "Flinz" facies. A summary of the lithostratigraphic subdivision of the Brilon area is given in Fig. 3.

Materials and methods

A detailed bed-by-bed description of the Burgberg sections (Figs. 4, 5) and sampling was performed, with average sampling rate of one sample per 25 cm (a total of 340 samples for thin-sections). The textural classification used to characterize the microfacies follows Dunham (1962) and Embry and Klovan (1972). Estimation of sorting is based on the visual charts of Pettijohn et al. (1972), while visual percentage estimation is based on the comparison charts of Bacelle and Bosellini (1965). Thin-sections were stained using Dickson solution (1965) to differentiate calcite, dolomite, ferroan calcite, and ferroan dolomite. Fourteen samples (±400 g) from pelagic facies were taken for conodont investigation. Conodonts are common, most samples containing 25–50 specimens/kg.

Analyses of $\delta^{13}C_{carb}$ were done using bulk mudstone-wackestone samples. Powdered samples reacted with phosphoric acid in an online carbonate preparation (Kiel III

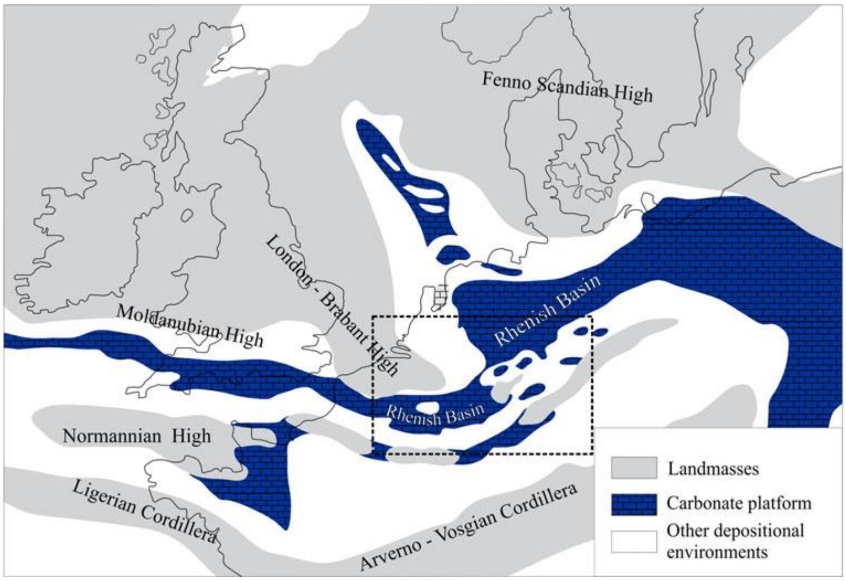

Fig. 1 Paleogeographical setting showing the large carbonate platform developed in northern Europe during the Middle Devonian (modified after Ziegler 1982; McKerrow and Scotese 1990). The enlargement of the *dotted line area* is illustrated in Fig. 2a

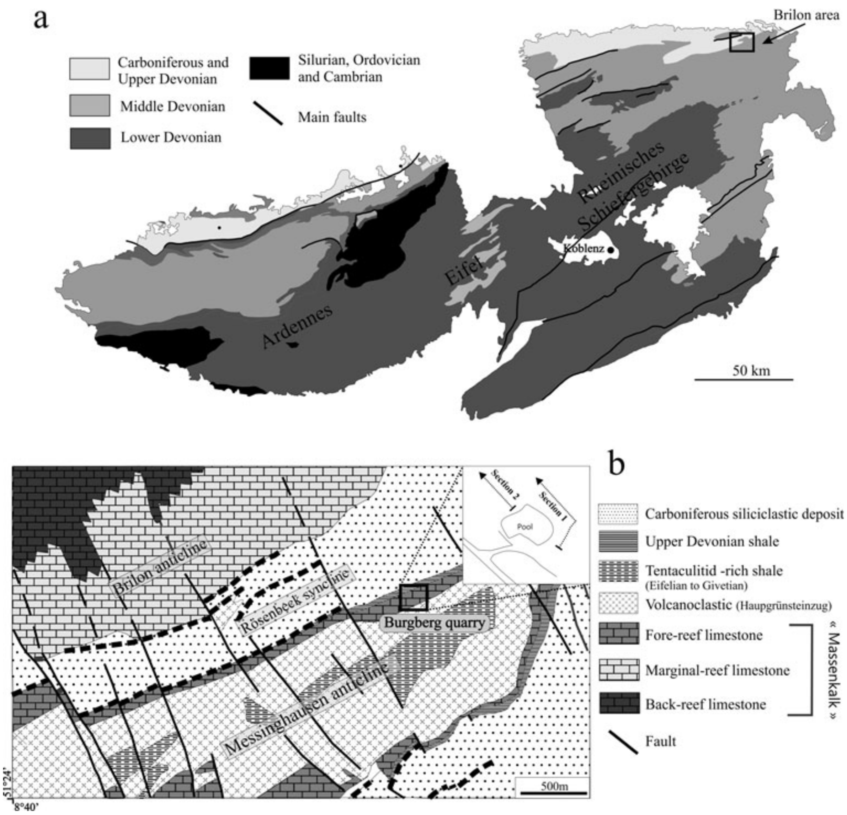

Fig. 2 **a** Location of the Brilon Reef Complex on a simplified geological map of the Rhenohercynian Massif, modified after Wehrmann et al. (2005). **b** Simplified geological map of the Messinghausen anticline with position and enlargement of the Burgberg quarry showing the two studied sections (modified from Ribbert et al. 2006)

carbonate device) connected to a Thermo-Delta^{plus}XL mass spectrometry instrument at the Vrij Universiteit Brussel, Belgium. Samples were calibrated to the NBS19 standard ($\delta^{13}C$ = 1.95 promille VPDB).

Results

Biostratigraphy

Several conodont biostratigraphic studies were conducted at the Burgberg quarry (Stritzke 1990; Aboussalam 2003). Nevertheless, they were not sufficient to provide a precise conodont biostratigraphy for this work considering the difficulties for fitting the published lithological columns with our work, as well as the recent changes in conodont terminology. Therefore, additional conodont samples were collected from the Middle Givetian (middle *varcus* Zone) to the Viséan (*bilineatus* Zone). Recognition of this last conodont zone is based on the occurrence of the *Crenistria* Limestone (Nicolaus 1963), a time-equivalent marker horizon (Korn and Kaufmann 2009) of the *bilineatus* Zone within the eastern Rheinisches Schiefergebirge (Warnke 1997). Complete biostratigraphic data resulting from the combination of previously published work (Stritzke 1990, Korn and Kaufmann 2009), new conodont data, and $\delta^{13}C$ measurements around the Frasnian/Famennian boundary (Fig. 6b) allowed the recognition of the Lower and Upper Kellwasser events, which in turn confirms our results for the Frasnian-Famennian boundary.

Description of the section

The succession exposed at Burgberg is overturned and the strata are oriented N110°E with an average dip of 70°SSE. The description of the Burgberg quarry is based on a combination of two sections called section 1 and section 2, respectively (for location of sections, see inset in Fig. 2b), which are partly superposed and provide a stratigraphically continuous succession of strata. The composite section is 117 m thick (Fig. 6) and covers a well-constrained stratigraphic interval (see above 1). The studied section begins with a thick limestone bed (Fig. 4b) overlying a 60-cm-thick outcrop gap. Below the gap, rocks corresponding to the uppermost part of spillitic tuffs of the so-called “Hauptgrünsteinzug” (Clausen and Korn 2008) were found.

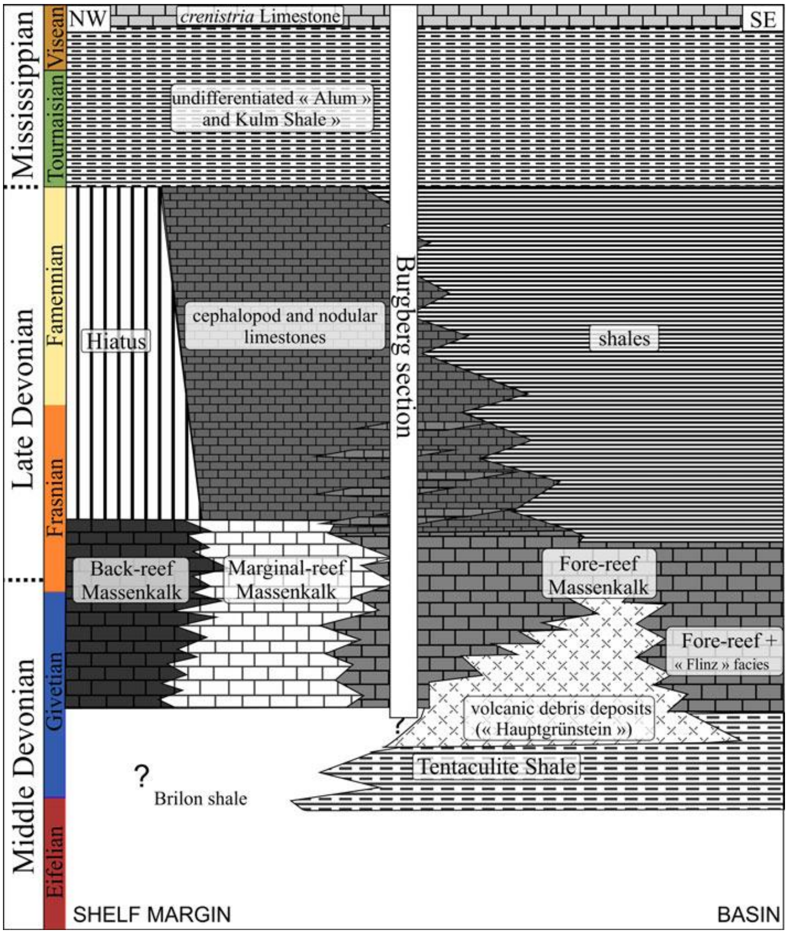

Fig. 3 Stratigraphy and facies relationships of the Brilon Reef Complex area, modified after Malmsheimer et al. (1990) with the stratigraphic interval of the Burgberg section

Five lithological units have been after defined:

– Unit 1 (~4.5 m thick; Figs. 4a, 6). The lower part of this unit (from 0 to 2.15 m) corresponds to several-dm to m-thick dark grey, lenticular-shaped, coarse-bioclastic limestone beds intercalated within black carbonaceous shale layers (Fig. 4a). Bioclasts in the limestone are dominated by several-cm-sized fragments of stromatoporoids, tabulate corals, brachiopods, and crinoids. In the upper part of this unit, a 50-cm-thick alternation of dm-thick dark-grey, fine-grained limestone beds and cm-thick shaly interbeds are observed (from 2.15 to 2.65 m). Within the middle part of the last bed belonging to this unit, a deeply weathered tuff occurs.
– Unit 2 (~55.5 m thick, between 4.5 and 60 m) is mainly composed of grey to blue lenticular to slightly lenticular-bedded bioclastic limestone. The average thickness of the beds is about 60 cm, but m-thick beds occur commonly. A conspicuous character of this unit is the local presence of erosional features on the lower bed surfaces (Fig. 4b). The main bioclasts are crinoids and fragments of reef builders (mainly stromatoporoids). From the middle to the upper part of this unit, stromatoporoid fragments can reach 25 cm in size, while in the lower part these fragments are generally smaller.
– Unit 3 (~29.1 m thick, between 60 and 89.1 m) consists of grey, well-bedded limestone. The main difference with the underlying unit is the strong decrease in the abundance and size of bioclasts, the scarcity of stromatoporoids, and the decrease in bed thickness. Only two massive m-thick beds are observed, located between 79.4 and 82.4 m (bed 166 and 167). These beds are light grey and show common occurrences of spar-filled fractures and irregular cm- to dm-sized cavities filled with calcite.
– Unit 4 (~12.1 m thick, between 89.1 and 112.5 m) corresponds mainly to a several-m-thick succession of

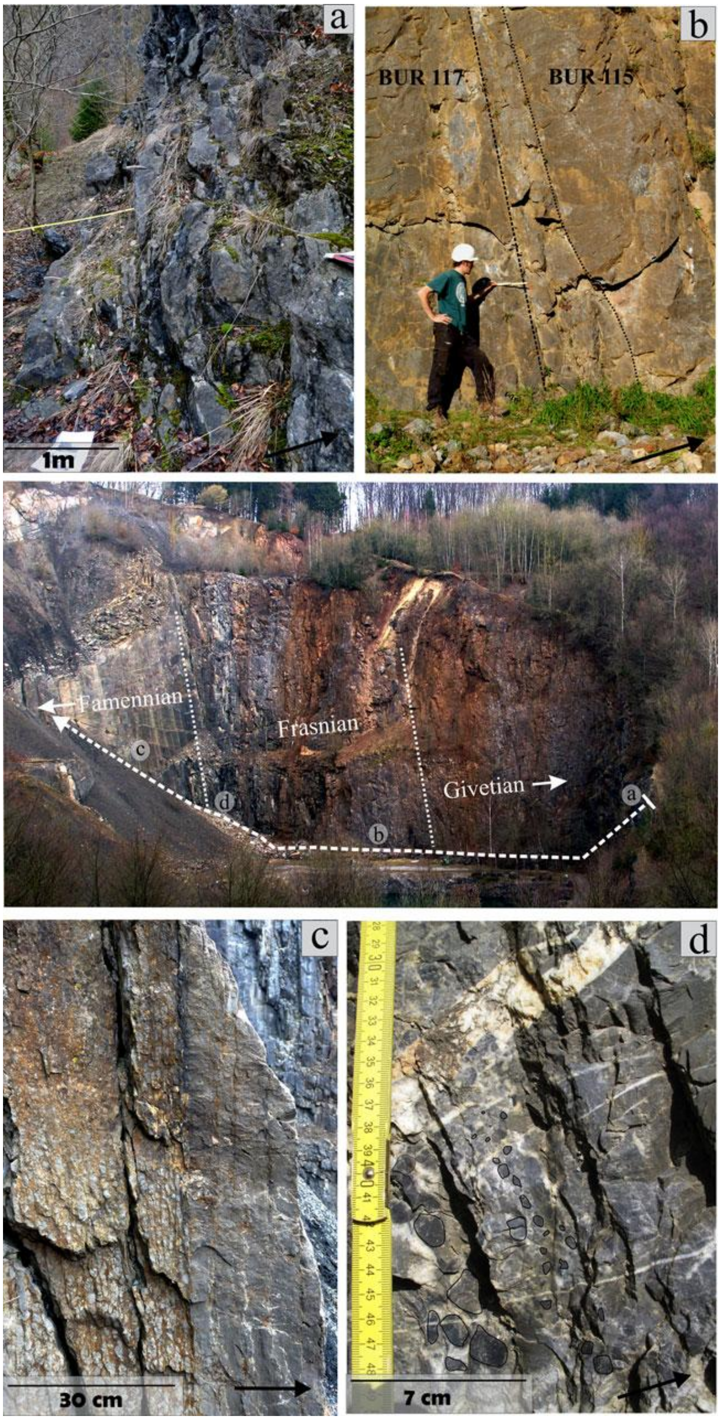

Fig. 4 In the center of the figure: Section 1 of the Burgberg quarry (view from the south) with location of the photographs **a–d** (the *arrow* in the *lower right* of the pictures points to the stratigraphic base). **a** Alternation of *thick lenticular-shaped* coarse-grained limestone with thin carbonaceous black shale characterizing the base of the section (microfacies MF3–4). **b** Channel-like structure within bed number 116 (microfacies MF8–9). **c** Thin-bedded limestone passing upward into nodular limestone (MF3). **d** Breccia texture showing coarsening-upward sorting of lithoclasts (delimited by *black lines*) and highly fractured facies (microfacies breccia, MF5)

monotonous light-grey, fine-grained limestone with numerous pressure-solution surfaces (lithologically termed "Flaserkalk"; e.g., Bandel 1974) passing upward into nodular limestone (Fig. 4c). The light-grey, fine-grained limestone is characterized by the common occurrence of thin-shelled bivalves and cephalopods (both shells are several mm in sizes). The nodular limestone is composed of mm- to cm-sized ovoid nodules, which are oriented parallel to the bedding and are highlighted by the contrast of color with the argillaceous dolostone matrix. This uppermost part of the section encompasses the Frasnian-Famennian boundary, located between 96 and 97 m (Fig. 6). A particular character of this unit is the occurrence of a brecciated level between 93 and 94 m (bed number 189; Fig. 6a, b) with inverse grading (Fig. 4d) and black, angular-shaped clasts from 0.5 to 3 cm in size (see Section "Description of the section" for a complete description of this bed). This level and the following ones are affected by numerous calcite-filled veins, crossing the bedding (Fig. 4d).

– Unit 5 ($\sim$4.5 m thick, between 112.5 and 117 m) corresponds to the last part of the section and consists mainly of dark-brown to black shale ("Alum and Kulm Shale" of the German literature). In the RS, the Devonian-Carboniferous boundary is marked by the first appearance of the "Lower Alum Shale" overlying fine-grained and nodular limestone (Fig. 5a). The topmost section is marked by the occurrence of three dm-sized limestone beds (so-called *Crenistria* Limestone; Nicolaus 1963; Warnke 1997) (Fig. 5b) named after the occurrence of *Goniatites crenistria*, stratigraphically belonging to the Early Late Viséan (Korn 1996; Korn and Horn 1997). These particular limestone beds are a lithologic marker horizon recognized within the entire eastern RS basin (Korn and Kaufmann 2009).

Microfacies

The field observations and petrographic analyses of thin-sections allowed the discrimination of nine microfacies. The microfacies were compared with other existing microfacies models such as those of Mamet and Préat (1985), Tucker (1974), Wendt and Aigner (1985), May (1994), and Casier and Preat (2007).

MF1: brown to black shale (Figs. 5b, 7a)

This microfacies occurs in the uppermost part of the section between 112.5 and 117 m within Unit 5 and corresponds to dark-brown to black shale with rare limestone nodules. Nodules are cm- to dm-sized and locally appear to coalesce into beds. MF1 is characterized by being laminated and by containing abundant clay particles, common silt-sized quartz grains (average size around 5 µm), and mica flakes. Locally, mm-thick layers enriched in silt-sized quartz occur. Bioclasts are absent.

Interpretation

Shale is generally thought to be deposited in basinal settings (Krebs 1967; Stow and Piper 1984; Piecha 1993; Boulvain et al. 2004) where the main sedimentary process is the settling of suspended particles likely below the storm wave-base (SWB). The absence of bioclasts within this sediment suggests an environment located far from shallow-water influence.

MF2: microbioclastic mudstone to wackestone

This microfacies forms thin-bedded limestone beds with an average thickness of 4 cm, which alternate with nodular/mottled limestone (Fig. 7b, c). It occurs only in the upper part of the section (from 80 to 112.5 m). The thin limestone beds are mostly characterized by the occurrence of pelagic/hemipelagic microfossils, such as goniatites and tentaculitids, thin-shelled pelagic bivalves, entomozoacean ostracods, and sponge spicules. These fossils are scattered in a micritic matrix. The micrite is light grey to grey in color with an average crystal size of around 4 µm. Even if goniatite shells (Fig. 7d) occur, tentaculitids and shells of juvenile pelagic bivalves are the most commonly observed microfossils (Fig. 7e). Locally, fine-grained crinoid debris is common and may be densely packed (local packstone texture). Bioturbation is well developed in this microfacies and is highlighted by selective dolomitization. Dolomitization is common and affects the nodular/mottled fabric (Fig. 7b) mostly where clay minerals are present.

Interpretation

In various sedimentological studies, Devonian cephalopod limestone in Europe has been thought to have accumulated on submarine rises at depths reaching several tens to about 100 m (e.g., Wendt and Aigner 1985; Rabien 1956; Tucker 1973, 1974). Wendt and Aigner (1985) suggested that these carbonates most probably formed during times of reduced sedimentation. A similar setting and faunal composition has also been described from the Gondwana shelf in a Late Devonian section in Thailand (Königshof et al. 2012, cum lit.). The predominance of deep-water fossils such as goniatites, tentaculitids, thin-shelled bivalves, entomozoacean ostracod shells, and sponge spicules points to a hemipelagic/pelagic environmental setting. The very fine grained sediment of microfacies MF2 points to a low-energy setting, probably located below the SWB where the main sedimentary process is the settling of suspended particles. The vertical evolution from a thin-bedded to a nodular/mottled fabric at the outcrop scale can be easily explained by changes in the bioturbation intensity, carbonate/clay ratio and pressure solution processes. The selective dolomitization commonly occurring in the nodular/mottled fabric is an argument in favor of bioturbation. Gingras et al. (2004) and Clari and Martire (1996) have shown that bioturbation promotes selective dolomitization by increasing the permeability and porosity (e.g., incorporation of organic matter, winnowing of the sediment, remobilization of the clay). Furthermore, according to Möller and Kvingan (1988) and Bathurst (1987), pressure solution processes are also considered to play an important role in the formation of the nodular fabric.

MF3: Carbonaceous microbioclastic wackestone to packstone (Fig. 7f)

This microfacies occurs in up to several cm-thick calcareous shale layers in the first 4 m of the section, alternating with the several-dm-thick dark bioclastic limestone beds of the MF4 (Unit 1, Fig. 4a). They are mainly characterized by common occurrence of bioclast hash (average size ~100 μm), a generally good sorting of the sediment, thin lamination, and black color of the matrix. Most of the bioclasts are undeterminable but locally thin shells of tentaculitids, ostracods, brachiopods, and crinoid debris (average size around 2 μm) can be recognized. Between the fine-grained bioclasts, insoluble residue and clay and silt-sized quartz are observed while matrix is mostly absent; this corresponds to the "stylocumulate texture" of Logan and Semenuik (1976). Locally, mm- to cm-thick irregular and discontinuous layers of MF4 with lower sharp erosional boundary are intercalated in this microfacies (Fig. 7g). As shown below, several-dm-thick layers of MF3 can also be intercalated in this microfacies. Maletz (2006) described a Middle Devonian graptolite fauna (*Dictyonema* and *Ruedemannograptus*) originating from these black calcareous shales from the Brilon reef.

Interpretation

The good sorting of bioclasts, the fine lamination, and the presence of a graptolite fauna suggest a calm sedimentary setting below SWB where deposition is controlled by the settling of particles. Moreover, the presence of thin-shelled tentaculitids, ostracods, bivalves, and brachiopods suggests an open-marine hemipelagic environment. The intercalation of mm- to several-cm-thick layers of MF4 are related to debris-flow deposits originating from the marginal reef area (see MF4), which indicates that episodic downslope transport significantly influenced the Brilon reef.

Fig. 5 *Top of the figure*: Section 2 of the Burgberg quarry (view from the north) showing the transition from the top of the Frasnian, to the lower part of the Carboniferous and location of pictures (**a**) and (**b**). The *arrow* in the *lower right* of the pictures points to the stratigraphic base. **a** Transition from thin-bedded limestone (MF2) with very thin shaly interbeds to the "Lower Alaun Shale" (MF1). This transition corresponds to the petrographic Devonian-Carboniferous boundary. **b** Intercalation of three limestone beds (delimited by *black* and *dotted lines*) called the "*Crenistria* beds" (Rüdiger Stritzke, pers. comm.). These beds contain specimens of *G. crenistria*, a typical goniatite of the Lower Carboniferous ▶

MF4: coarse-grained bioclastic packstone (Fig. 7h)

Bioclastic packstone occurs only in a few dark beds within the first 4 m of the section, and corresponds to the first appearance of limestone after the thick volcanic debris deposits ("Hauptgrünsteinzug"). MF4 alternates with sharp or gradual transition with MF3 carbonaceous microbioclastic packstone levels (Unit 1, Fig. 4a), or occurs as mm- to cm-thick intercalations within MF3 (Fig. 7g). MF4 is a black coarse-bioclastic limestone occurring in several-dm-thick lenticular beds and showing slumping features (thick beds in Fig. 4a). MF4 limestone beds contain stromatoporoid fragments (locally dm-sized), tabulate corals, and brachiopods. Bioclasts are poorly sorted, usually broken, and commonly mm to cm in size. They are represented, in descending order, by crinoids, brachiopods, tabulate corals, bivalves, trilobite shells, bryozoans (Fenestellidae), stromatoporoids, rugose corals, and tentaculitids. Other grains are micritic clasts (average size around 2 mm) and sub-angular mm- to cm-sized lithoclasts of wackestone. Occasionally cm-sized lithoclasts of tuff occur. The allochems commonly show pressure solution structures such as concave-convex and sutured contacts. The matrix of this packstone is a dark-brown micrite, although in some places, insoluble residue and clay occurs between the bioclasts and lithoclasts, while the texture is grain-supported. This corresponds to the "stylocumulate texture" of Logan and Semenuik (1976).

Interpretation

The thickness variations and lenticular shape of the beds (Fig. 4a), the poor sorting and preservation of bioclasts (variable size and shape), the presence of lithoclasts of different origins, and the matrix consisting of micrite and argillaceous material are features commonly linked to debris-flow deposits (Flügel 2004). Regarding the faunal assemblage, two sources of sediment can be distinguished: (1) a shallow-water source indicated by the common presence of reef-builder debris such as stromatoporoids, rugose and tabulate corals, and bryozoans, and (2) a deeper-water source indicated by trilobites, brachiopods, and


Devonian/Carboniferous boundary
Famennian
Carboniferous
Frasnian
a
b
10 cm
50 cm
Crenistria beds

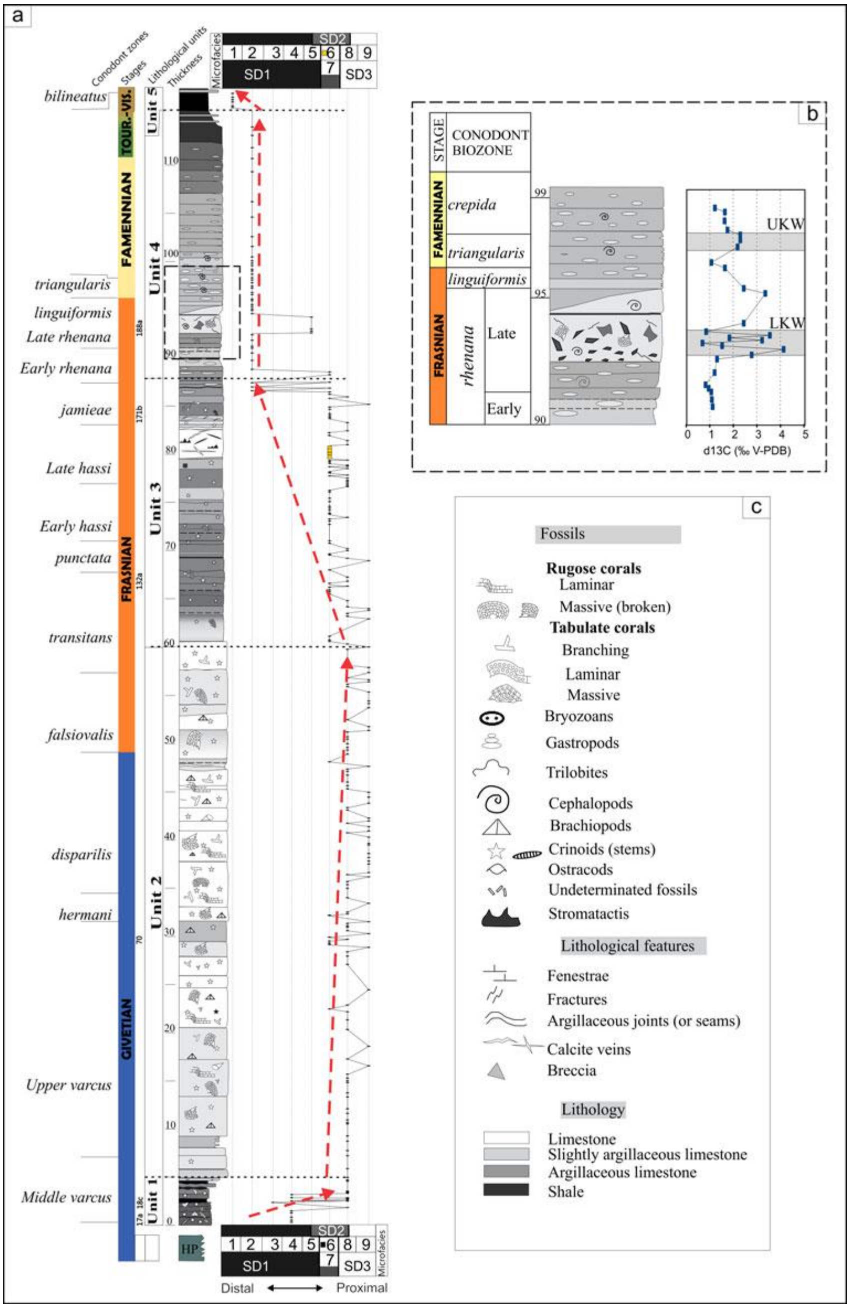

Fig. 6 **a** Schematic sedimentological log showing lithological units (U1–U5) and microfacies curve with main aggrading, prograding, and retrograding trends (*arrows*). The enlargement of the *dotted line area* is illustrated in Fig. 6b. *HP* Hauptgrünstein pyroclastics. **b** $\delta^{13}C$ isotopic trends in the *rhenana* and *triangularis* conodont zones at the Burgberg section. *Grey areas* highlight the Lower (LKW) and Upper (UKW) Kellwasser events. **c** Key of symbols used in this figure

tentaculitids. This mixture between shallow- and deeper-water biota is also commonly observed in debris flows. The intercalations of these thick coarse-grained bioclastic lenticular beds within the black carbonaceous beds (e.g., MF3) indicate deposition below the SWB (see also interpretation of MF3) most probably in a fore-reef setting as indicated by the abundant reefal debris. Volcanic lithoclasts within this microfacies are related to reworking processes of the underlying volcaniclastic rocks. Similar deposits corresponding to the development of reefs on volcaniclastic deposits have been described in the Lahn syncline in the middle v*arcus* Zone at several places (Buggisch and Flügel 1992; Braun et al. 1994; Königshof et al. 2010). The MF4 microfacies corresponds to a debris-flow deposit, which was deposited in an off-reef sedimentary environment and is related to reworking of debris from the newly developed reef on the volcanic substrate of the Hauptgrünstein.

MF5: breccia (Fig. 8a)

At the quarry scale, a single laterally continuous brecciated limestone bed of ~70 cm in thickness was observed in unit 4 between 93 and 94 m (beds 189 and 190), overlying a succession of thin-bedded limestones of MF2. The brecciated bed shows a sharp, slightly erosional contact overlying a fine-grained fabric corresponding to MF2. A coarsening-upward sorting with clasts grading from 0.5–3 cm is observed. Clasts are mainly angular to sub-rounded and consist of peloidal grainstone with tabulate coral debris and clasts of microfacies MF2 and MF6, interpreted as deposited in intermediate reef slope to off-reef carbonate settings. Crinoids and bryozoan debris are also observed. Usually, clasts are matrix-supported but within the upper part of the level, where the largest clasts occur, the fabric is clast-supported with blocky calcite cement.

Interpretation

The dm-thick brecciated level is intercalated between thin-bedded MF2 limestones interpreted as deposited in a quiet depositional setting. However, micro- and macroscopic characters of this microfacies such as the mixture of shallow-marine and deep-marine clasts (mostly matrix-supported), as well as their size, the sharp (slightly erosional) base, and the coarsening-upward nature (Fig. 4d) are indicative of mass-flow or debris-flow deposits. We assume that the larger reefal lithoclasts suffered downslope transport from a shallow platform, which may be related to a rapid sea-level fall.

MF6: Renalcis boundstone (Fig. 8b)

This microfacies was observed only in the upper part of the section, around 80 m within the lithological unit 3. It has been identified as a single m-thick bed intercalated within dm-thick greyish limestone beds of MF7. The massive bed shows common up to several-cm-sized fenestrae and horizontal fractures. The main organisms are *Renalcis* and *Izhella* embedded in a micritic matrix. These calcimicrobes are mostly disseminated but locally they are also densely packed (Fig. 8b). Other observed bioclasts are tabulate corals (around 1 cm in diameter), poorly preserved lamellar stromatoporoid fragments, bryozoan fragments, and tentaculitids. Usually, fenestrae are filled with two generations of cement: a radiaxial calcite at the rim and a blocky sparite in the center. Geopetal infilling by fine micrite at the base of the fenestrae occurs locally.

Interpretation

The abundance of the micritic matrix as well as the good preservation of *Renalcis* and *Izhella* (Fig. 8b), which have been regarded as calcified cyanobacteria by Riding (1991), support a very calm environment below SWB. According to Mamet and Préat (1985), Givetian *Renalcis* in Belgium could create small micritic buildups. The lenticular shape of the bed, its intercalation in bedded limestone MF7, as well as the abundance of *Renalcis* and micritic matrix highlights the depositional character of this microfacies, which corresponds to a small micritic-*Renalcis* mound.

MF7: fine-grained wackestone-packstone with cricoconarid shells and crinoids (Fig. 8c)

This microfacies is mostly observed within Unit 3, in association with microfacies MF8, with sharp transitions (Fig. 8d) or as lenses (mm to several-mm in thickness). Cricoconarids and fine-grained crinoid debris show variable abundance. Cricoconarids (average size around 0.05 mm) are locally concentrated in styliolinid packstone (Fig. 8e). Crinoids are disarticulated and fractured showing an average size of around 0.15 mm even though in some levels they can reach 1 mm. Within these levels, crinoids (Fig. 8f) are commonly oriented parallel to bedding. Other bioclasts are relatively rare and consist of calcispheres, ostracods, entomozoacean ostracods, brachiopods, trilobite fragments, *Amphipora*, stromatoporoids, and *Renalcis* lumps. The average size of these allochems is around 0.15 mm. Bioclasts are commonly associated with rounded peloids with an average size around 0.2 mm. Locally, the proportion of crinoids and cricoconarids is lower and fine-grained peloids dominate the assemblage. Several-mm-sized fenestrae filled with a granular sparite occur. The texture is a wackestone to packstone, although, several-mm- to cm-thick layers of MF8 fine- to coarse-grained grainstones are commonly observed. The lower boundary between the wackestone-packstone texture and the overlying grainstone is usually sharp and erosional. Episodically, lithoclasts of wackestone-packstone occur within the lower part of the overlying grainstone (Fig. 8g), but the uppermost part of the grainstone layers generally grades into packstone and then wackestone. Dolomitization commonly affected the micrite and is characterized by fine-grained equigranular dolomite crystals.

Interpretation

The common to abundant occurrence of cricoconarid shells embedded in a micritic matrix points to a hemipelagic depositional environment. In this microfacies, however, cricoconarids are associated with shallow-marine bioclasts such as reef-builders, which indicates an occasional input of material from a shallow-marine setting. The mixture of biota could be explained by winnowing of the sediment during high-energy events such as storms. The wackestone-packstone mixture of bioclasts from deep and shallow settings is similar to what is observed in intermediate and distal tempestites described by Wendt and Aigner (1985) and Casier and Preat (2007). The regular occurrence of grainstone layers (MF8) with erosional bases intercalated between the wacke- and packstones also strongly suggests event deposits from turbulent flows such as tempestites or turbidites. The absence of shell layers and the local gradation from grainstone to packstone and then wackestone confirms a turbiditic influence. These sediments were deposited in a hemipelagic intermediate reef slope environment.

MF8: bioclastic and lithoclastic grainstone (Fig. 9 a, b, d)

This microfacies is mainly characterized by the gradual transition from coarse- to fine-grained grainstone, a generally good sorting, and abundant crinoids and micritic clasts of variable size which locally can represent more than 80 % of the assemblage. The average size of micritic clasts is around 0.2 mm, although locally they can reach 2 cm in size. When they are small (0.1–0.2 mm), heterogeneous size distinguishes them from peloids, which show very little variability in size and shape (Tucker and Wright 1990). Large micritic clasts (larger than 0.2 mm) resemble micritized aggregate grains (lumps), and small micritic clasts (0.1–0.2 mm) resemble irregular-shaped peloids (“lithic peloid”, Flügel 2004). Lithoclasts of bioclastic grainstone (MF8) or wacke- to packstone (MF7) may occur. They are sub-angular to sub-rounded in shape and usually less than 0.5 mm in size. Another character of MF8 is its common occurrence as several-mm- to cm-thick layers in the wacke- to packstone texture of the MF7. The lower boundary between the wackestone-packstone texture and the overlying MF8 is usually sharp and erosional, and

Fig. 7 Microfacies from the fore-reef deposits (SD1) of the Burgberg section, Germany. Photomicrographs of thin-sections oriented perpendicular to the bedding. *Numbers preceded by “BUR”* correspond to bed numbers. **a** MF1 off-reef deposits: silty shale (BUR 212, transmitted light). **b** MF2 distal reef slope to off-reef: microbioclastic mudstone-wackestone showing nodular/mottled fabric highlighted by the Dickson staining (scanned thin-section BUR 196b). **c** MF2 distal reef slope to off-reef deposit: Nodular texture (scanned thin-section BUR 183b). **d** MF2 distal reef slope to off-reef deposit: fine-grained mudstone with a goniatite shell (BUR 192a, transmitted light). **e** MF2 distal reef slope to off-reef: microbioclastic mudstone with juvenile shells of pelagic bivalves (BUR 197a, transmitted light). **f** MF3 distal reef slope to off-reef deposit: carbonaceous microbioclastic wackestone to packstone overlying coarse-grained crinoidal packstone of MF4 (BUR 18d, transmitted light). **g** MF3 distal reef slope to off-reef deposit: microbioclastic wackestone to packstone showing intercalations of coarse-grained bioclastic packstone of MF4 (scanned thin-section BUR 18d). **h** MF4 distal reef slope to off-reef: coarse unsorted crinoidal packstone with brachiopod shells (BUR 17d, transmitted light) ▶

lithoclasts of MF7 described above mainly occur within the lower part of the overlying grainstone (Fig. 8g). The uppermost part of the grainstone layers generally grades into packstone and then wackestone (Fig. 8d). Crinoids are abundant and crinoidal remains (from 0.2 to 5 mm, with an average size around 1.5 mm) are angular to sub-angular and commonly show syntaxial cement or micritization. Other skeletal grains are rare to common and consist of broken reef builders (*Amphipora*, lamellar and massive stromatoporoids, and tabulate corals), bryozoans, calcispheres, bispheres, ostracods, brachiopods, trilobites, and *Renalcis* lumps. Reef-builder fragments are sub-angular to sub-rounded, range from 0.2–5 mm in diameter, and are commonly surrounded by a micritic envelope (biogenic encrustation of irregular to regular size). Locally, lamination consists of an alternation of light, coarse bioclastic levels dominated by crinoids and darker fine-grained levels dominated by micritic clasts.

Interpretation

The grainstone texture, with a generally good to moderate sorting and the absence of fine-grained particles, suggests a high-energy depositional setting. The presence of crinoids and reef-builder fragments is either related to reworking of the shallower sediments during higher energy events such as storm waves or by downward transport along the proximal fore-reef slope by gravity currents. The occurrence of MF6 and MF7 lithoclasts advocates hydrodynamic conditions strong enough to rework the lithified sediment. The presence of lamination, local fining-upward sequences, and erosional bases strongly support deposition by turbidity currents. MF8 belongs to a turbiditic sequence deposited in the proximal part of a fore-reef environment. Considering the presence of MF7 wackestone-packstone intraclasts, the

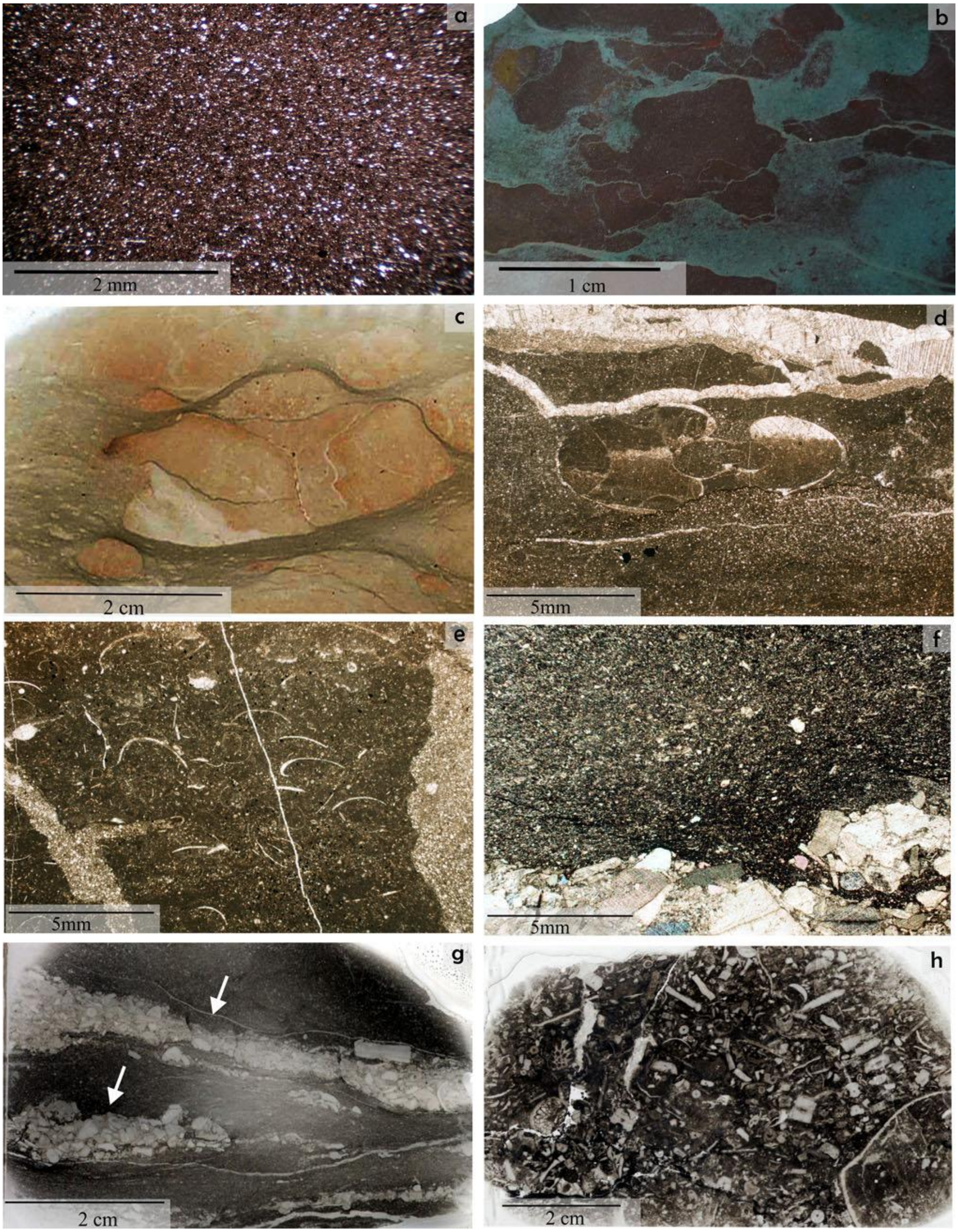
a
2 mm
b
1 cm
c
2 cm
d
5mm
e
5mm
f
5mm
g
2 cm
h
2 cm

depositional setting was located below the fair-weather wave-base (FWWB) (see interpretation of MF7 above).

MF9: reef-builder rudstone (Fig. 9d)

This microfacies corresponds to well to moderately sorted accumulations of crinoids and reef-builder debris and by the presence of micritic clasts (and/or micritized aggregate grains). The dominant texture of this microfacies is rudstone, and the spaces between large reef-builder fragments are commonly filled by smaller grains cemented by sparite (MF8). Skeletal grains ranging from 0.01 mm to more than 50 mm are mainly represented by crinoid debris (0.1–0.8 mm with an average size about 0.5 mm) and sub-angular to sub-rounded several-cm- to dm-sized reef-builder debris (mostly *Amphipora*, laminar stromatoporoids, and tabulate corals). Porostromate and spongiostromate crusts as well as encrusting stromatoporoids and bryozoans occur. Reef-builder debris is commonly surrounded by a thin irregular-micritized layer. Other skeletal grains were identified as bryozoan debris, fragmented brachiopods, calcispheres, bispheres, rugose coral fragments, and trilobites. Lithoclasts are also commonly observed and are angular to sub-rounded with an average size of 0.25 mm, even though some can reach more than 2 mm. They are either composed of mud-, wacke-, pack-, or grainstone. Locally, pack- and grainstone intraclasts are larger than 2 cm. The main cement of this microfacies is a blocky sparite, although a ferroan sparite calcite may occur locally. Large cavities (centimeter-sized) located under reef builders are showing a succession of radiaxial fibrous cement followed by a blocky sparite. Geopetal micritic infilling also occurs. Generally, MF9 gradually transform into MF8 through a decrease in grain size and in the proportion of reef builders. At the outcrop scale, this microfacies is observed in dm- to m-thick beds showing channel-like structures (Fig. 4b).

Interpretation

The rudstone texture associated with reef-builder debris embedded in a sparitic cement indicates an environment mainly influenced by shallow-water biota (lagoonal such as *Amphipora* and/or reefal such as laminar stromatoporoids). With respect to the good-to-moderate sorting and the common occurrence of syntaxial cement, the MF9 was deposited in a high-energy environment. The presence of reef-builder fragments is either related to reworking of the sediment by storms or by downward transport along the proximal fore-reef slope by turbidity currents. The absence of bivalve shell layers, the homogeneity of biota, and the relatively constant composition of the fauna, suggest deposition influenced by turbidite or grain-flow processes rather than by tempestites. A meter-scale channel-like structure observed in the outcrop (Fig. 4b) and the local gradual transition from coarse rudstone (MF9) to grainstone (MF8) support this assumption. The described sequence is comparable to other sections (May 1994), which have been interpreted to represent parts of allodapic limestone turbidites (Meischner 1964). This microfacies corresponds to the basal part of a proximal limestone turbidite deposited on the proximal part of a fore-reef environment below the FWWB. Regarding the MF8 and MF9 intraclasts exposed in this microfacies, it is suggested that older lithified turbidites were reworked during deposition.

Fig. 8 Microfacies from the fore-reef deposits (SD1 and 2) of the Burgberg section, Germany (continued). Photomicrographs of thin-sections oriented perpendicular to bedding. *Numbers preceded by "BUR"* correspond to bed numbers. **a** MF5 distal reef slope setting: breccia with tabulate coral (Tc), lithoclasts of tabulate coral partially surrounded by black, well-sorted peloidal grainstone (Li-A) and lithoclasts of MF2 (mudstone; Li–B). With numerous calcite-filled veins crossing the breccia texture (scanned polished slab, BUR 189b). **b** MF6 mound facies: *Renalcis*/*Izella* algal aggregates with micritic matrix (BUR 166b, transmitted light). **c** MF7 intermediate reef slope: fine-grained crinoidal packstone with some cricoconarid shells (BUR 146, transmitted light). **d** MF7 intermediate reef slope: transition between MF8 bioclastic grainstone and MF7 fine-grained crinoidal packstone (BUR 122, transmitted light). **e** MF7 intermediate reef slope: styliolinid packstone (BUR 132a, transmitted light). **f** MF7 intermediate reef slope: crinoid debris within a micritic matrix (BUR 57, transmitted light). **g** MF8 proximal reef slope: bioclastic to lithoclastic grainstone with lithoclasts of facies MF7 (BUR 131, transmitted light)

Discussion (Figs. 6a, 10, 11)

Petrographic analyses from the Burgberg section led to the definition of nine microfacies representing a fore-reef to off-reef setting (Fig. 10). In this model, three sedimentary domains (SD) are defined. SD1 corresponds to the most distal setting observed and is characterized by off-reef to distal reef slope sedimentation temporarily influenced by storm and gravity-flows (MF1–5). MF1 and MF2 were located in the most distal setting, while MF3 and MF4 were associated with a slightly more proximal environment. The breccia level (MF5) corresponds to the most proximal setting of SD1. On the intermediate reef slope (SD2), sediments are composed of a mixture of deeper-water autochthonous and shallow-water allochthonous debris (MF7), and in this setting *Renalcis* mound-like structures developed locally (MF6). On the upper reef slope (SD3), the most proximal facies of the succession are observed (MF8-9).

The temporal changes in microfacies point to five main paleoenvironmental trends, which correspond to the five lithological units defined in the Burgberg section. Unit 1 marks the Middle Givetian (middle *varcus* Zone) initiation

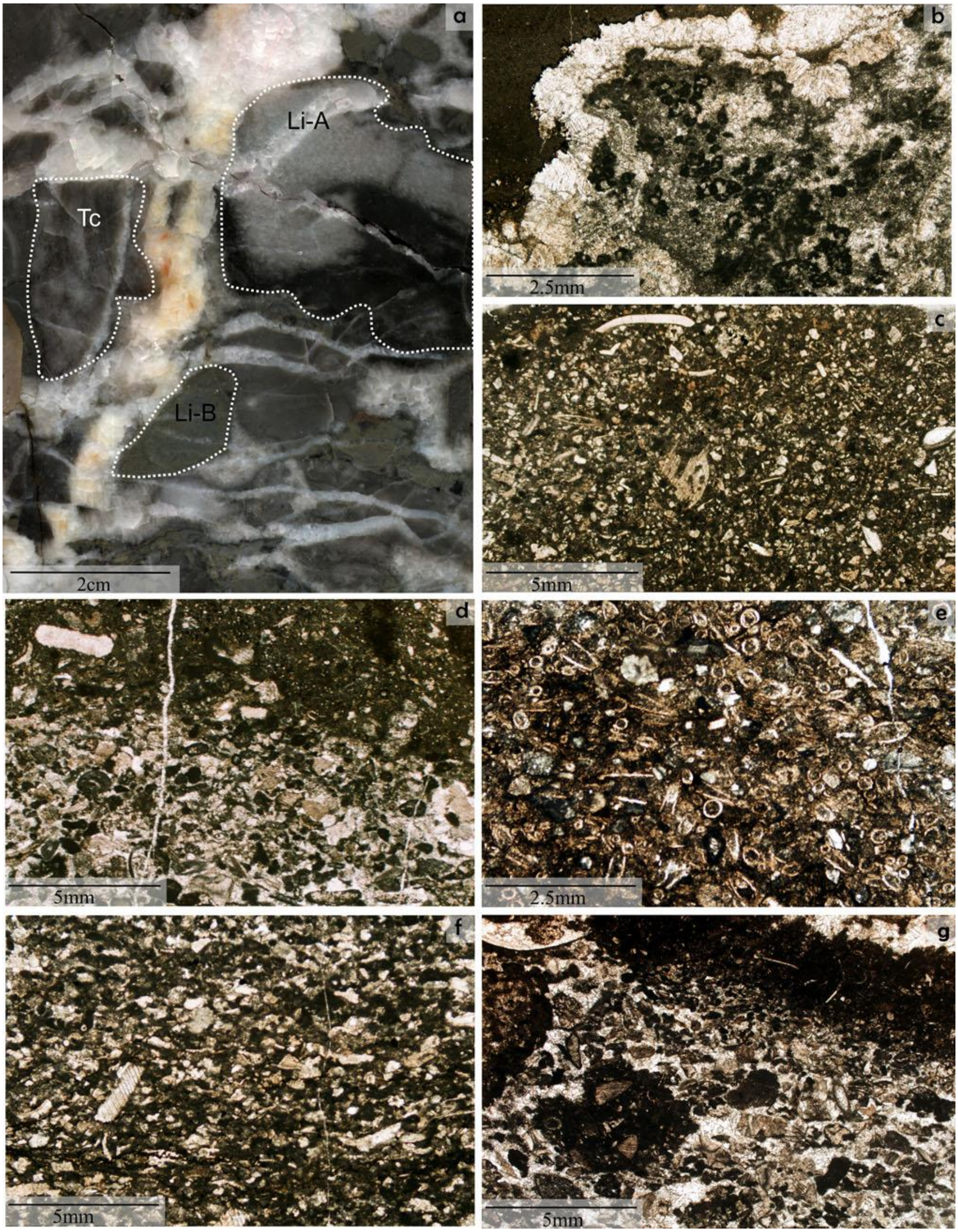
a
Li-A
Tc
Li-B
2cm
b
2.5mm
c
5mm
d
5mm
e
2.5mm
f
5mm
g
5mm

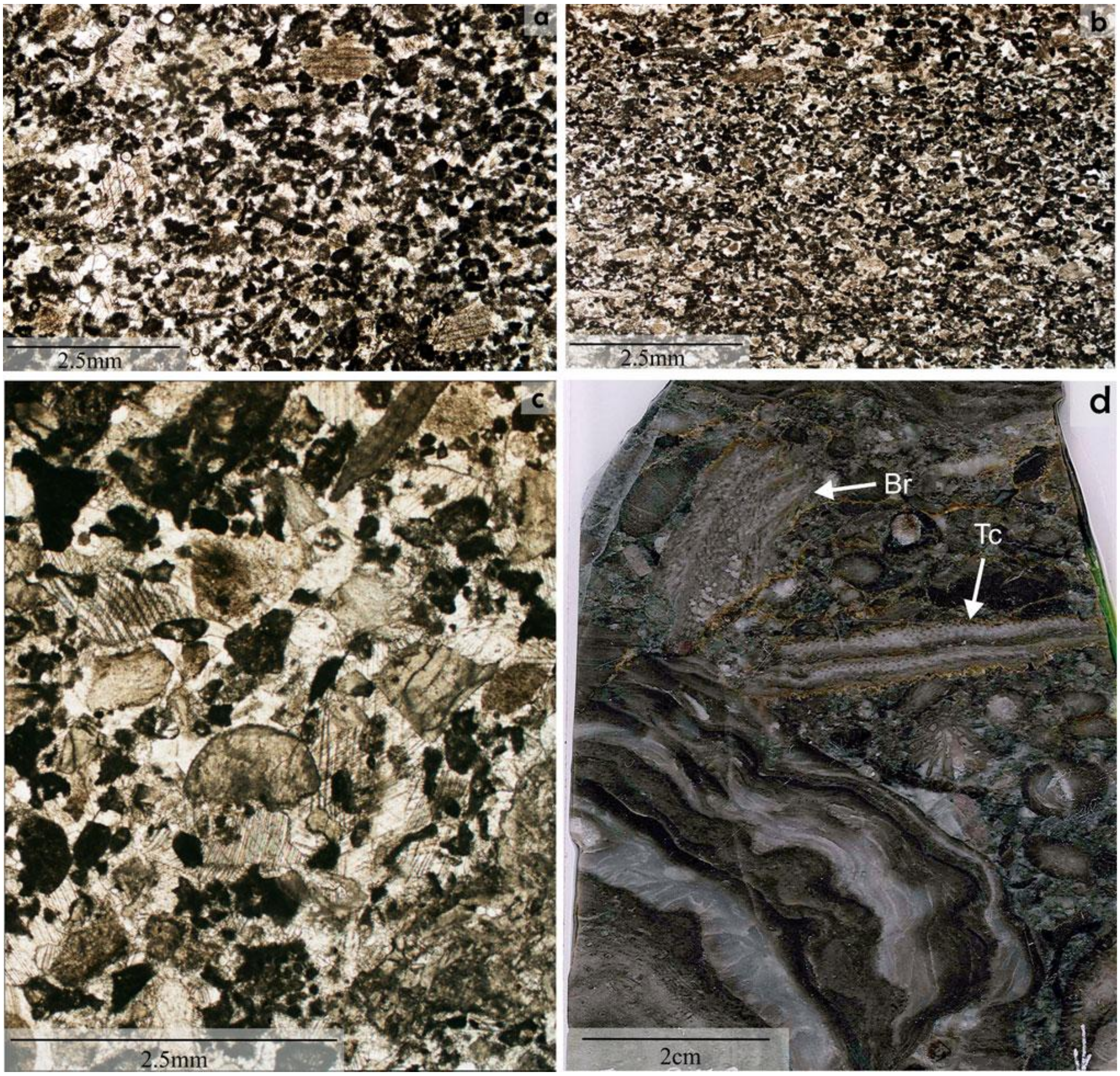

Fig. 9 Microfacies from the fore-reef deposits (SD3) of the Burgberg section, Germany (continued). Photomicrographs of thin-sections oriented perpendicular to bedding. *Numbers preceded by "BUR"* correspond to bed numbers. **a** MF8 proximal reef slope: fine-grained peloidal grainstone (BUR 36, transmitted light). **b** MF8 proximal reef slope: fine-grained lithic peloidal grainstone with crinoids (BUR 128, transmitted light). **c** MF9 proximal reef slope: coarse-grained grainstone with numerous dark-colored lithoclasts (BUR 97c, transmitted light). **d** MF9 proximal reef slope facies: reef-builder rudstone with bryozoan (Br), tabulate coral (Tc), and, in the *lower-left part*, multiple stromatoporoid and bryozoan crusts (scanned thin-section, BUR 73)

of the reefal platform on volcanic debris deposits of the "Hauptgrünstein" (Fig. 11a). A middle *varcus* age was also assigned by Malmsheimer et al. (1990) for the first debris flows covering large areas in the southeast margin of the reef complex. During Middle and Late Givetian times, numerous reef structures developed related to submarine volcanoes in the Rheinisches Schiefergebirge and the Harz Mountains (e.g., Königshof et al. 1991, 2010; May 1993; Gischler 1995, 1996; Nesbor 2004). The onset of carbonate production in the Burgberg area is thus likely related to the end of the volcanic activity in basinal areas, which gave rise to the development of reefal structures and corresponding off-reef deposits. The reefal origin of the debris flow occurring in Unit 1 is linked to the onset of reef growth in the Burgberg area. Furthermore, according to Aboussalam and Becker (2011), the black color of the

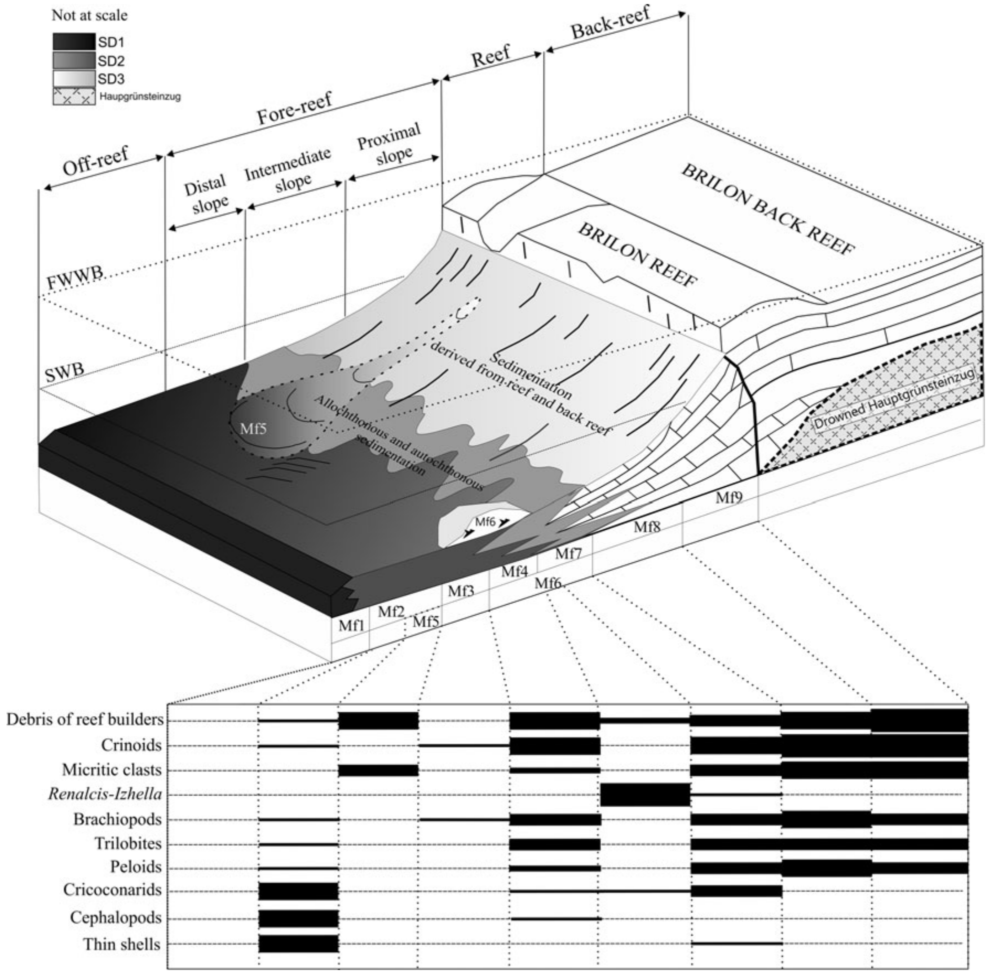

Fig. 10 Sedimentary model of the Burgberg succession showing the relative position of the nine microfacies described. The Brilon reef and the back-reef have not been observed in the Burgberg section but are inferred from literature and from the nature of the debris observed. The *lower part* of the figure depicts the distribution of the main fossils and allochems throughout the different microfacies

sediment (Figs. 4a, 7f–h) occurring in the lower part of the Burgberg section is most likely related to the Taghanic Event at the end of the Middle Givetian, which triggered oxygen-depleted conditions in distal slope environment. This first unit records an abrupt shallowing-upward, which is related to the transition from the distal reef slope (Unit 1; MF3, MF4) to the proximal reef slope of the second unit (Unit 2; MF7, MF8 and MF9). The microfacies curve corresponding to Unit 2 mainly records a prograding trend in the intermediate to proximal reef slope setting (MF7, MF8, and MF9), which is marked by the progressive increase in the proportion of MF9 in comparison to MF7-8 through the top of the Unit 2. A progradational pattern was also recognized by Machel (1990) and Städter and Koch (1987) in the south of the Brilon reef towards the Upper Givetian and can be linked with the global second-order sea-level rise recognized by Johnson et al. (1985) and Haq and Schutter (2008) during the Givetian. Relative sea-level rise may also have been influenced by cooling-related subsidence of the volcanic bodies. The higher proportion of MF9 (interpreted as the most proximal setting) through the top of Unit 2 (*disparilis* and *falsiovalis* conodont zones) marks a higher influence of shallow-water habitats. During this interval, the rate of carbonate accumulation exceeded the rate of subsidence, resulting in the progradation of shallow-water depositional environments over deeper-water ones. Climax of the reefal development and thus the maximum of progradation towards the southeastern part of

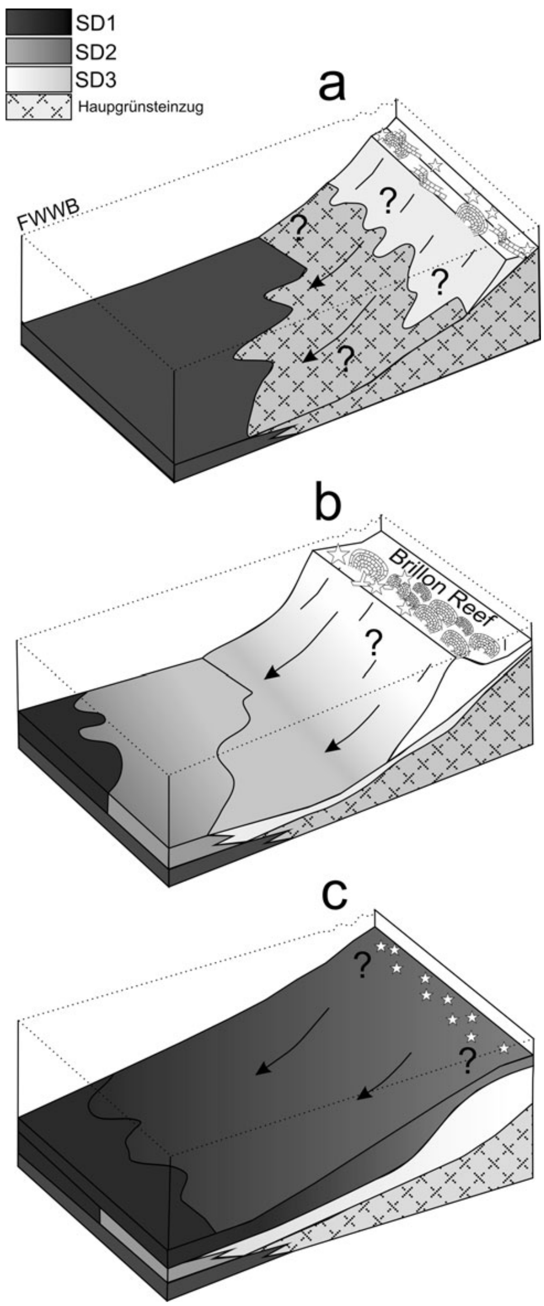

◀ **Fig. 11** Temporal evolution of the southeastern fringe of the Brilon Reef Complex from the Middle Givetian to the Viséan. **a** Unit 1: deposition of MF3-4 in the Burgberg area, with alternating microbioclastic wackestone and packstone including reefal debris. This corresponds to the onset of the carbonate production and the initial phase of reef growth on the "Hauptgrünstein" volcaniclastics during the middle *varcus* Zone. **b** Unit 2: deposition of MF7 (SD2) and MF8-9 (SD3) in the Burgberg area, with bioclastic rudstone and grainstone with abundant reefal debris and fine-grained bioclastic packstone. This corresponds to the extension of the Brilon reef from the middle *varcus* Zone to the *falsiovalis* Zone. **c** Units 4 and 5: deposition of MF1-2 (SD1) in the Burgberg area with thin-bedded limestone and dark shale. This corresponds to the deepening of the Burgberg area after the demise and drowning of the Brilon Reef Complex at the Frasnian-Famennian boundary. *Arrows* represent downslope transport of reefal debris towards the fore-reef area. Key of symbols in Fig. 6c

the Brilon Reef Complex extended from the Late Givetian to the Early Frasnian. The long-lasting and significant influence of the shallow-water habitats in the fore-reef setting of Burgberg, mainly characterized by *Amphipora*, tabulate corals, and stromatoporoids, indicates that conditions were favorable for reef development during the equivalent period of time in the shallow-water area of the Brilon Reef Complex (Fig. 11b). In the reef complexes of the Australian Canning Basin (Playford 1980), the Late Givetian to Early Frasnian time span is also characterized by an increasing amount of reefal material deposits in the marginal slope setting and has been interpreted as the result of an increase in the rate of transgression. The overlying third unit corresponds to a deepening-upward trend extending from the *transitans* to *jamieae* conodont zones, which is characterized by a progressive decrease in deposits of shallow-water origin (MF8 and MF9). Furthermore, an increase in the amount of hemipelagic/pelagic biota associated with fine-grained sediments (MF7) is visible. The changes in biota are related either to an increase in the global sea-level rise, an increase in the subsidence, or to a combination of both which finally led to the progressive retrogradation and back-stepping of the Brilon Reef Complex and corresponding off-reef deposits. This back-stepping has also been recorded in the fore-reef setting of the Australian Canning Basin (Playford 1980) and in the Canadian Rocky Mountains (Whalen 2000) around the Middle to Late Frasnian. Back-stepping of carbonate platforms at that time is a general trend recorded on a global scale and it is commonly correlated with several Frasnian pulses in the eustatic sea-level rise (Johnson et al. 1985; T-R cycle IId). However, the global sea-level fall documented by Haq and Schutter (2008) for the Frasnian stage is inconsistent with the deepening trend recorded in our data. The development of *Renalcis* mound-like structures (MF6) within the fore-reef area of the Brilon Reef Complex may be correlated with the progressively decreasing influx of reef debris to open-marine reef slope setting, which may confirm an increasing distance between the Burgberg fore-reef depositional setting and the shallow-water areas. The deepening trend characterizing the Unit 3 ends within the *jamieae* conodont Zone with sediments belonging to the distal reef slope to off-reef setting (MF2). The following aggrading trend (Unit 4) in the distal reef slope to off-reef setting is characterized by thin-bedded nodular and cephalopod-rich limestones (MF2) extending from the Late Frasnian to the Late Famennian stages. The breccia level (MF5) in the lower part of Unit 4 represents a strong shallowing-upward episode within the general aggrading trends in off-reef setting. The biostratigraphic position of this breccia in the late *rhenana* conodont Zone as well as the major positive $\delta^{13}C$ excursions (amplitude +4.14 ‰ and +3.56 ‰; Fig. 6b), correspond to the Lower Kellwasser Event (LKW). Similar positive $\delta^{13}C$ excursions were described from other European sections (Buggisch and Joachimski 2006). The Upper Kellwasser Event is also present in our section (Fig. 6b). The $\delta^{13}C$ excursions are usually associated with black shale levels and are interpreted to correspond to deepening events, although our breccia level, associated with high $\delta^{13}C$ values, is likely to be related to a shallowing event. This breccia level could thus correspond to the strong sea-level fall occurring worldwide (Johnson et al. 1985; Wendt and Belka 1991; Chen et al. 2002; Bond and Wignall 2008) after the Lower Kellwasser Event in the Late Frasnian, which generated exposure and collapse of shallow platform settings (e.g., George and Powell 1997; Bond et al. 2004). A global eustatic sea-level fall associated with the end of the Frasnian is recognized in many areas, such as on the East European Platform (Alekseev et al. 1996; Antoshkina 2006), in Western Canada (Geldsetzer et al. 1993) and in Southern China (Chen and Tucker 2004). The high values of $\delta^{13}C$ recorded in the breccia level suggest a reworking of the Lower Kellwasser sediments triggered during the deposition of this breccia level. The reef-derived bioclasts in the breccia level are the last occurrence of the shallow-water influxes within the Burgberg section and therefore confirm the existence of shallow-water areas south of the Brilon Reef Complex, at least until the late *rhenana* conodont Zone. For comparison, reef development in the Harz Mountains (Iberg reef) ranges from the *varcus* conodont Zone to the *rhenana* conodont Zone (Franke 1973). The dominance of MF2 within Unit 4 indicates the end of the shallow-water influx, which seems to be related to the demise and drowning of the shallow-water habitats in the Burgberg area as a result of the Late Frasnian sea-level rise. According to Eder and Franke (1982) and Johnson et al. (1985), the Late Frasnian eustatic sea-level rises caused the drowning of carbonate platforms on a global scale. They appear to be connected to the Kellwasser event interval at the end of the Frasnian, which is considered to be one of the major extinction events of the Phanerozoic (Sepkoski 1995) and marks the end of the Devonian reef communities. The beginning of the last unit (Unit 5; Fig. 6a) records a significant deepening trend related to the transition from bedded cephalopods and nodular limestone (MF2) to poorly oxygenated pelagic shale of MF1. In the Burgberg section, pelagic shale extends from the Late Famennian to the Viséan (Fig. 11c), which indicates poorly oxygenated bottom water conditions in the Burgberg area during a long stratigraphic interval. A similar aggrading facies development has been described in other parts of the Rhenish Massif, such as the Harz Mountains (e.g., Gischler 1996). The occurrence of the *Crenistria* Limestone beds (Fig. 5b) in the topmost part of the section corresponds to a change in the environmental conditions dominating in the basin. Indeed, the *Crenistra* Limestone beds are interpreted as a phases of bottom water oxygenation (Warnke et al. 1997).

Conclusions

(1) The Burgberg section provides an outstanding continuous succession of about 40 Ma in a fore-reef facies and can serve as an important contribution to the understanding of reef development in the Mid-Paleozoic. The stratigraphic framework of the entire section is well documented by conodont biostratigraphy.

(2) The section ranges from the Middle Givetian (middle *varcus* Zone) to the Viséan (*bilineatus* Zone) and contains the global Kellwasser events as shown by biostratigraphic and carbon-isotope data.

(3) The main sedimentary processes documented in the Burgberg section are gravity flows (turbidite, debris, and grain flows) and pelagic sedimentation (settling). Reworking by storms and bioturbation are locally important.

(4) Based on a detailed study of the microfacies, the development of the off-reef facies and corresponding Brilon reef can be reconstructed. The major evolutionary phases are (a) initial development of the Brilon reef on top of volcanic deposits which started within the middle *varcus* conodont Biozone, (b) the establishment of the reef structure lasting from the Middle Givetian to Early Frasnian with a culmination recorded from the *disparilis* to *falsiovalis* conodont biozones, (c) the stepwise withdrawal of the reef development from the Middle to the Late Frasnian, (d) the end of the reef development as a result of the global Kellwasser events, and finally (e) significant deepening of the Burgberg area starting in the Late Famennian, characterized by pelagic shale sedimentation overlying nodular limestones.

(5) The detailed sedimentological study of the Burgberg section demonstrates the potential of fore-reef sequences for the reconstruction of major paleoenvironmental changes that can occur in shallow-water reefal habitats.

Acknowledgments Financial support for this project from the sedimentary laboratory of the University of Liège is gratefully acknowledged. The authors would like to thank Philippe Claeys and David De Vleeschouwer (Earth System Sciences, Vrije Universiteit

Brussel) for the instrumental help provided for the stable isotope measurements. Many thanks to Rüdiger Stritzke for all the information and comments provided for conodont investigation. This paper is a contribution to IGCP 580 "Application of magnetic susceptibility in paleoenvironmental reconstruction" and to IGCP 596 "Climate change and biodiversity patterns in the Mid-Palaeozoic". Helpful comments from Dr. Thomas Suttner (Karl-Franzens University of Graz, Austria) and an anonymous journal reviewer are gratefully acknowledged.

References

Aboussalam ZS (2003) Das" Taghanic-Event" im höheren Mitteldevon von West-Europa und Marokko. Münstersche Forsch Geol Paläont 97:1–332

Aboussalam ZS, Becker RT (2011) The global Taghanic biocrisis (Givetian) in the eastern Anti-Atlas, Morocco. Palaeogeogr Palaeoclimatol Palaeoecol 304:136–164

Alekseev AS, Kononova LI, Nikishin AM (1996) The Devonian and Carboniferous of the Moscow Syneclise (Russian Platform): stratigraphy and sea level changes. Tectonophysics 268:149–168

Antoshkina AI (2006) Palaeoenvironmental implications of Palaeomicrocodium in Upper Devonian microbial mounds of the Chernyshev Swell, Timan-northern Ural region. Facies 52:611–625

Bacelle L, Bosellini A (1965) Diagrammi per la stima visiva della composizione percentuale nelle rocce sedimentarie. Ann Univ Ferrara Sez 9 Sci Geol Paleont 1:59–62

Bandel K (1974) Deep-water limestones from the Devonian-Carboniferous of the Carnic Alps, Austria. Spec Publ Int Assoc Sediment 1:93–115

Bär P (1968) Die ober-devonisch/unter-karbonische Schichtlücke über dem Massenkalk des Briloner und Messinghäuser Sattels (Ost-Sauerland). N Jb Geol Paläont Abh 131:263–288

Bathurst RGC (1987) Diagenetically enhanced bedding in argillaceous platform limestones: stratified cementation and selective compaction. Sedimentology 34:749–778

Bond DPG, Wignall PB (2008) The role of sea-level change and marine anoxia in the Frasnian–Famennian (Late Devonian) mass extinction. Palaeogeogr Palaeoclimatol Palaeoecol 263:107–118

Bond DPG, Wignall PB, Racki G (2004) Extent and duration of marine anoxia during the Frasnian-Famennian (Late Devonian) mass extinction in Poland, Germany, Austria and France. Geol Mag 141:173–193

Boulvain F, Cornet P, da Silva AC, Delaite G, Demany B, Humblet M, Renard M, Coen-Aubert M (2004) Reconstructing atoll-like mounds from the Frasnian of Belgium. Facies 50:313–326

Braun R, Oetken S, Königshof P, Kornder L, Wehrmann A (1994) Development and biofacies of reef-influenced carbonates (Lahnsyncline, Rheinisches Schiefergebirge). Cour Forschungsinst. Senckenberg 169:351–386

Brinckmann J (1981) Projekt Rhenoherzynikum: Untersuchung der Metallverteilung in geosynklinalen Sedimenten des Rhenoherzynikums in stratiformen Konzentrationen; Bericht über das Kernbohrprogramm im Briloner Riffkalk-Komplex. Bundesanstalt für Geowissenschaften und Rohstoffe

Buggisch W, Flügel E (1992) Mittel- bis oberdevonische Karbonate auf Blatt Weilburg (Rheinisches Schiefergebirge) und in Randgebieten: Initialstadien der Riffentwick-lung auf Vulkanschwellen. Geol Jb Hessen 120:77–97

Buggisch W, Joachimski MM (2006) Carbon isotope stratigraphy of the Devonian of central and southern Europe. Palaeogeogr Palaeoclimatol Palaeoecol 240:68–88

Casier J, Preat A (2007) Ostracodes et lithofacies du stratotype de la limite Devonien moyen/Devonien superieur (Puech de la Suque, Montagne Noire, France). Bull Soc Geol France 178:293–304

Chen D, Tucker M (2004) Palaeokarst and its implication for the extinction event at the Frasnian–Famennian boundary (Guilin, South China). J Geol Soc Lond 161:895–898

Chen D, Tuker M, Shen Y, Yans J, Preat A (2002) Carbon isotope excursions and sea-level change: implications for the Frasnian–Famennian biotic crisis. J Geol Soc Lond 159:623–626

Clari P, Martire L (1996) Interplay of cementation, mechanical compaction, and chemical compaction in nodular limestones of the Rosso Ammonitico Veronese (Middle-Upper Jurassic, northeastern Italy). J Sediment Res 66:447–458

Clausen CD, Korn D (2008) Höheres Mitteldevon und Oberdevon des nördlichen Rheinischen Schiefergebirges (mit Velberter Sattel und Kellerwald). In: Deutsche Stratigraphische Kommission (eds) Stratigraphie von Deutschland VIII. Devon. Schriftenreihe dtsch Ges Geowiss Heft 52:439–481

Copper P (2002) Silurian and Devonian reefs: 800 million years of global greenhouse between two ice ages. In: Kiessling W, Flügel E, Golonka J (eds) Phanerozoic reef patterns. SEPM Spec Publ, vol 72, pp 181–238

Dickson J (1965) A modified staining technique for carbonates in thin section. Nature 205:587

Dunham RJ (1962) Classification of carbonate rocks according to depositional texture. Mem Am Assoc Petrol Geol 1:108–121

Eder W, Franke W (1982) Death of Devonian reefs. N Jb Geol Paläont Abh 163:241–243

Embry AF, Klovan JE (1972) Absolute water depth limits of Late Devonian paleoecological zones. Geol Rundsch 61:672–686

Erben HK (1962) Zur Analyse und Interpretation der rheinischen und hercynischen Magnafazies im Devon. In: Erben HK (ed) International Arbeitstagung über die Silur/Devon Grenze und die Stratigraphie von Silur und Devon. Symposium Band, Schweizerbart, Stuttgart, pp 42–61

Flügel E (2004) Microfacies analysis of carbonate rocks. Analysis, interpretation and application. Springer, Berlin Heidelberg New York

Franke W (1973) Fazies, Bau und Entwicklungsgeschichte des Iberger Riffes (Mitteldevon bis Unterkarbon III NW-Harz, W-Deutschland). Geol Jb A 11:27–31

Geldsetzer HHJ, Goodfellow WD, McLaren DJ (1993) The Frasnian-Famennian extinction event in a stable cratonic shelf setting: Trout River, Northwest Territories, Canada. Palaeogeogr Palaeoclimatol Palaeoecol 104:81–89

George AD, Powell CMA (1997) Paleokarst in an Upper Devonian reef complex of the Canning basin, western Australia. J Sediment Res 67:935–944

Gingras MK, Pemberton SG, Muelenbachs K, Machel H (2004) Conceptual models for burrow-related, selective dolomitization with textural and isotopic evidence from the Tyndall Stone, Canada. Geobiology 2:21–30

Gischler E (1995) Current and wind induced facies patterns in a Devonian atoll: Iberg Reef, Harz Mts. Germany. Palaios 10:180–189

Gischler E (1996) Late Devonian-early Carboniferous deep-water coral assemblages and sedimentation on a Devonian seamount: Iberg Reef, Harz Mts. Germany. Palaeogeogr Palaeoclimatol Palaeoecol 123:297–322

Haq BU, Schutter SR (2008) A chronology of Paleozoic sea-level changes. Science 322:64–68

House MR (1985) Correlation of Mid-Palaeozoic ammonoid evolutionary events with global sedimentary perturbations. Nature 313:17–22

Johnson JG (1970) Taghanic onlap and the end of North American Provinciality. Geol Soc Am Bull 81:2077–2106

Johnson JG, Klapper G, Sandberg CA (1985) Devonian eustatic fluctuations in Euramerica. Geol Soc Am Bull 96:567–587

Jux U (1960) Die devonischen Riffe im Rheinischen Schiefergebirge. N Jb Geol Paläont Abh 110:186–258

Königshof P, Gewehr B, Kornder L, Wehrmann A, Braun R, Zankl H (1991) Stromatoporen-Morphotypen aus einem zentralen Riffbereich (Mitteldevon) in der südwestlichen Lahnmulde. Geol Palaeont 25:19–35

Königshof P, Nesbor HD, Flick H (2010) Volcanism and reef development in the Devonian: a case study from the Lahn syncline, Rheinisches Schiefergebirge (Germany). Gondwana Res 17:264–280

Königshof P, Savage N, Lutat P, Sardsu A, Dopieralska J, Belka Z, Racki G (2012) Late Devonian sedimentary record of the Palaeotethys Ocean—the Mae Sariang succession, northwestern Thailand. J Asian Earth Sci 52:146–157. doi:10.1016/j.jseaes.2012.03.006

Korn D (1996) Revision of the Late Visean goniatite stratigraphy. Ann Soc Geol Belg 117:205–212

Korn D, Horn K (1997) The Late Visean (early Carboniferous) goniatite stratigraphy in the South Portuguese Zone, a comparison with the Rhenish Massif. Newsl Stratigr 35:97–113

Korn D, Kaufmann B (2009) A high-resolution relative time scale for the Viséan Stage (Carboniferous) of the Kulm Basin (Rhenish Mountains, Germany). Geoll J 44:306–321

Krebs W (1967) Reef development in the Devonian of the eastern Rhenish Slate Mountains, Germany. In: Oswald DH (ed) International symposium on the Devonian system, vol 1. Alberta Society of Petroleum Geologists, Calgary, pp 295–306

Krebs W (1971) Devonian reef limestones in the eastern Rhenish Schiefergebirge. Sedimentology of parts of Central Europe guidebook, 8th international sedimentology congress, Heidelberg, pp 45–81

Krebs W (1974) Devonian carbonate complexes of central Europe. In: Laporte LF (ed) Reefs in time and space. SEPM Spec Publ, vol 18, pp 155–208

Kroner U, Hahn T, Romer RL, Linnemann U (2007) The Variscan orogeny in the Saxo-Thuringian zone—heterogenous overprint of Cadomian/Palaeozoic peri-Gondwana crust. In: Linnemann U, Nance RD, Kraft P, Zulauf G (eds) The evolution of the Rheic Ocean: From Avalonian-Cadomian active margin to Alleghenian-Variscan collision. Geol Soc Am Spec Pap 423: 153–172

Logan BV, Semenuik V (1976) Dynamic metamorphism: processes and products in Devonian carbonate rocks, Canning Basin, Western Australia. Geol Soc Australia Spec Publ 138

Machel H-G (1990) Faziesinterpretation des Briloner Riffs mit Hilfe eines Faziesmodells für devonische Riffkarbonate. Geol Jb D 95:43–83

Maletz J (2006) Middle Devonian dendroid graptolites from the Brilon Reef area (Rheinisches Schiefergebirge, Germany). Paläont Z 80:221–229

Malmsheimer KW, Mensink H, Stritzke R (1990) Beginn der Riffschutt-Produktion und Knollenkalk-Sedimentation in Südosten des Briloner Riffes/Ostsauerland. Geol Jb D 95:177–182

Mamet B, Préat A (1985) Sur la présence de *Palaeomicrocodium* (Algue?, Incertae sedis?) dans le Givétien inférieur de Belgique. Geobios 18:389–395

May A (1993) Stratigraphie, Stromatoporen-Fauna und Palökologie von Korallenkalken aus dem Ober-Eifelium und Unter-Givetium (Devon) des nordwestlichen Sauerlandes (Rheinisches Schiefergebirge). Geol Paläont Westfalen 24:1–93

May A (1994) Microfacies controls on weathering of carbonate building stones: Devonian (northern Sauerland, Germany). Facies 30:193–208

McKerrow WS, Scotese CR (1990) Palaeozoic palaeogeography and biogeography. Geol Soc Lond Mem 12:1–433

Meischner KD (1964) Allodapische Kalke. Turbidite in riff-nahen Sedimentations-Becken. Developm Sediment 3:156–191

Möller NK, Kvingan K (1988) The genesis of nodular limestones in the Ordovician and Silurian of the Oslo Region (Norway). Sedimentology 35:405–420

Nesbor HD (2004) Paläozoischer Intraplattenvulkanismus im östlichen Rheinischen Schiefergebirge—Magmenentwicklung und zeitlicher Ablauf. Geol Jb Hessen 131:145–182

Nicolaus HJ (1963) Zur Stratigraphie und Fauna der *crenistria*-Zone im Kulm des Rheinischen Schiefergebirges. Beih Geol Jahrb 53:1–246

Paeckelmann W (1922) Der mitteldevonische Massenkalk des Bergischen Landes. Preuss Geol Landesanst Abh 91:1–112

Paeckelmann W (1936) Geologische Karte von Preussen 1: 25000. Blatt Brilon (2659)

Pettijohn FJ, Potter PE, Siever R (1972) Sand and sandstone. Springer, Berlin Heidelberg New York

Piecha M (1993) Stratigraphie, Fazies und Sedimentpetrographie der rhythmisch und zyklisch abgelagerten, tiefoberdevonischen Beckensedimente im Rechtsrheinischen Schiefergebirge (Adorf Bänderschiefer). Cour Forsch Inst Senckenberg 163:1–153

Playford PE (1980) Devonian "Great Barrier Reef" of Canning Basin, Western Australia. Am Assoc Petrol Geol Bull 64:814–840

Rabien A (1956) Zur Stratigraphie und Fazies des Ober-Devons in der Waldecker Hauptmulde. Abh Hess LA Bodenforsch 16:1–83

Ribbert K-H, Skupin K, Oesterreich B (2006) Geologische Karte von Preussen und benachbarten Gebieten, von Nordrhein-Westfalen, 1:25000. Blatt Madfeld (4518)

Riding R (1991) Calcareous algae and stromatolites. Springer, Berlin Heidelberg New York

Salamon M, Königshof P (2010) Middle Devonian olistostromes in the Rheno-Hercynian (Rheinisches Schiefergebirge)—an indication of back arc rifting on the passive margin of Laurussia? Gondwana Res 17:281–291. doi:10.1016/j.gr.2009.10.004

Sepkoski JJ Jr (1995) Patterns of Phanerozoic extinctions: a perspective from global data bases. In: Walliser OH (ed) Global events and event stratigraphy. Springer, Berlin Heidelberg New York, pp 35–51

Städter T, Koch R (1987) Mikrofazielle und diagenetische Entwicklung einer devonischen Karbonatfolge (Givet) am SW-Rand des Briloner Sattels. Facies 17:215–229

Stow DAV, Piper DJW (1984) Fine-grained sediments: deep water processes and facies. Geol Soc Lond Spec Publ 15:1–659

Stritzke R (1990) Die Karbonatsedimentation im Briloner Vorriffbereich. Geol Jb D 95:253–315

Sunkel G (1990) Devonischer submariner Vulkanismus im Ostsauerland (Rheinisches Schiefergebirge): Vulkanaufbau, Magmenzusammensetzung und Alteration. Bochumer geol geotechn Arb 34:1–250

Tucker ME (1973) Sedimentology and diagenesis of Devonian pelagic limestones (Cephalopodenkalk) and associated sediments of the Rhenohercynian Geosyncline, West Germany. N Jb Geol Paläont Abh 142:320–350

Tucker ME (1974) Sedimentology of Palaeozoic pelagic limestones: the Devonian Griotte (Southern France) and Cephalopodenkalk (Germany). Spec Publ Int Assoc Sediment 1:71–92

Tucker ME, Wright VP (1990) Carbonate sedimentology. Blackwell, London

von Dechen H (1858) Geologische Karte der Rheinprovinz und der Provinz Westfalen 1: 80.000. (Hrsg.) Kgl Minist Handel Gewerbe öff Arbeit, Sect 18, Berleburg, Berlin

Warnke K (1997) Microbial carbonate production in a starved basin: the crenistria Limestone of the upper Viséan German Kulm facies. Palaeogeogr Palaeoclimatol Palaeoecol 130:209–225

Wehrmann A, Blieck A, Brocke R, Hertweck G, Jansen U, Königshof P, Plodowski G, Schindler E, Schultka S, Wilde V (2005) Palaeoenvironment and palaeoecology of intertidal deposits in a

Lower Devonian siliciclastic sequence of the Mosel Region, Germany. Palaios 20:101–120
Wendt J, Aigner T (1985) Facies patterns and depositional environments of Palaeozoic cephalopod limestones. Sediment Geol 44:263–300
Wendt J, Belka Z (1991) Age and depositional environment of Upper Devonian (early Frasnian to early Famennian) black shales and limestones (Kellwasser facies) in the eastern Anti-Atlas, Morocco. Facies 25:51–89
Ziegler AP (1982) Geological atlas of western and central Europe. Shell, Den Haag

Second part

Magnetic susceptibility and geochemistry of the Burgberg section

1. Introduction

This section describes and discusses the large amount of unpublished magnetic susceptibility and geochemical data collected from the Burgberg section. The following text is therefore in continuity with published sedimentological results by Pas et al. (2013).

As mentioned in Pas et al. (2013), the Burgberg section covers a million year stratigraphic interval that extend from the Middle Devonian (Middle Givetian) to Mississippian. This interval represents the largest among the fourth selected sections investigated through this PhD. It is thus worth of interest to analyses and highlight what are the major links between the large-scaled palaeoenvironmental evolution characterizing the Burgberg section (Pas et al., 2013) and the unpublished magnetic susceptibility and geochemical data from this section. Prior to provide our main results and conclusions, the previously published methodology by Pas et al. (2013) is supplemented here above.

2. Materials and methods

Magnetic susceptibility samples were collected bed by bed, simultaneously than thin-section samples, with an average sampling interval of one sample per 25 cms. Magnetic susceptibility measurements were undertaken on more than 340 rock samples. Each sample was analysed three times with KLY-3 (Kappabridge) and weighed with a precision of 0.01g. This allows the definition of the mass-calibrated magnetic susceptibility for each sample and the construction of magnetic susceptibility plots. Major and trace elements were measured using X-ray Fluorescence (ARL 9400 XP XRF instrument, University of Liège) on 34 samples regularly spaced through the studied part of the Burgberg section. The analysed rock samples were carefully cleaned prior to all treatment: weathered surfaces were removed. The major elements (in this paper SiO_2, TiO_2, Al_2O_3 and K_2O) were analysed on lithium tetra- and meta-borate fused glass discs, with matrix corrections following the Traill-Lachance algorithm and are expressed in elemental oxide concentration. Trace elements such as Zr were measured on pressed powder pellets and data were corrected for matrix effects by Compton peak monitoring and expressed in elemental concentration. Precision and accuracy were both shown to be better than 1% for major elements and 5% for trace elements as proved by international standards and analyses of replicate samples, respectively.

3. Results

3.1. Magnetic susceptibility (χ_{in})

As summarized in Da Silva et al. (2013), the application of χ_{in} as a palaeoenvironmental proxy or as a tool for correlation is pertinent only if the recorded χ_{in} signal reflects primary depositional conditions.

Indeed, primary recorded χ_{in} pattern can be strongly affected during post-depositional processes (e.g., diagenesis and remagnetization) and therefore damaged by a secondary χ_{in} component. It is thus important to assess whether the analyzed samples represent primary depositional imprint or secondary post-depositional conditions. This assessment is even more necessary in our case as Devonian rocks from NE Rhenish Massif were affected by a remagnetization event driven by the Variscan orogeny (Zwing et al., 2005). In a recent study dedicated to the origin of the χ_{in} signal in Devonian sections of Belgium, (Da Silva et al., 2012, 2013) established that the χ_{in} signal is mainly transported by fine-grained PSD magnetite in relation with the remagnetization event. Nevertheless, Da Silva et al. (2013) also showed that on six Devonian outcrops four were still reflecting syn-sedimentary conditions as pointed out by the relatively good relationship between χ_{in} and reliable siliciclastic input proxies such as Ti, Zr, Al and Si. In a recent paper Pas et al. (2014) also demonstrated the good relationship between siliciclastic input tracers and magnetic susceptibility signal for a study conducted in remagnetized rocks from the Devonian of western Belgium. The conclusion of these last authors is that the magnetic signal reflects primary depositional-induced conditions, despite remagnetization.

3.2. Magnetic susceptibility evolution in the Burgberg section

The magnetic susceptibility curve established for the Middle Devonian to Mississipian Burgberg section (Fig. 1) can be divided into four successive million year-scaled χ_{in} trends (A, B, C and D). Trends A and B correspond to the units 1 and 2 while the trends C and D characterize the units 3, 4 and 5. These χ_{in} trends show a relatively well-visible opposition with the main microfacies trends (I, II, III and IV) described in Pas et al. (2013; fig. 6) and presented above in Fig. 1. The χ_{in} values for the Middle Devonian to Mississippian Burgberg section record important variability ranging from 4.22 x 10^{-10} m^3/kg to 9.25 x 10^{-8} m^3/kg with a low average value of 2 x 10^{-8} m^3/kg. This values is lower than the χ_{in} marine standard of 5.5 x 10^{-8} m^3/kg defined by Ellwood et al. (2011) on the basis of ~11000 marine rock samples.

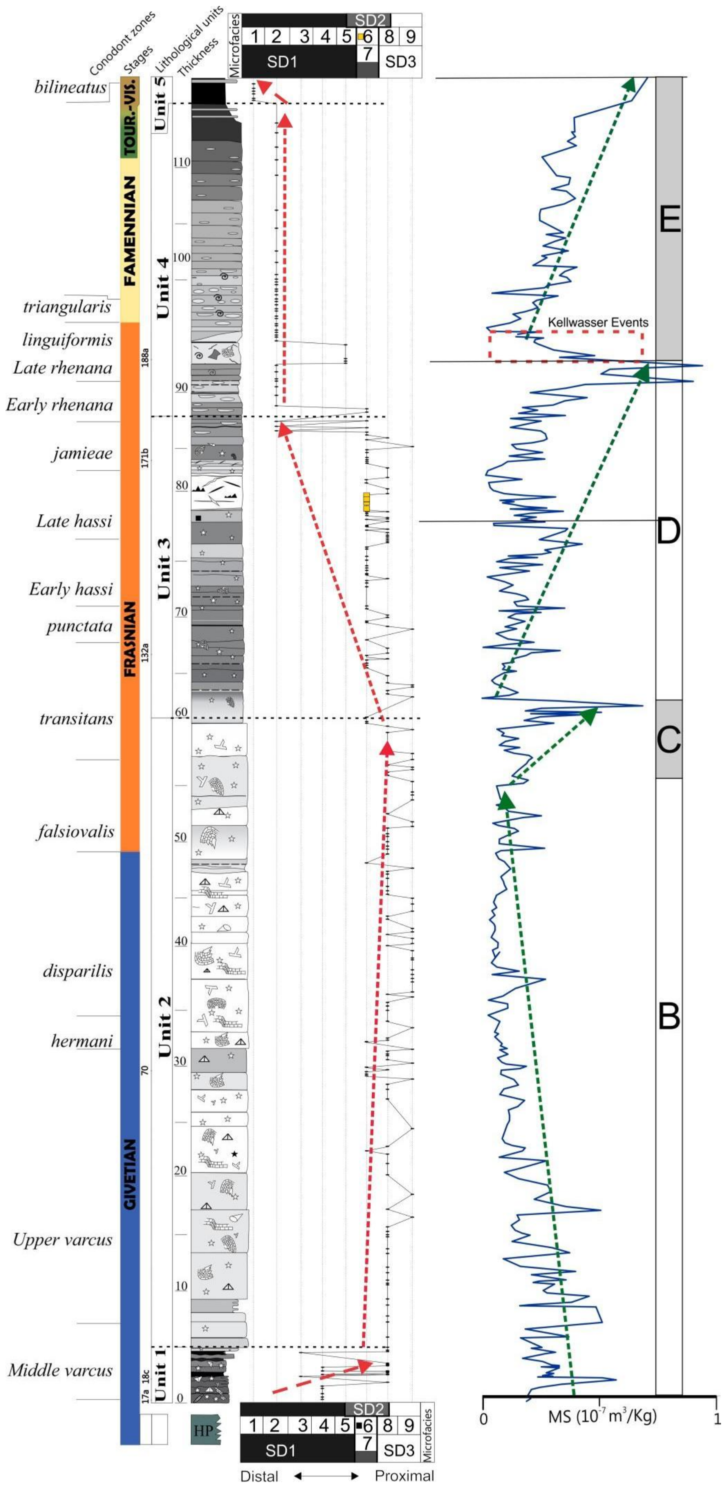

Fig. 1 ***a*** *Schematic sedimentological log showing lithological units (U1-5) and microfacies curves. Arrows represent trends in MF curves. The enlargement of the dotted line area is illustrated in.* ***b*** *Magnetic susceptibility curve with the major decreasing and increasing trends represented by green dotted lines. For the legend of the sedimentological log refers to Pas et al. (2013; fig. 6).*

Such a low average χ_{in} value is consistent with the depositional setting of the Burgberg section, corresponding the fore-reef fringe of the Brilon atoll reef system (e.g., far from terrestrial input), allowing a relatively pure carbonate deposition. The purity of carbonate is well-attested by the depletion in some detrital input proxies measured for the Burgberg section and presented in this complementary section. In the Frasnian fore-reef depositional setting of the Mont Freikofel section (Carnic Alps), Pas et al. (2014) even described a lower average χ_{in} values associated with a more significant depletion in siliciclastic input proxies. The trend A starts within the Middle *varcus* Zone with χ_{in} values close to 0.5 10^{-7} m^3/kg and ends toward the upper half of the *falsiovalis* Zone with very low value (3 10^{-9} m^3/kg). The base of the second trend (Trend B) is defined with the low value of the previous trend and record a general increase to reach high values (6.7 x 10^{-8} m^3/kg) corresponding to the base of the Unit 3 within the *transitans* Zone. Base of the trend C starts up to the drop in the χ_{in} value registered at the top of the trend B, and is characterized by a general increase of the value reaching the highest value of the succession (9.25 x 10^{-8} m^3/kg), associated with the lower portion of the Unit 4 within the *Late rhenana/linguiformis* Zone. The base of the last trend (Trend D) is defined by the significant fall in the χ_{in} value recorded up to the previous trend. This last trend records a general increase of the χ_{in} value to reach high value (7 x 10^{-8} m^3/kg) associated with the shale sequence that characterize the uppermost part of the section.

As mentioned above, the major shallowing and deepening trends that are recorded in microfacies are almost anti-correlated respectively with decreasing and increasing long-term trends in χ_{in}. As described in Pas et al. (2013) the Burgberg section recorded five major evolutionary phases that characterize the Brilon Reef Complex. The evolutionary phases are (1) initial development of the Brilon reef which started within the middle *varcus* conodont biozone, (2) the establishment of the reef structure lasting from Middle Givetian to Early Frasnian with a culmination recorded from the *disparilis* to *falsiovalis* conodont biozones, (3) the stepwise withdrawal of the reef development from the Middle to the Late Frasnian, (4) the end of the reef development as a result of the global Kellwasser events, and finally (5) significant deepening of the Burgberg area starting at the Late Famennian, characterized by pelagic shale sedimentation overlying the nodular limestone deposits. Each of these phases is defined by specific combination of syn-sedimentary processes such as siliciclastic influx, sedimentary rate and water turbulence which control the magnetic susceptibility variations as we have shown previously. Weight of each of these processes is dependent of the main depositional settings. Thus, the main increasing and decreasing χ_{in} trends can be explained using the three main sedimentary domains that were defined for the Burgberg section.

A relatively simple analyse of the average χ_{in} value for each sedimentary domains (SD1, SD2 and SD3; Pas et al., 2013; fig. 10) established for the Burgberg section provide robust key for understanding the primary mechanisms responsible of the opposition between long-term χ_{in} trends and microfacies trends. The graph illustrated in the Fig. 2 below indicates that the average χ_{in} values increase from the proximal towards the distal setting.

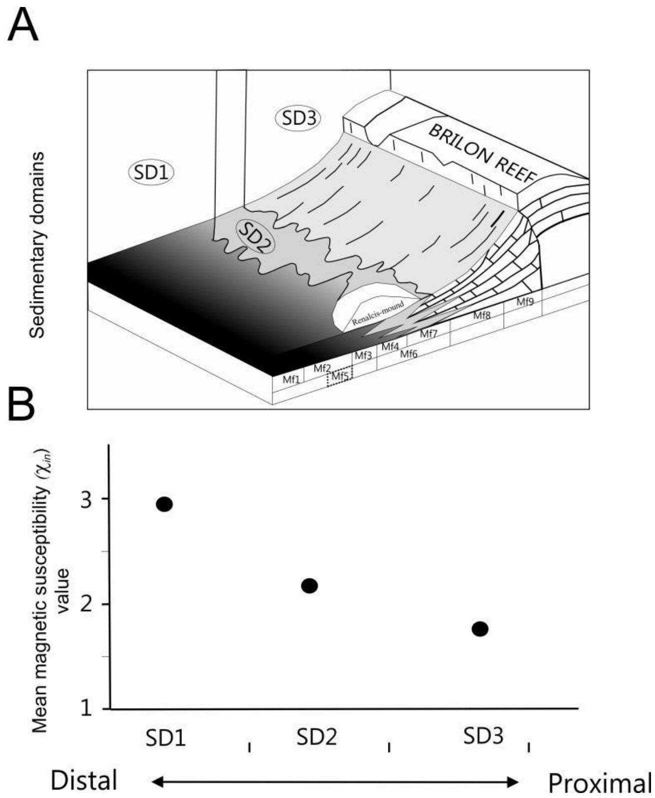

Fig. 2 a *Simplified sedimentological model defined for the Burgberg section showing the three main sedimentary domains (SD1, SD2 and SD3).* **b** *Mean magnetic susceptibility (χ_{in}) value on relative proximity transect illustrated by the position of the three sedimentary domains from proximal to distal location.*

Average χ_{in} values correspond to 3.8 x 10^{-8} m^3/kg for SD1, 1.4 x 10^{-8} m^3/kg for SD2 and 1.36 x 10^{-8} m^3/kg for SD3. Usually, data in the literature support the notion that proximal microfacies possess a higher value of χ_{in} than distal ones (Crick et al., 1997). This is related to the proximity with a terrestrial source. In our case, the average χ_{in} value shows the opposite trends. This situation has already been noticed for Belgian Eifelian fore-reef sedimentary environment (Mabille and Boulvain, 2007), in the for Belgian and Canadian Frasnian mounds and atolls platform (Da Silva et al., 2009) and also recently in the Frasnian fore-reef environment of the Carnic Alps (Pas et al., 2014). This behaviour can be easily explained with respect to the location of the Burgberg depositional setting compared to the continent. Indeed, if the depositional environment is far enough from terrestrial supplies as it is the case the Burgberg section we can consider that the siliciclastic input are homogenized and have the same influence on each microfacies. In such case, carbonate productivity/sedimentary rate processes must play a predominant role in the χ_{in} signal variations. Setting such as the distal fore-reef and the off-reef belonging to the sedimentary domain 1 (SD1) are characterized by a low sedimentary rate, which leads to condensed levels and thus to a concentration of magnetic minerals. This explains the higher average χ_{in} value recorded for SD1. High level of water agitation is suggested mainly for SD1 which is strongly influenced by turbidity current and thus a high level of water turbulence which prevent the deposition of χ_{in} carrying minerals. The sedimentary domain 2 (SD2) is located in an intermediate position between SD3 and SD1 and corresponds to an intermediate to distal slope setting influenced by both gravity flow and hemipelagic/pelagic sedimentation. Furthermore, this setting is marked by the development a *Renalcis* mound (MF6). Average χ_{in} value of SD2 is therefore mainly characterized by a low sedimentary rate where the water agitation and the carbonate productivity are temporarily high explaining its intermediate position.

3.3. Majors and traces elements analyses (Fig. 3)

In order to complement and strengthen interpretation derived from sedimentology and magnetic susceptibility we measured trace and major elements from a collection of samples regularly spaced throughout the section. As explained below, rocks from the NE Rhenish Massif were affected by a remagnetization event (Zwing et al., 2005). It is thus imperative to assess whether or not the recorded χ_{in} signal represent primary depositional conditions. To do so we plotted the χ_{in} curve established for Burgberg against the curves of reliable siliciclastic input tracers such as Zr, Ti, Al, K and Si (Riquier et al., 2010; Śliwiński et al., 2010).

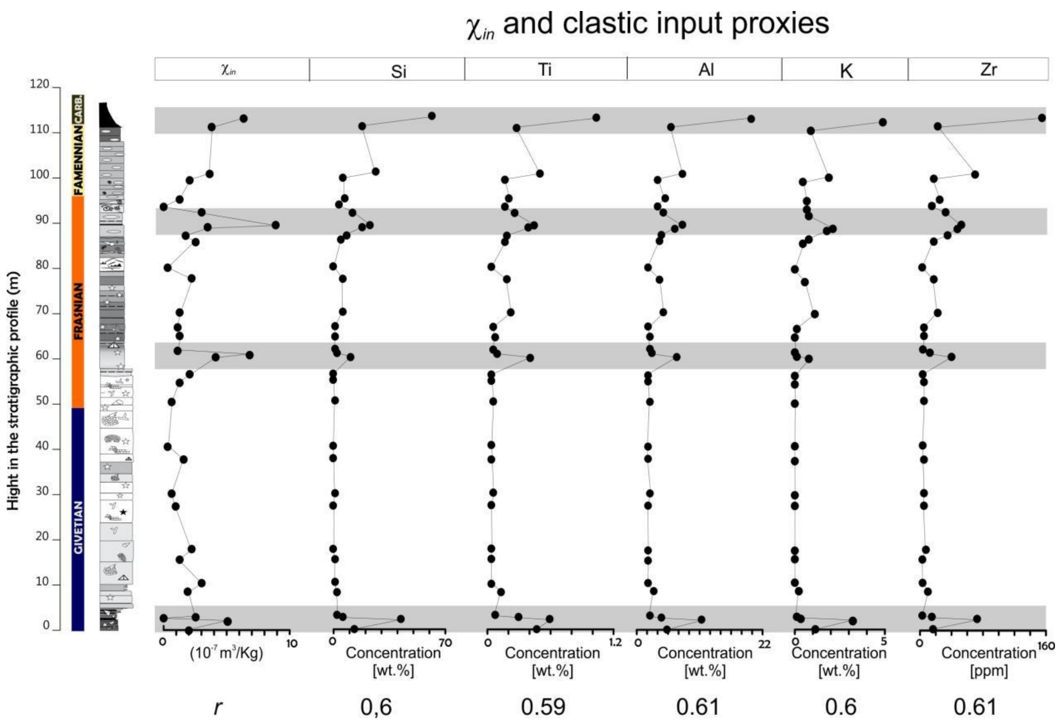

Fig. 3 *Chemostratigraphic profiles of elements used as proxies for terrigenous clastic influxes into marine depositional basins. Plotted also is the corresponding magnetic susceptibility (χ_{in}) profile. Shaded areas are meant to help visualize common trends.*

The distribution of these elements follows the same uniform large-scaled trend than χ_{in} and calculated coefficient correlation value *r* vary between 0.59 and 0.61 indicating an inherent link between the χ_{in} and the siliciclastic proxies variation. These good correlations attest for the preservation of the primary depositional χ_{in} signal despite the remagnetization event highlighted in the studied area. The low average χ_{in} values attest thus of an average very low terrestrial influx seaward during the deposition of the Burgberg section. The isolated location of the Brillon atoll reef within the NE portion of the Rhenohercynian Ocean, likely far from any continental source area, enables the formation of an almost pure carbonate deposition.

4. Conclusions

The χ_{in} values for the Middle Devonian to Mississippian Burgberg section range from 4.22 x 10^{-10} m^3/kg to 9.25 x 10^{-8} m^3/kg with a low average value of 2 x 10^{-8} m^3/kg. This χ_{in} average lower than χ_{in} for marine standard is in agreement with the depositional context of the Burgberg section, corresponding to the fore-reef fringe of the Brilon atoll reef (e.g., far from terrestrial influence).
Throughout the Burgberg section four large-scaled χ_{in} trends in relatively well-visible opposition with the main trends in microfacies. This opposition between major χ_{in} trends and microfacies trends is related to the specific weight of syn-sedimentary processes such as siliciclastic influx, sedimentary rate and water turbulence active the three main sedimentary domains defined for this section. In the most distal setting (e.g., off-reef seeting) defined for the Burgberg section sedimentary rate and water turbulence are low, allow the concentration of χ_{in} carrying particles resulting in a higher χ_{in} values. Meanwhile, in the most proximal setting (e.g., fore-reef proximal setting), sedimentary rate and turbulence are high, diluting χ_{in} carrying minerals and hampering the χ_{in} carrying minerals to settle, resulting in a higher χ_{in} signal in these proximal contexts.

5. References

Crick, R.E., Ellwood, B.B., El Hassani, A., Feist, R. and Hladil, J. (1997) Magnetosusceptibility event and cyclostratigraphy (MSEC) of the Eifelian - Givetian GSSP and associated boudary sequences in north Africa and Europe. *Episodes*, **20,** 167-175.

Da Silva, A.-C., Potma, K., Weissenberger, J.A.W., Whalen, M.T., Humblet, M., Mabille, C. and Boulvain, F. (2009) Magnetic susceptibility evolution and sedimentary environments on carbonate platform sediments and atolls, comparison of the Frasnian from Belgium and Alberta, Canada. *Sedimentary Geology*, **214,** 3-18.

Da Silva, A.C., De Vleeschouwer, D., Boulvain, F., Claeys, P., Fagel, N., Humblet, M., Mabille, C., Michel, J., Sardar Abadi, M., Pas, D. and Dekkers, M.J. (2013) Magnetic susceptibility as a high-resolution correlation tool and as a climatic proxy in Paleozoic rocks - Merits and pitfalls: Examples from the Devonian in Belgium. *Marine and Petroleum Geology*, **46,** 173-189.

Da Silva, A.C., Dekkers, M.J., Mabille, C. and Boulvain, F. (2012) Magnetic susceptibility and its relationship with paleoenvironments, diagenesis and remagnetization: Examples from the Devonian carbonates of Belgium. *Studia Geophysica et Geodaetica*, **56,** 677-704.

Ellwood, B.B., Tomkin, J.H., El Hassani, A., Bultynck, P., Brett, C.E., Schindler, E., Feist, R. and Bartholomew, A.J. (2011) A climate-driven model and development of a floating point time scale for the entire Middle Devonian Givetian Stage: A test using magnetostratigraphy susceptibility as a climate proxy. *Palaeogeography, Palaeoclimatology, Palaeoecology*, **304,** 85-95.

Mabille, C. and Boulvain, F. (2007) Sedimentology and magnetic susceptibility of the Upper Eifelian-Lower Givetian (Middle Devonian) in SW Belgium: Insights into carbonate platform initiation. *Geological Society Special Publication*, **275,** 109-123.

Pas, D., Da Silva, A.C., Cornet, P., Bultynck, P., Königshof, P. and Boulvain, F. (2013) Sedimentary development of a continuous Middle Devonian to Mississippian section from the fore-reef fringe of the Brilon Reef Complex (Rheinisches Schiefergebirge, Germany). *Facies*, **59,** 969-990.

Pas, D., Da Silva, A.C., Suttner, T., Kido, E., Bultynck, P., Pondrelli, M., Corradini, C., De Vleeschouwer, D., Dojen, C. and Boulvain, F. (2014) Insight into the development of a carbonate platform through a multi-disciplinary approach: A case study from the Upper Devonian slope deposits of Mount Freikofel (Carnic Alps, Austria/Italy). *International Journal of Earth Sciences*, **103,** 519-538.

Riquier, L., Averbuch, O., Devleeschouwer, X. and Tribovillard, N. (2010) Diagenetic versus detrital origin of the magnetic susceptibility variations in some carbonate Frasnian-Famennian boundary sections from Northern Africa and Western Europe: Implications for paleoenvironmental reconstructions. *International Journal of Earth Sciences*, **99,** 57-73.

Śliwiński, M.G., Whalen, M.T. and Jed, D. (2010) Trace element variations in the middle Frasnian Punctata zone (Late Devonian) in the Western Canada Sedimentary Basin - changes in oceanic bioproductivity and paleoredox spurred by a pulse of terrestrial afforestation? *Geologica Belgica*, **13,** 459-482.

Zwing, A., Matzka, J., Bachtadse, V. and Soffel, H.C. (2005) Rock magnetic properties of remagnetized Palaeozoic clastic and carbonate rocks from the NE Rhenish massif, Germany. *Geophysical Journal International*, **160,** 477-486.

Rainbow over the Lochkovian-Givetian succession of Mt. Gamspitz, Carnic Alps, Austria-Italy

Chapter 3

Depositional environment of the Early Frasnian to Early Famennian slope deposits of Mount Freikofel (Carnic Alps, Austria/Italy)

Based on: Pas, D., Da Silva, A-C., Suttner, T., Pondreli, M., Kido, E., Corradini, C., Bultynck, P., De Vleeschouwer, D., Boulvain, F. (2013) : Depositional environment of the Early Frasnian to Early Famennian slope deposits of Mount Freikofel (Carnic Alps, Austria/Italy). *International Journal of Earth Sciences*, 103, 519-538.

Insight into the development of a carbonate platform through a multi-disciplinary approach: a case study from the Upper Devonian slope deposits of Mount Freikofel (Carnic Alps, Austria/Italy)

Damien Pas · Anne-Christine Da Silva · Thomas Suttner · Erika Kido · Pierre Bultynck · Monica Pondrelli · Carlo Corradini · David De Vleeschouwer · Claudia Dojen · Frédéric Boulvain

Received: 26 July 2013 / Accepted: 6 October 2013

Abstract The development and behavior of million year-scaled depositional sequences recorded within Palaeozoic carbonate platform has remained poorly examined. Therefore, the understanding of palaeoenvironmental changes that occur in geological past is still limited. We herein undertake a multi-disciplinary approach (sedimentology, conodont biostratigraphy, magnetic susceptibility (MS), and geochemistry) of a long-term succession in the Carnic Alps, which offers new insights into the peculiar evolution of one of the best example of Palaeozoic carbonate platform in Europe. The Freikofel section, located in the central part of the Carnic Alps, represents an outstanding succession in a fore-reef setting, extending from the Latest Givetian (indet. *falsiovalis* conodont zones) to the Early Famennian (Lower *crepida* conodont zone). Sedimentological analysis allowed to propose a sedimentary model dominated by distal slope and fore-reef-slope deposits. The most distal setting is characterized by an autochthonous pelagic sedimentation showing local occurrence of thin-bedded turbiditic deposits. In the fore-reef slope, in a more proximal setting, there is an accumulation of various autochthonous and allochthonous fine- to coarse-grained sediments originated from the interplay of gravity-flow currents derived from the shallow-water and deepwater area. The temporal evolution of microfacies in the Freikofel section evolves in two main steps corresponding to the Freikofel (Unit 1) and the Pal (Unit 2) limestones. Distal slope to fore-reef lithologies and associate changes are from base to top of the section: (U1) thick bedded litho- and bioclastic breccia beds with local fining upward sequence and fine-grained mudstone intercalations corresponding, in the fore-reef setting, to the dismantlement of the Eifelian–Frasnian carbonate platform during the Early to Late Frasnian time (*falsiovalis* to *rhenana* superzones) with one of the causes being the Late Givetian major rift pulse; (U2) occurrence of thin-bedded red nodular and cephalopod-bearing limestones with local lithoclastic grainstone intercalations corresponding to a significant deepening of the area and the progressive withdrawal of sedimentary influxes toward the basin, in relation with Late Frasnian sea-level rise. MS and geochemical analyses were also performed along the Freikofel section and demonstrate the inherent parallel link existing between variation in MS values and proxy for terrestrial input. Interpretation of MS in terms of palaeoenvironmental processes reflects that even though distality

D. Pas (✉) · A.-C. Da Silva · F. Boulvain
Sedimentary Petrology, B20, University of Liège (ULg), Sart-Tilman, 4000 Liège, Belgium
e-mail: dpas@ulg.ac.be

T. Suttner · E. Kido
Institute for Earth Sciences (Geology and Paleontology), University of Graz, Heinrichstrasse 26, 8010 Graz, Austria

P. Bultynck
Department of Paleontology, Royal Belgian Institute of Natural Sciences, Rue Vautier 29, 1000 Brussels, Belgium

M. Pondrelli
Dipartimento di Ingegneria e Geologia, International Research School of Planetary Sciences, Università d'Annunzio, viale Pindaro 42, 65127 Pescara, Italy

C. Corradini
Dipartimento di Scienze Chimiche e Geologiche, Università di Cagliari, via Trentino 51, 09127 Cagliari, Italy

D. De Vleeschouwer
Earth System Science, Vrije Universiteit Brussel, Pleinlaan 2, 1050 Brussels, Belgium

C. Dojen
Landesmuseum für Kärnten, Museumsgasse 2, 9021 Klagenfurt, Austria

remains the major parameter influencing MS values, carbonate production and water agitation also play an important role.

Keywords Carbonate platform · Cellon-Kellerwand Nappe · Magnetic susceptibility · Geochemistry · Stable carbon isotope · Mid–Late Devonian

Introduction

The Carnic Alps represent one of few places within the alpine range where an almost continuous sedimentary record from the Ordovician to the Permo-Carboniferous is preserved. One of the largest Devonian carbonate complexes known in Europe is exposed in the central part of the mountain chain. This extended carbonate complex has been the focus of many researcher dealing with taxonomy, stratigraphy, sedimentology, and geochemistry, e.g., of von Gaertner (1931), Walliser (1964), Bandel (1969, 1972, 1974), Pölsler (1969a, b), Schönlaub (1971, 1980), Pohler (1982), Galli (1985), Kreutzer (1989), Oeckentorp-Küster and Oeckentorp (1992), Joachimski et al. (1994), Perri and Spalletta (1998), Schönlaub and Histon (2000), Schönlaub et al. (2004), Hüneke (2006, 2007), Hubmann and Suttner (2007), Suttner (2007), Corradini and Corriga (2010, 2012), and Corradini et al. (2012). According to Kreutzer (1992a, b) and Schönlaub (1992), Devonian reefs of the Carnic Alps had their climax during the Givetian and Early Frasnian prior to decline within the Late Frasnian. Coral and stromatoporoid patch reefs already started to produce a several hundred-meter-thick carbonate platform during the Early Devonian (Suttner 2007). In general, Devonian deposits of the Carnic Alps are divided into five S–SE to N–NE-directed facies belts: (1) southern shallow-water facies; (2) transitional facies; (3) pelagic limestone facies; (4) offshore, pelagic basinal facies; and (5) northern shallow-water facies. The reef-related sedimentation took place within a differently subsiding basin during a period of extensional regime. This was highlighted by significant variation in carbonate thickness of about one thousand meters occurring between the shallow-water (belt 1) and the pelagic (belt 3) facies. Between these two facies belts, a transitional environment with varying thickness, corresponding to the facies belt 2, was developed. More than thirteen microfacies types were identified by Kreutzer (1990, 1992a, b) discriminating all the different lithologies occurring during the Lochkovian to Frasnian interval.

Although Middle and Upper Devonian deposits of the Carnic Alps have been studied since the second half of the nineteenth century, a lot of uncertainties remain regarding the size and evolution of the Devonian platform. Geometrical complexity resulting from the Variscan and Alpine orogenies, hardly accessible outcrops, and lack of a precise biostratigraphic control within the shallow-water setting have slowed down further palaeoenvironmental investigations and therefore our knowledge about the evolution of life on Earth. In order to get a better understanding of the Devonian platform/basin evolution, including a reliable stratigraphical framework, we need new data within the so-called transitional facies defined by Kreutzer (1990). As indicated by their name, these "transitional" facies closely connect the shallow with the open-sea facies, and despite the possible reworking occurring in this setting (occurrence of breccias), they are datable by conodonts as the standard biozone sequence remains undisturbed (e.g., Spalletta et al. 1983). Therefore, biostratigraphic studies based on conodont from the "transitional" facies could bring a considerable improvement in deciphering the age of the shallow-water units. A remarkable succession recorded within those "transitional" facies is well exposed and preserved at Mount Freikofel (Austria/Italy border). In this paper, we document a detailed sedimentological study of the continuous Latest Givetian–Early Famennian succession (Freikofel Limestone and Pal Limestone) observed in the upper part of the Freikofel section in order to provide a detailed analysis and illustration of the Upper Devonian "transitional" and pelagic facies within the Carnic Alps. We present a new dataset including conodont biostratigraphy, geochemistry (major and trace element analysis and $\delta^{13}C$ stable isotopes), and magnetic susceptibility (MS) analyses in order to gain a better understanding of the depositional and environmental changes in a fore-reef setting within the Carnic Alps. Moreover, the biostratigraphic control of the succession offers the first opportunity to establish a reliable timing for the reworking and demise/drowning of the reefal structure within the Cellon-Kellerwand Nappe. Therefore, it allows to improve our knowledge of global changes over a long timescale in Palaeozoic. Geochemistry and MS measurements taken on the Freikofel succession in the fore-reef setting might help to establish further correlation between Upper Devonian transitional lithologies throughout the Carnic Alps and elsewhere.

Location and geological context

The Carnic Alps are situated at the southern margin of the European Variscides and belong to an east–west striking South Alpine domain of the Alps, extending across the Italy–Austrian border. The pre-Variscan sequence of the Carnic Alps is composed of an almost continuous sequence of sedimentary rocks ranging from Ordovician to Late–Early Carboniferous (compare Austrian Stratigraphic Chart of Piller et al. 2004; Hubmann et al. 2013) and belongs to the "Proto Alps" depositional basin north of Gondwana (Schönlaub and

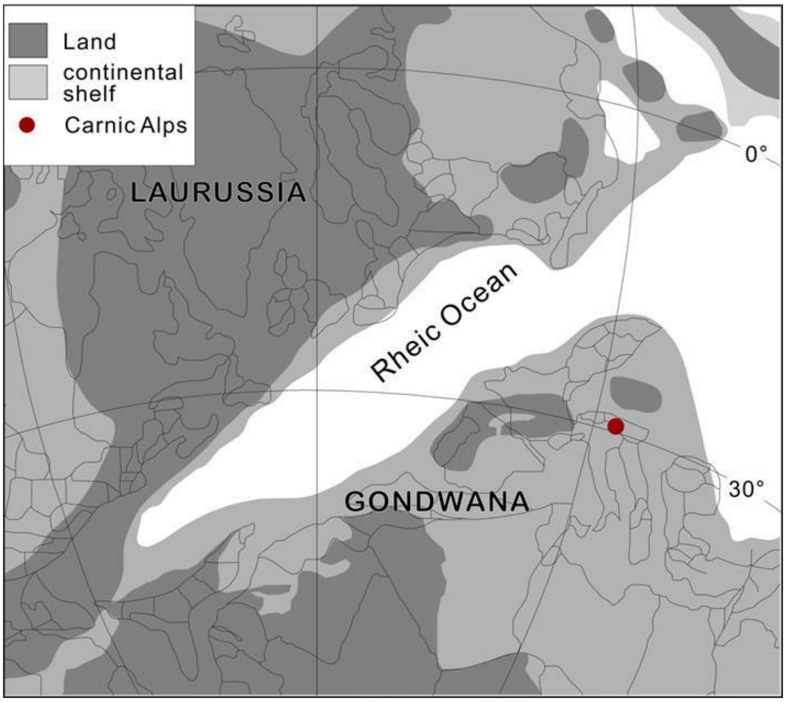

Fig. 1 Palaeogeographical reconstruction showing the location of the Carnic Alps during the Middle Devonian (modified after Scotese 2002)

Histon 2000) (Fig. 1). Overlying the Variscan sequence, Late Carboniferous to Triassic units (post-Variscan Sequence) were deposited. Post-Variscan sequence consists of non- to low-metamorphic substratum of the following Alpine cycle (Vai 1975). The entire Palaeozoic sequence was subjected to both Variscan and Alpine orogenies. Both orogenies resulted in the formation of several thrust sheets, imbricate nappe systems, and dislocations. The Variscan orogeny is interpreted as formed at considerable crustal depth, which leads to more ductile deformations, including recumbent folding (Venturini 1990; Brime et al. 2008). The resultant structural setting has been sketched by Läufer et al. (2001) who defined four major tectonic units (Fig. 2). From west to east, they are, respectively, named Late Alpine transpressive blocks, Fleons Nappe, Cellon-Kellerwand Nappe, and the Hochwipfel Nappe. These four tectonic units differ from each other in regard to their stratigraphy, grade of metamorphism, and deformation. In the Cellon-Kellerwand Nappe (Fig. 2), an almost continuous sedimentary record extending from the Late Ordovician to the Early Carboniferous with low-grade metamorphism and several tectonic deformations are revealed. This succession is mainly calcareous but includes shallow- to deepwater siliciclastic deposits. Starting from the Early Devonian, a reef complex and associated facies, encompassing all facies belts ranging from shallow-water to off-reef basinal facies, are exposed within the Cellon-Kellerwand Nappe (Bandel 1974; Vai 1975; Schönlaub 1979, 1985; Kreutzer 1992b). The significant reef development in the area is remarkably shown by the thickness ratio of 12:1 between shallow-water sedimentary pile and the contemporary pelagic cephalopod limestone deposits (Kreutzer 1989). It ended during the Frasnian Upper *rhenana* Zone (=Upper *gigas* Zone; Kreutzer 1990), following a general transgression possibly caused or enhanced by local extensional tectonics (Spalletta and Vai 1984).

According to regional settings, the fore-reef area consists of massive limestone including reefal debris and lithoclasts (Cellon Limestone), which gradually changes toward the east into bedded allodapic limestone (Freikofel Limestone). Both units are overlain by pelagic cephalopod limestone (Pal Limestone). The geographical distribution of the transitional facies related to the Freikofel Limestone can be traced from Mount Kleiner Pal (Schönlaub 1991: p. 39) toward east, with best outcrops at Mount Freikofel (Lischka 2007; Stark 2007; Schnellbächer 2007, 2010a, b) and Pramosio area (Spalletta and Perri 1998). According to geological maps (Schönlaub 1991), deposition of transitional facies initiated somewhere between Mount Cellon and Mount Kleiner Pal. On the Mount Cellon, the Cellon Limestone is directly overlain by the Pal Limestone lacking deposits characteristic for the Freikofel Limestone. According to Austrian authors (Piller et al. 2004), a summary of the Devonian stratigraphy of the Cellon-Kellerwand Nappe with the location of the Freikofel section is

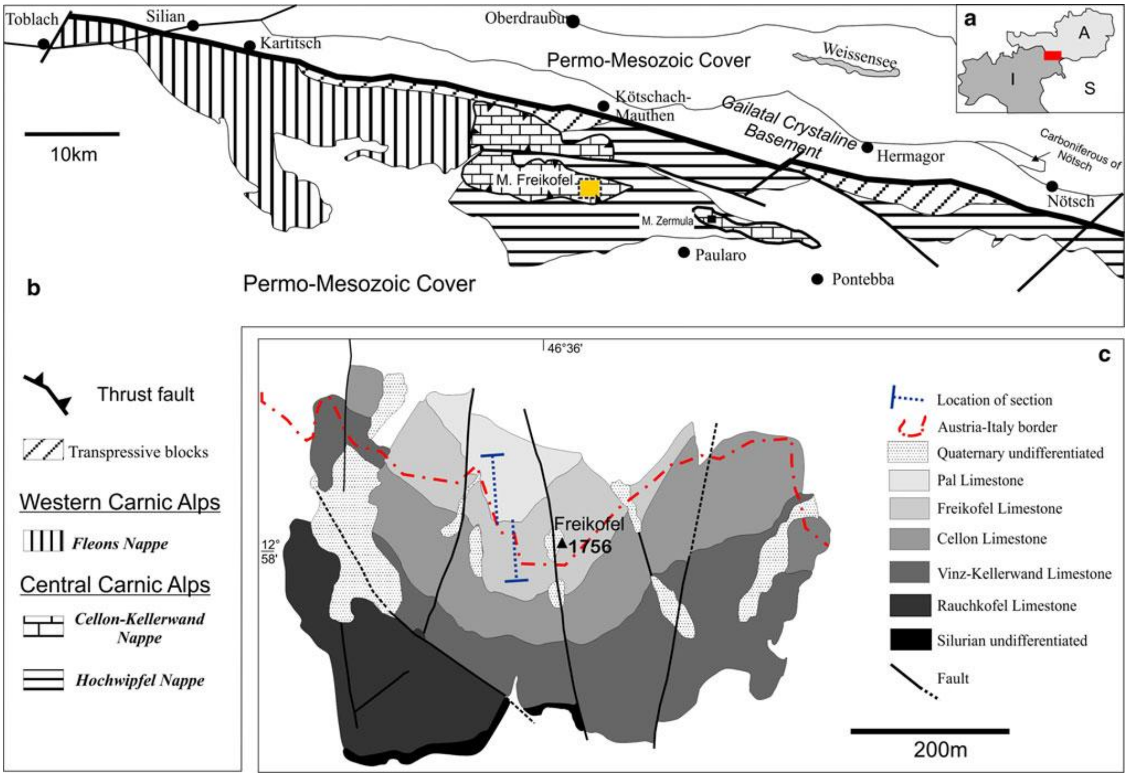

Fig. 2 **a** Location of the Carnic Alps area at the Austria–Italy border. **b** Location of Mount Freikofel in the carnic chain (redraw from Läufer et al. 2001). **c** Simplified geological map of Mount Freikofel with location of the studied sections (modified from M. Pondrelli, unpublished)

Fig. 3 General stratigraphic scheme and facies relationship of Devonian units in the Carnic Alps according to Austrian authors (Piller et al. 2004). Modifications are made for the Freikofel Limestone according to its age and relation with the cellon limestone (*red dotted line*) based on the age range mentioned in Brime et al. (2008), on the geological map of Venturini et al. (2009), and the new conodont data obtained for this study

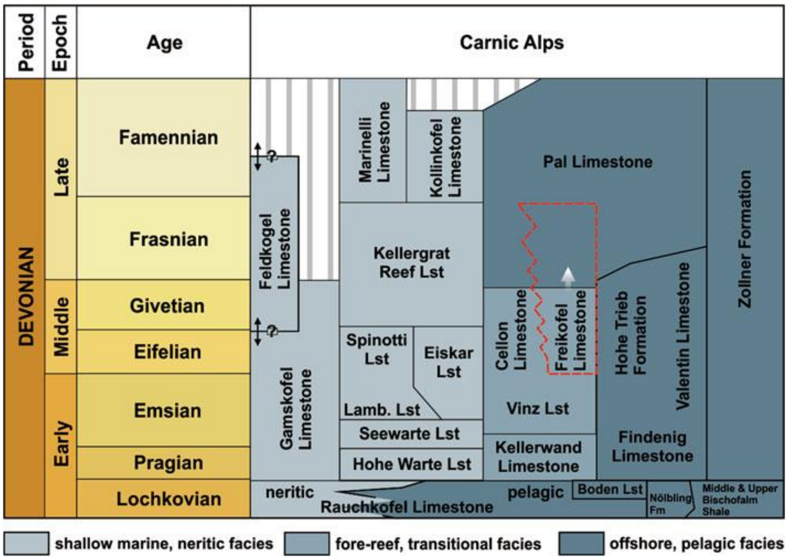

illustrated in the Fig. 3. In the Italian literature (i.e., Venturini et al. 2009), a stratigraphic unit named "Calciruditi del Freikofel" ranging from Pragian to Famennian is described but, it has to be mentioned that this unit has a different meaning of the Freikofel Limestone as used in this paper. Therefore, comparison between Austrian and Italian stratigraphic units is not straightforward.

Methods

A detailed bed-by-bed description and sampling of the Freikofel sections (Figs. 4, 6) were performed with an average sampling rate of one sample per 20 cms (except for the massive breccia levels where the sampling rate is one sample per meter). For microfacies analysis, 200 samples were collected. The textural classification used to characterize the microfacies follows Dunham (1962) and Embry and Klovan (1972). Estimation of sorting is based on the visual charts of Pettijohn et al. (1972). Thin sections were stained using Dickson solution to differentiate calcite, dolomite, feroan calcite, and feroan dolomite (Dickson 1965). Eighteen samples (±400 gr) belonging to intermediate slope and pelagic facies were taken for conodont investigation. Conodont frequency is poor to good, depending of the facies (from 10 to 50 specimens/kg). Thin sections and conodont samples are stored in the sedimentary petrology building (B20, University of Liège). Analyses of $\delta^{13}C_{carb}$ were done on 35 samples collected around the proposed Frasnian–Famennian boundary interval using bulk mudstone–wackestone. Powdered samples reacted with phosphoric acid in an online carbonate preparation (Kiel III carbonate device) connected to a Thermo-Delta plus XL mass spectrometry instrument at the Vrij Universiteit Brussel, Belgium. Samples were calibrated to the NBS19 standard ($\delta^{13}C = 1.95$ promille VPDB). MS measurements were undertaken on more than 200 rock samples. Each sample was analyzed three times with KLY-3 (Kappabridge) and weighed with a precision of 0.01 g. This allows the definition of the mass-calibrated MS for each sample and the construction of MS plots. Major and trace elements were measured using X-ray Fluorescence (ARL 9400 XP XRF instrument, University of Liège) on 15 samples regularly spaced through the studied part of the Freikofel section. The analyzed rock samples were carefully cleaned prior to all treatment: weathered surfaces were removed. The major elements (in this paper, SiO_2, TiO_2, K_2O, and Al_2O_3) were analyzed on lithium tetra- and meta-borate-fused glass discs, with matrix corrections following the Traill-Lachance algorithm and are expressed in elemental oxide concentration. Trace elements (in this paper, Zr, Cu, Ni, and Sr) were measured on pressed powder pellets, and data were corrected for matrix effects by Compton peak monitoring and expressed in elemental concentration. Precision and accuracy were both shown to be better than 1 % for major elements and 5 % for trace elements as proved by international standards and analyses of replicate samples, respectively.

Results

Description of section

The outcrop exposed at Mount Freikofel (46°36′05.2″N, 12°58′37.1″E) provides a stratigraphically continuous succession of strata, which starts within the Lochkovian and ends during the Lower Famennian. The entire section encompasses six formations: Rauchkofel, Kellerwand, Vinz, Cellon, Freikofel, and Pal Limestones (Figs. 3, 4). For the purpose of this investigation, we focused on the upper part of the Freikofel section including the upper part of the Freikofel Limestone and the base of the overlying Pal Limestone. The measured section is continuous, about 62 meters thick (Figs. 5, 6), and covers a stratigraphic interval extending from the Latest Givetian–Early Frasnian to Early Famennian. The measured succession of strata is oriented N110°E with an average dip of 52°NE. Strata usually show a strongly weathered surface, a covering by lichens and in the lower part a massive aspect. Despite those limiting factors, the main lithostratigraphic units have been recognized and mapped (Fig. 2).

Description of the lithological units

Unit 1 (~32.5 m-thick, upper portion of the Freikofel Limestone; Fig. 4)

This lower portion of the measured section mainly consists of several-m-thick (Fig. 4b) gray to blue beds of coarse-grained lithoclastic and bioclastic limestones locally intercalated by dm to several-dm-thick limestone beds. Lithoclasts are commonly sub-angular to rounded, cm to several tens-cm-sized (Fig. 4c, d). They are loosely to densely packed, are moderately sorted and of various color; some are dark gray in color, similar to the matrix. Where the texture is not concealed by alteration and/or lichens, a fining upward grading of lithoclasts is observed. Bioclasts are scarce, cm to dm in size, and mainly represented by stromatoporoid, crinoid and tabulate, and rugose coral fragments. Through the upper part of Unit 1, the thickness of beds decreases.

Unit 2 (~29.5 m-thick, lower and middle portions of the Pal Limestone; see Fig. 4)

The boundary between the Freikofel and the Pal Limestones is defined by the predominance of mudstone over

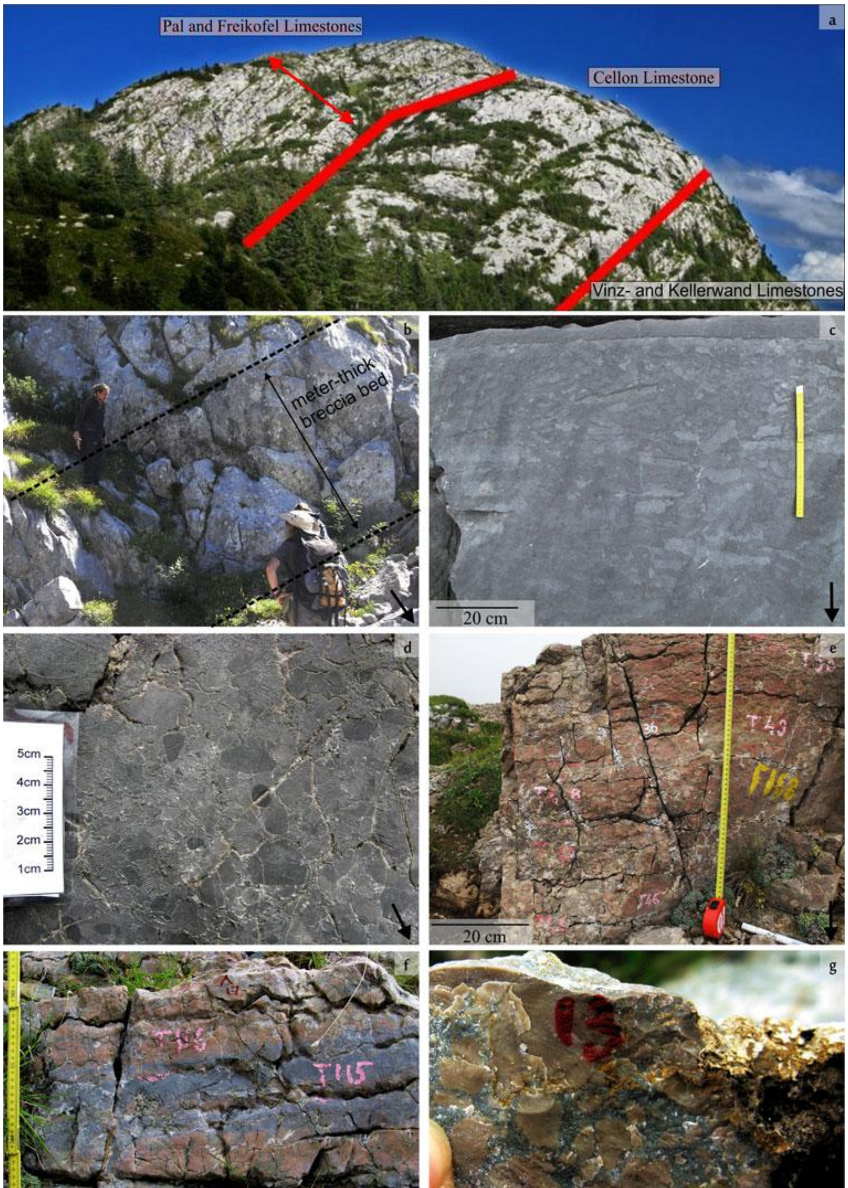

Fig. 4 **a** View of Mount Freikofel showing the studied interval (Freikofel Limestone and Pal Limestone; view from the west) and the underlying Cellon Limestone and undifferentiated Vinz and Kellerwand Limestones. **b** Several-m-thick breccia bed belonging to the Freikofel Limestone. *Dashed lines* indicate the bedding plan. **c** Close-up on a breccia bed with well-visible *light gray* elongated lithoclasts (MF6). **d** Close-up on a breccia levels exposing different types of subrounded lithoclasts. **e** Thin-bedded *red* to *pink* nodular limestone characterizing the Pal Limestone. **f** *Pink* to *red* thin-bedded limestone showing *blue gray* coarse-grained limestone horizon (MF3). **g** Close-up on a coarse-grained limestone intercalation (MF3) showing well-visible infra-centimeter reddish lithoclasts from the underlying thin-bedded limestone (MF1). The *arrow* on the lower right of the pictures points to the stratigraphic base

grainstone facies. Unit 2 corresponds mainly to a succession of thin-bedded several-cm to tens of cm-thick grayish, pinkish to reddish fine-grained burrow-mottled limestone with numerous stylolite-like structures along the stratification planes (Fig. 4e). These fine-grained limestones correspond to the so-called Flaserkalk of Bandel (1974). A particular character of Unit 2 is the common occurrence in these fine-grained sediments of two different types of coarser-grained limestone levels: (1) cm to several-cm-thick bluish grainstone horizons showing locally well-visible infra-cm reddish lithoclasts (Fig. 4g) and (2) several-dm to m-thick beds showing several-cm-sized lithoclasts of various lithologies locally displaying a fining upward grading. In the first case, lateral continuity of intercalation can be followed for several tens of meters.

Bio- and chemostratigraphy

In order to provide a biostratigraphic framework for the microfacies/sedimentology works performed on the Freikofel section, we selected 18 samples from the “transitional” (Freikofel Limestone) and the pelagic facies (Pal Limestone) for conodont analysis. They reveal a stratigraphic interval ranging from the Latest Givetian to Early Famennian. The occurrence of *Mesotaxis falsiovalis* and *Polygnathus dubius* near the base of the section (sample: FK93b) indicates a Latest Givetian age and constrains the sampled bed to an interval ranging from the Lower *falsiovalis* (FAD: *Mesotaxis falsiovalis*) or *transitans* zone (LAD: *Polygnathus dubius*). A 2-meter-thick interval near the 10-m-mark yields P1 elements of *Ozarkodina trepta* (samples: FK82a, b; FK83; FK85a, b and FK86), which indicate the Lower *hassi* zone. The occurrence of *Palmatolepis rotunda* (sample: FK62′) and *Pa.* aff. *subrecta* (sample: FKS22-28) around the 40-m-mark documents the Late Frasnian age as the total range of both taxa is constricted from the Early–Late *rhenana* zone until late in the *linguiformis* zone. Sample FKS74 from the lower part of the Pal Limestone yields in addition to Late Frasnian conodont elements like *Palmatolepis rotunda* elements of *Polygnathus timorensis,* which indicate reworking of Givetian deposits from the platform at least until the Late Frasnian. P1 elements identified as *Palmatolepis* cf. *crepida* (sample: FK07) near the top of the section document the upper limit of the sequence at Mount Freikofel within the *crepida* Zone (*indet*. zonation). Some diagnostic Middle and Late Devonian conodont elements are illustrated in Fig. 5. Furthermore, a distinctive positive shift of about 3 promille in the δ^{13}C trend is related to the Upper Kellwasser event and indicates the Frasnian–Famennian boundary in the section (Fig. 6b).

Microfacies

MF1: bioturbated microbioclastic mudstone-wackestone (Fig. 7a–f)

This microfacies mostly occurs in the uppermost part of the section between 41 and 60 m (Unit 2) and consists of grayish to red thin-bedded limestone (Fig. 4e–f). It is mostly characterized by the occurrence of pelagic/hemipelagic microfossils such as thin-shelled bivalves, goniatites (Fig. 7a), entomozoan ostracods, styliolinids, and trilobites. These fossils are scattered in a dark brown micritic matrix and are commonly associated with unidentifiable filaments and sponge spicules (Fig. 7d). A significant characteristic of this microfacies is bioturbation (Fig. 7b–c), which is locally intense and show lighter color compared to the non-disturbed surrounding sediments and lower amount in bioclasts. Rarely, burrows filled with grainstone (corresponding to MF3) occur. Another particular character of this microfacies is the local intercalation of several-mm to several-cm-thick layers of well-sorted lithoclastic grainstone (Fig. 7e) with lower sharp erosional boundary (Fig. 7f) and fining upward grading. Locally inverse grading with erosive base also occurs. Mottled nodular structures are frequent and highlighted by reddish-brown Fe oxides envelopes. Locally, an iden-supported fabric is very well exposed.

Interpretation

In numerous sedimentological studies (Rabien 1956; Tucker 1973; Vai 1980; Wendt and Aigner 1985; Pas et al. 2013; Königshof et al. 2012), the Devonian thin-bedded cephalopod limestone in Europe has been interpreted as being accumulated upon submarine rises at depths reaching several tens to about one hundred meters. Wendt and Aigner (1985) also suggested that thin-bedded cephalopod limestones were probably formed during times of reduced sedimentation rate. Indeed, the common occurrence of bioturbation likely indicates low accumulation rate, as well as oxygenated bottom water (Flügel 2004). The predominance of deepwater fossils attests an hemipelagic/pelagic environmental setting. Furthermore, the very fine-grained sediment of this microfacies points to a low energy setting located below the storm wave base (SWB) where the main sedimentary process is the product of settling of a very fine turbid tail and of periplatform oozes. This microfacies was thus deposited in a distal slope setting oxygenated environment with a low accumulation rate episodically influenced by distal turbidites (see MF3 below).

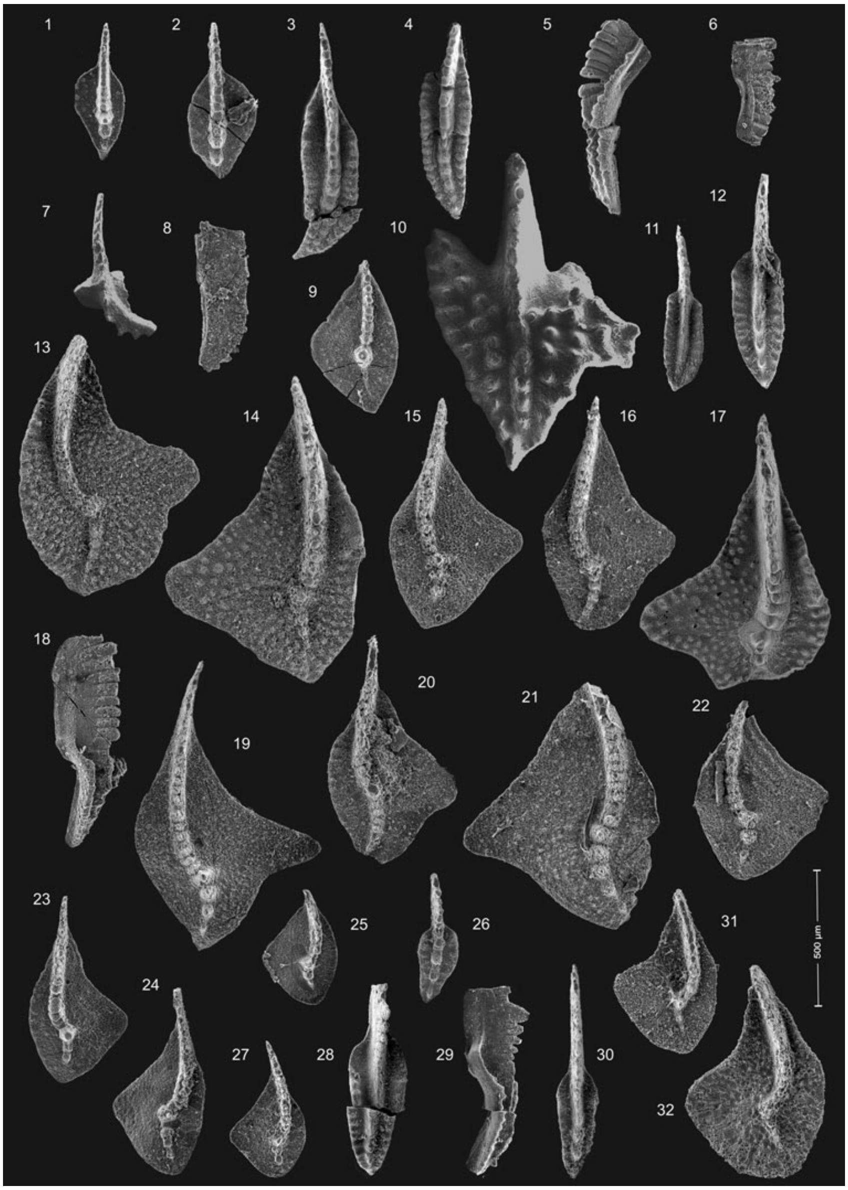

MF2: fine-grained bioclastic styliolinid wackestone-packstone (Fig. 7h)

This microfacies is mainly observed within Unit 1 either as decimeter-sized interbeds or as constituting part of the m-thick breccia beds (see description of Unit 1). This microfacies also occurs as lithoclasts within the MF6, or with MF4 through vertical grading. Locally, lenticular grainstone texture (corresponding to MF5) occurs within this wackestone-packstone (Fig. 7g). Styliolinids (average size around 0.05 mm diameter) are generally disseminated but locally concentrated in styliolinid wackestone to packstone lenses (Fig. 7h). From time to time, a well-preserved fining upward grading from MF2 toward MF1, followed by bioturbated MF1, is also observed. Other significant characteristics of MF2 are the finely broken character of allochems (average size: 0.15 mm), which make most of them unidentifiable, and the dominance of pelagic

◀ **Fig. 5** Some important conodonts of the Freikofel section. **1** *Mesotaxis falsiovalis*, oral view of P1 element from FK93b. **2** *Mesotaxis falsiovalis*, oral view of P1 element from FK93b. **3** *Polygnathus dubius*, upper view of P1 element from FK93b. **4** *Polygnathus dubius*, upper view of P1 element from FK93b. **5** *Polygnathus dubius*, lateral view of P1 element from FK93b. **6** *Tortodus intermedius*, oral view of P1 element from FK93b. **7** *Ozarkodina trepta*, upper view of P1 element from FK85a. **8** *Ozarkodinia bidentata*, lateral view of P1 element from FK93b. **9** *Palmatolepis* sp., oral view of a juvenile P1 element from FK93b. **10** *Ancyrodella lobata*, upper view of P1 element from FK87b. **11** *Polygnathus xylus*, upper view of P1 element from FK93b. **12** *Polygnathus dubius*, upper view of P1 element from FK81. **13** *Palmatolepis rotunda*, upper view of P1 element from FK62′. **14** *Palmatolepis hassi*, non-adult specimen, upper view of P1 element from FK62′. **15** *Palmatolepis* aff. *hassi*, upper view of P1 element from FK62′. **16** *Palamtolepis* aff. *hassi*, upper view of P1 element from FK62′. **17** *Palamtolepis* cf. *hassi*, upper view of the P1 element from FK50. **18** *Polygnathus decorosus*, lateral view of P1 element from FK50. **19** *Palmatolepis nasuta*, upper view of P1 element from FK50. **20** *Palmatolepis hassi*, upper view of the P1 element from FK50. **21** *Palamtolepis hassi*, upper view of P1 element from FK46a. **22** *Palmatolepis* cf. *gigas*, upper view of P1 element from FK07. **23** *Palmatolepis* aff. *subrecta*, non-adult specimen, upper view of P1 element from FK07. **24** *Palmatolepis* aff. *subrecta*, upper view of P1 element from FKS22-28. **25** *Palmatolepis* sp., juvenile specimen upper view of P1 element from FKS22-28. **26** *Polygnathus* sp., juvenile specimen, upper view of P1 element from FKS74. **27** *Palmatolepis delicatula*, upper view of P1 element from FK07. **28** *Polygnathus decorosus*, upper view of P1 element from FKS98. **29**: *Polygnathus decorosus* lateral view of P1 element from FKS74. **30** *Polygnathus* aff. *timorensis*, upper view from P1 element from FKS96-98. **31** *Palmatolepis rotunda*, upper view of P1 element from FKS74. **32** *Palmatolepis rotunda*, upper view of P1 element from FKS96-98

organisms over shallow-water ones. Recognized organisms are infra-millimeter in size and in order to the abundance represented by styliolinids, crinoids, thin-shelled bivalves, calcispheres, ostracods, entomozoacean ostracods, and trilobites. The sorting of this sediment is moderate to good and bioturbations occur.

Interpretation

The common to abundant occurrence of styliolinid shells and finely broken bioclasts in micritic matrix points to a hemipelagic depositional setting where the prominent sedimentary process is the periplatform oozes settling. Even if locally styliolinid shells are the dominant biogenic components and thus represent the background sedimentation, the common association with finely broken unidentifiable bioclasts is thought to reflect a mixture with materials derived from shallower marine realms. This mixture of biota from different origin can be explained by a winnowing of the sediment during more turbulent events such as gravity flow or storm. The well-preserved fining upward grading MF2 toward MF1, followed by bioturbated MF1, points to a turbiditic origin of these sequences; MF2–MF1 corresponds to the final sedimentation step recognized in the Bouma sequence (Td–Te interval of Bouma). Indeed, ideal turbiditic sequence of Bouma (1962), Piper (1978) and Stow and Shanmugam (1980) usually shows a final phase of sedimentation with a fining upward succession ending with bioturbated pelagic fine sediment. The common occurrence of MF2 lithoclasts within rudstone texture of MF6 (see below) indicates a depositional setting influenced by temporarily strong bottom current such as gravity flow. The local occurrence of MF2 in the top of meter thick fining upward sequences occurring in the breccia beds of Unit 1 also supports our interpretation.

MF3: lithoclastic grainstone (Fig. 7e–f)

This microfacies only occurs in Unit 2 as mm- to cm-sized lithoclastic grainstone intercalation within the mudstone-wackestone beds of MF1 (Figs. 5f, 7e). The cement of this grainstone is a sparite. Where outcrop conditions are good, it is possible to follow these intercalations laterally for several tens of meters. Where the pressure solution processes does not affect the sediment, the lower boundary of these grainstone layers appears sharp and with erosional contact, with scours and fills (Fig. 7e–f). Lithoclasts are mostly well-rounded even if some are angular, relatively well-sorted (locally bimodal) and their size ranges from 0.5 to 2 mm. Fining upward grading occurs locally (Fig. 8a). The lithoclasts are composed of mudstone and wackestone textures, respectively, corresponding to MF1 or MF2. Lithoclasts are associated with crinoid fragments and less frequent bioclasts such as brachiopods, ostracods, and stromatoporoids.

Interpretation

The intercalation of this thin-bedded lithoclastic grainstone (MF3) horizons within the hemipelagic/pelagic setting (MF1), the abundance of lithoclasts, their relatively good sorting, the fining upward, and the lateral persistence of the layers are diagnostic features of distal slope thin-bedded turbiditic deposits (Mutti 1977; Flügel 2004). According to Mutti (1977), thin-bedded turbiditic deposits are the product of waning and relatively dilute turbidity currents that carry fine-grained sand and silt-sized particles. According to Flügel (2004), the absence of shells concentration and flat top/base as well as the presence of grading allow to exclude an accumulation by distal tempestites. This MF3 corresponds to the “redeposited beds” occurring in pelagic limestone sequence described by Bandel (1972) in the Carnic Alps. Bandel (1972, 1974) considered the “pelagic limestone with common redeposited beds” as transitional between the basin floor and the shallow-water platform. The major source of lithoclasts is interpreted as bottom reworking of sediment during downslope movement.

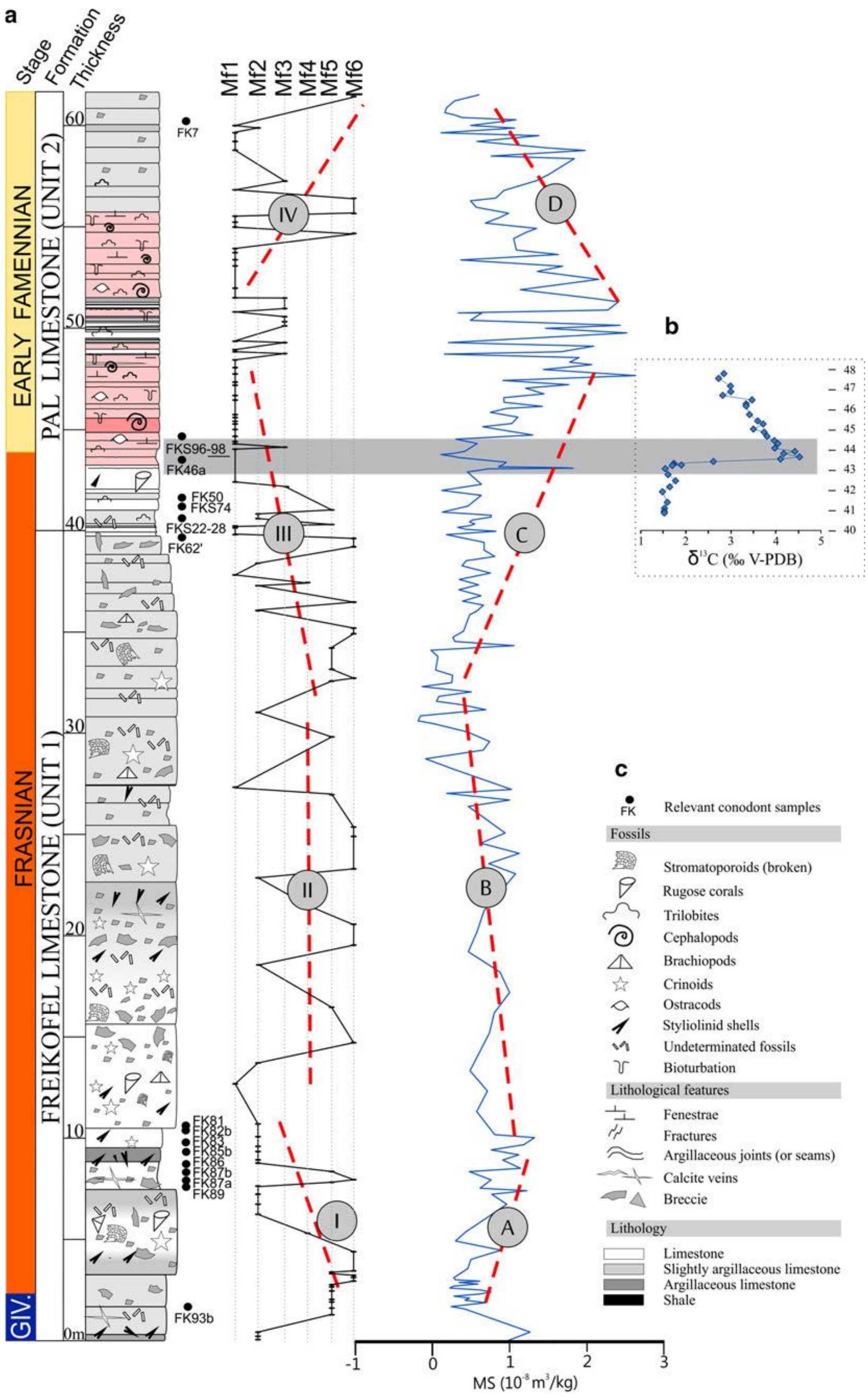

a
Stage
Formation
Thickness
EARLY FAMENNIAN
FRASNIAN
GIV.
PAL LIMESTONE (UNIT 2)
FREIKOFEL LIMESTONE (UNIT 1)
Mf1
Mf2
Mf3
Mf4
Mf5
Mf6
FK7
FKS96-98
FK46a
FK50
FKS74
FKS22-28
FK62'
FK93b
FK89
MS (10⁻⁸ m³/kg)
b
δ13C (‰ V-PDB)
c
Relevant conodont samples
Fossils
Stromatoporoids (broken)
Rugose corals
Trilobites
Cephalopods
Brachiopods
Crinoids
Ostracods
Styliolinid shells
Undeterminated fossils
Bioturbation
Lithological features
Fenestrae
Fractures
Argillaceous joints (or seams)
Calcite veins
Breccie
Lithology
Limestone
Slightly argillaceous limestone
Argillaceous limestone
Shale

◀ **Fig. 6** **a** Schematic sedimentological log, lithostratigraphic units, microfacies trends, and magnetic susceptibility curves. *Red dash line* represents trends in microfacies (I–IV) and magnetic susceptibility (*A*, *B*, *C*, and *D*) evolution. **b** Stable carbon isotope curve across the Frasnian—Famennian boundary. **c** Legend for symbols used in figures

MF4: crinoidal bioclastic packstone (Fig. 8b)

This microfacies is not frequent and mainly occurs in Unit 1 in association either with MF5 and MF2 through vertical grading or as lithoclasts in MF6. Except for crinoid debris, bioclasts are rare and often unidentifiable but the sorting is good. Crinoids are surrounded by syntaxial cement and have an average size around 0.35 mm. The bioclasts are commonly associated with irregularly shaped peloids with an average size around 0.2 mm. However, the peloids included in a packstone texture are sometimes difficult to be distinguished from the matrix.

Interpretation:

The general good sorting of the allochems suggests a depositional setting where the water agitation is, at least, temporarily high. Although, the packstone texture and its micritic matrix need relatively quiet conditions, likely under fair weather wave base (FWWB), to be deposited. The significant proportion of crinoids over other biogenic components suggests either a setting located in the vicinity of crinoidal meadows or a mechanical sorting of the allochems prior to deposition. The occurrence of this microfacies in association with MF5, interpreted as belonging to a turbiditic sequence (see below), and the vertical grading from MF5 through MF4 and also from MF4 through MF2 supports a mechanical sorting of the crinoids during turbulent flow such as turbidite. Sedimentological criteria observed in this microfacies are interpreted as part of the ideal turbiditic deposition occurring in Bouma sequence (e.g., Tb–c interval; Bouma 1962). Equivalent interval for “allodapic” limestone of Meischner (1964) corresponds to Zone 1c, 2a, and b.

MF5: mud peloids crinoidal grainstone (Fig. 8c, d, f, i)

This microfacies is observed within Unit 1, in association with microfacies MF6 either as filling the inter-lithoclastic voids in the rudstone texture (Fig. 8d) or as large lithoclasts (Fig. 8e). Less frequently, MF5 can be observed in association with MF4 either through a graded or sharp transition or as lenticular occurrences (Fig. 7g). Peloids (average size of 0.25 mm) are abundant and locally very well-sorted (Fig. 8f). They commonly display different size and shape (“lithic” or “mud” peloids). According to Flügel (2004), mud peloids are variously shaped micritic grains caused by the reworking of lithified carbonate mud and micritic clasts. Locally, thin laminations underlined by the alternation of small- and larger-sized peloid levels occur. These laminations are often planar but cross-laminations are locally observed. Local fining upward grading from MF5 toward packstone and wackestone (MF4, MF2) are observed. Crinoids are usually disarticulated with an average size around 0.3 mm and usually show syntaxial cement. Calcispheres are frequent (Fig. 8g) while brachiopods, foraminifera (*Frondilina tailferensis*; Mamet et al. 1985, Fig. 8h), and unidentifiable bioclasts are poorly represented.

Interpretation

The grainstone texture, with a generally good sorting and the local thin- and cross-lamination as well as the absence of fine-grained particles, suggests a depositional setting where water agitation was significant. The common occurrence of calcispheres and crinoids supports a depositional setting influenced by shallow-water setting. Indeed, calcispheres and crinoids are, respectively, found in lagoon and back- to fore-reef setting within the FWWB. These allochems are thus interpreted as reworking of the shallower sediments during more energetic events such as storm waves, or downward transport along the fore-slope environment by gravity currents. The local fining upward grading toward wackestone-packstone (MF2, MF4) and the presence of wackestone-packstone intraclasts in the grainstone texture are arguments in favor of gravity-flow deposit such as turbidite. Indeed, storm deposits do not display grading. Considering the presence of wackestone-packstone intraclasts (MF2), which are interpreted as background sedimentation (see interpretation of MF2), the depositional setting of MF5 might be located under the FWWB. Similar microfacies have been described by May (1994) and Pas et al. (2013) for the fore-reef-slope environment from the Rhenisches Schiefergebirge (Germany) and are interpreted as a part of the general pattern visible in “allodapic” limestone (Zone 1b; Meischner 1964) and in the ideal turbiditic sequence of Bouma (division Tb; Bouma 1962). Other sedimentological criteria such as the presence of lamination, local fining upward sequences also support a deposition related to turbidity currents.

MF6: lithoclastic rudstone (Figs. 8d, e and 9)

This microfacies occurs mainly in Unit 1 and appears as several-dm to several-m-thick beds (Fig. 4b) intercalated within dm-thick beds of MF2 and MF4. At the outcrop scale, a fining upward grading occurs locally depending of the alteration. MF6 corresponds to a moderately sorted

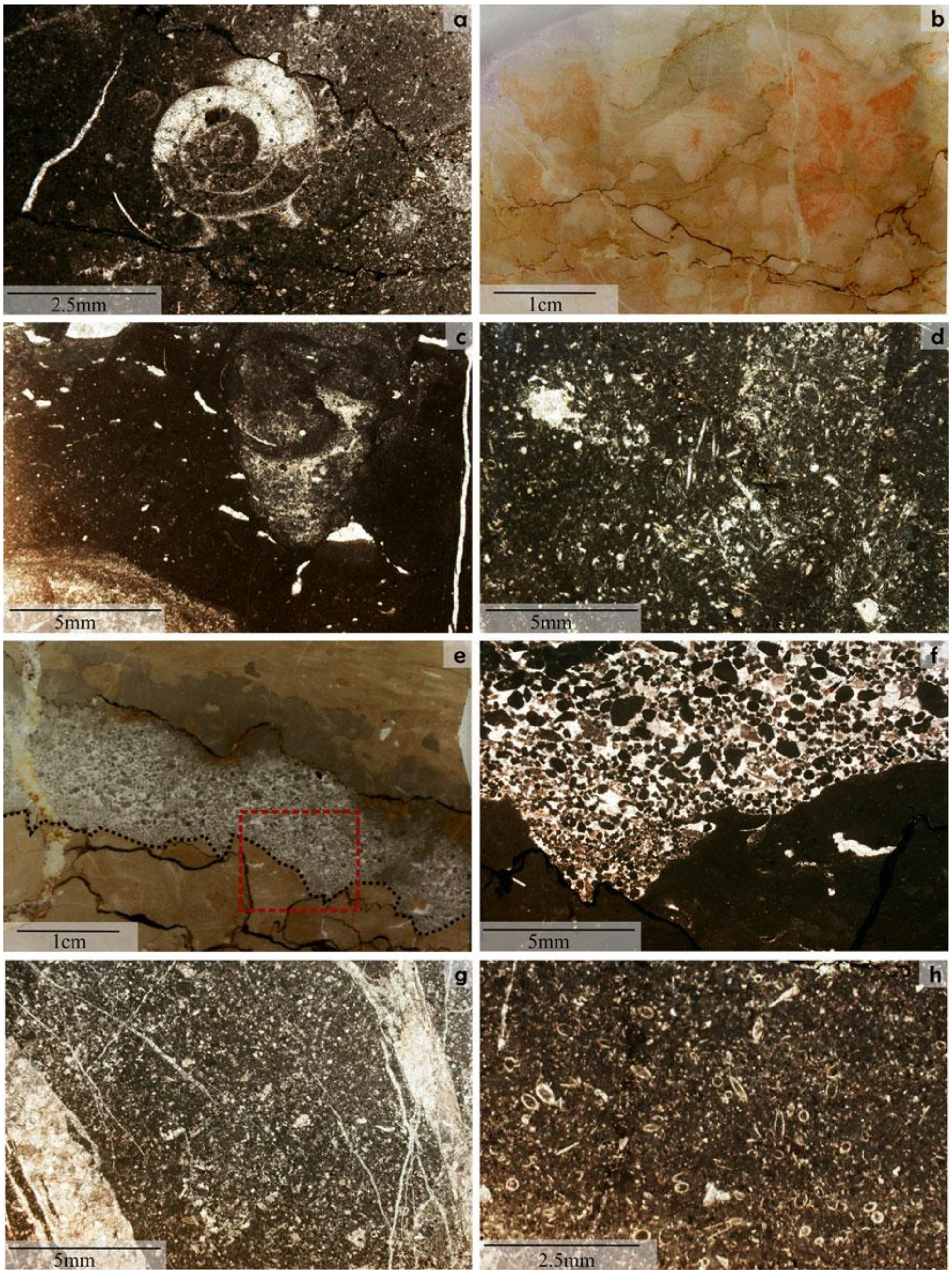

accumulation of various rounded to sub-angular-shaped several-mm to tens of cm-sized lithoclasts corresponding to MF1, MF2, MF4, and MF5 (Figs. 8e, 9b). The dominant texture of this microfacies is rudstone even if a floatstone texture occurs (Fig. 9a). In the rudstone, the space between lithoclasts is usually filled with smaller grains with a grainstone texture cemented by sparite (Figs. 8d, 9c). These grains have an average size of 0.3 mm and are mainly represented by mud peloids (locally 70 % of the filled space), calcispheres, brachiopod and ostracod shell

◀ **Fig. 7** Microfacies from the distal fore-reef deposits of the Freikofel section. Photomicrographs of thin sections oriented perpendicular to the bedding. Numbers preceded by FK correspond to bed numbers. **a** MF1 distal reef-slope deposits: fine-grained mudstone with a goniatite shell (FK 47a, transmitted light). **b** MF1 distal reef-slope deposits: fine-grained bioturbated mudstone (FK 41, scanned thin section). **c** MF1 distal reef-slope deposits: fine-grained mudstone with fenestrae and bioturbation (FK44a, transmitted light). **d** MF1 distal reef-slope deposits: accumulation of sponge spicule in a bioturbated mudstone (FK01, transmitted light). **e** MF1 distal reef-slope deposits: intercalation of a lithoclastic grainstone layer (MF3) within a mudstone (FK30, scanned thin section). **f** MF1 distal reef-slope deposits: close-up on a lithoclastic grainstone layer intercalation occurring in MF1 mudstone (for location, see inset in **e**) (FK30, transmitted light). **g** MF2 intermediate to distal reef-slope deposits: fine-grained bioclastic wackestone-packstone with peloidal grainstone intercalation (FK97, transmitted light). **h** MF2 intermediate to distal reef-slope deposits: fine-grained rich styliolinid packstone (FK93, transmitted light)

fragments, and styliolinids. Locally, centimeter-sized stromatoporoid and rugose coral debris occur. Unidentifiable bioclasts are common. In the floatstone, the inter-lithoclastic voids are also filled with grainstone texture even if locally a packstone texture occurs.

Interpretation

This facies was first described as "Lithoklastkalk" by Bandel (1972) and later as "intraclast parabreccia" by Spalletta et al. (1983) and Spalletta and Vai (1984). These authors interpret these facies as the result of the concurrent action of relevant seismic shocks that induced tsunamis, back currents, and related turbidity current. The m-thick lithoclastic beds characterizing MF6 combined with local occurrence of fining upward sequences passing upward to wackestone and mudstone interbeds are diagnostic features of turbiditic sequence (Bouma 1962; Mutti 1977). However, the rare occurrence of a floatstone texture might reveal a deposition rather influenced by debris flow. The local intercalation of wackestone and mudstone (MF2) interbeds corresponding to autochthonous sedimentation confirms a depositional setting located below the SWB, in an off-reef pelagic/hemipelagic environment for MF6. The abundance of lithoclasts originated from intermediate slope and off-reef pelagic/hemipelagic environment (see MF2, MF3, and MF4) indicate a reworking of lithified materials from different sources located in a fore-reef-slope setting. The low ratio between reef-builder remains and lithoclasts indicates rather gravity flow originated from the fore-reef slope than the shallow-reef habitat. This microfacies corresponds to the Zone 1a in the ideal "allodapic" sequence of Meischner (1964) and division Ta in the ideal turbiditic sequence of Bouma (1962). To conclude, this microfacies is mostly in relation with turbiditic flow even when debris flow likely plays a role as well.

Discussion

Depositional environments

Petrographic analyses from the upper part of the Freikofel section led to the definition of six microfacies representing fore-reef slope to distal-reef floor depositional setting where gravity-flow processes play a significant role during the sedimentation (Fig. 10). In this simplified model, the more distal setting is characterized by deeper slope to distal reef floor autochthonous sedimentation (MF1, MF3), temporarily influenced by distal turbiditic current (MF3). These distal turbidites are comparable to turbiditic fringe lobe developed in basin floor environment (e.g., Mutti 1977). In the intermediate to distal fore-reef-slope area, an interplay of various gravity processes (debris and turbiditic flow) dominates the depositional style and corresponds to an accumulation of various autochthonous and allochthonous sediments (MF6, MF5, MF4, and MF2); these sediments represent different portions of deposition occurring in Bouma (e.g., Ta, Tb, Tc, Td–e; Bouma 1962) or Meischner sequence; it is equivalent for carbonate environment (e.g., Zones 1, 2, and 3; Meischner 1964). Therefore, these microfacies could reflect a deposition in a channel lobe system in an outer fan turbiditic model (e.g., Mutti 1977).

The temporal evolution of microfacies throughout the studied section (Fig. 6) demonstrates two major palaeoenvironmental trends corresponding to Unit 1 (Freikofel Limestone) and Unit 2 (Pal Limestone), respectively. During the sedimentation of Unit 1, the microfacies curve (Fig. 6) shows mainly an aggrading trend with numerous oscillations between MF6, MF5, MF4, and MF2, which are interpreted as transitions between parts of the Bouma sequence recognized in turbiditic deposits. The occurrence of a mixed Late Eifelian–Early Givetian and Early Frasnian conodont fauna in the lower part of Unit 1 proves that the thick breccia levels are likely connected to the Late Givetian major rift pulse recognized in the Carnic Alps (Ebner et al. 1980; Spalletta et al. 1980; Vai 1980). This rift phase would have deeply altered the morphology of the fore-reef setting from a gentle slope to a steep fault scarps, resulting in a severe reworking of slope and/or platform margin settings. According to various authors (Vai 1976; Kreutzer 1992a, b; Schönlaub and Histon 2000), the maximum development of the Devonian carbonate platform in the Carnic Alps seems to have occurred in the Givetian and Early Middle Frasnian periods (Kreutzer 1992a; Vai 1998), which is consistent with the worldwide blossoming of Devonian carbonate platform (Copper 2002). Therefore, this period is interpreted here as the interval where the production of reef-derived debris susceptible to move downward reached its maximum. For instance, in the fore-reef setting of the Brilon Reef

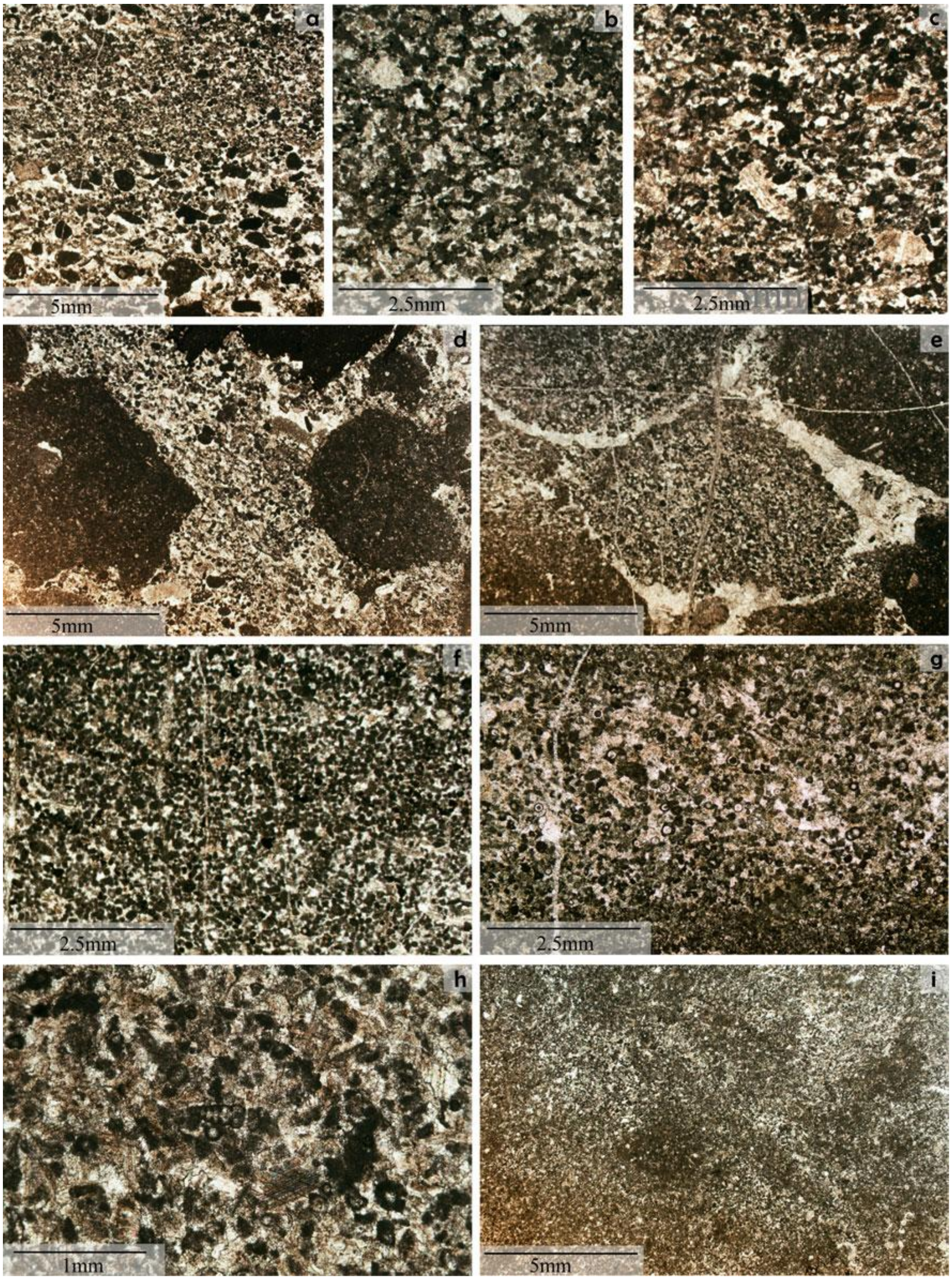

Complex (eastern Rheinisches Schiefergebirge), the highest proportion in reef-related debris extends from the Late Givetian to the Early Frasnian period (Pas et al. 2013), which is consistent with the maximal extension of the platform. This relationship between maximal extension of platform and highest proportion of reef-related debris was also recognized in the reef complex of the Australian Canning Basin (Playford et al. 1980). However, in the Freikofel section, the Lower Frasnian succession records low occurrence of reef-builder debris and/or shallow-water-derived allochems compared to the high proportion of fore-reef-slope-derived lithoclasts (e.g., MF2, MF4, and

◀ **Fig. 8** Microfacies from the intermediate to distal reef slope of the Freikofel section. Photomicrographs of thin section oriented perpendicular to the bedding. **a** MF3 distal reef-slope deposits: fining upward sequence in a lithoclastic grainstone (FK11, transmitted light). **b** MF4 intermediate reef-slope deposits: crinodal packstone (FK64, transmitted light). **c** Intermediate to distal reef-slope deposits: crinoidal grainstone (FK87, transmitted light). **d** MF6 intermediate to distal reef-slope deposits: lithoclastic rudstone with an inter-lithoclastic void filled with a peloidal grainstone (FK13a, transmitted light). **e** MF6 intermediate reef-slope deposits: lithoclastic grainstone showing three types of lithoclasts (pgl; cpl; wpl) (FK79a", transmitted light). **f** Well-sorted peloidal grainstone (FK93c, transmitted light). **g** MF5 intermediate reef-slope deposits: calcispheres-rich peloidal grainstone (FK75c", transmitted light) **h** MF5: intermediate reef-slope deposits: fine-grained micritic clasts grainstone showing foraminifera *Frondilina tailferensis*; Mamet et al. (1985) (FK87b, transmitted light). **i** MF5 intermediate reef-slope deposits: rich fine-grained peloidal grainstone corresponding to a pelsparite (FK79a, transmitted light)

MF5). This situation rather suggests a deposition during a period of low carbonate productivity within the shallow-water setting. This hypothesis is supported by the data from Schnellbächer (2010) who reported that the highest proportion of reef-builder debris in the Freikofel section (Cellon Limestone; see Fig. 4) occurs during the Emsian–Eifelian interval. There is thus a contradiction between the literature and our new data. Indeed, the low occurrence of shallow-water remains within the Unit 1 might signify that the early Frasnian reefs of the Carnic Alps were in decline earlier than in most of the reef localities throughout the Middle–Upper Devonian world. This might be related to the active extensional tectonic regime (Ebner et al. 1980; Spalletta et al. 1980; Vai 1980; Spalletta and Vai 1984), which increased the subsidence rate leading progressive drowning of reef and in the Carnic Alps locality to important reworking of the platform.

Throughout the upper part of Unit 1, the thickness of beds and proportion in MF6 and MF5 decreases in favor of MF4 and MF2. The transition from Unit 1 to Unit 2 is marked by a strong deepening, which is characterized by the transition from an intermediate fore-reef slope intensely influenced by gravity-flow deposits to a hemipelagic/pelagic environment in the distal slope to off-reef areas, less influenced by gravity-flow processes. The microfacies curve corresponding to the Pal Limestone records mainly an aggrading trend in distal reef-slope to off-reef settings (MF1, MF2), characterized by pink to red thin-bedded limestone extending from the upper Frasnian into the lower Famennian. The occurrence of thin-turbiditic interbeds reflects a depositional setting still influenced by fore-reef slope reworking

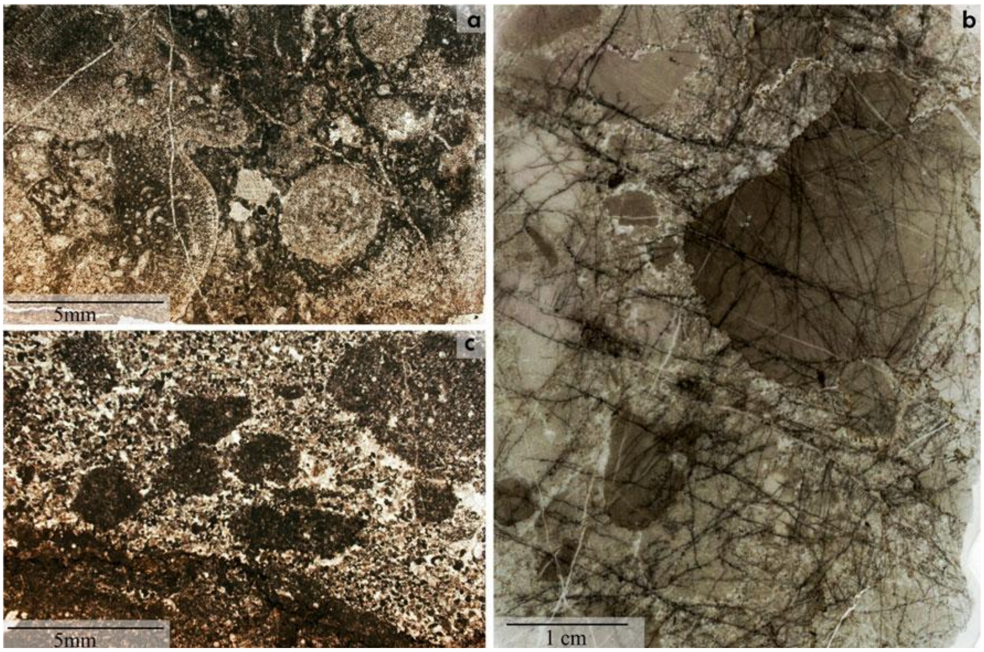

Fig. 9 Microfacies from the intermediate to distal reef-slope of the Freikofel section. Photomicrographs of thin section oriented perpendicular to the bedding. **a** MF6: flaotstone with stromatoporoids encrusted with *Renalcis* (FK 74c, transmitted light). **b** MF6 intermediate reef-slope deposits: lithoclastic rudstone showing several types of lithoclasts, which can be differentiated on the basis of color (FK93i, scanned thin section). **c** Transition between MF2 bioclastic wackestone-packstone and MF6 lithoclastic rudstone (lithoclasts are reworking of MF2) (FK66b, transmitted light)

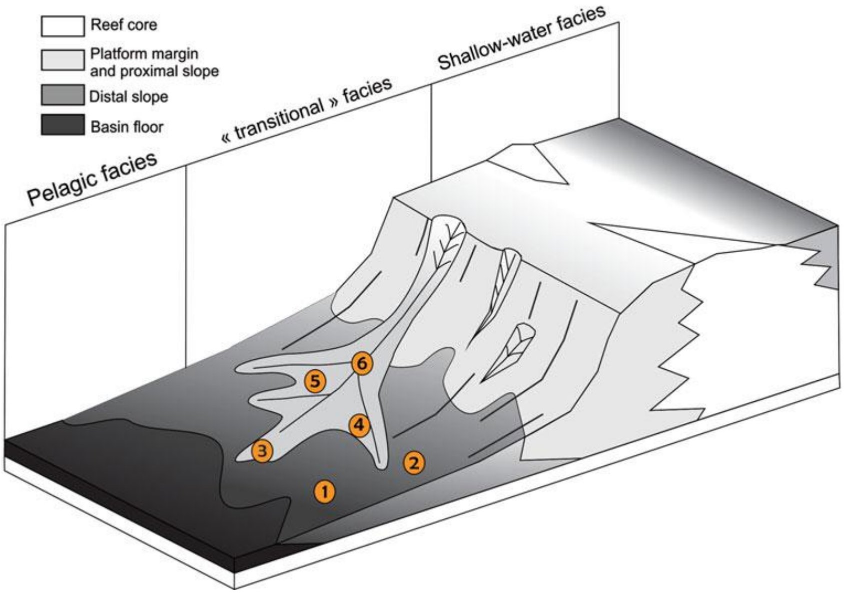

Fig. 10 Sedimentary model of the Freikofel section showing the distal slope sedimentary domain described herein. *Numbers* correspond to microfacies (see text for more information)

transported downslope by gravity currents. The predominance of the MF1 within the Unit 2 indicates both an increase in water depth and a strong decrease within the reef- and fore-reef-slope-related influxes toward the basin. This decrease in reef- and fore-reef might be related to the Late Frasnian sea-level rise (Johnson et al. 1985). In comparison with the thick breccia level of Unit 1, the thin-turbiditic layers of Unit 2 suggest a change from a steep erosional slope to either a backstepping margin or a just more depositional rather than erosional margin. The margin backstepping is easily supported by the long-term Frasnian eustatic sea-level rise recognized worldwide, causing the demise and drowning of the shallow-water carbonate platform in a global scale (Eder and Franke 1982; Johnson et al. 1985). Furthermore, in the Carnic Alps area, eustatic sea-level rise is likely enhanced by the tectonically active subsidence starting during the Late Givetian major extensional pulse (Ebner et al. 1980; Spalletta et al. 1980; Vai 1980). These global and local changes appear to be connected to the Kellwasser event interval at the end of the Frasnian, which is considered to be one of the major extinction events of the Phanerozoic (Sepkoski 1995; McGhee et al. 2013) and marks the end of the Devonian reef communities. The two positive δ^{13}C excursions commonly observed for the Kellwasser event interval were recognized in the Carnic Alps (Wolayer Glacier section) by Joachimski et al. (1994). Although black shale levels do not occur in the Freikofel section, a distinctive positive shift of about 3 promille in the δ^{13}C trend within the upper part of the *linguiformis* conodont Zone confirms the evidence of the Upper Kellwasser event. The significance of the Late Frasnian sea-level rise is also highlighted by the widespread deposition of red nodular limestone overlying the thick sequence of reef and fore-reef "transitional" facies of the Devonian Carnic Alps carbonate platform (Schönlaub and Histon 2000; Vai 1998).

Magnetic susceptibility and trace and major element geochemistry

The MS and geochemical curves prepared for the section studied are shown in Figs. 11 and 12. The MS values for the Middle and Upper Devonian Freikofel Limestone (Unit 1) and Pal Limestone (Unit 2) are very low, ranging from -0.18 to 2.7×10^{-8} m^3/kg with an average value of $7.73 \times 7 \times 10^{-9}$ m^3/kg. These MS values are much lower than the $MS_{\text{marine standard}}$ of 5.5×10^{-8} m^3/kg defined by Ellwood et al. (2011) on the basis of $\sim$11,000 marine rock samples. They are also lower than average MS values of time-equivalent fore-reef setting from the Rhenohercynian basin in Belgium (3.3×10^{-8} m^3/kg; Da Silva et al. 2009). The stratigraphic distribution of some selected elements commonly used as reliable tracers of the lithogenic input (Zr, Al, K, Si, and Ti) (Sliwinsky and Whalen 2010) was plotted against the MS curve (Fig. 11). The distribution of these elements follows the same large-scaled trend than MS. This relatively parallel evolution points to a MS signals linked to the amount of terrestrial input. Furthermore, there is a strong positive correlation ($r = 0.95$) between Al and Ti. According to Pratt et al. (1986), since Ti is not incorporated in the clay minerals fraction formed during diagenesis (e.g., illite), a good correlation between Ti and Al points to primary clay mineral assemblages was not transformed by diagenesis. MS

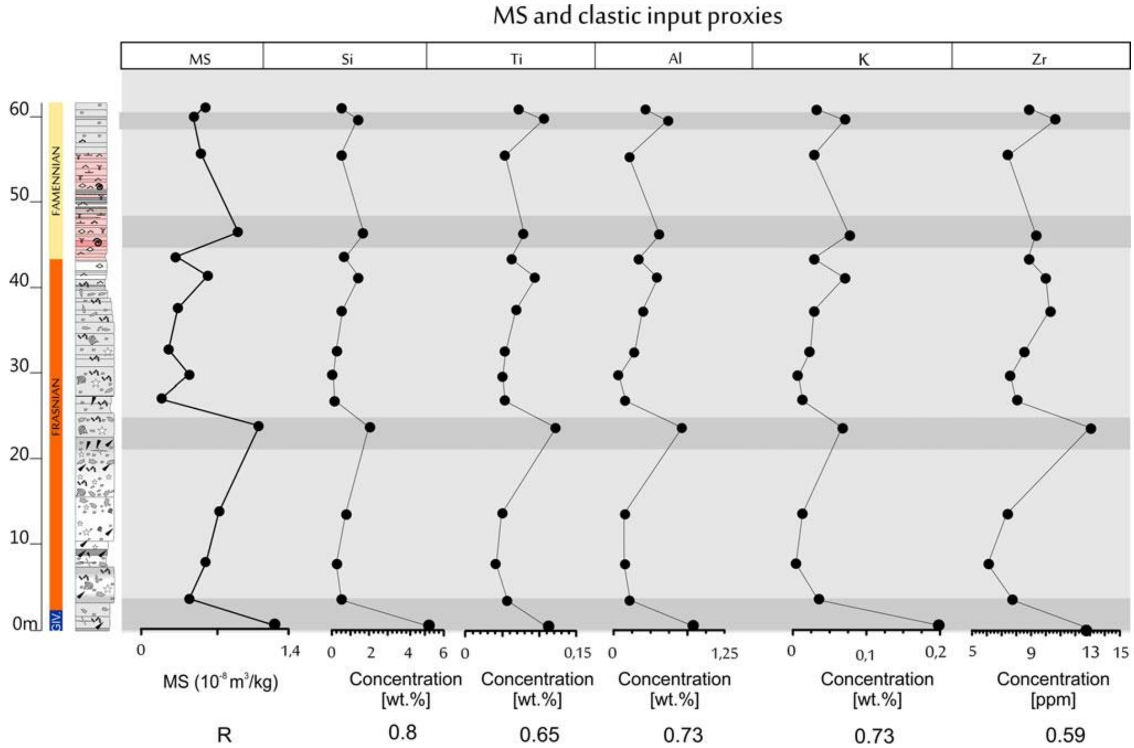

Fig. 11 Chemostratigraphic profiles of elements used as proxies for terrigenous clastic influxes into marine depositional basins. Plotted also is the corresponding magnetic susceptibility (MS) profile. Shaded areas are meant to help visualize common trends

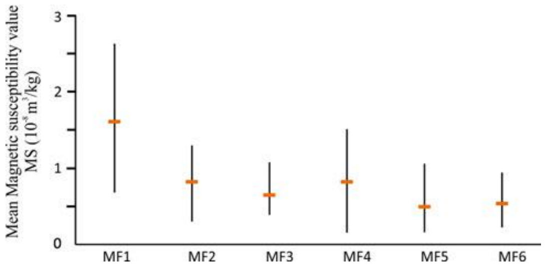

Fig. 12 Mean MS values on relative proximity transect illustrated by the position of microfacies from proximal to distal location

values attest thus of an average very low terrestrial influx seaward during the deposition of the Freikofel and Pal Limestones. The location of the "Proto Alps" basin around 30°S (Schönlaub 1992; see Fig. 1) during Middle and Late Devonian times was likely far from a continental or volcanic source area, which enabled the formation of an almost pure carbonate system. In the Rhenohercynian basin in Belgium, the vicinity with the Old Red Continent in the north might have triggered the higher values of MS recorded in the Givetian and Frasnian times.

At a large scale, the MS curve performed for the Freikofel section can be divided in four successive trends, respectively, called A, B, C, and D in Fig. 6. Trends A and B correspond to Unit 1 while trends C and D depict the evolution of Unit 2. Comparison between long-term trends in microfacies (MF I, II, III, and IV) and MS profiles mainly are in opposition. In order to get a better understanding of the parameters influencing long-scaled trends and the opposition between MS and microfacies (MF) profiles, we coupled MS, MF, and geochemical analyses. Average MS values for each microfacies (Fig. 12) display a general increase from proximal to distal setting excepted the slight decrease from MF4 to MF3 and MF5 to MF6. In the Freikofel area, the distality appears to be one of the most significant parameters influencing MS variations, but water turbulence and reworking also seem to play an important role. Usually, data related to carbonate platform (Da Silva and Boulvain 2006) support the notion that proximal microfacies possess a higher value of MS than distal ones because of vicinity with a terrestrial source. In our case, the average MS value shows just the opposite trends (increase in the average MS value with the distality). This situation has already been remarked for Belgian Eifelian fore-reef environment (Mabille and Boulvain 2007) as well as for Belgian and Canadian Frasnian mound and atoll (Da Silva et al. 2009), and this can be reasonably explained considering the location of the depositional setting compared to the continent. Indeed, if the sedimentary environment is far enough from terrestrial supplies, which is assumed for the Freikofel section, we can consider that the detrital inputs are homogenized and have the same influence on each microfacies. In such case, the carbonate productivity/sedimentary rate will play a more significant role in the MS variations. Low sedimentary rate (e.g., MF1, MF2, and MF4) will lead to condensed levels and thus to a concentration of magnetic minerals while higher sedimentary rate will decrease the concentration in MS carrying minerals by dilution. Water agitation is suggested mainly for MF6, MF5, and MF3, which are influenced by high turbulence of water preventing the settlement of MS carrying minerals. The higher mean MS value for MF6 compared to MF5 is thought to be related to the abundant occurrence of lithoclasts from MF2 and MF4 integrated within the MF6. In conclusion, MS variations in Freikofel can be explained using palaeoenvironmental parameters such as carbonate productivity/sedimentary rate and water agitation.

Conclusions

1. The Freikofel section provides an outstanding continuous succession of about 10 Ma in a fore-reef setting and delivers an important contribution to the understanding of the Carnic Alps platform/basin evolution during the Mid–Late Devonian. The stratigraphic framework of the entire section is well documented by conodont biostratigraphy.
2. Based on the detailed microfacies and field observations, the development of the Latest Givetian to Early Famennian fore-reef to distal slope facies of the Freikofel section can be reconstructed. Two major evolutionary phases are recognized such as (a) dismantlement of the Eifelian–Frasnian platform starting during the Early Frasnian with one of the causes being the Late Givetian major rift pulse recognized in the area. The dismantlement lasted till Late Frasnian; (b) stepwise withdrawal of the shallow-water influxes during the Late Frasnian and significant deepening of the Carnic Alps area during the Latest Frasnian and Early Famennian as a result of the Kellwasser event.
3. Though the Upper Kellwasser event layer does not show the specific lithological characteristics (e.g., shales), $\delta^{13}C$ values show a major positive excursion.
4. The detailed sedimentological study of the Freikofel section demonstrates the use of the "transitional" facies as reliable tool for temporal consideration where the occurrence of datable fossils is limited in shallow-water area.
5. The Freikofel and Pal Limestones show MS values (from -0.18 to 2.7 10^{-8} m^3/kg) much lower than (1) $MS_{marine\ \ standard}$ of 5.5×10^{-8} m^3/kg defined by Ellwood et al. (2011) on the basis of $\sim$11,000 marine rock samples and (2) time-equivalent fore-reef setting from the Rhenohercynian basin in Belgium (3.3×10^{-8} m^3/kg; Da Silva et al. 2009).
6. Parallelism between MS and proxy suites for terrestrial input suggests an inherent interdependence and changes in detrital input as the main driver of the oceanographic changes, which produced the observed geochemical variations. MS coupled with MF analyses demonstrates distality as the main palaeoenvironmental parameter leading to variation in the MS signal. In addition, two other MS controlling processes are also underlined such as (1) water agitation likely hampers MS carrying minerals to settle and (2) carbonate productivity that lowers the MS intensity by diluting the MS responsible minerals.

Acknowledgments This paper is a contribution to the UNESCO International Geoscience Program (IGCP) number 580; entitled "Application of magnetic susceptibility as a palaeoclimatic proxy on Paleozoic sedimentary rocks and characterization of the magnetic signal" and number 596 (Climate change and biodiversity patterns in the Mid-Paleozoic). This study was financially supported by the Grants IGCP 580 and NAP0017 (DP, ACDS), the FWF P 23775-B17 (TS and EK). This work was supported by a PhD fellowship awarded by the Research Foundation–Flanders (FWO) assigned to DDV. Philip Schnellbächer (Geognos Bertle, Austria) is thanked for providing his master thesis. The magmatic petrology laboratory of Liège University (N. Delmelle and J. Vander Auwera) is thanked for access and help on the geochemical measurement. For discussion on conodont biostratigraphy of the Freikofel area, we thank Maria Cristina Perri and Claudia Spalletta (University of Bologna, Italy). Finally, we gratefully acknowledge the two reviewers (Hans Peter Schönlaub and Claudia Spalletta) for their helpful and pertinent remarks that significantly improved the quality of this manuscript.

References

Bandel K (1969) Feinstratigraphische und biofazielle Untersuchungen unterdevonischer Kalke am Fuß der seewarte (Wolayer see: zentrale Karnische Alpen). Jb Geol B A 112:197–234

Bandel K (1972) Palökologie und Paläogeographie im Devon und Unterkarbon der zentralen Karnischen Alpen. Palaeontographica A 141(1–4):1–117

Bandel K (1974) Deep-water limestones from the Devonian-carboniferous of the Carnic Alps, Austria. Spec Publ Int Assoc Sediment 1:93–115

Bouma A (1962) Sedimentology of some flysch deposits. Elsevier, New York, p 168

Brime C, Perri MC, Pondrelli M, Spalletta C, Venturini C (2008) Polyphase metamorphism in the eastern Carnic Alps (N Italy–S Austria): clay minerals and conodont colour alteration index evidence. Int J Earth Sci 97:1213–1229

Copper P (2002) Silurian and Devonian reefs: 800 million years of global greenhouse between two ice ages. In: Kiessling W, Flügel

E, Golonka J (eds) Phanerozoic reef patterns. SEPM special publication, vol 72, pp 181–238

Corradini C, Corriga MG (2010) Silurian and lowermost Devonian conodonts from the Passo Volaia area (Carnic Alps, Italy). Boll Soc Paleontol Italy 49(3):237–253

Corradini C, Corriga MG (2012) A Pridoli-Lochkovian conodont zonation in Sardinia and the Carnic Alps: implications for a global zonation scheme. Bull Geos 87(4):635–650. doi:10.3140/bull.geosci.1304

Corradini C, Pondrelli M, Corriga MG, Simonetto L, Kido E, Suttner TJ, Spalletta C, Carta N (2012) Geology and stratigraphy of the Cason di Lanza area (Mount Zermula, Carnic Alps, Italy). Berichte des Institutes für Erdwissenschaften, Karl-Franzens-Universität Graz 17:83–103

Corriga MG, Corradini C (2009) Upper silurian and lower Devonian conodonts from the Monte Cocco II section (Carnic Alps, Italy). Bull Geosci 84(1):155–168. doi:10.3140bull.geosci.1112

Da Silva AC, Boulvain F (2006) Upper Devonian carbonate platform correlations and sea level variations recorded in magnetic susceptibility. Palaeogeog Palaeoclimatol Palaeoecol 240:373–388

Da Silva AC, Mabille C, Boulvain F (2009) Influence of sedimentary setting on the use of magnetic susceptibility: examples from the Devonian of Belgium. Sedimentology 56(5):1292–1306

Dickson J (1965) A modified staining technique for carbonates in thin section. Nature 205:587

Dunham RJ (1962) Classification of carbonate rocks according to depositional texture. Mem Am Assoc Petrol Geol 1:108–121

Ebner F, Fenninger A, Holzer HL (1980) Die Rannach-Fazies des Grazer Paläozoikums. Mitt Abt Geol Paläontol Bergb Landesmus Joanneum 41:249–269

Eder W, Franke W (1982) Death of Devonian reefs. N Jb Geol Palaönt Abh 163:241–243

Ellwood BB, Tomkin JH, El Hassani A, Bultynck P, Brett CE, Schindler E, Feist R, Bartholomew AJ (2011) A climate-driven model and development of a floating point time scale for the entire middle Devonian givetian stage: a test using magnetostratigraphy susceptibility as a climate proxy. Palaeogeog Palaeoclimatol Palaeoecol 304(1–2):85–95

Embry AF, Klovan JE (1972) Absolute water depth limits of Late Devonian paleoecological zones. Geol Rundsch 61(2):672–686

Flügel E (2004) Microfacies analysis of carbonate rocks. Analysis, interpretation and application. Springer, Berlin

Galli G (1985) Depositional environments in the devonian limestone succession of the Cima Ombladet (Camic Alps, Italy). Facies 12(1):97–111

Hubmann B, Suttner T (2007) Siluro-Devonian Alpine reefs and pavements. Geol Soc Lond Spec Pub 275(1):95–107

Hubmann B, Ebner F, Ferretti A, Histon K, Kido E, Krainer K, Neubauer F, Schönlaub HP, Suttner TJ (2013) The Paleozoic Era (them). In: Piller WE (ed) The lithostratigraphic units of the Austrian stratigraphic chart 2004 (sedimentary successions). Abh Geol B A 66(1):9–133

Hüneke H (2006) Erosion and deposition from bottom currents during the Givetian and Frasnian: response to intensified oceanic circulation between Gondwana and Laurussia. Palaeogeog Palaeoclimatol Palaeoecol 234:146–167

Hüneke H (2007) Pelagic carbonate ooze reworked by bottom currents during Devonian approach of the continents Gondwana and Laurussia. Geol Soc Lond Spec Pub 276:299–328

Joachimski MM, Buggisch W, Anders T (1994) Mikrofazies, Conodontenstratigraphie und Isotopengeochemie des Frasne-Famenne-Grenzprofils Wolayer Gletscher (Karnische Alpen). Abh Geol B A 50:183–195

Johnson JG, Klapper G, Sandberg CA (1985) Devonian eustatic fluctuations in Euramerica. Geol Soc Am Bull 96:567–587

Königshof P, Savage NM, Lutat P, Sardsud A, Dopieralska J, Belka Z, Racki G (2012) Late Devonian sedimentary record of the Paleotethys Ocean—The Mae Sariang section, northwestern Thailand. J Asian Earth Sci 52:146–157

Kreutzer LH (1989) Reef-basin distance in the Devonian of the Carnic Alps. Ann Soc Geol Belg 112:159–163

Kreutzer LH (1990) Mikrofazies, stratigraphie und Paläogeographie des Zentralkarnischen Hauptkammes zwischen Seewarte und Cellon. Jb Geol B A 133(2):275–343

Kreutzer LH (1992a) Photo-Atlas of the variscan carbonate sequences in the Carnic Alps (Austria/Italy). Abh Geol B A 47:1–129

Kreutzer LH (1992b) Palinspastische Entzerrung und Neugliederung des Devons in den Zentralkarnischen Alpen aufgrund von neuen Untersuchungen. Jahrb Geol Bundesanstalt 135(1):261–272

Läufer AL, Hubich DH, Loeschke JL (2001) Variscan geodynamic evolution of the Carnic Alps (Austria/Italy). Int J Earth Sci 90(4):855–870

Lischka M (2007) Hangschuttsedimente einer devonischen Karbonatplattform—Mikrofazies und Provenienz des Detritus (Freikofel, Karnische Alpen). Universität Greifswald. Greifswald [unpublished BSc thesis], pp 1–54

Mabille C, Boulvain F (2007) Sedimentology and magnetic susceptibility of the Couvin Formation (Eifelian, South Western Belgium): carbonate platform initiation in a hostile world. Geol Belg 10(1–2):47–67

Mamet B, Naisse F, Perez S, Préat A (1985) Frondilina tailferensis, n. sp. Un foraminifère nouveau du Frasnien de la Belgique. Bull Soc Belg Geol 94(4):269–271

May A (1994) Microfacies controls on weathering of carbonate building stones: Devonian (northern Sauerland, Germany). Facies 30(1):193–208

McGhee GR, Clapham ME, Sheehan PM, Bottjer DJ, Droser ML (2013) A new ecological-severity ranking of major phanerozoic biodiversity crises. Palaeogeog Palaeoclimatol Palaeoecol 370:260–270

Meischner KD (1964) Allodapische Kalke. Turbidite in riff-nahen Sedimentations-Becken. Developm Sediment 3:156–191

Mutti E (1977) Distinctive thin-bedded turbidite facies and related depositional environments in the Eocene Hecho Group (South-central Pyrenees, Spain). Sedimentology 24(1):107–131

Oeckentorp-Küster P, Oeckentorp C (1992) Rugose Korallenfaunen des Mittel und Ober-Devons der zentralen Karnischen Alpen. Jb Geol B A 135(1):233–260

Pas D, Da Silva AC, Cornet P, Bultynck P, Königshof P, Boulvain F (2013) Sedimentary development of a continuous middle Devonian to mississippian section from the fore-reef fringe of the Brilon reef complex (Rheinisches Schiefergebirge, Germany). Facies 59(4):969–990. doi:10.1007/s10347-012-0351-z

Perri MC, Spalletta C (1998) Updating of the conodont biostratigraphy in the Carnic Alps (Italy). In: Perri M, Spalletta C (eds) Southern Alps field trip guidebook. ECOS VII. Giorn Geol 60 (spec issue), pp 116–119

Pettijohn FJ, Potter PE, Siever R (1972) Sand and sandstone. Springer, Berlin

Piller WE, Egger H, Erhart CW, Gross M, Harzhauser M, Hubmann B, van Husen D, Krenmayr H-G, Krystyn L, Lein R, Lukeneder A, Mandl GW, Rögl F, Roetzel R, Rupp C, Schnabel W, Schönlaub HP, Summesberger H, Wagreich M, Wesseley G (2004) Die stratigraphische Tabelle von Östereich 2004 (sedimentäre Folgen). Kommission für die paläontologische und stratigraphische Erforschung Österreichs, Österreichische Akademie der Wissenschaften und Österreichische Stratigraphische Kommission, Wien

Piper DJW (1978) Turbidite muds and silts on deepsea fans and abyssal plains. In: Stanley DJ, Kelling G (eds) Sedimentation and submarine canyons, fans, and trenches. Dowden, Hutchinson and Ross, Stroudsburg, pp 163–176

Playford PE (1980) Devonian “Great Barrier Reef” of Canning Basin, Western Australia. Am Assoc Petrol Geol Bull 64:814–840
Pohler S (1982) Die Entwicklung der Flachwasserkarbonate im Mittel- und Oberdevon der Zentralen Karnischen Alpen (Seewartesockel zum S-Abfall der Hohen Warte). Rhenish Friedrich-Wilhelm University Bonn [unpublished diploma thesis], p 134
Pölsler P (1969a) Stratigraphie und Tektonik im Nordabfall des Findenigkofels (Silur bis Karbon; Karnische Alpen, Österreich). Jb Geol B A 112:355–398
Pölsler P (1969b) Conodonten aus dem Devon der Karnischen Alpen (Findenigkofel, Österreich). Jb Geol B A 112(2):399–440
Pratt LM, Claypool GE, King JD (1986) Geochemical imprint of depositional conditions on organic matter in laminated—Bioturbated interbeds from fine-grained marine sequences. Mar Geol 70(1–2):67–84
Rabien A (1956) Zur Stratigraphie und Fazies des Ober-Devons in der Waldecker Hauptmulde, Abh Hess L. Amt Bodenforsch 16:1–83
Schnellbächer P (2007) Hangschuttsedimente einer devonischen Karbonatplattform (Freikofel, Karnische Alpen)—Sedimentfazies und transportmechanismen. Universität Greifswald. Greifswald [unpubl BSc thesis], pp 1–61
Schnellbächer P (2010a) Kartierung des Freikofel in den Karnischen Alpen. Bericht zur Masterkartierung, Universität Greifswald. Greifswald [unpubl mapping report], pp 1–41
Schnellbächer P (2010b) Stratigraphy, transport mechanisms and provenience of Devonian carbonate slope deposits (Freikofel, Carnic Alps). Universität Greifswald. Greifswald. [unpubl. master thesis], pp 1–124
Schönlaub HP (1971) Die fazielle Entwicklung im Altpaläozoikum und Unterkarbon der Karnischen Alpen. Zeitschrift der Deutschen Geologischen Gesellschaft 122:97–111
Schönlaub HP (1979) Das Paläozoikum in Österreich. Abh Geol B A 33:1–124
Schönlaub HP (1980) Carnic Alps. Field trip A. With contributions from Jaeger H, House MR, Price JD, Göddertz B, Priewalder H, Walliser OH, Kříž J, Haas W, Vai GB. In: Schönlaub HP (ed) Second European conodont symposium, ECOS II, guidebook, abstracts. Abh Geol B A 35:5–57
Schönlaub HP (1985) Das Paläozoikum der Karnischen Alpen. In: Daurer A, Schönlaub HP (eds) Arbeitstagung der Geologischen Bundesanstalt 1985 in Kötschach-Mauthen. Geol Bundesanstalt, Wien, p 87
Schönlaub HP (1991) Vom Urknall zum Gailtal—500 Millionen Jahre Erdgeschichte in der Karnischen Region. Geol Bundesanstalt, Wien, p 169
Schönlaub HP (1992) Stratigraphy, biogeography and paleoclimatology of the Alpine Paleozoic and its implications for plate movements. Jb Geol B A 135(1):381–418
Schönlaub HP, Histon K (2000) The Palaeozoic evolution of the southern Alps. Mitt Österr Geol Ges 92:15–34
Schönlaub HP, Histon K, Pohler S (2004) The palaeozoic of the Carnic Alps. In: Schönlaub, HP (ed) Field trip Carnic Alps guidebook, 23–24 June 2004, Carinthia Austria. Geol Bundesanstalt 40, pp 2–32
Scotese C (2002) The Paleomap Project. http://www.scotese.com/
Sepkoski JJ Jr (1995) Patterns of Phanerozoic extinctions: a perspective from global data bases. In: Walliser OH (ed) Global events and event stratigraphy. Springer, Berlin, pp 35–51
Sliwinsky G, Whalen MT (2010) Trace element variations in the middle Frasnian *punctata* zone (Late Devonian) in the western Canada sedimentary basin—changes in ocean bioproductivity and paleoredox spurred by a pulse of terrestrial afforestation? Geol Belg 13(4):459–482
Spalletta C, Perri MC (1998) Stop 2.1B—Givetian and Frasnian conodonts from the Pramosio 327 section (Carnic Alps, Italy). In: Perri MC, Spalletta C (eds) Southern Apls field trip guidebook. Seventh international conodont symposium held in Europe. Giorn di Geol s3 60 (spec issue), pp 190–197
Spalletta C, Vai GB (1984) Upper Devonian intraclast parabreccias interpreted as seismites. Mar Geol 55:133–144
Spalletta C, Vai GB, Venturini C (1980) Il Flysch ercinico nella geologia dei Monti Paularo e Dimon (Alpi Carniche). Mem Soc Geol It 20:243–265
Spalletta C, Perri MC, Vai GB (1983) Pattern of conodont reworking in the Upper Devonian of the Alps: palaeoenvironmental and palaeotectonic implications. Lethaia 16(1):51–66
Suttner TJ (2007) Conodont stratigraphy, facies-related distribution patterns and stable isotopes (carbon and oxygen) of the uppermost Silurian to Lower Devonian Seewarte Section (Carnic Alps, Carinthia, Austria). Abh Geol B A 59:1–111
Stark A (2007) Hangschuttsedimente einer devonischen Karbonatplattform—Conodonten-stratigraphie (Freikofel, Karnische Alpen)—Universität Greifswald. Greifswald [unpublished BSc thesis], pp 1–70
Stow DAV, Shanmugam G (1980) Sequence of structures in fine-grained turbidites: comparison of recent deep-sea and ancient flysch sediments. Sediment Geol 25(1–2):23–42
Tucker ME (1973) Sedimentology and diagenesis of Devonian pelagic limestones (Cephalopodenkalk) and associated sediments of the Rhenohercynian Geosyncline, West Germany. N Jb Geol Paläont Abh 142:320–350
Vai GB (1975) Hercynian basin evolution of the Southern Alps. Geology of Italy, ESSLA R II:293–298
Vai GB (1976) Stratigrafia e paleogeografia ercinica delle Alpi. Mem Soc Geol Italy 13:7–37
Vai GB (1980) Sedimentary environment of Devonian pelagic limestones in the Southern Alps. Lethaia 13(1):79–91
Vai GB (1998) Field trip through the Southern Alps: an introduction with geological settings, palaeogeography and Palaeozoic stratigraphy. In: Perri MC, Spalletta C (eds) Southern Alps field trip guidebook. Seventh international conodont symposium held in Europe. Giorn di Geol s3 60(3)(spec issue), pp 1–38
Venturini C (1990) Geologia delle Alpi Carniche centro-orientali. Comune di Udine 36:1–220
Venturini C, Spalletta C, Vai GB, Pondrelli M, Delzotto S, Fontana C, Longo Salvador G, Carulli GB (2009) Note illustrative del foglio 031 Ampezzo, Carta geologica d'Italia alla scala 1:50000; ISPRA (ex-APAT, Servizio Geologico d'Italia), pp 7–232
von Gaertner HR (1931) Geologie der Zentralkarnischen Alpen. Denkschrift der Österreichischen Akademie der Wissenschaften, mathematisch-naturwissenschaftliche Klasse, Abteilung 102: 113–199
Walliser OH (1964) Conodonten des Silurs. Abh Hess L Amt Bodenforsch 41:1–106
Wendt J, Aigner T (1985) Facies patterns and depositional environments of Palaeozoic cephalopod limestones. Sediment Geol 44(3–4):263–300

Strong help for field work in Fromelennes-Flohimont section, France

Chapter 4

Dinant Syncline sections (Ardennes; Belgium and France)

First part

Sedimentary development and magnetic susceptibility correlations of the Givetian in the La Thure and Fromelennes-Flohimont sections

1 Introduction

The Belgian Givetian sedimentary sequence of the Ardennes area represents one of the thickest and best-known Palaeozoic reef-related deposits of Europe. The relatively large quarries within Givetian rocks and the numerous valleys crossing the Ardennes area offer easy access to a number of outstanding outcrops, allowing detailed sedimentological, biostratigraphical and taxonomic research (Lecompte, 1951; Lecompte, 1952; Errera et al., 1972; Bultynck, 1974; Préat and Boulvain, 1982; Préat et al., 1984; Boulvain and Préat, 1986; Coen-Aubert et al., 1986; Bultynck, 1987; Préat et al., 1987; Bultynck et al., 1991; Casier and Préat, 1991; Coen-Aubert, 1992; Préat and Kasimi, 1995; Coen-Aubert, 2000; Bultynck and Dejonghe, 2001; Coen-Aubert, 2002; Gouwy and Bultynck, 2003; Poulain, 2006; Boulvain et al., 2009; Casier and Préat, 2013; Maillet et al., 2013). The Belgian Givetian carbonate platform shows important north-south and east-west facies variations (Bultynck and Dejonghe, 2001; Boulvain et al., 2009). As a result of the remarkable outcropping conditions, the south and north-eastern portion of the Dinant Syncline (DS) have been the focus of most of the investigations cited above whereas its north-western area has suffered a lack of interest. Consequently, the reconstruction of lateral and vertical facies belts development within this platform has remained incomplete and hampers further palaeogeographic and palaeoenvironmental implications.

Over the last decade, magnetic susceptibility (MS) has been used extensively as a palaeoenvironmental, palaeoclimatic proxy and as a correlation tool (Bábek et al., 2010; Boulvain et al., 2010; Michel et al., 2010; Whalen and Day, 2010; Da Silva and Boulvain, 2012) and an extended database of MS measurements is available for numerous Devonian sections in Belgium (Da Silva et al., 2013; Pas et al., 2014a) and worldwide (Hladil et al., 2006; Whalen and Day, 2008; Koptíková et al., 2010; Koptíková, 2011; Pas et al., 2014b). Moreover, a recent IGCP project (IGCP-580, UNESCO funding) has focused on the application of MS as a palaeoclimatic proxy, specifically on the Devonian. This has allowed a better understanding of the use of MS techniques as a tool for high-resolution correlation and palaeoenvironmental reconstructions (e.g., IGCP 580 project; Da Silva et al., 2014). However, MS measurements need to be combined with the outcomes of other techniques such as geochemical data (Riquier et al., 2010; Da Silva et al., 2013), magnetic properties analyses (Devleeschouwer et al., 2010; Da Silva et al., 2012), sedimentology (Mabille et al., 2008b; Da Silva et al., 2009a), biostratigraphy, etc. to provide robust insight on the applicability of this proxy as a correlation-tool or as a palaeoclimatological indicator. Indeed, it is essential to decipher whether the recorded MS signal represents primary depositional-induced imprint (e.g., change in detrital supply basinward, leading to a link between MS and independent geochemical proxies related to detrital inputs such as Zr, Al, Rb, etc.) or post-depositional secondary signature (e.g., diagenesis and metamorphism).

This Chapter focuses on two sections from the Dinant Syncline: The La Thure section from the north-western margin of the DS and the Fromelennes-Flohimont section located in the southern margin.

Both sections are worthy of interest for the following reasons: 1) they provides a relatively continuous records of a several million-year-long stratigraphic interval, 2) they are deposited in the same basin but in a different position along the platform deepening and 3) they were separated by nearly 75 km during the time of deposition. Furthermore, the La Thure section is an outstanding outcrop in an area where outcrops are rare it has not been subject to sedimentological study.

This Chapter proposes detailed sedimentological analyses and illustrates the fascinating facies diversity that shaped the Early-Late Givetian platform in the north-western and southern margins of the DS. A thorough comparison between the two sections was done in combination with literature in order to improve the knowledge on the main facies belts distribution and their evolution over million year-scales within the Dinant Basin. Moreover, we have setup a large set of MS and geochemical data in order to clearly constraint the link between MS and siliciclastic input proxies for each section, and to build a robust high-resolution MS reference profile for the shallow-water of the Early- to Late-Givetian platform in Belgium.

The MS million-year trends that are recorded in these two profiles will allow us to further test the applicability of MS as a correlation tool within the Rhenohercynian Basin, but also with other basins. The geochemical dataset is also used to gain a better understanding of the palaeoredox and facies change history within the Dinant Basin. Moreover, this large set of data (including MS and geochemistry) will serve to increase knowledge of the applicability and limitation of MS as a tool for palaeoenvironmental reconstruction.

2. Geological context

During the Middle Devonian, Belgium was situated around 20°S (Torsvik et al., 2012) along Laurussia's south-eastern margin (Fig.1a). During the Givetian, this area was part of a wide carbonate platform along the northern passive margin of the Rhenohercynian Ocean. In terms of modern gography, the Givetian carbonate platform extends from the Avesnois Basin (northern France) to Aachen (western Germany) in the east. In addition, isolated carbonate complexes grew in the east and the southwest, i.e. the Rhenish Massif (Rheinisches Schiefergebirge e.g., Brilon Reef Complex; Pas et al., 2013) and Torbay Reef Complex of SW England respectively (Torbay Reef Complex; Garland et al., 1996). In Belgium, Givetian sediments crop out all along the border of the Dinant and Vesdre Synclines, in the Philippeville Anticline and along the southern border of the Brabant Massif, within the Brabant Para-Autochthonous area and the Haine-Sambre-Meuse Overturned Thrust sheets (for precise location see Belanger et al., 2012; fig. 5), which are all large-scaled units of the Rhenohercynian fold-and-thrust belt (Fig. 1b). This extensive tectonic structure was formed during the Carboniferous to Permian as a consequence of the collision between the Laurussia and Gondwana super continents during the Variscan orogeny. Several authors (e.g., Molina Garza and Zijderveld, 1996; Zwing et al., 2005; Da Silva et al., 2012) highlighted that during this orogeny, the rocks belonging to the Rhenohercynian fold-and-thrust belt were affected by remagnetization.

The La Thure section is located in south-western Belgium (50°17'11"N, 4°09'40"E) and belongs to the north-western border of the Dinant Syncline (DS; Fig. 1b). The section covers sediments ranging from the Givetian to the Frasnian. Recently, the Frasnian part of the La Thure section has been the topic of a multi-disciplinary study (sedimentology, geochemistry and magnetic susceptibility) published by Pas et al. (2014a). The Fromelennes-Flohimont section is located in northern France (50°07'04", N 4°51'26"E) and belongs to the southern border of the Dinant Syncline (DS, Fig. 1b). The section records sediments ranging from Early Givetian to Early Frasnian. Considering the tectonic shortening of pre-Mesozoic sequences of 33% (Burchette, 1981) and the present day distance of 50 km separating the La Thure quarry from the Fromelennes-Flohimont road sections, a distance of 75 km must have separated these two sites at time of deposition.

The Givetian lithostratigraphic units, according to the Belgian Givetian lithostratigraphic chart defined in Bultynck and Dejonghe (2001) were established for the southern border of the Dinant Syncline. They are associated with conodont zones (Bultynck, 1974; Bultynck, 1987; Gouwy and Bultynck, 2003) and to the main transgression – regression cycles (Johnson et al., 1985) (Fig. 1c). Five formations (Fm) lying in the Givetian are outcropping in the southern border of DS. From base to top those formations are respectively (Fig. 1c-d): (1) upper part of Hanonet; (2) Trois-Fontaines; (3) Terres d'Haurs; (4) Mont d'Haurs and (5) Fromelennes formations. Lateral equivalents of these five formations in the northern border of the DS are the Nèvremont and Le Roux formations (Fig. 1d). In the La Thure section, the upper part of the Terre d'Haurs Fm, the Mont d'Haurs and Fromelennes formations are observed (see also local geological map of Hennebert, 2008), and their lithologies remain relatively similar compared to DS southern border. However, The Mont d'Haurs and Fromelennes formations show reduced thickness respectively of ~50% and ~25% in comparison with the formations as defined in the type area. Considering the similar lithologies, we assume that the Givetian conodont biostratigraphy developed in the southern border of the Dinant Syncline (Bultynck, 1974; Bultynck, 1987; Gouwy and Bultynck, 2003) can convey an idea of the conodont zones extension. According to this, the La Thure section likely covers an interval extending from the lower Givetian *Polygnathus varcus* Zone to the middle Frasnian *Palmatolepis hassi* s.l. Zone while the interval covered in the Fromelennes-Flohimont section extends from the lower Givetian *Polygnathus hemiansatus* Zone to the early Frasnian *Palmatolepis falsiovalis* Zone. Based on Givetian sections from the Avesnes (northern France), Dinant and Namur Basins, which belong to the Dinant Syncline, Haine-Sambre-Meuse Overturned Thrust sheets and Brabant Para-Autochthonous, Préat and Mamet (1989) defined thirteen microfacies covering a large range of environments extending from open-marine, under wave action zone, to reefal complexes, lagoons and evaporitic sabkhas including laminites and palaeosoils.

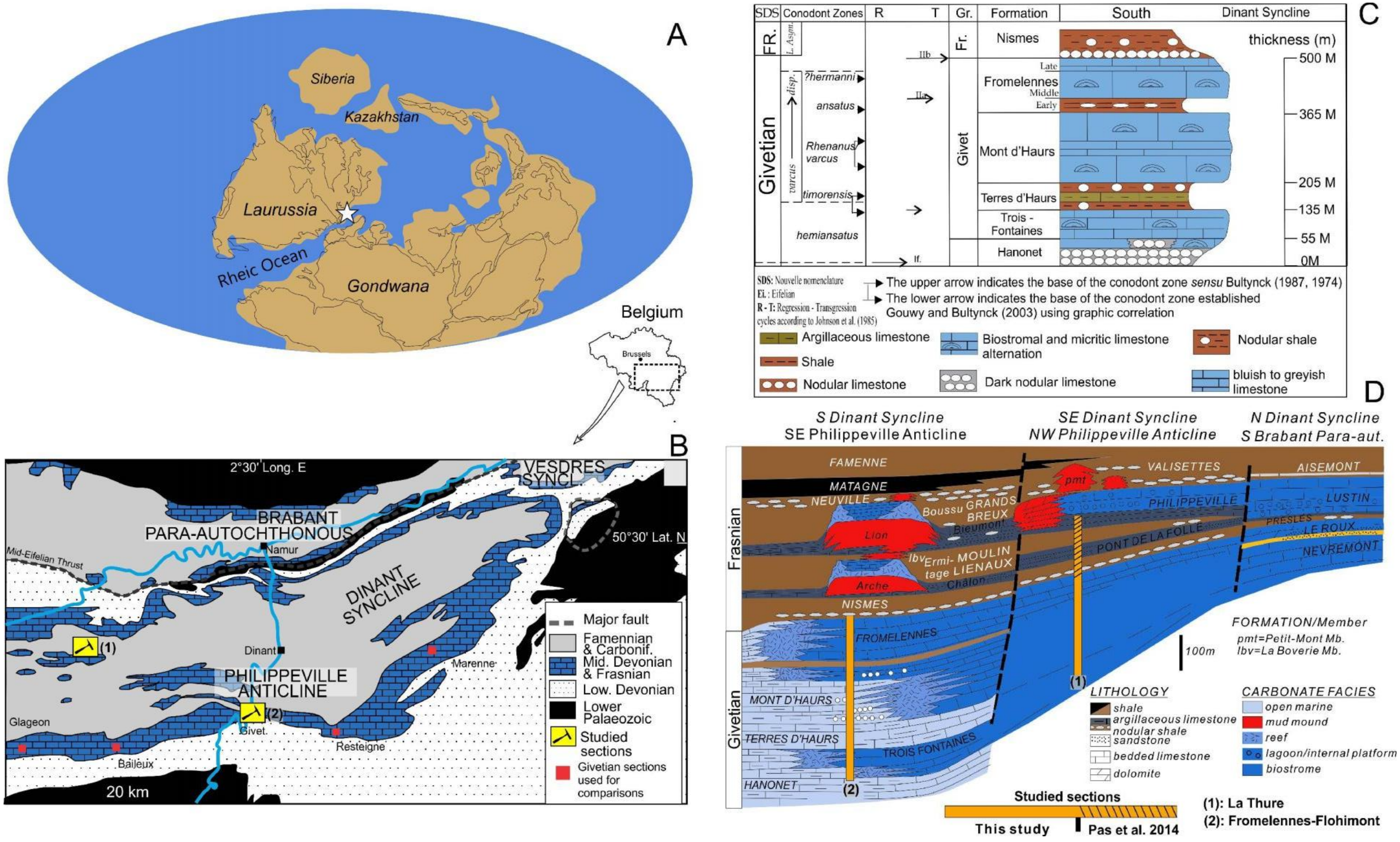
A
Siberia
Kazakhstan
Laurussia
Rheic Ocean
Gondwana
Belgium
Brussels
B
2°30' Long. E
VESDRES SYNCL.
BRABANT PARA-AUTOCHTHONOUS
Namur
Mid-Eifelian Thrust
50°30' Lat. N
DINANT SYNCLINE
Dinant
(1)
PHILIPPEVILLE ANTICLINE
(2)
Givet
Glageon
Baileux
Resteigne
Marenne
20 km
Major fault
Famennian & Carbonif.
Mid. Devonian & Frasnian
Low. Devonian
Lower Palaeozoic
Studied sections
Givetian sections used for comparisons
C
SDS
Conodont Zones
R
T
Gr.
Formation
South
Dinant Syncline
FR.
L. Asym.
Givetian
varcus
disp.
?hermanni
ansatus
Rhenanus/varcus
timorensis
hemiansatus
IIb
IIa
If.
Fr.
Givet
Nismes
Fromelennes
Late
Middle
Early
Mont d'Haurs
Terres d'Haurs
Trois - Fontaines
Hanonet
thickness (m)
500 M
365 M
205 M
135 M
55 M
0M
SDS: Nouvelle nomenclature
Ei.: Eifelian
R - T: Regression - Transgression cycles according to Johnson et al. (1985)
The upper arrow indicates the base of the conodont zone sensu Bultynck (1987, 1974)
The lower arrow indicates the base of the conodont zone established Gouwy and Bultynck (2003) using graphic correlation
Argillaceous limestone
Shale
Nodular limestone
Biostromal and micritic limestone alternation
Dark nodular limestone
Nodular shale
bluish to greyish limestone
D
S Dinant Syncline
SE Philippeville Anticline
SE Dinant Syncline
NW Philippeville Anticline
N Dinant Syncline
S Brabant Para-aut.
Frasnian
Givetian
FAMENNE
MATAGNE
NEUVILLE
Boussu
GRANDS BREUX
Bieumont
Lion
Ibv
Ermi-tage
MOULIN LIENAUX
Châlon
Arche
NISMES
pmt
VALISETTES
PHILIPPEVILLE
PONT DE LA FOLLE
AISEMONT
LUSTIN
PRESLES
LE ROUX
NEVREMONT
FROMELENNES
MONT D'HAURS
TERRES D'HAURS
TROIS FONTAINES
HANONET
(1)
(2)
100m
FORMATION/Member
pmt=Petit-Mont Mb.
lbv=La Boverie Mb.
LITHOLOGY
shale
argillaceous limestone
nodular shale
sandstone
bedded limestone
dolomite
CARBONATE FACIES
open marine
mud mound
reef
lagoon/internal platform
biostrome
Studied sections
This study
Pas et al. 2014
(1): La Thure
(2): Fromelennes-Flohimont

Fig. 1 **a** *Location of Belgium in the eastern margin of Laurussia during Devonian (simplified from Kiessling et al. (2003).* **b** *Simplified geological map of southern Belgium with location of the La Thure (NW of the Dinant Syncline, 1) and Fromelennes-Flohimont (South of the Dinant Syncline, 2) sections. For the location of the Haine-Sambre-Meuse Overturned Thrust sheets refer to the map of Belanger et al. (2012)* **c** *Givetian lithostratigraphic column established for the southern border of the Dinant Syncline showing conodont zones (Bultynck, 1974; Bultynck, 1987; Gouwy and Bultynck, 2003) and the main transgression – regression cycles (Johnson et al., 1985).* **d** *Integrated lithostratigraphical and palaeogeographical framework for the Givetian and Frasnian of Belgium. Relative position of the reefs shows the retrogradation-progradation patterns of the carbonate platforms (modified after Boulvain et al., 2009).*

According to these authors, the Belgian Givetian carbonate platform was composed of several km-sized faulted blocks. Furthermore, as summarized by Boulvain et al. (2009), the Givetian deposits in Belgium can be divided into three ENE-WSW directed facies belts (Fig.1d): one the most distal part of the platform ("southern belt") located along the southern margin of the Dinant Syncline is characterized by ramp and off-reef to internal platform deposits; two the "central belt" outcropping in the Philippeville Anticlinorium and SE of the Dinant Syncline (DS) which is poorly known and three a "northern belt", in the north of the DS and in the south of the Brabant Para-Autochthonous, characterized mainly by shallowest and alluvial deposits. Shallowest to deepest depositional environment of the Givetian platform are consistent with the general northerly transgressive sea-level evolution, which progressively submerged the Old Red Continent from Emsian to Late Frasnian (Préat and Bultynck, 2006).

3. Methodology

A detailed bed by bed description and sampling of the La Thure (153 m-thick; Fig. 3) and Fromelennes-Flohimont sections (461 m-thick; Fig. 4) was performed with a sampling interval of 25 to 45 cm, depending on outcrop condition. Magnetic susceptibility measurements were undertaken on all the collected samples (~400 samples for the La Thure section and ~800 samples for the Fromelennes-Flohimont section). Each sample was measured three times with KLY-3 (Kappabridge from AGICO) and weighted with a precision of 0.01g. This allows the definition of the low-field mass-calibrated magnetic susceptibility for each sample and the establishment of the magnetic susceptibility curves (Fig 14 and 15). Concerning microfacies analysis, around 200 thin-sections were studied for the La Thure section and around 550 thin-sections for the Fromelennes-Flohimont section. Thin-sections are stored at the sedimentary petrology laboratory of the University of Liège (TUR 100 - TUR 311 and FRO-18 – FRO400). The textural classification used to characterise the microfacies follows Dunham (1962) and Embry and Klovan (1972). Estimation of sorting is based on the visual chart of Pettijohn et al. (1972) and visual percentage estimation is based on Baccelle and Bosellini (1965). Several, thin-sections were stained using Dickson solution to distinguish from calcite, dolomite, ferroan calcite and ferroan dolomite (Dickson, 1965). For the La Thure section, a group of 30 samples (~1 sample per 5 m) were analysed for major and trace element concentration at Activation Laboratories Ltd (Ancaster, Ontario, Canada). Analyses were performed by ICP-MS (major, minor and trace elements). The samples were prepared by fusion with sodium peroxide Na_2O_2, which totally solubilizes all the minerals analysed in an aqueous solution after treatment. For the Fromelennes-Flohimont section, a group of 43 samples (~1 sample per 5 m) were analysed for major and trace element concentrations using X-ray Fluorescence (ARL 9400 XP XRF instrument) at the University of Liège. All rock samples were carefully cleaned prior treatment. The major elements (SiO_2, TiO_2, K_2O, and Al_2O_3) were analysed on lithium tetra and meta-borate-fused glass discs, with matrix corrections following the Traill-Lachance algorithm and are expressed in elemental oxide concentration. Trace elements (in this chapter, Zr, Th) were measured on pressed powder pellets, and data were corrected for matrix effects in elemental concentration. Precision and accuracy were both shown to be better than 1% for major elements and 5% for trace elements as proved by international standards and analyses of replicate samples, respectively.

4. Results

4.1 Description of the section

La Thure section (Fig. 2)

The measured section is ~153 meters thick with strata oriented N90°E and a dip of 70°S. It can be divided into five lithological units (LTU1-LTU5). According to the Belgian Givetian lithostratigraphic charts defined by Préat and Bultynck (2006) and data from the geological map of Hennebert (2008), the Terres d'Haurs (THR), Mont d'Haurs (MHR) and Fromelennes (FRO) formations (Fm) can be identified. In the La Thure section, only the upper part of the Terre d'Haurs Fm is observed. It is followed by the Mont d'Haurs and Fromelennes formations. These last two formations show reduced thickness, respectively, of of ~50% and ~25% in comparison with the formations defined in the type area. The lithological unit LTU1 can be assimilated to the Terre d'Haurs, LTU2 to Mont d'Haurs and LTU3-5 to Fromelennes formations.

Terres d'Haurs Fm (~8 m-thick; LTU1; Figs. 1-2) corresponds mainly to cm- to dm-thick dark-grey highly argillaceous limestone beds intercalated with dm-thick limestone locally rich in crinoid debris.

Mont d'Haurs Fm (~56 m-thick; LTU2; Figs. 1-2) is mainly composed of several-dm well-bedded black to dark grey limestone. Conspicuous within lower and middle part are abundant of gastropod shells (scattered within the sediment or organized into packed dm-thick levels parallel to the bedding; Fig. 2a). Other observed fossils include are tabulate corals, stromatoporoids, crinoids and brachiopods. Locally, a well-developed bioturbated fabric can be observed (Fig. 2b).

Fromelennes Fm (~85 m-thick; LTU3-5; Figs. 1-2) can be divided into three lithological units (LTU3-LTU5). Unit 3 (LTU3; from 64 to 93 m) is characterized by grey dm- to m-thick beds. The proportion of gastropods is low and the abundance of reef-builder debris such as tabulate and rugose corals, lamellar, branching and bulbous stromatoporoids is significant. Crinoids and brachiopods are also a major component of the faunal assemblage. The topmost part of LTU3 is characterized by two m-thick limestone beds showing abundant and large debris of reef-building organisms. Locally, stromatoporoids reach more than 50-cm in size. Unit 4 (LTU4; from 93 to 150 m) is mainly composed of dm-sized light grey to yellow-earth limestone beds (corresponding to dolomitized beds). The conspicuous characteristic of this LTU4 is the abundance of thin mm- to cm-sized laminar fabric (Fig. 2c). The fauna is usually poorly represented throughout the unit, whereas within the upper part, cm- to dm-thick, well-sorted, laminated levels enriched in branching stromatoporoids such as *Stachyodes* and *Amphipora* occur (Fig. 2d). These levels are usually overlying laminated limestone or dolostone throughout a sharp erosive lower boundary. Locally, a well-preserved intraformational breccia developed from the laminated limestone can be observed (Fig. 1e).

Throughout LTU4, organisms are essentially debris of reef-builders, such as branching and bulbous stromatoporoids and branching tabulate corals. The overlying Unit 3 (LTU5; from 150 to 153 m) is mainly characterized by dm- to m-thick dark grey to dark blue beds locally showing abundant brachiopod shells and crinoids. LTU5 is overlain by yellow-earth limestone interlayered with black carbonaceous limestone belonging to the Nismes Fm of Frasnian age (for a detailed description see Pas et al., 2014a).

Fromelennes-Flohimont section (Fig. 3)

The measured section is ~460 meters thick with strata oriented N65°E and a dip of 63°S. It can be divided into seven lithological units (FFU1-7). According to the Belgian lithostratigraphic chart defined by Préat and Bultynck (2006) and the geological map of Mansy et al. (2006), The Trois-Fontaines (TRF), the Terres d'Haurs (THR), Mont d'Haurs (MHR) and Fromelennes (FRO) formations can be identified. FFU1-2 corresponds to the Trois-Fontaines, FFU3-4 to Terre d'Haurs, FFU5 to Mont d'Haurs and FFU6-7 to the Fromelennes formations. Thickness of the above mentioned formations in the Fromelennes-Flohimont section are consistent with their thicknesses defined in the type area (see Fig. 1c). Trois-Fontaines Fm (~70 m-thick; TRF) encompasses the lithological Units 1 and 2 (FFU1-2). FFU 1 extends from 0 to 42 m and is characterized by dm- to m-sized beds showing a poor faunal assemblage mostly corresponding to crinoids, brachiopods and solitary rugose corals. A particularity of this formation is the occurrence of m- to pluri m-sized hummocky cross stratification (HCS; Fig. 3a) and local beds showing occurrence of lumachelle rich in brachiopod shells, crinoids and branching tabulate corals. The lowermost portion of this unit corresponds to the lower part of the Trois-Fontaine Fm but do not represent the lowermost part because the boundary between Trois-Fontaines Fm and the underlying Hanonet Fm do not outcrop in this section.

Fig. 2 *Top of the figure: view of the Givetian section in the La Thure quarry with the two investigated Formations and the location of photographs.* **a-e** *Close up on different facies, the black arrows point to the stratigraphic base.* **a** *Gastropods rich levels in the lower portion of the Mont d'Haurs Formation.* **b** *Laminated limestone, showing vertical burrows filled by calcite exposed within the lower portion of the Unit 1, Mont d'Haurs Fm.* **c** *Slightly yellowish laminated limestone commonly occurring within the Fromelennes Fm (LTU4).* **d** *Dm-thick level (delimited by dashed lines) enriched in branching stromatoporoids (note that the lower boundary of this level is characterized by an erosion surface while the upper boundary is overlain by a thin laminated fabric) - erratic block near upper portion of the section corresponding to the Fromelennes Fm.* **e** *Intraformational breccia overlying a level of laminated limestone.*

Fig. 3 *Top of the figure: view of the Givetian section in the Fromelennes-Flohimont road section showing the four investigated formations and the exact location of pictures below.* **a-c** *Close up on some specific clearly visible field characteristics.* **a** *Hummocky-cross stratification within limestone belonging to the lowest part of the Trois-Fontaines Fm (FFU1).* **b** *Blue-grey limestone showing abundant cm-sized beige vertical burrows belonging to the upper part of the Trois-Fontaines Fm (FFU2).* **c** *M-thick stromatoporoids-rich limestone beds characteristic of the Mont d'Haurs Fm.*

The lowermost portion of this unit corresponds to the lower part of the Trois-Fontaine Fm but do not represent the lowermost part because the boundary between Trois-Fontaines Fm and the underlying Hanonet Fm do not outcrop in this section. FFU2 extends from 42 to 70 m and starts with the dark micritic limestone overlying the HCS which characterize Unit 1. The dominant lithology of this unit is the fine-grained grey to black limestone occurring in dm- to pluri dm-thick beds. Three particular aspects of these beds are: 1) the locally abundant ostracod shells, 2) the occurrence of some remarkable vertical bioturbations as shown in Figure 3b and 3) the occurrence of well-developed palaeosoils with the uppermost portion of FFU2.

Terres d'Haurs Fm (~67 m-thick; TRH) encompasses the lithological units 3 and 4 (FFU3-FFU4). FFU3 extends from 70 to 108 m and is characterized in the lowermost part by the alternation of dm-sized dark-blue and argillaceous limestone showing poor fauna represented by crinoids, brachiopods and ostracods. Progressively towards the upper part of this Unit 3, pluri-dm to m-thick blue to grey limestone beds are dominant. They show similar faunal assemblage to the lower part. FFU4 extends from 108 to 137 m and is mainly characterized by m-thick blue limestone beds dominated by crinoids and brachiopods. Bulbous and lamellar stromatoporoids, branching tabulate and local solitary rugose corals occur towards the top of Unit 4. Reef-builders are never observed in living position and they are mostly broken.

Mont d'Haurs Fm (~178 m-thick; MHR) corresponding to Unit 5 (FFU5), extends from 108 to 315 m and is mainly characterized by m-thick very rich reef-builder limestone beds (e.g., biostrome) alternating with poor fauna-related limestone. Outcrops of Unit 5 are not easily accessible as it is a built-up area. Biostromal facies corresponds mainly to a pluri-m to pluri dm-thick accumulation of bulbous stromatoporoids (dm- to pluri dm-sized) and in a lesser degree to lamellar and encrusting stromatoporoids, branching and lamellar tabulate corals, fasiculate and solitary rugose corals, ostracods, brachiopods, gastropods and crinoids. The other beds are generally m-thick limestone showing a faunal assemblage mainly composed of crinoids, ostracods and brachiopods. Towards the top of Unit 5, an increasing amount in crinoids and argillaceous content is observed.

Fromelennes Fm (~148 m-thick; FRO) encompasses two lithological units (FFU6 and FFU7). Unit 6 mainly consists in an alternation of dm- to m-thick biostromal and non-biostromal limestone beds and extend from 315 to 432 m. Biostromal limestone is mainly represented by cm-sized branching stromatoporoids and bulbous stromatoporoids (pluri dm-sized). In this Unit, reefal organisms are better preserved (hardly broken) than in Unit 5. The m-thick non-biostromal limestone beds are fine-grained and grey to ochre in colour. It shows abundant mm- to cm-sized laminar fabrics. The rare organisms occurring in these beds are ostracods and crinoids. Outcrops gaps of 20 and 35 m-thick respectively occur at the base and at the top Unit 6. Unit 7 ranges from 432 to 461 m and shows numerous outcrop gaps. This lithological unit 7 corresponds mainly to grey or blue pluri dm-thick limestone alternating with local argillaceous grey-coloured beds. Organisms are poorly-diversified and mainly represented by brachiopods and crinoids. Locally, dm-sized solitary rugose corals can be observed at the base of FFU7. The first occurrence of large-sized brachiopods within shale corresponds to the overlying Nismes Fm of Frasnian age.

4.2 Description and interpretation of microfacies

This section presents an inventory of the remarkable diversity of microfacies characterizing both the Early-Late Givetian succession along the Fromelennes-Flohimont road and the La Thure quarry section. In order to emphasize local depositional variations that can occur between the La Thure and the Fromelennes-Flohimont sections we have established a relevant description of microfacies for both sections and built two sets of microfacies. The description of texture, faunal and floral assemblages, preservation and sorting of organisms, in combination with selected literature (Neumann et al., 1975; Strasser, 1986; Préat et al., 1987; Skompski and Szulczewski, 1994) have allowed us to distinguish eighteen microfacies for the La Thure section (DR-LT1; RP-LT1-2 and PF2-6-LT1-15) and seventeen for the Fromelennes-Flohimont section. Five microfacies occur in both sections (PF-LT1, 2, 4, 10 and 15) and they will be described and interpreted within the paragraph dedicated to the La Thure section. Following the definition of Read (1985) on carbonate platform models, we have filed microfacies into three carbonate platform profiles: (1) a homoclinal ramp, (2) a rimmed shelf and (3) a drowned shelf. The homoclinal ramp can be divided into two belts (RP1-RP2) corresponding to the mid- and outer-ramp settings. Due to the complexity and diversity of depositional settings which define the rimmed shelf profile, we have divided it into seven facies belts (PF1-PF7): (PF1) fore-reef to off-reef shelf; (PF2) biostromal and fore-reef shelf; (PF3) bioclastic shoals; (PF4) internal shelf with fair circulation; (PF5) internal restricted shelf; (PF6) internal evaporitic shelf and (PF7) supratidal shelf setting. Facies belts PF1 and PF7 do not occur in the La Thure section while the facies belt PF4 is not observed in the Fromelennes-Flohimont section. The drowned shelf is characterized by one microfacies. Tab. 1 and 2 provide a summary of the main features characterizing the microfacies that are defined below.

Our microfacies classification follows approximately a distal to proximal depositional setting (considering that some microfacies could be lateral equivalents). Furthermore, some microfacies represent event-like features, and are thus not limited to one or another depositional setting. For example, limestone with a concentration of shell material can be formed in different shallow-marine and deep-marine facies zones (e.g., Flügel, 2004; p. 799). Therefore, our classification of microfacies in a distal – proximal transect considers the stratigraphic position, the lateral extension and the taphonomy of fossils that characterize the shell beds within the sedimentary sequence (e.g., Kidwell and Bosence, 1991; Fürsich and Oschmann, 1993). The obtained microfacies curves demonstrate a complex evolution of carbonate platform types throughout the Early – Late Givetian interval. Starting with a homoclinal ramp profile the carbonate platform evolves through a discontinuously rimmed shelf to a drowned shelf in the Latest Givetian. Interpreted microfacies are thus considered to belong to a wide spectrum of carbonate platform profiles with two-end members. The subdivisions between carbonate platform types and related interpretations are discussed in the next section (discussion – platform models).

La Thure section (LT; Figs 4-10)

Drowned carbonate shelf - DR Microfacies

DR-LT1: Mudstone and wackestone with densely-packed brachiopod-bivalve shell levels (Fig. 4)

This microfacies exclusively occurs within Unit 3 of the Fromelennes Fm. It is mainly characterized by mudstone and wackestone textures, but, locally, densely-packed cm-thick brachiopod-bivalve shell packstone and rudstone levels occur. The transition from mudstone-wackestone to these packed levels is gradual (erosional surfaces are not observed). Packed levels correspond to cm-sized accumulations of brachiopod (dominant), bivalve and gastropod shells embedded in a micritic matrix and showing clear bioturbated fabrics. Shells of brachiopods and bivalves are relatively well-preserved (locally articulated shells occur) and expose sizes varying from 0.3 to 2.5 cm with an average around 0.6 cm. Large gastropod shells are commonly broken but juveniles are better preserved. Sorting is poor to moderate and bioturbation commonly affects the sediment; this is underlined by the reorganization of shells (“nesting”). Other organisms are common crinoid ossicules and plates, rare *umbella,* solitary rugose corals, ostracods, stromatoporoids debris and unidentified bioclasts. Crinoids are relatively well-preserved and often mm in size. The matrix is a fine-grained micrite, locally dolomitized.

Interpretation:

Brachiopod and bivalve shells embedded in a micritic matrix and common occurrence of crinoids point to an open-marine setting with relatively quiet conditions prior deposition. The poor- to moderate-sorting of shells and the vertical bioturbation corroborate this interpretation. According to Fürsich and Pandey (1999) the significant density of shell may be the result of several processes: a high productivity combined with low sedimentary rate and occasional winnowing. According to Mamet (1970) the occurrence of *umbella* indicates a vicinity with coastline and abnormal level of salinity (high or poor) while echinoderms and brachiopods are in favour of open-marine conditions. Considering the thick inter- to supratidal lagoonal sequence developed beneath (e.g., Unit 2), deposition of DR-LT1 should have occurred within a drowned lagoon concurrently with the re-establishment of open-marine conditions. This hypothesis is also confirmed by the overlying open-marine Frasnian shale sequence (Pas et al., 2014a). The occurrence of bioclasts from various environments might be the result of distal tempestites. However, the high-rate of bioturbation that affected the sediment after deposition destroyed the original fabric and hampers to testing of this hypothesis. In conclusion, this microfacies could correspond to an accumulation of shells in a calm open marine setting during a time of low sedimentary rate, subjected to storm-related winnowing and bioturbations.

Mid- to outer-ramp - RP Microfacies

RP-LT1: Bioclastic mudstone to packstone

This microfacies only occurs at the base of the studied section attributed to the Terre d’Haurs Fm. It is characterized by a commonly dolomitized fine-grained matrix, an open-marine faunal assemblage and the occurrence of mm- to cm-thick layers rich in poorly-preserved crinoids and finely-broken skeletal debris (Fig. 5a). Fossils are poorly- to moderately-preserved, except for some larger tabulate corals and stromatoporoids. The main fauna is represented by brachiopods (locally complete cm-sized shells) and other unidentified shells (often finely-broken and strongly recrystallized) and crinoid debris (from 0.4 to 2 mm). Less common organisms are gastropods, ostracods, branching bryozoans, worm tubes and rare tabulate corals and stromatoporoids. Locally, the sediment is significantly bioturbated and shows clear examples of circular burrows filled by peloidal grainstone (Fig. 5b). In other cases, bioturbation is recognized by the re-organization of bioclasts. Rarely, brachiopod shells show infra mm-thick encrustation by porostromates. Finely-broken unidentifiable shells are locally the main constituent of sediment corresponding to shell hash. Crinoidal rich layers, associated with fine-grained brachiopod and ostracod shells, show a packstone texture and the transition from mudstone –

wackestone in those layers is gradual. Insoluble residues are commonly observed between the fine-grained bioclasts.

Interpretation:

Crinoids, brachiopods and bryozoans indicate a depositional environment below the fair weather wave base (FWWB) within open-marine conditions. Common occurrence of gastropods implies a shallow-marine environment while moderate- to poorly-preserved levels of bioclasts indicate that organisms were subjected to relatively long exposure on the sea-floor prior deposition. Occurrence of mm- to cm-thick layers mainly characterized by crinoid debris accumulation indicates high energy events such as tempestite, triggering transport and concentration of debris basinward. The dominance of crinoid debris in those layers also suggests the occurrence of a crinoidal meadow in a shallower location. The lack of clues from microfacies RP-LT1 make it difficult to determine whether environment represents a homoclinal ramp or an external shelf reef for this microfacies. Occurrences of this microfacies within lithologies belonging to Terre d'Haurs Fm, which are commonly interpreted as ramp-related in southern Belgium (Mabille et al., 2008a; Boulvain et al., 2009), suggest deposition on a ramp profile for this microfacies. In conclusion, the depositional setting might correspond to a mid- to distal ramp located below FWWB and locally influenced by higher energy events such as storms, that triggered the transport of these bioclasts towards deeper marine area.

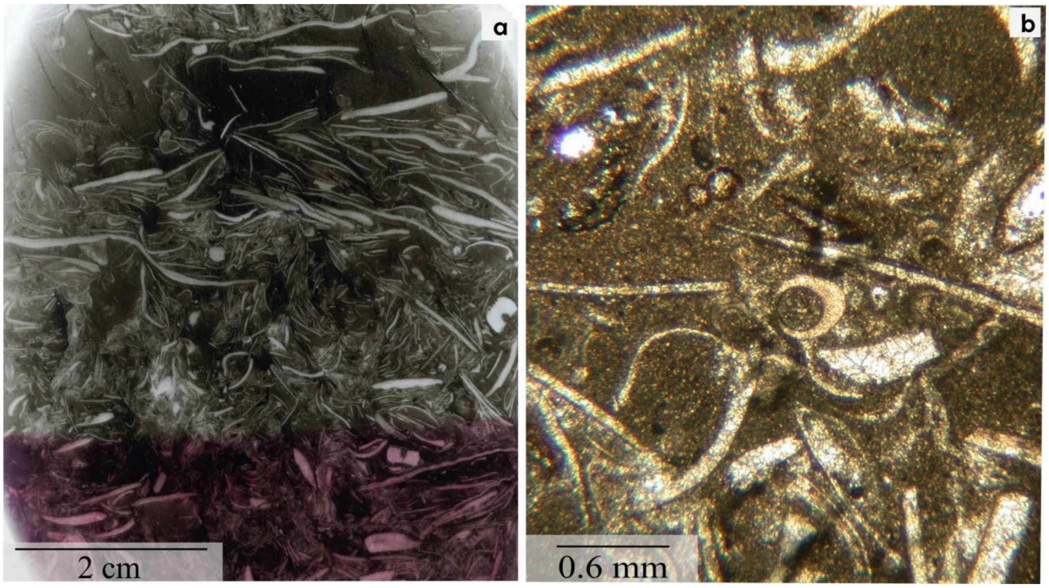

Fig. 4 *Microfacies DR-LT1 - drowned shallow-water carbonate platform from the Givetian of the La Thure section, Belgium. Photomicrographs of thin-section are oriented perpendicular to the bedding. Numbers preceded by "TUR" correspond to bed numbers.* **a** *Shell packstone and rudstone (TUR 310, scanned thin-section, with alysarine staining).* **b** *Shell packstone including umbella (TUR 293b, centre of the photograph, transmitted light).*

RP-LT2: Crinoidal packstone-grainstone (Fig. 5c)

This microfacies only occurs in few dm-thick beds located at the base of the studied section attributed to the Terre d'Haurs Fm. and is intercalated within microfacies RP-LT1. This microfacies is commonly dolomitized but texture and faunal assemblage are preserved locally. When dolomitization does not affect the main characteristics of this microfacies, the abundance of crinoid ossicules and plates showing a micritized rim (Fig. 5c) is typical. Crinoids range from 0.5 to 2 mm with an average size around 1 mm. Other fossils are generally broken and represented by gastropods, brachiopods, ostracods, rare bryozoans and finely-broken unidentifiable debris. Gastropods commonly display an internal mold filled by micritic matrix (Fig. 5d). Burrows occur and are underlined by a core filled with finely-broken organisms in a micritic matrix.

Interpretation:

Abundance of crinoids and occurrence of brachiopods and bryozoans within packstone-grainstone texture suggest an open-marine environment likely close to crinoidal meadows and within the fair weather wave zone (FWWZ). Crinoids debris and gastropods packed in cm-thick levels surrounded by microfacies RP-LT1 suggest a deposition related to high energy events, and in the vicinity of the setting assumed for RP-LT1. Indeed, RP-LT2 is surrounded by microfacies RP-LT1 and RP-LT1 is interpreted as deposited in an open-marine mid- to distal ramp setting below the FWWB.

Carbonate shelf: Microfacies PF

The complexity and diversity of depositional settings occurring in this carbonate shelf profile leads to the subdivision into seven facies belts (PF1-PF7): (PF1) fore-reef shelf and off-reef (PF2) biostrome and fore-reef shelf; (PF3) bioclastic shoals; (PF4) internal shelf with fair circulation; (PF5) internal restricted shelf, (PF6) internal evaporitic shelf and (PF7) supratidal shelf setting. In the La Thure section, facies belts PF1 and PF7 do not occur.

Facies Belt 2: Biostrome and fore-reef shelf

PF2-LT1: open-marine bioclastic wackestone and packstone (Fig. 5e-f)

This microfacies is characterized by open-marine faunal assemblages, embedded in a micritic matrix, showing poor- to moderate-sorting. Fossils are mostly broken and are represented in decreasing order of abundance by crinoids, brachiopods, ostracods (thick and thin-shelled), bivalves, gastropods, branching and fenestellid bryozoans, trilobites, tentaculitids, palaeosiphonocladales (e.g., issinellids; Fig. 5f) and abundant unidentifiable shells. Locally, debris of branching tabulate corals, rugose corals and poorly-preserved branching stromatoporoids occur. From time to time, bioclasts are crushed and very poorly-preserved displaying an average size of 0.2 mm. Bivalve shells locally show an irregular micritic envelope up to 0.5 mm. Thin-shells represent up to 80% of the biological constituents. Complete brachiopod shells are locally filled by a clotted fabric. Pressure-solution processes forming horse-tail and iden-supported fabric commonly occur. “Iden-supported” is a fabric where idens (bodies that behave as homogeneous entities under chemical and physical conditions) are densely packed and bound by irregular, anastomosing microstylolites (Logan and Semenuik, 1976) (see also caption of fig. 7.18b in p.318; Flügel, 2004). Argillaceous-rich mm-thick layers and seams parallel to the bedding also occur from time to time.

Interpretation:

The abundance of open-marine biota such as trilobites, tentaculitids, bryozoans and crinoids embedded in poorly to moderately-sorted micritic sediment indicates deposition within a relatively quiet open marine setting, likely below the FWWB. The occurrence of reef-building organisms and shallow-water biota/flora, such as gastropods and palaeosiphonocladales suggests an influence of shallow-marine assemblages towards deeper setting. Furthermore, the occurrence of reef-building organisms is in favour of a setting located in vicinity of reefal constructions such as patch- or barrier-reefs.

PF2-LT2: coral-stromatoporoids rudstone/floatstone (Fig. 5g)

This microfacies occurs mainly in m-thick beds in the upper part of the Mont d’Haurs Fm and lowermost part of the Fromelennes Fm. It is characterized by the dominance of several dm-scaled laminar and bulbous stromatoporoids, branching tabulate corals, encrusting stromatoporoids and solitary rugose corals. Those reef-builders are always reworked and broken. The area between skeletal debris is filled by small and commonly unidentifiable bioclasts embedded in a dark micritic matrix showing a wackestone to packstone texture and commonly dolomitized. Identified bioclasts are trilobites, brachiopods, gastropods, ostracods and rare palaeosiphonocladales. The sediment filling the space between large organisms contains detrital quartz and is relatively similar to PF2-LT1.

Interpretation:

The abundance of various and large-sized (several dm-sized) coral-stromatoporoids debris in a rudstone/floatstone texture indicates a depositional setting strongly influenced by close shallow-marine reefal constructions. Wackestone-packstone texture and bioclasts characterizing the space between large reef-builders are in favour of an environment located below the FWWB in the vicinity of PF2-LT1. The poor- to moderate preservation and sorting of reef-builder organisms suggest a reworking likely by wave action and a downward transport by gravity process such as storm or debris-flow.

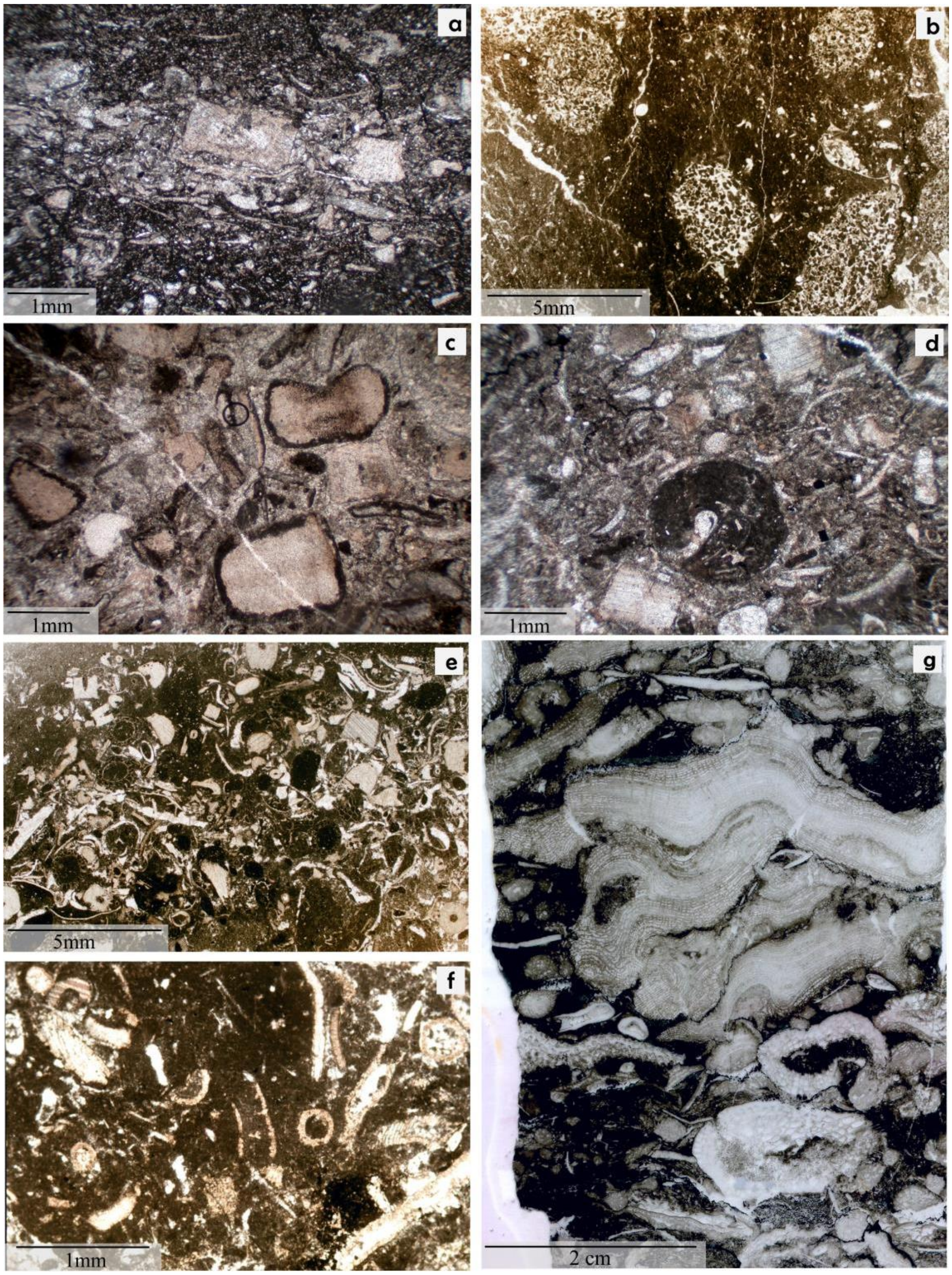

Fig. 5 *Microfacies RP-LT1-2 and PF1-LT1-2 from the Givetian of the La Thure section, Belgium. Photomicrographs of thin-sections are perpendicular to the bedding. Numbers preceded by "TUR" correspond to bed numbers.* **a** *RP-LT1 - mid- to distal-ramp setting: crinoidal packstone rich layer within a dolomitized mudstone and wackestone (TUR 100b, transmitted light).* **b** *RP-LT1 - mid- to distal-ramp setting: bioclastic mudstone – wackestone showing peloidal grainstone filling of burrows (TUR 108, transmitted light).* **c** *RP-LT2 - mid- to distal ramp setting: coarse-grained grainstone, with crinoids showing micritized rim (TUR 100, transmitted light).* **d** *RP-LT2 mid- to distal-ramp setting: gastropods crinoidal packstone showing gastropod internal molds filled by micrite (TUR 100, transmitted light).* **e** *PF1-LT1 – biostrome and fore-reef shelf: bryozoans crinoidal packstone (TUR 181c, transmitted light).* **f** *PF-LT1 external reef and fore-reef shelf: bioclastic packstone showing remains of issinellid algae (TUR 195, transmitted light).* **g** *PF1-LT2 biostrome and fore-reef shelf: lamellar stromatoporoids rudstone (TUR 202, scanned thin-section).*

Interpretation:

The abundance of various and large-sized (several dm-sized) coral-stromatoporoids debris in a rudstone/floatstone texture indicates a depositional setting strongly influenced by close shallow-marine reefal constructions. Wackestone-packstone texture and bioclasts characterizing the space between large reef-builders are in favour of an environment located below the FWWB in the vicinity of PF2-LT1. The poor- to moderate preservation and sorting of reef-builder organisms suggest a reworking likely by wave action and a downward transport by gravity process such as storm or debris-flow.

Facies Belt 3: Bioclastic shoals

PF3-LT3: Calcimicrobial bio- lithoclastic grainstone

This microfacies is characterized by the common occurrence of calcimicrobe *Girvanella*/ *Sphaerocodium* (Fig. 6a) as encrusters and oncoids/lumps builders. *Girvanella* encruster mainly occurs on gastropod shells and can reach up to several mm in thickness. Oncoids and lumps are also frequent and locally mm-scaled. Other skeleton are poorly-preserved and consist of gastropods (locally complete), brachiopods, worm tube debris (with encrusting *Sphaerocodium*), rare stromatoporoids and crinoids.

Another major characteristic of this PF-LT is the common occurrence of sub-angular to rounded, variously-sized (0.3 to 2 mm) lithoclasts (Fig. 6b) constituted either of peloidal grainstone (e.g., PF3-LT4) or mudstone-wackestone (e.g., PF4-LT5). Locally, calcimicrobial encrustation surrounds lithoclasts of bio- and lithoclastic packstone.

Interpretation:

The common occurrence of the calcimicrobe *Girvanella* as coating on gastropods and oncoids point to a euphotic internal shelf setting. According to Scholle and Ulmer-Scholle (2003) oncoid-like *Girvanella* can form in a setting episodically subjected to strong wave action. The grainstone texture and the occurrence of lithoclasts concur with this interpretation. Local occurrence of brachiopods and crinoids argues for an open-marine environment. This microfacies is likely formed adjacent to external shelf, subjected to strong wave action. The uncommon occurrence of reef builders indicates that this depositional setting was little influenced by reefal construction.

PF3-LT4: Peloidal – lithoclastic grainstone with gastropods (Fig. 6c-d)

Peloids represent over 80% of the grain assemblage; according to the variable size (from 50 to 200µm) and shape (from sub-angular to sub-rounded) most of them are considered as lithic peloids (variable shape and size ranging between 50 and 150µm; Flügel 2004, p.112). Micritic lithoclasts (e.g., micritic allochems larger than 200 µm) are commonly observed. Common poorly-preserved and rounded gastropod debris, brachiopods, crinoids, rare ostracod shells and rare tabulate corals, stromatoporoids, bryozoans are observed. When bioclasts are smaller than 500 µm they show intense micritization. Mud-coated grains are common and sorting of the sediment is moderate to good within a grainstone texture although local packstone texture occur.

Interpretation:

The main characteristic of PF2-LT4 is the abundance of lithic peloids and micritic lithoclasts. The origins of such allochems are interpreted as syn-sedimentary and post-sedimentary reworking of carbonate mud and micrite. The origins of the other peloids is varied: faecal, micritised grains, direct algal origin, and intraclasts (Tucker, 2001). Regarding the locally intense micritization of bioclasts, the origin of much of these other peloids could be related to micritization. Common occurrence of gastropods points to an internal shelf environments. Relatively good sorting and grainstone texture without any sedimentary structure may suggest the occurrence of peloids bars near the margin of internal shelf where agitation is important within the FWWB. Mud-coated grains are in favour of this interpretation. Furthermore, the occurrence of tabulate corals and stromatoporoids indicates a reefal influence. Local pelmicritic texture might be related to periods of lower energy allowing micritic mud to settle.

Facies Belts 4: Internal shelf with fair circulation

PF4-LT5: Mudstone to packstone with lithoclastic – brachiopods rudstone-grainstone layers

This mudstone – packstone is characterized by a well-developed stylonodular fabric, which commonly hampers a good observation of the original texture. Locally, a significant proportion of clay particles and insoluble residues occur. Faunal assemblages are dominated by brachiopod shells, gastropods, thick-walled ostracods and worm tubes (Fig. 6e). Irregular fenestrae (Fig. 6f) are a common occurrence in the mudstone texture. Peloidal grainstone (e.g., PF3-LT4) commonly fills the internal molds of brachiopod shells. Another dominant character of this microfacies is the local occurrence of brachiopod-rich – lithoclastic grainstone – rudstone layers (Fig. 6g). Within these layers both lithoclasts and brachiopod shells are abundant (Fig. 7a). Locally, there are also a few grainstone-rudstone pockets, dominated by lithoclasts. Lithoclasts are essentially micritic, well-rounded and infra-mm to mm-scaled while brachiopods range from 0.3 to 1 cm in size and are locally articulated. Grainstone – rudstone layers and pockets are cm-scaled and their boundary with the mudstone – wackestone is not clearly visible due to pressure-solution processes. Within this microfacies, bioturbation and local clotted fabric occur. When argillaceous material is abundant, dolomitization is well-developed.

Interpretation:

The mudstone – wackestone texture, the faunal assemblage and its relatively good preservation indicate a quiet depositional setting for this microfacies, allowing mud settling of mud and the preservation of organisms as in microfacies PF2-LT3. However, faunal assemblage infers an internal shelf with fair circulation. Grainstone-rudstone layers or pockets occurring in this microfacies suggest a temporary storm induced increase of the water-energy level allowing an accumulation of brachiopods and reworking micritic clasts in a grainstone – rudstone texture.

PF4-LT6: Magnella shell grainstone and rudstone (Fig. 7b-c)

This microfacies only occurs within three cm-sized beds in the lower portion of the Mont d'Haurs Fm. These beds are intercalated within PF3-LT5 mudstone-wackestone. The conspicuous characteristic of this microfacies is the abundance of whole *Magnella* shells (i.e. attributed to pteropods by Neumann et al. (1975); plate 3), associated with brachiopod shells. *Magnella* shells are always complete, they show an average size around 0.2 mm and can locally represent 80% of the sediment. Millimetre-sized Brachiopod shells are mostly articulated but often strongly deformed. Space between organisms is filled with sparitic cement. Peloids are locally abundant; they are spread within the sediment or occur as mm-sized pockets. Where deformed brachiopod shells occur it is common to observe argillaceous seams and pressure solution fabric. Molds of brachiopod shells are commonly filled with conical shells of *Magnella*. Rare lumps of *Girvanella* occur.

Interpretation:

The characteristics of this microfacies point to an environment where energy is high enough to prevent the deposition of micrite (grainstone texture). The limited thickness interval of this microfacies and its intercalation with PF3-LT5 mudstone and wackestone suggest event like deposition as tempestites. Indeed, overlying and underlying microfacies indicate a subtidal internal shelf setting. The scarcity of the literature mentioning "*Magnella*" does not allow for the inference of further details on the ecological interpretation.

PF3-LT7: Stromatoporoid rudstone

These rudstones are relatively similar to those described in PF2-LT2. Differences are mainly the absence of open-marine organisms, such as crinoids and trilobites, the occurrence of the branching tabulate, *Stachyodes,* fasiculate rugose corals and frequent palaeosiphonocladales. Stromatoporoids are locally encrusted by *Sphaerocodium* and serpulids. As for PF2-LT2, the matrix is often dolomitized and rich in insoluble residues.

Interpretation:

The occurrence of reef-builder remains encrusted by calcimicrobes and serpulids, and the occurrence of *Stachyodes* are in favour of back-reef and near-reef environments (Flügel, 2004; p. 500). Furthermore, the absence of crinoids and trilobites suggests limited connection to fully marine setting. This microfacies could correspond to small patch reefs developed in an internal shelf setting.

PF4-LT8: Palaeosiphonocladales wackestone – packstone

The main characteristics of this microfacies are the dark colour of the sediment, the commonly dolomitized matrix and the abundance of variously-preserved issinellid and palaeoberesellid algae (Fig. 6d). Other organisms are broken brachiopod shells, ostracods and locally mm-sized *Girvanella* oncoids (Fig. 7e), rugose corals and branching stromatoporoids. Shells commonly expose spongiostromate encrustation. Irregular mm-sized grainstone lenses rich in micritic lithoclasts in grainstone texture occur locally.

PF4-LT8: Palaeosiphonocladales wackestone – packstone

The main characteristics of this microfacies are the dark colour of the sediment, the commonly dolomitized matrix and the abundance of variously-preserved issinellids and palaeoberesellids algae (Fig. 6d). Other organisms are broken brachiopod shells, ostracods and locally mm-sized *Girvanella* oncoids (Fig. 7e), rugose corals and branching stromatoporoids. Shells commonly expose spongiostromate encrustation. Locally, mm-sized irregular lenses rich in micritic lithoclasts in grainstone texture occur.

Interpretation:

The abundance of issinellids and palaeoberesellids in a wackestone to packstone texture suggests a relatively quiet setting in the vicinity of palaeoshiphonocladale grass. In a paper dedicated to the Belgian Givetian platform, Mamet and Préat (1986) established that these algae mostly occur in barrier and lagoonal setting. Considering the absence of reef-builder remains we suggest deposition in a location distant from the reefal influence.

PF4-LT9: Burrowed calciphere mudstone (Fig. 3b)

The main characteristic of this mudstone is the occurrence of frequent calcispheres floating in a dark-brown micritic matrix and the common occurrence of cm-sized vertical burrows filled with sparitic cement. Other organisms are rare and represented by palaeoberesellid algae, ostracod shells and pteropods like *Magnella* shells (see also PF4-LT6). Locally, mm-sized pockets displaying a clotted texture and small fenestrae are observed.

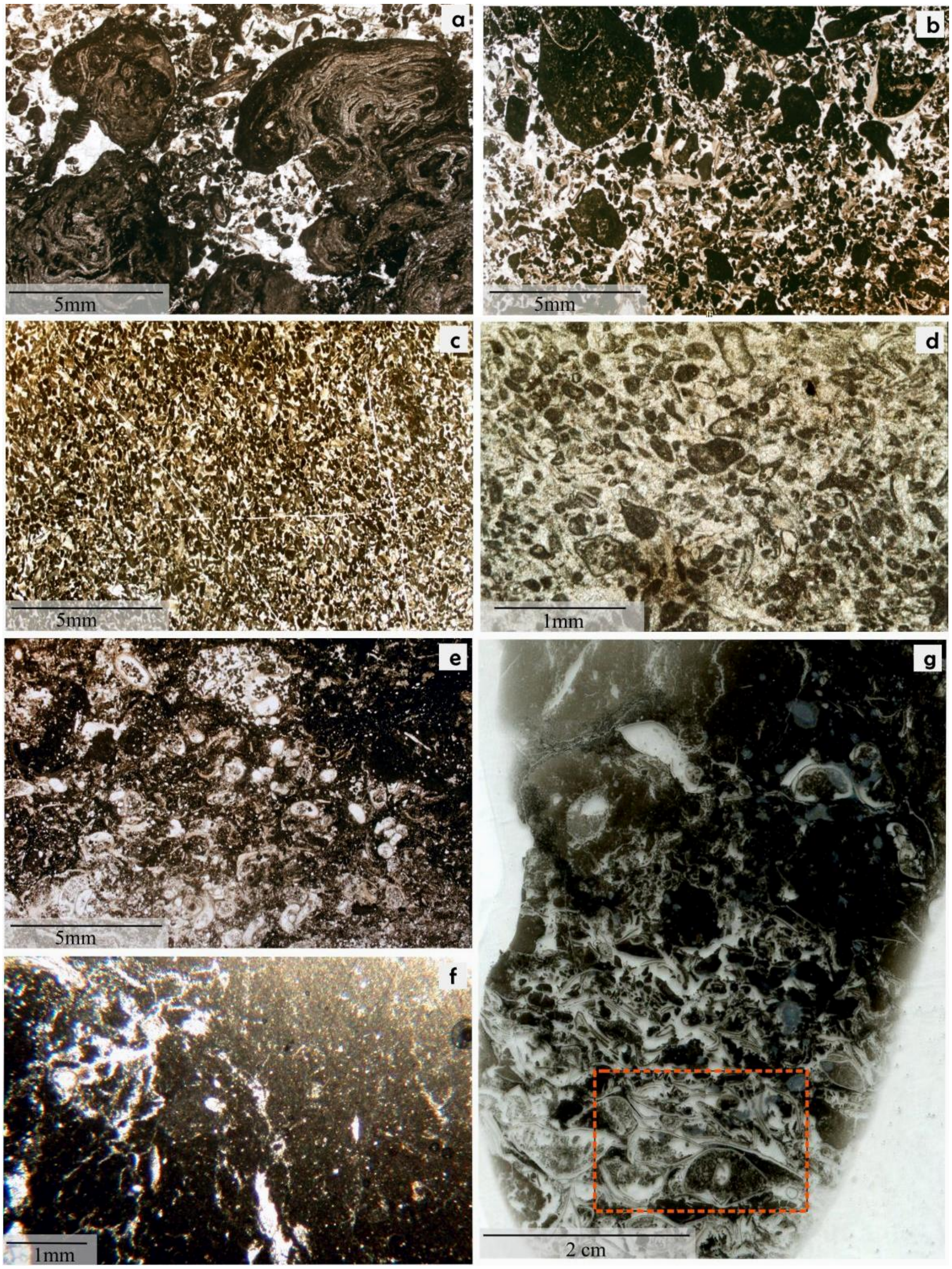

Fig. 6 *Microfacies PF2-LT3-4 and PF3-LT5 from the Givetian of the La Thure section. Photomicrographs of thin-sections are oriented perpendicular to the bedding. Numbers preceded by "TUR" correspond to bed numbers.* **a** *PF2-LT3 bioclastic shoals: calcimicrobe Sphaerocodium oncoidal grainstone – rudstone (TUR 200b, transmitted light).* **b** *PF2-LT3 bioclastic shoals: lithoclastic grainstone – rudstone (TUR 189, transmitted light).* **c** *PF2-LT4 bioclastic shoals: fine-grained peloidal bioclastic grainstone (TUR 163c, transmitted light).* **d** *PF2-LT4 bioclastic shoals: peloidal grainstone with mud-coated grains (TUR 138b, transmitted light).* **e** *PF3-LT5 internal shelf with good circulation: wackestone showing worm tubes accumulation (TUR 157, transmitted light).* **f** *PF3-LT5 internal shelf with fair circulation: mudstone – wackestone with fenestrae (TUR 176, transmitted light).* **g** *PF3-LT5 internal shelf with good circulation: coarse-grained brachiopod shells level overlain by a fenestral mudstone – wackestone (TUR 176, scanned thin-section).*

Interpretation:

The abundance of micritic matrix and vertical burrows infer a very quiet depositional setting likely located in a subtidal setting characterized by a low sedimentation rate; where settling is the main sedimentary process. Calcispheres are recognized as common constituents of Middle Devonian lagoonal and back-reef carbonate settings (Mamet, 1991; Flügel, 2004). Furthermore, the occurrence of palaeoberesellid algae is also in favour of a lagoonal setting. This microfacies is thus interpreted as deposition in a lagoonal setting, likely above the FWWB but in sheltered setting.

PF4-LT10a and PF5-LT10b-c: Oolitic grainstone-packstone

This microfacies is characterized by the abundance of ooids and the good- to moderate-sorting of sediment. Based on their texture, the occurrence of various types of ooids (Type 1, 2, 3 and 4; Strasser, 1986) and the abundance of bioclasts and lithoclasts, this microfacies can be divided into three categories: (PF4-LT10a) oolitic peloidal grainstone; (PF4-LT10b) oolitic lithoclastic grainstone – packstone and (PF5-LT10c) oolitic shelly packstone – wackestone.

PF4-LT10a and PF5-LT10b-c: Oolitic grainstone-packstone

This microfacies is characterized by the abundance of ooids and the good- to moderate-sorting of sediment. Based on their texture, the occurrence of various types of ooids (Type 1, 2, 3 and 4; Strasser, 1986) and the abundance of bioclasts and lithoclasts, this microfacies can be divided into three categories: (PF4-LT10a) oolitic peloidal grainstone; (PF4-LT10b) oolitic lithoclastic grainstone – packstone and (PF5-LT10c) oolitic shelly packstone – wackestone.

PF4-LT10a: Oolitic peloidal grainstone – packstone (Fig. 7f-g)

The main character of this microfacies is the moderate to good sorting of sediment, the abundance (80-90%) of Type 3 and 1 ooids of Strasser (1986) and the regular occurrence of peloids. Type 1 corresponds to spherical micritic ooids with thinly laminated tangential cortices while Type 3 corresponds to ooids with thinly laminated fine-radial cortices. The ooids observed feature an average size of 0.4 mm and are cemented by sparitic cement even if locally micritic matrix occurs. Oolitic grainstone overlies PF4-LT5 mudstone-packstone with a sharp and erosional boundary. Lithoclasts of mudstone occur within the lower part of the overlying oolitic grainstone. Aggregate grains and micritic lithoclasts (infra-mm to mm-sized) occur and locally the space between ooids is dolomitized.

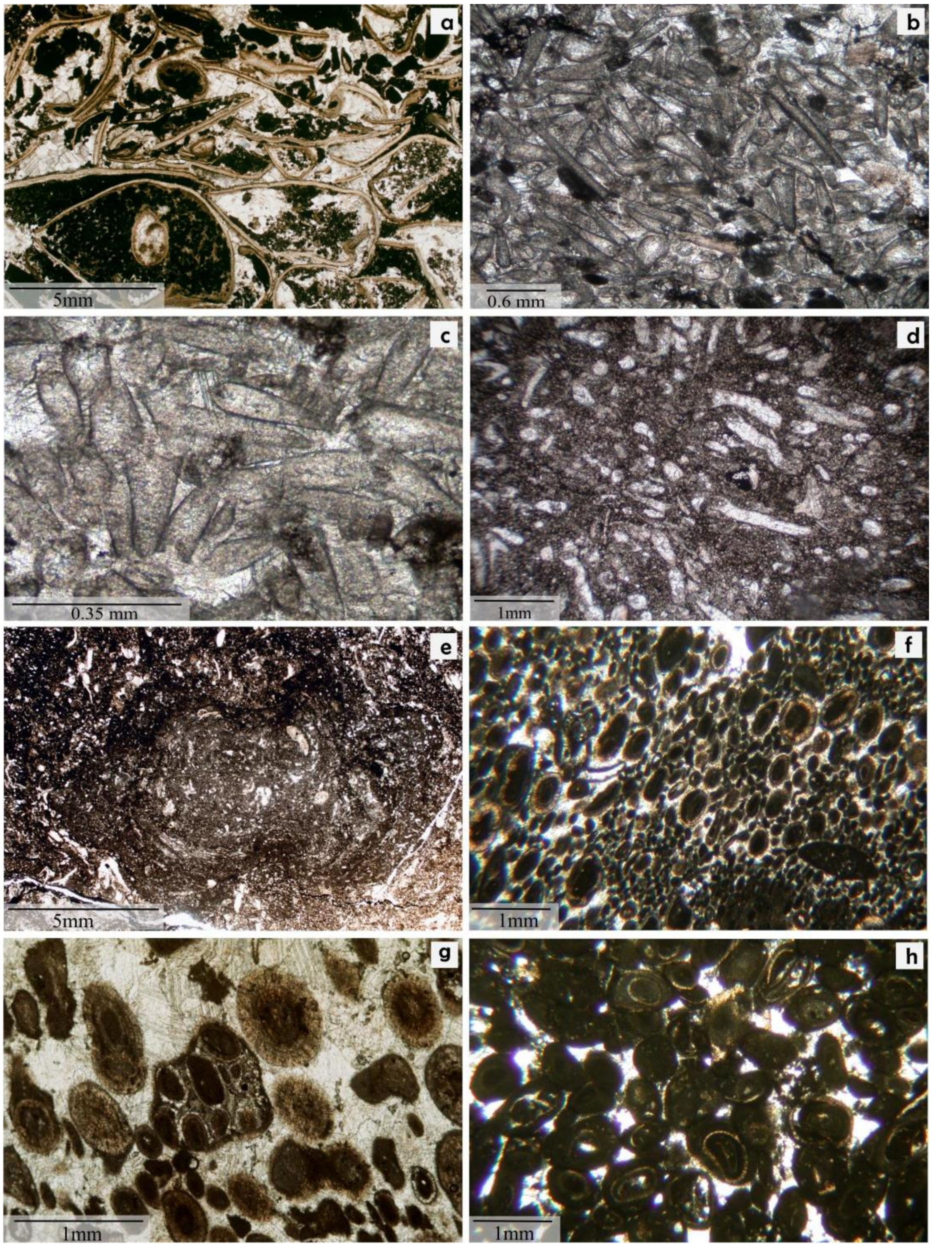

Fig. 7 *Microfacies PF3-LT5-7-10a and PF4-LT10b-c from the Givetian of the La Thure section, western Belgium. Photomicrographs of thin-section are oriented perpendicular to the bedding and were all made in transmitted light.* **a** *PF3-LT5 internal shelf with fair circulation: Brachiopod shells rudstone showing whole shell filled by a clotted fabric (for location see inset in* **Fig. 6g***) (TUR 176).* **b** *PF3-LT6 internal shelf with fair circulation: whole Magnella shells grainstone (TUR 133).* **c** *PF3-LT6 internal shelf with fair circulation: focus on conical shells like Magnella (TUR 133).* **d** *PF3-LT7 internal shelf with good circulation: dolomitized packstone rich in palaeoberesellid (TUR 149b).* **e** *PF3-LT7 internal shelf with fair circulation: Girvanella oncoid within a issinellid rich packstone (TUR 156).* **f** *PF3-LT10a internal shelf shoals setting: moderately-sorted oolitic grainstone (oolite Type 3) with common peloids (TUR 159c).* **g** *PF4-LT10b internal restricted shelf shoals setting: detail on Type 3 oolite (Strasser, 1986), peloids and aggregate grains within a moderately-sorted oolitic grainstone (TUR 159a).* **h** *PF4-LT10b internal restricted shelf lagoonal setting: micritized oolite grainstone (oolite are mainly of Type 2 and 4 - TUR 180).*

Interpretation:

The abundance of well- to moderately-sorted Type 1 and 3 ooids (Strasser, 1986) in a grainstone points to a depositional setting where water turbulence was relatively high thus allowing for the sorting of grains, likely within the FWWZ. Furthermore, according to Strasser (1986), Type 1 ooids are formed in intertidal conditions with high water-energy while Type 3 ooids (dominant) are interpreted as formed within an intermittently agitated and moderate water energy (see fig. 10 in Strasser, 1986). This environment might correspond to an oolitic shoal or bar developed in a shallow lagoonal setting. Within his rimmed carbonate platform model, Wilson (1975) defined several SMF Types (e.g., SMF15) referring to the occurrence of shoals in a platform interior. Occurrence of this microfacies overlying mudstone and wackestone (e.g., PF4-LT5) indicates that the suggested shoal was likely developed in internal shelf settings, in the vicinity of microfacies PF4-LT5.

Facies Belt 5: Internal restricted shelf

PF5-LT10b: Oolitic lithoclastic grainstone – packstone (Fig. 7h)

The main characteristics of this microfacies are the moderate sorting, the dominance of micritized Type 2 and 4 ooids (Strasser, 1986), and the occurrence of lithoclasts and bioclasts. Type 2 corresponds to irregular micritic ooids with thinly laminated cortices while Type 4 corresponds to ooids with a few fine-radial laminae. Observed ooids have an average size around 0.5 mm and they commonly show a nucleus constituted either of micrite or broken shells. Lithoclasts, constituted either of mudstone or oolitic grainstone/packstone, are usually rounded and range from 0.3 to 7 mm. Other observed allochems are rare and correspond to aggregate grains and broken brachiopod/bivalve shells. When the matrix is micritic, the sorting is moderate to poor. Micritization of allochems is generally significant.

Interpretation:

Type 2 ooids are formed within normal marine salinity condition while Type 4 ooids are made within hypersaline condition. However, these two types of ooids develop within calm- to moderately-agitated water likely within a lagoonal environment (Strasser, 1986). In comparison with PF4-LT10a, especially in the case of Type 4 ooids, this microfacies might be located in a more proximal setting PF4-LT10a.

PF5-LT10c: Oolitic shells packstone and wackestone (Fig. 8a)

This microfacies is mainly characterized by well- to moderately-sorted Type 4 ooids embedded in a micritic matrix (Fig. 8a). These oolites show an average size around 0.4 mm with micritic nucleus. Oolites are usually moderately packed but locally occur as densely packed oolitic levels, parallel to the bedding. Bioclasts only consist of broken bivalve and ostracod shells. This microfacies only occurs in the upper part of the Fromelennes Fm (LTU4), with PF6-LT14 and 15.

Interpretation:

Type 4 oolite indicates restricted salinity condition and intermittently agitated water condition (Strasser, 1986). The abundance of micritic matrix resulting of mud settlement within calm water and the common occurrence of bivalve shells are in accordance with this interpretation. Local occurrence of this microfacies within the intraclastic breccia characterizing PF6-LT14 attests to restricted conditions during deposition.

In conclusion, submicrofacies PF4-LT10a, PF5-LT10b and PF5-LT10c were all deposited on shoals inside an internal shallow shelf in a context of various levels of water energy and restriction. From PF4-LT10a to PF5-LT10c the proximality or the restriction degree of the lagoon increased. The occurrence of shoals in internal platform setting is also supported by the extended width of the internal platform (e.g., from the coastline to the barrier), estimated about ~60 km by Préat (2004). This significant width therefore contributes to the development of a large range hydrodynamic conditions.

PF4-LT11: Lithoclastic rudstone (Fig. 8b)

This microfacies is characterized by variously-sized (0.3 to 7 mm) angular to sub-rounded lithoclasts (Fig. 8b) cemented by sparitic cement. Lithoclasts are mainly composed of peloidal and oolitic grainstone (e.g., PF4-LT10a and PF5-LT10a-b) although locally, micritic lithoclasts can occury. A laminated fabric is underlined by the alternation of coarse- and fine-grained lithoclasts. Within the layers dominated by fine-grained lithoclasts abundant peloids occur. Type 1 and 3 ooids (Strasser, 1986) are commonly visible within the sediment and the fabric is clast-supported with blocky sparite cement.

Interpretation:

The rudstone texture and the abundance of oolitic grainstone (PF4-LT10a) and micritic lithoclasts indicate the reworking of microfacies PF4-LT10a likely during a rapid increase of water energy. The limited occurrence of those sediments attests to the event-like character of this microfacies which can be related to stronger tidal currents or storm. The distinction between those two processes is not obvious but in general an increasing proximity with the coastline is marked by an increasing influence of tidal current. Thus, the depositional setting of this microfacies might have been located in the vicinity of PF4-LT10a and related to a rapid increase in water energy caused by storm or tidal current.

Facies Belt 5: Internal evaporitic shelf

PF6-LT12: Dendroid stromatoporoid rudstone – floatstone (Figs. 2d and 8c-d)

Cm-sized dendroid (*Stachyodes and Amphipora*) and bulbous stromatoporoids lying parallel to the bedding and fine-grained yellow-earth dolomitized matrix characterize this microfacies. *Stachyodes* are mm- to cm in size and commonly show encrustation by mm-scaled encruster stromatoporoids. Rare moderately- to poorly-preserved allochems such as brachiopods, peloids, lithoclasts, *Girvanella*, *Renalcis* lumps, tabulate corals and unidentified bioclasts are observed between large organisms. Locally, cm-sized bulbous stromatoporoids can be frequent. The sediment is moderately- to well-sorted. Locally, this microfacies is intercalated with sediment from PF6-LT14 (laminated mudstone – peloidal grainstone) with sharp and erosive lower contact (Fig. 3d).

Interpretation:

According to several authors (Cornet, 1975; Pohler, 1998a; Wood, 2000) *Amphipora and Stachyodes* are characteristic of shallow-water back-reef lagoonal settings and growth on soft substrate. Occurrence of abundant *Stachyodes* and *Amphipora* in a rudstone/floatstone texture intercalated with laminated mudstone PF6-LT14 (defined above) suggests significant reworking of dendroid stromatoporoids, which grew in the relative vicinity of PF6-LT12 and PF6-LT14 depositional settings. According to Flügel (2004; p. 500) branching stromatoporoids are frequently swept into other environments by storms. Furthermore, local erosive bases at the boundaries between PF6-LT14 and PF6-LT12 and the good-sorting of dendroid stromatoporoids indicate an important increase of water energy enabling the reworking and landward transport of stromatoporoids patch-reef within a location characterizing PF6-LT14.

PF6-LT13: Algal microbial boundstone (Figs. 8e-h and 9a-b)

This microfacies occurs in the lower portion of the Mont d'Haurs Fm and overlies beds formed by PF6-LT14. It is mainly characterized by the numerous occurrences of micritic tubular structure (diameter of tubes is around 0.2 mm), the abundance of cement and the common occurrence of peloids arranged in a clotted fabric. Locally, ostracods (showing thick-walled valves) and recrystallized worm tubes occur. Thin micritic tubes are usually surrounded by a fringe of fibrous cement (Fig. 8f-g) which fills the interparticle pores. This microfacies is also characterized by numerous stylotitic seams rich in insoluble residues locally forming a "horse tail" structure and on a larger scale an iden-supported fabric.

Interpretation:

The abundance of sparitic cement and clotted fabric is in favour to a microbial/bacterial mediation (e.g. thrombolitic fabric: "peloidal micrite", exhibiting a distinct clotted fabric; Flügel, 2004; p.86). The abundance of sparitic cement filling the interparticle pores between thin micritic walled tubes is in a favour of a relatively shallow-marine protected setting allowing the development of those thin tubes. Indeed, considering the diameter of micritic tubes (~2 mm) they would have been destroyed by any energetic event. According to a personal communication (Stjepko Golubic), diameter of these tubes are out of size range for cyanobacteria. Intercalation of this microfacies between PF6-LT14, interpreted as lagoonal restricted environment, suggests an internal evaporitic setting for this microfacies.

PF6-LT14: Laminated mudstone – peloidal grainstone (Fig. 9a-f)

One of the most specific aspect of this microfacies is the common occurrence of both wrinkled and regular laminae (Fig. 10a) underlined by a couplet of micrite alternating with fine-grained peloidal grainstone (Fig. 10b). Laminae can be arranged either in dense or sparse growth patterns (mm- to cm-sized). Within grainstone layers, sizes of peloids are relatively homogeneous although from one layer to the next it can vary substantially (0.1 to 2 mm). Mm-sized vertically pronounced fenestral fabrics (Fig. 10a) crossing lamination and fenestrae showing horizontal patterns occur in this microfacies. Dolomitization is common and when affecting the sediment, the laminae are less clearly visible. Lamination can be locally underlined by silt-sized rich quartz grains layers alternating with micritic rich layers (Fig. 9c). Occasionally, lamination displays mm-scaled protuberance (Fig. 10d) locally filled with coarse calcite cement (Fig. 10e). Issinellids and *Amphipora* fragment floating in micritic mud (Fig. 10f) and gypsum evaporitic pseudomorphes are also observed. In this microfacies, fine-grained micritic clasts grainstone layers occur locally and silt-sized quartz grains and clays are occasionally an important constituent of the sediment.

Interpretation:

The abundance of laminae (locally wrinkled), the occurrence of fenestrae and peloids and fine-grained micritic matrix characterize microbially modified sediments (Aitken, 1967). In the Middle Devonian carbonate platform of Poland, Skompski and Szulczewski (1994) interpreted similar microfacies as formed within the shallow intertidal to supratidal restricted shelf. Similar Upper Givetian sediments in Belgium are interpreted as having been deposited in extensive tidal flat complexes including channel, levee and back-levee systems (see microfacies Type 1', 2' and 3' and fig. 7 of Boulvain and Préat, 1986). Furthermore, the occurrence of laminae crossed by vertical fenestral fabric corresponding to desiccation crack and occurrence of evaporitic pseudomorph both in point to a setting temporarily subjected to emersion and an arid climate, triggering the desiccation of soft sediments. According to Scholle and Ulmer-Scholle (2003; p.6) and Purser (1980; p.98), laminae protuberances relate to th

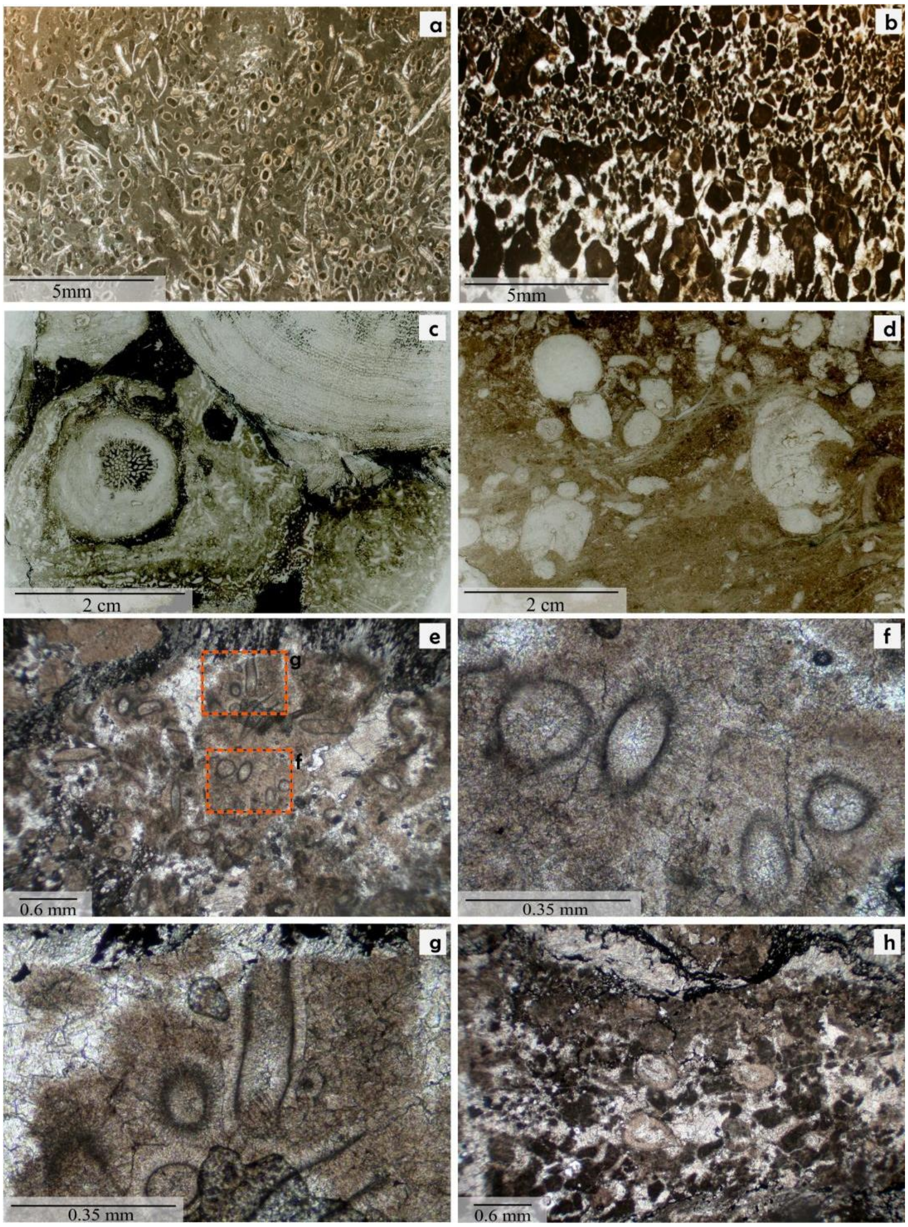

Fig. 8 *Microfacies (PF4-LT10-11, PF5-LT12) from the Givetian of the La Thure section, western Belgium. Photomicrographs of thin-sections are oriented perpendicular to the bedding.* **a** *PF4-LT10c internal restricted shelf setting: wackestone – packstone with oolites (mainly of Type 4) and shells (TUR 268, transmitted light).* **b** *PF4-LT11 internal restricted shelf setting: coarse- to fine-grained lithoclastic rudstone – grainstone (large lithoclasts are constituted of oolitic grainstone) (TUR 226a, transmitted light).* **c** *PF5-LT12 internal shelf setting: stromatoporoids rudstone (TUR 285, scanned thin-section).* **d** *PF5-LT12 internal evaporitic shelf setting: dendroid stromatoporoids rudstone (TUR 279c, scanned thin-section).* **e** *PF5-LT13 internal evaporitic shelf setting: boundstone (TUR 119, transmitted light).* **f** *PF5-LT13 internal evaporitic lagoonal setting: focus on micritic tubular structure with rims of fibrous cement (for location see inset in* **Fig. 6e***) (TUR 119, transmitted light).* **g** *PF5-LT13 internal evaporitic lagoonal shelf setting: focuse on the elongated tubular structure (note the polygonal aspect of the fibrous cement) (for location see inset in* **Fig. 6e***) (TUR 119, transmitted light).* **h** *PF5-LT13 internal evaporitic shelf: peloidal and ostracods accumulation observed within PF5-LT13 algal boundstone (TUR 123a, transmitted light).*

growth of evaporitic minerals (e.g., anhydrite) within the sediment. The rare occurrence of fauna corresponds to a hostile evaporitic environment and is characteristic of an inter- to supratidal restricted evaporitic setting.

PF6-LT15: Intraclastic rudstone – grainstone (Figs. 2d and 8g-h)

This microfacies is characterized by the mm- to cm-sized angular to rounded-elongated fenestral mudstone lithoclasts. Lithoclasts are locally surrounded by wrinkled laminae and space between lithoclasts is filled either by ooids, clay or coarse-grained sparitic cement. Pressure-solution processes produced iden-like textures.

Interpretation:

Mm- to cm-sized elongated fenestrae associated with mudstone lithoclasts, corresponding to lithified algal mats, indicate the reworking of supratidal deposits likely during an increase of water energy (e.g., storms). The wrinkled laminae surrounding lithoclasts argues for re-deposition in intertidal to supratidal settings. Oolites are likely allochthonous and derived from an oolitic sand bar located seaward (e.g., PF4-LT10a). Skompski and Szulczewski (1994; plate 49) interpreted relatively similar deposits as tide-channel breccias. This microfacies might thus be deposited within upper intertidal to supratidal location (e.g., tidal flat) and related to a change in the water energy triggering a reworking of the sediment and the transport of oolites through the PF6-LT15 depositional setting.

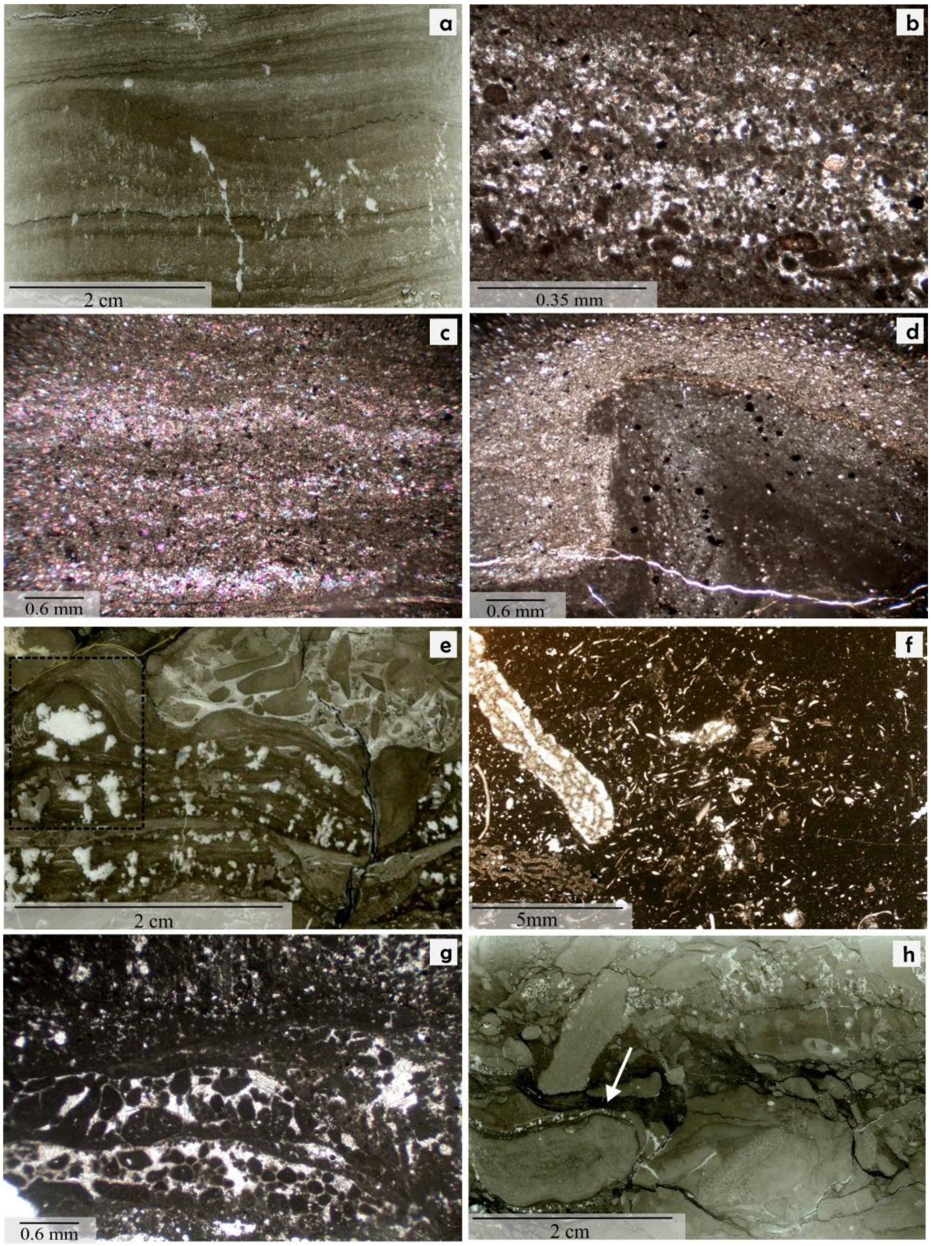

Fig. 9 *Microfacies PF5-LT14 and PF5-LT15 – inter- to supratidal internal evaporitic shelf from the Givetian of the La Thure section, western Belgium. Photomicrographs of thin-section are oriented perpendicular to the bedding.* **a** *PF5-LT14: alternation of dark and lighter laminae locally crossed by vertical fenestrae (TUR 158, scanned thin-section).* **b** *PF5-LT14: fine-grained peloidal grainstone alternating with mudstone texture (TUR 287, transmitted light).* **c** *PF5-LT14: alternation between silt-sized rich quartz and micritic rich levels (TUR 117, crossed light).* **d** *PF5-LT14: laminae marked by a well-developed protuberance (TUR 117, transmitted light).* **e** *PF5-LT14: wrinkled laminae showing stacked protuberance filled by coarse-calcite cement (note the intraclastic breccia in the upper right of the thin-section)(TUR 293b, scanned thin-section).* **f** *PF5-LT14: abundant palaeoberesellid floating in a micritic matrix (TUR 282, transmitted light).* **g** *PF5-LT15: partly reworked algal mat (TUR 120, transmitted light)* **h** *PF5-LT15: intraclastic grainstone – rudstone (note the lithoclasts surrounded by algal layer arrowed)(TUR 291d), scanned thin-section).*

***Table 1**. Synthesis of microfacies for the Givetian in the La Thure section (NW Belgium).*

Micro-facies number	Name	Main diagnostic features	Bedding, color and sedimentary structures	Depositional setting
Drowned shelf model (DR)				
DR-LT1	Brachipod-bivalve shells packstone-rudstone	Limestone with brachiopods, bivalves, gastropods, crinoids. Poorly- to moderatly-sorted. Common bioturbations	Dm-thick homogeneous dark-grey to black limestone beds	Drowned lagoon below the FWWB
Carbonate ramp model (RP)				
RP-LT1	Bioclastic mudstone to packstone	Limestone rich in insoluble residues commonly dolomitized. With poorly-preserved crinoids, brachiopods and unidentified shells,gastropods, ostracods, bryozoans, worm tubes, tabulate corals and stomatoporoids	Cm- to dm-thick black to dark-grey argillaceous beds	Mid- to distal-ramp below the FWWB with storm deposit occurrences
RP-LT2	Crinoidal packstone-grainstone	Coarse-grained crinoids (with micritized rims), gastropods (with common micrite filling internal molds) and bioturbations	Cm- to dm-thick argillaceous black to dark-grey limestone beds	Mid- to distal-ramp below the FWWB with storm deposit occurrences
Carbonate shelf model (PF)				
Facies belt 1: Biostrome and fore-reef shelf				
PF1-LT1	Open-marine bioclastic wackestone-packstone	Crinoids, brachiopods, ostracods, trilobites, bryozoans, Tentaculitids and local debris of branching tabulate and rugose corals, and stromatoporoids	Dm-thick coarse-grained dark-blue limestone beds	Open-marine setting located below the FWWB slightly influenced by reefal-construction (barrier-reef or patch-reef)
PF1-LT2	Coral-Stromatoporoid rudstone and floatstone	Dm-sized stromatoporoids (laminar and bulbous), solitary rugose corals, branching tabulate corals, crinoids, brachiopods, trilobites	Coarse-grained dark-blue to dark-grey limestone with large and broken reef-builders in non-living position	Open-marine setting located below the FWWB strongly influenced by reefal construction (barrier-reef or patch-reef)

Facies belt 2: Bioclastic shoals				
PF2-LT3	Calcimicrobial bio-lithoclastic grainstone	*Girvanella*, *Sphaerocodium,* gastropods, rare and poorly-preserved brachiopods, worm tubes, stromatoporoids	Dm-thick dark-blue to dark-grey limestone beds	Open-marine temporarily agitated setting located in the internal shelf margin
PF2-LT4	Peloidal – lithoclastic grainstone with gastropods and mud-coated grains	Peloids and micritic lithoclasts, gastropods, brachiopods, crinoids, ostracods and rare tabulate corals and bryozoans	Dm-thick dark blue to dark-grey limestone	Peloid bars within the FWWB at the of internal shelf margin
Facies belt 3: Internal shelf with good circulation				
PF3-LT5	Mudstone to packstone with lithoclastic - brachiopods rudstone-grainstone layers/pockets	Brachiopod shells, thick-walled ostracods, gastropods, worm tubes and micritic lithoclasts within grainstone	Dm-thick dark-blue limestone	Internal shelf with open-water circulation located under the FWWB but likely subject to tides or storm flow
PF3-LT6	*Magnella* shell grainstone and rudstone	*Magnella* shells and peloids	Pluri cm thick beds	Storm deposits within an internal shelf setting
PF3-LT7	Stromatoporoid rudstone	Broken bulbous and dendroid stromatoporoids, branching tabulate, fasiculate rugose corals, *Sphaerocodium* and frequent palaeosiphonocladales	Dm-thick dark-blue beds	Setting with limited connection to fully-marine setting
PF3-LT8	Palaeosiphonocladales wackestone – packstone	Abundance of issinellid and palaeoberesellid algae, brachiopod shells, ostracods and *Grivanella* oncoids	Dm-thick dark-blue beds	Subtidal setting in the vicinity of palaeosiphonocladale grass
PF3-LT9	Burrowed calcisphere mudstone	Vertical burrow filled by calcite	Dm-thick dark-blue beds	Protected setting below the FWWB
PF3-LT10a	Oolitic grainstone-packstone	Type 3 ooids and locally Type 1 of Strasser (1986)	Cm- to dm-sized light- to dark-grey bed	Oolitic shoal developed intermittently agitated water in internal shallow platform setting
Facies belt 4: Internal restricted shelf				
PF4-LT10b	Oolitic peloidal grainstone-packstone	Type 2 and 4 ooids of Strasser (1986)	Cm- to dm-sized light- to dark-grey bed	Lagoonal setting with calm- to moderately-agitated water energy

PF4-LT10c	Oolitic lithoclatic grainstone-packstone	Type 4 ooids of Strasser (1986)	Cm- to dm-sized light- to dark-grey bed	Lagoonal setting with local higher energy-event
PF4-LT11	Lithoclastic rudstone	Peloidal and oolitic grainstone lithoclasts	Cm- to dm-sized light- to dark-grey bed	Lagoonal setting in the vicinity of PF3-LT10a
Facies belt 5: Evaporitic internal shelf				
PF5-LT12	Dendroid stromatoporoid rudstone – flaotstone	*Stachyodes* and *Amphipora*, *Girvanella*, *Renalcis* lumps and stromatoporoids	Pluri-dm-sized beds with local erosive base	Reworked stromatoporoids patch-reef in internal setting
PF5-LT13	Algal microbial boundstone	Micritic tubular structures, clotted fabric, ostracods and worm tubes	Cm- to dm-sized beds	Shrub-like structure in quiet shallow-marine internal setting
PF5-LT14	Laminated mudstone - peloidal grainstone-packstone	Alternation of peloidal grainstone and mudstone layer or light and darker micritic laminae with locally well-spread silt-sized quartz	Dm-thick beds	Tidal-channel and levees bordering channel and intertidal pounds in supratidal setting
PF5-LT15	Intraclastic rudstone - grainstone	Cm-sized mudstone and grainstone intraclasts, oolite and sparitic cement	Dm-thick yellow-earth beds	Reworking in tidal-channel setting

Fromelennes-Flohimont section (FF; Figs. 10-14, Tab. 2)

Drowned carbonate shelf model: Microfacies DR

DR-LT1: Mudstone and wackestone with densely-packed brachiopod-bivalve shells packstone-rudstone levels and pockets (Fig. 4)

This microfacies characterizes the upper part of the Fromelennes Fm and its description is similar to the description made for the La Thure section. However, in the Fromelennes-Flohimont road section, this microfacies exposes cm-thick layers corresponding to mudstone and wackestone with small amount of bioclasts. The combination of observation from Fromelennes-Flohimont and La Thure localities allows to implement description of this microfacies.

Ramp model: Microfacies RP

RP-FF1: Palaeosiphonocladale and shell-rich bioclastic wackestone-packstone (Fig. 10a-d)

Main characteristics of this microfacies are the common occurrence of shells such as brachiopods, gastropods, trilobites (Fig. 10a) and abundance of palaeosiphonocladales such as issinellid and palaeoberesellid (Fig. 10b-c). Widespread bioclastic hash (i.e. unidentifiable fine-grained organisms) is an important characteristic of this microfacies. The organisms observed are commonly broken, showing moderately-rounded shape and displaying a size varying from 0.5 to 2 cm. Algae show a range between 0.1 and 0.4 cm (entire longitudinal section), are poorly-preserved and recognized by the yellowish color of their thallus, which is usually bowed. Locally, internal part of the thallus is filled by a darker micrite contrasting with the lighter surrounding micrite. In this case, it is common to observe infra-mm sized micritic lithoclasts. Other allochems are *Girvanella* lumps, peloids, calcisphere, bryozoan, wackestone-packstone intraclasts and rare branching tabulate corals (*Hilaepora*; Fig. 10d) and stromatoporoid debris. Preservation of bioclasts varies: crinoids often show pitting and micritic rim while gastropods are locally encrusted by spongiostromate. Locally, mm- to pluri-mm-sized pockets or grainstone layers with sparitic cement including peloids, gastropods (mold filled by micrite), micritic clasts and mud-coated grains occur (this is similar to the RP-LT2 defined for the La Thure section). Densely-packed areas where shells are oriented parallel to the bedding can be seen. In this microfacies, bioturbations are common and usually underlined by the circular-shape and the reorganization of bioclasts cemented by sparite. A significant character of this microfacies is also the occurrence of mm- to cm-thick rich argillaceous horizons and occurrence of disseminated silt-sized quartz. Dolomitization is also common.

Interpretation:

The wackestone and packstone texture and the biotic influence from both semi-restricted (e.g. issinellid, palaeoberesselid; Mamet, 1991) and more open marine setting (e.g., crinoids) indicate a depositional setting with two biotic influences. The general poor-sorting of this sediment and the micritic matrix attest of a deposition in a relatively quiet setting, but the occurrence of locally well-sorted shells and bioclastic layers as well as intraclasts are in favor of high-energy events such as storm waves. Thus, this sediment is likely deposited within the storm wave base (SWB) close to the fair weather wave zone (FWWZ). The rare occurrence of tabulate corals and stromatoporoids advocates either for a setting located out of reefal influence or to the scarcity of reefal structure. In such carbonate setting, the local occurrence of siliciclastic materials (clay, mica and silt-sized quartz) demonstrates the land to basinwards supply of detrital material and low-energy water condition enabling the settlement of these particles. The locally abundant argillaceous materials and the dissemination of silt may indicate a direct connection with the landmass bordering this marine setting.

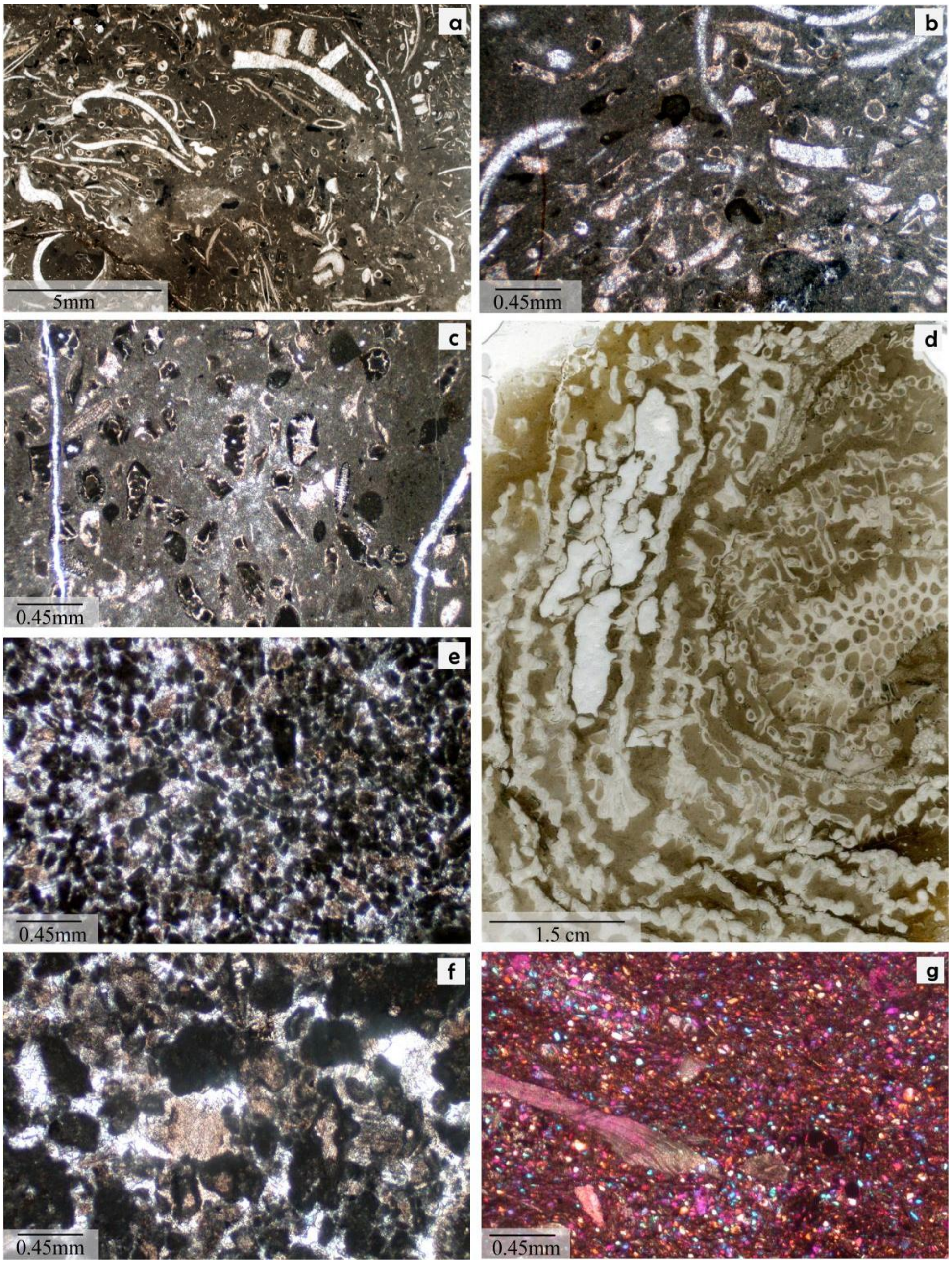

Fig. 10 *Microfacies RP-FF1 and RP-FF2a-b outer- to mid-ramp settings, and PF1-FF1 off-reef shelf belt. Givetian sediments of the Fromelennes-Flohimont section, southern Belgium. Photomicrographs of thin-sections are oriented perpendicular to the bedding. Numbers preceded by "FRO" correspond to bed numbers.* **a** *RP-FF1: shell-rich bioclastic wackestone-packstone (FRO 140, transmitted light).* **b** *RP-FF1: close-up on palaeosiphonocladale in a packstone texture (FRO 129, transmitted light).* **c** *RP-FF1: thallus of palaeosiphonocladale filled by a darker micrite contrasting with the lighter surrounding micrite (FRO 89, transmitted light).* **d** *RP-FF1: branching tabulate corals Hilaepora characteristic of the Terres d'Haurs Fm (FRO 151, scanned thin-section).* **e** *RP-FF2a: fine-grained peloidal grainstone (FRO -3, transmitted light).* **f** *RP-FF2b: coarse-grained peloidal and crinoidal grainstone (FRO -2, transmitted light).* **g** *PF1-FF1 off-reef shelf: brachiopods and rare crinoids in a argillaceous matrix rich in silt-sized quartz grains (FRO 219, crossed nicols with gypsum blade).*

RP-FF2: Peloidal grainstone (Fig. 10e-f)

This microfacies is characterized by the abundance of peloids, the grainstone texture and a general good-sorting of the allochems. Based on the size and shape of peloids and occurrence of palaeosiphonocladales we divided this microfacies into two groups: (1) fine-grained peloidal grainstone and (2) peloidal bioclastic grainstone with palaeosiphonocladales.

RP-FF2a: Fine-grained peloidal grainstone (Fig. 10e)

This microfacies is mainly characterized by the abundance of fine-grained and well-rounded peloids (size ranging between 0.1 and 0.2 mm), very good-sorting and the occurrence of local planar and oblique lamination. Other allochems show a variable preservation state ranging from moderately-preserved to poorly-preserved and intensively micritized crinoids, brachiopods, gastropods, palaeosiphonocladales and unrecognized bioclasts. Their size is similar to or slightly bigger than peloids size. Planar and oblique laminations are underlined by mm- to cm-thick layers enriched in crinoids, brachiopods, ostracods and trilobites. These layers are oblique to the bedding and locally correspond to cross-stratification. A laminar fabric underlined by the alternation of darker and lighter levels may occur locally. The cement of this grainstone is microsparitic

Interpretation:

This abundance of well-rounded peloids and the good sorting of this sediment indicate a setting where water energy is high, likely within the FWWB. Furthermore, the local occurrence of hummocky cross stratification observed at the outcrop scale and planar and oblique laminations attest of a setting influenced by storms. The grainstone texture coupled with the preservation of the sedimentary structures and bioclastic layers suggest a location around the FWWB (Burchette and Wright, 1992). Peloids probably have a shallow-water low-energy origin (Tucker and Wright, 1990). Layers enriched in crinoids, brachiopods in a grainstone texture correspond to a concentration of bioclasts in relation with storms. In this microfacies, crinoids and brachiopods (open-marine biota) are associated with palaeosiphonocladales and gastropods (semi-restricted to marine biota). The occurrence of a mixture of bioclasts from open-marine and semi-restricted water also suggests a location halfway between semi-restricted and open-water environment. This microfacies could correspond to peloidal sand bar in a homoclinal ramp setting.

RP-FF2b: Peloidal bioclastic grainstone with palaeosiphonocladales (Fig. 10f)

The main difference with RP-FF2a is the extensive occurrence of palaeosiphonocladales such as issinellid, the abundance of peloids showing various sizes (between 0.1 and 0.4) and shapes (e.g., lithic peloid; Flügel, 2004) and the higher occurrence of preserved bioclasts such as crinoids, brachiopods, mollusks and bryozoans. Micritization of bioclasts is also important in this microfacies but relics of former bioclasts are preserved locally. The size of bioclasts varies from 0.1 to 1 mm (locally pluri-mm in size). Rare reef-builders debris such as tabulate corals and stromatoporoids occur.

Interpretation:

Abundant occurrence of issinellids likely indicates lagoonal or at least restricted marine environment. Indeed, according to Mamet and Préat (1986) palaeosiphonocladales occur in various shallow-water setting but they are mostly associated with semi-restricted environment such as lagoons. An abundance of lithic peloids and bioclasts such as crinoids, gastropods and bryozoans showing a better preservation level than in the RP-FF2a, indicates a more protected setting compared to RP-FF2a and probably closer to palaeosiphonocladales meadows considering their abundance. This microfacies must be located in a more proximal location than RP-FF2a.

Carbonate shelf model: Microfacies PF

Facies belt 1: Fore-reef shelf and off-reef

PF1-FF1: Argillaceous crinoidal – brachiopods mudstone (Fig. 10g)

This microfacies only occurs in the Mont d'Haurs Fm. Moreover, they are collected from deeply weathered and argillaceous beds, which are barely outcropping. It overlays beds characterized by microfacies PF2-LT2 and PF2-FF3 and underlays microfacies PF6-LT12 (internal restricted belt). Microfacies PF1-FF1 is mainly characterized by a mudstone texture and local occurrence of crinoids, brachiopods and trilobites. These organisms are mm in size and show a moderate- to poor-sorting. Locally, wackestone-packstone layer showing similar faunal assemblage occur. Bioturbation is visible and is either underlined by circular reorganization of bioclasts or by a contrast of colour in relation with quartz content. The matrix is a slightly argillaceous micrite with significant dissemination (locally 30 %) of silt-sized quartz grains (Fig. 10g). According to Flügel (2004; p.74) this matrix is called "calcisiltite". Mica sheets and insoluble residue also occur commonly.

Interpretation:

The mudstone texture and the faunal assemblage attest to an open-marine environment located in a low-energy setting likely below the FWWB. The low energy setting is also attested by the occurrence of clay. Bioturbation suggests oxygenated bottom-water conditions. According to the occurrence of this microfacies overlying PF2-LT2 and PF2-FF3 and underlying PF6-LT12, it is assumed that these argillaceous crinoidal – brachiopods mudstone belongs to the shelf model.

Facies belt 2: External reef shelf and fore-reef

PF2-LT1: Open-marine bioclastic wackestone-packstone (Fig. 5e-f)

This microfacies is similar to the one described for the La Thure section

PF2-FF2: Fine- to coarse-grained crinoidal bioclastic packstone (Fig. 11a)

This microfacies occurs mainly within the uppermost part of the Terres d'Haurs Fm and in the lower part of Mont d'Haurs Fm, prior the m-thick biostromal accumulation (e.g., PF2-LT2; see Fig. 4 for an outcrop overview). It is mainly characterized by the extensive occurrence of crinoids, the common occurrence of bioclasts such as brachiopods, and the bioturbations. Crinoids display a size ranging from 0.2 to 3 mm and a poorly- to moderate-preservation (e.g. they are either broken, intensively micritized or show pitting). In order of decreasing abundance other bioclasts are brachiopods, gastropods and ostracods, bryozoans, stromatoporoids, rugose corals, *Girvanella* lumps, palaeosiphonocladales, worm tubes and trilobites. Fine-grained peloids are also recognized in the sediment with respect to the low contrast with the dark-brown micritic matrix. Gastropod remains are commonly encrusted by *Girvanella* or show their mold filled by a dark brown micrite. Bioturbations are circular, mm-sized and mainly underlined by reorganization of finely-broken unidentifiable bioclasts. From time to time, the sediment of this microfacies is affected by pressure-solution processes underlined by an iden-supported fabric and the occurrence of insoluble rich residue observed into pressure-solution seams. The matrix is micritic, pale brown in color and quartz grains occur occasionally.

Interpretation:

The large occurrence of crinoids within packstone texture intercalated into PF2-LT2 microfacies indicates a setting in the vicinity of crinoidal meadow and strongly influenced by reefal construction. The occurrence of trilobite and brachiopods suggests a fully-marine setting though gastropods, *Girvanella* and palaeosiphonocladales are rather in favor of more restricted water conditions. Occurrence of both biotic assemblages might be related to mixing due to eworking which affects the shallow-marine environment. This microfacies likely represents a crinoidal meadow flanking a fore-reef slope below the FWWB.

PF2-LT2: Coral-stromatoporoid flaotstone and rudstone (Figs. 3c, 5g and 11b)

This microfacies is similar to the one described for the La Thure section (Fig. 5g) although much thicker and better developed in the Fromelennes-Flohimont section (see Fig. 3c).

PF2-FF3: Dendroid stromatoporoid and bioclast-rich rudstone

This microfacies occurs mainly in the upper portion of the Mont d'Haurs Fm intercalated within PF2-LT2 microfacies. It is characterized by the occurrence of dendroid stromatoporoids such as *Amphipora* and *Stachyodes* embedded in a bioclastic wackestone to packstone texture showing poor-sorting. *Amphipora* are mm- to cm in size while *Stachyodes* are larger (cm to pluri-cm). Bulbous stromatoporoids are also locally clearly exposed and better preserved; they are over 1 cm in size. When the sediment is not affected by dolomitization, the space between stromatoporoids is filled by wackestone-packstone sediment rich in poorly-preserved bioclast such as crinoids, brachiopods, stromatoporoids, rugose and tabulate corals. Peloids, thick-shelled ostracods, *Girvanella* like-encruster or lumps, palaeosiphonocladales and unidentified shells are also observed. Pressure-solution processes underlined by concavo-convex contact, stylolithes and insoluble rich residue seams occur.

Interpretation:

As mentioned above (PF5-LT12), *Amphipora* and *Stachyodes* are characteristic of back-reef and lagoonal settings (Cornet, 1975; Pohler, 1998b; Wood, 2000) and their accumulation in the Belgian Givetian limestone is interpreted as enhanced by storm waves reworking lagoonal setting. In this case, a mixture of dendroid stromatoporoids with numerous open-marine organisms (e.g., reef-builders, crinoids, brachiopods), as observed in this microfacies, reflects either a seaward transport via storm wave action or the vicinity with the open-marine reefal construction or a landward transport of open-marine organisms. The second hypothesis fits with the intercalation of PF2-FF3 in PF2-LT2 reef-builders rudstone. In comparison with PF2-LT2, this microfacies must be located in location close to open-marine reefal construction, and considering the texture, deposited within the FWWZ.

Facies belt 3: Bioclastic shoals

PF3-LT4: Peloidal – lithoclastic grainstone with gastropods and mud-coated grains (Figs. 11c-d and Figs. 6c-d for La Thure equivalent microfacies)

This microfacies is similar to the one described for the La Thure section.

Facies belt 5: Internal restricted shelf

PF5-LT10b-c: Oolite lithoclastic grainstone – packstone (Figs. 11e-g and Figs. 7f-h for La Thure

This microfacies is similar to the one described for the La Thure section.

Facies belt 6: Internal evaporitic shelf

PF6-LT12: Dendroid stromatoporoid floatstone to rudstone (Fig. 12a and Figs. 2d and 8c-d for La Thure equivalent facies)

This is a similar microfacies to the La Thure section.

PF6-FF4: Micritic lithoclasts and peloidal grainstone (Fig. 12b)

This microfacies only occurs within the Fromelennes Fm. It is mainly characterized by the abundance of variously-sized and shaped peloids (e.g., lithic peloid; Flügel, 2004; p.112) and lithoclasts that also display a large range of shape and size (sub-angular to sub-rounded, and mm to pluri-cm in size). Both allochems represent up to 90% of the sediment. Lithoclasts are either micritic mudstone or peloidal grainstone. Locally a rim of fibrous calcite surrounds these allochems. Ooids and micritized ooids scattered within the sediment are observed. More rarely, these ooids are concentrated within peloidal – oolitic layers (Fig. 11g; likely allochthonous ooids). Other allochems are not common and represented by *Amphipora,* thick-shelled ostracods, calcisphere, broken brachiopod shells, unidentified conical shells and palaeosiphonocladales. Exception for some brachiopod shells, which are cm in size, most of the remaining allochems are mm in size. The cement of this sediment is sparitic and locally dolomitized; this is highlighted by the occurrence of infra-mm dolomite rhombohedra. Locally, this microfacies overlies thick layer of mudstone texture. Transition between mudstone and grainstone is either sharp or gradual. Sometime, the occurring mudstone shows circular or irregular burrows filled by peloidal grainstone (Fig. 12d). A similar microfacies was described by Boulvain and Préat (1986; Type 5) for Upper Givetian sequences in southern Belgium.

Interpretation:

Abundant lithic peloids and mudstone lithoclasts in a grainstone texture suggest intense reworking of a lithified micritic mud or micrite either by tidal flooding or storm wave. Furthermore, the limited occurrence of organisms indicates restricted environment hostile to forms of life. The local occurrence of brachiopods and *Amphipora* suggests a reworking triggered by storm capable of transporting such organisms landward. Local occurrence of PF6-FF6 underlying this microfacies indicates vicinity with inter- to subtidal ponds (see description of PF6-FF6 below). Occurrence of Type 4 ooids (Strasser, 1986) indicates restricted environment and lithic peloids with rim of calcite cement points to meteoric phreatic environment (Flügel, 2004; p.300).

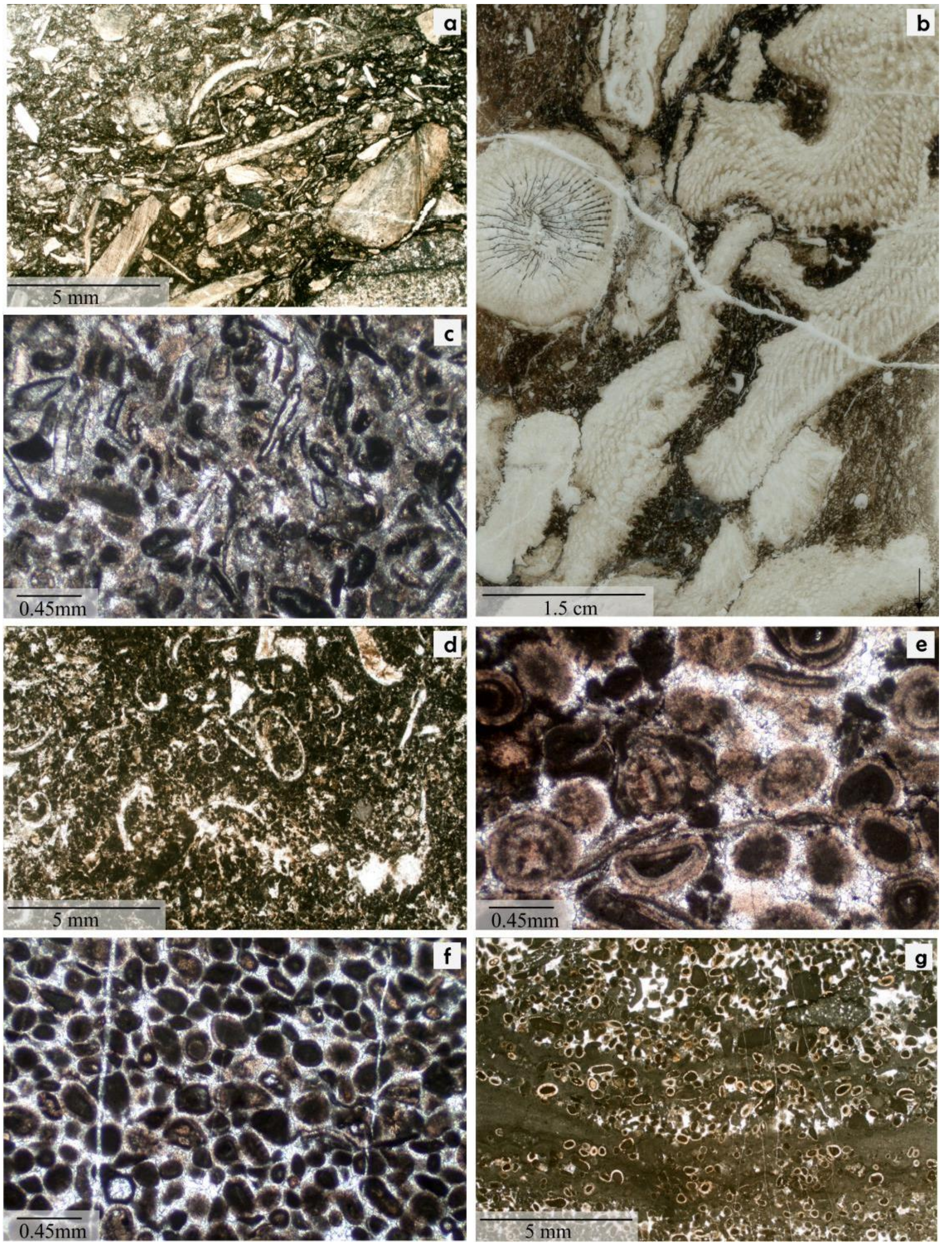

Fig. 11 *Microfacies PF2-LT2 – biostrome and fore-reef belt, PF3-LT4 – bioclastic shoals belt and PF5-LT10b-c – internal restricted shelf belt. Givetian sediments of the Fromelennes-Flohimont section, northern France. Photomicrographs of thin-sections are oriented perpendicular to the bedding. Numbers preceded by "FRO" correspond to bed numbers.* **a** *PF2-FF2: fine- to coarse-grained crinoidal bioclastic packstone (FRO 227a, transmitted light).* **b** *PF2-LT2: reef-builders rudstone showing tabulate and rugose corals (FRO 170, scanned thin-section).* **c** *PF3-LT4: mud-coated and micritized grains grainstone (FRO 177a, transmitted light).* **d** *PF3-LT4: fine-grained peloidal grainstone with gastropod shells (FRO 227d, transmitted light).* **e** *PF5-LT10b: oolite grainstone (according to Strasser (1986), oolite are mainly of Type 2 and 4) (FRO 247, transmitted light).* **f** *PF5-LT10b-c: oolitic grainstone (oolite of Type 4) (FRO 247, transmitted light).* **g** *PF5-LT10c: wackestone-packstone with oolites (mainly of Type 4) (FRO 312a, transmitted light).*

PF6-FF5: Mudstone-wackestone with green algae, ostracods and gastropods (Fig. 12c)

This microfacies occurs in the Trois-Fontaines Fm. It is characterized by a wide spectrum of texture between two end-members and by frequent occurrence of green algae such as *kamaena, triangulinella* and thick-shelled ostracods. Green algae are characterized by various preservation stages; from well- to poorly-preserved and with a size oscillating between 0.3 and 0.5 mm. They are always easily recognizable by their yellowish calcite forming thallus. Ostracods are mostly represented by thick-shelled specimens while a few thin-shelled can be found locally. Their size ranges from 0.3 to 1 mm. Other allochems are gastropods, *Amphipora*, peloids (e.g., reworked cyanobacteria mat), calcispheres, bispheres, *labyrinthoconus*, *ortonella,* irregular fenestrae and unidentifiable bioclastic hash. From time to time, irregular-shaped pockets are filled with dolomite crystals. Fenestrae are commonly mm- to cm-sized and locally feature geopetal fabric (lower part is filled by micrite while upper part by sparite). Locally, unidentifiable micro-bioclasts are spread in the micritic mud.

Interpretation:

The mudstone-wackestone texture indicates a quiet depositional setting allowing fine-grained particles to settle down. The frequent occurrence of well-preserved palaeosiphonocladales is in favor of lagoonal sedimentation (Mamet and Préat, 1986) and might result from palaeosiphonocladales bafflestone dismantling. Occurrence of other algae such as *labyrinthoconus* and *Amphipora*, thick-shelled ostracods and calcispheres confirms a lagoonal deposition for this microfacies. It is likely deposited in a subtidal location within a lagoonal setting influenced by episodic high energy event such as storm waves which are reflected by the local bioclastic hash deposition.

PF6-FF6: Mudstone

This microfacies is mainly characterized by a limited fauna and flora, the common manifestation of irregular-shaped pockets filled by peloids in grainstone texture, and the dark micritic matrix. Rare whole and dislocated ostracod shells and unidentified fine-grained bioclasts are the only organisms occurring in this micritic mud. Irregular- or circular-shaped mm- to cm-sized pockets corresponding likely to bioturbation filled by peloids in a grainstone texture commonly occur (Fig. 12d). Peloids are variously-sized and rounded in shape. The fringe of pockets is dull and it is common to observe peloids embedded in the surrounding micritic mud. Irregular and circular mm- to cm-sized fenestrae filled by sparitic cement are also occurring locally. This sediment is locally overlain by PF3-LT7 throughout sharp or gradual contact.

Interpretation:

Similar microfacies from the Upper Givetian of southern Belgium have been interpreted by Boulvain and Préat (1986; Type 4) as deposited in intertidal to subtidal pond located in an internal lagoonal setting. According to Boulvain and Préat (1986) those ponds act as sediment trap and were covered by peloidal sand and algal or lithic debris in relation with successive flooding of the tidal complex. Texture of the sediment, common occurrence of bioturbation filled by peloidal sand and the locally overlying peloidal and lithoclastic grainstone are in agreement with interpretations of (Boulvain and Préat, 1986). The cm-sized lithoclasts occurring from time to time may be the result of desiccation cracks reworking. Further, the limited occurrence of fauna and flora reflects a restricted environment hostile to live. This microfacies is thus deposited in lagoonal setting within inter- to subtidal location.

PF6-LT14: Laminated mudstone – peloidal grainstone

This is a similar microfacies to the one observed in La Thure section. However, in the Fromelennes-Flohimont section this microfacies is mainly characterized by couplets of micrite alternating with peloidal grainstone arranged in a spar growth pattern. Indeed, variability is less marked in the Fromelennes-Flohimont road section.

Within the Fromelennes-Flohimont section PF6-LT14a microfacies is dominant with microfacies PF6-FF5 and 6 while in the La Thure section PF6-FF5 and 6 are absent at time-equivalent periods. Furthermore, time-equivalent facies in the La Thure section are richer in silt-sized and quartz grains.

Facies Belt 7: Supratidal internal shelf

PF7-FF7: Palaeosoils (Fig. 12e)

At the outcrop scale this microfacies is characterized by breccia fabric constituted of angular mm- to cm intraclasts floating in argillaceous matrix. These intraclasts show a mudstone texture and a poor faunal assemblage (c.f. PF6-FF5) characterized by palaeosiphonocladales algae, ostracods and calcispheres. Peloids and mudstone lithoclasts are also observed locally. Vertical fenestrae filled by calcite follow the rim of intraclasts. The matrix is argillaceous and rich in silt-sized quartz grains. Pressure solution seams are frequent and can locally show a haematitic coating. Hematite is frequently observed within the argillaceous matrix, either as cubic or xenomorphic crystal.

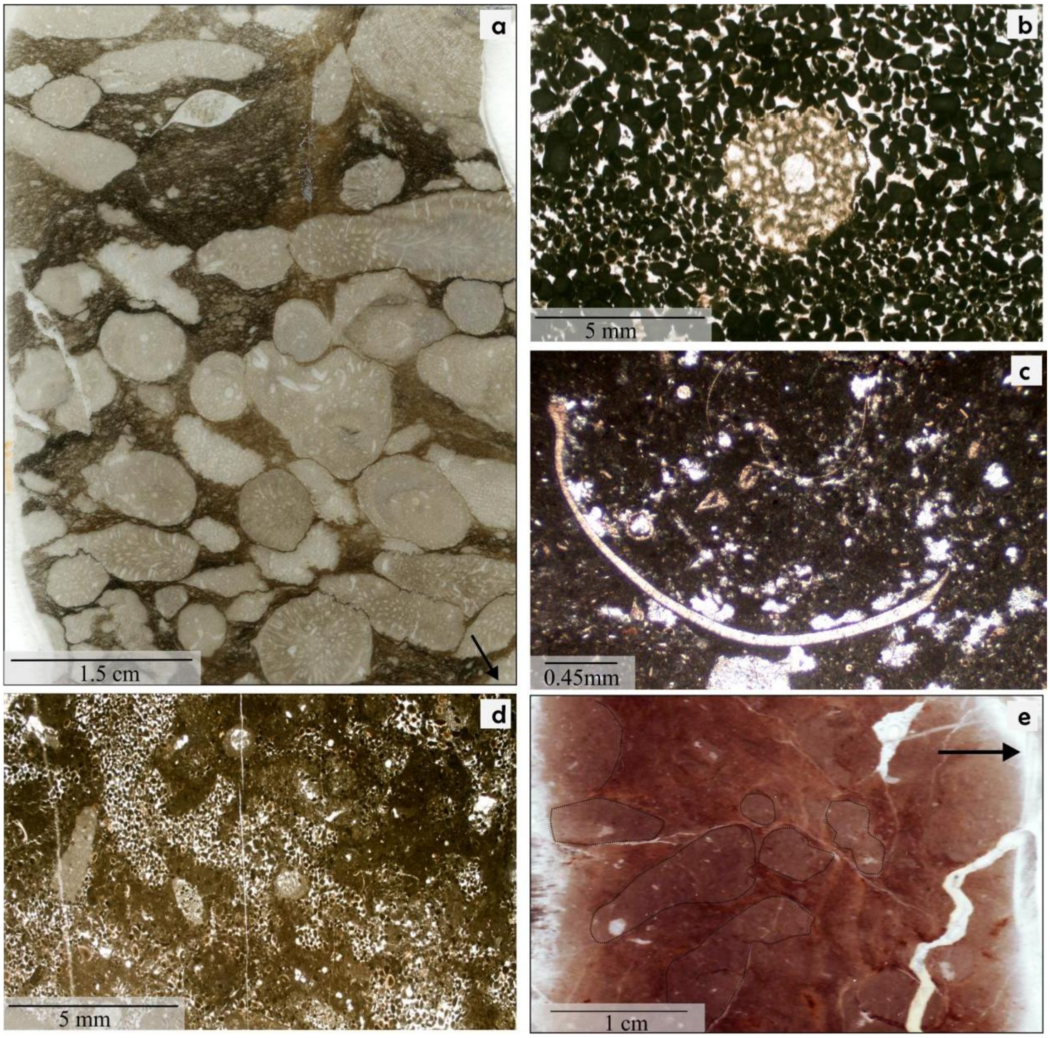

Fig. 12 *Microfacies PF6-LT12, PF6-FF4-6 internal evaporitic shelf belt and PF7-FF7 internal supratidal shelf belt. Givetian sediments of the Fromelennes-Flohimont section, France. Photomicrographs of thin-section are oriented perpendicular to the bedding. Numbers preceded by "FRO" correspond to bed numbers.* **a** *PF6-LT12: Stachyodes and Amphipora rudstone (FRO 289a, scanned thin-section).* **b** *PF6-FF4: micritic lithoclasts and peloidal grainstone with normal section of an Amphipora in the center of the photomicrograph (FRO 313b, transmitted light).* **c** *PF6-FF5: microbioclastic mudstone and wackestone showing a thick-shell of ostracod (leperditia) and numerous fenestrae filled by calcite (FRO 40, transmitted light).* **d** *PF6-FF6: densely bioturbated mudstone with bioturbations filled by a peloidal grainstone texture (FRO 299a, transmitted light).* **e** *PF7-FF7: red clay showing numerous occurrence of mm- to cm-sized intraclast floating in the matrix (FRO 39a, transmitted light).*

Interpretation:

The mudstone texture, the typical restricted fauna and the occurrence of intraclasts indicate an inter- to supratidal setting similar to the one described for PF6-LT15. According to Bhattacharyya and Chakraborty (2000), an abundance of argillaceous materials filling space between the intraclasts is characteristic of illuviation processes specific to palaeosoils. Furthermore, the breccia fabric is a common characteristic of palaeosoils (Tucker and Wright, 1990).

Tab. 2 *Synthesis of microfacies for the Givetian in the Fromelennes-Flohimont road section (N France).*

Micro-facies number	Name	Main diagnostic features	Bedding, color and sedimentary structures	Depositional setting
Drowned shelf				
DR-LT	Brachipod-bivalve shells packstone-rudstone	Limestone with brachiopods, bivalves, gastropods, crinoids. Sediment is poorly- to moderatly-sorted and bioturbations are common	Decimetre thick homegeneous dark-grey to black limestone beds	Drowned lagoonal setting above the FWWB
Homoclinal ramp				
RP-FF1	Palaeosiphonocladale and shell-rich bioclastic wackestone-packstone	Abundance of palaeosiphonocladales and crinoids. Common occurrence of brachiopods, gastropods, trilobiltes. Abundant bioclastic hash	Cm- to dm-thick fine-grained beds	Mid- to distal-ramp below the FWWB with storm deposits
RP-FF2a	Fine-grained peloidal grainstone	Coarse-grained crinoids (with micritized rims), gastropods (with common micrite filling internal molds) and bioturbations	Cm- to dm-thick argillaceous black to dark-grey limestone beds	Mid- to distal-ramp below the FWWB with storm deposits
RP-FF2b	Peloidal bioclastic grainstone with palaeosiphonocladales	Abundance of peloids and palaeosiphonocladaes within a grainstone texture	Cm- to dm-thick fine-grained beds	Mid-ramp within the FWWB
Rimmed shelf				
Facies belt 1: Fore-reef shelf and off-reef				
PF1-FF1	Argillaceous crinoida - brachiopods mudstone	Crinoids, brachiopods and trilobites. Slightly argillaceous micrite rich in silt-sized quartz grains and local mica sheets	Strongly weathered argilaceous limestone	Fore-reef to off-reef setting below the FWWB
Facies belt 2: marginal reef and fore-reef shelf				
PF-LT1	Open-marine bioclastic wackestone-packstone	Crinoids, brachiopods, ostracods, trilobites, bryozoans, *tentaculitids* and local debris of branching tabulate and rugose corals, and stromatoporoids	Dm thick coarse-grained dark-blue limestone beds	Open-marine setting located below the FWWB and influenced by reefal-construction (barrier-or patch-reef)

PF2-FF2	Fine- to coarse-grained crinoidal bioclastic packstone	Abundant large-sized crinoids, common brachiopods and bioturbations, ostracods, peloids, gastropods, bryozoans, rugose corals, girvanella lumps, trilobites	Dm-thick coarse-gained beds	Crinoidal meadow flanking fore-reef slope below FWWB
PF2-LT2	Coral-stromatoporoid rudstone and floatstone	Dm-sized stromatoporoids (laminar and buldous), solitary rugose corals, bracnhing tabulate corals, crinoids, brachiopods, trilobites	Coarse-grained dark-blue to dark-grey limestone with large and broken reef-builders in non-living position	Open-marine setting located below the FWWB in the vicinity of reef
PF2-FF3	dendroid stromatoporoid and bioclast-rich rudstone	*Stachyodes, Amphipora* and open-marine bioclasts such as brachiopods, *crinoids.* Rugose and tabulate corals, peloids, grivanella and palaeosiphonocladales	Dm-thick coarse-gained beds with visible reef-builder organisms	Fore-reef open-marine setting influenced by internal shelf setting
Facies belt 3: marginal shelf sand shoals				
PF3-LT4	Peloidal – lithoclastic grainstone with gastropods and mud-coated grains	Peloids and micritic lithoclasts, gastropods, brachiopods, crinoids, ostracods and rare tabulate corals and bryozoans	Dm-thick dark blue to dark-grey limestone	Peloid bar in within the FWWB
Facies belt 5: internal restricted shelf				
PF5-LT10	Oolite lithoclastic grainstone – packstone	Type 4 ooids of Strasser (1986)	Cm- to dm-sized light- to dark-grey bed	lagoonal setting with local higher energy-event
Facies belt 6: Internal evaporitic - brackish shelf				
PF6-LT12	dendroid stromatoporoid floatstone to rudstone	*Stachyodes* and *Amphipora*, *Girvanella*, *Renalcis* lumps and stromatoporoids	Pluri-dm-sized beds with local erosive base	Dendroid stromatoporoids patch-reef reworked in lagoonal setting
PF6-FF4	Micritic lithoclast and peloidal grainstone	Abundance of variously-shaped and sized peloids and lithoclasts (micritic or peloidal grainstone. Locally, *Amphipora, ostracods, calcisphere, allocthtonous ooids*	Dm-to pluri dm-sized beds	Tidal channel in the vicinity of intertidal pond and *Amphipora* patch-reefs
PF6-FF5	Mudstone-wackestone with green algae, ostracods and gastropods	*Abundance of kamaena, triangulinella and* ostracods. Locally gastropods, *labyrinthoconus*, *Amphipora, peloids, calcisphere,* ortonella and fenestrae	Cm- to dm-thick beds	Evaporitic lagoonal setting under the FWWB

PF6-FF6	Mudstone	Limited flora and fauna, bioturbation filled with peloids and rare ostracods	Dm-thick beds	Evaporitic intertidal ponds
PF6-LT14	laminated mudstone – peloidal grainstone	Alternation of peloidal grainstone and mudstone layer or light and darker micritic laminae with locally well-spread silt-sized quartz	Dm-thick beds	Tidal-channel and levees bordering channel and intertidal pounds in supratidal setting
Facies belt 7: Supratidal shelf				
PF7-FF7	Palaeosoils	Intraclast in argillaceous matrix. Intraclasts are mudstone in texture and show palaeosiphonocladale, ostracods, calciphere	Dm-thick bed showing brecciated fabric	Palaeosoils in internal supratidal shelf setting

Summary of microfacies interpretation: palaeoenvironmental model (Fig. 13 and 14)

Field and petrographic analyses have led to the definition of eighteen microfacies for the La Thure section and seventeen for the Fromelennes-Flohimont section. A summary of the main features and interpretations characterizing these two sections is available in Tables 1 and 2. Microfacies occurring throughout both La Thure and Fromelennes-Flohimont sections are an outstanding example of the wide range of depositional settings that shaped a shallow carbonate platform setting during the early- to late-Givetian time. All, these microfacies represent different types of carbonate platform and show a remarkable evolution through the early- to late-Givetian times. Following the definition of Read (1985) for carbonate platform models, we have distinguished three main platform profiles for the Belgian Givetian deposits: (1) a homoclinal ramp; (2) a rimmed-shelf; (3) a drowned shelf. Repartition of the microfacies through the ramp and the rimmed-shelf models are synthetized in Figs. 13 and 14.

The establishment and differentiation of the three sedimentological models is based on the combination of field, microfacies criteria (e.g., marked lithological changes, faunal assemblage, matrix nature, terrigenous content and sediment texture) and an abundant literature mentioned through the previous sections. A major criterion for the establishment of the rimmed shelf model during the middle Givetian is the significant occurrence of biostromal deposits in the Fromelennes-Flohimont section (western margin of the DS). These deposits were interpreted as having originated from a barrier-reef (Poulain, 2006; Boulvain et al., 2009).

The carbonate ramp model can be divided into an inner-ramp, a mid-ramp and an outer-ramp. Bioclastic mudstone to packstone (RP-LT1) and crinoidal packstone – grainstone (RP-LT2) characterize the outer-ramp setting and are interpreted as being deposited within a SWB location. Palaeosiphonocladale and shell-rich bioclastic wackestone – packstone (RP-FF1) is deposited in an intermediate location between the mid- and the outer-ramp setting. The fine-grained peloidal grainstone (RP-FF2a) and the peloidal bioclastic grainstone with palaeosiphonocladale (RP-FF2b) are characteristic of the mid-ramp depositional setting. Inner-ramp deposits are lacking in both sections. For the rimmed shelf profile the situation is more complex. Indeed, in order to underline the diversity of depositional settings we have divided this profile into seven facies belts (PF1-PF7). These belts extend from an off-reef to an internal supratidal shelf setting with local palaeosoil development. Argillaceous crinoidal – brachiopods mudstone (PF1-FF1) represent the most distal setting defined for this shelf model. Open-marine bioclastic wackestone-packstone (PF2-LT1), fine- to coarse-grained crinoidal bioclastic packstone (PF2-FF2), coral-stromatoporoid rudstone and floatstone (PF2-LT2) and dendroid stromatoporoids and bioclast-rich rudstone (PF3-FF3) represent the biostromal to the fore-reef portion of the shelf (PF2). Calcimicrobial bio-lithoclastic grainstone (PF3-LT3) and peloidal – lithoclastic grainstone with gastropods (PF3-LT4) correspond to sediments that are deposited in the bioclastic shoals belt, developed at the margin of the shelf interior (PF3). In a landward location, the internal shelf with fair circulation belt (PF4) is characterized by a large set of microfacies: a) mudstone to packstone with lithoclastic-brachiopods rudstone – grainstone layers (PF4-LT5), b) *Magnella* shell grainstone and rudstone (PF4-LT6), c) stromatoporoid rudstone (PF4-LT7), d) palaeosiphonocladales wackestone – packstone (PF4-LT8) and burrowed mudstone (PF4-LT9) and e) oolitic peloidal grainstone – packstone (PF4-LT10a). Oolitic lithoclastic grainstone – packstone (PF5-LT10b), oolitic shells packstone and wackestone (PF5-LT10c) and the lithoclastic rudstone (PF5-LT11) characterize the internal restricted shelf belt. Dendroid stromatoporoids rudstone-floatstone (PF5-LT12), algal microbial boundstone (PF5-LT13), micritic lithoclast and peloidal grainstone (PF6-FF4), mudstone-wackestone with green algae, ostracods and gastropods (PF6-FF5), laminated mudstone – peloidal grainstone (PF6-LT14) and intraclastic rudstone – grainstone (PF6-LT15) correspond to the evaporitic internal shelf belt (PF6). Palaeosoils (PF7-LT16) represent the most proximal setting of the rimmed-shelf (PF7). The drowned carbonate shelf model is characterized by mudstone and wackestone with densely-packed brachiopod-bivalve shell levels (DR-LT1). Microfacies stacking patterns drawn for the Givetian sequences in La Thure and Fromelennes-Flohimont sections permit recognition of respectively five (III-VII) and seven (I-VII) main depositional intervals (Fig. 14 and Fig. 15).

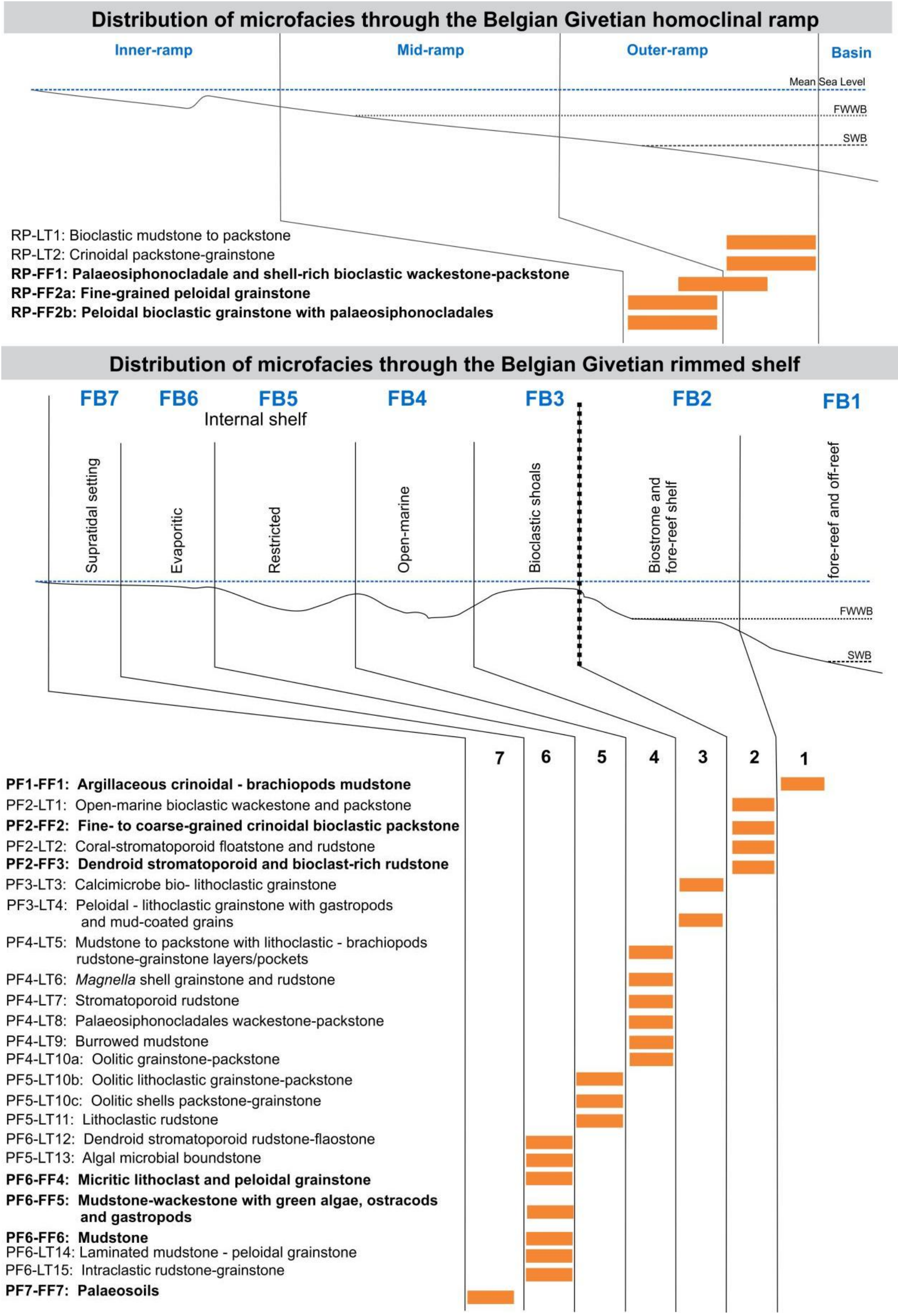

Fig. 13 *Synthetic distribution of microfacies from La Thure and Fromelennes-Flohimont along the homoclinal ramp and the rimmed shelf models.*

4.3 Magnetic susceptibility (Figs. 14, 15 and 17)

In order to apply magnetic susceptibility (MS) as a palaeoenvironmental proxy or as a tool for correlation, it is necessary to assess whether the MS signal reflects primary depositional conditions or secondary post-depositional imprint (synthesis in Da Silva et al., 2013). This assessment is imperative in this case as Devonian rocks in Belgium underwent a remagnetization event driven by the Variscan orogeny (Zegers et al., 2003; Zwing et al., 2005). In a recent study dedicated to the origin of the MS signal in Devonian sections of Belgium, (Da Silva et al., 2012, 2013) established that the MS signal is mainly carried by fine grained PSD magnetite formed during this remagnetization event. Nevertheless, Da Silva et al. (2013) also demonstrated that four of on six Devonian outcrops still reflected variations of detrital inputs as pointed out by the relatively good relationship between MS and siliciclastic input proxies such as Ti, Zr, Al and Si. Similar results on the Devonian of western Belgium were recently published by Pas et al. (2014a).

Based on ~1200 samples (sampling interval of about 0.25 and 0.45 cm depending outcrop conditions), we have drawn a magnetic susceptibility curve for the La Thure and the Fromelennes-Flohimont sections (Figs. 14-15). As synthetized in Fig. 17, the MS curve of each section exposes similar trends and events for the assumed time-equivalent deposits. Considering to these similarities, each MS curve is divided into several magnetic susceptibility units (MSU) which are separated by comparable increases and decreases of the MS average value. The Fromelennes-Flohimont section, which covers a stratigraphic interval extending from *Polygnathus hemiansatus* to *Polygnathus disparilis/Palmatolepis falsiovalis* Zones, contains eight MSU (MSU-I - MSU-VII). The La Thure section is covering a shorter stratigraphic interval (from *Polygnathus rhenanus/varcus* to *Polygnathus disparilis/Palmatolepis falsiovalis* Zones), contains the time-equivalent MSU-III to MSU-VII.

Description of the magnetic susceptibility curves

La Thure section: The MS values for the Lower – Upper Givetian part of the La Thure section range from -5.64 $x10^{-9}$ to 2.97 $x10^{-7}$ m^3/kg with an average value of 4.15 $x10^{-8}$ m^3/kg. The entire MS curve provided for the Givetian of the La Thure section can be divided into six main MS units (MSU-III - MSU-VII; Fig. 14). A vertical dotted line indicates the average MS value for each MSU on Figure 10. The six main MS units correspond to the sedimentary intervals established from the microfacies curve. The THR Fm locally shows fairly high values (1.5 $x10^{-7}$ m^3/kg) and an average close to 1 $x10^{-7}$ m^3/kg (MSU-III). The overlying MHR Fm records the lowest average MS value (0.2 $x10^{-7}$ m^3/kg; MSU-IV) and is locally punctuated by peaks reaching 1.3 $x10^{-7}$ m^3/kg. In this internal shelf setting MS values are homogeneous and relatively low. In the upper section, within the base of the FRO Fm, MS value increases and shows an average of 0.75 $x10^{-7}$ m^3/kg (MSU-V). Locally, peaks reaching 1 $x10^{-7}$ m^3/kg also occur. The middle portion of the FRO Fm, Interval IV, shows lower mean values (0.3 $x10^{-7}$ m^3/kg; MSU-VIa) but, throughout the upper part of the FRO Fm (upper part of the Unit 2) these values increase rapidly and reach 3 $x10^{-7}$ m^3/kg. Within this portion, MS values oscillate strongly between 0.7

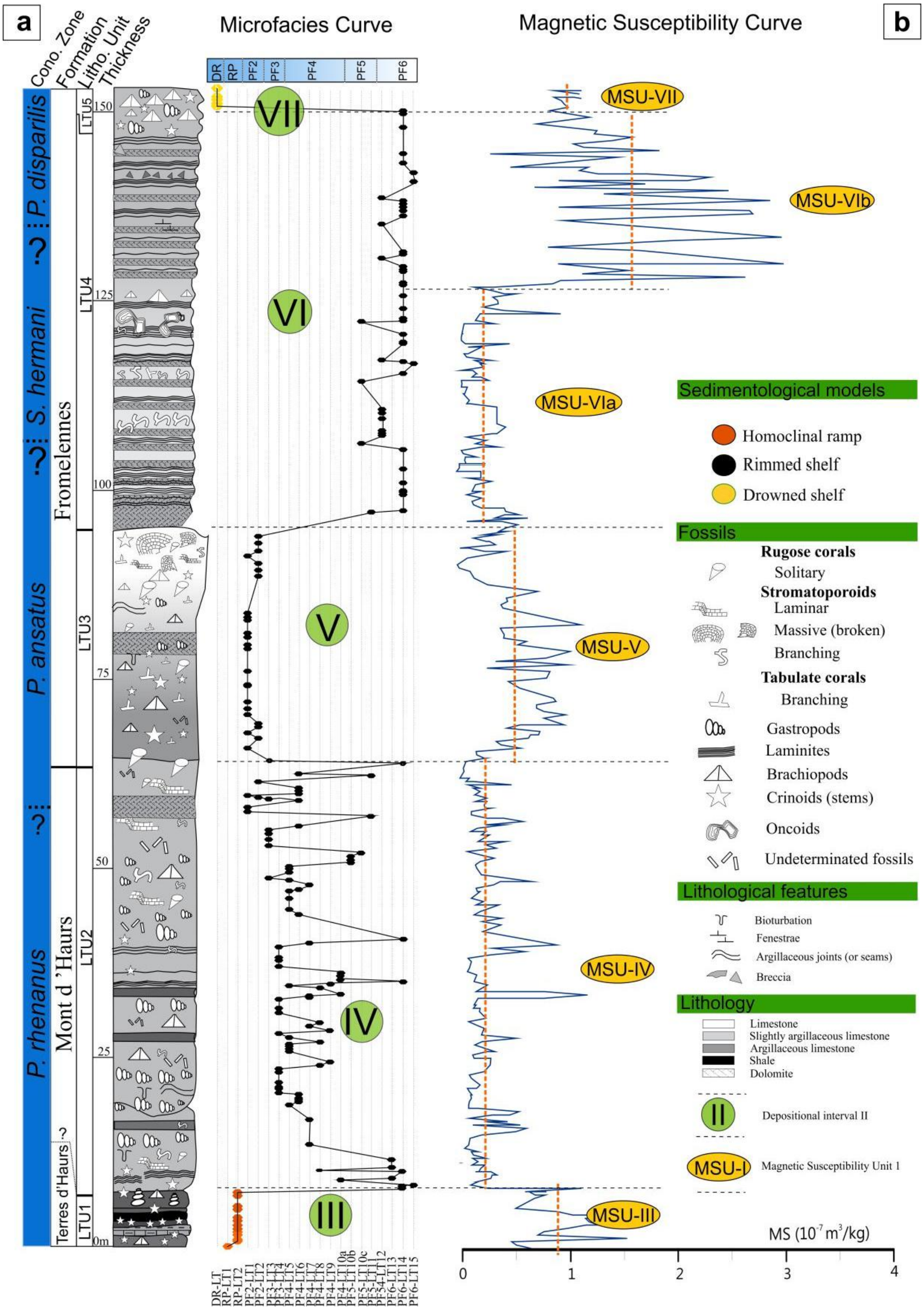

Fig. 14 a *Schematic sedimentological log showing formations, lithological units (LTU1-LTU5) and microfacies curve with the five main depositional intervals (III-VII; intervals are separated by horizontal dotted lines).* **b** *Magnetic susceptibility evolution showing the six main magnetic susceptibility Units (MSU-III to MSU-VII). Vertical dotted lines correspond to average MS values for each MS interval. Legend is also in use for the Figs. 15 and 16.*

and 3 x10^{-7} m^3/kg (MSU-VIb). Then they decrease to reach intermediate values of 0.9 x10^{-7} m^3/kg (MSU-VII) within the uppermost portion of the FRO Fm corresponding to Unit 3.

Fromelennes-Flohimont section: MS values for the Early – Late Givetian Fromelennes-Flohimont section record extend MS signal variations that range from -5.64 x10^{-9} to 4 x10^{-7} m^3/kg with an average value of 4.66 x10^{-8} m^3/kg. In term of biostratigraphy, the MS curve produced for this section covers the largest range within the Givetian of the Dinant Syncline, extending from *hemiansatus* to *disparilis/falsiovalis* Zones. The MS curve provided for the Fromelennes-Flohimont section can be divided into height MS units (MSU-I – MSU-VII). MSU-I corresponds to the lower half of the Trois-Fontaine (TRF) Fm and exposes average MS values close to 0 whereas the upper half of this Formation corresponding to the MSU-II records the highest average MS value of the entire section (~2 x10^{-7} m^3/kg). The overlying Terre d'Haurs (TRH) Fm records the second highest values of the section (~1 x10^{-7} m^3/kg; MSU-III) and towards the upper half, prior the Terres d'Haurs (THR) – Mont d'Haurs (MHR) boundary, a significant decrease, ends with very low values close to 0. The THR Formation shows important variation in the MS values ranging from 0 to 2 x10^{-7} m^3/kg. Up in the section, the Mont d'Haurs and Fromelennes Fm show a discontinuous signal due to poor- to moderate outcropping conditions whereas large-scaled trends remain visible. The MHR Fm shows a low and monotonous signal with an average of 0.3 x10^{-7} m^3/kg (MSU-IV). The Fromelennes (FRO) Fm includes the last four MS Units (MSU-V – MSU-VII). MSU-V corresponds to the lowermost of the FRO Fm and records an average MS value of 0.5 10^{-7} m^3/kg. The Interval MSU-VI is divided into MSU-VIa and MSU-VIb. MSU-VIa exposes low MS values (~0.35 x10^{-7} m^3/kg) while the interval MSU-VIb, corresponding to the base of upper portion of the Fromelennes Fm, shows an outcrop gap of several meters. MSU-VII shows a relatively high average MS value close to 1 x10^{-7} m^3/kg.

Average magnetic susceptibility values for the La Thure (4.15 x10^{-8} m^3/kg) and the Fromelennes-Flohimont (4.66 x10^{-8} m^3/kg) sections are relatively close, and the median value of 4.4 x10^{-8} m^3/kg is in the classical MS range of marine sediments (5.5 x10^{-8} m^3/kg) defined by Ellwood et al. (2011) on the basis of ~11000 marine rocks including siltstone, limestone, shale and argillaceous limestone samples.

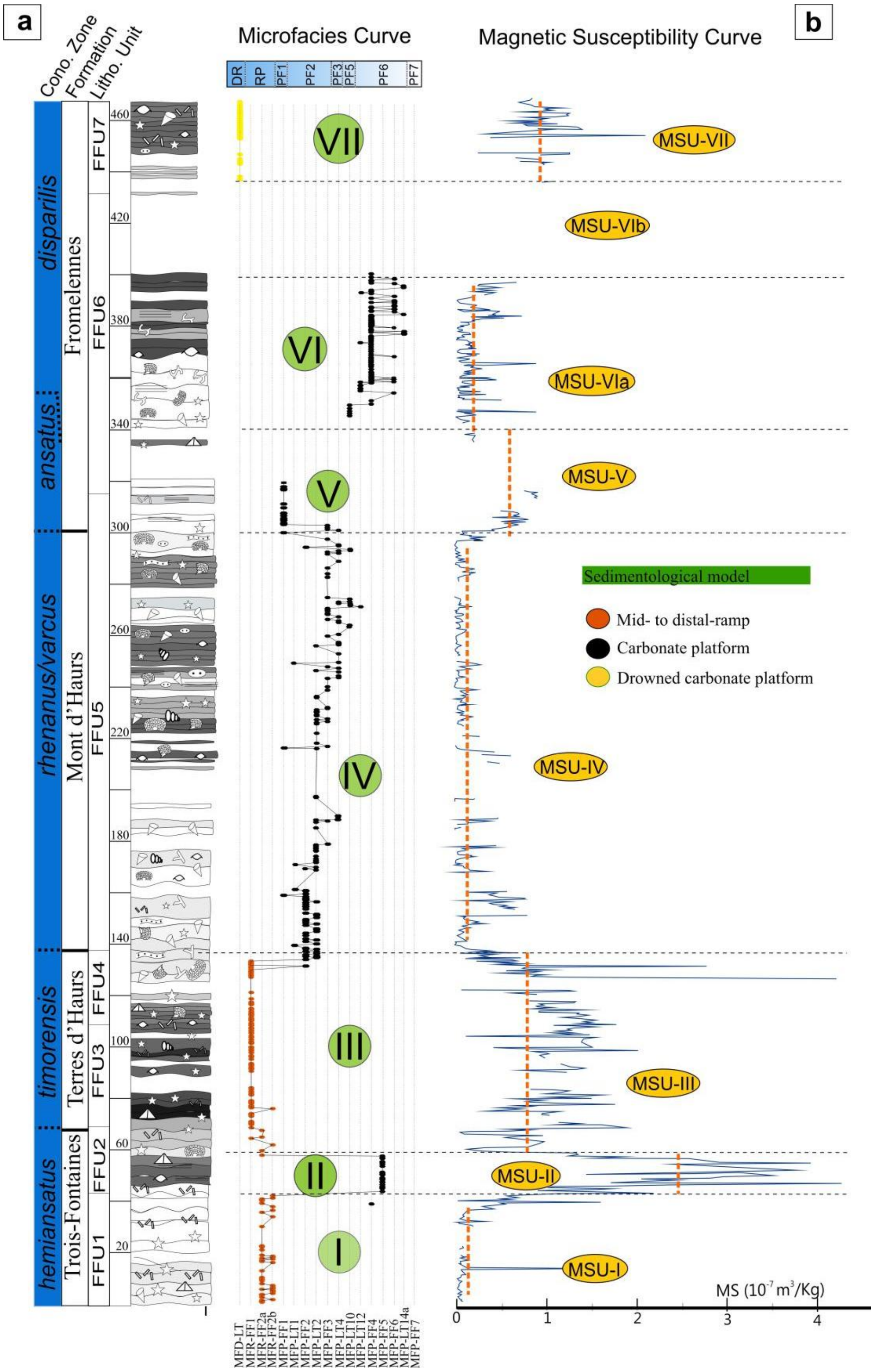

Fig. 15 a *Schematic sedimentological log showing formations, lithological units (FFU1-FFU7), conodont zonation and microfacies curve with the seven main depositional intervals (I-VII; intervals are separated by horizontal dotted lines).* **b** *Magnetic susceptibility evolution showing the eight main MS Units (MSU-I to MSU-VII). Vertical dotted lines correspond to average MS values for each MS interval. See Fig. 14 for legend of symbols.*

5. Discussions

5.1 Comparison between the La Thure and Fromelennes-Flohimont sections: implication for the early-late Givetian platform development in the Dinant Basin (Figs. 16 and 17)

Comparison of microfacies curves constructed for the Givetian sequences recorded in both La Thure and Fromelennes-Flohimont sections reveals marked similarities between time-equivalent large-scaled shallowing and deepening trends (Fig.16). These similarities can be observed despite the distance separating the sections (~75 km) and the difference in depositional background in each sites. Microfacies stacking patterns extracted from microfacies curves together with published data (Boulvain and Préat, 1986; Préat et al., 1987; Préat and Boulvain, 1988; Bultynck et al., 1991; Boulvain et al., 1995; Préat, 2006; Préat and Bultynck, 2006; Boulvain et al., 2009; Maillet et al., 2011; Maillet et al., 2013) suggest correlation between the La Thure and Fromelennes-Flohimont section and help to decipher the main evolutionary phases characterizing the Belgian Givetian platform evolution. Moreover, the proposed correlation leads to a better understanding of the extension and repartition of the main facies belts responsible for structuration of this extended Givetian shallow-water platform. This sedimentological study has also permitted to gain a meaningful understanding the key depositional changes characterizing the Givetian platform in the Dinant Basin. A summary of our interpretations and illustrations of the palaeogeographic history for the Dinant Basin during the early- to late-Givetian interval, including southward – northward migration of reefal bodies, is shown in Fig. 17.

Temporal evolution of microfacies over the early- to late-Givetian from both Fromelennes-Flohimont and La Thure sections is marked by seven major depositional intervals (I-VII), which are separated by noteworthy shallowing – deepening trends. These depositional intervals represent the main evolutionary phases that gradually built the Givetian platform. Considering that the shallowest depositional settings in the Dinant Basin are located to the north (see model orientation in Fig. 17), sedimentary rocks from the La Thure section, cropping out in the north-western margin of the Dinant Syncline, must have been deposited in shallower settings than sediments belonging to the Fromelennes-Flohimont section (e.g., southern margin of the Dinant Syncline, see geological map Fig. 1b).

The Lower Givetian TRF Fm and most of the THR Fm only outcrop in the Fromelennes-Flohimont section. As a result, our discussion on the early Givetian platform evolution is mostly based on the data collected in Fromelennes-Flohimont section. However, owing to the continuous character of the La Thure sequence, from upper Lower to Upper Givetian most of the discussion will combine results from both La Thure and Fromelennes-Flohimont sections.

The TRF and THR Fm record three depositional intervals (I-III) and four intervals (IV-VII) are depicted from the microfacies curve corresponding to MHR and FRO Fm. According to our interpretations, the base of TRF Fm represents a deposition within the SWB into a homoclinal ramp model. This ramp-related setting is unusual for the base of Trois-Fontaines Fm in the southern margin of the DS. Indeed, the classical sections in this area (e.i. Glageon, Resteigne, Baileux; see location on Fig. 1b) expose m-thick accumulations of reef-related deposits, commonly called “premier” biostrome. The absence of reef-builder organisms for time-equivalent facies in the Fromelennes-Flohimont section points to local changes in the environmental conditions, hampering reef-related deposition. According to De Wilde (2005) and Mabille et al. (2008a) an increase of detrital input seaward could have inhibited reef to growth. Indeed, they studied time-equivalent deposits located in the “Marenne Est” section (south-eastern part of the DS; see Fig. 1b) and mentioned that the important proportion of quartz grains in the limestone was responsible for the absence of the “premier” biostrome. According to De Wilde (2005) the higher proportion of quartz grains was related to the vicinity between “Marenne Est” depositional setting and the emerged Stavelot Massif. Another hypothesis explaining the absence of biostrome could be that the Fromelennes-Flohimont depositional area was located in a fore-reef setting, south of the barrier reef.

The transition from the interval I to II, in the upper part of the TRF Fm, is characterized by an important shallowing-upward shift corresponding to the first occurrence of restricted lagoonal setting and environment with palaeosoil developments (FB6 and FB7). This abrupt shallowing trend is likely related to a sea-level fall which had triggered a basinward drift of the reef-building communities. The development of a new reefal structure basinward (e.g., southward) is likely responsible for the lagoonal deposits occurring in the TRF Fm (Boulvain et al., 2009). Considering the thickness of carbonate characterizing this specific environment in the Fromelennes-Flohimont section, and in other location in the southern margin of the DS (c.f., Resteigne, Marenne, Glageon), the reefal or palaeo-high structures (responsible for that division between internal and external shelf) should have been continuous and stable for a relatively long period of time. According to the lack of outcrops, the location of the “barrier” responsible for this biostrome, has never been observed. Although, we might presume that this “barrier” should be located a few kilometres southward of the DS southern margin. Hypothetical extension of the “barrier” controlling deposition of lagoonal sedimentation in the upper part of the Trois-Fontaines Fm is shown in Boulvain et al. (2009; fig. 16). In this figure, the barrier responsible for the “premier” biostrome as mentioned below is also exposed. Upward in the section, the transition from the upper part of the TRF Fm (Interval II) to the TRH Fm (Interval III), corresponding to the transition from *hemiansatus* to *timorensis* conodont Zones, registers a deepening trend and the return to a ramp-related deposition (e.g., microfacies RP). The TRH Fm represents the ramp-related model which is anterior to the extensive Mid-Late Givetian carbonate shelf development in the Dinant Syncline (Boulvain et al., 2009; Casier et al., 2013). The homogenous deposits occurring throughout the THR Fm are the consequence of a stable mid- to distal ramp environment influenced by storm, and locally by the development of patch-reefs. Uppermost part of the THR Fm is also exposed in the La Thure section and records similar environments.

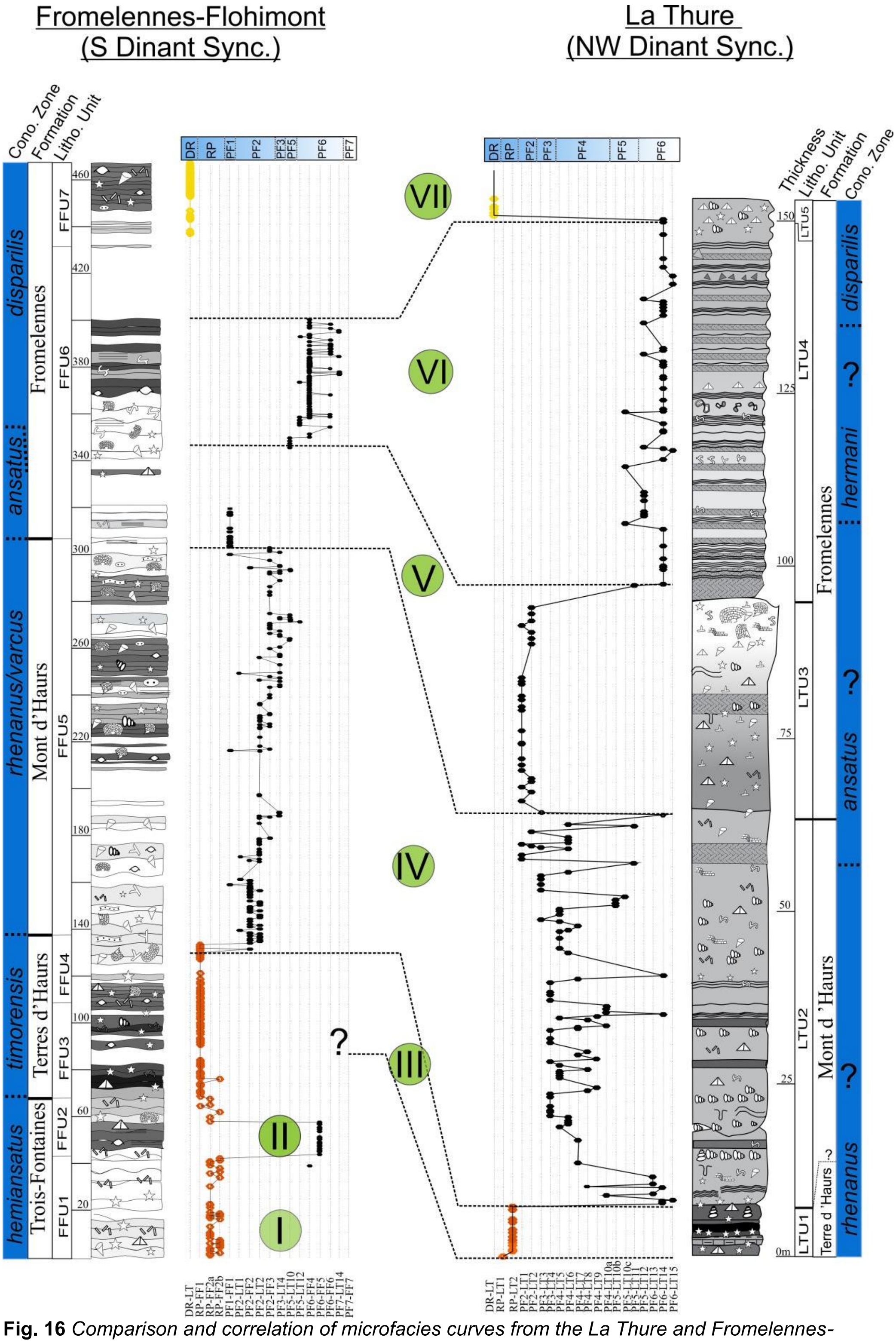

Fig. 16 *Comparison and correlation of microfacies curves from the La Thure and Fromelennes-Flohimont sections. See Fig. 14 for legend of symbols.*

The transition from the THR Fm (Interval III) to MHR Fm (Interval IV) corresponds to a shift from mid-ramp (Interval III) to internal shelf or biostrome and fore-reef setting (Interval IV), depending on the section. In the Fromelennes-Flohimont section this trend corresponds to the transition from mid- and outer-ramp related sedimentation (RP-FF1) to biostromal and fore-reef shelf facies (FB2). In the La Thure section, this transition corresponds to a more marked change which is characterized by a shift from mid-ramp (RP-LT2) to internal shelf deposits (FB3, FB4 and FB5). This abrupt transition can be explained by the well-marked north to south facies deepening within the Dinant Syncline (Préat and Boulvain, 1988; Bultynck et al., 1991; Poulain, 2006; Préat and Bultynck, 2006) (see Fig. 1d). At the Fromelennes-Flohimont section and in most sites belonging to the southern margin of the DS, extensive biostromal deposits are documented throughout the Mont d'Haurs Fm (*rhenanus/varcus* Zone). The progressive development of large patches and barrier-reefs that resulted in the formation of the thick-bedded biostromal limestones of the MHR Fm in the southern margin of the DS (c.f. Poulain, 2006; Boulvain et al., 2009) must have progressively divided the Middle Givetian platform into an internal and an external shelf setting. These conditions created the sedimentary conditions which allowed for the deposition of lagoonal and bioclastic shoals facies (e.g., PF3-LT3 to PF5-LT10c) in the north-western La Thure area. These biostromal deposits are interpreted as the result of barrier-reef debris transported southward by debris-flow or storm reworking processes (Boulvain et al., 2009). Considering this interpretation, the location of the barrier-reef separating the north-western margin (La Thure) from the southern margin (Fromelennes-Flohimont, see map in Fig. 1b) of the DS might exist in the subsurface near the axis of the Dinant Syncline. In the Fromelennes-Flohimont section, the MHR Fm exposes sediments belonging to the FB2 even if toward the top, sediments related to FB3, attesting a shallowing of the facies are more frequent. The MHR Fm as exposed in the La Thure section records numerous oscillations of microfacies which correspond to alternating small-scale regressive cycles (see Fig. 10 interval II). As mentioned by several authors (Playford, 1980; Tourneur, 1985; Boulvain and Préat, 1986; Préat and Carliez, 1994; Skompski and Szulczewski, 1994; Da Silva and Boulvain, 2004; Boulvain et al., 2009), the records of cyclic sedimentation are a common characteristic of Devonian shallow-marine sequences. Moreover, De Vleeschouwer et al. (2014, see their fig. 3) related the 6 to 8 m-thick oscillations in the microfacies curve in this part of the La Thure section with 100-kyr eccentricity.

On a larger scale, MHR Fm as exposed in the La Thure and Fromelennes-Flohimont areas can be considered as an aggrading trend in internal shelf setting. The transition from interval IV to V (Fig. 16) is characterized by a deepening-upward trend leading to the occurrence of off-reef and fore-reef deposits (PF1-FF1) in the Fromelennes-Flohimont and biostromal and fore-reef facies (PF2-LT2-3) in the La Thure section. In the Fromelennes-Flohimont section the deepening upward is characterized by the occurrence of the most distal facies belt of the shelf model (PF1) corresponding mainly to argillaceous limestone with intercalations of clay layers. These clay layers are well-visible in the Glageon quarry (Boulvain et al., 1995). In the Fromelennes type area, in the southern margin of the DS, this transgressive trend is also marked by the occurrence of argillaceous limestone with intercalation of clay (Préat and Bultynck, 2006) overlying thick-bedded limestone of the MHR Fm. In the Fromelennes-Flohimont section these lithologies are poorly-outcropping. In the La Thure section, clay layers do not occur but some strata show a distinct argillaceous character within the interval V. According to Boulvain et al. (2009), this abrupt shift between intervals IV and V is interpreted as a transgressive pulse. The absence of clay deposits in the La Thure section is explained with respect to the north-western location within the DS. Indeed, this transgressive pulse must have been represented by shallower sedimentation in the north-western margin of the DS. Shortly after this important transgressive pulse, both sections record a shallowing-upward shift observed between the depositional Interval V and VI, corresponding roughly to the *ansatus* to *hermani* conodont Zones transition. This sea-level drop likely favoured a seaward shift of the reefal structure that had provided the materials deposited during interval V (e.g., biostromal and fore-reef deposits). This sea-level drop corresponds to a similar shift of facies from fore-reef (FB1 and FB2) to internal shelf (FB5, FB4) in both sections, although characterized by slightly different microfacies. In the Fromelennes-Flohimont section dominant deposits show a marked influence of water energy (see section microfacies; PF5-FF4) while sedimentation in the La Thure took place in a calm protected-like area (see section microfacies; PF6-LT14). In both La Thure and Fromelennes-Flohimont sections, sediments are characteristic of the restricted and the evaporitic internal shelf belts (FB5 and FB6) confirming shallow semi-protected to protected marine conditions. The transition to such internal facies signifies two substantial changes within the Belgian Upper Givetian shelf: firstly, a significant sea-level fall at the *rhenanus/varcus – ansatus* boundary and secondly the edification of a palaeo-high structure like a barrier-reef in a seaward location. The development of this reefal structure in a seaward location allowed initiation and deposition of lagoonal deposits landward (e.g., explained for interval III to IV transition). According to several authors (Bultynck, 1974; Préat and Carliez, 1994) as synthetized in Boulvain et al. (2009), the Middle – Upper Givetian in the south and south-eastern margin of the DS is also characterized by lagoonal sedimentation (e.g., Fromelennes Fm) and interpreted by Boulvain et al. (2009) as related to the occurrence of a barrier-reef located southward. The occurrence of locally thick levels of *Amphipora* rudstone (e.g., PF4-LT12; microfacies section) could indicate a malor increase of the water energy in internal setting suggesting a discontinuous barrier. Toward the upper half of the Fromelennes Fm in both sections, the transition from Interval VI to VII corresponds to a significant transgressive pulse, which is marked by the transition from internal restricted lagoon-like deposits to drowned shelf sedimentation (e.g., RP-LT1). These drowned deposits are several tens of meters thick in Fromelennes-Flohimont but only several meters thick in the La Thure section. The significant difference in these limestones thickness might be the results of a lower accommodation space in the La Thure section. This rapid sea-level rise occurs a few meters below the first shale of Frasnian age (Pas et al., 2014a). Thus, the uppermost half of the Fromelennes Fm is considered as a part of the Late Givetian transgression that resulted in the withdrawal of the carbonate production and the demise of shallow-water sedimentation in Belgium before Middle Frasnian. Synthetic models showing distribution of microfacies along the homoclinal ramp and the rimmed shelf profiles are shown in Fig. 13.

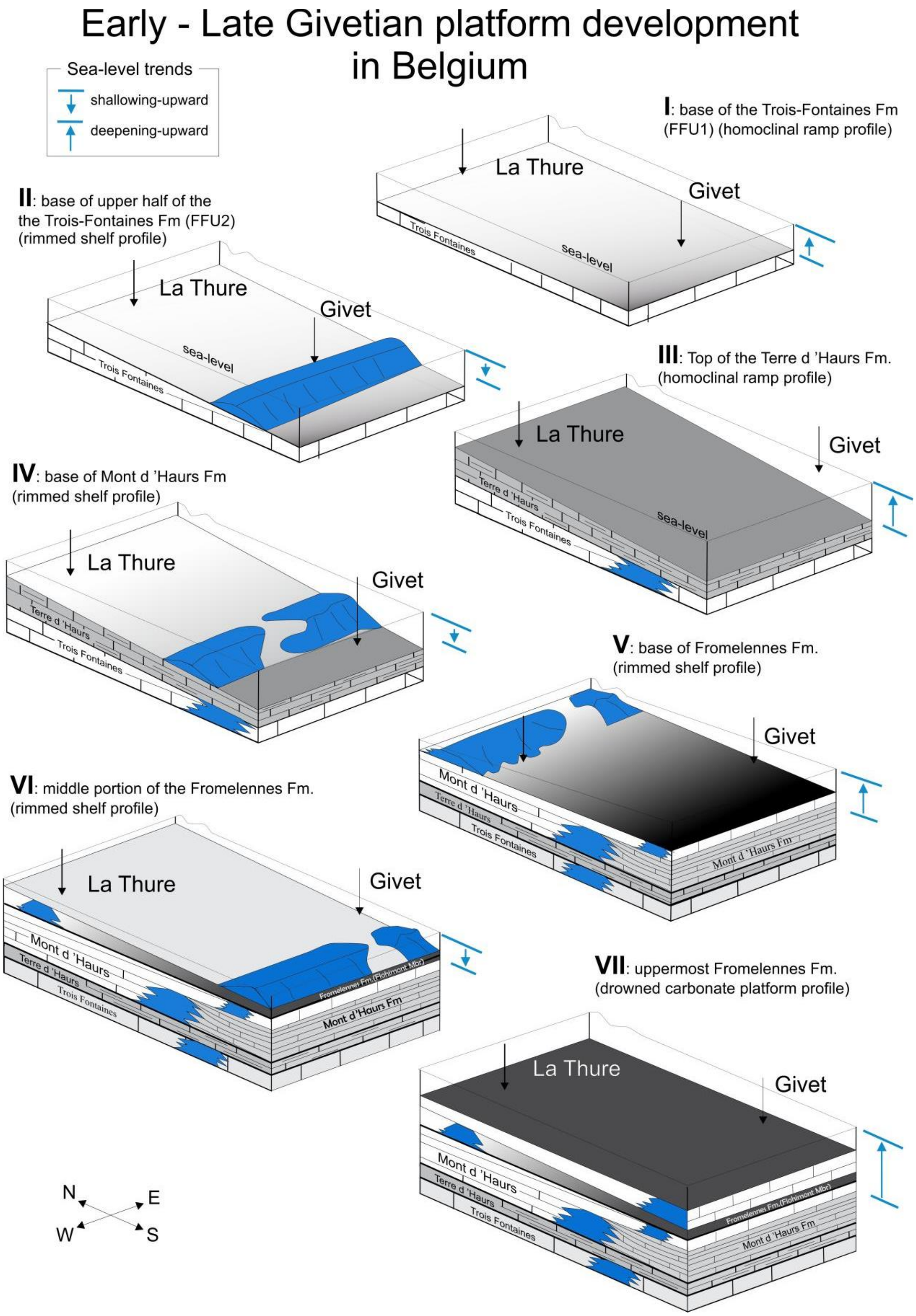

Fig. 17 *Early – Late Givetian carbonate platform development within the Dinant Basin showing main basinward vs landward migrations of the reefal body in relation with the sea-level variations.*

5.2 Comparison and interpretation of magnetic susceptibility versus geochemistry and microfacies from La Thure and Fromelennes-Flohimont sections: implication for MS as a correlation tool for the Belgian Givetian platform (Figs. 18 and 19)

Magnetic susceptibility and geochemistry

Before MS records can be interpreted faithfully in terms of sea-level variation or palaeoclimatic proxies it must be established that the MS signal still contains original palaeoenvironmental information. This is not trivial and even less so in the Belgian Ardennes where a remagnetization event was recognized by Zegers et al. (2003). In order to estimate the preservation of the recorded MS signal in the La Thure and Fromelennes-Flohimont sections we have analysed the stratigraphic distribution of reliable proxies for siliciclastic input such as SiO_2, TiO_2, Al_2O_3, K_2O, Zr and Rb (Calvert and Pedersen, 2007; Śliwiński et al., 2012) along both profiles and compared it with MS evolution (Figs. 18 and 19). Indeed, the detrital supply basinward is considered as the main MS primary-controlling factor. (Vanderaveroet et al., 1999; Ellwood et al., 2000; Tribovillard et al., 2006; Śliwinski et al., 2010; Śliwiński et al., 2012). Therefore the correlation between MS signal and siliciclastic input proxies will reflect the preservation level of the primary recorded MS signal. As illustrated in Figs. 18 and 19, siliciclastic input proxies and MS follow the same large-scaled trends. Moreover, calculated correlation coefficient *r*, respectively for the Fromelennes-Flohimont and the La Thure sections ranges between 0.66 and 0.62 (n = 42) and 0.51 to 0.61 (n = 30). According to Riquier et al. (2010) such correlation demonstrates the inherent-parallel link existing between variations in MS values and proxies for siliciclastic input. Thus, despite the remagnetization event affecting the Rhenohercynian fold-and-thrust belt, the MS signal is preserved as it still reflects primary depositional-induced conditions. Therefore, the large-scaled MS trends in both sections can serve as a proxy for siliciclastic input variations and therefore as a tool for correlation purpose. The origin of the magnetic susceptibility signal and implications on its application as a correlative tool and paleoenvionmental proxy will be discussed in more detail in Chapter 6.

The magnetic susceptibility (MS) curves of both sections have been divided into several MS Units: Six MS Units (MSU3-8) were recognized for the La Thure section (Fig. 14) and height MS Units (MSU1-7) for the Fromelennes-Flohimont section (Fig. 15). When we compare the long-term MS and microfacies evolution for the two studied sections (Fig.19), similar trends and events are observed between time-equivalent deposits. In addition, the behaviour of the MS signal in comparison to microfacies is also similar in each section. Based on the analogous pattern between MS and microfacies between the two sections we propose a correlation which is synthetized in Fig. 20. This synthesis illustrates the remarkable similarities in large-scaled MS trends that exist between the south and north-western margin of the Dinant Syncline despite the distance separating each site (~75 km) before the folding of the area during the Variscan orogeny and the difference in terms of depositional background.

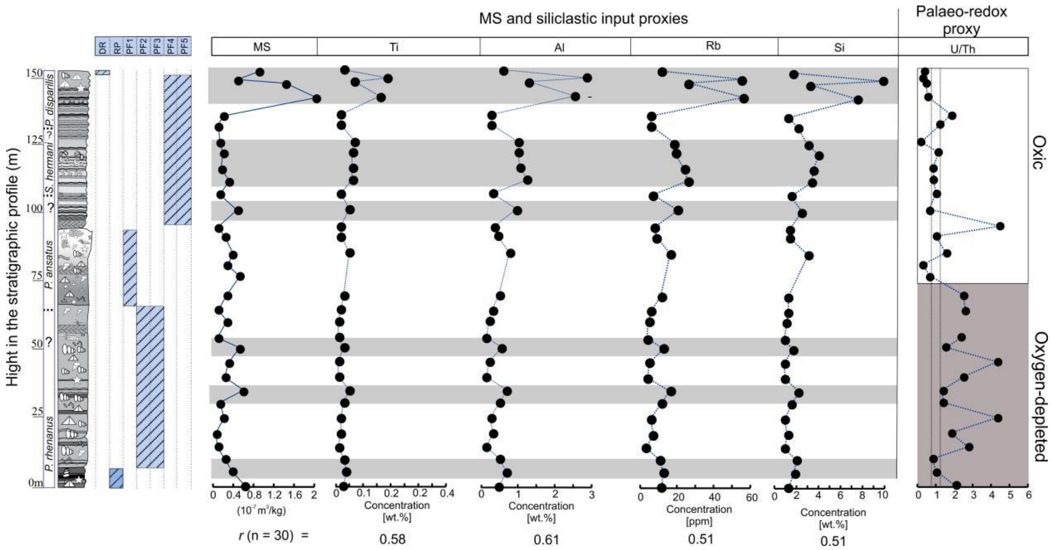

Fig. 18 *Chemostratigraphic profile of magnetic susceptibility (MS), Ti, Al, Rb and Si. Ti, Al, Rb and Si concentrations are considered as proxy for detrital inputs and show moderate correlation with MS variations. Shaded areas highlight major or trace element enrichment. U/Th ratio is considered as a proxy for redox condition at the sediment-water interface. Based on the marked drop in U/Th ratio recorded around the mid-late Givetian boundary we subdivided the La Thure section into two parts characterized by different bottom water redox condition: a lower half part with less oxic condition (shaded area) and an upper half with more oxic condition. Vertical dotted lines in the U/Th graph represent the threshold values for redox condition based on Jones and Manning (1994; <0.75 = oxic, 0.75-1.25 = dysoxic, >1.25 = anoxic). Main facies belts occurring throughout this section are represented by hatched areas along the lithological log.*

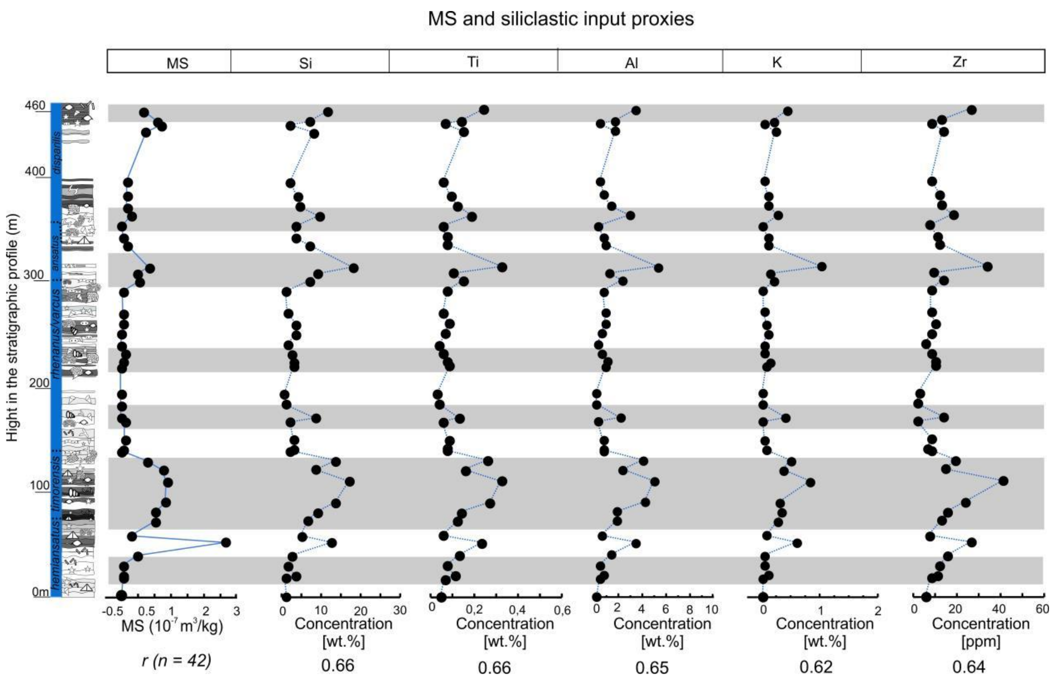

Fig. 19 *Chemostratigraphic profile of magnetic susceptibility (MS) and proxies for siliciclastic input into marine depositional basin (Si, Ti, Al, K and Zr) from Fromelennes-Flohimont section. Shaded areas highlight major or trace element enrichments.*

Comparison of MS with facies and lithologies: As already demonstrated in various studies, the behaviour of the magnetic susceptibility signal is strongly related to microfacies and therefore to depositional induced parameters such as water agitation, sedimentation rate, carbonate productivity and siliciclastic supply (Boulvain and Coen-Aubert, 2006; Bábek et al., 2007; Mabille et al., 2008b; Da Silva et al., 2009b; Whalen and Day, 2010; Pas et al., 2014a; Pas et al., 2014b). In order to discriminate the main depositional induced parameters acting for the MS variations we have compared MS with microfacies.

As mentioned below, Lower Givetian only occurs in the Fromelennes-Flohimont section hampering comparison between the two sections for this period of time.

Sediments characterizing the base of the Trois-Fontaines Fm in Fromelennes-Flohimont are deposited in a mid-ramp context (see distribution of microfacies in Fig. 13). The low average MS value (MSU-I) characterizing this part of the Trois-Fontaines Fm agree with the permanent water energy in such setting, which prevent settlement of MS carrying minerals.

The strong MS increase toward the upper part of the Trois-Fontaines Fm is explained by the change from a mid-ramp to an internal restricted shelf setting. Low water energy condition and vicinity with continental emerged area favour both the concentration of MS carrying mineral and likely an increasing detrital supply basinward.

The Terres d'Haurs Fm in the south and north-western Dinant Syncline is dominated by mixed carbonate and argillaceous lithologies deposited in a mid- to distal-ramp setting corresponding to one of the deepest facies of our succession. The high average MS value (MSU-III) corresponding to this formation supports the model of ramp-related deposition of Mabille and Boulvain (2007). In the Belgian Upper Eifelian – Lower Givetian ramp profile Mabille and Boulvain (2007) showed a general increase of the averaged MS values from inner to outer ramp. This increase in the MS values is explained by the decrease in carbonate productivity related to the increasing depth and the decreasing hydro-energy. Both parameters allow increasing settlement of fine-grained MS carrying particles. Data available on the Terres d'Haurs Fm are limited to two microfacies and therefore further consideration on the MS behaviour would be inappropriate.

Higher up in the section, the sediments characterizing the Mont d'Haurs Fm in the La Thure section mainly represent an internal shelf deposition (facies belt PF3-6) dominated by relatively pure carbonate and characterized by low average MS value (MSU-IV). In the Fromelennes-Flohimont section, the equivalent MS Unit is also characterized by a very low average MS value. This is explained by the occurrence of external shelf reefs and fore-reef deposits characterized by high carbonate productivity. The low mean MS value expressed for this Formation (MSU-IV) is therefore mainly attributed to the dilution of MS-carrying minerals by carbonate.

The MSU-V is characterized by a significant increase of the average MS value in the lowermost part of the Fromelennes Fm in both sections. This increase is related to a substantial change in the depositional setting from internal shelf to biostrome and fore-reef in La Thure, and biostrome and fore-reef to off reef setting in Fromelennes-Flohimont. Therefore, this MS increase should probably be explained by the decreasing water energy and the drop in carbonate productivity that characterize these external settings. The first parameter enhances the settlement of fine-grained MS carrying particles while the second condenses MS carrying minerals into the sediments.

Transition from MSU-V to MSU-VI corresponds to a decrease of average MS values in both locations. This decrease coincides with the transition from off-reef and fore-reef shelf deposits (facies belts PF1 and PF2) to internal restricted sediments (facies belt PF5-6) and likely related to the permanent water agitation and the confinement that characterize this inter- to supratidal environment dominated by a thick accumulation of internal evaporitic/brackish deposits (PF6).

In the north-western margin, the transition from MSU-VI to MSU-VII corresponding to the transition from lower half to upper half of the Fromelennes Fm is characterized by a substantial increase of the average MS value while the depositional setting remains relatively similar. In the southern margin of the DS, the base of the upper half of the Fromelennes Fm mostly corresponds to a m-thick outcropping gap, whereas – where MS values are recorded – they are as high as the values logged in the La Thure section (MSU-VII). The significant increase in averaged MS value between MSU-VI and MSU-VII occurs despite the occurrence of remarkable deviations in microfacies. Based on a detailed comparison with recent tropical sediment, Boulvain and Préat (1986) have demonstrated that during the Upper Givetian in Belgium (e.g., Fromelennes Fm) shore-face realm depositional processes were mainly dictated by arid conditions similar to those found today in the Persian Gulf. Local occurrence of desiccation crack and evaporitic crystal like pseudomorphe (e.g., PF6-LT14-15) indicating aridic climate are also observed in the Givetian La Thure sediments. Since the role of climatic conditions implies changes within the sediments transport processes we consider that an increase of the aridity on the main landmass (cf. Old Red Sandstone) that bordered the Belgian Givetian carbonate platform might have favoured the amount of wind-related MS carrying particles transported towards the marine realm. For instance, in a contemporary study dedicated to the evolution of climate during the Mesopotamian Empire, Cullen et al. (2000) performed various mineralogical and geochemical analyses on marine sediments core from the Gulf of Oman which is downwind of Mesopotamian dust source areas. Their results document a very abrupt increase in eolian dust parallel to Mesopotamian aridification. This increase in eolian dust is similarly-marked in MS (10^{-6} SI units) and eolian dolomite (% wt.) curves. During the Givetian, evidences of evaporitic plains, semi-arid deserts and continental redbeds are recognized worldwide (Scotese, 2005). Recently Hladil et al. (2006) published important gamma-ray spectroscopy (GRS) and MS data obtained in mid-Eifelian to end-Frasnian Moravian isolated carbonate platform (Czech Republic) and underlined the important role played by eolian inputs and aridic conditions for the MS signal intensity in carbonate rocks. In addition, by the combination of GRS and MS measurement Hladil (2006, fig. 3) showed an increasing amount of atmospheric dust between late Givetian and middle Frasnian on the Moravian carbonate platform. Therefore, we assume that the significant increase of the MS signal throughout the upper half of the Fromelennes Fm (Unit 2; Fig. 9) could be related to an increase of wind-blown dust deposition in shallow-water triggered by an aridification of the main land during Mid-Late Givetian time. Nevertheless, as mentioned by Sur et al. (2010) the geological record of eolian dust in ancient carbonate is only consistent if all non-atmospheric sources of silica can be confidently eliminated from consideration (e.g., isolated platform, oceanic basin) for the investigated time interval. This means that only isolated platform or oceanic basin sedimentary records are consistent with such a hypothesis. According to various palaeogeographic reconstructions of Western Europe during the Middle Devonian (Ziegler, 1982; McKerrow and Scotese, 1990) the south of Belgium was located in immediate vicinity of the Old Red Sandstone continent (e.g., London-Brabant Hight) and non-atmospheric sources of silica cannot be eliminated. However, until the present time siliciclastic facies or riverine deposits have never been mentioned throughout the Late Givetian in Belgium. Hence, the hypotheses of an increasing MS value in relation with higher amount of eolian-related dust deposition could be envisaged after prudent consideration as consistent proofs of the separation between the Belgian platform and the main continent have not been documented. At present, it is therefore preferable to envisage a combination of eolian dust and riverine input to explain the recorded MS changes toward the Late Givetian within the north-western margin of the Dinant Basin.

In our results for the Belgian Givetian platform, as described below, we have also underlined a strong link between the evolution of microfacies and the magnetic susceptibility signal. However, we observed that this link varies between the homoclinal ramp and the rimmed shelf profiles as defined in this study. This observation is consistent with recent publication by Da Silva et al. (2013) summarizing a large number of Mid-Upper Devonian Belgian sections and settings (e.g., carbonate ramp, shelf and mud mounds models) in which the authors outlined a significant difference in MS behaviour for each carbonate platform model. Considering the large number of microfacies defined in this study and in order to compare our results with published data, we have analysed the link between MS and microfacies separately for the rimmed-shelf and the homoclinal ramp models. However, an analysis of the drowned shelf profile could not be relevant as the model is only represented by one microfacies (DR-LT).

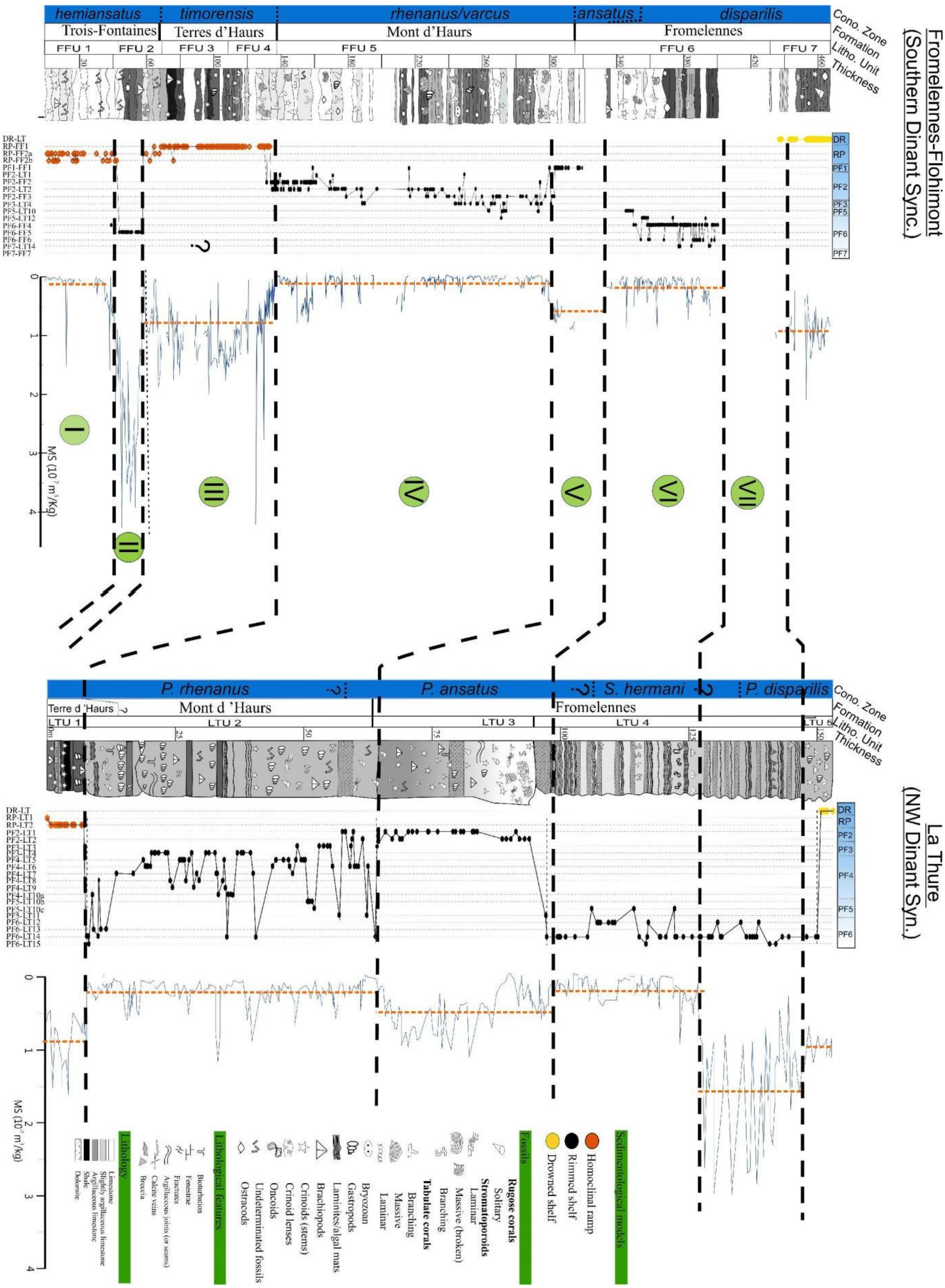
Fromelennes-Flohimont
(Southern Dinant Sync.)
Cono. Zone
Formation
Litho. Unit
Thickness
hemiansatus
timorensis
rhenanus/varcus
ansatus
disparilis
Trois-Fontaines
Terres d'Haurs
Mont d'Haurs
Fromelennes
FFU 1
FFU 2
FFU 3
FFU 4
FFU 5
FFU 6
FFU 7
DR
RP
PF1
PF2
PF3
PF5
PF6
PF7
MS (10⁻⁷ m³/Kg)
I
II
III
IV
V
VI
VII
La Thure
(NW Dinant Syn.)
P. rhenanus
P. ansatus
S. hermani
P. disparilis
Terre d'Haurs
Mont d'Haurs
Fromelennes
LTU 1
LTU 2
LTU 3
LTU 4
LTU 5
PF4
Lithology
Limestone
Slightly argillaceous limestone
Argillaceous limestone
Shale
Dolomite
Lithological features
Bioturbation
Fenestrae
Fractures
Argillaceous joints (or seams)
Calcite veins
Breccia
Fossils
Rugose corals
Solitary
Stromatoporoids
Laminar
Massive (broken)
Branching
Tabulate corals
Branching
Massive
Laminar
Bryozoan
Gastropods
Laminites/algal mats
Brachiopods
Crinoids (stems)
Crinoid lenses
Oncoids
Undeterminated fossils
Ostracods
Sedimentological models
Homoclinal ramp
Rimmed shelf
Drowned shelf

Fig. 20 *Comparison and correlation of magnetic susceptibility curve for the studied sections.*

Homoclinal ramp: sediments belonging to this profile are exposed throughout the Lower Givetian Trois-Fontaines and Terres d'Haurs formations. A general increase of the mid- to outer-ramp setting can be observed in the Fig. 20a showing the average MS values for each microfacies. Microfacies RP-FF1 located on the margin between mid- and outer-ramp settings record an exceptionally high average MS value. Nevertheless, the MS general behaviour coincides with the model of Mabille and Boulvain (2007) for the Eifelian – Givetian ramp in south-western Belgium. These authors record a general increase of the average MS values along a proximal – distal profile. Similar comportment of the MS signal was also observed by Mabille et al. (2008b) in an Eifelian ramp-related setting in the Eifel area.

Carbonate shelf model: the characteristic sediments of this model correspond to the middle portion of the Trois-Fontaines, the Mont d'Haurs and the Fromelennes formations. Owing to the large diversity of depositional settings for the rimmed shelf defined herein, we have carried out an analysis of the average MS variations for each facies belts (Fig. 20b). In both La Thure and Fromelennes-Flohimont sections, external (FB1 and FB2) and internal shelf belts (FB3, FB4, FB5, FB6 and FB7) deposits are characterized by different MS behaviour (see Fig. 20). A general decrease of the average MS signal from the off-reef to biostromal belts characterizes the external shelf. In the internal shelf a general increase is observed between the bioclastic shoals and the supratidal setting. The internal shelf oolitic shoal is marked by a decrease of the average MS value. This decrease might be driven by the high hydro-energy characterizing shoals in shelf interior, preventing MS-carrying minerals from settling. The MS varying behaviour in the internal and external shelf settings is also clearly visible on the MS curves constructed for both sections (Figs. 14 and 15). Each deepening upward trend in microfacies that leads to deposition of external shelf deposits is characterized by an increasing MS trend. The similar pattern between MS and microfacies evolution in La Thure and Fromelennes-Flohimont sections has been used to propose a correlation between Fromelennes-Flohimont and La Thure sections based on the MS results.

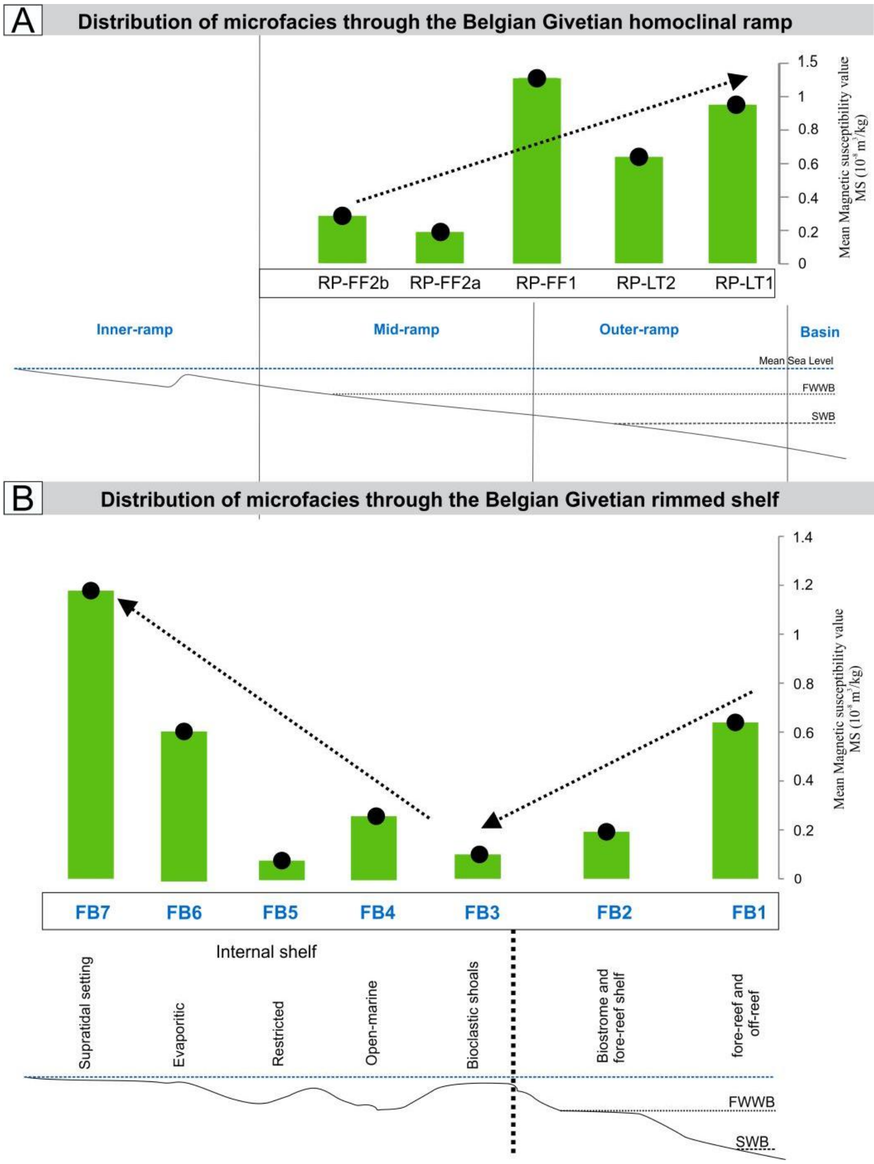

Fig. 21 a *Mean values on relative proximity transect illustrated by the position ramp-related microfacies from proximal to distal location.* **b** *Mean values on relative proximity transect illustrated by the position of the main facies belts (FB1-FB7) defined for the rimmed-shelf model.*

Palaeoredox conditions within an Early-Late Givetian platform in the north-western Dinant Basin

The following discussion is based on the elemental data set provided in the La Thure section. In Fromelennes-Flohimont section, all reliable trace elements used for palaeoredox reconstruction are below the limit of detection.

Redox sensitive elemental ratios commonly used to interpret palaeo-oxygenation in bottom water conditions are Ni/Co, V/Cr, V/(V+Ni) and U/Th (Hatch and Leventhal, 1992; Jones and Manning, 1994). The concentrations of the trace elements (Ni, Co, V, and Cr) recorded in our data set is below the detection limit. The concentrations of U and Th, on the other hand, are within this limit and the calculated redox element ratio U/Th profile through the section is shown in Fig.18. The general evolution of calculated U/Th ratio through the profile can be assigned to the anoxic-dysoxic-oxic threshold values of Jones and Manning (1994; <0.75 = oxic, 0.75-1.25 = dysoxic, >1.25 = anoxic), although these calculations should be viewed as relative. Indeed, as was mentioned by Rimmer (2004) and other authors (Riquier et al., 2005; Śliwiński et al., 2010), these threshold values should only be used as a relative scale to interpret the degree of palaeo-oxygenation. Since, these threshold values are based either on contemporary disoxic-anoxic basin analogues or they were developed for a specific palaeobasin. In line with the arguments of Rimmer (2004) and Śliwiński et al. (2010), the evolution of calculated U/Th ratio for the La Thure section reveals a significant large-scale change in the oxygenation level of bottom water (Fig. 18) from oxygen-depleted conditions throughout the lower half of the section to more oxic condition within upper half. This lowering in the U/Th ratio is concurrent with the onset of the extensive development of lagoonal – evaporitic setting in the La Thure section (see interval IV in Fig. 10) but also in the Fromelennes-Flohimont section (e.g., FFU6) but also all over the Dinant Basin in Belgium and France (Boulvain and Préat, 1986). On a more global scale, lagoonal – evaporitic sediments were also recorded in the Middle and Late Givetian of the eastern Rheinisches Schiefergebirge (Brilon Reef; Machel, 1990), Harz Mountain (Iberg Reef; Krebs, 1974), Brunai Platform in Czech Republic (Gischler, 1995; Hladil et al., 2006) and in the Carnic Alps (Schönlaub and Histon, 2000). These data support peaks in palaeo-temperature near the onset of the Late Devonian as established by Joachimski et al. (2009, 2004) on the basis of a large $\delta^{18}O$ dataset from biogenic calcite and conodont apatite collected in different location bordering the Rheic Ocean (see fig. 1 in Joachimski et al., 2004). In La Thure, the relation existing between the depositional setting and the low U/Th ratio value presumably indicates an aridification of the climate as the driving process for bottom water oxygenation has changed. Indeed, the aridic climate characterizing Middle and Late Givetian must have dropped the amount in organic matter (OM) and nutriments transported seaward. Considering that oxygen dissolved in water is consumed during the decay of the OM, a decreasing amount in OM flux toward the marine realm will automatically lead to an oxygen enrichment of the bottom water, resulting in oxidizing water conditions. In such conditions, redox sensitive trace metals (e.g., U, V and Mo) are more soluble (Tribovillard et al., 2006) and their concentration as well as the U/Th ratio in the sediment-water interface will decrease proportionally. The intensity of ocean water circulation is another process that might account for the significant change recorded in bottom water oxygenation at the mid-late Givetian boundary. The intensity of ocean circulation is highly dependent on the temperature gradient between the poles and the equator. As pointed out by Joachimski et al. (2009) during the Early-Middle Givetian, the tropics were relatively cool, meaning that the temperature gradient between the poles and the equator was relatively weak at that time. As a consequence, the ocean circulation was weaker and thus more prone to anoxia. The dramatic increase of temperature within the tropical areas at the mid-late Givetian boundary (Joachimski et al., 2004) favoured a better ocean circulation between the poles and the equator and a system less prone to anoxia.

6. Conclusions

In the first part of Chapter 4, we have focused on two remarkable sections from the Dinant Syncline: The La Thure section located in the north-western margin of the Dinant syncline and the Fromelennes-Flohimont section situated in the southern margin of the same syncline. The La Thure section cuts through a continuous early- to late-Givetian carbonate sequence belonging to the Belgian carbonate platform and includes the Terre d'Haurs, Mont d'Haurs and Fromelennes formations. The Fromelennes-Flohimont section covers a stratigraphic interval extending from the early- to late-Givetian encompassing the Trois-Fontaines, Terre d'Haurs, Mont d'Haurs and Fromelennes formations. In total, ~1200 samples were collected from these two sections and measured for magnetic susceptibility, ~600 samples were selected for thin-section analyse and a group of 72 samples were analysed for major- and trace elements concentration. The main conclusions of this pluri-disciplinary investigation are as follows:

- Petrographic analyses has allowed for the delineation of twenty microfacies for the La Thure section and seventeen for the Fromelennes-Flohimont section. These microfacies represent a remarkable carbonate platform evolution through early- to late-Givetian, ranging from a homoclinal ramp to a discontinuously rimmed shelf and finally to a drowned shelf. This facies model highlights the fascinating environmental diversity that characterized one of the largest carbonate platforms of Europe and provide an up to date model of the vertical and lateral development of the Belgian/France Givetian platform.
- Sedimentary development throughout the La Thure and The Fromelennes-Flohimont sections can be divided into five and seven major depositional intervals, respectively separated by significant sea-level fluctuation. The drowning that caused the demise of the Belgian Givetian platform is well-marked by the re-establishment of open-marine conditions and the subsequent deposition of the overlying lower Frasnian shale visible in both sections.
- Major depositional intervals recorded in the southern and north-western margin of the Dinant Syncline can be correlated despite a different background in the main depositional settings and the distance of nearly 75 km separating the sections. A thorough comparison of our sedimentological data from both locations with an abundant literature permitted to better decode the delineation of main facies belts distribution and the major depositional changes within the Dinant Basin for the early-late Givetian interval.
- According to the moderate to good correlation ($r_{La\ Thure}$ = 0.51-0.61; $n_{La\ Thure}$ = 30; $r_{Fromelennes\text{-}Flohimont}$ = 0.61-0.66; $n_{Fromelennes\text{-}Flohimont}$ = 42) observed between magnetic susceptibility (MS) and proxies for siliciclastic influx we can deduce that the magnetic signal is still carrying some primary depositional-induced information. As a result of this, we can conclude that MS technique can serve as a proxy for siliciclastic input variations toward the basin. Moreover, the

behavior of MS for the homoclinal and rimmed shelf profiles compared to microfacies have turned out to be similar, which means that the MS curves drawn for each section can be used for correlation purpose in the Dinant Syncline.

- Observations made throughout the late Givetian in the La Thure section indicate that eolian-dust related deposition might have a major influence on the MS signal.
- In term of palaeo-oxygenation, the U/Th proxy record in the La Thure section points to a significant change in the oxygenation level of bottom water condition prevailing in the platform, from oxygen-depleted throughout the Middle Givetian to more oxic conditions within the Late Givetian. This change towards more oxic condition is thought to have been driven either by an increasing aridity on the continent or a better ocean circulation toward the Late Givetian. Furthermore, we can conclude that these two hypotheses are concurrent with the increase palaeo-temperature near the onset of the Late Givetian.

7. References

Aitken, J.D. (1967) Classification and environmental significance of cryptalgal limestones and dolomites, with illustrations from the Cambrian and Ordovician of southwestern Alberta. *Journal of Sedimentary Petrology*, **37,** 1163-1178.

Bábek, O., Kalvoda, J., Aretz, M., Cossey, P.J., Devuyst, F.X., Herbig, H.G. and Sevastopulo, G. (2010) The correlation potential of magnetic susceptibility and outcrop gamma-ray logs at Tournaisian-Viséan boundary sections in Western Europe. *Geologica Belgica*, **13,** 291-308.

Bábek, O., Přikryl, T. and Hladil, J. (2007) Progressive drowning of carbonate platform in the Moravo-Silesian Basin (Czech Republic) before the Frasnian/Famennian event: facies, compositional variations and gamma-ray spectrometry. *Facies*, **53,** 293-316.

Baccelle, L. and Bosellini, A. (1965) Diagrammi per la stima visiva della composizione percentuale nelle rocce sedimentarie. *Annali della Università di Ferrara, Sezione IX, Science Geologiche e Paleontologiche*, **1,** 59-62.

Belanger, I., Delaby, S., Delcambre, B., Ghysel, P., Hennebert, M., Laloux, M., Marion, J.-M., Mottequin, B. and Pingot, J.-L. (2012) Redéfinition des unités structurales du front varisque utilisées dans le cadre de la nouvelle Carte géologique de Wallonie (Belgique). *Geologica Belgica*, **15,** 169-175.

Bhattacharyya, A. and Chakraborty, C. (2000) *Analysis of Sedimentary Successions. A field manual*, Rotterdam, 408 pp.

Boulvain, F. and Coen-Aubert, M. (2006) A fourth level of Frasnian carbonate mounds along the south side of the Dinant Synclinorium (Belgium). *Bulletin de l'Institut Royal des Sciences Naturelles de Belgique*, **76,** 31-51.

Boulvain, F., Coen-Aubert, M., Mansy, J.L., Proust, J.N. and Tourneur, F. (1995) Le Givetien en Avesnois (Nord de la France): Paléoenvironnements et implications paléogéographiques. *Bulletin de la Société belge de Géologie*, **103,** 171-203.

Boulvain, F., Da Silva, A.C., Mabille, C., Hladil, J., Gersl, M., Koptikova, L. and Schnabl, P. (2010) Magnetic Susceptibility Correlation of Km-Thick Eifelian-Frasnian Sections (Ardennes and Moravia). *Geologica Belgica,* **13,** 309-318.

Boulvain, F., Mabille, C., Poulain, G. and Da Silva, A.C. (2009) Towards a palaeogeographical and sequential framework for the givetian of Belgium. *Geologica Belgica*, **12,** 161-178.

Boulvain, F. and Préat, A. (1986) Les calcaires laminaires du Givétien Supérieur du bord sud du Bassin de Dinant (Belgique, France): Témoins d'une évolution paléoclimatique. *Annales de la Societé Géologique de Belgique*, **109,** 609-619.

Bultynck, P. (1974) Conodontes de la formation de Fromelennes du Givetien de l'Ardenne franco-belge. *Bulletin De L'Institut Royal Des Sciences Naturelles De Belgique, Sciences De La Terre*, **50,** 1-30.

Bultynck, P. (1987) Pelagic and neritic conodont successions from the Givetian of pre-Sahara Morocco and the Ardennes. *Bulletin De L'Institut Royal Des Sciences Naturelles De Belgique, Sciences De La Terre*, **57,** 149-181.

Bultynck, P., Coen-Aubert, M., Dejonghe, L., Godefroid, J., Hance, L., Lacroix, D., Preat, A., Stainier, P., Steemans, P., Streel, M. and Tourneur, F. (1991) Les formations du Dévonien moyen de la Belgique. *Mémoires pour servir à l'explication des cartes géologiques et minières de la Belgique*, **30,** 1-105.

Bultynck, P. and Dejonghe, L. (2001) Devonian lithostratigraphic units (Belgium). In: *Guide to a revised lithostratigraphic scale of Belgium* (Eds P. Bultynck and L. Dejonghe), **4**, pp. 39-69, Geologica Belgica.

Burchette, T.P. (1981) European Devonian reefs ; a review of currents concepts and models. In: *European fossil reef models, S.E.P.M. Special Publication* (Ed D.F. Toomey), **30**, pp. 85-142.

Burchette, T.P. and Wright, V.P. (1992) carbonate ramp depositional systems. *Sedimentary Geology*, **79,** 3-57.

Calvert, S.E. and Pedersen, T.F. (2007) Chapter Fourteen Elemental Proxies for Palaeoclimatic and Palaeoceanographic Variability in Marine Sediments: Interpretation and Application. In: *Developments in Marine Geology* (Eds H.M. Claude and V. Anne De), **Volume 1**, pp. 567-644. Elsevier.

Casier, J.G., Devleeschouwer, X., Maillet, S., Petitclerc, E. and Préat, A. (2013) Ostracods and rock facies across the Givetian/Frasnian boundary interval in the Sourd d'Ave section at Ave-et-Auffe (Dinant Synclinorium, Belgium). *Bulletin of Geosciences*, **88,** 241-264.

Casier, J.G. and Préat, A. (1991) Evolution sédimentaire et Ostracodes de la base du Givetien à Resteigne (bord sud du Bassin de Dinant, Belgique). *Bulletin de L'Institut Royal des Sciences Naturelles de Belgique, Sciences de la Terre*, **61,** 157-177.

Casier, J.G. and Préat, A. (2013) Ostracodes et lithologie du stratotype de la Formation du Mont d'Haurs (Givetien, Synclinorium de Dinant). *Revue de Paléobiologie.*

Coen-Aubert, M. (1992) Rugueux coloniaux mésodevoniens du fondry des chiens à nismes (Ardennes, Belgique). *Bulletin de l'Institut Royal des Sciences Naturelles de Belgique, Sciences de la Terre*, **62,** 5-21.

Coen-Aubert, M. (2000) Stratigraphy and additional rugose corals from the givetian mont d'haurs formation in the Ardennes. *Bulletin de l'Institut Royal des Sciences Naturelles de Belqique, Sciences de la Terre*, **70,** 5-24.

Coen-Aubert, M. (2002) Temnophyllids and spinophyllids (Rugosa) from the givetian mont d'Haurs formation in Belgium. *Bulletin de l'Institut Royal des Sciences Naturelles de Belqique, Sciences de la Terre*, **72,** 5-24.

Coen-Aubert, M., Preat, A. and Tourneur, F. (1986) Compte rendu de l'excursion de la Société belge de Géologie du 6 novembre 1985 consacrée à l'étude du sommet du Couvinien et du Givetien au bord sud du Bassin de Dinant, de Resteigne à Beauraing. *Bulletin de la Société belge de Géologie*, **95,** 247-256.

Cornet, P. (1975) *Morphogenèse, caractères écologiques et distribution des stromatoporoïdes dévoniens au bord sud du bassin de Dinant (Belgique)*, Université Catholique de Louvain, Leuven.

Cullen, H.M., De Menocal, P.B., Hemming, S., Brown, F.H., Guilderson, T. and Sirocko, F. (2000) Climate change and the collapse of the Akkadian empire: Evidence from the deep sea. *Geology*, **28,** 379-382.

Da Silva, A.-C., Potma, K., Weissenberger, J.A.W., Whalen, M.T., Humblet, M., Mabille, C. and Boulvain, F. (2009a) Magnetic susceptibility evolution and sedimentary environments on carbonate platform sediments and atolls, comparison of the Frasnian from Belgium and Alberta, Canada. *Sedimentary Geology*, **214,** 3-18.

Da Silva, A.C. and Boulvain, F. (2004) From paleosols to carbonate mounds: facies and environments of Middle Frasnian carbonate platform in Belgium. *Geological Quarterly*, **48,** 253-266.

Da Silva, A.C. and Boulvain, F. (2012) Analysis of the Devonian (Frasnian) platform from Belgium: A multi-faceted approach for basin evolution reconstruction. *Basin Research*, **24,** 338-356.

Da Silva, A.C., De Vleeschouwer, D., Boulvain, F., Claeys, P., Fagel, N., Humblet, M., Mabille, C., Michel, J., Sardar Abadi, M., Pas, D. and Dekkers, M.J. (2013) Magnetic susceptibility as a high-resolution correlation tool and as a climatic proxy in Paleozoic rocks - Merits and pitfalls: Examples from the Devonian in Belgium. *Marine and Petroleum Geology*, **46,** 173-189.

Da Silva, A.C., Dekkers, M.J., Mabille, C. and Boulvain, F. (2012) Magnetic susceptibility and its relationship with paleoenvironments, diagenesis and remagnetization: Examples from the Devonian carbonates of Belgium. *Studia Geophysica et Geodaetica*, **56,** 677-704.

Da Silva, A.C., Mabille, C. and Boulvain, F. (2009b) Influence of sedimentary setting on the use of magnetic susceptibility: Examples from the Devonian of Belgium. *Sedimentology*, **56,** 1292-1306.

Da Silva, A.C., Whalen, M.T., Hladil, J., Koptikova, L., D., C., Spassov, S., Boulvain, F. and Devleeschouwer, X. (2014) Application of magnetic susceptibility as a paleo-climatic proxy on Paleozoic sedimentary rocks and characterization of magnetic signal - IGCP-580 project and events. *Episodes*, **37,** 87-95.

De Vleeschouwer, D., Boulvain, F., Da Silva, A.-C., Pas, D., Labaye, C. and Claeys, P. (2014) The astronomical calibration of the Givetian (Middle Devonian) timescale (Dinant Synclinorium, Belgium). *Geological Society, London, Special Publications*, **414**.

De Wilde, C. (2005) *Sédimentologie de la Formation de Trois-Fontaines à Marenne*, Université de Liège, unpublished master thesis.

Devleeschouwer, X., Petitclerc, E., Spassov, S. and Préat, A. (2010) The Givetian-Frasnian boundary at nismes parastratotype (Belgium): The magnetic susceptibility signal controlled by ferromagnetic minerals. *Geologica Belgica*, **13,** 351-366.

Dickson, J. (1965) A modified staining technique for carbonates in thin section.

Dunham, R.J. (1962) Classification of carbonate rocks according to depositional texture. *Amercian Association of Petroleum Geologists Memoir*, **1,** 108-121.

Ellwood, B.B., Crick, R.E., Hassani, A.E., Benoist, S.L. and Young, R.H. (2000) Magnetosusceptibility event and cyclostratigraphy method applied to marine rocks: Detrital input versus carbonate productivity. *Geology*, **28,** 1135-1138.

Ellwood, B.B., Tomkin, J.H., El Hassani, A., Bultynck, P., Brett, C.E., Schindler, E., Feist, R. and Bartholomew, A.J. (2011) A climate-driven model and development of a floating point time scale for the entire Middle Devonian Givetian Stage: A test using magnetostratigraphy susceptibility as a climate proxy. *Palaeogeography, Palaeoclimatology, Palaeoecology*, **304,** 85-95.

Embry, A.F. and Klovan, J.E. (1972) Absolute water depth limits of Late Devonian paleoecological zones. *Geologische Rundschau*, **61,** 672-686.

Errera, M., Mamet, B. and Sartenaer, P. (1972) Le calcaire Givetien à Givet. *Bulletin de l'Institut Royal des Sciences Naturelles de Belgique, Science de la Terre*, **48,** 1-59.

Flügel, E. (2004) *Microfacies analysis of carbonate rocks. Analysis, Interpretation and Application*. Springer-Verlag, Berlin, 976 pp.

Fürsich, F.T. and Oschmann, W. (1993) Shell beds as tools in basin analysis: the Jurassic of Kachchh, western India. *Journal of the Geological Society (London)*, **150,** 169-185.

Fürsich, F.T. and Pandey, D.K. (1999) Genesis and environmental significance of Upper Cretaceous shell concentrations from the Cauvery Basin, southern India. *Palaeogeography, Palaeoclimatology, Palaeoecology*, **145,** 119-139.

Garland, J., Tucker, M.E. and Scrutton, C.T. (1996) Microfacies analysis and metre-scale cyclicity in the Givetian back-reef sediments of southeast Devon. *Proceedings - Ussher Society*, **9,** 31-36.

Gischler, E. (1995) Current and wind induced facies patterns in a Devonian atoll; Iberg Reef, Harz Mts., Germany. *Palaios*, **10,** 180-189.

Gouwy, S. and Bultynck, P. (2003) Conodont based graphic correlation of the Middle Devonian formations of the Ardenne (Belgium): Implications for stratigraphy and construction of a regional composite. *Revista Española de Micropaleontologia*, **35,** 315-344.

Hatch, J.R. and Leventhal, J.S. (1992) Relationship between inferred redox potential of the depositional environment and geochemistry of the Upper Pennsylvanian (Missourian) Stark Shale Member of the Dennis Limestone, Wabaunsee County, Kansas, U.S.A. *Chemical Geology*, **99,** 65-82.

Hennebert, M. (2008) Carte géologique de Wallonie, Merbes-Le-Château - Thuin n°52/1-2, à 1/25000 et sa notice explicative. Ministère de la région Wallonne.

Hladil, J., Gersl, M., Strnad, L., Frana, J., Langrova, A. and Spisiak, J. (2006) Stratigraphic variation of complex impurities in platform limestones and possible significance of atmospheric dust: a study with emphasis on gamma-ray spectrometry and magnetic susceptibility outcrop logging (Eifelian-Frasnian, Moravia, Czech Republic). *International Journal of Earth Sciences*, **95,** 703-723.

Joachimski, M.M., Breisig, S., Buggisch, W., Talent, J.A., Mawson, R., Gereke, M., Morrow, J.R., Day, J. and Weddige, K. (2009) Devonian climate and reef evolution: Insights from oxygen isotopes in apatite. *Earth and Planetary Science Letters*, **284,** 599-609.

Joachimski, M.M., van Geldern, R., Breisig, S., Buggisch, W. and Day, J. (2004) Oxygen isotope evolution of biogenic calcite and apatite during the Middle and Late Devonian. *International Journal of Earth Sciences*, **93,** 542-553.

Johnson, J.G., Klapper, G. and Sandberg, C.A. (1985) Devonian eustatic fluctuations in Euramerica. *Geological Society of America Bulletin*, **96,** 567-587.

Jones, B. and Manning, D.A.C. (1994) Comparison of geochemical indices used for the interpretation of palaeoredox conditions in ancient mudstones. *Chemical Geology*, **111,** 111-129.

Kidwell, S.M. and Bosence, D.W. (1991) Taphonomy and time-averaging of marine shelly faunas. *Taphonomy: releasing the data locked in the fossil record. Plenum, New York*, 115-209.

Kiessling, W., Flügel, E. and Golonka, J.A.N. (2003) Patterns of Phanerozoic carbonate platform sedimentation. *Lethaia*, **36,** 195-225.

Koptíková, L. (2011) Precise position of the Basal Choteč event and evolution of sedimentary environments near the Lower–Middle Devonian boundary: The magnetic susceptibility, gamma-ray spectrometric, lithological, and geochemical record of the Prague Synform (Czech Republic). *Palaeogeography, Palaeoclimatology, Palaeoecology*, **304,** 96-112.

Koptíková, L., Bábek, O., Hladil, J., Kalvoda, J. and Slavík, L. (2010) Stratigraphic significance and resolution of spectral reflectance logs in Lower Devonian carbonates of the Barrandian area, Czech Republic; a correlation with magnetic susceptibility and gamma-ray logs. *Sedimentary Geology*, **225,** 83-98.

Krebs, W. (1974) Devonian Carbonate Complexes of Central Europe. In: *Reefs in Time and Space: Selected Examples from the Recent and Ancient* (Ed L.F. Laporte), pp. 155-208. Special Publication of the Society for Economic Paleontologists and Mineralogists.

Lecompte, M. (1951) Les stromatoporoïdes du Dévonien moyen et supérieur du Bassin de Dinant: première partie. *Mémoires de l'Institut Royal des Sciences Naturelles de Belgique*, **116,** 1-215.

Lecompte, M. (1952) Les stromatoporoides du Dévonien moyen et supérieur du bassin de Dinant: deuxième partie. *Mémoires de L'Institut Royal Des Sciences Naturelles De Belgique*, **117,** 216-359.

Logan, B.V. and Semenuik, V. (1976) Dynamic Methamorphism: Processes and Products in Devonian Carbonate Rocks, Canning Basin, Western Australia. *Geological Society of Australia Special Publication*, **6,** 138.

Mabille, C. and Boulvain, F. (2007) Sedimentology and magnetic susceptibility of the Upper Eifelian-Lower Givetian (Middle Devonian) in SW Belgium: Insights into carbonate platform initiation. *Geological Society Special Publication*, **275,** 109-123.

Mabille, C., De Wilde, C., Hubert, B., Boulvain, F. and Da Silva, A.C. (2008a) Detailed sedimentological study of a non-classical succession for Trois-Fontaines and Terres d'Haurs formations (Lower Givetian, Marenne, Belgium) - Introduction to the Marenne Member. *Geologica Belgica*, **11,** 217-238.

Mabille, C., Pas, D., Aretz, M., Boulvain, F., Schröder, S. and Silva, A.C. (2008b) Deposition within the vicinity of the Mid-Eifelian High: Detailed sedimentological study and magnetic susceptibility of a mixed ramp-related system from the Eifelian Lauch and Nohn formations (Devonian; Ohlesberg, Eifel, Germany). *Facies*, **54,** 597-612.

Machel, H.G. (1990) Faziesinterpretation des Briloner Riffs mit Hilfe eines Faziesmodells für devonische Riffkarbonate. *Geologische Jahrbuch Reihe D*, **95,** 43-83.

Maillet, S., Milhau, B. and Dojen, C. (2013) Stratigraphical distribution of Givetian ostracods in the type-area of the Fromelennes Formation (Fromelennes, Ardennes, France) and their relationship to global event. *Bulletin of Geosciences*, **88,** 865-892.

Maillet, S., Milhau, B. and Pinte, E. (2011) The Fromelennes Formation in the type-area (Fromelennes, Ardennes, France). *Annales de la Société Géologique du Nord*, **18,** 9-34.

Mamet, B. (1991) Carboniferous Calcareous Algae. In: *Calcareous Algae and Stromatolites* (Ed R. Rober), pp. 370-451. Springer Berlin Heidelberg.

Mamet, B. and Préat, A. (1986) Algues givetiennes du bord sud du bassin de Dinant et des régions limitrophes. *Annales de la Société Géologique de Belgique*, **109,** 431-454.

Mamet, B.L. (1970) Sur les Umbellaceae. *Canadian Journal of Earth Sciences*, **7,** 1164-1171.

Mansy, J.L., Lacquement, F., Meilliez, F. and Van Vliet-Lanoë, B. (2006) Carte géologique de Givet (1/50000). In: *Carte géologique de la France* (Ed B.d.R.G.e. Minière).

McKerrow, W.S. and Scotese, C.R. (1990) *Paleozoic Palaeogeography and biogeography*. Geological Society of London, Memoir, 433 pp.

Michel, J., Boulvain, F., Philippo, S. and Da Silva, A.C. (2010) Palaeoenvironmental Study and Small Scale Correlations Using Facies Analysis and Magnetic Susceptibility of the Mid-Emsian (Himmelbaach Quarry, Luxembourg). *Geologica Belgica*, **13,** 447-458.

Molina Garza, R.S. and Zijderveld, J.D.A. (1996) Paleomagnetism of Paleozoic strata, Brabant and Ardennes Massifs, Belgium: Implications of prefolding and postfolding Late Carboniferous secondary magnetizations for European apparent polar wander. *Journal of Geophysical Research B: Solid Earth*, **101,** 15799-15818.

Neumann, M., Pozaryska, K. and Vachard, D. (1975) Remarques sur les microfacies du Devonién de Lublin (Pologne). *Revue de Micropaléontologie*, **18,** 38-52.

Pas, D., Da Silva, A.C., Cornet, P., Bultynck, P., Königshof, P. and Boulvain, F. (2013) Sedimentary development of a continuous Middle Devonian to Mississippian section from the fore-reef fringe of the Brilon Reef Complex (Rheinisches Schiefergebirge, Germany). *Facies*, **59,** 969-990.

Pas, D., Da Silva, A.C., Devleeschouwer, X., De Vleeschouwer, D., Labaye, C., Cornet, P., Michel, J. and Boulvain, F. (2014a) Sedimentary development and magnetic susceptibility evolution of the Frasnian in Western Belgium (Dinant Synclinorium, La Thure section). *Geological Society, London, Special Publications*, **414**.

Pas, D., Da Silva, A.C., Suttner, T., Kido, E., Bultynck, P., Pondrelli, M., Corradini, C., De Vleeschouwer, D., Dojen, C. and Boulvain, F. (2014b) Insight into the development of a carbonate platform through a multi-disciplinary approach: A case study from the Upper Devonian slope deposits of Mount Freikofel (Carnic Alps, Austria/Italy). *International Journal of Earth Sciences*, **103,** 519-538.

Pettijohn, F.J., Potter, P.E. and Siever, R. (1972) *Sand and sandstone*. Springer, Berlin, 618 pp.

Playford, P.E. (1980) Devonian "Great Barrier Reef" of Canning Basin, Western Australia. *The American Association of Petroleum geologists Bulletin*, **64,** 814-840.

Pohler, S.M.L. (1998a) Devonian carbonate buildup facies in an intra-oceanic island arc (Tamworth Belt, New South-Wales, Australia). *Facies*, **39,** 1-34.

Pohler, S.M.L. (1998b) Devonian carbonate buildup facies in an intra-oceanic island arc (Tamworth Belt, New South-Wales, Australia). *Facies***,** 1-34.

Poulain, G. (2006) *Etude sédimentologique du Groupe de Givet à Givet*, Université de Liège, unpublished master thesis, 49 pp.

Préat, A. (2004) Le Givétien franco-belge: moteur de la sédimentation eustatisme vs subsidence? . *Géologie de la France* **1-2,** 45-51.

Préat, A. (2006) Le Givétien franco-belge: moteur de la sédimentation eustatisme vs subsidence? *Géologie de la France***,** 45-51.

Préat, A. and Boulvain, F. (1982) Etude sédimentologique des calcaires givetiens à Vaucelles (bord Sud du Synclinorium de Dinant). *Annales de la Société Géologique de Belgique*, **105,** 273-282.

Préat, A. and Boulvain, F. (1988) Middle and upper Devonian carbonate platform evolution in Dinant and Namur Basins (Belgium, France). In: *Excursion A-1, IAS 9th European Regional Meeting: Excursion Guidebook*, pp. 1-25.

Préat, A. and Bultynck, P. (2006) Givetian. In: *Chronostratigraphic units named from Belgium* (Eds P. Bultynck and L. Dejonghe), pp. 9-18. Geologica Belgica.

Préat, A. and Carliez, D. (1994) microfaciès et cyclicité dans le givetien supérieur de Fromelennes (Synclinorium de Dinant, France). *Annales de la Société Géologique de Belgique*, **117,** 227-243.

Préat, A., Ceuleneer, G. and Boulvain, F. (1987) Etude sédimentologique des calcaires du Givétien Inférieur d'Olloy-sur-Viroin (bord Sud du Bassin de Dinant, Belgique). *Annales de la Société Géologique du Nord*, **106,** 251-265.

Préat, A., Coen-Aubert, M., Mamet, B. and Tourneur, F. (1984) Sédimentologie et paléoécologie de trois niveaux récifaux du Givetien inférieur de Resteigne (bord sud du Bassin de Dinant, Belgique). *Bulletin de la Société belge de Géologie*, **93,** 227-240.

Préat, A. and Kasimi, R. (1995) Sédimentation de rampe mixte silico-carbonatée des couches de transition eifeliennes-givetiennes franco-belge. Deuxième partie : cyclostratigraphie et paléostructuration. *Bulletin des Centres de Recherches et d'Exploration-Production. Elf-Aquitaine*, **19,** 329–375.

Préat, A. and Mamet, B. (1989) Sédimentation de la plate-forme carbonatée Givetienne Franco-belge. *Bulletin des Centres de Recherches et d'Exploration-Production. Elf-Aquitaine*, **13,** 47-86.

Purser, B.H. (1980) *Sédimentation et diagenèse des carbonates néritiques récents*. Edition Technip, Paris, 367 pp.

Read, J.F. (1985) Carbonate Platform Facies Models. *The American Association of Petroleum Geologists Bulletin*, **69,** 1-21.

Rimmer, S.M. (2004) Geochemical paleoredox indicators in Devonian–Mississippian black shales, Central Appalachian Basin (USA). *Chemical Geology*, **206,** 373-391.

Riquier, L., Averbuch, O., Devleeschouwer, X. and Tribovillard, N. (2010) Diagenetic versus detrital origin of the magnetic susceptibility variations in some carbonate Frasnian-Famennian boundary sections from Northern Africa and Western Europe: Implications for paleoenvironmental reconstructions. *International Journal of Earth Sciences*, **99,** 57-73.

Riquier, L., Tribovillard, N., Averbuch, O., Joachimski, M.M., Racki, G., Devleeschouwer, X., El albani, A. and Riboulleau, A. (2005) Chapter 8: Productivity and bottom water redox conditions at the Frasnian-Famennian boundary on both sides of the Eovariscan Belt: constraints from trace-element geochemistry. *Developments in Palaeontology and Stratigraphy*, **20,** 199-224.

Scholle, P.A. and Ulmer-Scholle, D.S. (2003) *Color Guide to the Petrography of Carbonate Rocks: Grains, Texture, Porosity, Diagenesis*. American Association of Petroleum Geologist Memoir 77, 474 pp.

Schönlaub, H.P. and Histon, K. (2000) The Palaeozoic evolution of the Southern Alps. *Mitteilungen der Österreichischen Geologischen Gesellschaft*, **92,** 15-34.

Scotese, C.R. (2005) Paleomap project, climate history.

Skompski, S. and Szulczewski, M. (1994) Tide-dominated Middle Devonian sequence from the northern part of the Holy Cross Mountains (Central Poland). *Facies*, **30,** 247-265.

Śliwinski, M.G., Whalen, M.T. and Day, J. (2010) Comparison of magnetic susceptibility (MS) and other geochemical proxies from the Middle-Late Frasnian of the Canadian Rocky Mountains: Implications for paleoenvironmental and paleoclimatic analyses and interpretations of the punctata Event. *Przeglad Geologiczny*, **58,** 1152-1160.

Śliwiński, M.G., Whalen, M.T. and Jed, D. (2010) Trace element variations in the middle Frasnian Punctata zone (Late Devonian) in the Western Canada Sedimentary Basin - changes in oceanic bioproductivity and paleoredox spurred by a pulse of terrestrial afforestation? *Geologica Belgica*, **13,** 459-482.

Śliwiński, M.G., Whalen, M.T., Meyer, F.J. and Majs, F. (2012) Constraining clastic input controls on magnetic susceptibility and trace element anomalies during the Late Devonian punctata Event in the Western Canada Sedimentary Basin. *Terra Nova*, **24,** 301-309.

Strasser, A. (1986) Ooids in Purbeck limestones (lowermost Cretaceous) of the Swiss and French Jura. *Sedimentology*, **33,** 711-727.

Sur, S., Soreghan, M.J., Soreghan, G.S. and Stagner, A.F. (2010) Extracting the silicate mineral fraction from ancient carbonate: Assessing the geologic record of dust. *Journal of Sedimentary Research*, **80,** 763-769.

Torsvik, T.H., Van der Voo, R., Preeden, U., Niocaill, C.M., Steinberger, B., Doubrovine, P.V., van Hinsbergen, D.J.J., Domeier, M., Gaina, C., Tohver, E., Meert, J.G., McCausland, P.J. and Cocks, L.R.M. (2012) Phanerozoic polar wander, palaeogeography and dynamics. *Earth-Science Reviews*, **114,** 325-368.

Tourneur, F. (1985) *Contribution à l'étude des tabulés du Dévonien moyen de la Belgique. Systématique et stratigraphie*, Université Catholique de Louvain, Leuven, 568 pp.

Tribovillard, N., Algeo, T.J., Lyons, T. and Riboulleau, A. (2006) Trace metals as paleoredox and paleoproductivity proxies: An update. *Chemical Geology*, **232,** 12-32.

Tucker, M.E. (2001) *Sedimentary Petrology. An introduction to the Origin of the Sedimentary Rocks, 3rd Edition*. Blackwell, London, 272 pp.

Tucker, M.E. and Wright, V.P. (1990) *Carbonate Sedimentology***,** 482.

Vanderaveroet, P., Averbuch, O., Deconinck, J.F. and Chamley, H. (1999) A record of glacial/interglacial alternations in Pleistocene sediments off New Jersey expressed by clay mineral, grain-size and magnetic susceptibility data. *Marine Geology*, **159,** 79-92.

Whalen, M.T. and Day, J.E. (2008) Magnetic susceptibility, biostratigraphy, and sequence stratigraphy: Insights into Devonian carbonate platform development and basin infilling, western Alberta, Canada. *Society for Sedimentary Geology*, **89,** 291-314.

Whalen, M.T. and Day, J.E. (2010) Cross-basin variations in magnetic susceptibility influenced by changing sea level, paleogeography, and paleoclimate: Upper Devonian, western Canada sedimentary basin. *Journal of Sedimentary Research*, **80,** 1109-1127.

Wilson, J.L. (1975) *Carbonate Facies in geologic history*. Springer-Verlag, Berlin, Heidelberg, New York, 473 pp.

Wood, R. (2000) Palaeoecology of a Late Devonian back reef: Canning Basin, Western Australia. *Palaeontology*, **43,** 671-703.

Zegers, T.E., Dekkers, M.J. and Baily, S. (2003) Late Carboniferous to Permian remagnetization of Devonian limestones in the Ardennes: Role of temperature, fluids, and deformation. *Journal of geophysical research*, **108,** 5/1 - 5/19.

Ziegler, A.P. (1982) *Geological Atlas of Western and Central Europe*. Shell Internationale Petroleum Maatschappij, 130 pp.

Zwing, A., Matzka, J., Bachtadse, V. and Soffel, H.C. (2005) Rock magnetic properties of remagnetized Palaeozoic clastic and carbonate rocks from the NE Rhenish massif, Germany. *Geophysical Journal International*, **160,** 477-486.

Second part

Sedimentary development and magnetic susceptibility evolution of the Frasnian in Western Belgium (Dinant Synclinorium, La Thure section)

Based on: Pas, D., Da Silva, A.C., Devleeschouwer, X., De Vleeschouwer, D., Labaye, C., Cornet, P., Michel, J., Boulvain, F. (2014): Sedimentary development and magnetic susceptibility evolution of the Frasnian in Western Belgium (Dinant Synclinorium, La Thure section). *Geological Society of London, Special Publication*, 414.

Sedimentary development and magnetic susceptibility evolution of the Frasnian in Western Belgium (Dinant Synclinorium, La Thure section)

D. PAS[1]*, A. C. DA SILVA[1], X. DEVLEESCHOUWER[2], D. DE VLEESCHOUWER[3,4], C. LABAYE[1], P. CORNET[1], J. MICHEL[5] & F. BOULVAIN[1]

[1]*Pétrologie sédimentaire, B20, Liège University, B-4000 Liège, Belgium*

[2]*O.D. Earth and History of Life, Royal Belgian Institute of Natural Sciences, 13 Rue Jenner, B-1000, Brussels, Belgium*

[3]*Earth System Science and Department of Geology, Vrije Universiteit Brussel, Pleinlaan 2, B-1050, Brussels, Belgium*

[4]*Present address: MARUM – Center for Marine Environmental Sciences, Leobener Straße, D-28359 Bremen, Germany*

[5]*Département de géologie, Rue de Bruxelles, 61, Namur University, B-5000, Namur, Belgium*

**Corresponding author (e-mail: dpas@ulg.ac.be)*

Abstract: Recent opening of the La Thure quarry in Western Belgium allowed the collection of new data from a poorly outcropping area of the Belgian Frasnian platform. The studied section covers an interval extending from the *falsiovalis* to *hassi* s.l. Zones. Sedimentological analyses allowed the reconstruction of depositional settings in the northwestern part of the Dinant Synclinorium after the demise of the extended Givetian carbonate platform. Two depositional models are distinguished: (a) siliciclastic drowned platform during the Early Frasnian; and (b) a fore-reef depositional setting belonging to a rimmed shelf during the Middle Frasnian. Moreover, interpreted depositional settings in the northwestern part of the Dinant Synclinorium allowed to constraint the direction of the main facies belts for the Belgian Frasnian platform. Combination of MS and geochemistry demonstrates the inherent-parallel link existing between variation in MS values and proxy for terrestrial input (such as Si and Al). This observation means that, despite the remagnetization occurring within the Belgian Frasnian lithologies, the main trends in the MS signal from the La Thure section still reflect some syn-sedimentary conditions. The increase in MS and clastic input proxies recorded in distal fore-reef deposit within the *punctata* Zone are likely to be considered as enhanced by rapid and strong shallowing events recognized in the '*puncata* Event' interval.

The Frasnian platform in Belgium shows important north–south and east–west facies variations (Boulvain *et al.* 1999; Bultynck & Dejonghe 2001). The lasts decade's advances in biostratigraphy (Gouwy & Bultynck 2000), sedimentology (Da Silva & Boulvain 2004; Boulvain 2007), geochemistry (Da Silva & Boulvain 2008), palaeoecology (Da Silva *et al.* 2011*a*, *b*) and magnetic susceptibility (Da Silva *et al.* 2009; Devleeschouwer *et al.* 2010) resulted in an improved understanding of the timing and relationship between sea-level changes, water circulation, sediment supply and facies distribution of the Belgian Frasnian carbonate platform (synthesis in Da Silva & Boulvain 2012). Nonetheless, the northwestern part of the platform did not receive as much attention as the southern and northeastern part. As a consequence some weak points remained, hampering a full understanding of the facies belt's geometry within the Belgian Frasnian basin. Furthermore, the Lower Frasnian and the base of the Middle Frasnian in Belgium are dominated by shaly lithologies, often resulting in very poor outcropping conditions. Consequently, very few data are available for this crucial period of time, characterized by the initiation of the Frasnian carbonate factory subsequent to the drowning and demise of the prominent Givetian rimmed shelf at the Givetian–Frasnian boundary. This paper proposes a detailed sedimentological study of the outstanding and continuous Frasnian section recorded in the La Thure quarry and provides a sedimentological model covering the entire sequence of facies in the northwestern margin of the Dinant Synclinorium (DS). Lithostratigraphic and biostratigraphic datasets from the literature have been combined with new sedimentological and geochemical analyses in order to gain a better understanding of the depositional and environmental changes that occur within the Early and Middle Frasnian interval in the northwestern fringe of the Frasnian platform. Moreover, geochemistry and magnetic susceptibility measurements helped to establish further correlation between long-term trends recorded in Upper Devonian lithologies and other sections from the Rhenohercynian Basin.

Geological context

During the Late Devonian time, Belgium was situated at near 20° south of the equator (Torsvik *et al.* 2012) along Laurussia's southeastern margin (Fig. 1a) and was a site of extensive reefal development. Frasnian sediments crops out in the Philippeville Anticlinorium, and along the border of the Versdres and Dinant Synclinoria, which are all large-scaled units of the Rhenohercynian fold-and-thrust belt (Fig. 1b). This extensive tectonic structure was formed during the Carboniferous to Permian, as a consequence of the collision between Laurussia and Gondwana, during the Variscan orogeny. Several authors (e.g. Molina Garza & Zjiderveld 1996; Zwing *et al.* 2005) have highlighted that, during this orogeny, rocks belonging to Rhenohercynian fold-and-thrust belt were affected by remagnitization.

The La Thure section is located in southwestern Belgium (50°17′11″N, 4°09′40′E) and belongs to the northwestern border of the DS (Fig. 1b). Throughout recent decades, extensive studies dealing with sedimentology, palaeontology and magnetic susceptibility have allowed a platform model

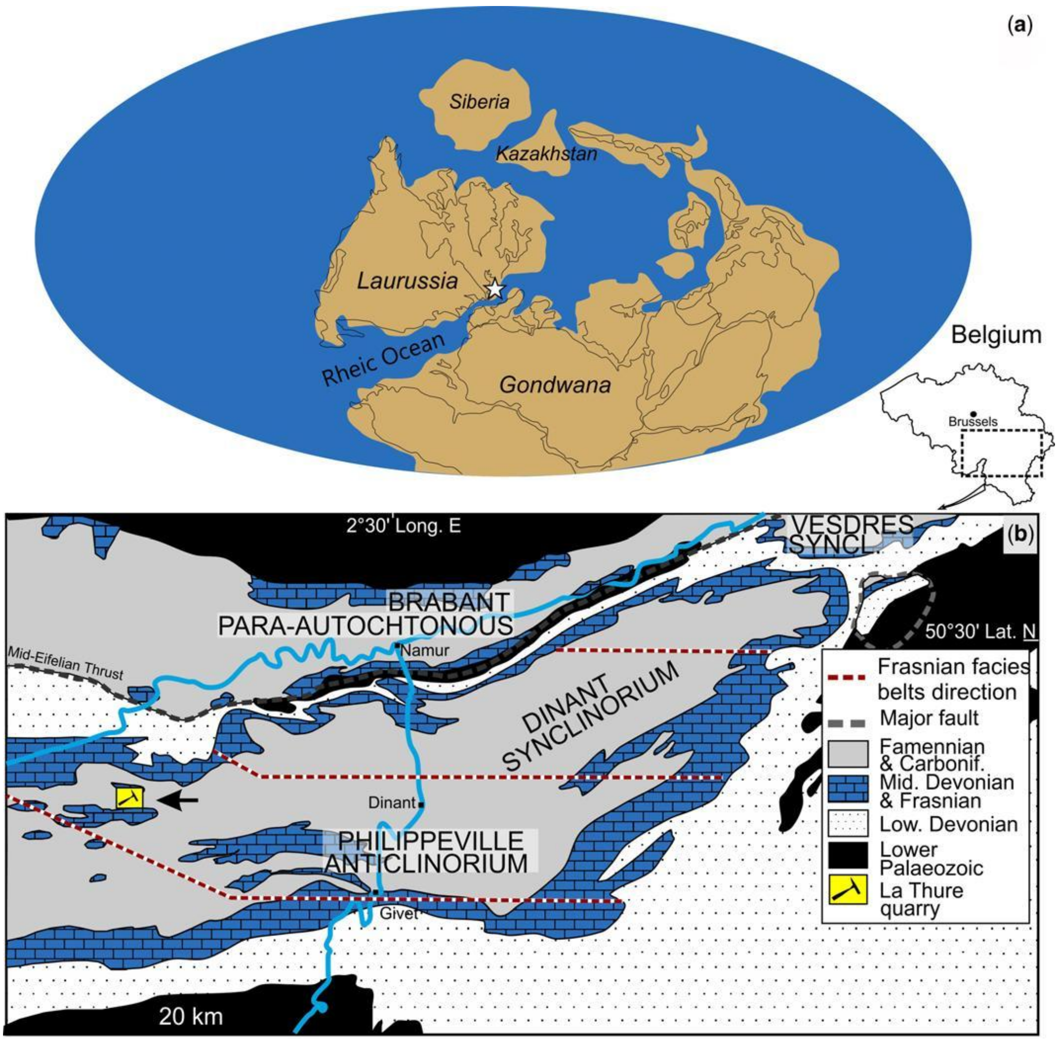

Fig. 1. (**a**) Location of Belgium in the eastern margin of Laurussia during Devonian (simplified from Kiessling *et al.* 2003). (**b**) Simplified geological map of Belgium with location of the main tectonic structures.

to be established for the Frasnian of Belgium (synthesis in Da Silva & Boulvain 2012). This model includes three main facies belts (Fig. 2) covering a large range of environments, from lagoonal-supratidal to off-reef settings, with significant development of carbonate mud mounds. During the early Frasnian, each belt is dominated by shale deposition as a result of the late Givetian transgressive event that led to the drowning of the extensive Givetian platform (Boulvain *et al.* 2009; Fig. 2). During the Middle Frasnian an outstanding diversification appears between the different facies belts. Each belt is characterized by a specific facies association, carbonate production and sedimentation style. The most distal part of the platform ('southern belt'), located along the southern border of the Dinant Synclinorium, is characterized by carbonate mound build-ups with associated flank and off-mound facies (Boulvain 2001). Three distinct levels of carbonate mounds are recognized in the middle part of the Frasnian (a summary is given in Boulvain 2001). In the Philippeville Anticlinorium ('central belt'), the carbonate mound-bearing levels are replaced by argillaceous and nodular crinoidal marls with local lenses of stromatoporoid–coral coverstones and dark crinoidal argillaceous bedded limestone, representing open-marine and biostromal facies. Along the northern border of the Dinant Synclinorium ('northern belt'), the Middle Frasnian consists of bedded limestones, exhibiting a distinct proximal aspect with biostromes alternating with lagoonal facies. As for the Lower Frasnian, the Upper Frasnian Belgian platform is characterized by the widespread deposition of shales corresponding to the final Frasnian transgressive pulse. For the following discussion, the Belgium Frasnian conodont zonation established by Gouwy & Bultynck (2000) will be used.

Methods

A detailed bed to bed description and sampling of the La Thure section (Figs 3 & 4) was performed with a sampling rate of 25–45 cm, depending the outcrop condition. For instance, for the massive stromatoporoid limestone level the sampling rate is one sample per metre. For microfacies analysis around 100 thin sections were studied. Thin sections are stored at the sedimentary petrology laboratory of the University of Liège (TUR 311–429b). The textural classification used to characterize the microfacies follows Dunham (1962) and Embry & Klovan (1972). Estimation of sorting is based on the visual charts of Pettijohn *et al.* (1972) and visual percentages estimation is based on Baccelle & Bosellini (1965). Thin sections were stained using Dickson solution to differentiate calcite, dolomite, ferroan calcite and feroan dolomite (Dickson 1965). Magnetic susceptibility measurements were undertaken

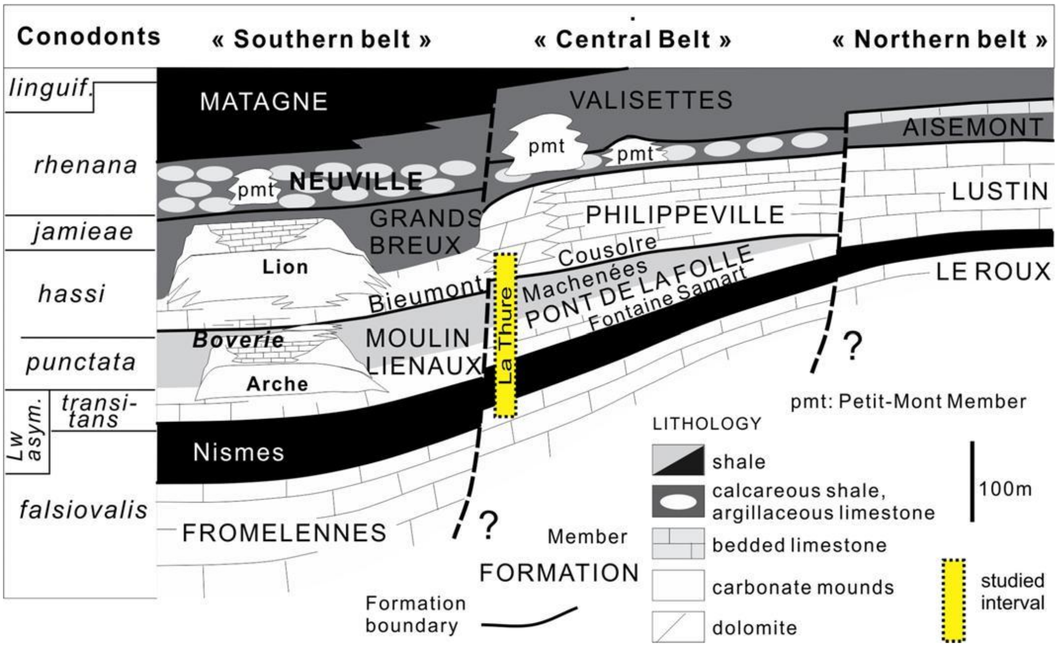

Fig. 2. Stratigraphy and facies relationships of the Frasnian basin in Belgium prior Variscan orogeny (Boulvain 2001) with location and stratigraphic interval of the La Thure section. Conodonts Zones after Bultynck *et al.* (1998).

Fig. 3. Top of the figure: view of the Nismes Formation (view from the West) showing the prevailing shale sequence corresponding to the Lower Frasnian, and location of ⓐ and ⓑ. (**a**) Transition from uppermost Givetian thick-bedded limestone to the lower Frasnian shale and yellow-earth limestone beds. (**b**) Upper portion of the Nismes Formation showing the rapid change from shale to carbonate lithologies which are corresponding to the initiation of the Frasnian carbonate factory within the northwestern margin of the Belgium Frasnian basin.

on more than 350 rock samples. Each sample was analysed three times with KLY-3 (Kappabridge) and weighed with a precision of 0.01 g. This allows the definition of the low-field mass-calibrated magnetic susceptibility for each sample and the establishment of the magnetic susceptibility stacking pattern. A group of 24 samples (*c.* 1 sample per 5 m) was analysed for major- and trace-element concentrations at Activation Laboratories Ltd (Ancaster, Ontario, Canada). Analyses were performed by inductively coupled plasma mass spectrometry (ICP-MS; major, minor and trace elements). The samples were prepared by fusion with sodium peroxide, Na_2O_2, which totally solubilizes all of the minerals analysed in an aqueous solution after treatment.

Results

Description of the section (Figs 3 & 4)

The outcrop exposed at the La Thure quarry provides a stratigraphically continuous succession of strata that starts within the Middle Givetian and ends during the Middle Frasnian. Throughout the entire section seven lithological units were recognized. Similarity of these lithological units with the formal lithostratigraphic units described in the Givetian and Frasnian lithostratigraphic charts of Belgium (e.g. Boulvain *et al.* 1999; Préat *et al.* 2006) led us to use the formal lithostratigraphic names in the present study. This paper focusses on the last four lithological units (Figs 3 & 4), corresponding to Nismes, Pont de La Folle (Fontaine Samart and des Machenées members) and Philippeville formations (PHV in Fig. 5) of Frasnian age. The measured section is *c.* 135 m thick and covers a stratigraphic interval extending from the Early to the Middle Frasnian (*P. falsiovalis* to *P. hassi s.l.* Zones). Strata are oriented N90°E with an average dip of 70°S in the lower portion and 85°S in the upper portion. Sampling starts with the first carbonaceous shale bed, which corresponds to the base of the Nismes Formation (e.g. Frasnian lithostratigraphic chart of Belgium; Boulvain *et al.* 1999).

Description of formations and members for the La Thure quarry (Fig. 5)

Nismes Formation (32 m thick; Nismes Formation, Figs 3 & 4) corresponds mainly to brownish and greenish shales. The lower part (from 0 to 1.2 m) corresponds to several decimetre-thick yellow-earth limestone beds interbedded with black carbonaceous shale layers (Fig. 3a), followed (from 1.2 to 6.5 m) by several decimetre-sized yellow-earth bioclastic limestone beds that show crinoids and shell remains. From 6.5 to 27 m, the Nismes Formation is essentially characterized by brownish to greenish shale showing few brachiopod shells. The top of the Nismes Formation (from 27 to 32 m) is marked by the occurrence of six weathered coarse-grained limestone beds (several decimetres to metres thick, Figs 3b & 4a) containing very abundant and relatively well-preserved fauna such as large-sized crinoids (stems and ossicles, Fig. 4a), brachiopod shells, solitary rugose corals and branching bryozoans.

The lower and middle part of the Fontaine Samart Member (*c.* 17 m thick; lower part of the Pont de La Folle Formation, Fig. 4) consists of a single massive light grey limestone (Fig. 4). The base of this massive limestone lies up to an outcrop hiatus of 7 m corresponding to a gully covered by rubble. The lower part is mainly characterized by a remarkable accumulation of several decimetre-sized lamellar stromatoporoids (locally they can reach 40 cm in length and be several centimetres thick; Fig. 4b) that bind the sediment in association with a coarse sparitic cement. Brachiopods, crinoids, solitary rugose corals and other unidentified bioclasts also occur. In the upper part, the accumulation of stromatoporoids gradually decreases and the limestones become fine-grained and easily visible organisms are exposed such as brachiopods (commonly complete shells), rugose corals and fenestrae (centimetre-sized) filled by calcite.

The upper part of the Fontaine Samart Member and the Machenées Member (*c.* 47 m thick; Pont de La Folle Formation, Fig. 4) start with several decimetre-thick blackish limestone beds showing scattered crinoid remains. These beds belong to the upper part of the Fontaine Samart Member (Fig. 4d). The remainder of this lithological unit mainly consists of dark-grey marly limestone showing scattered crinoids, brachiopods and solitary rugose corals altogether belonging to the Machenées Member. In the middle part, a dark fine-grained limestone bed interval occurs. Towards the top, the succession becomes more calcareous with well-developed bedding (Fig. 4c). The Machenées Member is commonly affected by an oblique cleavage.

The lower part of the Philippeville Formation (Fig. 4; *c.* 10 m thick) starts with a 3 m-thick massive light-grey dolomite containing phantoms of reef-builder debris, crinoids, brachiopods and local cavities corresponding to dissolved shells. It is overlain by a succession of centimetre- to several decimetre-thick dark-grey, fine-grained and well-bedded limestones with crinoids and brachiopod shells (Fig. 4c).

The main differences between the formations and members described herein and the formal lithostratigraphic units described in the Frasnian lithostratigraphic chart of Belgium mainly concern the thickness. In the La Thure section, all formations and members show a reduced thickness compared with stratotype area.

Microfacies (Figs 6 & 7; Table 1)

Numerous criteria are available for interpreting the palaeoenvironmental setting of sedimentary rocks and microfacies. Faunal association and depositional texture provide direct insight in the main biotope and hydrodynamic conditions. Sorting, terrigenous content, the nature of the matrix and the degree of bioclasts preservation allow palaeoenvironmental interpretations and provide a tool for estimating the distance between the source area of observed fauna and the depositional setting. Moreover, comparison with other existing microfacies models defined in the literature (Tucker & Wright 1990; Préat & Kasimi 1995; Da Silva & Boulvain 2006) allows the interpretations to be reinforced. The combined use of these criteria allowed to define six microfacies (MFLT1-MFLT6) and six sub-microfacies (MFLT4a–b, MFLT5a–b, MFLT6a–b). Their description follows the order from the most distal to the most proximal area. A summary of the main microfacies diagnostic features and interpretation is provided in Table 1.

In the studied Frasnian sequence two main faunal assemblage have been described: (a) open-marine fauna (trilobites, bryozoans, crinoids, brachiopods and ostracods); and (b) shallow-water reef-building organisms (rugose corals, tabulate corals and stromatoporoids).

Fig. 4. Top of the figure (A): view of the Fontaine Samart Member (view from the East) showing the massive character of the Member, and location of ⓐ and ⓑ. (**a**) Upper bed surface belonging to the uppermost portion of the Nismes Formation showing crinoid stems (cs), brachiopod shell (bs) and solitary rugose coral (src). (**b**) Accumulation of lamellar stromatoporoids characterizing most of the the Fontaine Samart Member. A large lamellar stromatoporoids is

MFLT1: brownish and greenish shales (Fig. 6a). This microfacies occurs within the Nismes Formation (Figs 3–5). The shale is laminated and mainly consists of clay particles with well-spread silt-sized quartz grains. At the outcrop scale, rare brachiopod shells occur.

Interpretation. Shale such as that characterizing the Nismes Formation is generally thought to be deposited in basinal settings (Krebs 1967; Stow & Piper 1984; Piecha 1993; Boulvain *et al.* 2004) where the main sedimentary process is the settling of suspended clay particles, probably below the storm wave base (SWB). The Lower Frasnian shale is usually interpreted as related to the late Givetian transgressive event, resulting in the drowning and demise of the Givetian platform (Boulvain *et al.* 2009; Casier & Préat 2009; Devleeschouwer *et al.* 2010; Casier *et al.* 2013). The quasi-absence of bioclasts from shallow- or deeper-water origins points to an environment hostile to life. Therefore, MFLT1 is considered to be deposited on the flat drowned Givetian platform below the SWB and, as mentioned by Casier *et al.* (2013), in an environment with no true barrier or topographic differentiation.

MFLT2: Carbonaceous wackestone–packstone with densely packed lumachelle levels (Fig. 6b). This microfacies occurs within the first calcareous black shale layers at the very base of the Nismes Formation, which overlies the Givetian limestone. The main characteristic of this microfacies is the presence of millimetre-sized densely packed bivalve shell (probably 'filament') levels occurring in wackestone texture (Fig. 6b). Shells are commonly centimetre-sized and mostly oriented parallel to the bedding. Other characteristics are the abundance of insoluble residue and organic matter, and the presence of well-rounded limestone lithoclasts (*c.* 5 mm) including gastropods with spongiostromate encrustation (Fig. 6b). These lithoclasts are found in the shelly levels. Bioclasts that occur in the wackestone–packstone are often broken and difficult to identify. However, brachiopod shells, bivalves, ostracods, crinoids, rare *umbella*, branching bryozoan and goniatite were identified. The matrix is neomorphized and microsparitic. The abundant insoluble residues and organic matter filling the space between crystals are probably responsible for the blackish colour of the sediment.

Interpretation. The wackestone texture with densely packed 'filament' levels and occurrence of crinoids, brachiopods, goniatites and bryozoans attests to a tempestite-related deposition (Flügel 2004) within an open-marine hemipelagic/pelagic environment (Conti & Morani 1992). Limestone lithoclasts including gastropods with spongiostromate encrustation, as well as the occurrence of *umbella*, suggest that materials were transported seaward during storms, which probably reworked previously deposited lagoonal sediment (e.g. lagoon of the Givetian platform). The occurrence of this microfacies, intercalated between Givetian limestone and Frasnian shale of MFLT1, suggests a deposition within a drowned carbonate platform environment above the SWB.

MFLT3: Marly crinoidal-brachiopod mudstone–wackestone with local packstone levels (Fig. 6c–e). This microfacies occurs within the Machenées Member of the Pont de La Folle Formation. It is characterized by the dark-brown micritic slightly argillaceous matrix commonly containing bioclast debris and well-preserved organisms. Fossils are millimetre-sized and mainly represented by crinoids (ossicles and stems; Fig. 6c) and brachiopod shells, with a few fenestrate bryozoans (Fig. 6d), ostracods, pelagic bivalves, pelagic crinoids, tentaculitids, trilobites and rare goniatites. A conspicuous character of this microfacies is the occurrence of centimetre-thick well-sorted packstone levels with the same fauna as described above but enriched in pelagic crinoids (Fig. 6e). The matrix is mostly a carbonate mud or microspar, but locally mainly composed of clay particles. Bioturbation and pyrite occur locally.

Interpretation. The well-preserved morphology of bioclasts embedded in a mudstone–wackestone texture indicates a low-energy setting dominated by deposition of fine turbid tails and probably periplatform oozes. Furthermore, faunal assemblage attests to an open-marine hemipelagic/pelagic environment. Levels enriched in pelagic echinoderms reveal turbulent events such as storms triggering bottom current responsible either for the accumulation of organisms by removing part of the matrix or for reworking of pelagic echinoderm meadows. Local occurrence of pyrite suggests a sediment water–interface temporarily depleted in oxygen. This microfacies is thought to be deposited in an intermediate to distal open-marine

Fig. 4. (*Continued*) highlighted by the black dotted line. In the centre of the figure (B): panorama displaying the Fontaine Samart Member, the des Machennées Member and the Philippeville Formation (view from the West) and the location of ⓒ and ⓓ. (**c**) Transition from massive limestone (Fontaine Samart Member) to blackish bedded limestone and then marly limestone belonging to the Machenées Member. (**d**) Transition between marly limestone of the Machenées Member and the Philippeville Formation starting with the Couslore Member (massive dolomitized limestone bed) which is directly overlain by thin-bedded limestone.

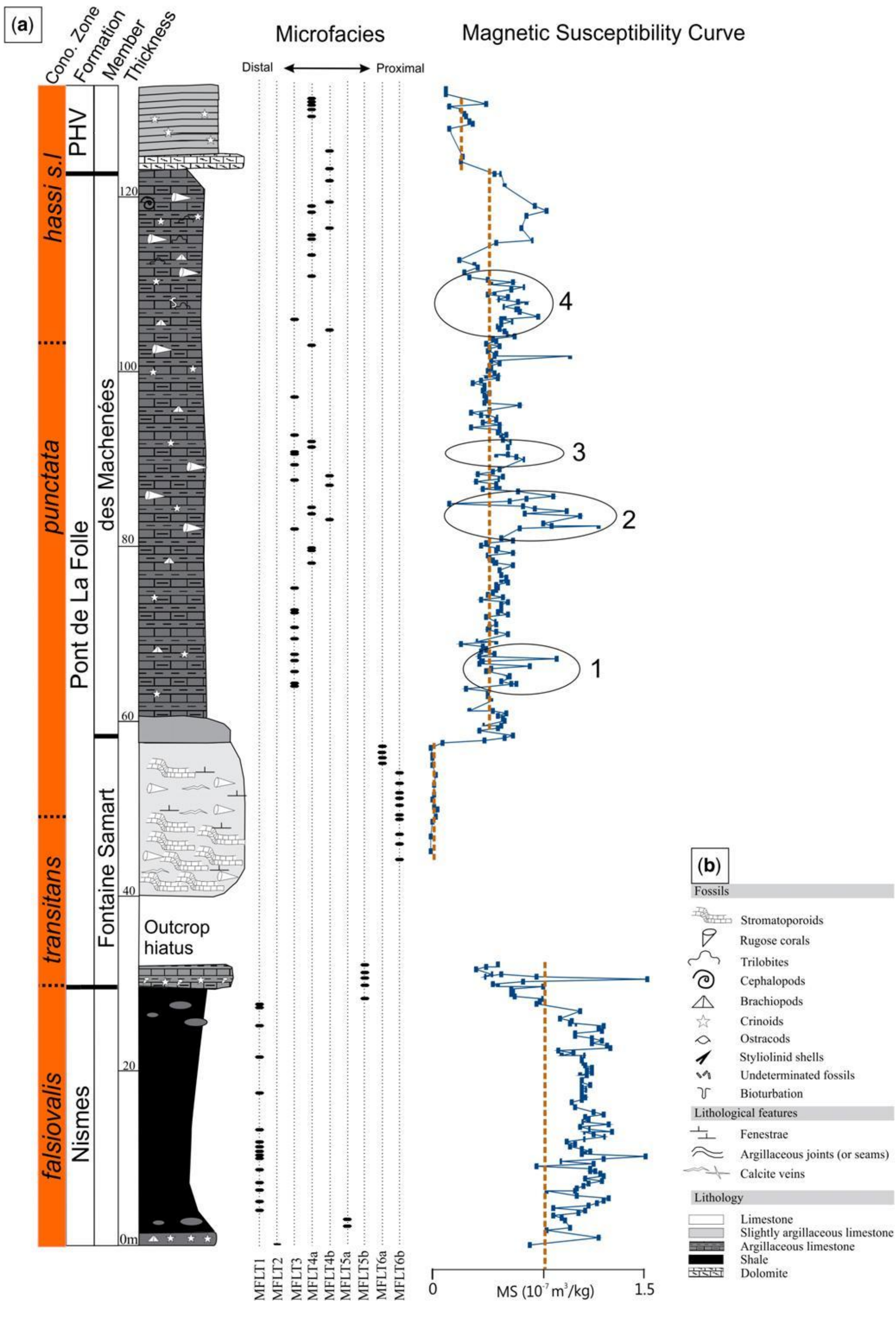

Fig. 5. (**a**) Schematic sedimentological log showing formations, members and microfacies stacking pattern. (**b**) Legend for symbols used in figures. Vertical dashed lines correspond to the average MS value for each formations and members outcropping in the section and discussed in the main text.

hemipelagic/pelagic fore-reef environment slightly above the SWB according to the local occurrence of bottom current.

MFLT4: argillaceous bioclastic wackestone–packstone (Fig. 6f–h)

MFLT4a: argillaceous shelly wackestone–packstone with local floatstone texture. This microfacies occurs within the Machenées Member (middle and upper part of the Pont de la Folle Formation) as marly limestone without easily visible bedding. It is characterized by diversified fine- to coarse-grained bioclasts with various preservation levels and showing moderate to good sorting. The faunal assemblage is characterized by prevalent broken shells of bivalves and gastropods, and crinoids. Other allochems are fenestrate and branching bryozoans (locally *c.* 5 cm; floatstone texture; Fig. 6g), ostracods, tentaculites, trilobites, pelagic echinoderms and, locally, rugose (Fig. 6h) and tabulate corals. The matrix is a brown argillaceous micrite showing local bioturbation (commonly underlined by the re-organization of broken shells within the sediment). Argillaceous material also occurs within seams oriented parallel to bedding, and centimetre-sized clay levels occur locally. The sediment is locally affected by an oblique cleavage (depending the concentration of argillaceous material).

Interpretation. The wackestone–packstone texture and the moderate to good sorting of bioclasts suggest a variable energy level probably between the SWB and the fair weather wave base (FWWB) during deposition. The diversified fauna with prevailing occurrence of brachiopods, crinoids, bryozoans and trilobites points to an open-marine environment. Furthermore, locally well-preserved branching and fenestrate bryozoans floating in a micritic matrix are thought to reflect a vicinity to bryozoan meadows during deposition. Shallow-water influence is established by local occurrence of organisms such as gastropods, and rugose and tabulate corals. The commonly bioturbated matrix reflects the occurrence of an active endofauna and therefore oxygenated bottom-water conditions. This microfacies reveal an intermediate open-marine fore-reef environment located between the SWB and the FWWB in the vicinity of bryozoan meadows.

MFLT4b: bioclastic wackestone–packstone with reef-builder remains in a partly dolomitized matrix (Fig. 6h). MFLT4b occur in the upper part of the Machenées Member within marly limestone beds. Wackestone and packstones of the MFLT4b are similar to those described in MFLT4a. The main difference concerns the presence of reef-builder remains, the common dolomitization of the matrix associated with clay seams and the general larger size of gastropods, brachiopods and crinoids. Reef-builder remains are represented by solitary rugose corals, branching tabulate corals and lamellar stromatoporoids. In addition, rare *Girvanella* are also observed. Another difference from MFLT4a is the occurrence of pyrite associated with a darker matrix. The sediment is locally affected by an oblique cleavage (depending the concentration of argillaceous material).

Interpretation. Interpretation of this microfacies is similar to that of MFLT4a. The significant difference is related to the amount of shallow-water fauna such as stromatoporoids, solitary rugose and tabulate corals suggesting a stronger influence of shallow-water settings towards the open-marine fore-reef environments compared with MFLT4a. Poorly oxygenated sediment–water interface is indicated by the occurrence of pyrite.

MFLT5: crinoidal limestone (Fig. 7a–c). This facies occurs within the both lower and upper parts of the Nismes Formation as pluri-decimetre-sized coarse-grained yellow-earth limestone beds. It is characterized by common to abundant crinoid remains (stems and ossicles) and brachiopods and the occurrence of ostracod shells. Based on bioclasts preservation stage, brachiopod abundance and bryozoan occurrence, this microfacies can be divided into two categories: MFLT5a, fine- to medium-grained crinoidal packstone; and MFLT5b, fine- to coarse-grained crinoidal, brachiopod, bryozoan wackestone and packstone.

MFLT5a: fine- to medium-grained crinoidal packstone (Fig. 7a). This microfacies occurs within decimetre-thick beds intercalated in shale belonging to the lowermost part of the Nismes Formation It is characterized by the abundance of poorly preserved crinoid remains associated with broken brachiopod shells, ostracod and rare trilobite remains. Bioclast size averages 0.05 mm with a moderate sorting; they are embedded within a light-brown micritic partly dolomitized matrix rich in silt-sized quartz grains.

Interpretation. The abundance of poorly preserved crinoids and common relatively well-sorted broken shells indicates an open-marine setting. Intercalation of this microfacies in between Nismes shale (MFLT1) points to an environment where water agitation increases quickly. Indeed, the overlying and underlying shale lithologies are considered to be deposited in quiet water conditions below the FWWB. Préat & Kasimi (1995) interpreted similar microfacies from the Eifelian–Givetian boundary in Belgium as related to storm-deposit.

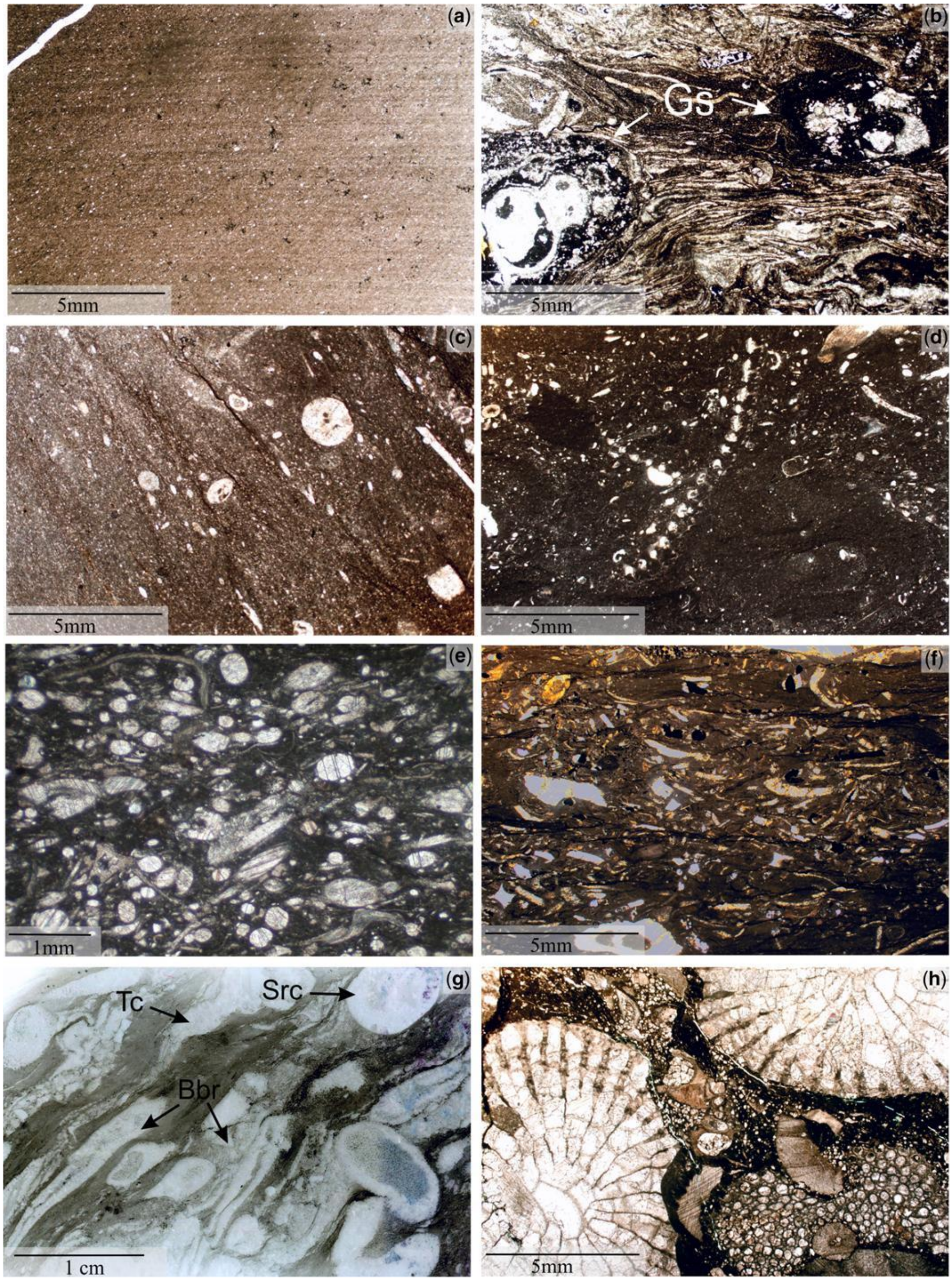

Fig. 6. Microfacies from the Frasnian of the La Thure section, Belgium. Photomicrographs of thin-sections are oriented perpendicular to the bedding. Numbers preceded by 'TUR' correspond to bed numbers. (**a**) MFLT1 outer ramp setting: brown silty shale (TUR 317, transmitted light). (**b**) MFLT2 distal tempestite in outer ramp setting: very dense accumulation of pelagic bivalve ('filaments') including lithoclasts of spongiostromate encrusting gastropod (Gs) (TUR 311, transmitted light). (**c**) MFLT3 distal fore-reef: crinoidal mudstone (TUR 363f, transmitted light). (**d**) MFLT3 distal fore-reef: mudstone–wackestone with bioclastic hashes bryozoans and crinoids (TUR 378, transmitted light).

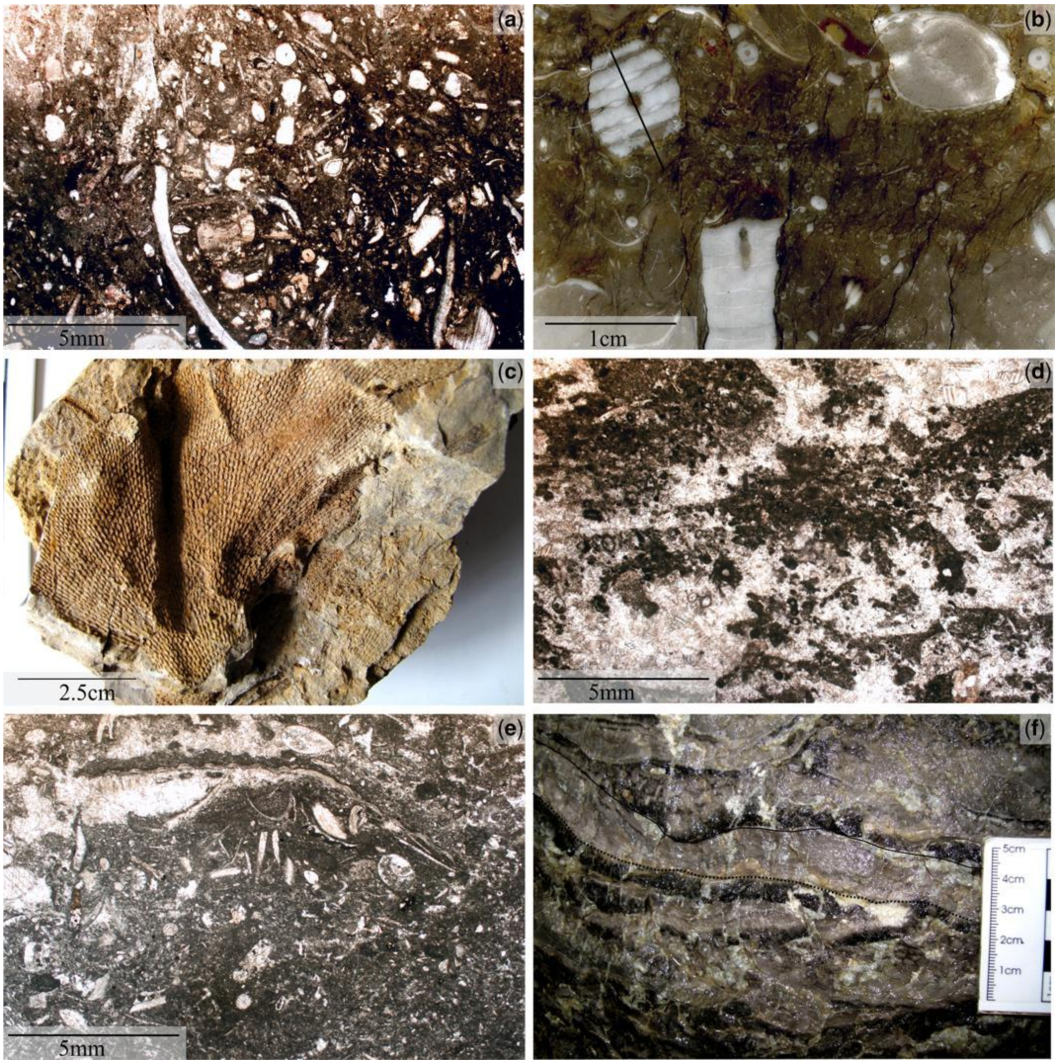

Fig. 7. Microfacies from the Frasnian of the La Thure section, Belgium (continued). Photomicrographs of thin-sections are oriented perpendicular to the bedding. Numbers preceded by 'TUR' correspond to bed numbers. (**a**) MFLT5a mid-ramp setting: fine-grained crinoidal packstone (TUR 315, transmitted light). (**b**) MFLT5b mid-ramp setting: coarse-grained crinoidal–brachiopod packstone (scanned thin-section, TUR 337). (**c**) MFLT5b mid-ramp bryozoan meadow setting: sample of large-sized branching bryozoans collected in the upper surface of bed 'TUR 334'. (**d**) MFLT6a stromatoporoid build-up setting: fine-grained bioclastic wackestone–packstone (TUR 347 M, transmitted light). (**e**) MFLT6a stromatoporoid build-up setting: mudstone–wackestone with irregular and stromatactoid fenestrae (TUR 347 T, transmitted light). (**f**) MFLT6b stromatoporoids build-up setting: large-sized lamellar stromatoporoids (light-grey colour) alternating with fibrous calcite cement (black colour) forming a framestone texture (erratic block near lower portion of the Fontaine Samart Member).

Fig. 6. (*Continued*) (**e**) MFLT3 distal fore-reef: distal tempestite forming densely packed level enriched in pelagic 'free swimming' crinoids (TUR 361b, transmitted light). (**f**) MFLT4a intermediate fore-reef: packstone rich in gastropod and bivalve shells and showing dissemination of pyrite (TUR 418, transmitted light). (**g**) MFLT4a intermediate fore-reef: local flaotstone texture within MFLT4a packstone showing tabulate coral (Tc), solitary rugose corals (Src) and branching bryozoans (Bbr), note the well-developed oblique cleavage (scanned thin-section; TUR 368a). (**h**) MFLT4b intermediate fore-reef: packstone with solitary rugose corals and bryozoans (TUR 369a, transmitted light).

Table 1. *Synthesis of microfacies for the Frasnian in the La Thure quarry section (western Belgium)*

Microfacies	Name	Formation/ Member	Main diagnostic allochems	Bedding, colour and sedimentary structures	Depositional setting
Model 1: Drowned platform					
MFLT1	Brownish and greenish shales	Nismes Formation	Laminated argillaceous shale which consists in clay particle and silt-sized quartz. Rare brachiopod occur	Thin beds of homogeneous greenish to brownish shales	Drowned platform below the SWB
MFLT2	Carbonaceous wackestone – packstone with densely packed lumachelle levels	Nismes Formation	Microsparitic matrix rich in insoluble residue. Occurrence of densely packed bivalve shell level and bioclasts such as brachiopod, bivalve, ostracod, crinoid, bryozoan and goniatite	Thin-beds (centimetre-thick) intercalated between MFLT1 shale and givetian limestones	Drowned platform below the SWB and influenced by gravity flow currents
MFLT5a	Fine- to medium-grained crinoidal packstone	Nismes Formation	Micritic partly dolomitized matrix rich in silt-sized quartz. Abundant poorly preserved and sorted crinoid remain and local brachiopod, ostracod and rare trilobite	Brownish and yellowish decimetre-thick beds intercalated in MFLT1 shales	Drowned platform influenced by storms
MFLT5b	Fine- to coarse-grained crinoidal, brachiopods, bryozoan packstone and floatstone	Nismes Formation	Micritic matrix with well-preserved bryozoan, crinoid, brachiopod and rare ostracod and trilobite	Yellow-earth decimetre-thick argillaceous limestone beds overlying MFLT1 shales	Crinoidal – bryozoan meadow below the FWWB

Model 2: Fore-reef of a rimmed shelf					
MFLT3	Marly crinoidal – brachiopod mudstone – wackestone with local packstone levels	des Machenées Member (Pont de la Folle Formation)	Micritic slightly argillaceous matrix with fenestrate bryozoan, ostracod, pelagic bivalve and echinoderm, tentaculite, trilobite and goniatite	Dark-grey marly limestone. The bedding is not easily visible	Distal to intermediate fore-reef setting locally influenced by storms
MFLT4a	Argillaceous shelly wackestone – packstone with local floastone texture	des Machenées Member (Pont de la Folle Formation)	Micritic slightly argillaceous matrix with prevalent crinoid, bivalve and gastropod. Fenestrate bryozoan, trilobite, pelagic echinoderm and rare tabulate and rugose corals	Dark-grey marly limestone with decimetre- to metre-thick limestone intercalation. The bedding is not well-visible	Intermediate fore-reef located between the FWWB and the SWB, in the vicinity of bryozoan meadows and influenced by shallower setting
MFLT4b	Bioclastic wackestone – packstone with reef-builder remains in a partly dolomitized matrix	des Machenées Member (Pont de la Folle Formation) and Philippeville Formation	Similar to MFLT4a with branching tabulate, solitary rugose coral, lamellar stromatoporoids and rare Girvanella. Pyrite and dolomite occur	Dark-grey marly limestone with decimetre- to metre-thick limestone intercalation. Bedding is well-visible within limestone	Similar depositional setting than MFLT4a but with a stronger influence of the shallow-water setting
MFLT6a	Mudstone – packstone with fenestrae and bioclasts	Fontaine Samart Member (Pont de la Folle Formation)	Light-grey micritic matrix with fenestrae and bioclasts. Ostracod, calcisphere, brachiopod, crinoid, stromatoporoid, solitary rugose coral	Light-grey massive limestone	Open-marine setting located below the FWWB and associated to stromatoporoid biostrome
MFLT6b	lamellar stromatoporoids boundstone	Fontaine Samart Member (Pont de la Folle Formation)	Similar characteristics as MFLT6a with a high accumulation of lamellar stromatoporoid (centimetre- to several decimetre-sized) and abundant cement	Decimetre-thick dark-blue to grey limestone	Open-marine stromatoporoids biostrome below FWWB

MFLT5b: fine- to coarse-grained crinoidal, brachiopods, bryozoan packstone and floatstone (Fig. 7b, c). This microfacies occurs within the uppermost part of the Nismes Formation. Compared with MFLT5a, it is characterized by better preservation of the bioclasts and the occurrence of bryozoans (branching and fenestrate). Bioclasts are mainly crinoids (0.05–2 cm in size), brachiopod shells (often complete; 2–3 cm in size), branching and fenestrate bryozoans (0.1–10 cm in size; Fig. 7c) and, subordinate to these, ostracods and trilobites. These bioclasts are embedded in a micritic matrix and show moderate to poor sorting. Locally, the proportion of clay particles is significant.

Interpretation. The packstone texture of MFLT5b implies a setting where agitation is moderate (Wright & Burchette 1996) and influenced by open-marine water as proven by the faunal assemblage. The proportion and generally good preservation of crinoids and bryozoans suggest a deposition in the vicinity of crinoidal–bryozoan meadows above the FWWB. The occurrence of MFLT5b characterizing the first limestone beds overlying shales of Nismes (MFLT1) probably indicates a change from siliciclastic to carbonate sedimentation within the study area and therefore confirms recovery of the carbonate production. According to Burchette (1981), crinoidal sands are common substratum of biostrome. Therefore, MFLT5b microfacies is interpreted as the first colonization step allowing development of the overlying stromatoporoid build-up (MFLT6; Fontaine Samart Member).

MFLT6: lamellar stromatoporoids limestone (Fig. 7d–f). This microfacies occurs in a single several metre-thick light-grey massive limestone intervals (Fontaine Samart Member) overlying the coarse-grained crinoidal limestone of the uppermost part of the Nismes Formation (e.g. MFLT5b). Based on the abundance of stromatoporoids, this microfacies can be divided into two categories: MFLT6a, mudstone–packstone with fenestrate and bioclasts; and MFLT6b, stromatoporoids boundstone. In both microfacies the occurrence of a clotted fabric and small bioclasts such as ostracod and brachiopod shells is common.

MFLT6a: mudstone–packstone with fenestrae and bioclasts. This microfacies occur mainly in the upper part of the single metre-thick limestone bed (corresponding mainly to MFLT6b). It is characterized by the abundance of light-grey micritic matrix commonly showing small fenestrae (stromatactoids and irregular; Fig. 7d) and various sized (from 0.2 mm to 5 cm) bioclasts with moderate to poor sorting (Fig. 7e). Fenestrae are usually millimetres to several centimetres in size and mostly filled by one blocky sparite cement generation. Organisms are represented, in order of abundance, by ostracods (often completely preserved specimen), calcispheres, bispheres, brachiopods (commonly complete shells), crinoids, lamellar and branching stromatoporoids and rugose corals. These two reef-builders are usually well-preserved and are commonly surrounded by an irregular thin microbial encrustation.

Interpretation. One of the main characteristic of this MF is the abundance of micrite that suggests a low-energy setting. Common occurrence of complete ostracod and brachiopod shells attests our first interpretation, and further suggests an open-marine environment. Moreover, the preservation of a clotted fabric and occurrence of small fenestrae, usually interpreted as related to microbial origin (Pratt 1982; Tsien 1985; Boulvain 2001) attests to a depositional setting, allowing organic community development. However, local packstone texture with poorly sorted bioclasts indicates a quiet environment located close to the FWWB where the sediment was sometimes reworked by storm action above the SWB, as shown by the reworked bioclasts and stromatoporoids in non-living positions.

MFLT6b: lamellar stromatoporoids boundstone (Fig. 7f). This microfacies shows similar characteristics to MFLT6a. Nevertheless, an important difference is the large amount of lamellar stromatoporoids (several centimetre- to several decimetre-sized) and the abundance of both cement and micrite. Lamellar stromatoporoids are mostly oriented parallel to bedding. The interval between stromatoporoids is filled either by mudstone–packstone texture with small bioclasts (e.g. MFLT6a) or by radiaxial calcite and blocky sparite cements. These two different cements also occur in cavities located underneath stromatoporoids. Saddle dolomite is also commonly observed within this microfacies.

Interpretation. The dominant character of this microfacies compared with MFLT6a is the significant accumulation of lamellar stromatoporoids. Similar microfacies have already been described in other Belgian Frasnian localities (Tailfer and Villers; Da Silva *et al.* 2011*b*; Da Silva & Boulvain 2012) and interpreted as biostrome developed in an outer/intermediate zone (fore-reef setting). The good preservation of stromatoporoids (not reworked), the local occurrence of complete ostracod and brachiopod shells, and the local clotted fabric are in agreement with a relatively quiet depositional setting, probably below the FWWB. Our interpretation is also supported by the abundance of lamellar stromatoporoids, which are known to live under relatively protected conditions and on soft substrate where sedimentary rate and detrital supply are relatively low (Cornet 1975; Kershaw 1998).

The combined characteristics of MFLT6a and b such as the clotted fabric, abundance of fenestrae, micritic matrix and accumulation of stromatoporoids are all arguments in favour to a depositional setting intimately related to the development of a stromatoporoid biostrome in fore-reef setting.

Magnetic susceptibility

Based on 350 samples (sampling interval of about between 0.25 and 0.45 cm depending on outcrop conditions) from the La Thure quarry section, we prepared an MS curve (Fig. 5). The MS values for the Lower and Middle Frasnian of the La Thure section record high variability ranging from -8.05×10^{-10} to $1.5 \times 10^{-7}\ m^3\ kg^{-1}$ with an average value of $5.87 \times 10^{-8}\ m^3\ kg^{-1}$. This value is relatively close to the $MS_{marine\ standard}$ of $5.5 \times 10^{-8}\ m^3\ kg^{-1}$ defined by Ellwood *et al.* (2011) on the basis of *c.* 11 000 marine rock samples. It is also relatively similar to average MS values recorded within the time-equivalent fore-reef setting from other Belgium localities ($3.3.10^{-8}\ m^3\ kg^{-1}$; Da Silva *et al.* 2009).

It is important to note that all of the descriptions underlined above are specifically made for the formations and members outcropping in the La Thure quarry. Throughout the section, both formations and members expose distinctive magnetic susceptibility behaviour (Fig. 5). The Nismes Formation starts at the base of the section with relatively high values ($1.2 \times 10^{-7}\ m^3\ kg^{-1}$). Then values slightly increase prior a strong decrease to reach low values ($0.5 \times 10^{-7}\ m^3\ kg^{-1}$) at the top. It is interesting to underline that, even if monotonous shale without clear sedimentological changes dominates the Nismes Formation, numerous oscillations are highlighted in the MS signal.

The Fontaine Samart Member shows the lowest MS values of our profile ($0.04 \times 10^{-8}\ m^3\ kg^{-1}$). In these relatively shallow facies compared with the rest of the section, magnetic susceptibility values are homogeneous and very low. High in the section, the evolution of the MS in the succession of the Machenées Member is depicted. This member presents relatively low MS values (around $0.47 \times 10^{-7}\ m^3\ kg^{-1}$) even if several groups of peaks (1–3; Fig. 5) occur (around $1.2 \times 10^{-7}\ m^3\ kg^{-1}$) between 60 and 120 m. The lower part of the Philippeville Formation exposed in the uppermost part of the section presents similar values (around $3.76 \times 10^{-7}\ m^3\ kg^{-1}$) to those in the Machenées Member.

Discussion

Depositional environments

Petrographic analyses from the La Thure section led to the definition of six microfacies and six submicrofacies characterizing the sedimentary environments of the northwestern margin of the DS during the early to middle Frasnian interval. Microfacies palaeoenvironmental interpretations allowed two depositional models to be distinguished for the studied succession: (a) a siliciclastic drowned carbonate platform (during the Early Frasnian, Nismes Formation), with prevailing shale and carbonates with open-marine fauna, including storm-related deposits (MFLT1, MFLT2 and MFLT5); and (b) a fore-reef depositional setting belonging to a rimmed shelf (during the Middle Frasnian, Pont de la Folle and Philippeville formations), characterized by mudstone to packstone including open- and shallow-marine fauna (MFLT3, MFLT4) and stromatoporoids biostrome facies (MFLT6). Transition from depositional model (a) to (b) took place in the early *transitans* Zone.

Vertical evolution of the microfacies highlights four main palaeoenvironmental trends corresponding to the four formal lithological units observed in this study (Fig. 5). The Nismes Formation corresponds to the drowned platform shale facies occurring everywhere in Belgium during the Lower Frasnian. The shale deposition is related to a transgressive event starting within the late Givetian, resulting in the drowning and demise of the Givetian carbonate platform (Boulvain *et al.* 2009; Casier & Préat 2009; Casier *et al.* 2013). According to Gouwy & Bultynck (2000), shale lithologies in Belgium extend from lower *falsiovalis* to lower *transitans* conodont Zones. According to the late Middle to Late Devonian sea-level curve established by Sandberg *et al.* (2002), Lower Frasnian shale in Belgium could be the result of a eustatic sea-level rise occurring at the Givetian–Frasnian boundary. Indeed, in other localities such as NW Africa (Lüning *et al.* 2004) and NE America (upstate New York area; House 2002), for example, lower/lowermost Frasnian is also characterized by shale lithologies. However, this lithology is not recognized worldwide at the base of the Frasnian stage, as in the eastern Rhenish Massif in Germany (e.g. Brilon area; Pas *et al.* 2013), in the Caning Basin in Australia (Chow *et al.* 2013) and in the Carnic Alps in Austria/Italy (Schönlaub & Histon 2000), where Lower Frasnian shows bioclastic limestone lithologies. Therefore, the transgressive event recorded for instance in Belgium, NW Africa and NE America is more marked and might be enhanced by the peculiar regional geology. In Belgium, syn-sedimentary faults are highlighted by the north–south lateral thickness and facies variations of the Frasnian sequence (Da Silva & Boulvain 2012). These faults have probably enhanced the effect of transgression. The vicinity of the Belgian Frasnian basin with the London–Brabant High (e.g. McKerrow & Scotese 1990) characterized by humid tropical climate (Copper 2002; Joachimski *et al.* 2009) allowing an increase in the terrestrial influx seaward could also have contributed to deposition of shale.

The upper part of Nismes Formation shows a significant shallowing-upward trend evidenced by bioclastic limestone beds (MFLT5b) overlying the shale sequence. The shift from shale to carbonate deposition and the occurrence of a rich open-marine shallow-water fauna are in agreement to the re-establishment of favourable conditions for the development of a carbonate factory within the Belgium Frasnian basin. Similar time-equivalent changes have been observed in most of the Belgium Frasnian localities (Boulvain *et al.* 1999).

After a gap in observation, the shallowing trend continues, with the transition to massive stromatoporoid boundstone (MFLT6b). Development of a lamellar stromatoporoid build-up within the northwestern margin of the DS is biostratigraphically correlated with the base of the Arche buildups (Boulvain 2007) occurring in basinal setting (see Fig. 2; southern belt). These reefal structures appear in the upper *transitans* to lower *punctata* conodont Zones within one of the lowest relative sea-levels recorded during the Early Frasnian (Boulvain 2007, fig. 8).

The top of the Fontaine Samart Member shows a slight deepening trend characterized by the occurrence of MFLT6a (mudstone–packstone with fenestrae). This deepening continues towards the base of the Machenées Member, and is marked by the evolution from stromatoporoids limestone (MFLT6) to mudstone and wackestone with hemipelagic fauna (MFLT3). A relative sea-level rise is also observed within time-equivalent facies in the southern margin (southern belt) of the Dinant Synclinorium (Boulvain 2007).

After the deepening recorded at the very base of the Machenées Member, the remainder of this lithological unit mainly records an aggrading trend in fore-reef setting, with two *c.* 5 m-thick intervals near the 80 and 110 m-mark, recording a slight shallowing trend (transition from MFLT3 to MFLT4b). The occurrence of MFLT4b (bioclastic wackestone–packstone with reef-builder remains) indicates an obvious increase in shallower influence towards the fore-reef setting. The transition from fore-reef setting to massive dolomitized bioclastic limestone bed of Philippeville Formation indicates a shallowing trend. The outcrop finishes with MF4a (argillaceous shelly wackestone–packstone) corresponding to a last deepening trend.

A comparison between deepening and shallowing trends occurring in the La Thure section and the sea-level curve proposed for the Frasnian stage in the south margin of the Dinant Synclinorium (Boulvain 2007, fig. 8) reveals remarkable similarity despite different palaeogeographic location

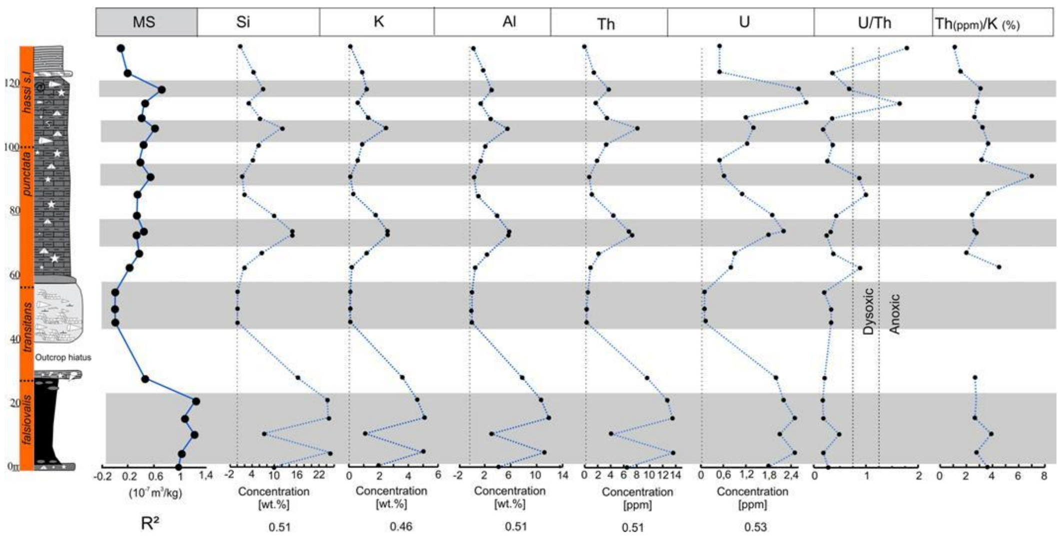

Fig. 8. Chemostratigraphic profiles of elements used as proxies for terrigenous clastic influxes into marine depositional basins and ratio (U/Th) for redox condition in the sediment–water interface (distinction between oxic, anoxic and dysoxic bottom-water condition represented by vertical dotted line is based on Jones & Manning 1994). Detection limit of elemental proxies is represented by the vertical dotted lines.

and depositional setting. As mentioned above, the shallowest depositional settings of the DS are located to the north, while the deepest are recognized in the south (Da Silva & Boulvain 2012), suggesting a general east–west orientation for the facies belts. With respect to observations, sedimentary rocks from the La Thure section should have been deposited in a relatively shallow-water setting as they are located in the northwestern margin of the DS. However, our study shows that the early-middle Frasnian sediments were deposited in an open-marine, relatively deep (hemipelagic/pelagic) setting: siliciclastic drowned platform during the early Frasnian, and fore-reef setting during the middle Frasnian. Therefore we suggest that the main direction of facies belts for the Frasnian platform are east–west within the eastern part of the Dinant Synclinorium and bend towards an ENE–WSW orientation to the western part (see dashed lines in Fig. 1).

Comparison of magnetic susceptibility, facies and major element geochemistry

In order to apply magnetic susceptibility as a palaeoenvironmental proxy or as a tool for correlation, it is important to assess the origin of the magnetic susceptibility signal and to decipher the primary origin from the secondary origin of the magnetic minerals (see a synthesis in Da Silva *et al.* 2013). This is even more important in these Devonian sections from Belgium, which were affected by a remagnetization event (Zegers *et al.* 2003; Zwing *et al.* 2005) related to the Variscan orogeny. In a detailed study on the origin of the magnetic susceptibility signal in Devonian sections, Da Silva *et al.* (2012, 2013) showed that the MS signal is carried by fine-grained PSD magnetite, related to this remagnetization event. However, Da Silva *et al.* (2013) showed that, of six outcrops, four are still carrying a relatively good correlation between MS and elemental detrital proxies (Ti, Zr, Rb and Al), and this indicates that the primary detrital signal is reasonably well preserved in the MS signal despite the remagnetization. Thus, primary trends can be retained despite remagnetization, although on two outcrops the correlation is not observed, indicating that the impact of the remagnetization was probably stronger for these. In order to obtain insight into the origin of the magnetic minerals, we propose a comparison of MS trends with another detrital input proxy (selected chemical elements) and with another palaeoenvironmental proxy (facies).

Comparison with geochemical selected elements. Some selected elements commonly used as reliable tracers of the lithogenic input (Th, K, Al and Si; see Riquier *et al.* 2010; Sliwinski *et al.* 2012) were plotted against the MS curve (Fig. 8). Distribution of these elements follows the same large-scale trend as MS. This parallelism indicates an MS signal inherently linked to the concentration in terrestrial input proxies. Variation of Al concentration in relation to diagenetic formation of clay is unlikely, because there is a strong positive correlation ($r^2 = 0.99$) with Ti, which is not assimilated during authigenic clay mineral formation (Pratt *et al.* 1986). Thus, despite the remagnetization occurring within the Belgian Frasnian lithologies, the main trends in the MS signal from the La Thure section still reflect some syn-sedimentary conditions. Moreover, the general low values of lithogenetic input tracers in the Middle Frasnian Pont de la Folle and Philippeville formations are in agreement with the occurrence of reef-related systems in shallower part of the platform (e.g. 'central belt') within the Middle Frasnian. Indeed, it is trivial but reef-related systems behave as filter and confine the basin from terrigenous influx.

Comparison with facies, lithologies and geochemistry. Until now, few data have been collected within the shaly lithologies characterizing the Lower Frasnian in Belgium (Casier & Préat 2009; Devleeschouwer *et al.* 2010). The behaviour of MS signals in comparison to microfacies evolution throughout the entire section can be explained using environmental parameters such as wave agitation, sedimentary rate, carbonate production and terrestrial supply (see Da Silva *et al.* 2009).

The Nismes Formation, dominated by shale lithologies, is interpreted as one of the deepest facies occurring in the Belgian Frasnian carbonate platform together with the Upper Frasnien 'Matagne' shale related to the Kellwasser events. Magnetic susceptibility evolution and facies are relatively well correlated, and an increase in the MS values corresponds to a deepening in microfacies. Evolution of the MS curve can probably be explained by the low sedimentary rate characterizing shale deposition, which leads to increasing concentration of terrigenous elements and therefore triggers an increase in the MS carrier accumulation (e.g. Si, Th, K and Al). This situation has already been reported for the Belgian Eifelian–Givetian ramp system (Mabille & Boulvain 2007; Da Silva *et al.* 2009) and in the Upper Devonian fore-reef depositional setting in the Carnic Alps (Pas *et al.* 2014).

Concerning the Fontaine Samart Member, which corresponds to the shallowest depositional setting, the very low MS values are probably related to the significant carbonate production, which acted as a dilution process (e.g. Mabille *et al.* 2008; Da Silva *et al.* 2009).

The evolution of the MS and MF curves throughout the Machenées Member, deposited in fore-reef environment, shows that shallowing trends in microfacies are correlated with increasing MS (see group of peaks 1–4; Fig. 5) and detrital inputs proxies (Fig. 8) values. This situation is contrary to what was observed in Pas *et al.* (2014) for a Middle and Upper Devonian fore-reef setting in the Carnic Alps. In this setting, shallowing trends are associated with decreasing MS values related to higher carbonate production/supply, which enhanced the dilution of MS carrying minerals. This contrary situation might be explained by considering the stratigraphic interval corresponding to the Machenées Member. Indeed, this member was partly deposited during the *punctata* Zone. This conodont Zone is characterized by the so-called '*punctata* event', a sharp C-isotope negative excursion identified in Belgium (Yans *et al.* 2007), but also in Poland (Pisarzowska *et al.* 2006), Nevada (Morrow *et al.* 2009), South China (Ma *et al.* 2008) and western and northeastern Alberta (Holmden *et al.* 2006; Sliwinski *et al.* 2011). Its fundamental mechanism seems to be a specific combination of vascular plant developments on the continent coupled with uplift and weathering of orogens, triggering an increase in terrestrial supply that deregulates the nutriment balance in epeiric seaways (synthesis in Sliwinski *et al.* 2011).

In the lateral equivalent deposits of the Machenées Member, the mud mound facies from the Moulin Liénaux Formation (southern facies belt; see Fig. 2), Da Silva *et al.* (2010) described sedimentary structures such as a karstic surface, a sharp transition from deep to shallow facies and brecciated facies, and interpreted those as related to significant regressive trends within the specific T–R cycle pattern associated with the '*punctata* event' (Fig. 9). In the Machenées Member the increasing MS values (group of peaks 1–4) might relate to the shallowing trends described by Da Silva *et al.* (2010) (Fig. 9). Indeed, during an important sea-level fall, there is a seaward facies shift, increasing the size of continental area and therefore enabling an increasing amount of terrestrial materials to move seaward, leading to higher MS values. The thorium/potassium (Th/K) ratio may also help to get insight into sea-level variations (e.g. Kozlowski & Sobien 2012). For instance, during a sea-level fall the amount of terrigenous inputs towards the basin increases, leading to an increase in the heavy mineral admixture and therefore an increase in Th in comparison to K because heavy minerals contain a very low percentage of K (see Quirein *et al.* 1982). Moreover, in many cases (Ellwood *et al.* 2000), MS rises resulting from maximum terrestrial input are induced by intensive erosion during sea-level fall. In conclusion, a concurrent increase in Th/K and MS values can be interpreted as a typical signal of a sea-level fall. However, considering the locally very low content in K (close to the detection limit, see dotted line in Fig. 8) throughout the *punctata* interval, the Th/K ratio should be regarded with caution (e.g. Th/K peak at the 90 m-thick mark). For a more detailed description of the use and limitation of Th/K ratio in sea-level reconstruction see Ruffell & Worden (2000) and Kozlowski & Sobien (2012).

Recently, Sliwinski *et al.* (2011, 2012) completed a detailed study on the '*punctata* event' interval in a fore-reef setting of the Western Canada Sedimentary Basin using a large magnetic susceptibility and geochemical dataset. These authors demonstrated that during the *punctata* interval trace element variations within a sequence stratigraphic perspective reveal that T–R cycles exerted a strong control on the terrigenous influx. Furthermore, they highlighted a strong statistical correlation between terrigenous input proxies and MS variations. In a similar fore-reef setting, Whalen & Day (2008) indicated that MS is generally high during third- and fourth-order sea-level lowstand, early transgression and late highstand. According to these results, concurrent increases in MS and lithogenic input proxies (Fig. 8) recognized in the Machenées Member can be taken to imply increasing clastic input driven by regressive events, as outlined in Da Silva *et al.* (2010) in the southern facies belt of the Belgian Frasnian platform. Moreover, the remarkable similarity between Belgian and NE Alberta $\delta^{13}C_{(carb)}$ curve (Sliwinski *et al.* 2011; fig. 10) through *punctata* Zone show that major changes affecting Middle Frasnian marine realm are of supraregional extent and therefore were probably driven by similar combination of causes (e.g. afforestation, intense weathering, uplift and T–R cycles).

Variation in U/Th ratio, considered as a sensitive proxy of palaeo-oxygenation in the depositional environment (Jones & Manning 1994), in the *punctata* interval points to changes in redox condition from oxic to dysoxic in the sediment–water interface (see Fig. 8). The U/Th ratio in *punctata* interval from Western Alberta (Sliwinski *et al.* 2011) also shows variation in redox condition but of higher amplitude, rather from oxic to anoxic than oxic to dysoxic as in the Machenées Member.

Data available for the Philippeville Formation are limited but the slight deepening trends in MF concomitant with decreasing trends in MS and terrestrial proxies can probably be explained by the occurrence of extensive lagoonal deposit observed in a time-equivalent shallower setting (e.g. Lustin Formation in Fig. 2). The occurrence of these deposits attests to the existence of true barrier-reef systems, which therefore must have prevented distal setting from terrestrial input. The uppermost part of the Philippeville Formation also records

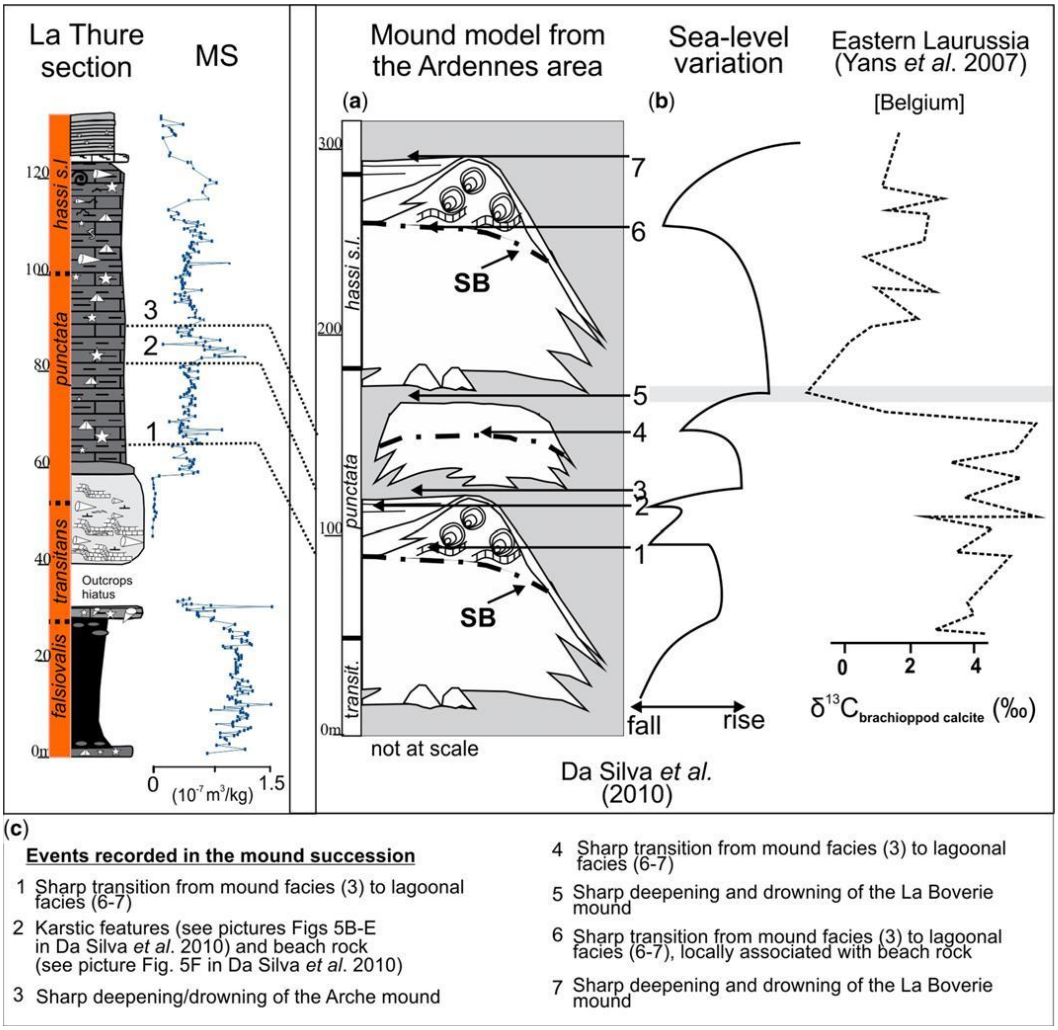

Fig. 9. Synthetic model, mound succession from Ardennes area and main sedimentological events. (**a**) Conodont zonation from Bultynck & Dejonghe (2001). (**b**) Main events (defined in c) and sedimentological observations. (**c**) Description of the events described in (b). Figure modified from Da Silva *et al.* (2010).

the highest U/Th ratio of the section (Fig. 8), indicating anoxic conditions during the deposition. These anoxic conditions are also confirmed by the occurrence of pyrite dissemination within the sediment (e.g. Fig. 6f).

Conclusions

This paper presents environmental analyses of an Early–Middle Frasnian succession in Western Belgium by combining new sedimentological and geochemical datasets with data from the literature. Petrographic analyses and field observations allowed reconstruction of the palaeoenvironemental evolution of that period of time within the poorly studied northwestern margin of the Dinant Synclinorium. In addition, the particularly well outcropping Lower Frasnian in the La Thure section provided the first opportunity to gain better knowledge of the transition from the drowned platform shale deposits, overlying the Givetian–Frasnian boundary, to the new flourishing Frasnian carbonate platform. To characterize this sedimentological evolution, two depositional models have been defined: (a) a siliciclastic drowned platform including Lower Frasnian shales; and (b) a rimmed platform including fore-reef depositional setting of the Middle Frasnian Pont de la Folle and Phillipeville. Comparison of these results combined with data from the literature allowed the main direction of the facies belts recognized in the Belgian Frasnian platform to be drawn. The main directions are east–west within the eastern part of the DS and ENE–WSW orientation within the western part. Integration of results from magnetic susceptibility (MS) and geochemistry highlight an MS signal inherently connected with the concentration in siliciclastic input proxies (Si, Al, K and Th) and that, despite the strong remagnetization event affecting rocks from the Rhenohercynian fold-and-thrust belt, the MS signal still reflects primary trends. For instance, this allowed inference of the specific MS behaviour in the fore-reef environment in the La Thure section during the *punctata* Zone as probably related to enhanced siliciclastic influx in response to severe and rapid sea-level fluctuations occurring in the '*punctata* event' interval.

This study is a contribution to UNESCO International Geoscience Program (IGCP 580 and 596 projects). This work was supported by a PhD fellowship awarded by the Research Foundation–Flanders assigned to D. D. V. We sincerely thank W. Kozlowzki (University of Warsaw) and T. Suttner (University of Graz) for their thoughtful reviews and relevant suggestions. J. P. Cullus is acknowledged for the preparation of thin-sections. This research would not have been possible without the cooperation of the 'S. A. carrières de La Thure', which provided access and permission to sample.

References

Baccelle, L. & Bosellini, A. 1965. Diagrammi per la stima visiva della composizione percentuale nelle rocce sedimentarie. *Annali della Università di Ferrrara, Sezione IX, Science Geologiche a Paleontologiche*, **1**, 59–62.

Boulvain, F. 2001. Facies architecture and diagenesis of Belgian Late Frasnian carbonate mounds. *Sedimentary Geology*, **145**, 269–294.

Boulvain, F. 2007. Frasnian carbonate mounds from Belgium: sedimentology and paleoceanography. *In*: Alvaro, J. J., Aretz, M., Boulvain, F., Munnecke, A., Vachard, D. & Vennin, E. (eds) *Paleozoic Reefs and Bioaccumulations: Climatic and Evolutionary Controls*. Geological Society, London, Special Publications, **275**, 124–142.

Boulvain, F., Bultynck, P. *et al.* 1999. Les formations du Frasnien de la Belgique. *Memoirs of the Geological Survey of Belgium*, **44**, 1–125.

Boulvain, F., Cornet, P. *et al.* 2004. Reconstructing atoll-like mounds from the Frasnian of Belgium. *Facies*, **50**, 313–326.

Boulvain, F., Mabille, C. *et al.* 2009. Towards a palaeogeographical and sequential framework for the Givetian of Belgium. *Geologica Belgica*, **12**, 161–178.

Bultynck, P. & Dejonghe, L. 2001. Devonian lithostratigraphic units (Belgium). *In*: Bultynck, P. & Dejonghe, L. (eds) *Guide to a Revised Lithostratigraphic Scale of Belgium. Geologica Belgica*, **4**, 39–60.

Bultynck, P., Helsen, S. & Hayduckiewich, J. 1998. Conodont succession and biofacies in upper Frasnian formations (Devonian) from the southern and central parts of the Dinant Synclinorium (Belgium) — (timing of facies shifting and correlation with Late Frasnian events). *Bulletin de l'Institut Royal des Sciences Naturelles de Belgique*, **68**, 25–75.

Burchette, T. P. 1981. European Devonian reefs: a review of current concepts and models. *In*: Toomey, D. F. (ed.) *European Fossil Reef Models*. Society of Economic Paleontologists and Mineralogists, Tulsa, OK, Special Publications, **25**, 5–17.

Casier, J.-G. & Préat, A. 2009. Late givetian to middle Frasnian ostracods from Nismes (Dinant Synclinorium, Belgium) and their lithological context. *Bulletin de l'Institut royal des Sciences Naturelles de Belgique*, **79**, 87–115.

Casier, J.-G., Devleeschouwer, X. *et al.* 2013. Ostracods and rock facies across the Givetian/Frasnian boundary interval in the Sourd d'Ave section at Aveet-Auffe (Dinant Synclinorium, Ardenne, Belgium). *Bulletin of Geosciences*, **88**, 241–264.

Chow, N., George, A. D. *et al.* 2013. Stratal architecture and platform evolution of an early Frasnian syntectonic carbonate platform, Canning Basin, Australia. *Sedimentology*, **60**, 1583–1620.

Conti, M. A. & Morani, S. 1992. Thin-shelled bivalves from the Jurassic Rosso Ammonotico and Calcari a Posidonia formations from Umbrian–Marachean Apennine (Central Italy). *Palaeopelagos*, **2**, 193–213.

Copper, P. 2002. Silurian and Devonian reefs: 80 million years of global greenhouse between two ice ages. *In*: Kiessling, W., Flügel, E. & Golonka, J. (eds) *Phanerozoic Reef Patterns*. Society of Economic Paleontologists and Mineralogists, Tulsa, OK, Special Publications, 181–238.

Cornet, P. 1975. *Morphogenèse, caractère ecologiques et distribution des stromatoporoïdes dévoniens au bord sud du bassin de Dinant (Belgique)*. Unpublished PhD thesis.

Da Silva, A. C. & Boulvain, F. 2004. From palaeosols to carbonate mounds: facies and environments of the middle Frasnian platform in Belgium. *Geological Quarterly*, **48**, 253–265.

Da Silva, A. C. & Boulvain, F. 2006. Upper Devonian carbonate platform correlations and sea-level variations recorded in magnetic susceptibility. *Palaeogeography Palaeoclimatology Palaeoecology*, **240**, 373–388.

Da Silva, A. C. & Boulvain, F. 2008. Carbon isotope lateral variability in a Middle Frasnian carbonate platform (Belgium): significance of facies, diagenesis and sea-level history. *Palaeogeograhy Palaeoclimatology Palaeoecology*, **269**, 189–204.

Da Silva, A. C. & Boulvain, F. 2012. Analyses of the Devonian (Frasnian) platform from Belgium: a multifaceted approach for basin evolution reconstruction. *Basin Research*, **23**, 338–356.

Da Silva, A. C., Mabille, C. & Boulvain, F. 2009. Influence of sedimentary setting on the use of magnetic susceptibility: examples from the Devonian of Belgium. *Sedimentology*, **56**, 1292–1306.

Da Silva, A. C., Yans, J. & Boulvain, F. 2010. Early–Middle Frasian (Early Late Devonian) sedimentology and magnetic susceptibility of the Ardennes area (Belgium): identification of severe and rapid sea-level fluctuations. *Geologica Belgica*, **13**, 319–332.

Da Silva, A. C., Kershaw, S. & Boulvain, F. 2011*a*. Sedimentology and stromatoporoid paleoecology of Frasnian (Upper Devonian) mud mounds from southern Belgium. *Lethaia*, **44**, 255–274.

Da Silva, A. C., Kershaw, S. & Boulvain, F. 2011*b*. Stromatoporoid palaeoecology in the Frasnian (Upper Devonian) Belgian platform, and its applications in interpretation of carbonate platform environments. *Palaeontology*, **54**, 883–905.

Da Silva, A. C., Dekkers, M. J., Mabille, C. & Boulvain, F. 2012. Magnetic susceptibility and its relationship with paleoenvironments, diagenesis and remagnetization: Examples from the Devonian carbonates of Belgium. *Studia Geophysica et Geodaetica*, **56**, 677–704.

Da Silva, A. C., De Vleeschouwer, D. *et al.* 2013. Magnetic susceptibility as a high-resolution correlation tool and as a climatic proxy in Paleozoic rocks-merits and pitfalls: examples from the Devonian in Belgium. *Marine and Petroleum Geology*, **46**, 173–189.

Devleeschouwer, X., Petitclerc, E. *et al.* 2010. The Givetian–Frasnian boundary at Nismes parastratotype (Belgium): the magnetic susceptibility signal controlled by ferromagnetic minerals. *Geologica Belgica*, **13**, 351–366.

Dickson, J. 1965. A modified staining technique for carbonates in thin section. *Nature*, **205**, 587.

Dunham, R. J. 1962. Classification of carbonate rocks according to depositional texture. *In*: Ham, W. E. (ed.) *Classification of Carbonate Rocks, A Symposium*. American Association of Petroleum Geologists, Tulsa, OK, Memoirs, **1**, 108–121.

Ellwood, B. B., Crick, R. E. *et al.* 2000. Magnetosusceptibility event and cyclostratigraphy method applied to marine rocks: detrital input v. carbonate productivity. *Geology*, **28**, 1135–1138.

Ellwood, B. B., Tomkin, J. H. *et al.* 2011. A climate-driven model and development of a floating point time scale for the entire Middle Devonian Givetian Stage: a test using magnetostratigraphy susceptibility as a climate proxy. *Palaeogeography Palaeoclimatology Palaeoecology*, **304**, 85–95.

Embry, A. F. & Klovan, J. E. 1972. Absolute water depth limits of Late Devonian paleoecological zones. *Geologische Rundschau*, **61**, 672–686.

Flügel, E. 2004. *Microfacies Analysis of Carbonate Rocks: Analysis, Interpretation and Application*. Springer, Berlin.

Gouwy, S. & Bultynck, P. 2000. Graphic correlation of Frasnian sections (Upper Devonian) in the Ardennes, Belgium. *Bulletin de l'Institut Royal des Sciences Naturelles de Belgique*, **70**, 25–52.

Holmden, C., Braun, W. K. *et al.* 2006. Carbon isotope chemostratigraphy of Frasnian sequences in Western Canada. *Saskatchewan Geological Survey, Summary of Investigation*, **1**, 1–6.

House, R. M. 2002. Strength, timing, setting and cause of mid-Palaeozoic extinctions. *Palaeogeography Palaeoclimatology Palaeoecology*, **181**, 5–25.

Joachimski, M. M., Breisig, S. *et al.* 2009. Devonian climate and reef evolution: insights from oxygen isotopes in apatite. *Earth and Planetary Science Letters*, **284**, 599–609.

Jones, B. & Manning, D. A. C. 1994. Comparison of geochemical indices used for the interpretation of paleoredox conditions in ancient mudstone. *Chemical Geology*, **111**, 111–129.

Kershaw, S. 1998. The application of stromatoporoid palaeobiology in palaeoenvironmental analyses. *Palaeontology*, **41**, 509–544.

Kiessling, W., Flügel, E. & Golonka, J. 2003. Patterns of Phanerozoic carbonate platform sedimentation. *Senckenbergiana Lethaia*, **36**, 195–226.

Kozlowski, W. & Sobien, K. 2012. Mid-Ludfordien coeval carbon isotope, natural gamma ray and magnetic susceptibility excursions in the Mielnik IG-1 borehole (Eastern Poland)-Dustiness as a possible link between global climate and the Silurian carbon isotope record. *Palaeogeography Palaeoclimatology Palaeoecology*, **339–341**, 74–97.

Krebs, W. 1967. Reef development in the Devonian of the eastern Rhenish Slate Mountains, Germany. *In*: Oswald, D. H. (ed.) *International Symposium on the Devonian System*. Alberta Society of Petroleum Geologists, Calgary, **1**, 295–306.

Lüning, S., Wendt, J. *et al.* 2004. Temporal – Spatial reconstruction of the early Frasnian (Late Devonian) anoxia in NW Africa: new field data from the Ahnet Basin (Algeria). *Sedimentary Geology*, **163**, 237–264.

Ma, X. P., Wang, C. Y., Racki, G. & Racki, M. 2008. Facies and geochemistry across the Early – Middle Frasnian transition (Late Devonian) on South China carbonate shelf: comparison with the Polish reference succession. *Palaeogeography Palaeoclimatology Palaeoecology*, **269**, 130–151.

Mabille, C. & Boulvain, F. 2007. Sedimentology and magnetic susceptibility of the Couvin Formation (Eifelian, South Western Belgium): carbonate platform initiation in a hostile world. *Geologica Belgica*, **10**, 47–67.

Mabille, C., Pas, D. *et al.* 2008. Deposition within the vicinity of the Mid-Eifel High: detailed sedimentological study and magnetic susceptibility of a mixed ramp-related system from the Eifelian Lauch and Nohn Formations (Ohlesberg, Eifel, Germany). *Facies*, **54**, 597–612.

McKerrow, W. S. & Scotese, C. R. 1990. *Palaeozoic Palaegeography and Biogeography*. Geological Society, London, Memoirs, **12**, 1–433.

Molina Garza, R. S. & Zjiderveld, J. D. A. 1996. Paleomagnetism of Paleozoic strata, Brabant and Ardennes Massifs, Belgium: Implications of prefolding and postfolding Late Carboniferous secondary magnetizations for European apparent polar wander. *Journal of Geophysical Research*, **101**, 15 799–15 818.

Morrow, J. R., Sandberg, C. A. *et al.* 2009. Carbon isotope chemostratigraphy and precise dating of middle Frasnian (lower Upper Devonian) Alamo Breccia, Nevada, USA. *Palaeogeography Palaeoclimatology Palaeoecology*, **282**, 105–118.

Pas, D., Da Silva, A. C. *et al.* 2013. Sedimentary development of a continuous Middle Devonian to Mississippian section from the fore-reef fringe of the Brilon Reef

Complex (Rheinisches Schiefergebirge, Germany). *Facies*, **59**, 969–990, http://dx.doi.org/10.1007/s10347-012-0351-z

Pas, D., Da Silva, A. C. *et al.* 2014. Insight into the development of a carbonate platform through a multi-disciplinary approach – a case study from Upper Devonian slope deposit of Mount Freikofel (Carnic Alps, Austria/Italy). *International Journal of Earth Sciences*, **103**, 519–538, http://dx.doi.org/10.1007/s00531-013-0969-2

Pettijohn, F. J., Potter, P. E. & Siever, R. 1972. *Sand and Sandstone*. Springer, Berlin.

Piecha, M. 1993. Stratigraphie, Fazies und Sedimentpetrographie der rhytmisch und zyklisch abgelagerten, tiefoberdevonischen Beckensedimente im Rechtsrheinischen Schiefergerbirge (Adorf Bänderschiefer). *Courier Forschung Institute Senckenberg*, **163**, 1–135.

Pisarzowska, A., Sobstel, M. & Racki, G. 2006. Conodont-based stratigraphy of the Early-Middle Frasnian transition on the South Polish carbonate shelf. *In*: Baliński, A., Olempska, E. & Racki, G. (eds) *Biotic Aspect of the Early–Middle Frasnian Eventful Transition. Acta Palaeontologica Polonica*, **51**, 609–646.

Pratt, B. R. 1982. Stromatolitic framework of carbonate mud-mounds. *Journal of Sedimentary Petrology*, **52**, 1203–1227.

Pratt, L. M., Claypool, G. E. & King, J. D. 1986. Geochemical imprint of depositional conditions on organic matter in laminated – bioturbated interbeds from fine-grained marine sequences. *Marine Geology*, **70**, 67–84.

Préat, A. & Kasimi, R. 1995. Sédimentation de rampe mixte silico-carbonatée des couches de transition eifeliennes-givétiennes franco-belges. Première partie: microfaciès et modèle sédimentaire. *Bulletin des Centres de Recherche Exploration-Production Elf Aquitaine*, **19**, 329–375.

Préat, A., Bultynck, P. & Brice, D. 2006. Givetian. *In*: Bultynck, P. & Dejonghe, L. (eds) *Chronostratigraphic Units Named from Belgium and Adjacent Areas. Geologica Belgica*, **9**, 9–18.

Quirein, J. A., Garden, J. S. & Watson, J. T. 1982. Combined natural gamma ray spectral/litho-density measurments aplied to complex lithologies. *Society of Petroleum Engineers*, **11143**, 1–14.

Riquier, L., Averbuch, O. *et al.* 2010. Diagenetic v. detrital origin of the magnetic susceptibility variations in some carbonate Frasnian–Famennian boundary sections from Northern Africa and Western Europe: implications for paleoenvironmental reconstructions. *International Journal of Earth Siences*, **99**, 57–73.

Ruffell, A. & Worden, R. 2000. Palaeoclimate analysis using spectral gamma-ray data from the Aptian (Cretaceous) of southern England and southern France. *Palaeogeography Palaeoclimatology Palaeoecology*, **155**, 265–283.

Sandberg, C. A., Morrow, J. R. & Ziegler, W. 2002. Late Devonian sea-level changes, catastrophic events, and mass extinctions. *In*: Koeberl, C. & MacLeod, K. G. (eds) *Catastrophic Events and Mass Extinctions: Impacts and Beyond*. Geological Society of America, Boulder, CO, Special Papers, **356**, 473–487.

Schönlaub, H. P. & Histon, K. 2000. The Palaeozoic evolution of the southern Alps. *Mitteilungen der Österreichische Geologische Gesellschaft*, **92**, 15–34.

Sliwinski, M. G., Whalen, M. T. *et al.* 2011. Stable isotope ($\delta^{13}C_{carb\ and\ org}$, $\delta^{15}N_{org}$) and trace element anomalies during the Late Devonian 'punctata Event' in the Western Canada Sedimentary Basin. *Palaeogeography Palaeoclimatology Palaeoecology*, **307**, 245–271.

Sliwinski, M. G., Whalen, M. T. *et al.* 2012. Contrasting clastic input controls on magnetic susceptibility and trace element anomalies during the Late Devonian punctata Event in the Western Canada Sedimentary Basin. *Terra Nova*, **24**, 301–309.

Stow, D. A. V. & Piper, D. J. W. 1984. Deep-water fine-grained sediments: facies models. *In*: Stow, D. A. V. & Piper, D. J. W. (eds) *Fine-grained Sediments: Deep-water Processes and Facies*. Geological Society, London, Special Publications, **15**, 611–646.

Torsvik, T. H., Van der Voo, R. *et al.* 2012. Phanerozoic polar wander, palaeogeography and dynamics. *Earth-Science Reviews*, **114**, 325–368.

Tsien, H. H. 1985. Algal-bacterial origin of micrites in mud mounds. *In*: Toomey, D. F. & Nitecki, M. H. (eds) *Paleoalgology: Contemporary Research and Applications*. Springer, Berlin, 291–296.

Tucker, M. E. & Wright, T. P. 1990. *Carbonate Sedimentology*. Blackwell, Oxford.

Whalen, M. T. & Day, J. E. 2008. *Magnetic Susceptibility, Biostratigraphy, and Sequence Stratigraphy: Insights into Devonian Carbonate Platform Development and Basin Infilling, Western Alberta, Canada*. Society of Economic Paleontologists and Mineralogists, Tulsa, OK, Special Publications, **89**, 291–314.

Wright, V. P. & Burchette, T. P. 1996. Shallow-water carbonate environments. *In*: Reading, H. G. (ed.) *Sedimentary Environments: Processes, Facies and Stratigraphy*, Blackwell, Oxford, 325–394.

Yans, J., Corfield, R. M. *et al.* 2007. Evidence for perturbation of the carbon cycle in the Middle Frasnian punctata Zone (Late Devonian). *Geological Magazine*, **144**, 263–270.

Zegers, T. E., Dekkers, M. J. & Baily, S. 2003. Late Carboniferous to Permian remagnetization of Devonian limestones in the Ardennes: role of temperature, fluids, and deformation. *Journal of Geophysical Research*, **108**, 5/1–5/19.

Zwing, A., Matzka, J. *et al.* 2005. Rock magnetic properties of remagnetized Palaeozoic clastic and carbonate rocks from the NE Rhenish massif, Germany. *Geophysical Journal International*, **160**, 477–486.

View on Dourbes landscape from the « Centre de Physique du Globe de Dourbes »

Chapter 5

Integration of magnetic hysteresis, magnetic susceptibility and elemental geochemistry measurements from all sections: implication on the nature and preservation of the initial magnetic susceptibility

1. Introduction

These last decades, magnetic susceptibility (here we will use χ_{in}) measurement has been developed and broadly used for environmental and climatic reconstructions of past sedimentary records (Hladil et al., 2006; Riquier et al., 2007; Whalen and Day, 2010; Koptíková, 2011; Da Silva et al., 2012; De Vleeschouwer et al., 2012; Da Silva et al., 2013) but also for Recent sediment (Bloemendal et al., 1988; Chen et al., 1997; Bloemendal and Liu, 2005; Larrasoaña et al., 2008). In the studies related to ancient limestones, variation in χ_{in} has been demonstrated to be driven by facies changes and to be likely comparable over relatively long-distance (e.g., intra- to extra-basinal) (Ellwood et al., 2001; Hladil et al., 2006; Mabille et al., 2008; Whalen and Day, 2008; Bábek et al., 2010; Boulvain et al., 2010; Riquier et al., 2010; Da Silva and Boulvain, 2012). These studies established that primary χ_{in} signal in ancient marine carbonate is possibly ruled by the amount of magnetic components inherited from condition that prevailed during deposition, such as climate, sea-level or tectonic variations. Indeed, these large-scaled fluctuations are the primary causes of changes in siliciclastic supply basinward, which is itself the strongest χ_{in} primary-controlling factor (Vanderaveroet et al., 1999; Ellwood et al., 2000; Tribovillard et al., 2006; Devleeschouwer et al., 2010; Śliwinski et al., 2010; Śliwiński et al., 2012). For instance, chemical weathering, its intensity and compositional trends, depends on terrestrial climate, and it is that fact that allows to use χ_{in} of marine sediments to be used as a recorder of climate changes over geological time. However, for such use as a climatic proxy, a good preservation of the primary inherited magnetic susceptibility signal is essential. This is valid as much in past than in recent sedimentary records. Ancient sedimentary sequences (e.g., Palaeozoic) can be affected by multiple post-depositional transformations such as diagenesis and metamorphism which often leads to obliteration or distortion of the primary depositional-induced χ_{in} signal (Schneider et al., 2004; Devleeschouwer et al., 2010; Riquier et al., 2010; Da Silva et al., 2012; Da Silva et al., 2013). In such cases, the recorded magnetic susceptibility signal can be the combined manifestation of (1) a primary detrital signature, (2) the precipitation of secondary mineralogical phases during early or late diagenesis and (3) later remagnetization. Numerous palaeomagetic studies dealing with Paleozoic rocks (Jackson, 1990; Elmore et al., 1993; Channell and McCabe, 1994; Szaniawski et al., 2003; Zegers et al., 2003; Zwing et al., 2005; Da Silva et al., 2012) clearly demonstrated the effect of the diagenesis like chemical remagnetization process. However, recently Da Silva et al. (2013) and Riquier et al. (2010) performed rock magnetic studies on numerous Devonian limestone sections respectively from the NE Rhenish Massif, Ardennes, France and Moroco. Despite the remagnetization highlighted in the NE Rhenish Massif and Ardennes (Molina Garza and Zijderveld, 1996; Zwing et al., 2002; Zegers et al., 2003; Zwing et al., 2005), Da Silva et al. (2013) and Riquier et al. (2010) underlined that in most of the case the primary depositional-induced χ_{in} signal was at least partly preserved, even if probably also partly blurred and could be used for palaeoenvironmental and palaeoclimatic reconstructions. Even if such case studies mainly exposed positive results, they also revealed that for reliable palaeoenvironmental reconstruction the respective influence of the primary-induced depositional setting versus secondary diagenetic signatures must be thoughtfully evaluated. In order to better estimate the respective influence of secondary and primary depositional processes on the initial magnetic susceptibility measurement (χ_{in}) we carried out magnetic hysteresis measurements for a representative set of 72 samples in the four sections studied for this PhD (Burgberg section: 18 samples; Freikofel section: 14 samples; La Thure section: 20 samples; Fromelennes-Flohimont section: 20 samples). These measurement are expected to improve our understanding of the origin of the χ_{in} variations recorded in our sections (and broadly to Palaeozoic limestone succession) and as a corollary, to establish the restriction and applicability of the χ_{in} measurements as palaeoenvironmental/palaeoclimatic proxy and correlative tool in marine limestone. To strengthen these results, a large geochemical dataset, including well-known detrital input proxies (Al_2O_3, SiO_2, TiO_2, K_2O, Zr, etc.), was measured for each section in order to evaluate the impact of the detrital primary signature on the χ_{in} signal. For the detailed results and discussion on the initial magnetic susceptibility (χ_{in}) and the link with depositional setting and the siliciclastic input proxies the reader is referred to Chapter 3, 4 and 5.

2. Analytical methods

Initial magnetic susceptibility measurements (χ_{in}) were performed on a KLY-3S instrument (AGICO, noise level 2 × 10^{-8} SI) at the University of Liège (Belgium). Magnetic susceptibility is expressed in m³/kg; each data point is the average of three measurements. In order to compare χ_{in} values with other data on exactly the same sample, χ_{in} was measured on samples prepared for hysteresis measurement as explained hereafter. Isothermal magnetisation curves (hysteresis loops) were realized on a cuboid rock weighted with a precision of 0.001 gr and the average mass of sample is 2.5 gr. These samples were packed in a small paper box and measured with a J-Coercivity “rotation” magnetometer developed by Kazan University (Burov et al., 1986) and sited at the Geophysical centre of the Royal Meteorological Institute. The magnetising field was increased every 0.5 mT from 0 to +500 mT, then decreased to zero and further decreased to –500 mT and induced and remanent magnetisation were measured at each field increment/decrement. Finally, the decay of the IRM_{500mT} was monitored for about 100 s. These measurements allowed the determination of the initial hysteresis curve (curve 1 in Fig. 1a), the descending branch of the hysteresis curve (curve 2 in Fig. 1a) as well as the Isothermal Remanent Magnetisation (IRM) acquisition (i.e., remanence from 0 to +500 mT, curve 3 in Fig. 1a) and backfield curve (remanence from 0 to -500 mT, curve 4 in Fig. 1a). The following parameters were extracted from hysteresis measurement and IRM acquisition curves: saturation magnetization M_s (Am²/kg); remanent saturation magnetization M_{rs} (Am²/kg) at a field of 500 mT; high-field magnetic susceptibility χ_{HF} (m³/kg); coercive force H_c (mT); remanent coercive force H_{cr} (mT). χ_{HF}, the high-field magnetic susceptibility provides a direct quantification of the combined paramagnetic and diamagnetic components for rock samples that does not contain high coercivity mineral such as hematite. The value χ_{ferro} (m³/kg) which corresponds to the ferromagnetic *s.l.* contribution is calculated by subtracting χ_{HF} from χ_{in} (e.g., Walden et al., 1999). M_s and H_c were determined after slope correction based on data point at field values < 0.5 T. Parameters extracted from the hysteresis loop are commonly interpreted using the so-called “Day” plot (Day et al., 1977) which corresponds to linear or logarithmic plot of M_{rs}/M_s versus H_{cr}/H_c values usually including single-domain (SD), pseudo-single domain (PSD) and multi-domain (MD) grain-size field delimitations. Thus, the “Day” plot allow to assess the main grain-size of magnetite particles for a given sample collection. Moreover, using logarithmic "Day" plot from Dunlop (2002) and curves for diagenesis-induced remagnetized and non-remagnetized established by Channell and McCabe (1994), it is possible to estimate whether or not the ferromagnetic signal is over-printed by diagenetic processes. However, when samples are composed of mixed grain-size mineralogy or bimodal grain-size distribution the "Day" plot is more difficult to interpret. This limitation can be partly overcome using Tauxe et al. (2002) diagram. Tauxe et al. (2002) performed numerical simulation for a great variety of rock samples and proposed to use M_{rs}/M_s vs. H_c instead of M_{rs}/M_s vs. H_{cr}/H_c plot. Indeed, M_{rs}/M_s vs. H_c plot allow to delineate with more accuracy the magnetic grain-size domains and shapes for a collection of samples. Another useful parameter which can be measured with a J-Coercivity "rotation" magnetometer is the magnetic decay viscosity coefficient (S_d, a dimensionless parameter) which is calculated on a remanence decay interval of 100 seconds (Fig. 1b). This parameter corresponds to the slope measured in the M_s/M_0 vs. Log_{10} (time[s]) plot (Fig. 1c). The relative decay viscosity coefficient (S_d) parameter provides an qualitative estimation of the magnetic viscosity of a samples and a qualitative estimation of superparamagnetic (SP) and viscous grains concentration. Magnetic viscosity is the time lag in the change of magnetic parameters of magnetic grains relative to change in the applied magnetic field. The qualitative estimation of viscous and superparamagnetic grains concentration in a rock sample can be evaluated with respect to the noise of the remanence decay curve. A remanence curve showing high noise (high amplitude variation) corresponds to a sample with low concentration in ferromagnetic mineral. Parameters extracted from the hysteresis loops and remanance decay curve that are obtained with the J-Coercivity "rotation" magnetometer (M_s, M_{rs}, H_c, H_{cr}, χ_{HF}, χ_{ferro}, χ_{in}, M_{rs}/M_s, H_{cr}/H_c and S_d) are reported in Fig. 2-11 and provided in Table 1 or Supplementary materials.

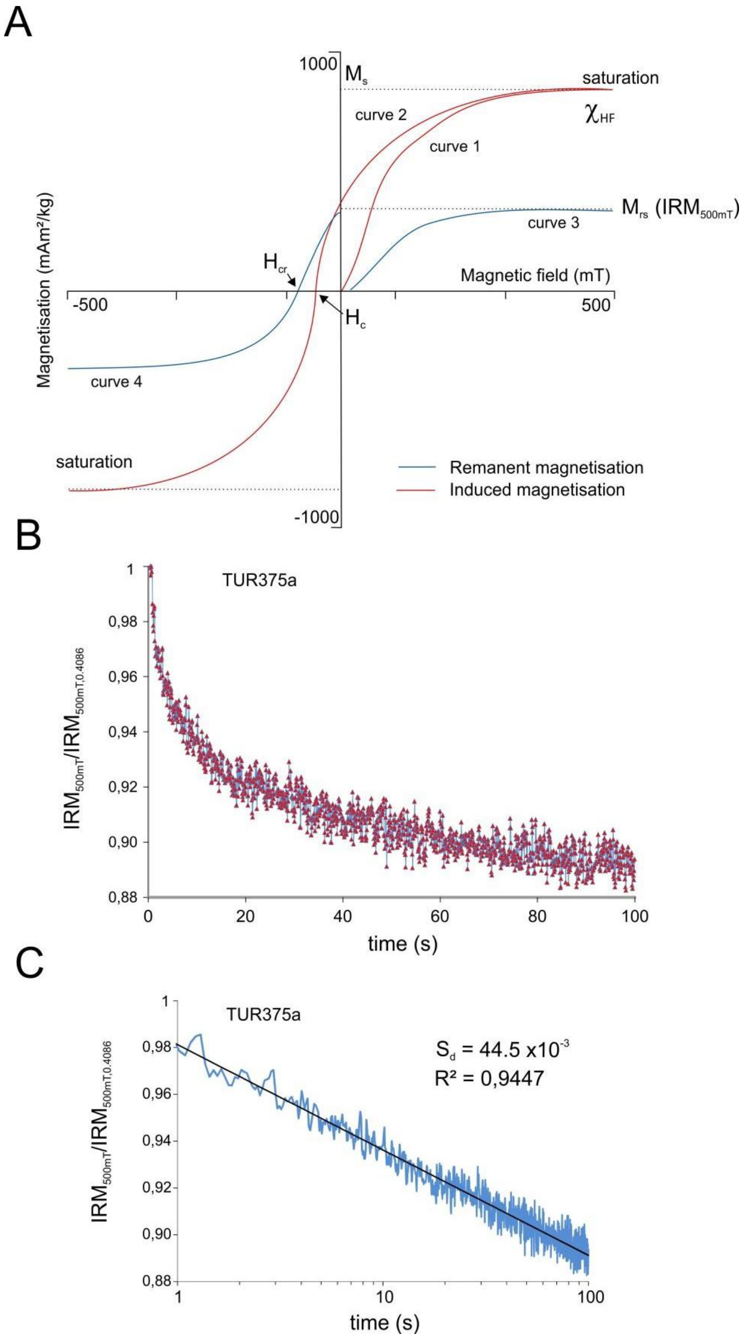

Fig. 1 ***a*** *Sketch of magnetisation curve measurements performed with the J-coercivity meter. Curve 1 (red) represents the initial hysteresis curve and curve 2 (red) the descending branch of the hysteresis loop. From these curves (slope-corrected) the saturation magnetisation Ms, the coercive force Hc and the high-field magnetic susceptibility χ_{HF} are calculated. Curve 3 (black) represents the IRM acquisition from 0 to 500 mT and curve 4 (black) is the backfield curve between 0 and -500mT. Saturation magnetisation at 500 mT (IRM_{500mT}) and coercivity of remanence Hcr were obtained from remanence measurements (redraw from Devleeschouwer et al., 2010).* ***b*** *IRM decay over 100 seconds for sample TUR375a. The IRM_{500mT} (t) is normalized to the initial IRM_{500mT} value at 0.4s after shutting off the applied field.* ***c*** *IRM decay over 100 seconds on a semi logarithmic scale for sample TUR375a. Sd coefficient corresponds to the slope measured in the IRM_{500mT} / $IRM_{500mT,0.4s}$ vs. Log_{10} (time[s]).*

3. Origin and nature of the initial magnetic susceptibility signal

3.1. Nature of minerals carrying the χ_{in} signal

Characteristic of the hysteresis loop measurements in the four Mid-Late Devonian carbonate succession are presented herein (Figs. 2-11 and Tab. 1). The M_s vs. χ_{in} plot (Fig. 2a) indicates that the χ_{in} signal for the Fromelennes-Flohimont (r = 0.98) and La Thure (r = 0.5) sections are more influenced by the ferromagnetic *s.l.* contribution than at the Burgberg (r = 0.2) and Freikofel (r = 0.28) sections. This is confirmed by the strong linear correlation between χ_{in} and χ_{ferro} (La Thure r = 0.98; Fromelennes-Flohimont r = 0.99; Freikofel r = 0.98; Fig. 2b). For the Burgberg section, the correlation is, as expected lower (r = 0.52). However, an unexpected very good correlation between χ_{in} and χ_{ferro} is recorded for the Freikofel section (r = 0.98) indicating that ferromagnetic *s.l.* contribution is finally higher than what was shown using M_s vs. χ_{in} plot.

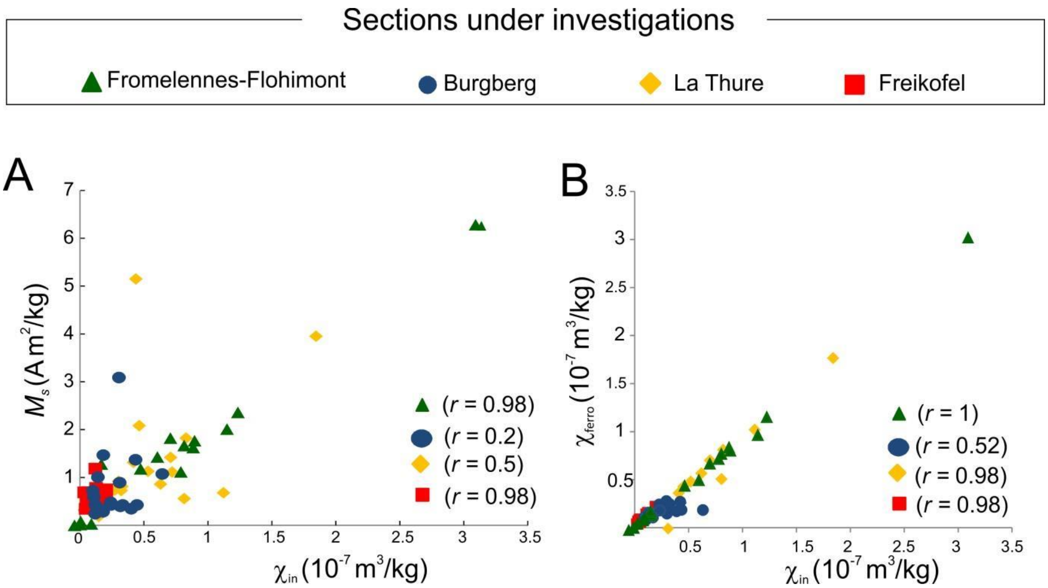

Fig. 2 *Comparison of initial magnetic susceptibility (χ_{in}) with parameters extracted from the hysteresis curves for the Fromelennes-Flohimont, La Thure, Burgberg and Freikofel sections.* ***a*** *Magnetization at saturation (M_s, Am²/kg) versus χ_{in} for the four sections under investigation.* ***b*** *Ferromagnetic susceptibility (χ_{ferro}, m³/kg) versus χ_{in} for the four sections under investigation.*

Though the ferromagnetic *s.l.* contributes significantly on the χ_{in} signal in the Freikofel dataset, the significant noise (Fig. 3a) observed in most of the remanent decay curve indicates a very low ferromagnetic minerals concentration. In contrast, the low noise in the remanent decay curve for a large number of the La Thure samples (Fig. 3b) indicates a higher ferromagnetic minerals concentration in this section. In the Burgberg and Fromelennes-Flohimont samples, both remanence decay behaviours are observed, depending of the analysed samples.

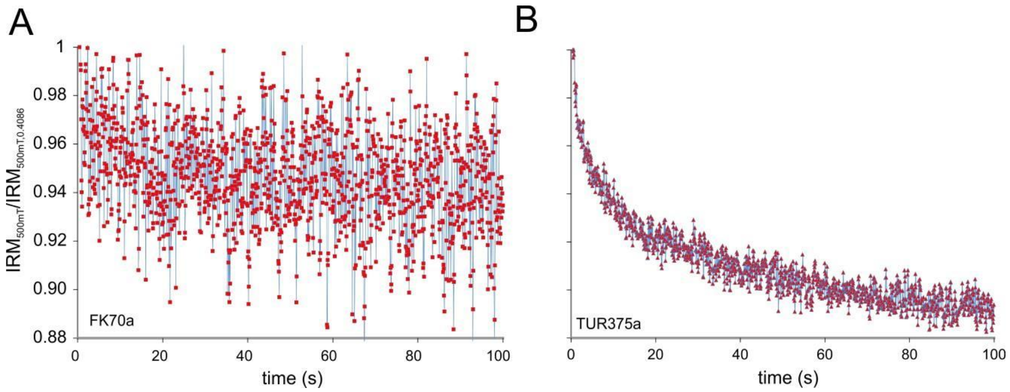

Fig. 3 a *IRM decay over 100 seconds for sample FK70a characteristic of the Freikofel section. Note the high noise recorded over the 100 seconds.* ***b*** *IRM decay over 100 seconds for samples TUR375a characteristic of most samples from the La Thure section. Note the very low noise recorded over the 100 seconds in comparison to the plot* **a**

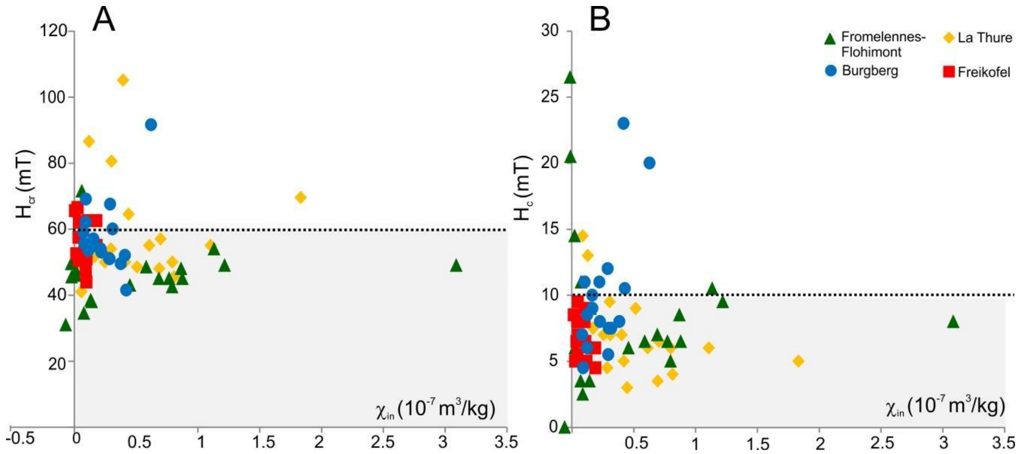

Fig. 4 *Comparison of initial susceptibility magnetic (χ_{in}) with parameters extracted from the hysteresis curves for the Fromelennes-Flohimont, La Thure, Burgberg and Freikofel sections.* **a** *Comparison of initial magnetic susceptibility (χ_{in})* with the remanent coercivity (H_{cr}). **b** *Comparison of initial magnetic susceptibility (χ_{in}) with the coercivity (H_c). Shaded bands correspond to domains coercivity and remanance coercivity values for magnetite.*

As established above, ferromagnetic *s.l.* components have a major influence in our data sets and it is therefore essential to better constrain the origin of these magnetic minerals. Majority of samples in our data sets display H_{cr} and H_c values respectively lower than 60 mT and 15 mT (Fig. 4). These observations suggest that the main ferromagnetic contributors are low-coercivity minerals like magnetite (Fe_2O_3) and therefore a χ_{in} signal mainly driven by varying concentration of such magnetite-type mineral. These observations concur with usual results from platform carbonates (Borradaile et al., 1993; Zwing et al., 2005; Riquier et al., 2010; Da Silva et al., 2012; Da Silva et al., 2013). As shown above, low-coercivity minerals like magnetite lead the χ_{in} in most of the analysed samples. χ_{HF} value can therefore be used with confidence in order to analyze the diamagnetic and paramagnetic contributions in our data sets. Concerning the Burgberg section, diamagnetic and paramagnetic contributions to the bulk χ_{in} are important as shown by the correlation (r = 0.74) between χ_{in} and χ_{HF} (Fig. 5a-b). Correlation between χ_{in} and χ_{HF} are also good for the Fromelennes-Flohimont section (0.64). Inversely, the low correlation between χ_{in} and χ_{HF} for the La Thure (r = 0.19) and Freikofel (r = 0.06) points to a weak influence of the paramagnetic and diamagnetic components on the χ_{in} signal. Also note that on the Fig. 5a-b, χ_{HF} values for Burgberg, La Thure and Fromelennes-Flohimont are all in the same range (0 to 5x10^{-8} m³/kg) and are mostly positive. This indicates that the χ_{HF} is dominated in this case by paramagnetic minerals. In the Freikofel section χ_{HF} values are all negative (Fig. 2b), pointing to a strong influence of diamagnetic minerals and low impact of the paramagnetic minerals.

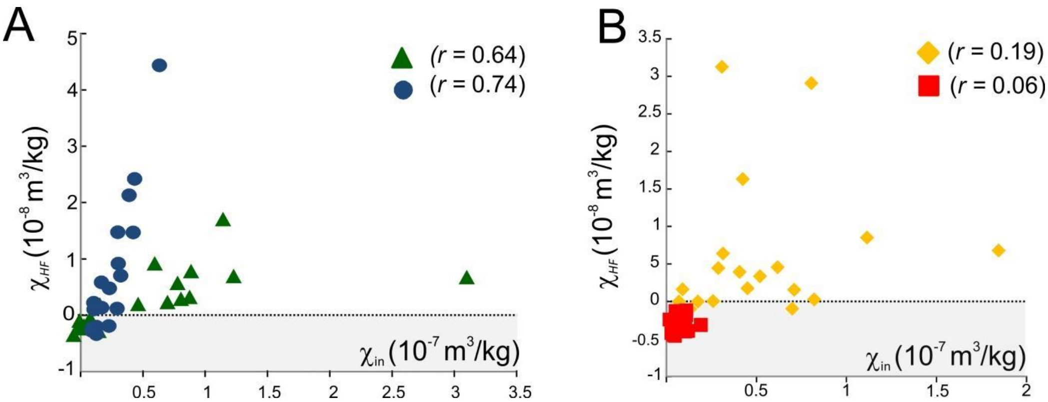

Fig. 5 a *High-field magnetic susceptibility (χ_{HF}, m³/kg) versus χ_{in} for the Fromelennes-Flohimont and Burgberg sections.* **b** *High-field magnetic susceptibility ($\chi_{HF,}$ m³/kg) versus χ_{in} for La Thure and Freikofel sections. Shaded bands correspond to χ_{HF} negative values.*

3.2 Grain size and origin of the ferromagnetic minerals

As we have seen earlier, χ_{in} signal is mainly driven by low-coercivity ferromagnetic grains. The assessment of the magnetic grain sizes that contribute to the χ_{in} is not easy to evaluate and this is mostly done by comparison with reference studies and comparable Devonian data sets (e.g., Jackson, 1990; Zwing et al., 2005; Devleeschouwer et al., 2010; Riquier et al., 2010; Da Silva et al., 2012; Da Silva et al., 2013; Konigshof et al., 2015). In order to further constraint the main magnetic grains size contributing to the χ_{in} signal, ratios of values M_{rs}/M_s and H_{cr}/H_c extracted from hysteresis loop were plot in bi-logarithmic "Day" plot. Empirical trends from Dunlop (2002) and Parry (1982) are respectively illustrated for the combination of various proportion of PSD and MD+SD, SP+SD grains and MD+SD (Figs. 6-8). Furthermore, our data sets are compared with other Devonian reported data, as mentioned above. To make the reading and comparison of data easier we divided data for comparison into two bi-logarithmic "Day" plots. "Day" plot in Fig. 6 shows only our data with empirical trends from Dunlop (2002) and mixing lines for MD+SD from Parry (1982). For comparison with Belgian Devonian data reported in Da Silva et al. (2013) (for which H_{cr} values was not measured and so comparison on a "Day" plot is not possible) we also contructed a squareness versus coercivity plot (SQC; Tauxe et al., 2002) (Fig. 8).

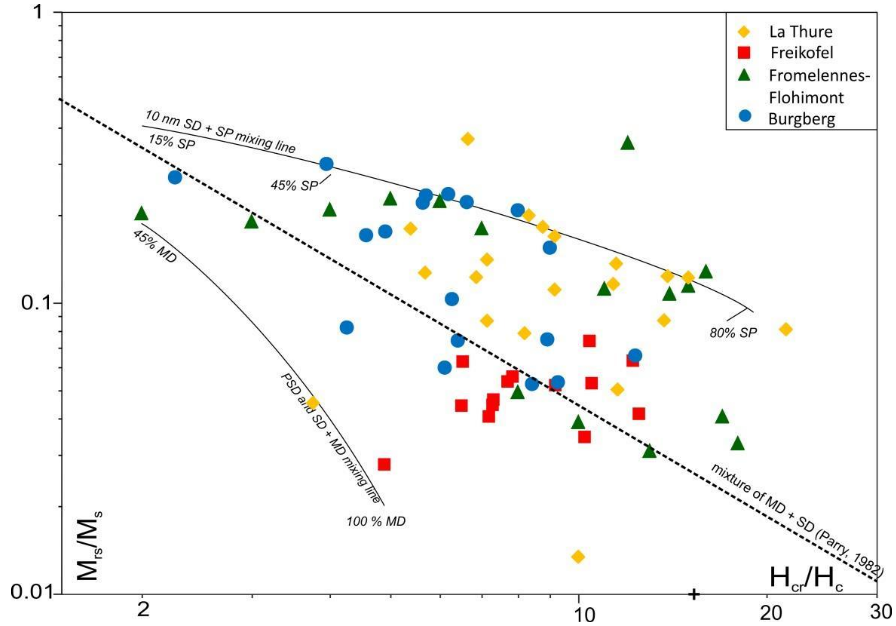

Fig. 6 *Bi-logarithmic Day plot (Day et al., 1977) for data sets from the four sections under investigation in this study. Empirical trends from Dunlop (2002) and Parry (1982) are respectively illustrated for the combination of various proportion of PSD and MD+SD, SP+SD grains and MD+SD.*

The "Day" diagram in figures 6 shows that Mid-Upper Devonian limestone from this investigation are mostly distributed between the SD+SP and PSD and SD+MD mixing curves of Dunlop (2002). Figures 7 and 8 also show that samples from the Rhenohercynian sections (Burgberg, La Thure and Fromelennes-Flohimont) are not homogeneously distributed. Samples from the La Thure and Fromelennes-Flohimont are scattered between the SD+SP and SD+MD lines, close to North America Paleozoic limestones reported by Jackson (1990), biohermal limestone investigated by Zwing et al. (2005) and values reported by Riquier et al. (2010) corresponding to Frasnian/Famennian limestone/shale. M_{rs}/M_s and H_{cr}/H_c values for Burgberg appear to be divided in two distinct areas. Half of the samples fall in or close of the SD+SP mixing line, adjacent the La Thure samples while the other half lie near SD+MD mixing line of Parry (1982), neighboring the hysteresis values of the Freikofel samples and remagnetized siliciclastic rocks studied by Zwing et al. (2005) (Fig. 9).

In the SQC plot our samples are mainly distributed along three trends corresponding mainly to the PSD and MD grains size domains (Fig. 9). This first observation is consistent with previous results based on the bi-logarithmic "Day" plots (Figs. 6-8) also showing distribution of samples in three main areas even if this is less well defined in the Fig. 9. Values for the Freikofel samples and half of the Burgberg and Fromelennes-Flohimont samples are clustered in the lower part of the SQC diagram (Trend 1), characteristic of the multi-domain (MD) grain size of detrital origin. Hysteresis values for the La Thure section and the second half of samples from the Burgberg section cluster in the Trend 2, similarly to the values published by Da Silva et al. (2013) for Belgium Devonian limestones. This result is indicating magnetic grains with size ranging from 70 nm to 115 nm and showing cubic to elongated shapes (aspect ratio 1:1 to 2:1). According to Da Silva et al. (2013), Trend 2 is indicative for the formation of fine-grained magnetite in our limestone related to remagnetization event. Remaining part of the samples belonging to the Fromelennes-Flohimont section fall in or close to the Trend 3, similarly to typical remagnetized samples studied by Zwing et al. (2005).

Values from Jackson (1990) illustrated in the “Day" plot were interpreted by Channell and McCabe (1994) as recording a fine-grained fingerprint typical of remagnetized limestone. Data from Riquier et al. (2010) used for comparison are from section in the NE Rhenish Massif (Steinbruch Schmidt and Beringhauser Tunnel sections) and are affected by deformation and burial diagenesis.

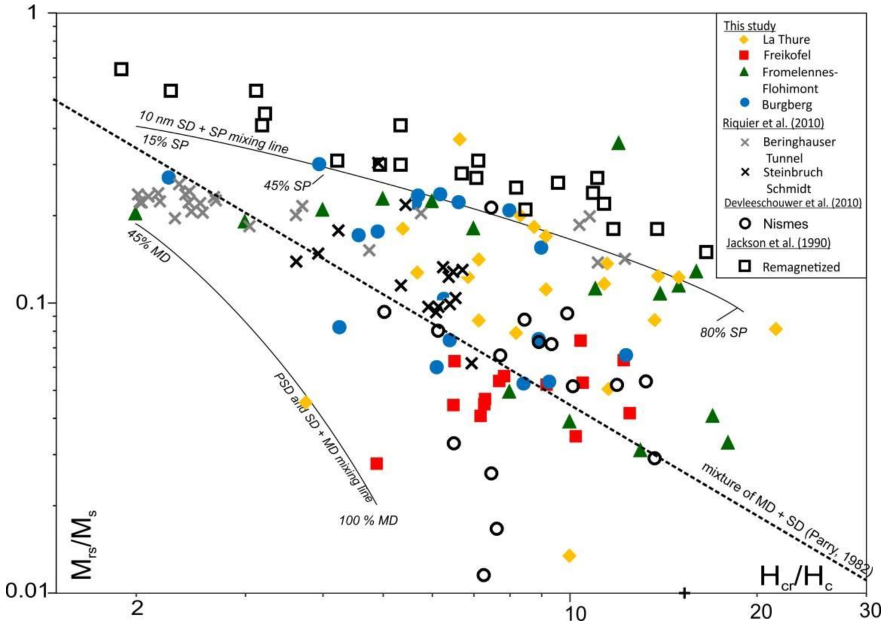

Fig. 7 *Bi-logarithmic Day plot (Day et al., 1977) for data sets from the four sections under investigation in this study compared with reported Palaeozoic data for remagnetized siliciclastic and carbonate rocks from Zwing et al. (2005) and limestone/shale from Konigshof et al. (2015). The lines are theoretical SD+SP and PSD and SD+MD curves from Dunlop (2002) that are based on 10 nm SP magnetite grains and coarse-grained magnetite end members, respectively. The dashed line corresponds to a mixture of MD+SD grains according to Parry (1982).*

Riquier et al. (2010) demonstrated that their data show a remagnetized fingerprint as observed by McCabe and Channell (1994) and Zwing et al. (2005) for remagnetized limestone from UK (Craven Basin) and Germany (NE Rhenish Massif) respectively. Riquier et al. (2010) interpreted the magnetic signature of their samples as the superimposition of a coarse-grained magnetite detrital fraction and a diagenetic fraction showing authigenic SD+SP fine-grained magnetite. Furthermore, based on a good correlation between χ_{in} and selected siliciclastic input proxies (Zr and Th), Riquier et al. (2010) claimed that the secondary authigenic magnetite formation do not disturb too much the initial magnetic susceptibility. Data from Da Silva et al. (2013) are all from Belgian Devonian limestone and interpreted as carrying a fine-grained PSD magnetite formed during the Variscan Orogeny as a consequence of the remagnetization triggered by clay diagenesis (Zegers et al., 2003). As for Riquier et al. (2010), the good correlation between χ_{in} signal and detrital input proxies for these Belgian limestones (Da Silva et al., 2012) suggests a preservation of the primary χ_{in} signal for these samples despite remagnetization recognized in these Palaeozoic lithologies. La Thure, Fromelennes-Flohimont and part of the samples from Burgberg falling close to data from Zwing et al. (2005), Riquier et al. (2010) and Da Silva et al. (2013) are therefore interpreted as carrying a secondary magnetite signal related to a remagnetization event.

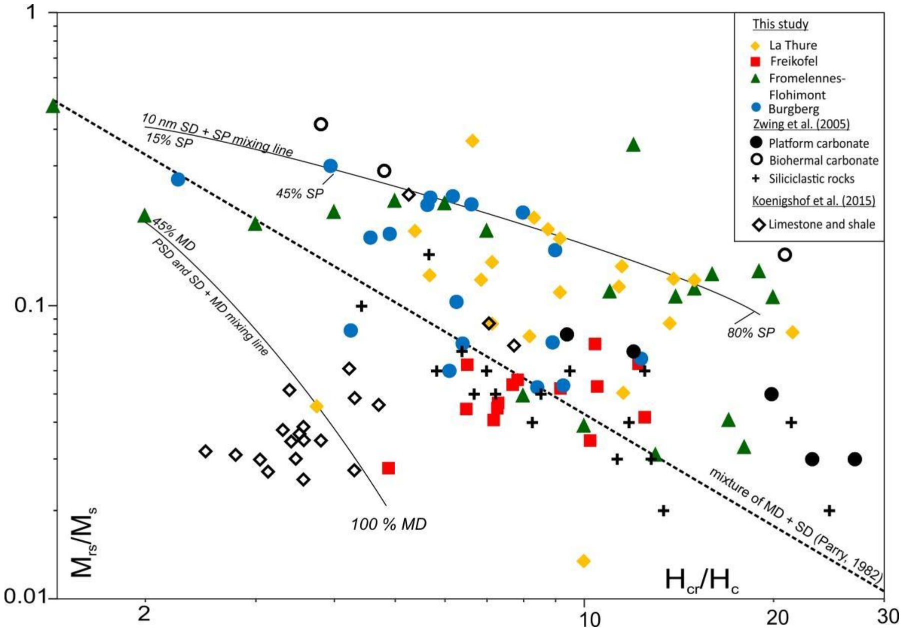

Fig. 8 *Bi-logarithmic Day plot (Day et al., 1977) for data sets from the four sections under investigation in this study compared with different Palaeozoic rocks from Riquier et al. (2010), Devleeschouwer et al. (2010) and samples from (Jackson, 1990) which correspond to classical remagnetized limestone (Channell and McCabe, 1994). The lines are theoretical SD+SP and PSD and SD+MD mixing curves from Dunlop (2002) that are based on 10 nm SP magnetite grains and coarse-grained magnetite end members, respectively. The dashed line corresponds to a mixture of MD+SD grains according to Parry (1982).*

Values corresponding to the Freikofel sections have hysteresis properties similar to the siliciclastic rocks studied by Zwing et al. (2005) (Fig. 6) and Givetian limestone reported by Devleeschouwer et al. (2010) and are tightly grouped along the line for mixture of SD and MD magnetic grains obtained by Parry (1982) and head towards MD domain and the values from Konigshof et al. (2015) indicative of limestone with a preserved primary coarse multi-domain (MD) detrital magnetic.

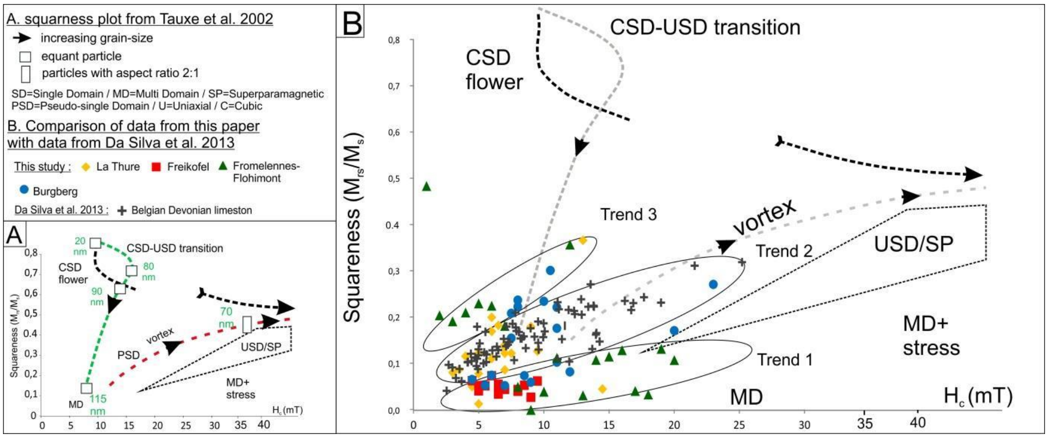

Fig. 9 *Squareness vs coercivity plot (SQC): plot of Mrs/Mr versus Hc (mT).* **a** *explanation of the different areas occurring in the SQC plot modified from Tauxe et al. (2002).* **b** *Comparison of data from this present research with Belgian Devonian remagnetized limestone data reported by Da Silva et al. (2013).*

As mentioned earlier, the Burgberg samples are characterized by a division in two distinct areas which is well exposed in the Fig. 10. This separation of M_{rs}/M_s, and H_{cr}/H_c values recorded in the Burgberg into two groups is also corresponding with two different facies. Indeed, the data plotting along the SD+SP mixing curves (Dunlop, 2002) are all intermediate and off-reef facies (SD2+SD3), while the data fitting along the mixture of MD+SD line of (corresponding to Parry, 1982) are all proximal fore-reef facies (SD3). These three main sedimentary domains were defined in Pas et al. (2013). In addition, the lowest M_{rs}/M_s values correspond to the weakest values of proxies for siliciclastic influx (Al, Ti and Zr) while the highest M_{rs}/M_s values record the opposite. As shown on the Fig. 9a, H_{cr}/H_c and M_{rs}/M_s values for the Burgberg proximal fore-reef limestone (SD3) are fitting with values for the Freikofel limestone samples. Besides being recording similar M_{rs}/M, and H_{cr}/H_c than the Burgberg proximal fore-reef samples (SD3) (see Fig. 10a), the Freikofel samples are also comparable in term of sedimentary setting (e.g., fore-reef setting; Pas et al., 2014) and average concentration in siliciclastic input proxies (Fig. 10b). The subdivision of the H_{cr}/H_c and M_{rs}/M_s values between intermediate+distal fore-reef limestone (SD2+SD1) and proximal fore-reef limestone (SD3) is very interesting because it allows us to highlight a facies-related process that seems to influence hysteresis behaviour. Indeed, hysteresis behaviour of the SD3 Burgberg samples follow the line of Parry (1982) for a typical coarse-grained MD magnetite of detrital signature [and correlatively for non-remagnetized limestone (Channell and McCabe, 1994)]. However SD1+SD2 Burgberg samples fall nearby Jackson (1990) limestone classically attributed to remagnetized limestone (Channell and McCabe, 1994).

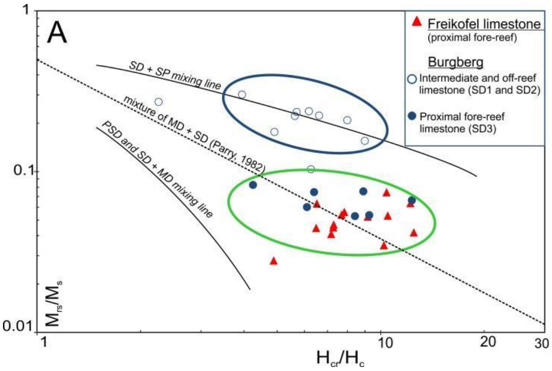

B

	Burgberg		Freikofel
	SD1-SD2 (n=11)	SD3 (n=7)	Freikofel (n=14)
Hcr/Hc	6.362	6.960	8.593
Mrs/Ms	0.191	0.097	0.050
Al (wt. %)	4.380	0.284	0.376
Ti (wt. %)	0.125	0.036	0.072
Zr (ppm)	18.718	5.515	9.113

Fig. 10 a *Bi-logarithmic Day plot (Day et al., 1977) showing split of the values between proximal fore-reef limestone (SD3) and intermediate and off-reef limestone (SD1 and SD2) belonging to the Burgberg section (Pas et al., 2013) and the hysteresis values for the proximal fore-reef limestone from the Freikofel section (Pas et al., 2014).* **b** *Comparison of average values for hysteresis ratio H_{cr}/H_c, M_{rs}/M_s and for siliciclastic input proxies between sedimentary domains defined in Burgberg and the Freikofel proximal fore-reef samples. Theoretical SD+SP line and PSD and SD+MD line from (Dunlop, 2002).*

This observation is hard to explain. However, our hypothesis would be that the occurrence of fine-grained magnetic fingerprint in relation with remagnetization occurs in all the samples belonging to the Burgberg section but would be disguised in the SD3 proximal fore-reef limestone where coarse-grained (MD) signal would be dominant. This type of hypothesis was proposed by Zwing et al. (2005) who studied various lithologies from the NE Rhenish Massif extending from siliciclastic rocks to biohermal and platform carbonate. The hysteresis ratio from siliciclastic rocks fall in or close to the field of MD magnetite (Fig. 8; Parry, 1982), indicative of detrital magnetite. The hysteresis parameters of biohermal rocks fall in the field of SD+SP magnetite of remagnetized rocks (Fig. 8; Jackson, 1990). Some fine grained clastic rocks and the platform carbonates have hysteresis properties between the biohermal carbonates and coarse clastic rocks (SD+MD mixture). For Zwing et al. (2005) this distribution points towards the presence of ultrafine grained materials in all lithologies, which supports a remagnetization. However, for Zwing et al. (2005), fine-grained magnetic fingerprint was increasingly masked by increasing amount of coarse-grained detrital magnetite (MD). In the case of SD3 Burgberg samples characterized by a very low concentration in siliciclastic (e.g., Al, Ti, Zr; Fig. 9b) we suggest that the masked fine-grained remagnetization is related to the weak formation of secondary fine-grained magnetite (directly dependant of clay content) and not to increasing detrital magnetite (MD) as suggested by Zwing et al. (2005). As demonstrated by Zwing et al. (2005) during the late Palaeozoic remagnetization the clay diagenesis (e.g., smectite - illite transition) was the main process enable to create fine-grained magnetite that are characteristic of remagnetized rocks. Thus, even if detrital (MD) magnetite likely occurs in very low concentration, this coarse-sized magnetite remains visible as a result of the very weak clay content recorded in this proximal fore-reef SD3 limestone. These results undoubtedly highlight that all type of limestone studied in the Burgberg section where affected by a remagnetization which is not visible in the case where clay content is very low. Now if we analyse the case of the Freikofel fore-reef limestone, either the MD detrital magnetite mask a remagnetization fingerprint or no remagnetization process occur. The similar hysteresis values and depositional setting that characterize the Freikofel limestone and the Burgberg proximal fore-reef (SD3) lead us to the conclusion that the Freikofel samples are also affected by a remagnetization. But, the magnetic fingerprint that could attest of it is disguised by the MD detrital grains, as explained for SD3 Burgberg samples.

The Carnic Alps area corresponds to the non- to low-metamorphic portion of the Variscan substratum of the Southern Alps. In this region, the CAI (conodont Colour Alternation Index) was studied by Brime et al. (2008) in numerous localities. In Freikofel area this CAI varies from 4 to 4.99, corresponding to low- to mid-Anchizone domain (Brime et al., 2008). According to these authors, CAI value between 1 and 5 corresponds to temperature from 50° to 300°C. This result indicates a maximal temperature of 300°C during the diagenesis in the Freikofel area. According to Urrutia-Fucugauchi (2007) thermic formation of magnetite based on detrital source requires temperature of 350°. This observation hamper to envisage a remagnetization in the Freikofel as suggested below. Nevertheless, if we analyse the case of the unmetamorphosed to very low grade metamorphic carbonate of the Brabant and Ardennes Massifs it appears that pressure solution process enhancing smectite to illite conversion and hence remagnetization is the most conceivable process in this area (Zegers et al., 2003). A remagnetization related to internal fluids caused by hydrothermalism is also possible (see Elmore et al., 2012 for a synthesis of remagnetization processes).

To support data on magnetic grain size provided through the bi-logarithmic “Day” and SQC plots we have analysed the normalized decay viscosity coefficient S_d indicative of fine-grained superparamagnetic (SP) and viscous grains. The normalized decay viscosity coefficient was calculated from the remanence decay measured during 100 s. S_d represents the slope in the IRM_{500mT} vs Log_{10} (time[s]) diagram. As presented in box-wisker (Fig. 11), the median S_d coefficient ranges between 20 and 35 $x10^{-3}$ for the studied sections in this research. These S_d coefficients are relatively high and comparable to S_d coefficient of SP grain containing in Tiva Canyon tuff reference samples TCO4-11M (Sd = 25 x 10-3, containing SP an SSD; Spassov and Valet, 2012). This result evidence the existence of high viscosity grains such as SP magnetic minerals, with relaxation times in the order of tens of seconds or below, in each section under investigation. The higher average S_d values for the Freikofel, La Thure and Fromelennes-Flohimont sections and the locally high S_d coefficients (~45 $x10^{-3}$) point to a larger occurrence of SP grain size in those sections, consistent with results provided in the bi-logarithmic “Day” plots (Figs 6-8).

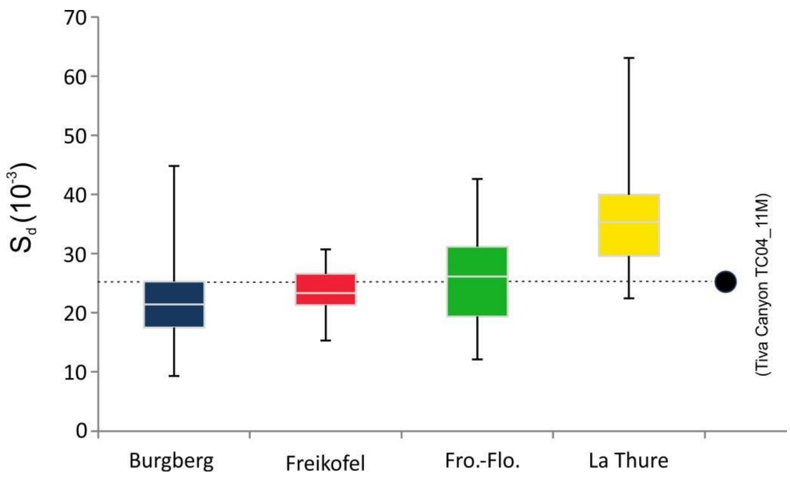

Fig. 11 *Box-wisker showing median (horizontal line), range of mean 50 per cent of results (shaded boxes) and extreme values (caps) of the normalized magnetic viscosity decay (S_d) for the sections under investigation in this research. Tiva Canyon tuff reference sample TC04_11M (S_d = 25 x10^{-3}) (Spassov and Valet, 2012) containing SP grain is plotted for comparison. The normalized magnetic viscosity decay in Freikofel, Fromelennes-Flohimont and La Thure sections is high compared to the Tiva Canyon tuff sample containing superparamagnetic (SP) grains. This result indicates a contribution of SP grains in the initial magnetic susceptibility for these sections. Locally, this contribution is significant.*

The combined analysis of "Day" and SQC plots with published Devonian data allowed us to highlight a typical fine-grained magnetic fingerprint in all the samples, classically attributed to remagnetization. Occurrence of these fine-grained fingerprints is also inferred by the analysis of normalized magnetic viscosity coefficient (S_d). This result means that our initial magnetic susceptibility signal is related to the combined effect of both a primary detrital signature and a remagnetization, which establish the necessity to control whether the primary depositional induced magnetic signature is still preserved. To constraint how we are allowed to interpret the primary character of our signal we have compared reliable proxies for siliciclastic input such as SiO_2, TiO_2, Al_2O_3, K_2O, Zr and Rb (Calvert and Pedersen, 2007; Śliwiński et al., 2012) with χ_{in} results. Fig. 12 and Table 1 summarized the coefficient correlation (*r*) for each set of samples obtained in the Freikofel, Burgberg, Fromelennes-Flohimont and La Thure sections. The coefficient correlation (r >0.5) indicates that χ_{in} signal for all the studied sections is mainly a primary depositional-induced magnetic susceptibility signal. This result point out a remagnetization fingerprint which do not significantly distort the χ_{in} signal and can thus be used as a tool for correlation and environmental purpose. Another option to consider the primary character of the χ_{in} signal is the link with facies variation. This question has been deeply investigated in Chapters 2, 3 and 4 and has also revealed that the primary signal was preserved in the initial magnetic susceptibility (χ_{in}).

Table 1
Mean value (mean) for each hysteresis parameters and selected siliciclastic input proxies and calculated coefficient correlation (r) between these two sets of data and initial magnetic susceptibility (χ_{in}, m³/kg). NM = not measured. For definition of each parameter refers to methodology.

	Hysteresis								Geochemistry					
	Number of sample (n)	χ_{hf} (10^{-8}) m³/kg	χ_{ferro} (10^{-8}) m³/kg	M_s (10^{-4}) Am²/kg	M_{rs} (10^{-4}) Am²/kg	H_c mT	H_{cr} mT	S_d (10^{-3})	Number of sample (n)	SiO_2 % wt.	Al_2O_3 % wt.	TiO_2 % wt.	K_2O % wt.	Zr ppm
Burgberg	**18**								**34**					
r		0.74	0.52	0.20	0.60	0.75	0.14	0.14		0.64	0.63	0.65	0.65	0.67
Mean		0.71	0.54	7.72	1.01	10.0	55.59	21.44		5.87	1.90	0.14	0.49	22.25
Freikofel	**14**								**15**					
r		0.06	0.98	0.28	0.48	0.37	0.13	0.28		0.81	0.74	0.66	0.73	0.59
Mean		-0.31	0.86	6.06	0.30	6.82	55.71	23.31		1.07	0.42	0.07	0.05	9.10
La Thure	**20**								**54**					
r		0.19	0.98	0.50	0.83	0.41	0.03	0.36		0.53	0.52	0.51	0.48	NM
Mean		0.58	4.45	12.49	1.26	6.80	58.40	35.34		5.00	2.00	0.10	1.01	NM
Fro.-Flo.	**20**								**42**					
r		0.64	1.00	0.98	0.98	0.19	0.13	0.35		0.66	0.65	0.66	0.62	0.64
Mean		0.24	5.25	12.53	1.94	9.00	46.30	26.14		5.49	1.42	0.11	0.18	15.74

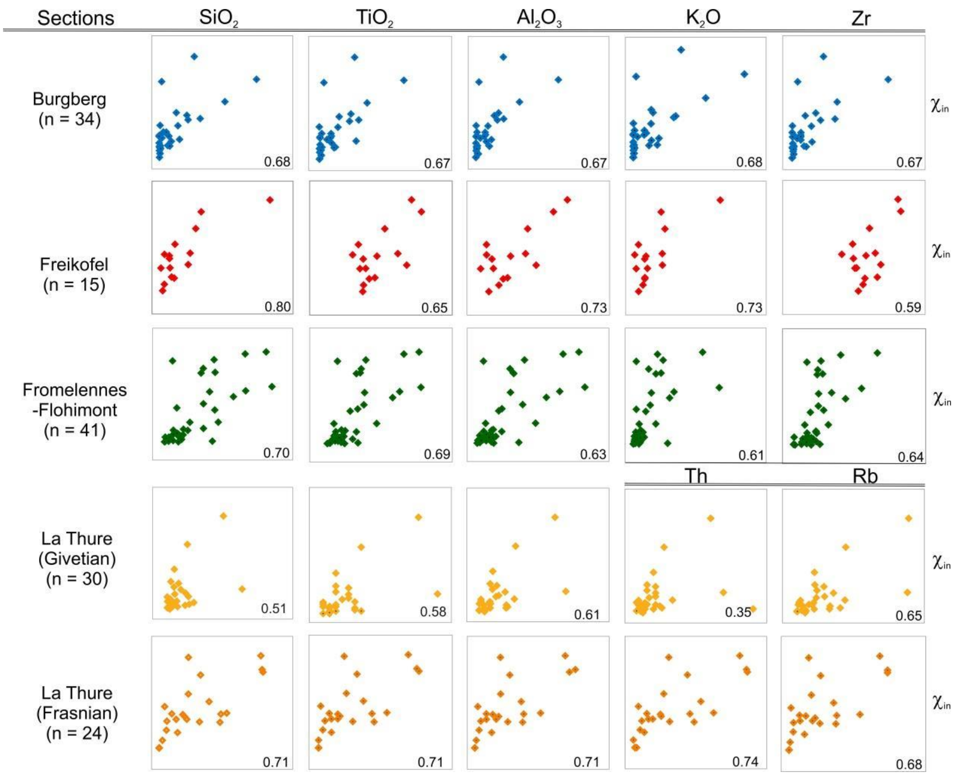

Fig. 12 *Correlation of* the initial magnetic susceptibility (χ_{in}) *with clastic input proxies measured for sections under investigation in this study.*

4. Synthesis and conclusions on the nature and preservation of the initial magnetic susceptibility

Parameters extracted from the hysteresis loops for each section indicate a relatively minor influence of diamagnetic and paramagnetic minerals in comparison to the influence of ferromagnetic minerals (Fig. 2). According to the general low values of remanent coercivity (Fig. 4), soft magnetic components, such as magnetite or pyrrhotite, have the main influence on χ_{in}. Plot of data sets within the bi-logarithmic "Day" plot, including the theoretical curves for mixing of different sized magnetic grains (Parry, 1982; Dunlop, 2002; Figs. 6-8), allowed us to constrain the main magnetic components controlling initial magnetic susceptibility (χ_{in}). Concerning the La Thure, Fromelennes-Flohimont sections and samples from the Burgberg section that correspond to distal fore-reef to off-reef and intermediate fore-reef setting (SD1+SD2), the H_{cr}/H_c and M_{rs}/M_s values indicate a χ_{in} signal mainly controlled by a mixture of SD and SP grains related to remagnetization. Concerning the SD3 proximal fore-reef, the H_{cr}/H_c and M_{rs}/M_s values point to a χ_{in} signal controlled by mixture of SD+MD but with a fine-grained remagnetization fingerprint likely masked by the coarse-grained detrital magnetite (MD). We have suggested that the masked fine-grained remagnetization is related to the weak formation of secondary fine-grained magnetite (directly dependant of clay content) and not to an increase of detrital magnetite (MD) as suggested by Zwing et al. (2005). The distinct hysteresis behavior between SD1+SD2 and SD3 Burgberg samples - belonging to a same carbonate section - clearly highlight a facies-related process influencing hysteresis behavior. In proximal fore-reef Freikofel samples, the ferromagnetic signal appears to be mainly controlled by a mixture of MD+SD grains as for the SD3 proximal-fore reef Burgberg samples. Considering the relatively similar sedimentary setting, hysteresis values and very low concentration in siliciclastic input proxies for both SD3 Burgberg and Freikofel samples we would like to suggest that the remagnetization fingerprint is also disguised by MD grains in the Freikofel section. Even if a remagnetization fingerprint is locally masked, it is obvious that all sections studied in this research were remagnetized. Transition from smectite to illite during diagenesis appeared to be the most convincing parameters enable to produce fine-grained magnetite, which is classically observed in remagnetized limestone. Hence, the recorded χ_{in} signal in our sections is constituted of both a primary depositional-induced and a secondary diagenesis-induced magnetic signal. The relatively good correlations observed between χ_{in} signal and siliciclastic input proxies for all the sections confirm the preservation of the primary depositional-induced character χ_{in} even the remagnetization must have influenced the final χ_{in} signature. Therefore we can use the recorded χ_{in} as a proxy for correlation and environmental reconstruction for all sections under investigation in this research.

5. References

Bábek, O., Kalvoda, J., Aretz, M., Cossey, P.J., Devuyst, F.X., Herbig, H.G. and Sevastopulo, G. (2010) The correlation potential of magnetic susceptibility and outcrop gamma-ray logs at Tournaisian-Viséan boundary sections in Western Europe. *Geologica Belgica*, **13,** 291-308.

Bloemendal, J. and Liu, X. (2005) Rock magnetism and geochemistry of two plio–pleistocene Chinese loess–palaeosol sequences—implications for quantitative palaeoprecipitation reconstruction. *Palaeogeography, Palaeoclimatology, Palaeoecology*, **226,** 149-166.

Bloemendal, J., Tauxe, L. and Valet, J.P. (1988) High-resolution,whole-core magnetic susceptibility logs from Leg 108 (ODP, Atlantic). *Proc., initial reports (part A), ODP, Leg 108, Eastern Tropical Atlantic, (Section 2)***,** 1005-1013.

Borradaile, G.J., Chow, N. and Werner, T. (1993) Magnetic hysteresis of limestones: facies control? *Physics of the Earth and Planetary interiors*, **76,** 241-252.

Boulvain, F., Da Silva, A.C., Mabille, C., Hladil, J., Gersl, M., Koptikova, L. and Schnabl, P. (2010) Magnetic Susceptibility Correlation of Km-Thick Eifelian-Frasnian Sections (Ardennes and Moravia). *Geologica Belgica*, **13,** 309-318.

Brime, C., Perri, M.C., Pondrelli, M., Spalletta, C. and Venturini, C. (2008) Polyphase metamorphism in the eastern Carnic Alps (N Italy'S Austria): Clay minerals and conodont Colour Alteration Index evidence. *International Journal of Earth Sciences*, **97,** 1213-1229.

Burov, B., Nurgaliev, D.K. and Jasonov, P.G. (1986) *Paleomagnetic Analysis* Kazan University Press, Kazan, 176 pp.

Calvert, S.E. and Pedersen, T.F. (2007) Chapter Fourteen Elemental Proxies for Palaeoclimatic and Palaeoceanographic Variability in Marine Sediments: Interpretation and Application. In: *Developments in Marine Geology* (Eds H.M. Claude and V. Anne De), **Volume 1**, pp. 567-644. Elsevier.

Channell, J.E.T. and McCabe, C. (1994) Comparison of magnetic hysteresis parameters of unremagnetized and remagnetized limestones. *Journal of Geophysical Research*, **99,** 4613-4623.

Chen, F.H., Bloemendal, J., Wang, J.M., Li, J.J. and Oldfield, F. (1997) High-resolution multi-proxy climate records from Chinese loess: evidence for rapid climatic changes over the last 75 kyr. *Palaeogeography, Palaeoclimatology, Palaeoecology*, **130,** 323-335.

Da Silva, A.C. and Boulvain, F. (2012) Analysis of the Devonian (Frasnian) platform from Belgium: A multi-faceted approach for basin evolution reconstruction. *Basin Research*, **24,** 338-356.

Da Silva, A.C., De Vleeschouwer, D., Boulvain, F., Claeys, P., Fagel, N., Humblet, M., Mabille, C., Michel, J., Sardar Abadi, M., Pas, D. and Dekkers, M.J. (2013) Magnetic susceptibility as a high-resolution correlation tool and as a climatic proxy in Paleozoic rocks - Merits and pitfalls: Examples from the Devonian in Belgium. *Marine and Petroleum Geology*, **46,** 173-189.

Da Silva, A.C., Dekkers, M.J., Mabille, C. and Boulvain, F. (2012) Magnetic susceptibility and its relationship with paleoenvironments, diagenesis and remagnetization: Examples from the Devonian carbonates of Belgium. *Studia Geophysica et Geodaetica*, **56,** 677-704.

Day, R., Fuller, M. and Schmidt, V.A. (1977) Hysteresis properties of titanomagnetites: Grain-size and compositional dependence. *Physics of the Earth and Planetary Interiors*, **13,** 260-267.

De Vleeschouwer, D., Da Silva, A.C., Boulvain, F., Crucifix, M. and Claeys, P. (2012) Precessional and half-precessional climate forcing of Mid-Devonian monsoon-like dynamics. *Climate of the Past*, **7,** 1427-1455.

Devleeschouwer, X., Petitclerc, E., Spassov, S. and Préat, A. (2010) The Givetian-Frasnian boundary at nismes parastratotype (Belgium): The magnetic susceptibility signal controlled by ferromagnetic minerals. *Geologica Belgica*, **13,** 351-366.

Dunlop, D.J. (2002) Theory and application of the Day plot (Mrs/Ms versus Hcr/Hc) 1. Theoretical curves and tests using titanomagnetite data. *Journal of Geophysical Research: Solid Earth*, **107,** 4-1 - 4-22.

Ellwood, B., Crick, R.E., Garcia-Alcalde Fernandez, J.L., Soto, F.M., Truyols-Massoni, M., El Hassani, A. and Kovas, E.J. (2001) Global correlation using magnetic susceptibility data from Lower Devonian rocks. *Geology*, **29,** 583–586.

Ellwood, B.B., Crick, R.E., Hassani, A.E., Benoist, S.L. and Young, R.H. (2000) Magnetosusceptibility event and cyclostratigraphy method applied to marine rocks: Detrital input versus carbonate productivity. *Geology*, **28,** 1135-1138.

Elmore, R.D., London, D., Bagley, D., Fruit, D. and Gao, G. (1993) Remagnetization by basinal fluids: Testing the hypothesis in the Viola Limestone, southern Oklahoma. *J. Geophys. Res.*, **98,** 6237-6254.

Elmore, R.D., Muxworthy, A.R. and Aldana, M. (2012) Remagnetization and chemical alteration of sedimentary rocks. *Geological Society Special Publication*, **371,** 1-21.

Hladil, J., Gersl, M., Strnad, L., Frana, J., Langrova, A. and Spisiak, J. (2006) Stratigraphic variation of complex impurities in platform limestones and possible significance of atmospheric dust: a study with emphasis on gamma-ray spectrometry and magnetic susceptibility outcrop logging (Eifelian-Frasnian, Moravia, Czech Republic). *International Journal of Earth Sciences*, **95,** 703-723.

Jackson, M. (1990) Diagenetic sources of stable remanence in remagnetized Paleozoic cratonic carbonates: a rock magnetic study. *Journal of Geophysical Research*, **95,** 2753-2761.

Konigshof, P., Da Silva, A.C., Suttner, T., Kido, E., Waters, J., Carmichael, S.K., Jansen, U., Pas, D. and Spassov, S. (2015) Shallow water facies setting around the Kacακ Εϖεντ – α μυλτιδισχιπλιναρψ αππροαχη *Geological Society, London, Special Publication* **423**.

Koptíková, L. (2011) Precise position of the Basal Choteč event and evolution of sedimentary environments near the Lower–Middle Devonian boundary: The magnetic susceptibility, gamma-ray spectrometric, lithological, and geochemical record of the Prague Synform (Czech Republic). *Palaeogeography, Palaeoclimatology, Palaeoecology*, **304,** 96-112.

Larrasoaña, J.C., Roberts, A.P. and Rohling, E.J. (2008) Magnetic susceptibility of eastern Mediterranean marine sediments as a proxy for Saharan dust supply? *Marine Geology*, **254,** 224-229.

Mabille, C., Pas, D., Aretz, M., Boulvain, F., Schröder, S. and Silva, A.C. (2008) Deposition within the vicinity of the Mid-Eifelian High: Detailed sedimentological study and magnetic susceptibility of a mixed ramp-related system from the Eifelian Lauch and Nohn formations (Devonian; Ohlesberg, Eifel, Germany). *Facies*, **54,** 597-612.

McCabe, C. and Channell, J.E.T. (1994) Late Paleozoic remagnetization in limestones of the Craven Basin (northern England) and the rock magnetic fingerprint of remagnetized sedimentary carbonates. *Journal of Geophysical Research*, **99,** 4603-4612.

Molina Garza, R.S. and Zijderveld, J.D.A. (1996) Paleomagnetism of Paleozoic strata, Brabant and Ardennes Massifs, Belgium: Implications of prefolding and postfolding Late Carboniferous secondary magnetizations for European apparent polar wander. *Journal of Geophysical Research B: Solid Earth*, **101,** 15799-15818.

Parry, L.G. (1982) Magnetization of immobilized particle dispersions with two distinct particle sizes. *Physics of the Earth and Planetary Interiors*, **28,** 230-241.

Pas, D., Da Silva, A.C., Cornet, P., Bultynck, P., Königshof, P. and Boulvain, F. (2013) Sedimentary development of a continuous Middle Devonian to Mississippian section from the fore-reef fringe of the Brilon Reef Complex (Rheinisches Schiefergebirge, Germany). *Facies*, **59,** 969-990.

Pas, D., Da Silva, A.C., Suttner, T., Kido, E., Bultynck, P., Pondrelli, M., Corradini, C., De Vleeschouwer, D., Dojen, C. and Boulvain, F. (2014) Insight into the development of a carbonate platform through a multi-disciplinary approach: A case study from the Upper Devonian slope deposits of Mount Freikofel (Carnic Alps, Austria/Italy). *International Journal of Earth Sciences*, **103,** 519-538.

Riquier, L., Averbuch, O., Devleeschouwer, X. and Tribovillard, N. (2010) Diagenetic versus detrital origin of the magnetic susceptibility variations in some carbonate Frasnian-Famennian boundary sections from Northern Africa and Western Europe: Implications for paleoenvironmental reconstructions. *International Journal of Earth Sciences*, **99,** 57-73.

Riquier, L., Averbuch, O., Tribovillard, N., Albani, A.E., Lazreq, N. and Chakiri, S. (2007) Environmental changes at the Frasnian–Famennian boundary in Central Morocco (Northern Gondwana): integrated rock-magnetic and geochemical studies. *Geological Society, London, Special Publications*, **278,** 197-217.

Schneider, J., de Wall, H., Kontny, A. and Bechstadt, T. (2004) Magnetic susceptibility variations in carbonates of the La Vid Group (Cantabrian Zone, NW-Spain) related to burial diagenesis. *Sedimentary Geology*, **166,** 73-88.

Śliwinski, M.G., Whalen, M.T. and Day, J. (2010) Comparison of magnetic susceptibility (MS) and other geochemical proxies from the Middle-Late Frasnian of the Canadian Rocky Mountains: Implications for paleoenvironmental and paleoclimatic analyses and interpretations of the punctata Event. *Przeglad Geologiczny*, **58,** 1152-1160.

Śliwiński, M.G., Whalen, M.T., Meyer, F.J. and Majs, F. (2012) Constraining clastic input controls on magnetic susceptibility and trace element anomalies during the Late Devonian punctata Event in the Western Canada Sedimentary Basin. *Terra Nova*, **24,** 301-309.

Spassov, S. and Valet, J.P. (2012) Detrital magnetizations from redeposition experiments of different natural sediments. *Earth and Planetary Science Letters*, **351-352,** 147-157.

Szaniawski, R., Lewandowski, M., Mansy, J.-L., Averbuch, O. and Lacquement, F. (2003) Syn-folding remagnetization events in the French-Belgium Variscan thrust front as markers of the fold-and-thrust belt kinematics. *Bulletin de la Societe Geologique de France*, **174,** 511-523.

Tauxe, L., Bertram, H.N. and Seberino, C. (2002) Physical interpretation of hysteresis loops: Micromagnetic modeling of fine particle magnetite. *Geochemistry, Geophysics, Geosystems*, **3,** 1055.

Tribovillard, N., Algeo, T.J., Lyons, T. and Riboulleau, A. (2006) Trace metals as paleoredox and paleoproductivity proxies: An update. *Chemical Geology*, **232,** 12-32.

Urrutia-Fucugauchi, J. (2007) Magnetic Susceptibility, Anisotropy, Effects Of Heating. In: *Encyclopedia of Geomagnetism and Paleomagnetism* (Eds D. Gubbins and E. Herrero-Bervera), pp. 560-564. Springer Netherlands.

Vanderaveroet, P., Averbuch, O., Deconinck, J.F. and Chamley, H. (1999) A record of glacial/interglacial alternations in Pleistocene sediments off New Jersey expressed by clay mineral, grain-size and magnetic susceptibility data. *Marine Geology*, **159,** 79-92.

Walden, J., Oldfield, F. and Smith, J. (1999) Environmental magnetism: A practical guide. *Technical Guide*, **6**.

Whalen, M.T. and Day, J.E. (2008) Magnetic susceptibility, biostratigraphy, and sequence stratigraphy: Insights into Devonian carbonate platform development and basin infilling, western Alberta, Canada. *Society for Sedimentary Geology*, **89,** 291-314.

Whalen, M.T. and Day, J.E. (2010) Cross-basin variations in magnetic susceptibility influenced by changing sea level, paleogeography, and paleoclimate: Upper Devonian, western Canada sedimentary basin. *Journal of Sedimentary Research*, **80,** 1109-1127.

Zegers, T.E., Dekkers, M.J. and Baily, S. (2003) Late Carboniferous to Permian remagnetization of Devonian limestones in the Ardennes: Role of temperature, fluids, and deformation. *Journal of geophysical research*, **108,** 5/1 - 5/19.

Zwing, A., Bachtadse, V. and Soffel, H.C. (2002) Late Carboniferous remagnetisation of Palaeozoic rocks in the NE Rhenish Massif, Germany. *Physics and Chemistry of the Earth, Parts A/B/C*, **27,** 1179-1188.

Zwing, A., Matzka, J., Bachtadse, V. and Soffel, H.C. (2005) Rock magnetic properties of remagnetized Palaeozoic clastic and carbonate rocks from the NE Rhenish massif, Germany. *Geophysical Journal International*, **160,** 477-486.

IGCP 596 field work caravan in Gobi-Altai desert, Mongolia

Chapter 6

Summary and discussions

Our multi-disciplinary study conducted onto four stratigraphically extended sections in the Ardennes, the Rheinisches Schiefergebirge and the Carnic Alps provided a significant amount of new data that have been subjected to an in-depth study reported in Chapters 2, 3, 4, 5 and 6. In each Chapter, results on sedimentology, biostratigraphy, geochemistry, and magnetic susceptibility have been discussed and allowed to gain a persuasive understanding of the environmental development over long-time scale for three of the most fascinating Devonian carbonate platform from Europe. Moreover, combination of magnetic hysteresis measurements, geochemistry and initial magnetic susceptibility data have allowed us to prove that our magnetic susceptibility signal still reflects trustworthy primary environmental condition. Such a well-preserved signal is the foundation to provide a meaningful assessment on the reliability of χ_{in} records for the correlation of long-term χ_{in} trends over long distance and to discuss the links existing between χ_{in} and environmental parameters at this large scale. These results are a major contribution to the first question that was raised in this PhD. What do the long-term sedimentary records from major Devonian carbonate successions in Europe teach us on the regional and global palaeoenvironmental development of some major European carbonate platforms over long time scale? What are the fundamental criteria to provide a meaningful analysis of past environmental changes and their correlation based on magnetic susceptibility records? Are the long-term correlations of χ_{in} records reliable on a large timescale? What is the link between χ_{in} and environmental parameters on this timescale?

Prior to go further in the discussion that concern the correlation of long-term χ_{in} trends over long distance, we first summarize the main results on depositional setting, biostratigraphy, long-term palaeoenvironmental changes, magnetic susceptibility, geochemistry and hysteresis measurements acquired for all the sections (Fig. 1 and Tab. 1).

1. Main results on biostratigraphy, depositional settings and long-term palaeoenvironmental changes

1.1 The Burgberg section (Germany)

The Burgberg section in the northeastern portion of the Rhenish Massif cut through the southeastern fore-reef fringe of the large atoll-like Brilon Reef Complex. It covers a stratigraphic interval extending from the Middle Givetian (middle *varcus* Zone) to the Viséan (*bilineatus* Zone) which is characterized by nine depositional settings organized into off-reef (SD1), intermediate fore-reef (SD2), and proximal fore-reef (SD3) main sedimentary domains (summary in Supplementary material). Majors sedimentary processes occurring on this portion of the platform are gravity flows (turbidite, debris and grain flows), pelagic sedimentation (settling) and reworking of sediments triggered by storms. The off-reef domain (SD1) is the most distal setting observed and is characterized by fine-grained sediments, dominated by pelagic biota and the local occurrence of gravity-flow deposits. The intermediate fore-reef (SD2) is characterized by a mixture of biota and sediments from deeper-water and shallower-water sources and is influenced by storm and gravity-flow currents. In this sedimentary domain, *Renalcis* mound-like structures developed. The proximal fore-reef (SD3) corresponds to the most proximal setting and is strongly affected by gravity-flow currents derived from the Brilon Reef Complex.

Based on the vertical evolution of our microfacies and the biostratigraphic framework, the million-year environmental evolution of the Brilon Reef Complex was reconstructed. It is characterized by five major trends in direct relation with the onset, general development and withdrawal/drowning of the Brilon Reef Complex. The five major evolutionary phases are (a) initial development of the Brilon reef on top of volcanic deposits which started within the middle *varcus* Zone, (b) establishment of the reef structure lasting from the Middle Givetian to Early Frasnian with a culmination recorded from the *disparilis* to *falsiovalis* Zones, (c) the stepwise withdrawal of the reef development from the Middle to the Late Frasnian, (d) the end of the reef development as a result of the global Kellwasser events (the lower and upper Kellwasser were identified through carbon isotope analyses and biostratigraphy) and gradual drowning of the area and finally (e) significant deepening of the Burgberg area starting in the Late Famennian, characterized by pelagic shale sedimentation overlying nodular limestones.

1.2 The La Thure section (Belgium)

The La Thure section in the northwestern Dinant Syncline cuts through a complex succession of really well-developed carbonate platform profiles. The entire section covers a stratigraphic interval extending from the Middle Givetian to the Middle Frasnian. Throughout this continuous section, astonishing depositional settings diversity was highlighted and a significant difference between the Givetian and Frasnian stages was revealed. For this reason we described each stage separately.

Givetian

Early- to late-Givetian (*varcus to disparilis* Zones) sediments in the La Thure section are remarkably diversified, distributed through twenty depositional settings (summary in Supplementary materials) belonging to three main carbonate platform profiles: (1) a homoclinal ramp; (2) a shallow-water rimmed shelf; and (3) a drowned shelf. The drowned shelf is characterized by only one microfacies. The homoclinal ramp includes two microfacies ranging from mid- to outer-ramp settings. The rimmed shelf is divided into five facies belts extending from an external fore-reef and biostrome to a supratidal internal shelf setting. Based on microfacies analyses, five long-term environmental trends were underlined through the Early- to Late-Givetian La Thure succession. By integrating these results with published ones, we reconstructed the platform development in the Dinant Syncline in five steps: (a) development of a sedimentation on a homoclinal ramp in the late Early Givetian, (b) establishment of a reef structure, southward, at the onset of the Middle Givetian, allowing internal facies to develop within the La Thure area ; (c) northward drift of this reef structure enabling fore-reef deposits within the La Thure area during the late Middle Givetian; (d) huge reef development in the southernmost Dinant

Syncline enabling thick deposition of internal evaporitic sediments in the La Thure from late Middleto latest Givetian and (e) drowning of the Givetian platform as a result of the Late Givetian sea-level rise attributed to the Frasnes Event.

Frasnian

Early- to middle-Frasnian (*falsiovalis* to *hassi s.l.* Zones) sedimentary record in the La Thure section in the northwestern Dinant Syncline is characterized by six main depositional settings belonging to two different profiles: (1) a mixed carbonate – siliciclastic ramp and (2) a rimmed shelf (summary in Supplementary materials). According to the vertical evolution of the depositional environments through time, from the early- to middle-Frasnian four major environmental trends were recorded and correspond respectively to: (a) deposition of shale on the drowned Givetian platform during the Lower Frasnian (from *falsiovalis* to Lower *transitans* Zones); (b) decrease of the siliciclastic input and development of a crinoidal-rich sedimentation; (c) establishment of lamellar stromatoporoids buildup between the Upper *transitans* and Lower *punctata* Zones and (d) thick intermediate to distal fore-reef deposition from the Lower *punctata* to the *hassi s.l.* Zones.

1.3 The Fromelennes-Flohimont section (France)

The sedimentary record in Fromelennes-Flohimont section extends from the Early-Givetian to Early-Frasnian (*hemiansatus to falsiovalis* Zones) and encompasses seventeen depositional environments (summary in Supplementary materials). The described depositional settings are belonging to three main platform profiles, similar than in the La Thure section: (1) a homoclinal ramp; (2) a shallow-water rimmed shelf and (3) a drowned shelf. The drowned shelf is characterized by only one microfacies (similarly than in the La Thure section) while the homoclinal ramp includes four microfacies ranging from mid- to outer-ramp settings. The rimmed shelf profile is divided into six facies belts which are ranging from an off-reef to an internal supratidal shelf setting including local palaeosoil developments. Throughout the Fromelennes-Flohimont section the vertical environmental evolution led to the observation of seven large-scaled palaeoenvironmental trends. The three first trends are observed within the Lower Givetian and the four last within the Middle and Upper Givetian. The three first Lower Givetian trends are respectively represented by: (a) deposition on a homoclinal ramp within the FWWB; (b) deposition of lagoonal and palaeosoils-like sediments related to a substantial shallowing sea-level tendency with development of a reefal structure basinward and (c) deepening-upward trends conducting to the re-establisheent of mid- to outer-ramp deposits within the platform. Mid-late Givetian shallowing and deepening trends recorded in the Fromelennes-Flohimont section are similar to time-equivalent trends in the La Thure (Fig. 1).

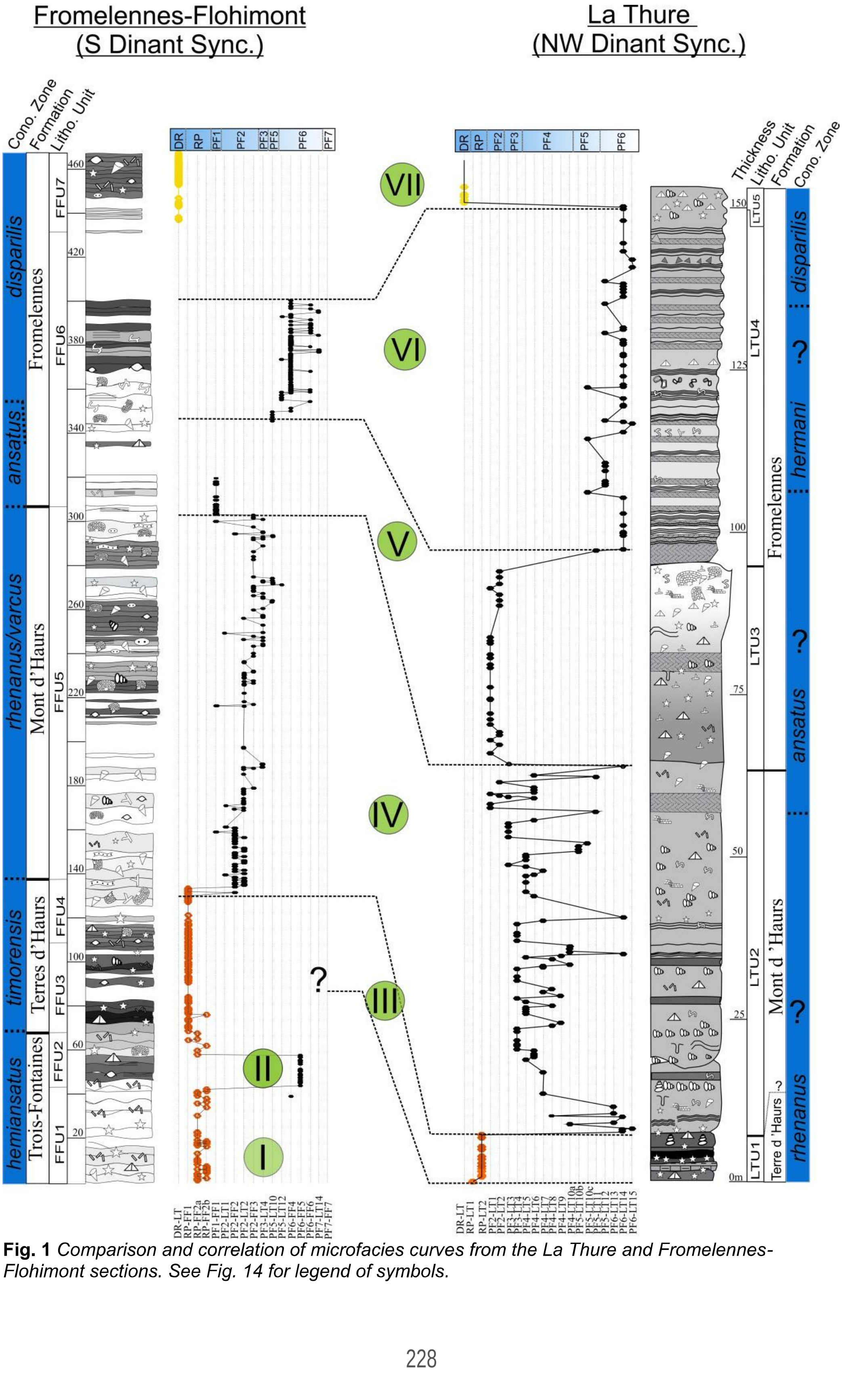

Fig. 1 *Comparison and correlation of microfacies curves from the La Thure and Fromelennes-Flohimont sections. See Fig. 14 for legend of symbols.*

1.4 The Freikofel section (Italy/Austria)

The Freikofel section in central Carnic Alps covers a succession through the so-called "transitional" facies (e.g., fore-reef) that range from the indet. *falsiovalis* Zones within the Latest Givetian to the Lower *crepida* Zone in Early Famennian. This carbonate succession is characterized by a detached rimmed shelf type carbonate platform model, with six depositional settings ranging from a distal reef floor dominated by autochthonous sedimentation and locally influenced by turbidites to a proximal The microfacies curve constructed from the vertical stacking of the environmental settings in combination with the biostratigraphic scheme led to the distinction of two major million-year scale environmental trends: (a) dismantlement of the Eifelian-Frasnian Carnic Alps platform starting during the Early Frasnian. One of the cause of this dismantlement being the Late Givetian major rift pulse recognized in the area and (b) stepwise withdrawal of the shallow-water influxes during the Late Frasnian and significant deepening of the Carnic Alps area during the Latest Frasnian as a result of the Kellwasser event. The $\delta^{13}C_{carb}$ values show a major positive excursion though the Upper Kellwasser event layer, but it does not show the specific lithological black shales.

1.5. Conclusions on biostratigraphy and platform types (Fig. 2)

The sections investigated in this research were measured and sampled in three of the best Devonian carbonate platform localities in Central Europe (Ardennes, Rheinisches Schiefergebirge and Carnic Alps). They all provide an extended and controlled stratigraphic interval in Devonian carbonate platform that developed within the shallow-water portion of the Rhenohercynian and Palaeotethys Oceans (Fig. 1). As described in Chapters 2, 3 and 4, and summarized here above, our investigation has provided an in-depth diving into the diverse carbonate platform depositional settings that shaped a large portion of the marine world during the Mid-Late Devonian Period. Following the definition of Wright and Burchette (1996), the Freikofel and Burgberg sections correspond to detached rimmed shelf such as atoll-like reef while the Fromelennes-Flohimont and La Thure sediments were deposited in attached rimmed shelf and homoclinal ramp profiles. Drowned carbonate platform sedimentation is also observed in all the sections either at the Givetian/Frasnian (e.g., Fromelennes-Flohimont and La Thure sections) or Frasnian/Famennian boundary (e.g. Burgberg and Freikofel sections). The vertical microfacies evolution constructed for all the sections provided meaningful insight on the long-term environmental evolution and changes that affected the various platform settings recognized in this study. The four sections investigated in this research present relatively similar 2nd order long-term sea-leveltrends. Indeed, all the sections including Givetian sediments show general 2nd order shallowing of the facies from the beginning to the end of this Period and then a general deepening upward between the early to the late Frasnian (observed at Freikofel and Burgberg sections where Upper Frasnian is recorded). These comparable 2nd order shallowing vs deepening upward trends indicate similar carbonate platform development within the Rhenohercynian and Palaeotethys Ocean. These global trend on the carbonate platform development were already mentioned in the review paper on the European Devonian reefs from Burchette (1981) and observed worldwide (Copper, 2002).

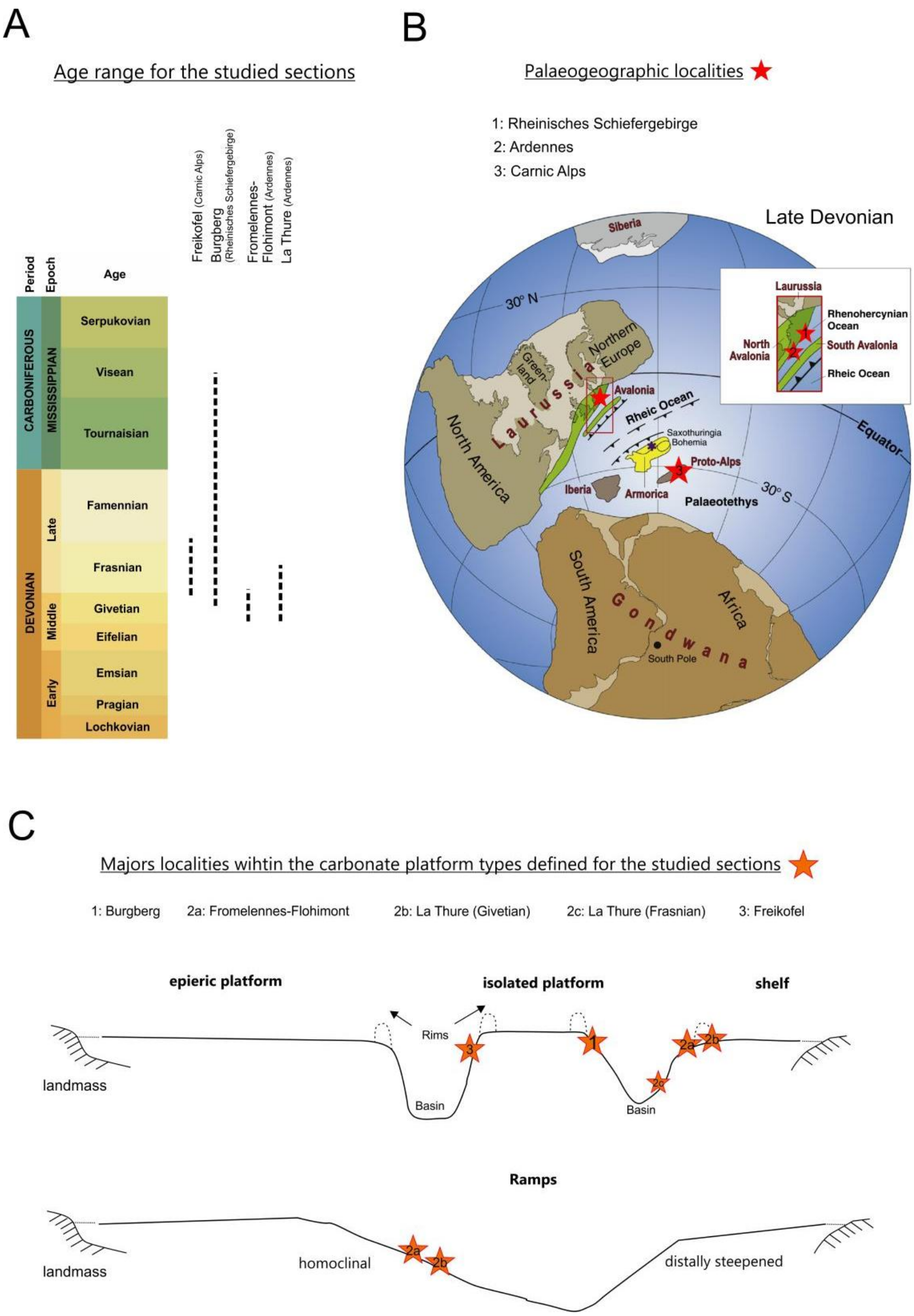

Fig. 2 a *time range extension for all the sections*. **b** *Location of three main palaeogeograhic contexts investigated in this study (map modified from Eckelmann et al., 2014)*. **c** *Location of our sections within the model of Wright and Burchette (1996) for the Types of carbonate platforms.*

2. Main results from magnetic susceptibility and major and trace elements geochemistry (Tab. 1 and Supplementary materials)

2.1. The Burgberg section (Eastern Rhenish Massif, Germany)

Middle Devonian to Mississippian Burgberg section records important magnetic susceptibility variability ranging from 4.22 x 10^{-10} m^3/kg to 9.25 x 10^{-8} m^3/kg with a low average value of 2 x10^{-8} m^3/kg which is consistent with the isolated depositional setting attributed for the Brilon Reef Complex (e.g., atoll reef). This values is lower than the χ_{in} marine standard of 5.5 x 10^{-8} m^3/kg defined by Ellwood et al. (2011) on the basis of ~11000 marine rock samples. The magnetic susceptibility curve constructed for the Middle Devonian to Mississippian Burgberg section can be divided into four large-scaled χ_{in} trends. These trends are opposed with the microfacies trends, with decreasing χ_{in} values towards shallowing upward. The most distal microfacies correspond to the highest χ_{in} values while the most proximal is characterized by the lowest χ_{in} values. The opposition between both magnetic susceptibility and microfacies trends is triggered by the specific influence of various syn-sedimentary processes that characterize the proximal-distal fore-reef transect. In the most distal setting (e.g., off-reef setting) defined for the Burgberg section, sedimentary rate, carbonate production and water turbulence are low, triggering a concentration of χ_{in} carrying particles and then resulting in a higher χ_{in} value. Meanwhile, in the most proximal setting (e.i., fore-reef proximal setting), sedimentary rate, turbulence and carbonate deposition are high, diluting χ_{in} carrying minerals and hampering the χ_{in} carrying minerals to settle, triggering lower χ_{in} signal in these proximal contexts. Such opposition between the χ_{in} and microfacies evolution was also reported for Belgian and Canadian mound and atoll (Da Silva et al., 2009a). The relatively good correlation (r >0.5) between χ_{in} and proxies for siliciclastic input for the Burgberg section indicates a χ_{in} signal is triggered by variations in Si, Al, Ti, Zr and K in the sediment.

2.2. The Dinant Syncline sections (La Thure and Fromelennes-Flohimont)

Givetian

The χ_{in} values for the Lower – Upper Givetian portion of the La Thure section range between 5.64 x10^{-9} and 2.97 x10^{-7} m^3/kg and show an average value of 4.15 x10^{-8} m^3/kg. In the Fromelennes-Flohimont section, the Lower – Upper Givetian succession records χ_{in} values ranging from -5.64 x10^{-9} to 4 x10^{-7} m^3/kg and an average value of 4.66 x10^{-8} m^3/kg. Average magnetic susceptibility values for the La Thure (4.15 x10^{-8} m^3/kg) and the Fromelennes-Flohimont (4.66 x10^{-8} m^3/kg) sections are relatively close, and the median value of 4.4 x10^{-8} m^3/kg is in the classical χ_{in} range of the marine sediments (5.5 x10^{-8} m^3/kg) defined by Ellwood et al. (2011) When we compare the long-term χ_{in} and microfacies evolution for both the Givetian Fromelennes-Flohimont and La Thure sections, similar trends and events are observed between time-equivalent deposits. In addition, a strong link between the χ_{in} signal and microfacies was highlighted for each section, depending of the platform types and the specific environmental conditions (e.g., rimmed shelf and homoclinal ramp). In summary, χ_{in} values for sediments deposited in the homoclinal ramp model increase from the mid- to outer-ramp setting. Concerning sediments that belong to the rimmed shelf the situation is more complex. The main observation on the link between magnetic susceptibility and facies belts underlines a decrease of the χ_{in} values from the fore-reef to the biostromal facies. In the internal shelf a general increase of the χ_{in} values is observed between the bioclastic shoal and the supratidal facies belts with a small decrease of values for the oolitic shoals belts. Our general results on the link between the depositional setting and the magnetic susceptibility are consistent with results from Da Silva et al. (2013) summarizing a large number of Mid-Upper Devonian Belgian sections and setting (e.g., carbonate ramp, shelf and mud mounds models) and in which the authors outlined a significant difference in χ_{in} behaviour for each carbonate platform model. In both Fromelennes-Flohimont sections, the long-term χ_{in} curves are relatively well-correlated (r > 0.5) with the curves constructed for siliciclastic proxy suite. Such a correlation indicates that the magnetic susceptibility signal in these two Givetian sections is triggered by the primary depositional conditions. In term of palaeo-oxygenation, U/Th proxy indicates an important change in bottom water oxygenation level prevailing in the carbonate platform, from oxygen-depleted throughout the middle Givetian to more oxic conditions toward the late Givetian. This change through more oxic condition is thought to be driven either by an increasing aridity on the continent or a better ocean circulation toward the late Givetian. These two hypotheses are concurrent with the increasing palaeo-temperature near the onset of the Late Givetian.

Frasnian

The χ_{in} values for the measured Frasnian portion of the La Thure section record high variability ranging from -8.05 x10^{-10} m^3/kg to 1.5 x10^{-7} m^3/kg with an average value of 5.87 x10^{-8} m^3/kg. This average value is in the classical χ_{in} range of the marine sediments (5.5 x10^{-8} m^3/kg) defined by Ellwood et al. (2011) and also relatively similar to time-equivalent fore-reef sediments from other Belgian localities (~3.3 x10-8 m3/kg; Da Silva et al., 2009a). The χ_{in} curves constructed for this Frasnian succession can be divided into four distinct units that correspond to both formations and members defined for this succession. In Frasnian of the La Thure section a parallelism (r > 0.5) is also recorded between proxy suites for terrestrial input and χ_{in} which indicate interdependence between both parameters and therefore, a χ_{in} variation that reflects the primary depositional-induced trends.

2.4. The Freikofel section (Carnic Alps, Italy-Austria)

The Latest Givetian to Early Famennian Freikofel section records χ_{in} values ranging from -0.18 x10^{-8} m^3/kg to 2.7 x10^{-8} m^3/kg with an average value of 7.73 x10^{-9}. These values are much lower than (1) the χ_{in} of marine standard of 5.5. x10^{-8} m^3/kg defined by Ellwood et al. (2011) and (2) time-equivalent fore-reef setting from the Rhenohercynian Basin in Belgium (~3.3 x10-8 m3/kg; Da Silva et al., 2009a). These low χ_{in} values are consistent with the commonly reported isolation of the Carnic Alps Reef Complex (e.g., Hubmann and Suttner, 2007). The magnetic susceptibility curve constructed for the Freikofel section can be divided into four successive long-term χ_{in} trends. As in the Burgberg section, the magnetic susceptibility and the microfacies curves opposed. The most distal microfacies correspond to the highest χ_{in} values while the most proximal is characterized by the lowest χ_{in} values. Such an opposition can be explained using environmental parameters that prevail during to deposition as already explained for the Burgberg section. As already explained for the Burgberg section, in the most distal setting (e.g., distal fore-reef), sedimentary rate, carbonate production and water turbulence are low triggering a concentration of χ_{in} carrying particles into condensed levels, resulting in a higher χ_{in} value. Meanwhile, in the most proximal setting (e.g., proximal fore-reef), sedimentary rate, turbulence and carbonate deposition are high, diluting χ_{in} carrying minerals and hampering the χ_{in} carrying minerals to settle, resulting in a lower χ_{in} signal in these proximal contexts. In the Freikofel section a good parallelism ($r > 0.5$) is observed between proxy suites for terrestrial input and χ_{in} which indicates interdependence between both parameters and therefore, a χ_{in} variation that directly reflects the primary depositional-induced trends.

2.5. Conclusion on magnetic susceptibility and geochemistry

All the sections under investigation for this PhD were abundantly sampled for geophysical measurements. The collected data sets have allowed us to build high-resolution χ_{in} curves for each section. Comparison between sedimentological and magnetic susceptibility data sets supports and confirm the models established by Da Silva et al. (2009b) concerning the link that exists between χ_{in} and environmental conditions during deposition (e.g., carbonate productivity, sedimentary rate, agitation and siliciclastic influx). In the fore-reef setting of atoll-like profile we record a general increase of the χ_{in} signal with the distallity. This magnetic susceptibility behavior is also observed for the homoclinal ramp setting. In internal shelf setting, general increase of the χ_{in} values is observed between the bioclastic shoal and the supratidal setting. Based on the construction of χ_{in} curves, we distinguished long-term χ_{in} trends in each section. The good correlation between χ_{in} and proxy suite for detrital input in all the sections indicated that our χ_{in} signal was controlled by the siliciclastic input concentration within the sediments and that original information on the depositional-induced magnetic signal was preserved.

3. Main results from hysteresis magnetic measurements

Parameters extracted from the hysteresis loops for each section point to the minor influence of paramagnetic and diamagnetic minerals in comparison to ferromagnetic minerals. Low-coercivity components such as magnetite or pyrrothite have the strongest influence on χ_{in} variation within the section under investigation. In the La Thure, Fromelennes-Flohimont sections and samples from the Burgberg section corresponding to distal fore-reef to off-reef and intermediate fore-reef setting (SD1+SD2), the H_{cr}/H_c and M_{rs}/M_s values indicate a χ_{in} signal mainly controlled by a mixture of SD and SP grains related to remagnetization. Considering the Burgberg and Freikofel samples, the remagnetization fingerprint is less clear but we have raised the hypothesis that it can be masked by coarse-grained MD magnetite. Transition from smectite to illite during diagenesis has appeared to be the most convincing parameter able to produce fine-grained magnetite that is classically observed in remagnetized limestone. When comparing the variations in the magnetic susceptibility signal with facies evolution, it appears that χ_{in} is influenced by proximality but also by the main depositional setting. Hence, the recorded χ_{in} signal in our sections is constituted of a primary depositional-induced and a secondary diagenesis-induced magnetic signal. The good correlation observed between χ_{in} signal and siliciclastic input proxies confirms the primary depositional-induced character of the recorded initial magnetic susceptibility and the low to weak distortion triggered by remagnetization. We can therefore use the initial magnetic susceptibility signal as a proxy for correlation and environmental reconstruction for all sections under investigation in our research.

	Burgberg	**Freikofel**	**La Thure (Givetian)**	**La Thure (Frasnian)**	**Fromelennes -Flohimont**
Country	Germany	Italy/Austria border	Belgium	Belgium	France
Geological locality	NE Rheinisches Schiefergebirg e	Carnic Alps	Ardennes	Ardennes	Ardennes
Thickness	125 m	62 m	153 m	135 m	460 m
Time-range	Middle Devonian to Mississippian	Latest Givetian to Early Famennian	Early Givetian to Early Frasnian	Early- to Middle Frasnian	Early Givetian to Early Frasnian
Number of microfacies	9	6	20	9	17
Main facies belts	Proximal fore-reef, intermediate fore-reef and distal fore-reef to off-reef	Proximal fore-reef to off-reef	Internal and external shelf	Fore-reef, stromatoporoid biostrome and drowned platform shale	Internal and external shelf
Platform types	Detached rimmed-shelf	Detached rimmed-shelf	Attached rimmed-shelf and homoclinal ramp	Attached rimmed-shelf and drowned platform	Attached rimmed-shelf and homoclinal ramp
χin range and average (m³/kg)	4.22 $\times 10^{-10}$ to 9.25 $\times 10^{-8}$	– 0.18 $\times 10^{-8}$ to 2.7 $\times 10^{-8}$	5.64 $\times 10^{-9}$ to 2.97 $\times 10^{-7}$	– 8.05 $\times 10^{-10}$ to 1.5 $\times 10^{-7}$	– 5.64 $\times 10^{-9}$ to 4 $\times 10^{-7}$
χin average (m³/kg)	2 $\times 10^{-8}$	7.73 $\times 10^{-9}$	4.15 $\times 10^{-8}$	5.87 $\times 10^{-8}$	4.66 $\times 10^{-8}$
Dominant ferromagnetic grain-size	SP+SD (SD1+SD2) and SD+MD (SD3)	SD+MD	SP+SD	SP+SD	SP+SD

Tab. 1 *Synthesis on the main results from biostratigraphy, depositional setting, magnetic susceptibility and magnetic hysteresis.*

4. The reliability of χ_{in} records for the long-distance correlation of long-term trends in the Devonian

In order to confirm the preliminary results provided by Boulvain et al. (2010) on the long-distance correlation of long-term χ_{in} trends between Devonian rocks from Belgium and Czech Republic, it would need substantial geochemical, hysteresis and conodont biostratigraphic control on the Czech material (Belgian material has been studied by Da Silva et al., 2013 and in this work). However, the research reported in Chapters 2, 3, 4 and 5 provided a large control on sections from different location. Results from magnetic susceptibility, sedimentology, geochemistry and magnetic hysteresis measurements from all the section are all pointing to a relatively well-preserved primary depositionally-induced χ_{in} signal despite the remagnetization fingerprint. In order to answer the question “Are the long-term correlations of χ_{in} records reliable on large scale and what are the links between χ_{in} and environmental parameters at this large scale?” we built a correlation chart showing the χ_{in} curves for each section measured during this research (Fig. 3). On this chart, we presented the thickness, the lithologies, the conodont zones and the χ_{in} curves. According to the main conodont zones, we delineate time-equivalent rock succession. As observed in Figure 3, the long-term χ_{in} trends recorded in the Givetian sequences are well-correlated within the Dinant Syncline (e.g., first part of Chapter 3). However, correlations of sections from the Ardennes with the Rheinisches Schiefergebirge and the Carnic Alps sections are not clear.

The absence of correlation between time-equivalent long-term trends in χ_{in} for sections from the Ardennes with the Rheinisches Schiefergebirge and the Carnic Alps sections is not in agreement with results from Ellwood et al. (2001) and Boulvain et al. (2010) stating that χ_{in} signal can be used as a global correlation tool. By analyzing the impact of the various parameters playing a role in the depositionally-induced χ_{in} signal in marine sedimentary rocks this situation can be clarified. These parameters are respectively: 1) the climate, 2) the global and local sea-level variations, 3) the tectonic variation, 4) the syn-sedimentary processes, 5) the resolution of the χ_{in} record or the resolution of the section, 6) the post-sedimentary processes and 7) the eolian input variation. The three first parameters were interpreted as the main drivers of lithogenic input basinward (e.g., Crick et al., 1997). Given that the χ_{in} signal is related to the siliciclastic materials concentration (cf. Chapter 5) these three factors have significant influence on the χ_{in} at inter-basinal scale. Theoretically, χ_{in} curve increase during a sea-level regression, and show high values at low levels; and decrease during sea-level transgression and low values during high levels. Increasing rainfall or ice sheets related to climate variations can trigger an increase of the magnetic susceptibility and tectonic variations can change magnetic mineral sources. However, we could see that local parameters such as water agitation and carbonate production would also influence the settlement of magnetic particles, as showed before by da Silva and Boulvain (2004); Da Silva and Boulvain (2005); Bábek et al. (2007); (Mabille et al., 2008); Da Silva et al. (2009a). In these papers, these authors showed a χ_{in} evolution as a function of proximality has been revealed to have a substantial influence on the χ_{in} signature in each section selected (see

Chapters 2, 3 and 4). For each section investigated in this research we explored the link existing between magnetic susceptibility signature and microfacies and/or facies belts (e.g., Chapters 2, 3 and 4). Implication of syn-sedimentary environmental parameters such as the carbonate productivity and/or sedimentary rate, the water agitation and siliciclastic content were proven to exert a significant role in the χ_{in} signature. Concerning the Givetian sections in the Dinant Syncline, two models of magnetic susceptibility evolution were envisaged. (e.g., homoclinal ramp and rimmed-shelf; see Chapter 4 for more detail). For the Frasnian part of the La Thure section, particular trends of χ_{in} signal in response to facies have not been clearly-observed. For both Burgberg and Freikofel sections, deposited in fore-reef and off-reef setting, χ_{in} trend for a relative proximity transect corresponds to a typical decrease of the values (see Chapters 2 and 3). The strong influence of the environmental parameters along a proximal – distal transect is also clearly-visible through the dependence occurring between χ_{in} and microfacies curves for each section. These disclosures have convinced us that the different χ_{in} behaviors along a distal to proximal transect is one of the most obvious parameter that favor the absence of correlation between the χ_{in} curves from the Dinant Syncline sections and the Rheinisches Schiefergebirge and Carnic Alps sections. In a regional scale and for a shorter time-interval (e.g., three to four conodont Zones), Da Silva et al. (2009b) observed a similar situation when trying to correlate time-equivalent χ_{in} curves obtained in the distal part of the Belgian Frasnian platform with the curves acquired in the intermediate and proximal areas of the same platform. Indeed, the distal portion of the Belgian Frasnian platform is ruled by one χ_{in} evolutionary model while the intermediate and internal platform setting is dictated by another model. Such observations clearly demonstrated that even within regional scale (e.g., Belgian Frasnian platform) local environmental parameters, driving magnetic susceptibility evolution, play a significant role and are able to obstruct the correlation of time-equivalent sedimentary sequences. In their work on the correlation of long-term χ_{in} curves over a long distance Boulvain et al. (2010) stated the relative independence between magnetic susceptibility and microfacies curves; this might be one reason that allowed correlation between Belgian and the Czech Republic.

The temporal resolution of our sections or the resolution of our χ_{in} records is also a major parameter that might be an element of answer on the lack of correlation. Indeed, in thick shallow-water succession such as for the Fromelennes-Flohimont and La Thure sections, the biostratigraphic constrain is relatively low compared to the Burgberg sections, which is well-constrained by conodont. Moreover average sampling rate for all the sections, even if relatively high, is the same whereas different sedimentary rates characterize each studied time-intervals. For instance, for the Givetian interval in the condensed Burgberg section, we collected around 200 samples while in the Fromelennes-Flohimont section for the same interval counts nearly 600 samples. This difference in the relative sampling rate has a direct impact on the χ_{in} signal resolution for the studied time interval and may reduce the visibility of the expected long-term trends in χ_{in}.

Concerning post-sedimentary processes such as remagnetization, they obviously have an influence on the χ_{in} since our signal is mostly carried by magnetic particles formed during such process. However, we could show that despite this remagnetization, the magnetic signal is still carrying some primary information and diagenesis seems to have a relatively minor impact on the preservation of primary depositionally-induced χ_{in} signal in our sections (see discussion in Chapter 5). Da Silva et al. (2013) have also showed that the magnetic minerals carrying the magnetic susceptibility signal in the Devonian of Belgium were having similar hysteresis properties as the remagnetization grains identified in the Ardennes by Zegers et al. (2003). These grains were interpreted as created during a remagnetization event related to a smectite to illite conversion (Zwing et al., 2002; Zegers et al., 2003; Zwing et al., 2009). Zegers et al. (2003) proposed that the iron released during the smectite-illite conversion would partly remain in situ in the clay aggregates, where it would crystallize as fine-grained magnetite. Da Silva et al. (2013) proposed that the persistence of a primary signal despite the remagnetization can be related to the fact that the Fe^{2+} would indeed remain in situ, which would then enhance the primary trends. However, as mentioned by Da Silva et al. (2013), in a few cases, the primary signal could be altered by remagnetization as for example the following cases: 1) the originally present clay mineral suite contained a considerably varying amount of smectite (unfortunately this remains hard to test); 2) early reductive diagenetic processes could have already influences the magnetic mineral composition and 3) during the smectite to illite transition, prolonged reaction could have blurred the original lithological expression, if a portion of the released iron had migrated over a larger distance, this could lead to a partially hidden primary signal.

As stated earlier, atmospheric circulation and associated eolian material is a parameter active over long- and short timescale and distance, and influence the siliciclastic budget to the ocean realm. In their work on the long-distance correlation of long-term trends in χ_{in}, Boulvain et al. (2010) advocate that global climatic-eustatic regime and variable atmospheric circulation during the Eifelian-Frasnian interval might be a parameter responsible of the long-term χ_{in} trends correlation This last decade a specific focus has been made on the use of the eolian related deposits, recorded in the deep-sea repository, for the reconstruction of past climate and atmospheric circulation (Ridgwell, 2002; Irino and Tada, 2003; Larrasoaña et al., 2008; Weber et al., 2012). Weber et al. (2012) highlighted a spectacular correlation between magnetic susceptibility signal and the proportion in eolian materials by comparing ice-core and time-equivalent deep-sea sediment core. These authors also indicate that the long-range of transport of wind-blow material may be used as a powerful tool for correlation over large distances. Nonetheless, a crucial element and common point of all these researches is that all the recent sedimentary successions analysed are located in deep-sea setting. Indeed, this repository is generally more complete and judicious site for collecting climate archives because it is not subject to severe alteration by chemical or physical processes and erosion and/or redeposition as observed in continental or shallow-marine context. In ancient carbonate, the study of eolian dust is even more perilous because necessitating a relevant palaeogeographic background that allows to be confident about magnetic minerals source for the investigated time interval (Sur et al., 2010). This means that only confidentially selected isolated platform or oceanic basin sedimentary record are reliable for such a hypothesis. As mentioned before, according to various palaeogeographic reconstruction of Western Europe during the Middle Devonian (Ziegler, 1982; McKerrow and Scotese, 1990), the south of Belgium was located in a relative vicinity with the Old Red Sandstone continent (e.g., London-Brabant High) and non-atmospheric sources of silica such as river cannot be eliminated. The hypothesis of Boulvain et al. (2010) stating that correlation of long-term χ_{in} between Belgium and Czech Republic might be linked to varying eolian-related dust through Eifelian-Frasnian is therefore poorly conceivable even if it cannot be completely sweep away. Detached platform context such as Freikofel and Burgberg are probably the best palaeogeographic and depositional context to envisage a relevant record of the eolian-related dust as they represent a pelagic/hemipelagic sedimentation. However, the prominence of reworking processes that were active in both sections (e.g. turbidite and debris flow), are a strong argument against a complete and meaningful palaeodsut record. Indeed, during gravity-flow process as turbidite, the primary depositional information is strongly altered.

Concerning the Belgian and France sections that belong to the Dinant Basin (separated by about 75 km), χ_{in} curves have been well-correlated despite the local changes in the syn-sedimentary processes which can cause variability in the χ_{in} signature and alter the magnitude or local trends of the χ_{in} signal. However, the general trend with peaks and troughs is maintained. In the Dinant Syncline, the correlation has been partly attributed to the similarity of the sedimentary model (e.g., attached platform) and its evolution through time and partly to the relative sea-level variations and associated siliciclastic influx variation (see Chapter 4). In intra-basinal/regional scale magnetic susceptibility tool has already been successfully used for the correlation of sections (Whalen and Day, 2010; Da Silva and Boulvain, 2012). In respect to their previously established sequence stratigraphic framework (Whalen et al., 2000), Whalen and Day (2010) correlated several Frasnian fore-reef to basin sections (locally separated by several tens of kilometers) into the Western Canadian sedimentary basin. In the Belgian Frasnian platform, χ_{in} based correlations have been observed only between sections characterized by similar model of χ_{in} evolution (fig. 3; Da Silva and Boulvain, 2012).

The Burgberg, Fromelennes-Flohimont and La Thure sections were located in the Rhenohercynian basin bordering the Old Red Continent in the north. At the present time, the Burgberg area is situated at ~280 km from the Fromelennes-Flohimont section and ~340 km from the La Thure section. Considering a Variscan compression with a NE-SW direction and that the Burgberg section is located in the southeast of the Ardennes, the distance between all these sections prior deformation should not be very different. Furthermore, in respect to Middle Devonian palaeogeographic reconstruction from McKerrow and Scotese (1990) these sites were located in a same palaeolatitude, near the equator (see fig. 7; Eckelmann et al., 2014). However, the La Thure and Fromelennes-Flohimont sections belong to an attached platform and are both deposited in internal marine setting while the Burgberg was defined as part of a detached/isolated platform (e.g., atoll reef system; see synthetic Fig. 1c and Tab. 1) and deposited in an open-marine fore-reef environment likely far from direct continental input. These differences in term of platform type/morphology and main depositional contexts have a direct influence on both sedimentary rate and water agitation parameters discussed above. During the middle- to late-Givetian times the Freikofel section, part of the Proto-Alps terrane (Fig.1b), was likely located around 30°S and likely far from a continental or volcanic source area (Schönlaub, 1992), which enabled the formation of an almost pure carbonate system (in comparison to the La Thure and Fromelennes-Flohimont sections bordering the Old Red Continent).

Considering the 2nd order timescale on which we examined the χ_{in} trends, we projected to have marked trends related to parameters playing a role over long-distance (e.g. inter-regional scale) such as climate, tectonic and global eustatic fluctuations. These parameters are considered as the primary trigger of erosion and siliciclastic fluctuation basinward, leading to χ_{in} variation. Thereby, we have expected that the imprint of these parameters on an extended stratigraphic interval would have been more visible between the section selected and would have permitted long-distance correlation. However, as presented herein, we have established that the syn-sedimentary parameters are strongly influencing our χ_{in} trends. The χ_{in} signature that we recorded throughout all the sections is most likely the combined result of the different parameters discussed above. However, it is still hard to understand the impact of syn-sedimentary parameters over parameters driving variations in continental erosion (e.g., tectonic, climate and sea-level changes), which are considered as the primary causes of χ_{in} variation in sedimentary rocks.

This part of our research aiming to test the reliability of magnetic susceptibility signal as tool for correlation between sedimentary basins has not yet proven to be reliable and more time-equivalent χ_{in} curves from other palaeogeographic settings are required. This will allow further comparisons with results presented herein and will provide a better understanding on the influence of the large-scale parameters and how they affect the χ_{in} signature.

5. Application of magnetic susceptibility as a palaeoclimatic proxy and the search for orbital forcing

Based on the integration of the χ_{in} records of 4 sections from the Dinant Syncline going through the whole Givetian (the La Thure, Fromelennes-Flohimont from this PhD and La Couvinoise and Baileux from Cédric Mabille's PhD (2008)), De Vleeschouwer et al. (2014) proposed a calibration of the Givetian time scale (see publication in Supplementary materials; De Vleeschouwer et al., 2014). Based on time-series analysis on the four sections (Fig. 3), this study revealed the imprint of the different Milankovitch astronomical parameters (eccentricity, obliquity, and precession) with a clear imprint of eccentricity (405 kyr cycles). The highly stable 405 kyr cycles allowed to constrain the duration of the Givetian Stage at 4.35 ±0.45 Myr, which is a significant improvement from previous cyclostratigraphic assessments of the duration of the Givetian (House, 1995; Ellwood et al., 2011) and in good agreement with the International Chronostratigraphic Chart (5.0 ±0.8 Myr).

Such study is an important application of the magnetic susceptibility (χ) of sedimentary rocks as proxy for climate change, allowing for the generation of high-resolution records in deep past sedimentary archives.

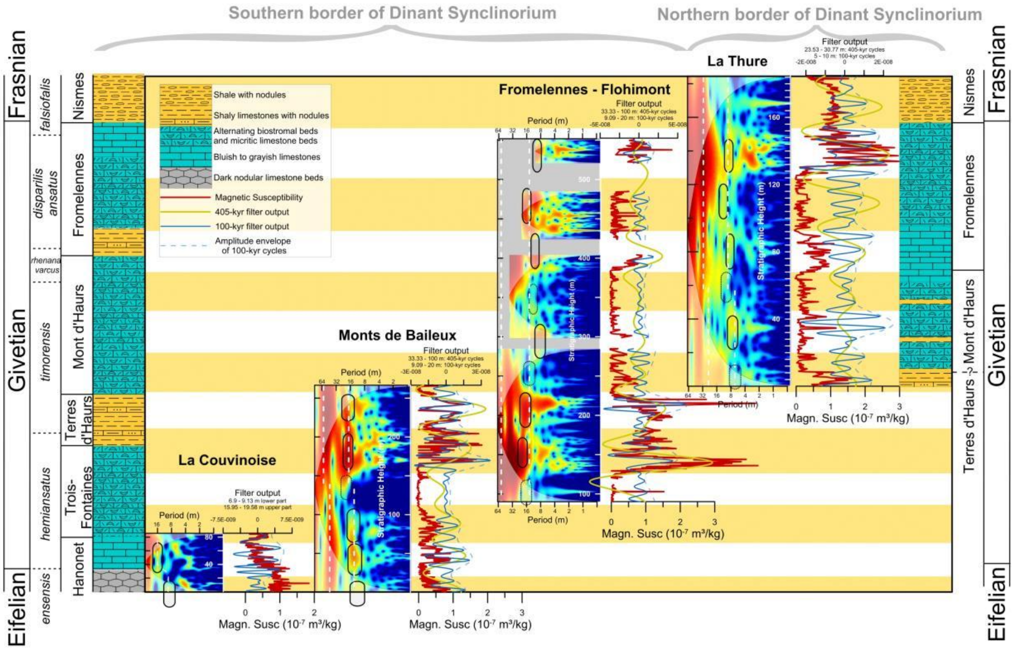

Fig. 3. Cyclostratigraphic interpretation of the continuous wavelet transforms (CWT) of the studied magnetic susceptibility signals. For each section, the magnetic susceptibility signal is plotted in red, along its CWT. On the CWT, the frequency range of 405 and 100 kyr eccentricity is denoted by a white dashed line. For the 100 kyr cycles, the rounded rectangles suggest zones of increased spectral power during 405 kyr maxima, caused by amplitude modulation of the 100 kyr cycles by 405 kyr eccentricity. Based on the filter outputs, alternating orange and white horizontal bands delineate the 405 kyr eccentricity cycles. Based on this figure, the Givetian contains 10.75 such cycles, that is, 4.35 Myr.

6. References

Bábek, O., Přkryl, T. and Hladil, J. (2007) Progressive drowning of carbonate platform in the Moravo-Silesian Basin (Czech Republic) before the Frasnian/Famennian event: Facies, compositional variations and gamma-ray spectrometry. *Facies*, **53,** 293-316.

Boulvain, F., Da Silva, A.C., Mabille, C., Hladil, J., Gersl, M., Koptikova, L. and Schnabl, P. (2010) Magnetic Susceptibility Correlation of Km-Thick Eifelian-Frasnian Sections (Ardennes and Moravia). *Geologica Belgica*, **13,** 309-318.

Burchette, T.P. (1981) European Devonian reefs ; a review of currents concepts and models. In: *European fossil reef models, S.E.P.M. Special Publication* (Ed D.F. Toomey), **30**, pp. 85-142.

Copper, P. (2002) Silurian and Devonian reefs: 80 million years of global greenhouse between two ice ages. In: *Phanerozoic Reef Patterns. SEPM, Special Publication* (Eds w. Kiessling, E. Flügel and J. Golonka), **72**, pp. 181-238.

Crick, R.E., Ellwood, B.B., El Hassani, A., Feist, R. and Hladil, J. (1997) Magnetosusceptibility event and cyclostratigraphy (MSEC) of Eifelian-Givetian GSSP and associated boundary sequences in North Africa and Europe. *Episodes*, **20,** 167-175.

Da Silva, A.-C., Potma, K., Weissenberger, J.A.W., Whalen, M.T., Humblet, M., Mabille, C. and Boulvain, F. (2009a) Magnetic susceptibility evolution and sedimentary environments on carbonate platform sediments and atolls, comparison of the Frasnian from Belgium and Alberta, Canada. *Sedimentary Geology*, **214,** 3-18.

da Silva, A.C. and Boulvain, F. (2004) From palaeosols to carbonate mounds: Facies and environments of the middle Frasnian platform in Belgium. *Geological Quarterly*, **48,** 253-266.

Da Silva, A.C. and Boulvain, F. (2012) Analysis of the Devonian (Frasnian) platform from Belgium: A multi-faceted approach for basin evolution reconstruction. *Basin Research*, **24,** 338-356.

Da Silva, A.C., De Vleeschouwer, D., Boulvain, F., Claeys, P., Fagel, N., Humblet, M., Mabille, C., Michel, J., Sardar Abadi, M., Pas, D. and Dekkers, M.J. (2013)

Magnetic susceptibility as a high-resolution correlation tool and as a climatic proxy in Paleozoic rocks - Merits and pitfalls: Examples from the Devonian in Belgium. *Marine and Petroleum Geology*, **46,** 173-189.

Da Silva, A.C., Mabille, C. and Boulvain, F. (2009b) Influence of sedimentary setting on the use of magnetic susceptibility: Examples from the Devonian of Belgium. *Sedimentology*, **56,** 1292-1306.

Da Silva, C. and Boulvain, F. (2005) Upper Devonian carbonate platform correlations and sea level variations recorded in magnetic susceptibility. *Palaeogeogr Palaeoclimatol Palaeoecol*.

De Vleeschouwer, D., Boulvain, F., Da Silva, A.-C., Pas, D., Labaye, C. and Claeys, P. (2014) The astronomical calibration of the Givetian (Middle Devonian) timescale (Dinant Synclinorium, Belgium). *Geological Society, London, Special Publications*, **414**.

Eckelmann, K., Nesbor, H.D., Königshof, P., Linnemann, U., Hofmann, M., Lange, J.M. and Sagawe, A. (2014) Plate interactions of Laurussia and Gondwana during the formation of Pangaea - Constraints from U-Pb LA-SF-ICP-MS detrital zircon ages of Devonian and Early Carboniferous siliciclastics of the Rhenohercynian zone, Central European Variscides. *Gondwana Research*, **25,** 1484-1500.

Ellwood, B., Crick, R.E., Garcia-Alcalde Fernandez, J.L., Soto, F.M., Truyols-Massoni, M., El Hassani, A. and Kovas, E.J. (2001) Global correlation using magnetic susceptibility data from Lower Devonian rocks. *Geology*, **29,** 583–586.

Ellwood, B.B., Tomkin, J.H., El Hassani, A., Bultynck, P., Brett, C.E., Schindler, E., Feist, R. and Bartholomew, A.J. (2011) A climate-driven model and development of a floating point time scale for the entire Middle Devonian Givetian Stage: A test using magnetostratigraphy susceptibility as a climate proxy. *Palaeogeography, Palaeoclimatology, Palaeoecology*, **304,** 85-95.

House, M.R. (1995) Devonian precessional and other signatures for establishing a Givetian timescale. *Geological Society, London, Special Publications*, **85,** 37-49.

Hubmann, B. and Suttner, T. (2007) Siluro-Devonian Alpine reefs and pavements. *Geological Society, London, Special Publications*, **275,** 95-107.

Irino, T. and Tada, R. (2003) High-resolution reconstruction of variation in aeolian dust (Kosa) deposition at ODP site 797, the Japan Sea, during the last 200 ka. *Global and Planetary Change*, **35,** 143-156.

Larrasoaña, J.C., Roberts, A.P. and Rohling, E.J. (2008) Magnetic susceptibility of eastern Mediterranean marine sediments as a proxy for Saharan dust supply? *Marine Geology*, **254,** 224-229.

Mabille, C. (2008) *Dynamique sédimentaire de l'Eifelien et de la base du Givétien en Belgique et dans les régions limitrophes*, Liège University, 185 pp.

Mabille, C., Pas, D., Aretz, M., Boulvain, F., Schröder, S. and Silva, A.C. (2008) Deposition within the vicinity of the Mid-Eifelian High: Detailed sedimentological study and magnetic susceptibility of a mixed ramp-related system from the Eifelian Lauch and Nohn formations (Devonian; Ohlesberg, Eifel, Germany). *Facies*, **54,** 597-612.

McKerrow, W.S. and Scotese, C.R. (1990) *Paleozoic Palaeogeography and biogeography*. Geological Society of London, Memoir, 433 pp.

Ridgwell, A.J. (2002) Dust in the Earth system: The biogeochemical linking of land, air and sea. *Philosophical Transactions of the Royal Society A: Mathematical, Physical and Engineering Sciences*, **360,** 2905-2924.

Schönlaub, H.P. (1992) Stratigraphy, biogeography and paleoclimatology of the Alpine Paleozoic and its implications for plate movements. *Jahrbuch der Geologischen Bundesanstalt*, **135,** 381-418.

Sur, S., Soreghan, M.J., Soreghan, G.S. and Stagner, A.F. (2010) Extracting the silicate mineral fraction from ancient carbonate: Assessing the geologic record of dust. *Journal of Sedimentary Research*, **80,** 763-769.

Weber, M.E., Kuhn, G., Sprenk, D., Rolf, C., Ohlwein, C. and Ricken, W. (2012) Dust transport from Patagonia to Antarctica - A new stratigraphic approach from the Scotia Sea and its implications for the last glacial cycle. *Quaternary Science Reviews*, **36,** 177-188.

Whalen, M.T. and Day, J.E. (2010) Cross-basin variations in magnetic susceptibility influenced by changing sea level, paleogeography, and paleoclimate: Upper

Devonian, western Canada sedimentary basin. *Journal of Sedimentary Research*, **80,** 1109-1127.

Whalen, M.T., Eberli, G.P., Van Buchem, F.S.P. and Mountjoy, E.W. (2000) Facies architecture of Upper Devonian carbonate platforms, Rocky Mountains, Canada. *Bull. Cent. Rech. Elf Explor. Prod. Mem.*, **24,** 139-178.

Wright, V.P. and Burchette, T.P. (1996) Shallow-water carbonate environments. In: *Sedimentary Environments: Processes, Facies and Stratigraphy* (Ed H.G. Reading). Blackwell Science, Oxford.

Zegers, T.E., Dekkers, M.J. and Baily, S. (2003) Late Carboniferous to Permian remagnetization of Devonian limestones in the Ardennes: Role of temperature, fluids, and deformation. *Journal of geophysical research*, **108,** 5/1 - 5/19.

Ziegler, A.P. (1982) *Geological Atlas of Western and Central Europe*. Shell Internationale Petroleum Maatschappij, 130 pp.

Zwing, A., Bachtadse, V. and Soffel, H.C. (2002) Late Carboniferous remagnetisation of Palaeozoic rocks in the NE Rhenish Massif, Germany. *Physics and Chemistry of the Earth, Parts A/B/C*, **27,** 1179-1188.

Zwing, A., Clauer, N., Liewig, N. and Bachtadse, V. (2009) Identification of remagnetization processes in Paleozoic sedimentary rocks of the northeast Rhenish Massif in Germany by K-Ar dating and REE tracing of authigenic illite and Fe oxides. *Journal of Geophysical Research: Solid Earth*, **114**.

Reminiscence of conodont Palmatolepis, Cap Blanc Nez, France

Chapter 7

Conclusions

The work achieved during this thesis mainly consisted in the characterization of long-term palaeoenvironmental development in three of the most remarkable European Devonian carbonate platforms. We also assessed the reliability of magnetic susceptibility records in marine carbonates as a tool for long-distance correlation.

In order to conduct this study we have selected four sections covering the longest possible stratigraphic interval in the Mid-Late Devonian of the Ardennes, Rheinisches Schiefergebirge and Carnic Alps Pre-Mesozoic massifs. We have analyzed the early-Givetian to middle-Frasnian in La Thure and the early-Givetian to early-Frasnian in Fromelennes-Flohimont, both sections located in the Ardennes. We have then carried out our investigations on the Middle Devonian (middle-Givetian) to Mississippian in the Burgberg section of the Rheinisches Schiefergebirge and on the late-Givetian to early-Frasnian in the Freikofel section of the Carnic Alps. Altogether these sections provide over 1 km of Devonian marine carbonate records.

Each section has been subjected to an in-depth multi-disciplinary study that includes sedimentology, conodont biostratigraphy, major and trace elements and carbon isotope geochemistry, magnetic susceptibility and hysteresis magnetic measurements.

The extended field works and petrographic analyses have provided an updated picture of the palaeoenvironmental diversity that shaped the Mid-Late Devonian off-reef to shallow-water reef in the Rhenohercynian and Palaeotethys oceans. This picture is based on ~1400 thin-sections and 61 microfacies that provide an eloquent illustration of carbonate platforms (e.g. homoclinal ramp, attached rimmed shelf, detached rimmed shelf and drowned shelf) that built the European tropical belt during the Mid-Late Devonian. Based on microfacies stacking patterns and conodont biostratigraphy we have reconstructed the long-term carbonate platform development for each selected section.

The Givetian La Thure and Fromelennes-Flohimont sections encompass a shallow-water attached rimmed shelf, a homoclinal ramp and a drowned shelf. Evolution throughout the early- to late-Givetian can be divided into seven major intervals separated by various shallowing-deepening upward events and resulting in complex platform development with rapid morphological changes. The late-Givetian transgressive trend caused the demise of this platform and the subsequent deposition of drowning shale characterizing the early Frasnian in the Ardennes.

In the La Thure section, the Frasnian is characterized by four major sea-level fluctuations and is dominated by deposition on a homoclinal ramp during the early Frasnian and in a fore-reef context during the middle Frasnian onward.

The Burgberg section represents a continuous deposition within the fore-reef fringe of the Brilon Reef Complex, which corresponds to a detached rimmed shelf, developed on a volcanic high within the Rhenohercynian Ocean. Sedimentation in the Burgberg section ranges from proximal to off-reef settings. The off-reef domain is the most distal setting observed and is characterized by fine-grained sediments, dominated by pelagic biota and the local occurrence of gravity-flow deposits. The intermediate fore-reef is characterized by a mixture of biota and sediments from deep-water and shallow-water sources and is influenced by storm and gravity-flow currents. In this sedimentary domain, *Renalcis* mound-like structures developed. The proximal fore-reef setting corresponds to the most proximal setting and is strongly affected by gravity-flow currents derived from the Brilon Reef Complex. The precise conodont biostratigraphic pattern established in this section has constrained the timing of the main evolutionary phases that shaped this huge detached platform in the Rheinisches Schiefergebirge, and also enabled us to highlight, with the help of $\delta^{13}C$ analyses, the Kellwaser events at the Frasnian – Famennian boundary in a breccia limestone.

.

The Freikofel section corresponds to a deposition in the fore-reef setting of the Carnic Alps detached platform. Sedimentation in the Freikofel section is commonly associated with “transitional” facies and ranges from proximal to distal fore-reef and also records drowning sedimentation. The most distal setting is characterized by an autochthonous pelagic sedimentation showing local occurrence of thin-bedded turbiditic deposits. In the fore-reef slope, in a more proximal setting, there is an accumulation of various autochthonous and allochthonous fine- to coarse-grained sediments originating from the interplay of gravity-flow currents derived from the shallow-water and deep-water area deposition in a fore-reef setting. The precise conodont biostratigraphic pattern established in this section provides a timing for the main environmental evolution that characterized deposition in the Freikofel section. The dismantlement of the Eifelian – Frasnian platform starting at the early-Frasnian up until the late-Frasnian and the stepwise withdrawal of the shallow-water influxes during the late Frasnian together with a significant deepening of the Carnic Alps platform at the Frasnian – Famennian boundary are the main environmental evolutions recorded within the fore-reef Freikofel succession. Conodont biostratigraphy combined with $\delta^{13}C$ measurements have revealed on of the global Kellwasser events in limestone lithologies.

Magnetic susceptibility (χ_{in}) has been measured on nearly 2000 samples in the four sections. This large set of measures has permitted to build four high-resolutions χ_{in} curves and gain a better understanding of the dependence between χ_{in} and environmental parameters such as water agitation, carbonate production and/or sedimentary rate (e.i., acting as dilution or concentration trigger). Four models of χ_{in} evolution on a proximal – distal transect were defined. These models coincide with the classical facies-dependent models defined for homoclinal ramp, and rimmed-shelf platform type. The combination of data sets from magnetic susceptibility and major and trace elemental geochemistry has brought up the inherent-parallel link between the siliciclastic input proxies variation and the χ_{in} signature in all the sections.

In most of the sections, the χ_{in} signal is mainly controlled by a mixture of SD and SP grains related to remagnetization. Transition from smectite to illite during diagenesis has appeared to be the most convincing parameter able to produce fine-grained magnetite that is classically observed in remagnetized limestone. When comparing the variations in the magnetic susceptibility signal with facies evolution, it appears that χ_{in} is influenced by proximality but also by the main depositional setting. Thus, the recorded χ_{in} signal in our sections is constituted of a primary depositionally-induced signal and likely a secondary diagenetically-induced magnetic signal. The relatively good correlation observed between χ_{in} signal in all the section and siliciclastic input proxies attest of a fairly good preservation of the primary depositional character of the χ_{in} signature, and the low to weak distortion triggered by remagnetization. These results have confirmed that χ_{in} records can be used for correlation and as a paleo-environmental proxy for all the sections analyzed.

The chart showing the long-term χ_{in} trends for each section measured in our PhD shows a strong correlation between Givetian sequences in the Dinant Syncline. However, correlations of sections from the Ardennes with the Rheinisches Schiefergebirge and the Carnic Alps sections are not clear. We analyzed the factors playing a role on the primary record of χ_{in} (e.g., syn-sedimentary parameters, sea-level fluctuation, climate, tectonic, eolian-related dust etc.) and have showed that intra-basinal χ_{in} based correlations are possible between sequences deposited in relatively similar carbonate platform model. However, the inter-basinal χ_{in} based correlations must be considered carefully because the situation is more complex and more time-equivalent χ_{in} curves from other palaeogeographic settings and platforms are required. These supplementary data would allow further understanding on the impact of syn-sedimentary parameters over the parameters driving variation in continental erosion (e.g., tectonic, climate and sea-level changes), which are considered as the primary trigger of siliciclastic input supplies. Beyond these results, the high-resolution χ_{in} records on extended timescales within the Dinant Syncline have proven to be a relevant tool for the search of orbital forcing parameters and allowed us to get significant improvement of the estimate of Givetian Stages duration.

View of Mt. Nilgiri from Syang village, Mustang, Nepal

Annexes

Based on: Pas, D., Da Silva, A.C., Boulvain, F., Dhital, M.R. (2011): Sedimentology of a Mid-Late Ordovician carbonate mud-mound complex from the Kathmandu nappe in Central Nepal. *Journal of Asian Earth Sciences*, 42(3), 451-466.

De Vleeschouwer D., Boulvain, F., Da Silva, A.C., Pas, D., Labaye, C., Claeys, P. (2014): astronomical interpretation of the magnetic signal signal of the Givetian sections in the Dinant Synclinorium (La Couvinoise, Monts de Baileux, Fromelennes-Flohimont and La Thure). *Geological Society of London*, *Special Publication,* 414

Contents lists available at ScienceDirect

Journal of Asian Earth Sciences

journal homepage: www.elsevier.com/locate/jseaes

Sedimentology of a Mid-Late Ordovician carbonate mud-mound complex from the Kathmandu nappe in Central Nepal

Damien Pas [a,*], Anne-Christine Da Silva [a], Megh Raj Dhital [b], Frédéric Boulvain [a]

[a] *Pétrologie Sédimentaire, B20, Université de Liège, Sart-Tilman, Liège, Belgium*
[b] *Central Department of Geology, Tribhuvan University, Kirtipur, Kathmandu, Nepal*

A R T I C L E   I N F O

Article history:
Received 25 August 2010
Received in revised form 12 May 2011
Accepted 24 May 2011
Available online 12 June 2011

Keywords:
Stratigraphy
Phulchauki Group
Godavari quarry
Diagenetic sequence
Stromatactis
Microstromatolites

A B S T R A C T

This sedimentological study of the Godavari quarry is the first relating to the Palaeozoic Tethyan sedimentary rocks of the Kathmandu nappe (Central Nepal). Sedimentological analyses led to the identification of six microfacies belonging to a large carbonate mud-mound complex, which can be divided into mound, flank and off-mound main depositional settings. Identification of two dasycladaceans (*Dasyporella* cf. *silurica* (Stolley, 1893) and *Vermiporella* sp.) in the mound facies gives a Mid-Late Ordovician age to this newly discovered Godavari carbonate mud-mound, which makes this mound one of the oldest ever described in the Asian continent.

The mound microfacies are characterized by a high micritic content, the presence of stromatactis and the prevalence of red coloured sediments (the red pigmentation probably being related to organic precipitation of iron). The flank microfacies are characterized by a higher crinoid and argillaceous content and the presence of bio- and lithoclasts concentrated in argillaceous lenses. Finally, the off-mound microfacies show very few bioclasts and a high argillaceous content. Palaeoenvionmental interpretation of microfacies, in terms of bathymetry, leads us to infer that the Godavari mud-mound started to grow in a deep environment setting below the photic and wave action zones and that it evolved to occupy a location below the fair weather wave base. Cementation of cavities within the mound facies underlines a typical transition from a marine to a burial diagenetic environment characterized by: (1) a radiaxial non luminescent feroan calcite cement (marine) showing a bright orange luminescent band in its middle part; (2) a bright zoned orange fringe of automorphic feroan calcite (meteoric phreatic); (3) a dull orange xenomorphic feroan calcite cement in the centre of cavities (burial) and (4) a saddle dolomite within the centre of larger cavities.

The faunal assemblage (diversity and relative proportion) of the Godavari mound facies is dominated by crinoids and ostracods, which makes this carbonate mud-mound comparable to the Meiklejohn Peak mounds (Nevada).

1. Introduction and aims of the study

The occurrence of Palaezoic sedimentary rocks which had not been completely transformed by metamorphism is really scarce in Nepal. Surprisingly, the Kathmandu nappe, which is one of the remarkable areas in Nepal where Palaeozoic sediment accumulations are exposed, has never been submitted to any detailed sedimentological analyses. Belonging to the Kathmandu nappe, the Phulchauki area is a relevant region to perform a sedimentological approach in regard to its well visible Palaeozoic accumulations (Stöcklin and Bhattarai, 1977; Stöcklin, 1980). In the Phulchauki area, the Godavari quarry is one of the largest outcrops. This quarry cuts through a carbonate mud-mound complex which is the focus of this paper. The Godavari mud-mound complex is observed within the sediment of the Phulchauki Group which belong to the Kathmandu Complex (Stöcklin, 1980).

The carbonates studied in the Godavari quarry have been exploited since the Rana period (~1850), while the first official geological assessment of the quarry was conducted in 1987 (unpublished report, Kansakar, 2003). This assessment revealed the "geological and structural complexity of the marble deposit in the area", describing lithological features of the relevant categories of rocks observed in the quarry. Despite relatively good outcrop conditions, in contrast to the surrounding area, no sedimentological or palaeontological study was performed in the Godavari quarry. Although, a few palaeontological papers concerning the Phulchauki area (area surrounding the quarry) have been published (Bordet et al., 1960; Funakawa, 2001), these ones disregard the succession of the Godavari quarry. According to Stöcklin

* Corresponding author. Tel.: +32 (0) 4 366 22 54.
E-mail address: dpas@ulg.ac.be (D. Pas).

1367-9120/$ - see front matter © 2011 Elsevier Ltd. All rights reserved.
doi:10.1016/j.jseaes.2011.05.008

(unpublished UNDP report, 1981), based on lithological features and aerial geology observations, the succession of the Godavari quarry belongs to the Chandragiri Formation (which is considered as Ordovician in age). In this context, the aims of this paper are as follows: (1) to provide a date for the strata exposed in the Godavari quarry; (2) to give a detailed description of the five most interesting sections exposed in the Godavari quarry and a definition of the different facies; (3) to provide an interpretation of the observed facies and the distribution of these facies in a depositional model; (4) to compare the Godavari carbonate mud-mound with some other well known Palaeozoic carbonate mud-mounds; and finally (5) to place the Godavari section within a palaeogeographic location.

2. Location and geological context

The Kathmandu nappe is located in Central Nepal (Fig. 1A) and is one of the five nappes identified within the Lesser Himalayan Zone (Hagen, 1951; Upreti and Le Fort, 1999). Tectonic, stratigraphic, and lithological studies conducted in Nepal (Hagen, 1951, 1969; Stöcklin, 1980) have shown that the Kathmandu nappe was thrust from the Tibetan-Tethys Zone into the Lesser Himalayan Zone during the Himalayan orogen. The rock succession of the Kathmandu nappe belongs to the Kathmandu Complex (Stöcklin and Bhattarai, 1977; Stöcklin, 1980), which is divided into the Bhimphedi Group and the Phulchauki Group (Fig. 1B). The Bhimphedi Group consists of an 8 km-thick sequence of variously metamorphosed lithologies. Towards the top of the Group, the grade of metamorphism decreases and gives way to the overlying sedimentary sequence of the Phulchauki Group. The Phulchauki Group consists of 5–6 km-thick Precambrian (?) and Lower Palaeozoic sedimentary rock succession encompassing four formations (Fig. 1B). In stratigraphic order, these four formations are respectively named the Tistung, Chandragiri, Chitlang and Godavari Formations. Rocks of the Phulchauki Group are well exposed in the Chandragiri-Phulchauki syncline (Fig. 1C), which forms the core of the Mahabarath Synclinorium (see Upreti, 1999 for an overview of the stratigraphy and tectonics of the Nepal Himalaya). The Godavari quarry is located 15 km SE of Kathmandu, on the northeastern flank of the Chandragiri-Phulchauki syncline, at the foot of Phulchauki hill next to the village of Godavari. On the basis of aerial photo interpretation and field mapping, Stöcklin (unpublished UNDP report, 1981) suggested that the succession exposed in the Godavari quarry belongs to the Chandragiri Formation (see discus-

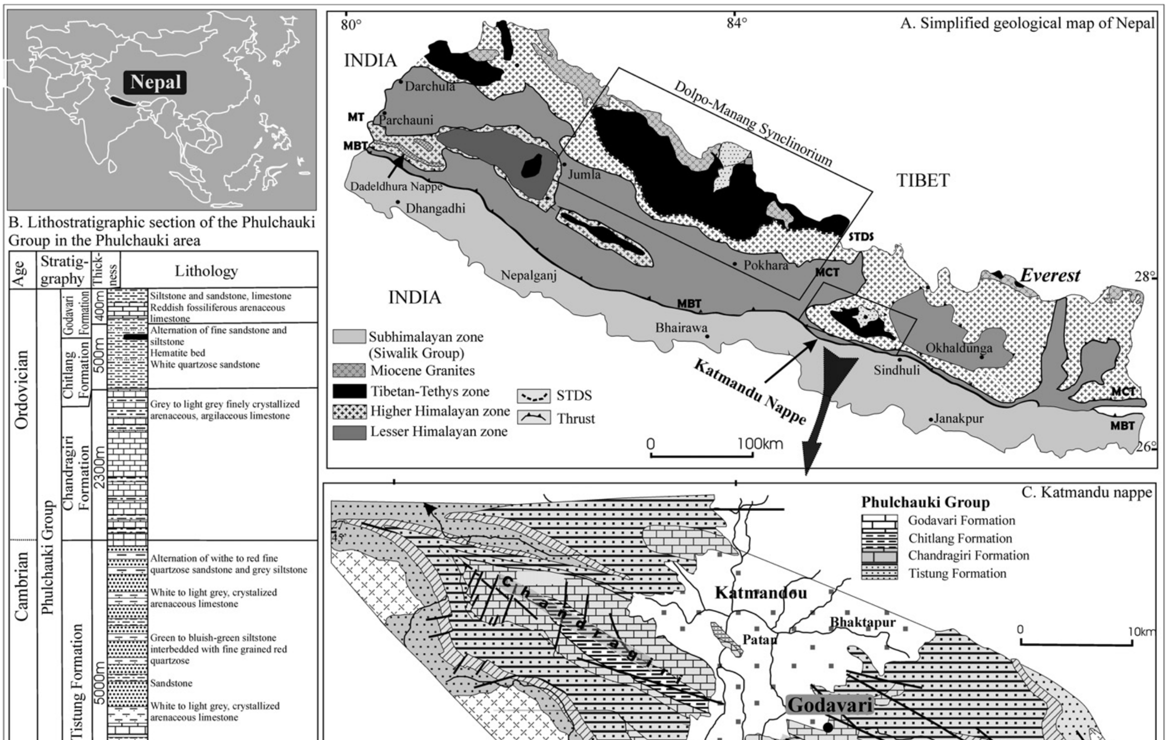

Fig. 1. Geological setting of the Godavari section. A. Simplified geological map of Nepal showing major tectonostratigraphic divisions (modified from Amatya and Jnawali, 1994). MBT: Main Boundary Thrust, MCT: Main Central Thrust, STDS: South Tibetan Detachment System. B. Generalized lithostratigraphic section of the Phulchauki Group in the Puhulchauki area (modified from Stöcklin (1980) and Funakawa (2001)). C. Simplified geological map of the Kathmandu nappe (Kathmandu area and central Mahabharat Range) (modified from Stöcklin (1980)).

sion in Section 4.2). It is a 2300 m-thick succession mainly composed of yellow or brown (when weathered) limestone of massive appearance from a distance but always well bedded. Crinoids, cystoids, bryozoans, brachiopods, bivalve shells and orthoceratids occur in the Formation. In the upper part of the Formation, a white 150 m-thick strata of thinly layered quartzite is observed (see Stöcklin, 1980 for a complete description of this Formation). Based on the identification of thecal cystoid plates (*Caryocrinites* s.l.) in the uppermost part of the Chandragiri Formation, in the type locality of Chandragiri (Stöcklin et al., 1977), a late Ordovician age has been assigned to the Chandragiri Formation. In the Tibetan-Tethys Zone and more particularly in the Palaeozoic–Mesozoic Tethyan sediments of the Dolpo-Manang Synclinorium (Fig. 1A), an equivalent of the Chandragiri Formation corresponding to the Nilgiri Limestone (Bordet et al., 1971) is observed (Stöcklin et al., 1977; Funakawa, 2001). The Nilgiri Limestone corresponds to a nearly 1600 m-thick ochre-weathering shallow-water limestone succession. It shows ripple marks, low- to high-angle cross-lamination and bioclastic layers with orthid brachiopods, gasteropods, bivalve shells, nautiloids and crinoids (see Fuchs et al., 1988 for a complete description of the Formation).

3. Methods

For the microfacies analysis of the mound, a bed-by-bed description and sampling was carried out, and about 100 thin-sections were prepared. Due to the massive and fractured aspect of section GE, samples were taken from each metre in stratigraphical order. The textural classification used to characterize the microfacies follows Dunham (1962) and Embry and Klovan (1972). Thin-sections were stained with Dickson solution (1965) to differentiate calcite, feroan calcite, dolomite and feroan dolimite. Stromatactis and fenestrae are described following Neuweiler et al. (2001). Estimation of sorting is based on the visual charts of Pettijohn et al. (1972). Pressure solution features are described following Logan and Semeniuk (1976) and Wanless (1979) modified by Choquette and James (1987). Cathodoluminescence imaging was performed at the University of Mons-Hainaut (UMH) using a CITL cold-cathode unit (model CL8200 Mk5) operating at 15 kV and 500 μA.

4. Results

4.1. Studied sections

Since it is not possible to describe a single continuous log from the base of the quarry to its top, the quarry was divided into five sections, which are, in ascending order: GA, GB, GC, GD and GE (see Fig. 2). The names are given according to the quarry benches and do not correspond to any stratigraphic order. According to field observations (geopetal structures, petrographic features, etc.) and an unpublished assessment report of the Godavari quarry including a basic geological map (unpublished report, Kansakar, 2003), the oldest section is GD followed by GC, GB and lastly GE. Section GA corresponds to a lateral equivalent of GB. Due to the presence of a fault zone, section GE is in abnormal tectonic contact with the other sections (Fig. 3). The strike of the strata in sections GA, GB, GC and GD is N 60° E with an average dip of 70° NNE. Due to the massive aspect of section GE, bedding was only clearly measured in one spot (N45–50° E with an average dip of 50° N). However, the presence of stromatactis (with geopetal structure) led both to confirmation of the measured dip and to confirm that the section GE was in the same stratigraphical order than the other sections. Tectonic deformation

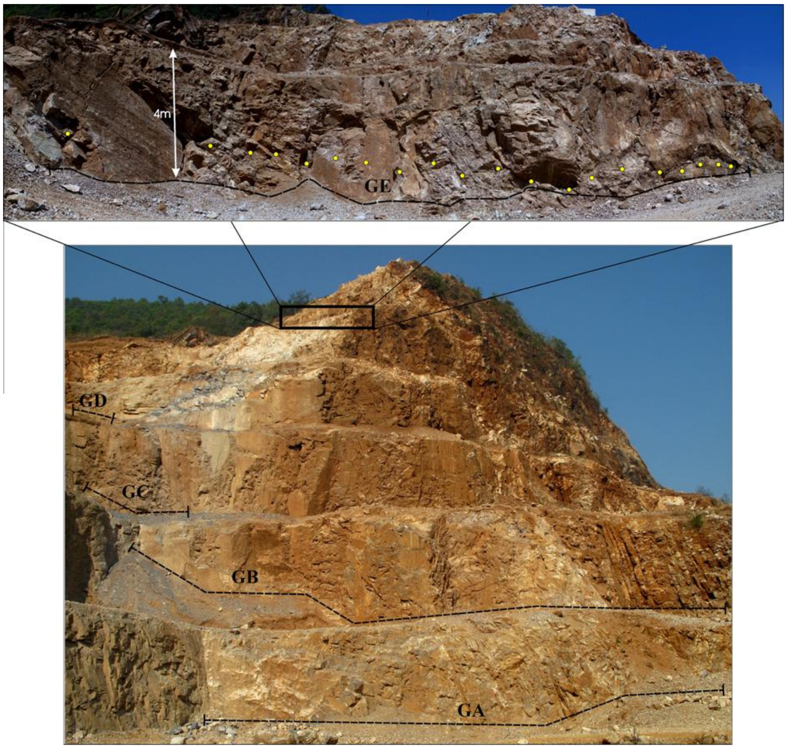

Fig. 2. The Godavari quarry showing the position of sections GA, GB, GC, GD and GE. Zoom on section GE, showing the position of collected samples (white dots). View from the East.

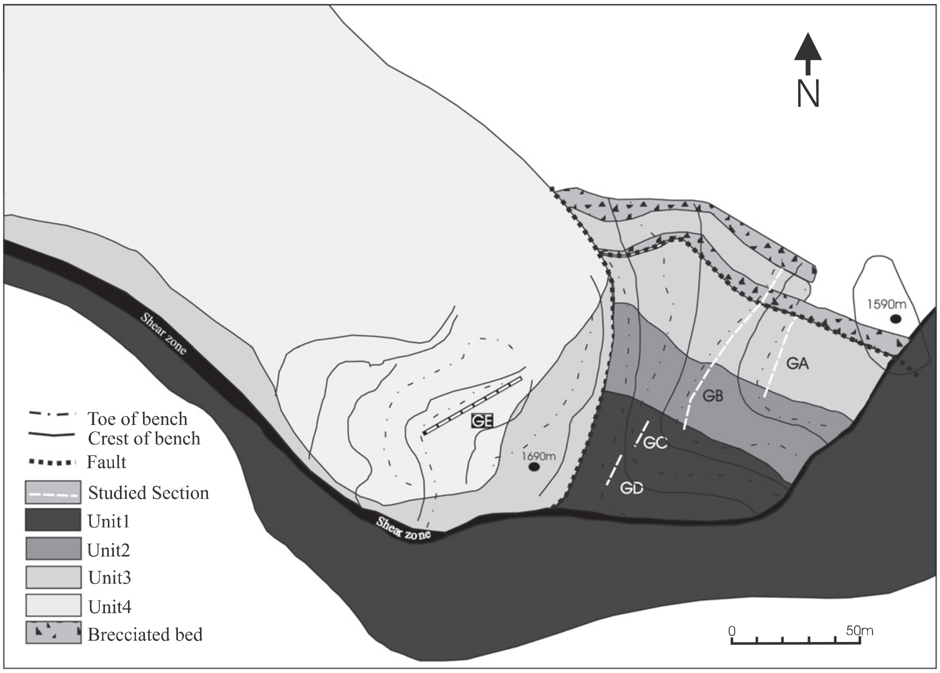

Fig. 3. Facies map of the Godavari quarry showing the location of the five studied sections (GA, GB, GC, GD and GE) (map modified from the unpublished report of Kansakar (2003)).

(schistosity, fracturing and recrystallization) experienced by the strata of the quarry as well as those of the surrounding area, has affected the original petrographic features of the rocks. In the studied part of the quarry, two faults and a shear zone have been recognized (unpublished report, Kansakar, 2003) (Fig. 3). Locally, in sections GA and GB, some beds are completely covered by cm-thick layers of calcite. Despite these limiting factors, a bed-by-bed description together with data from the assessment report (unpublished report, Kansakar, 2003) led to the definition of four lithological units through the studied sections.

The first three lithological units are observed within sections GD, GC, GB and GA, while Unit 4 corresponds to the whole of section GE (Fig. 4). Due to the absence of local tectonic reconstruction, the stratigraphic position of section GE is not well constrained. Nevertheless, the similarity in terms of petrographic features (colour, matrix, skeletal grains) between the upper part of section GB and section GE suggests that section GE corresponds to the top of the stratigraphic column defined for the Godavari quarry.

Unit 1 ($\sim$26 m-thick, corresponds to section GD, section GC and the first 5.45 m of section GB) consists of dark purplish to white shaly crystalline limestone in several tens of cm-thick, fractured and altered beds. The shaly limestones show an irregular lamination highlighted by light levels dominated by limestone and darker purplish levels corresponding to argillaceous phyllites. The boundary between the carbonated part and the argillaceous levels is microstylolithic (clearly visible in thin-section), suggesting that lamination was probably generated by pressure solution processes. Coarsely crystalline calcite occurs as vein fillings.

Unit 2 ($\sim$30 m-thick,, corresponding to the portion of section GB between 27.5 m and 45.60 m and to the first 10 m of section GA) mainly corresponds to dark brown to purplish massive and poorly bedded coarsely argillaceous recrystallized limestone. This limestone is thinly cleaved due to the presence of a thin phyllitic parting, which gives a darker colour to the rocks. A few millimetre- to centimetre-sized crinoid ossicles (intact and broken) and stems are observed scattered through the rock and locally concentrated in layers. Unidentified fossil grains are also observed. Argillaceous content decreases towards the top of the unit. The transition to the overlying unit is marked by a progressive variation in colour and by an increase in bioclastic content.

Unit 3 ($\sim$30 m-thick, corresponding to the last 40,7 m of section GB and the last 19 m of section GA) shows pinkish brown, fine- to medium-grained, recrystallized and fossiliferous, thick-bedded limestones. Fossils are abundant and mostly represented by crinoids (commonly mm-sized and locally a few cm in size) with less abundant recrystallized shells (bivalves and brachiopods). The lower part of this unit is greenish to purplish in colour (higher argillaceous content), while the upper part is pinkish to brownish. Coarsely crystalline calcite occurs as vein fillings and also as patches of irregular shapes. The upper part of the unit corresponds to thick- and well-bedded pinkish to slightly greenish, medium-grained recrystallized limestone, showing phyllitic layers on the bedding planes. Crinoid fragments are observed scattered through the rocks. Two brecciated beds (3 m-thick) are also observed, with well-cemented angular shaped fragments of different sizes (1–20 cm) derived from the underlying unit. According to Kansakar (unpublished report, 2003), this brecciated zone is related to a fault.

Unit 4 ($\sim$34 m-thick, section GE) is characterized by a pinkish to red-stained finely to medium crystalline massive and fractured limestone without clear bedding. Presence of fenestrae, stromatactis of varying sizes and veins filled either by white calcite or brown dolomite are the main characteristics of the unit. Locally, stromatactis and fenestrae form a laminar framework corresponding to the bedding plane. Crinoid fragments or stems and indeterminate fossils are occasionally observed.

4.2. Stratigraphy and dating of the mound

To our knowledge, there are no published palaeontological data concerning the Godavari mud-mound, only a few papers related to

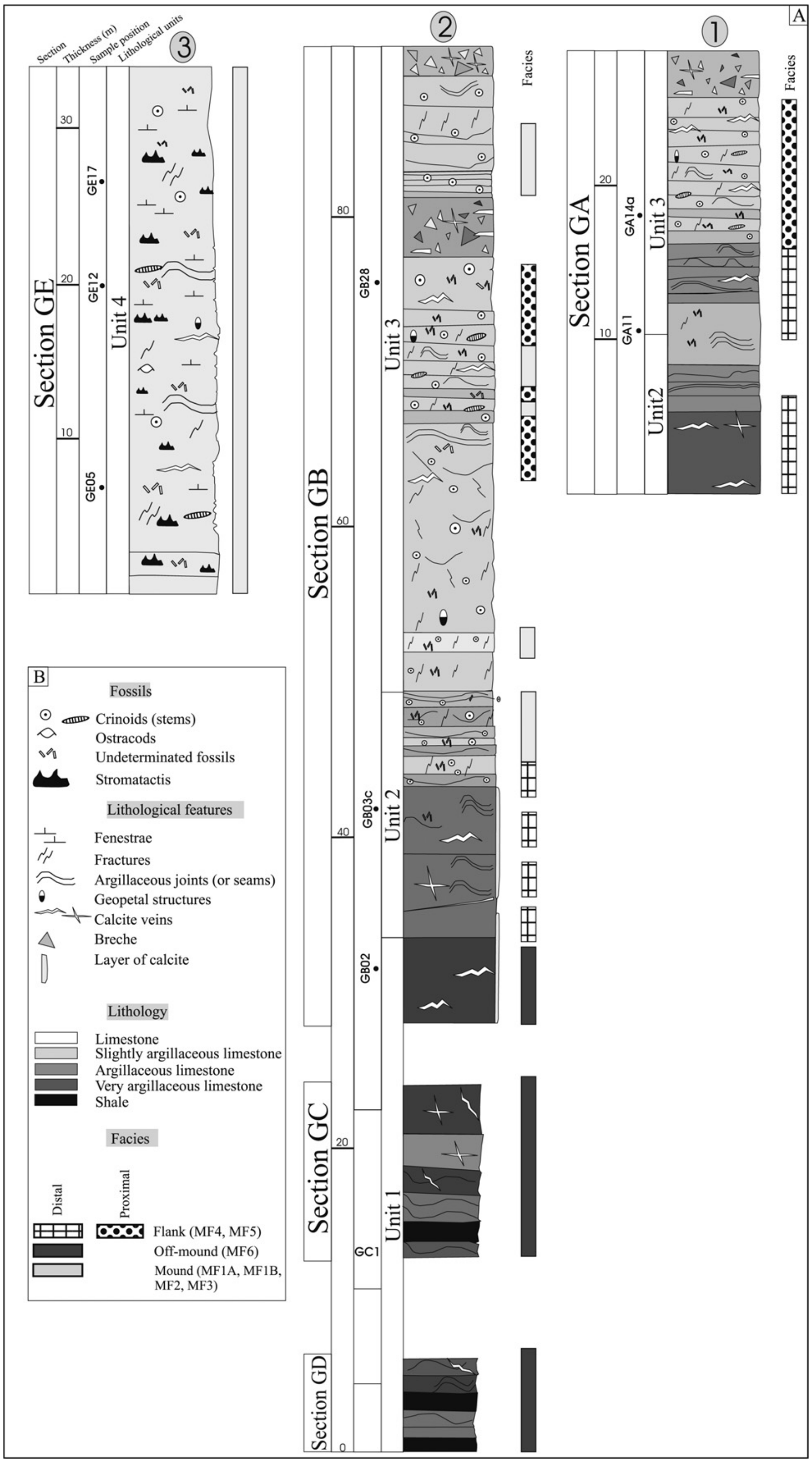

Fig. 4. A. Schematic sedimentological log showing lithological units and observed facies (log 2 is a composite log of sections GB, GC and GD). B. Legend for symbols used in figures.

the Chandragiri-Phulchauki area (Auden, 1935; Bordet et al., 1960; Stöcklin et al., 1977; Funakawa, 2001). So, even if the succession exposed in the Godavari quarry belongs to the Ordovician Chandragiri Formation (Stöcklin and Bhattarai, 1981; unpublished UNDP report), the lack of palaeontological data in this region does not allow a precise dating of the Godavari mud-mound. However, we observed two dasycladacean algae within a red stromatactis mudstone–wackestone (MF1a, section GE; see complete description of microfacies in Section 4.3). These dasycladaceans (Fig. 5E and F) have been identified as *Dasyporella* cf. *silurica* (Stolley, 1893) and *Vermiporella* sp. by Ioan Bucur (personal communication). These algae are known in the Hudson Bay in Canada (Poncet, 1986) and in the Tarim Basin in China (Riding and Fan, 2001) as Mid-Late Ordovician age. This Mid-Late Ordovician age, which is in accordance with the Late Ordovician age assigned by Stöcklin et al. (1977) for the uppermost part of the Chandragiri Formation

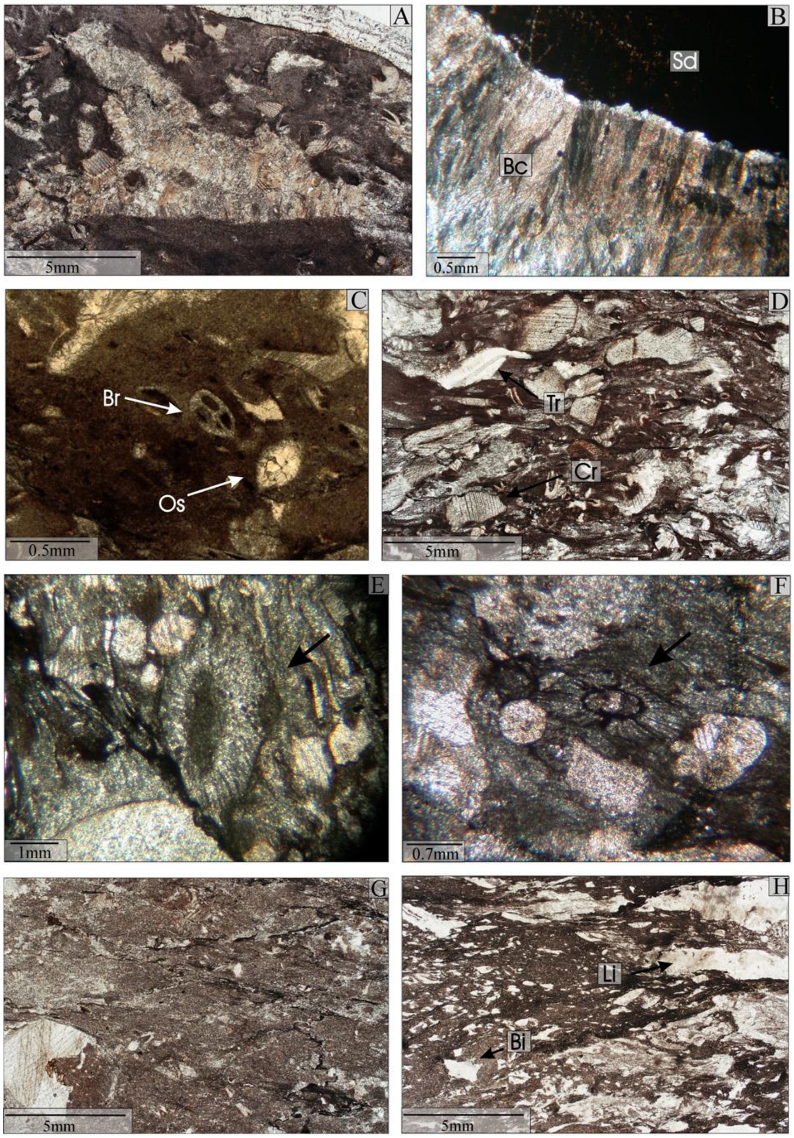

Fig. 5. Microfacies of the Godavari sections. *Numbers in brackets correspond to bed numbers in* Fig 4. See text for explanation. A. MF1a (mound facies): stromatactis cavity filled with an altered bladded calcite on the rim and a blocky calcite in its centre, in a micritic matrix, thin-section (GE17), normal light. B. MF1a: focus on a well developed bladded calcite (Bc) observed on the rim of a pluri-centimetre-sized stromatactis cavity and on a dark saddle dolomite (Sd) in its centre, thin section (GE17′), crossed nicols. C. MF1a (mound facies): Mudstone with (Br) bryozoan and (Os) ostracod, thin section (GE17), normal light. D MF1b (mound facies): bioclastic wackestone with crinoids (Cr) and trilobites (Tr), thin section (GE12), normal light. E. MF1a (mound facies): Dasycladacean (*Dasyporella* cf. *silurica* (Stolley, 1893) (black arrow), identified by Ioan Bucur (personal communication). Dimensions. Internal diameter 0.35–1.25 mm, external diameter 1.25–2 mm, thin section (GE05), normal light. F. MF1a (mound facies): *Vermiporella* sp. (black arrow), identified by Ioan Bucur (personal communication). Dimensions. Internal diameter 0.35–0.7 mm, external diameter 0.75–1.8 mm, thin section (GE05a) normal light. G. MF3 (mound facies): pinkish crinoidal mudstone, thin section (GB28), normal light. H. MF4 (flank facies): Argillaceous lenses showing recrystallized bioclasts (Bi) and lithoclasts (Li), thin section (GBO2), normal light.

in its type locality, makes the Godavari mound one of the oldest ever described in the Asian continent.

4.3. Microfacies

Our petrographic analyses led to the definition of six microfacies. These microfacies are placed in order with respect to a decrease both in the abundance of micritic matrix and in faunal diversity.

4.3.1. MF1: Red limestone with stromatactis

This microfacies (only observed in section GE, Unit 4) corresponds to a red to pink fine to medium crystalline limestone showing common stromatactis as well as fenestrae (irregular and stromatactoid). According to Bourque and Boulvain (1993), stromatactis are defined as a "spar network, whose elements have flat to undulose smooth lower surfaces and digitate upper surfaces, made up principally of isopachous crusts of centripetal cement and embedded in finely crystalline limestone" and following Neuweiler et al. (2001), stromatactoid fenestrae are defined as "unconnected cavities usually smaller than 5 mm width". As stromatactis, these fenestrae have a flat to undulose smooth lower surface and a digitate upper surface. By contrast, irregular fenestrae do not show any particularity at their lower and upper surface. At microscopic scale, this facies can be divided into two categories: (MF1a) mudstone–wackestone with common stromatactis and (MF1b) bioclastic fenestral wackestone-packtone with rare stromatactis.

4.3.2. MF1a: Red to pink mudstone–wackestone with stromatactis

This microfacies is characterized by the occurrence of stromatactis and fenestrae (stromatactoid and irregular). The dominant texture of the matrix is mudstone–wackestone, with a dark micrite (average size of micritic crystals around 4 μm), which has been locally recrystallized to pseudosparite (average size of crystals around 20 μm). Stromatactis may exceed tens of cm in size but are generally only a few cm (Fig. 5A). Usually, stromatactis are filled with radiaxial calcite cement, overlying an internal dark micritic matrix. When stromatactis cavities are pluri-centimetre-sized, they display well formed bladded calcite (Fig. 5B) and a core constituted of saddle dolomite. In a few cases, deformation has changed the stromatactis shape, and the base appears curved. Sporadically, stromatactoid fenestrae and irregular fenestrae occur, commonly mm-sized and cemented by an equigranular sparite. The faunal assemblage is characterized by a poor preservation and diversity, and is dominated by crinoids (~5% of the sediment). Other allochems are recrystallized ostracods (Fig. 5C), sponge spicules, bryozoan fragments, bivalve and/or brachipod shells (?), trilobites and very rare dasycladaceans (Fig. 5E and F). Fossil grains are dispersed within the matrix with a moderate sorting and show sub-angular to rounded shapes ranging from 0.2 to 4 mm (for the entire ossicle) with an average size of around 0.4 mm. Locally, small crinoids grains (~0.3 mm) are packed in mm-sized pockets. Occasionally, crinoids show a rim of syntaxial cement. Another characteristic of this microfacies is the occurrence of pressure solution and deformation structures represented by (1) stylolitic seams filled with insoluble residue, (2) "horse tail" and (3) pressure shadows filled with calcite.

4.3.3. MF1b: Red to pink bioclastic fenestral wackestone–packstone

This microfacies presents similar characteristics to MF1a but the main difference is observed in the type of cavity. Indeed, pluri-millimetre-sized irregular fenestrae can be regularly seen

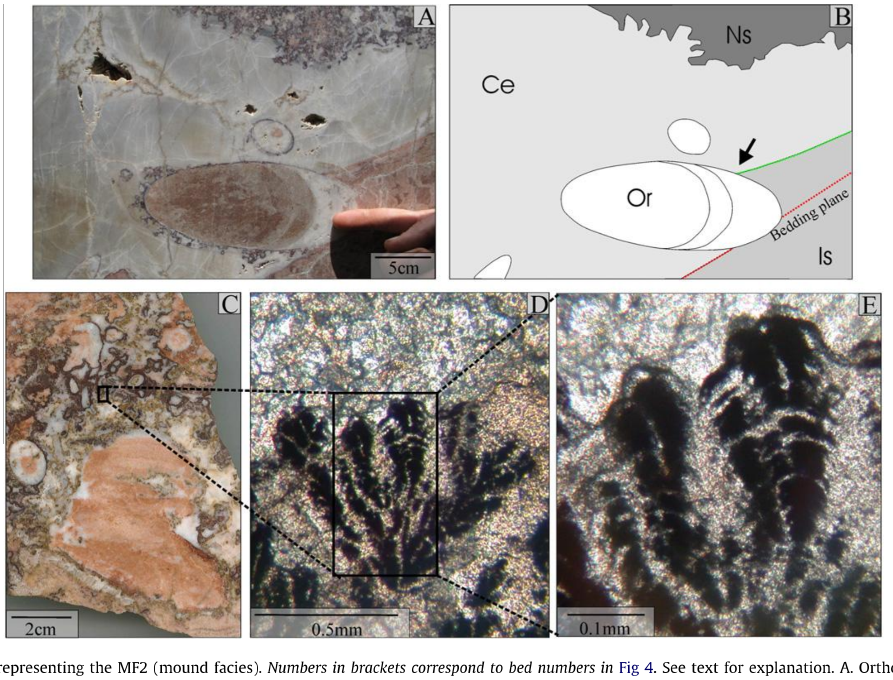

Fig. 6. Set of photos representing the MF2 (mound facies). *Numbers in brackets correspond to bed numbers in* Fig 4. See text for explanation. A. Orthoceratidea (Or) at the interface cement-internal sediment; polished slab, quarry showroom. B. Sketch of Fig. 6A emphasize the slight concave bend between the interface cement (Ce) – internal sediment (Is). Ns: "nebuloid" structure. C. Rudstone with lithoclast and "nebuloid" structures (erratic block), polished slab, near section GE. D. Hematitic branching dentrites in a sparitic cement (erratic block) thin section, normal light. E. Zoom on the central branch of the dendrite from picture D showing an alternation of hematitic and sparitic laminae (erratic block), thin section, normal light.

while stromatactis (mm-sized) are very rarely observed. Another difference is the increase in bioclasts (mostly crinoids, 7.5–10% of the sediment).

4.3.4. MF2: "Nebuloid" rudstone with orthoceratids and microstromatolites

This microfacies was observed only on erratic blocks near section GE and on a metre-sized polished slab in the quarry showroom (Fig. 6A). In macroscopic view, three components characterize this microfacies: (1) the light pink to red colour of the rock; (2) the presence of large (m-scale) and smaller cavities (cm to dm-scale), which show common cm- to tens of cm-scaled orthoceratids (Fig. 6A) and which are filled with dolomitic cement and (3) conspicuous structures consisting of cm- to tens of cm-sized irregular recrystallized (cemented) lenses commonly enclosed by a mm-thick red hematitic coating (Fig. 6B). A coating is also observed around bioclasts and millimetre- to centimetre-sized lithoclasts (cm- to tens of cm-sized lithoclasts also occur in this microfacies (Fig. 6C)). Similar structures have been termed "nebuloids" by Boulvain (2001). In thin-sections, this microfacies corresponds to an entirely dolomitized rudstone. Large cavities are cemented by mm-sized automorph dolomite, while litho- and bioclasts are constituted of smaller xenomorph to subautomorph dolomite. Locally, a fine-grained red to pink stained dolomite occurs at the base of the cavities (note the slight concave interface between cement and the fine-grained dolomite above the orthoceratid in Fig. 6A and B). Locally ferroan dolomite occurs within the centre of the cavities. Hematite occurs as blisters (sub-millimetre-sized to millimetre-sized) or as coatings around grains. Hematitic coatings are preferentially observed on the border of bio- and lithoclasts, forming two types of structure: (1) submillimetre-sized hematitic clusters separated by drusy calcite cement and (2) notable sub-millimetre-sized iron-bearing dendrites regularly spaced around the surfaces of clasts (Fig. 6C). In closer view (Fig. 6D), dendrites are constituted of branches (0.1–0.5 mm in height and 0.01–0.04 mm in width) becoming wider towards the top and showing thin lamination underlined by alternation of µm wide clear and dark hematitic bands.

4.3.5. MF3: Slightly pink recrystallized crinoidal mudstone–wackestone

This mudstone–wackestone mostly occurs interbedded with MF4 at the top of section GB (Unit 3). It is characterized by an uncommon fauna represented by only a few crinoids (Fig. 5G). The mudstone–wackestone with micritic matrix shows local pseudosparitic ferroan calcite and sparitic ferroan calcite (probably due to the recrystallization of former shells). Crinoids are mostly broken and range from 0.1 to 1 mm (although some reach 4 mm in diameter) and are generally disseminated, but locally they are packed within pluri-millimetre-sized lenses. Saddle dolomite occurs either as isolated crystals or as clusters. Detrital quartz of angular shape ranging from 0.1 to 0.3 mm is present but never reaches as much as 1%. A pressure solution process has produced stylolites. Millimetre- to centimetre-sized geopetal structures fitting with the bedding plane occur within completely recrystallized shells and are constituted of a brown microsparite at the base and a sparry calcite at the top.

4.3.6. MF4: Recrystallized crinoidal mudstone–wackestone with argillaceous bio and/or lithoclastic lenses and stylonodular fabric (Fig. 5H)

This mudstone–wackestone occurs within Unit 2 and in the lower part of Unit 3. It is characterized by a poor faunal diversity (often not determinable), and is dominated by crinoids, which are poorly preserved and are associated with rare broken mm-size brachiopods and recrystallized shells. Crinoids (ossicles or plates) are sub-angular to sub-rounded and mostly range from 0.2 to 1 mm, although some undislocated stems reach 1.5 cm. Crinoid

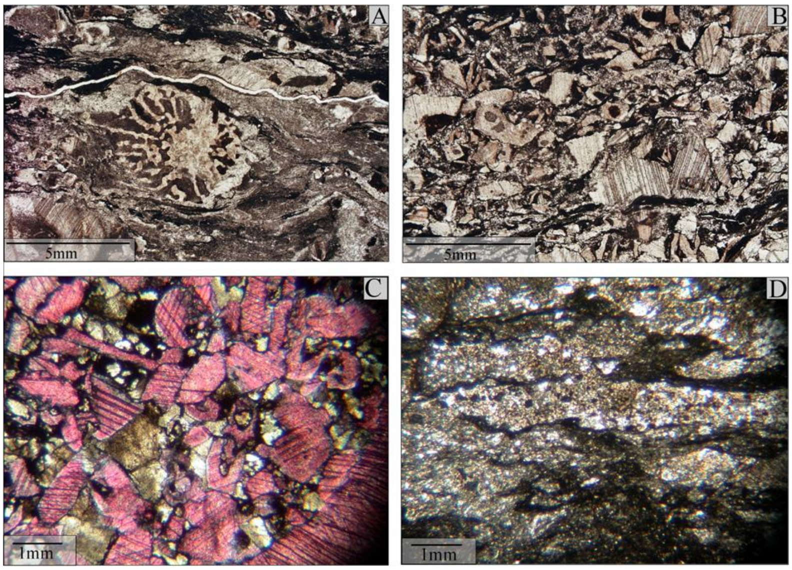

Fig. 7. Microfacies of the Godavari sections. *Numbers in brackets correspond to bed numbers in* Fig 4. See text for explanation. A. MF4 (flank facies): lower part: calcareous sponges (possibly *pharetronid*, Neuweiler F., personal communication) in a microsparitic matrix with crinoids, upper part: argillaceous lenses with bioclasts, thin section (GB03c), normal light. B. MF5 (flank facies): Diagenetic packstone showing important insoluble residues between crinoid grains, thin section (GA11), normal light. C. MF5 (flank facies): Lenses of diagenetically recrystallized crinoidal packstone–grainstone showing dolomitic replacement cement between crinoids, thin section stained by dickson solution (GA14a), normal light. D. MF6 (off-mound facies): Recrystallized argillaceous mudstone showing alternating dark and lighter parts corresponding respectively to microsparite with quartz and clay, thin section (GC1), normal light.

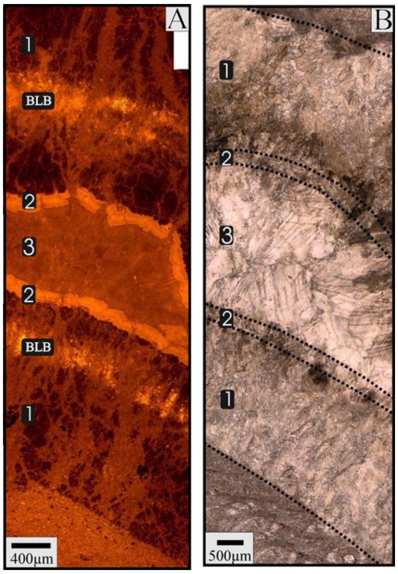

Fig. 8. Diagenetic sequence through cm-sized cavity of MF1a, thin section GE17. A. Cathodoluminescence 1: non luminescent radiaxial calcite cement showing BLB (Bright Luminescent Band) in its central part. 2: Bright luminescent granular calcite slightly zoned in its proximal part. 3: Dull luminescent xenomorphic calcite. B. Normal light.

plates are sub-angular to sub-rounded. Cm-sized crinoid stems are locally concentrated in lenses and regularly display deformed calcite macles. This mudstone–wackestone dominated by a microsparitic feroan matrix to a sparitic ferroan calcite underwent strong pressure solution, which produced stylonodular and stylolaminated fabrics, as well as concavo-convex and sutured contacts, gulfs of dissolution and microstylolithes. Irregular bedding seams and horse tails are also observed. Associated with the pressure solution fabric, a few millimetre- to several centimetre-thick clay lenses occur, containing or not variable proportions of bio- and lithoclasts. Lithoclasts are mostly mm-sized and are constituted by a microsparite to a pseudosparite and rarely by a granular sparite. Lithoclasts are locally pink recrystallized crinoidal mudstone–wackestone (MF3). All the lithoclasts are mainly of angular shape and are always oriented in a bedding-parallel direction. Locally, crinoids, trilobites and sponge spicules (?) are concentrated in lenses but are particularly poorly preserved. A calcareous sponge (possibly *pharetronid*, Neuweiler F., personal communication) (Fig. 7A) is observed. Lenses enriched by clay material show disseminated automorphic ferroan dolomite, with pressure shadows filled with calcite. Sub-angular to sub-rounded detrital quartz ranging from 0.1 to 0.3 mm is observed but never reaches 1% except, episodically, in the form of small lenses (~5 mm) where it can reach 10–15%. Crinoid ossicles or plates are sometimes silicified. Dolomite rhombs within silica replaced crinoids also occur.

4.3.7. MF5: Diagenetically recrystallized crinoidal wackestone–packstone with packstone–grainstone lenses

This microfacies occurs in Unit 3 (sections GA and GB). At the outcrop scale, it corresponds to a bedded purplish limestone, with coarse crinoids, representing up to 60% of the sediment (Fig. 7B). Apart from rare unidentifiable shells, crinoids are the only biological grains observed. Crinoid grains have an average size of around 1 mm (between 0.2 mm and 30 mm). These are often highly broken and are mostly angular to sub-angular. Generally their sorting is low to moderate whereas locally, a good sorting is observed often associated with the packstone–grainstone lenses (Fig. 7C). Locally, within these lenses, crinoids show a rim of syntaxial overgrowth cement. Frequently, crinoids are densely packed and show pressure solution structures such as concavo-convex and sutured contacts. Between these crinoids, insoluble residue, clay and, sporadically, chlorite are observed, while matrix is mostly absent; this corresponds to a "stylocumulate texture" (Logan and Semenuik, 1976). This microfacies is dominated by a wackestone to packstone texture with a matrix commonly recrystallized and mainly constituted of a microsparitic to pseudosparitic ferroan calcite whereas locally, the matrix is less recrystallized and constituted of a dark micrite. Ferroan dolomite is also present as replacement cement within the crinoidal packstone–grainstone lenses (Fig. 7C). Both crinoids and calcite grains display regularly deformed macles.

4.3.8. MF6: Recrystallized mudstone with argillaceous lenses (Fig. 7D)

This mudstone occurs in Unit 1 (section GC and GD). It is dominated by a dark brown microsparitic to pseudosparitic matrix, which shows regularly bedding-parallel anastomosing seams filled with insoluble residue and clay. This mudstone alternates irregularly with clay lenses (devoid of bioclasts) reaching episodically up to 4 cm in thickness. Bioclasts are particularly uncommon in the mudstone and are only represented by rare and completely recrystallized subangular crinoid fragments (~0.4 mm). Detrital quartz (0.03–0.1 mm) is only observed within the mudstone and is mostly disseminated, whereas quartz is able to form small lenses (millimetre-sized).

4.4. Diagenetic sequence in cm-scale cavities of mound facies

Petrographic and cathodoluminescence analyses of stromatactis cavities (cm-sized) mostly observed within MF1a revealed the following diagenetic sequence, from the rim to the centre of the cavity (Fig. 8): (1) non luminescent radiaxial calcite, with a bright luminescent band (BLB) (0.2 mm) in its central part; (2) slightly zoned bright orange luminescent (thin black zonations) automorphic calcite; directly followed by (3) a dull orange luminescent xenomorphic calcite. Locally, within larger cavities, a fourth stage of cement corresponding to a saddle dolomite (4) can be observed. The radiaxial calcite (1) occupies most of the cavities and shows inclusions of microscopic dolomite. Fractures cutting through the whole stromatactis are filled with a dull orange calcite, similar to the cement of stage (3).

5. Discussion – reconstruction of an Ordovician Asian mud-mound

5.1. Interpretation of microfacies – Palaeoenvironments

As stated earlier, deformation and diagenetic processes have modified or even erased some original petrographic features such as sedimentary structures and fossils which made the task of interpretation harder and occasionally hampers to provide well-constraint interpretations. However, meticulous petrographic analysis using different relevant criteria such as faunal association, the nature of the matrix, terrigenous content and the degree of preservation of bioclasts enabled and reinforce the interpretation of the palaeoenvironmental setting of each microfacies in terms of bathymetry and location in a mound model.

5.1.1. Mound facies

5.1.1.1. MF1a – red to pink mudstone–wackestone with stromatactis. One of the main characteristic of MF1a is the abundance of fine micrite indicates a low energy setting, allowing settling of the micritic mud. The fine micritic matrix associated with the small size of bioclasts (~0.4 mm) occurring in MF1a are in favour of a location under the storm wave base (SWB) and a position relatively far from source of bioclasts. The rare mm-sized pockets of packed crinoids may corresponds to a concentration of crinoids via slight turbulence (bottom current) removing part of the micritic matrix. The other main characteristic of this microfacies is the presence of common stromatactis. In various mud-mound studies (James and Bourque, 1992; Bourque and Boulvain, 1993; Bourque, 1997) the common occurence of stromatactis has been interpreted as being related to relatively deep settings. Further, stromatactis mudstone facies of Belgian Frasnian mud-mounds is considered to be the deepest facies of carbonate mud-mounds (Boulvain, 2007). The presence of sponge spicules indicates that the presence of stromatactis could be related to sponge. Indeed, Bourque and Boulvain (1993) described the stromatactis facies from Belgiam Frasnian mounds as rich in sponge spicules and they interpreted the stromatactis as related to sponge tissue decay and partial cementation of organic matter (Bourque and Boulvain, 1993 and Monty, 1995 for a complete discussion on the origin of stromatactis). The very rare occurrence of green algae, as well as their poor preservation, point to a position below the photic zone. Indeed, if this facies was deposited in the photic zone the occurrence of green algae will probably be higher. This could also suggest the occurence of a facies located in the photic zone where green algae were present during the deposition of MF1a. The transport and alteration of these green algae and their redeposition in the area of MF1a could be related either to a slope between both areas or to storm redeposition. This microfacies was probably formed in a location close to the SWB and under the photic zone.

5.1.1.2. MF1b – red to pink bioclastic fenestral wackestone–packstone. The higher bioclast content, mostly crinoids compared to MF1a, supposes either an increase in turbulence allowing a higher crinoid supply or a location closer to the flank facies. A study of the Waulsortian mud-mounds of New Mexico (Bolton et al., 1982) showed that the lower slope of the core facies and proximal flank facies are the major growth sites of crinoids. The close similarity in terms of matrix, fossil, colour and argillaceous content between MF1b and MF1a suggests rather slight and local variations in the environmental setting (i.e. due to turbulence) than a connection to the flank, which may be marked by a change in terms of texture, fossils and argillaceous content. The decrease in the abundance of stromatactis between MF1a and MF1b could be explained by the increase in bioclast content (mainly crinoids) (Hladil et al., 2005) or by the absence (or disarticulation) of sponges.

Both MF1a and MF1b mound facies are characterized by a high micritic content. According to Neuweiler et al. (1999), micrite could be related to three principal modes of accumulation: (1) autochthonous micrite "automicrite" (mineralization related to non-living organic substrates called organomineralization; sponge soft-tissue degradation followed by its calcification forms part of the total automicritic volume); (2) transported micrite "allomicrite", which represents a biodetrital fraction and (3) internal, geopetal carbonate mud, which reduces primary and secondary pore space. In the MF1 microfacies, the presence of sponge spicules, even in low proportion, suggests that a specific percentage of the micrite is related to sponge degradation and thus corresponds to autochthonous micrite. According to Neuweiler et al. (2001), it is most likely that the principal proportion of the micrite occurring in MF1a, MF1b and probably in MF3 is related to organomineralization. Indeed, these authors showed that Palaeozoic carbonate mud-mounds present a low degree of biological sediment recycling (bioerosion, deposit feeding) compared to Meso- and Cenozoic mud-mounds, and this suggests that most of the micrite observed in MF1 is related to non-living organic substrates (organomineralization).

In conclusion MF1a and MF1b are interpreted as being located below the photic zone and the fair weather wave base (FWWB) where MF1a appeared mostly during a quiet period and MF1b appeared in a slightly more turbulent setting.

5.1.1.3. MF2: "Nebuloid" rudstone with orthoceratids and microstromatolites. The abundance of cement occurring in MF2 as well as the common orthoceratids, locally pluri-decimetre-sized, suggest that this microfacies was formed within large cavities. The presence of cavities is supported by the occurence of the fine-grained red to pink dolomite which is considered as internal sediment. The internal origin is attested by the slight concave bend of the dolomite–cement interface above the orthoceratid (Fig. 6A and B)[1]. The red to pink staining of this internal sediment, by comparison to the staining of the micritic sediment occurring in the MF1, may argues that these cavities were developed into the mound facies. An important characteristic of MF2 is the presence of common orthoceratids interpreted as being related to a deep depositional setting (Flügel, 2004). This is in accordance with the relatively deep setting advocated for the MF1a and MF1b. It is important to note that MF2 was only observed, in the present study, on erratic blocks (in the vicinity of the section GE) and polished slabs. This does not allow to confirm that the cavities advocated for this microfacies were developed into the mound facies.

On a smaller scale, a particular characteristic of MF2 is the common occurrence of iron-bearing dendrites, clusters and blisters in the red coating surrounding recrystallized lenses, lithoclasts and bioclasts (Fig. 6C). These structures are suspected to be related to iron-bacterial activity. Indeed, in accordance with the cavity facies of Belgian Frasnian mud-mounds (Mamet and Boulvain, 1988), iron-bearing dentrite-like structures (Fig. 6D and E) were interpreted in the present study as microstromatolites. According to Boulvain (2001), microstromatolites are columnar structures reaching a few mm in height and showing thin internal lamination, often crenulated with an individual thickness oscillating between 4 and 10 μm. Microstromatolites have also been recognized in Devonian carbonate in Morocco (Préat et al., 2008), as well as in Devonian and Carboniferous griottes in France and Spain respectively (Mamet and Boulvain, 1991; Mamet and Perret, 1995). In all these localities, microstromatolites have mostly been interpreted as being related to iron-bacterial activity and to periods of low sedimentation rate. This microfacies was probably formed by the accumulation of sediment and cementation within cavities formed during the growth of the mound.

The red coloured sediment of the three microfacies discussed above (MF1a, MF1b and MF2) is a particular characteristic of the succession studied in the Godavari quarry. By comparison with several studies of Devonian carbonate mud-mounds (Préat et al., 1999a, 1999b; Bourque and Boulvain, 1993; Boulvain et al., 2001) the red colour of MF1a and MF1b and the local red coloured sediment in MF2 suggest the presence of available iron during their deposition. There are three main hypotheses explaining the origin of the ferruginous pigment (for the first two see Boulvain, 1993): (1) trapping of suspended hematite detrital particles on the carbonate mounds (Lecompte, 1936); (2) local production, possibly of microbial origin (Monty et al., 1982; Boulvain et al., 2001) and (3) a post-sedimentary alteration. In our mud-mound complex in Nepal, the red staining of the sediment is heterogeneously disseminated. Indeed, only the mound facies are red stained. This heterogeneous pigmentation through the mound is not in agreement

[1] For interpretation of color in Figs. 5 and 6, the reader is referred to the web version of this article.

with the first hypothese (1). Indeed, if the supply of iron was derived from continent, the homogeneous repartition of it in the epieric sea should be homogeneously deposited and distributed through contemporaneous facies of the mound complex. A nearly similar explanation could be used to refute the third hypotese (3). Indeed, if the post-sedimentary alteration was responsible for the red colour of the sediment, a red staining should also be observed for the flank and off-mound facies sediments.

In respect to the presence of several structures interpreted as being related to biological activity within MF2, such as hematitic clusters blisters and iron-bearing dendrites, the red pigment could easily be explained by a local microbial production (2). Another persuasive argument supporting the biological origin of the red pigment is the correlation between the red colour and the type of facies. Indeed, red coloured sediments only occur within the mound facies corresponding to the higher carbonate production of the Godavari mud-mound complex. The local red pigmentation of the sediments (matrix) could thus reflect the fulfilment of ecological conditions for pigment-producing micro-organisms. In the red Frasnian facies of the Belgian mud-mounds (Pm1 and Pm2, Boulvain, 2001), these pigment-producing micro-organisms exist in four forms: (1) microstromatolites and associated forms (blisters, veils, etc.); (2) hematitic coccoids; (3) hematitic filaments (resembling the iron bacteria *Sphaerotilus–Leptothrix* group); and lastly (4) networks of dichotomic filaments ascribable to fungi. Krumbein (1969) indicates that in desert environments and in soil, fungi play a major role in the precipitation of Mn and Fe. Filamentous fungi are known to be present in marine environments (Kohlmeyer and Kohlmeyer, 1979). These four forms of pigment-producing micro-organisms are known to live in environments where iron is available in reduced forms, but where the redox potential is sufficiently high to allow oxidation. For the red carbonate intervals in the Devonian in Tafilalt (Morocco), Préat et al. (2008) note that the presence of dysoxic conditions favoured the spread of iron-bacteria and fungi at water–sediment interfaces. These conditions induced the precipitation of Fe (and Mn), leading to the red pigmentation of the micritic matrix. Thus, the fulfilment of the ecological conditions for pigment-producing micro-organisms corresponded to an environment depleted of O_2 where iron was available at the time of the development of the red mound facies. Probably due to the diagenesis the iron-encrusted micro-organism have been destroyed in MF1a and MF1b and this does not allow to confirm the iron-bacterial activity for these two microfacies. However, probably due to the early cementation, the iron-bacterial activity is confirmed for the red pigmentation of MF2.

5.1.1.4. MF3 – slightly pink recrystallized crinoidal mudstone–wackestone. The poor faunal assemblage (scarce and broken crinoids, mainly disseminated within a fine micritic matrix) suggests a quiet depositional environment where the settling of mud was the main sedimentary process. The presence of packed crinoid fragments within small lenses may either correspond to a concentration of bioclasts by episodically more energetic periods reworking crinoids from their growing sites (lateral flank facies). This microfacies shows a pink colour and also a fine micritic matrix, which can be compared to the micritic matrix of MF1. These features suggest that the depositional setting of this microfacies is relatively close to the depositional setting of MF1. However, the absence of MF3 in section GE means that the exact link between MF3 and MF1 cannot be identified. The characteristics of MF3 indicate that it is probably located between the FWWB and the storm wave base (SWB).

5.1.2. Flank facies

5.1.2.1. MF4 – diagenetically recrystallized crinoidal wackestone–packstone with crinoidal packstone–grainstone lenses. The abundance of crinoids probably indicates a setting located in the vicinity of crinoidal meadows flanking mounds (Read, 1982). This type of community has been commonly reported on the flanks of Palaeozoic carbonate mounds (Burchette, 1981; Pratt, 1982). The local packstone–grainstone texture which seems, in this case, to be the original texture of the rock (good sorting of crinoids and local presence of crinoids showing a rim of syntaxial overgrowth cement) indicates an environment where agitation is periodically high, probably located around the FWWB. However, the dominant wackestone–packstone texture and the regular occurrence of stylocumulate (indicating an impure limestone), together with the presence of clay lenses, indicates instead an environment located below the FWWB, allowing the deposition of fine particles. The general low to moderate sorting of crinoids confirms this last statement. In conclusion, this microfacies is probably located on the flanks of the mound below the FWWB in a bathymetric position episodically subjected to a higher agitation (storms? grain flow?) leading the occurrence of small packstone–grainstone lenses. Due to the lower argillaceous content compared to MF5, this microfacies is probably located closer to the mound centre.

5.1.2.2. MF5 – recrystallized crinoidal mudstone–wackestone with bio-lithoclastic argillaceous lenses and stylonodular fabric (Fig. 5F). Due to its relative abundance of detrital content (mostly clay), this facies has been preferentially affected by pressure solution processes (Bathurst, 1987). These processes have modified the texture of the microfacies but, locally, the original texture has been preserved. The presence of litho- and bioclasts within argillaceous lenses suggests a reworking of the sediment either during (1) a more energetic event such as storm waves or (2) a downslope transport along the flanks of the mound. Indeed, Read (1982) stated for Virginian Ordovician mud-mounds that "locally steep slopes on flanks of downslope buildups promoted downslope movement of sediment into deeper water environment". However, the occasional presence of argillaceous lenses devoid of bio- and lithoclasts in MF5 suggests a slow deposition of suspended mud by settling on the flank (Flügel, 2004). The presence of undislocated crinoid stems also supports the hypothesis of the existence of low energy conditions. It is also possible that crinoid stems were picked up and transported over short distances by storm waves or currents around and between the growing mounds (Dreesen et al., 1985).

In conclusion, this microfacies seems to indicate either variable energetic conditions or a downslope transport along the flanks of the mound. MF5 may be located around the storm wave zone (SWZ) on the distal flank of the mound where sedimentation is mainly controlled by sediment coming from more proximal flank parts of the mound.

5.1.3. Off-mound facies (surrounding sediment)

5.1.3.1. MF6 – recrystallized mudstone with argillaceous lenses. The particularly fine-grained and terrigenous sediments characterizing this microfacies indicate a low energy setting probably located below the SWB where the main sedimentary process is the settling of suspended particles. The presence of cm-scale clay lenses (without bioclasts) confirms the last hypothesis. This kind of fine-grained sediment is often interpreted as "surrounding sediment" (e.g. Silurian reefs of the Great Lakes area (Textoris and Carozzi, 1964); Middle Devonian mounds of Algerian Sahara (Wendt et al., 1997); Silurian mounds of Gaspé and the Lower Devonian of Sardinia (Gnoli et al., 1981)). The particularly uncommon occurrence of bioclasts within this sediment suggest an environment located far from the mud-mound setting where the influence of the carbonate mound on the bioclasts budget is very low. The lower stratigraphic position of MF6 (off-mound facies, Unit 1) observed in the geological map (Fig. 3) represents another argument in favour of an external depositional setting compared to the mound facies. Indeed, in this geological map, the off-mound sediments (MF6, Unit 1) correspond to the more external position compared to mound facies sediments (mainly Unit 3).

5.2. Microfacies succession – palaeoecological evolution – "determination of mound type"

Each of the five studied sections presents different facies and palaeoenvironments. An analysis of microfacies succession in stratigraphic order (Fig. 4) will provide a better understanding of the relationships between facies in the Godavari carbonate mound and will offer a better understanding of the growth of the mound.

From the base to the top of the mound, the main characteristics of Units 1–4 are the gradual decrease in argillaceous content and the increasing bioclast diversity. Indeed, the base of the section (Unit 1) starts with MF6, characterized by significant argillaceous content and very few bioclasts, suggesting a distal location compared to the mound (surrounding sediments). Further up the section, Unit 2 is mostly characterized by MF5, corresponding to an increase in bioclast content (mostly crinoids) and a decrease in argillaceous material. Parallel to this is the appearance of lithoclasts (originating locally from the mound facies, MF3). This suggests a rapprochement to the buildup (similar interpretations have been made regarding the Belgian Frasnian mound, Boulvain, 2007).

The thick bedded overlying Unit 3 is mainly characterized by the appearance of MF4 (crinoidal wackestone–packstone with crinoidal grainstone lenses) which leads us to suppose a proximity to a crinoidal meadow flanking the mound. Indeed, MF4 shows the highest crinoid content recorded in the Godavary sections. The crinoidal meadow was probably located on the slope of the mound where agitation was occasionally higher, allowing the transport of bioclasts downslope. It is important to note that MF3 (mound facies) characterized by little bioclast content as well as by a pinkish colour and a micritic matrix is locally interbedded in Unit 3. This observation may suggest an environment located in the vicinity of a flank where mound and flank facies are interbedded.

Unit 4 (Fig. 3) is characterized by the presence of typical red stromatactis facies (deep mound), with an alternation between MF1a and MF1b, probably related to a slight variation in turbulence. Considering the thrusted (or faulted) contact between section GE and upper GB, the stratigraphic relationship between these two sections is unknown. Nevertheless, microfacies analysis suggests a relative proximity between two microfacies from section GE (MF1a, MF1b) and the one characterizing the upper part of section GB (MF3). Indeed these three microfacies show a prevalence of a fine red micritic matrix as well as a small amount of clay. This uppermost stratigraphic unit conspicuously corresponds to an environment located in the inner part of a carbonate mud-mound complex where the carbonate production is higher compared to flank and off-mound facies.

The description of facies, the relationships between facies and the facies succession lead us to propose a facies model for the Godavari studied sections (Fig. 9). This model is based on observed geometry (c.f. geological map of Kansakar, 2003; unpublished report), field observations and a comparison with mud-mound models proposed in the literature. The model illustrates the three main types of facies observed in the Godavari sections: the off-mound ("surrounding sediment"; MF6), the flank (MF4, MF5) and the mound (MF1, MF2 and MF3) facies. Almost every environment is associated with one or more lithological units (Fig. 4). Considering the limiting factors listed above (Section 4.1), it is difficult to propose a complete 3D architecture of the mound, such as the dipping of slopes, size and thickness. Nonetheless, the geological map of the quarry (Kansakar, 2003; unpublished report) and the surfaces of already exploited red marble (Unit 4; see Fig. 3), which is approximately 30,000 m^2, suggest that the Godavari mound probably had significant proportions.

Due to the sedimentological features of the mound facies (abundance of micrite, presence of stromatactis, absence of tabulate corals and rugose corals, etc.), it is reasonable to integrate the model proposed above into the "mud" mound category as defined by Riding (2002). Indeed, according to Riding (2002), carbonate mud-mounds are "carbonate mud-dominated (micrite and fine-silt) deposits with topographic relief and few or no stromatolites, thrombolites or in place skeletons". Further, the thick succession of flank facies occurring in the Godavari quarry (section GB) infers that the Godavari mound is a "high relief" carbonate mud-mound. Indeed, flank facies only appear when the mound facies is already sufficiently developed. This statement implies that flank and mound facies are not everywhere contemporaneous and deposited in different bathymetric position. The bathymetric interpretation suggests that the Godavari mound started to grow in a deep environmental setting below the photic and wave action zones and evolved to reach a location below the FWWB.

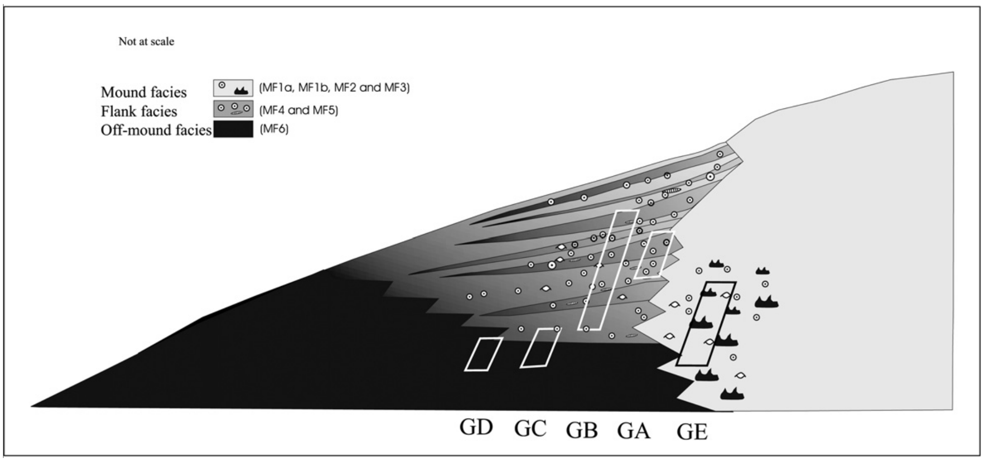

Fig. 9. Sedimentological model for the studied section of the Godavari quarry showing theoretical location of studied sections. Location of sections is based both on observed geometry and on the comparison with other mud-mounds.

5.3. Interpretation of the diagenetic sequence in cm-scale cavities

Petrographic analyses and cathodoluminescence observations of small cavities (cm-sized) observed within the mound facies revealed a particular sequence of cements (Fig. 8): (1) non luminescent radiaxial calcite, with a bright luminescent band (BLB); (2) bright zoned orange luminescent automorphic calcite; (3) a dull orange luminescent xenomorphic calcite and finally (4) saddle dolomite within the core of pluri- centimetre-sized cavities. Interpretation of these cements provides constraints on the evolution of the environment of sedimentation and post sedimentation of the Godavari carbonate mud-mound.

Radiaxial cements (1) have often been observed within Palaeozoic mounds (e.g. Newfoundland (Stenzel and James, 1995); Nevada (Krause, 2001); Australia (Kerans et al., 1986) and Belgium (Boulvain, 1993). This kind of cement was often interpreted as related to a precipitation from marine water (Tucker and Wright, 1990). However, a secondary origin related to the replacement of the primary marine fibrous cements has also been proposed (Kendall and Tucker, 1973; Kerans et al., 1986). The bright luminescent band (BLB) observed within the non luminescent radiaxial calcite is a particular characteristic of this first cementation stage. It probably suggests a decrease in the oxic conditions of marine water during cementation of stage (1). Indeed, the bright luminescence of this band is most probably caused by the presence of Mn^{2+} (the main activator causing cathodoluminescence), which is incorporated into the calcite framework during an increase in the reducing characteristic of fluids. This brighter luminescent band (BLB) could be related to a decrease in the supply of fluids into the cavities. Indeed, a decrease in marine water supply through the mound reduces the oxygen available for the oxidation–decomposition of organic matter present in the mound, and this leads to reduced conditions (and Mn incorporation).

Following radiaxial calcite (1), bright luminescent granular calcite cement with slight zonations occurs (2). Granular calcites are generally not considered as constituting cement of marine origin (Purser, 1980). Zonations observed in stage (2) are related to a fluctuation in the redox condition of diagenetic fluids. These fluctuations have often been interpreted as being associated with a meteoric diagenesis (Mountjoy and Krebs, 1983; Hurley and Lohmann, 1989).

In terms of diagenetic sequence, dull orange luminescence xenomorphic calcite (3) has often been interpreted as being related to a burial diagenesis (Walls and Burrowes, 1985; Boulvain, 1993). Indeed, the dull luminescence is in accordance with an increase in the reducing characteristics of diagenetic fluids, compared to stage (2) (incorporation of Fe^{2+}, the main inhibitor of cathodoluminescence). The dull luminescent network of fractures cutting through stages (1) and (2) is probably contemporaneous to the void-fill deposition of stage (3). Furthermore, the local occurrence of saddle dolomites (4) within larger stromatactis cavities also supports the idea of a burial diagenesis (Flügel, 2004).

Apart from the BLB identified in the radiaxial cement stage (1), the diagenetic evolution of Godavari mound cavities is identical to other Palaeozoic carbonate mounds and banks (Lees and Miller, 1995; Boulvain, 2001); and corresponding to a first cementation stage (cement 1) in the marine phreatic zone followed by a cementation controlled by meteoric water (cement 2) and finally burial cementation (cement 3 and dolomite 4).

5.4. Brief comparison with other Ordovician carbonate mud-mounds

Twelve Mid-Late Ordovician carbonate mud-mounds have been identified throughout the world (Pratt, 1995; Webby, 2002 for a general survey) and only five for the entire Asian continent. Only the most relevant ones have been taken into account in the following comparison. As mentioned before, due to the lack of data concerning geometry and size as well as limiting factors affecting the Godavari mud-mound, this comparison is limited.

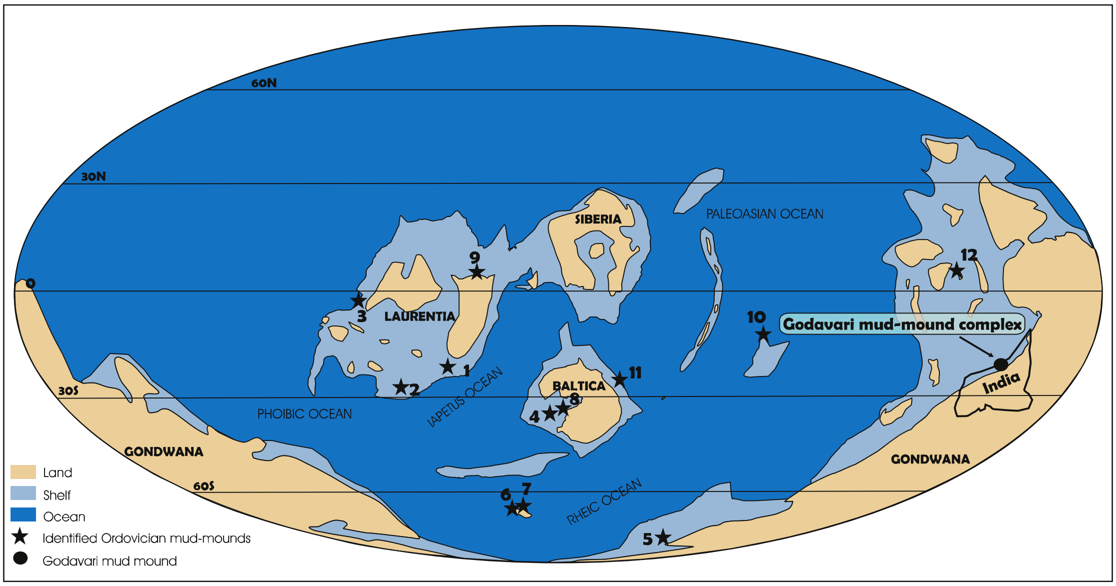

Fig. 10. Palaeogeographic map of the Middle to Late Ordovician (modified after Golonka (2002)) showing the location of the most intensively studied (1–5) Mid-Late Ordovician mud-mounds and of the newly discovered Godavari mud-mound complex. Accessory carbonate mud-mounds (6–12) referenced by Webby (2002) are also located on the map. Locality index (black cross): 1: Western Newfoundland, Canada (Pohler and James, 1989; Stenzel and James, 1995); 2: Virginia Appalachians, USA (Read, 1982); 3: Nevada, USA (Ross, 1977; Krause, 2001); 4: Lake Siljan, Sweden (Schmid et al., 2001); 5: Eastern Iberian Chain, Spain (Vennin et al., 1998).

In several aspects such as the abundance of stromatactis, the mud-dominated matrix, etc., the Godavari carbonate mud-mound resembles certain Mid-Late Ordovician mud-mounds such as those in Virginia (Read, 1982), Nevada (Ross et al., 1975), Sweden (Jaanuson, 1979) and Spain (Vennin et al., 1998).

In the Godavari example, as well as in these Mid-Late Ordovician carbonate mud-mounds, stromatactis is an important constituent. Faunal assemblage of the majority of the Mid-Late Ordovician mounds is dominated by crinoids (~30%) and bryozoans (~25%), compared to the rest of the faunal assemblage (ostracods, trilobites, bivalve shells, brachiopods, algae, and indeterminate items) representing often less than 10%. The Meiklejohn example (Ross et al., 1975) is an exception. Here, bryozoans are almost absent compared to ostracods and crinoids, which represent together nearly 80% of the fossil content. Most of the fossils present in the Mid-Late Ordovician carbonate mud-mounds are also observed in the Godavari mound. However, the faunal assemblage of the Godavari example, in terms of relative abundance is comparable to the Meiklejohn Peak mud-mounds, as crinoids and ostracods are the most abundant, while bryozoans are rare.

5.5. Palaeoenvironment and palaeogeographic reconstruction

The Mid-Late Ordovician age given in this study for the Godavari carbonate mud-mound enabled us to assign an age to the succession exposed in the Godavari quarry and thus to confirm the age of the thick carbonate succession of the Chandragiri Formation. Lithological description of this formation made by Stöcklin (1981, unpublished UNDP report) leads us to suggest a shallow water carbonate platform for the Chandragiri Formation. This is also suggested by Garzanti (1991) for the Nilgiri Formation (lateral equivalent of the Chandragiri Formation), localized in the Dolpo–Manang Synclinorium of the Tibetan-Tethys Zone of Nepal (Fig. 1A). Regarding facies, it is likely that the Godavari carbonate mud-mound grew in the deeper part of the carbonate platform suggested for the Chandragiri Formation. With respect to the palaeogeographic reconstruction made by Garzanti (1991) for the Nilgiri Formation (equivalent of the Chandragiri Formation), the carbonate platform represented by the succession of the Chandragiri Formation was probably localized in the northern epicontinental part of the Indian continent. This northern part belongs to the northern margin of the ancestral Gondwana landmass (Liu and Einsele, 1994). Thus, regarding Golonka's (2002) palaeogeographic reconstruction for the Mid-Late Ordovician period, the area of the Godavari mud-mound was located in the low latitude (0–30° S) of the eastern part of Gondwana. According to the palaeogeographic location pinpointed by Webby (2002) and Krause et al. (2004), the identified Mid-Late Ordovician carbonate mud-mounds are observed in the low latitude region of Laurentia and Baltica, in the higher latitude region of northern Gondwana and on the Avalonia, Kazakhstan and Indochina plates (Fig. 10). The uncommon eastern palaeogeographic location of our Godavari example, compared to most of the other Mid-Late Ordovician examples, is a new component in the distribution of carbonate mud-mounds. The eastern location of the Godavari as well as the Indochina mud-mound (see Fig. 10) is probably not particular in palaeoenvionmental terms but is rather due to the lack of studies in the areas constituting the vast eastern Gondwana regions.

6. Conclusion

This paper presents a sedimentological, diagenetic and palaeoecological analysis of a newly discovered carbonate mud-mound complex in Nepal (Godavari mud-mound). The main conclusions are as follows:

1. In the Godavari quarry, four lithological units were identified, including six microfacies representing a carbonate mud-mound complex. In this mound complex, three major facies were defined: (1) the mound facies, (2) the mound flank facies and (3) the off-mound facies, corresponding to surrounding sediments. The mound facies is characterized by significant micritic content, stromatactis and the prevalence of a red pigmentation of the sediment and is interpreted as being deposited below the SWB and below the photic zone. The origin of the red pigmentation of this facies is not well constrained but observation of preserved microstructures (microstromatolites) resulting from iron precipitating micro-organisms suggests a biological origin for the red pigmentation of the micritic matrix. The mound flank facies differs from the mound facies by an increase in crinoids as well as in argillaceous content and the presence of bio- and lithoclasts within argillaceous lenses. These different characteristics suggest a location in the vicinity of the crinoidal meadow flanking mound, in an intermediate agitation setting; probably between the FWWB and the SWB where reworking of sediments is conducted during either energetic events or downslope transport along the flanks of the mound. The off-mound facies is characterized by the quasi absence of bioclasts and an important terrigenous content (mostly clay), suggesting a location below the SWB where the bioclasts budget from the mound is low.
2. Sedimentological features of the mound facies (abundance of micrite, presence of stromatactis, absence of tabulate corals and rugose corals, etc.) confirm that the facies model proposed for the Godavari studied sections can be integrated into the "mud" mound category as defined by Riding (2002). Further, the thick succession of flank facies occurring in the Godavari quarry (section GB) infers that the Godavari mound is a "high relief" carbonate mud-mound. Finally, bathymetric interpretations suggest that this mound started to grow in an environmental setting located below the photic and wave action zones and that it is likely to grow to reach a location below the FWWB.
3. Identification of two dasycladacean algae (*Dasyporella* cf. *silurica* (Stolley, 1893) and *Vermiporella* sp.) by Ioan Bucur (personal communication) in the mound facies gave a Mid-Late Ordovician age for the succession of the Godavari quarry, which confirms the age of the thick limestone succession of the Chandragiri Formation and makes this mud-mound one of the oldest ever described in the entire Asian continent.
4. Cathodoluminescence analyses of cm-sized cavities localized in the mound facies led us to identify the following cement succession: (1) a non luminescent radiaxial calcite cement formed in the marine phreatic zone (oxic and suboxic) followed by (2) a bright cement related to the incoming of meteoric water, (3) a dull calcite cement formed during burial diagenesis and finally (4) a saddle dolomite cement (within the core of larger stromatactis cavities) also related to burial diagenesis. These four stages of cementation have already been identified in other mounds (Lees and Miller, 1995; Boulvain, 2001) and are typical of a transition from a marine to a burial diagenetic environment.
5. Regarding fossil diversity and lithological features, the Godavari carbonate mud-mound is relatively close to other Mid-Late Ordovician carbonate mud-mounds. The relative proportion of fossils in the mound facies makes this mud-mound mostly comparable to the Meiklejohn Peak mound (Nevada).

Acknowledgments

The Research and Development Administration (ARD) of the University of Liège (ULg) financed the project for fieldwork in Nepal. Additional financial support for this project from the sedimentary petrology laboratory of the University of Liège is gratefully acknowledged. Many thanks to Ioan Bucur (Babes-Bolyai University, Romania) for his help in the identification of algae and to Jean-Marc Baele (Mons-Hainaut University, Belgium) for his support in the cathodoluminescence imaging. We are grateful to Prabin Kayastha for his help during fieldwork and to the management of the Godavari quarry for giving us permission to study the section and for providing us a geological report. A.-C. da Silva acknowledges the Belgian National Science Foundation (FRS–FNRS) for her postdoctoral research position. Substantial improvements from an earlier manuscript resulted from the thoughtful anonymous reviews.

References

Amatya, K.M., Jnawali, B.M., 1994. Geological Map of Nepal. Scale: 1:1,000,000. Published by Department of Mines and Geology, Kathmandu, Nepal.
Auden, J.B., 1935. Traverses in the Himalaya. Records of the Geological Survey of India 62 (2), 123–167.
Bathurst, R.G.C., 1987. Diagenetically enhanced bedding in argillaceous platform limestones: stratified cementation and selective compaction. Sedimentology 34, 749–778.
Bolton, K., Lane, H.R., Le Mone, D.V., 1982. Symposium in paleoenvironmental setting and distribution of Waulsortian facies. El Paso Geological Society and the University of Texas, 202p.
Bordet, P., Cavet, P., Pillet, J., 1960. La faune Silurienne de Phulchauki près de Katmandou (Himalaya du Népal). Bulletin de la Société Géologique de France 7, 3–14.
Bordet, P., Colchen, M., Krummenacher, D., Le Fort, P., Mouterde, R., Remy, M., 1971. Recherches Géologiques dans l'Himalaya du Népal: Région de la Thakkhola. Editions du Centre National de la Recherche Scientifique, Paris, p. 279.
Boulvain, F., 1993. Sédimentologie et diagenèse des monticules micritiques frasniens "F2j" de l'Ardenne. Professional Paper of the Geological Survey of Belgium 260, 427p.
Boulvain, F., 2001. Facies architecture and diagenesis of Belgian Late Frasnian carbonate mounds. Sedimentary Geology 145, 269–294.
Boulvain, F., 2007. Frasnian carbonate mounds from Belgium: sedimentology and paleoceanography. In: Alvaro, J.J., Aretz, M., Boulvain, F., Munnecke, A., Vachard, D., Vennin, E. (Eds.), Paleozoic Reefs and Bioaccumulations: Climatic and Evolutionary Controls. Geological Society of London, pp. 124–142 (Special Publication 275).
Boulvain, F., De Ridder, Ch., Gillan, D., Mamet, B., Préat, A., 2001. Iron microbial communities in Belgium Frasnian carbonate mounds. Facies 44, 47–60.
Bourque, P.-A., 1997. Paleozoic finely crystalline carbonate mounds: cryptic communities, petrogenesis and ecological zonation. Facies 36, 250–253.
Bourque, P.A., Boulvain, F., 1993. A model for the origin and petrogenesis of the red stromatactis limestone of Paleozoic carbonate mounds. Journal of Sedimentary Petrology 63, 607–619.
Burchette, T.P., 1981. European Devonian reefs: a review of current concepts and models. In: Toomey, D.F. (Ed.), European fossil reef models. SEPM Special Publication 25, pp. 5–17.
Choquette, P.W., James, N.P., 1987. Diagenesis, 12, diagenesis in limestone-3, the deep burial environment. Geoscience Canada 14, 3–34.
Dickson, J.A., 1965. A modified staining technique for carbonate in thin section. Nature 205, 587.
Dreesen, R., Bless, M.J.M., Conil, R., Flajs, G., Laschet, C., 1985. Depositional environment, paleoecology and diagenesis history of the "marbre rouge a crinoids de Baelen" (Late Upper Devonian, Verviers Synclinorium, Eastern Belgium). Annales de la Société Géologique de Belgique 108, 311–359.
Dunham, R.J., 1962. Classification of carbonate rocks according to depositional texture. American Association of Petroleum Geologists Memoir 1, 108–121.
Embry, A.F., Klovan, J., 1972. Absolute water depth limits of Late Devonian paleoecological zones. Geologische Rundschau 61, 672–686.
Flügel, E., 2004. Microfacies of Carbonates Rocks: Analysis, Interpretation and Application. Springer, Berlin, 976p.
Fuchs, G., Widder, R.W., Tuladhar, R., 1988. Contributions to the Geology of the Annapurna Range (Manang Area, Nepal). Jahrbuch der Geologischen Bundesanstalt 131, 593–607.
Funakawa, S., 2001. Lower Paleozoic Tethys sediments from the Kathmandu Nappe, Phulchauki area, central Nepal. Journal of Nepal Geological Society 25, 123–134 (Special Publication).
Garzanti, E., 1991. Non-carbonate intrabasinal grains in arenites: their recognition, significance and relationship to eustatic cycles and tectonic setting. Journal of Sedimentary Petrology 61, 959–975.
Gnoli, M., Jaanusson, V., Leone, F., Serpagli, E., 1981. A lower Devonian stromatactis-bearing carbonate mound from southern Sardinia. Jahrbuch *für* Geologie und Paläontologie Mh. 6, 339–345.
Golonka, J., 2002. Plate-Tectonic maps of the Phanerozoic. In: Kiessling, W., Flügel, E., Golonka, J. (Eds.), Phanerozoic Reef Patterns. SEPM Special Publication 72, pp. 21–75.
Hagen, T., 1951. Preliminary Note on the Geological Structure of Central Nepal. Verhandlungen der Schweizerischen Naturforschenden Gesellschaft, Luzern, pp. 133–134.
Hagen, T., 1969. Report on Geological Survey of Nepal, vol. 1. Preliminary Reconnaissance, Zurich, Denkschriften der Schweizerischen Naturforchenden Gesellschaft, Memoires de la Societé Helvetique des Sciences Naturelles 86, p. 185.
Hladil, J., Ruzicka, M., Koptikova, L., 2005. The formation of stromatactis structures during the sedimentation of experimental slurries – a possible clue to a 120-year-old puzzle about stromatactis. Bulletin of Geosciences 80 (3), 193–211.
Hurley, N.F., Lohmann, K.C., 1989. Diagenesis of Devonian reefal carbonates in the Oscar Range, Canning Basin, Western Australia. Journal of Sedimentary Petrology 59 (1), 127–146.
Jaanuson, V., 1979. Karbonatnye postroyki v. ordovike shvetsii [Carbonate mounds in the Ordovician of Sweden]. Izvestiya Rossiiskoi Akademii Kazakh CCP. Service Geology 4, 92–99.
James, N.P., Bourque, P.A., 1992. Reefs and mounds. In: Walker and James (Eds.), Facies Models Response to Sea-Level Change. Geological Association of Canada, pp. 323–347.
Kansakar, D.R., 2003. Report on the Geological Assessment of the Godavari Marble Industry Quarry Lease Area, Godavari, Lalitpur District (unpublished).
Kendall, A.C., Tucker, M.E., 1973. Radiaxial fibrous calcite: a replacement after acicular carbonate. Sedimentology 20, 365–389.
Kerans, C., Hurley, N.F., Playford, P.E., 1986. Marine diagenesis in Devonian reef complexes of Canning Basin, Western Australia. In: Schroeder, J.H., Purser, B.H. (Eds.), Reef Diagenesis. Springer-Verlag, pp. 357–380.
Kohlmeyer, J., Kohlmeyer, E., 1979. Marine Mycology: The Higher Fungi. Academic Press, New-York, p. 690.
Krause, F.F., 2001. Genesis and geometry of the Meiklejohn Peak lime mud-mound, Bare Mountain Quadrangle, Nevada, USA: Ordovician limestone with submarine frost heave structures – a possible response to gas clathrate hydrate evolution. Sedimentary Geology 145, 189–213.
Krause, F.F., Scotese, C.R., Nieto, C., Sayegh, S.G., Hopkins, J.C., Meyer, R.O., 2004. Paleozoic stromatactis and zebra carbonate mud-mounds: global abundance and paleogeographic distribution. Geological Society of America 32, 181–184.
Krumbein, W.E., 1969. Über den Einfluss de Mikroflora auf die Exogen Dynamik (Verwitterung und Krustenbildung). Geologische Rundschau 58, 63–333.
Lecompte, M., 1936. Contribution à la connaissance des récifs du Dévonien de l'Ardenne. Mémoire de l'Institut Géologique de l'Université Catholique de Louvain 10, 30–113.
Lees, A., Miller, J., 1995. Waulsortian banks. In: Monty, C.L.V., Bosence, D.W.J., Bridges, P.H., Pratt, B.R. (Eds.), Carbonate Mud-Mounds: Their Origin and Evolution. International Association of Sedimentologists, pp. 191–271 (Special Publication 23).
Liu, G., Einsele, G., 1994. Sedimentary history of the Tethyan basin in the Tibetan Himalaya. Geologische Rundschau 83, 32–61.
Logan, B.V., Semenuik, V., 1976. Dynamic Metamorphism: Processes and Products in Devonian Carbonate Rocks, Canning Basin, Western Australia. Geological Society of Australia, p. 138 (Special Publication).
Mamet, B., Boulvain, F., 1988. Remplissage bactérien de cavités biohermales frasniennes. Bulletin de la Société Belge de Géologie 97, 63–78.
Mamet, B., Boulvain, F., 1991. Construction hématitiques des griottes carbonifères (Asturies, Espagne). Bulletin de la Société Belge de Géologie 99, 229–239.
Mamet, B., Perret, C., 1995. Bioconstructions hématitiques de Griottes dévoniennes (*Pyrénées centrales*). Géobios 28, 655–661.
Monty, C.L.V., 1995. The rise and nature of carbonate mud-mounds: an introductory actualistic approach. International Association of Sedimentologists 23, 11–48 (Special Publication).
Monty, C.L.V., Bernet-Rollande, M.C., Maurin, A.F., 1982. Re-interpretation of the Frasnian classical "reefs" of the southern Ardennes, Belgium. Annales de la Société Géologique de Belgique 105, 339–341 (Extended Abstract).
Mountjoy, W., Krebs, W., 1983. Diagenesis of Devonian reefs and buildups, Western Canada and Europe—a comparison. Zeitschrift der Deutsche Geologische Gesellschaft 134, 5–60.
Neuweiler, F., Bourque, P.A., Boulvain, F., 2001. Why is stromatactis so rare in Mesozoic carbonate mud mounds? Terra Nova 13, 338–346.
Neweiler, F., Gautret, P., Thiel, V., Langes, R., Michaelis, W., Reitner, J., 1999. Petrology of Lower Cretaceous carbonate mud mounds (Albian, N. Spain): insights into organomineralic deposits of the geological record. Sedimentology 46, 837–859.
Pettijohn, F.J., Potter, P.N., Siever, R., 1972. Sand and Sandstone. Springer, Berlin, p. 618.
Pohler, S.M.L., James, N.P., 1989. Reconstruction of a Lower/Middle Ordovician carbonate shelfmargin: cow head group, western newfoundland. Facies. 21, 189–262.
Poncet, J., 1986. Les algues calcaires du Paléozoïque inférieur de la Baie d'Hudson et de l'Archipel arctique canadien. Bulletin du Centres Recherche Exploration.-Production. Elf-Aquitaine 10 (2), 259–282.
Pratt, B.R., 1982. Stromatolitic framework of carbonate mud mounds. Journal of Sedimentary Geology 52 (2), 1203–1227.
Pratt, B.R., 1995. The origin, biota and evolution of deep-water mud-mounds. International Association of Sedimentologists 23, 49–123 (Special Publication).
Préat, A., Mamct, B., Bernard, A., Gillan, D., 1999a. Rôle des organismes microbiens dans la formation des matrices rougeâtres Paléozoïques: exemple du Dévonien, Montagne Noire. Revue de Micropaléontologie 42, 161–182.

Préat, A., Mamet, B., Bernard, A., Gilan, D., 1999b. Bacterial mediation, red matrices diagenesis, Devonien, Montagne Noire (southern France). Sedimentary Geology 126, 223–243.

Préat, A., El Hassani, A., Mamet, B., 2008. Iron bacteria in Devonian carbonates (Tafilalt, Anti-Atlas, Morocco). Facies 54, 107–120.

Purser, B.H., 1980. Sédimentation et Diagenèse des Carbonates Néritiques Récents. Tome1: Les Éléments de la Sédimentation et de la Diagenèse. Technip, Paris, p. 367.

Read, J.F., 1982. Geometry, facies, and development of middle Ordovician carbonate buildups, Virginia Appalachians. American Association of Petroleum Geologist Bulletin 66, 189–192.

Riding, R., 2002. Structure and composition of organic reefs and carbonate mud mounds: concept and categories. Earth-Sciences Reviews 58, 163–231.

Riding, R., Fan, J., 2001. Ordovician calcified algae and cyanobacteria, northern Tarim bassin subsurface, China. Paleontology 44, 783–810.

Ross, R.J.J., Jaanusson, V., Friedman, I., 1975. Lithology and Origin of Middle Ordovician Calcareous Mudmound at Meiklejohn Peak, Southern Nevada. Professional Paper. US Geological Survey 871, 48p.

Ross, R.J.J., 1977. Ordovician paleogeography of the western United States. In: Stewart, J.H., Stevens, C.H., Fritsche, A.E. (Eds.), Paleozoic Paleogeography of the Western United States, Pacific Coast Paleogeography Symposium 1. Society of Economic Paleontologists and Mineralogists, pp. 19–38.

Schmid, D., Leinfelder, R., Nose, M., 2001. Growth dynamics and ecology of Upper Jurassic mounds, with comparisons to Mid-Paleozoic mounds. Sedimentary Geology 145, 343–346.

Stenzel, S.R., James, N.P., 1995. Shallow-water stromatactis mud-mounds on a Middle Ordovician foreland basin platform, western Newfoundland. International Association of Sedimentologists 23, 127–149 (Special Publication).

Stöcklin, J., 1980. Geology of Nepal and its regional frame. Journal of the Geological Society of London 137, 1–34.

Stöcklin, J., Bhattarai, K.D., 1977. Geology of the Kathmandu area and central Mahabharat Range, Nepal Himalaya. In: Himalaya Report Department of Mines and Geology Kathmandu Nepal, New York, 86p (unpublished).

Stöcklin, J., Bhattarai, K.D., 1981. Geology of the Kathmandu area and central Mahabharat Range, Nepal Himalaya. In: Report of the Department of Mines and Geology/UNDP, New York, 64p (unpublished).

Stöcklin, J., Termier, G., Bhattarai, K., 1977. A propos des roches fossilifères de Chandragiri (Mahabharat, Himalaya du Nepal). Bulletin de la Société Géologique de France 7, 367–373.

Stolley, E., 1893. Ueber silurische Siphoneen. Neues Jahrbuch *für* Mineralogie, Geologie und Paläontologie 2, 135–146.

Textoris, D.A., Carozzi, A.V., 1964. Petrography and development of Danian bryazoan biomicrite mounds (Karlby Klint, Denmark). Sedimentology 23, 485–509.

Tucker, M.E., Wright, V.P., 1990. Carbonate Sedimentology. Blackwell Science, Oxford.

Upreti, B.N., 1999. An overview of the stratigraphy and tectonics of the Nepal Himalaya. Journal of Asian Earth Sciences 17, 577–606.

Upreti, B.N., Le Fort, P., 1999. Lesser Himalayan crystalline nappes of Nepal: problem of their origin. In: Macfarlane, A., Quade, J., Sorkhabi, R. (Eds.), Geological Society of America Special Paper 328, pp. 225–238.

Vennin, E., Álvaro, J.J., Villas, E., 1998. High latitude pelmatozoan–bryozoan mud-mounds from late Ordovician northern Gondwana platform. Geological Journal 33, 121–140.

Walls, R.A., Burrowes, G., 1985. The role of cementation in the diagenetic history of Devonian Reefs, Western Canada. In: Schneidermann, N., Harris, P.M. (Eds.), Carbonate Cements. SEPM Special Publication 36, pp. 185–220.

Wanless, H.R., 1979. Limestone response to stress: pressure solution and dolomitization. Journal of Sedimentary Petrology 49, 437–462.

Webby, 2002. Patterns of Ordovician reef development. In: Kiessling, W., Flügel, E., Golonka, J. (Eds.), Phanerozoic Reef Patterns. SEPM Special Publication 72, pp. 129–179.

Wendt, Z., Belka, B., Kaufmann, R., Kostrewa Hayer, J., 1997. The world's most spectacular carbonate mud mounds (Middle Devonian, Algerian Sahara). Journal of Sedimentary Research 67, 424–436.

The astronomical calibration of the Givetian (Middle Devonian) timescale (Dinant Synclinorium, Belgium)

DAVID DE VLEESCHOUWER[1]*, FRÉDÉRIC BOULVAIN[2], ANNE-CHRISTINE DA SILVA[2], DAMIEN PAS[2], CORENTIN LABAYE[2] & PHILIPPE CLAEYS[3]

[1]*MARUM – Center for Marine Environmental Sciences, Leobener Straße, D-28359 Bremen, Germany*

[2]*Pétrologie sédimentaire, B20, Université de Liège, Sart Tilman, B-4000 Liège, Belgium*

[3]*Earth System Sciences, Vrije Universiteit Brussel, Pleinlaan 2, B-1050 Brussels, Belgium*

**Corresponding author (e-mail: ddevleeschouwer@marum.de)*

Abstract: Recent advances in radiometric dating result in significant improvements in the geological timescale and provide better insight into the timing of various processes and evolutions within the Earth's system. However, no radiometric ages are contained within the Givetian. Consequently, the absolute ages of the Givetian Stage boundaries, as well as the stage's duration, remain poorly constrained. As an alternative, the analysis of sedimentary cycles allows for the estimation of the duration of this stage. We examined the high-resolution magnetic susceptibility signals of four Givetian outcrops in the Givet area for a possible astronomical imprint, to fully understand the rates of evolutionary and environmental change. All four sections are firmly correlated and wavelet analyses of the magnetic susceptibility signals reveal the imprint of astronomical eccentricity forcing. The highly stable 405 kyr cycles constrain the duration of the Givetian Stage at 4.35 $\pm$ 0.45 Myr, which is in good agreement with the International Chronostratigraphic Chart (5.0 Myr). The studied sections also exhibit an imprint of obliquity, suggesting a climatic teleconnection between low and high latitudes. The corresponding microfacies curves demonstrate similar astronomical imprint, and thereby indicate that the observed 10^5 year-scale cyclicity is the result of climatic and environmental change.

The Devonian period (*c.* 419.2–358.9 Ma; Gradstein *et al.* 2012) was a time of fundamental changes in both marine and terrestrial environments. During the Silurian and Early Devonian, land plants were still restricted to the outskirts of water bodies. However, by the Middle Devonian, arborescent vegetation developed an amazing complexity and successfully occupied various terrestrial ecosystems, forming the earliest forest (e.g. Stein *et al.* 2007, 2012; Mintz *et al.* 2010). In the marine realm, equally important events took place, including the appearance of air-breathing lungs, leading to the fish–tetrapod transition (Clack 2007, 2009), and the development of internal fertilization (Long *et al.* 2008, 2009). Despite these crucial events in the evolution of life on Earth, a reliable high-precision chronology for the Devonian is still lacking. Indeed, both accuracy and precision of the Devonian timescale are debated, as over recent years different authors have produced rather dissimilar chronologies, albeit all based on virtually the same set of a very limited number of radiometric ages (Gradstein *et al.* 2004; Kaufmann 2006; Becker *et al.* 2012). As a consequence, it remains extremely difficult to obtain a detailed understanding of the timing, magnitude and duration of geological events in the Devonian. The Givetian Stage can be considered the exponent of the Devonian timescale since it does not contain a single radiometric age. In recent Devonian timescales (Kaufmann 2006; Becker *et al.* 2012), the age of the Givetian Stage boundaries is estimated by linear interpolation between the Eifelian Tioga Ash bed B (390.0 $\pm$ 2.5 Ma; Klapper 1971; Roden *et al.* 1990) and the Frasnian Belpre Ash (381.1 $\pm$ 3.3 Ma; Tucker *et al.* 1998; Rotondo & Over 2000). It goes without saying that the Givetian chronology is extremely poorly resolved when taking into account the broad error bars on these radiometric ages, the stratigraphic uncertainty and the dubiousness of the relative spans of biostratigraphical conodont zones within each (sub)stage.

As an additional chronometer, next to chrono- and biostratigraphy, a cyclostratigraphic approach offers the opportunity to estimate the duration of a particular (sub)stage, conodont zone or geological event. The inclusion of cyclostratigraphic methods in the construction of timescales has resulted in the most precise and high-resolution Cenozoic and Mesozoic timescales (e.g. Lourens *et al.* 2004; Meyers 2008; Meyers *et al.* 2012). Only a few astrochronological studies have addressed Palaeozoic greenhouse periods such as the Devonian (Bai 1995; House 1995; Chlupáč 2000; Chen & Tucker 2003; Ellwood *et al.* 2011*a*, *b*; Garcia-Alcalde *et al.* 2012; De Vleeschouwer *et al.* 2012*b*, 2013). Two of these studies estimated the duration of the Givetian by counting astronomically forced sedimentary cycles: House (1995) estimated the Givetian duration at 6.5 Myr, assuming that the dominant microcyclicity at the Pic de Bissous (southern France) is forced by climatic precession. Unfortunately, when making an astrochronologic estimate of the duration of a stage, one should avoid counting precessional cycles. The reason for this is twofold: first, the precessional cycle does not have a stable periodicity, and second, the amplitude of climatic precession is very small (and thus indiscernible) under periods of low eccentricity. Ellwood *et al.* (2011*b*) estimated the Givetian duration at 5.6 Myr, by identifying fourteen 405 kyr eccentricity cycles in four different sections, including the two Givetian GSSP sections. However, several problems arise with the correlation between their studied sections. First, the base of the AKZO Core (Western New York) is ascribed to their MS Zone 'Gv5'. By doing this, Ellwood *et al.* (2011*b*) assume that the base of the AKZO Core precisely corresponds to the top of the Eifelian–Givetian GSSP section (Mech Irdane, Morocco). However, the authors do not provide any argument to justify the fact that they assume that both sections perfectly align. Of course, this assumption is highly debatable, as one needs different undisputed points of correlation to firmly correlate two sections. This clearly is not the case in the work of Ellwood *et al.* (2011*b*), as the AKZO core and the Mech Irdane section do not stratigraphically overlap (figure 10 in Ellwood *et al.* 2011*b*). Second, none of the four selected sections covers their MS Zone 'Gv22': in the AKZO Core, the last MS Zone before the major unconformity is 'Gv21', while the first MS Zone in the Tully Composite (New York) is 'Gv23' (figures 7 and 8 in Ellwood *et al.* 2011*b*). In other words, the authors recognize that there is a stratigraphic interval missing and they assume that it lasted for 200 kyr. However, no arguments for this assumption can be found in their paper. Third, the correlation between the 'New York Composite dataset' (i.e. the combination of the AKZO Core and the Tully Composite) and the Givetian–Frasnian GSSP is based on only 25 magnetic susceptibility values in the latter section (figures 4 and 10 in Ellwood *et al.* 2011*b*). This seems rather limited to correlate two sections from entirely different palaeolocations and environmental settings.

In this study, we estimate the Givetian duration by counting the extremely stable 405 kyr eccentricity cycles in four firmly correlated sections from the Dinant Synclinorium (southern Belgium). Correlation amongst the studied sections is considered accurate because of well-studied litho- and biostratigraphy in the historical type area of the Givetian. Also, magnetic susceptibility has proven to allow for high-resolution correlations in this area (Da Silva & Boulvain 2006; Mabille & Boulvain 2007; Boulvain *et al.* 2010*a*). Also the stratigraphic position of the Eifelian–Givetian and Givetian–Frasnian Stage boundaries is relatively well known thanks to the long biostratigraphic tradition in the Givet area. The latter, combined with the high-resolution magnetic susceptibility (MS) dataset that is available for this region, bear a high cyclostratigraphic and astrochronologic potential.

Geological setting

The present cyclostratigraphic study is based on existing magnetic susceptibility data from four different sections in the Dinant Synclinorium (Fig. 1). Combined, these four sections include limestones and shales from the uppermost Eifelian to the lower Frasnian. The Givetian Stage in the study area is depicted by the main part of the Hanonet Formation (Fm), the Trois-Fontaines Fm, the Terres d'Haurs Fm, the Mont d'Haurs Fm, the Fromelennes Fm and the lowest part of the Nismes Fm (Preat *et al.* 2006). The Eifelian–Givetian boundary is characterized by a mixed detrital–carbonate outer ramp, followed by a well-developed Givetian carbonate platform with environments ranging from external crinoidal facies to stromatoporoid-dominated biostromes and lagoonal facies. The demise of the carbonate factory and the generalization of argillaceous sedimentation marks the beginning of the Frasnian (Nismes Fm; Boulvain *et al.* 2010*b*).

The 'La Couvinoise' section (50°03′38″N, 4°29′18″E) exposes 85 m of the Hanonet Fm, and contains the Eifelian–Givetian boundary. This section has been subjected to detailed sedimentological and cyclostratigraphic studies and provides good knowledge of facies, environmental and sea-level variations (Mabille & Boulvain 2007; De Vleeschouwer *et al.* 2012*a*). The 'Monts de Baileux' section (50°02′25″N, 4°23′37″E) exposes a succession of strata from the Hanonet Fm to the base of the Mont d'Haurs Fm, and also encompasses the Eifelian–Givetian boundary (Mabille & Boulvain 2008). It has been firmly correlated with the 'La Couvinoise' section based on sedimentology (Mabille & Boulvain 2007) and cyclostratigraphy (figure 10 in Da Silva *et al.* 2013). The 'Fromelennes–Flohimont' section (50°07′06″N, 4°51′25″E) is more than 450 m thick, and covers all Givetian formations except the Hanonet Fm. Its sedimentology is well studied (Boulvain *et al.*

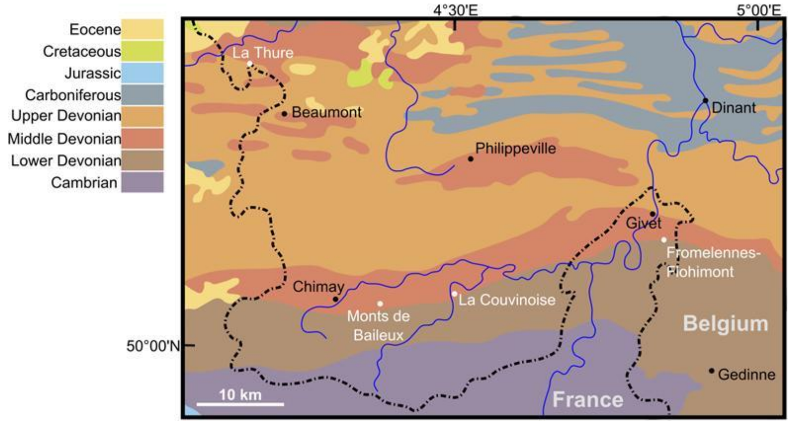

Fig. 1. Geological map of the Dinant Synclinorium and location of the four studied sections.

2009, 2010*b*), and the correlation to 'Monts de Baileux' is straightforward thanks to the highly parallel MS variations (Fig. 2). However, the many sampling breaks in the upper part of the 'Fromelennes–Flohimont' section limit the suitability for cyclostratigraphy between 400 and 550 m. However, in this stratigraphic interval, the 'La Thure' section (50°17′11″N, 4°09′40″E) provides a very detailed and continuous sampling. The correlation between the 'La Thure' and 'Fromelennes–Flohimont' sections is based on lithostratigraphy and the MS signal.

Conodont faunas are generally sparse in the study area, considering that most of these Givetian

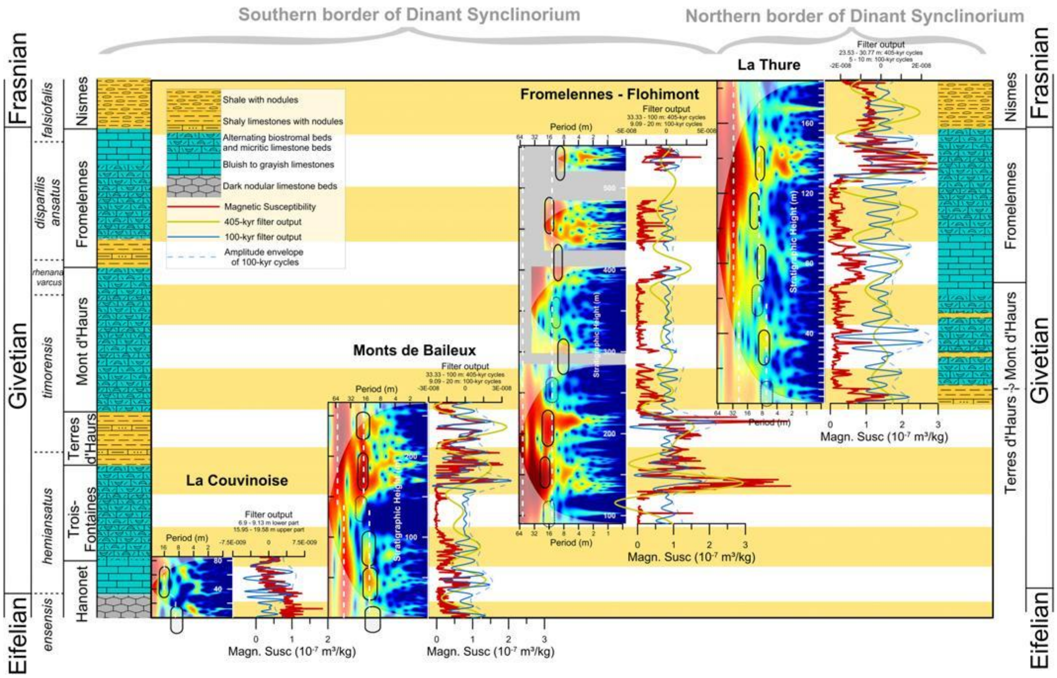

Fig. 2. Cyclostratigraphic interpretation of the continuous wavelet transforms (CWT) of the studied magnetic susceptibility signals. For each section, the magnetic susceptibility signal is plotted in red, along its CWT. On the CWT, the frequency range of 405 and 100 kyr eccentricity is denoted by a white dashed line. For the 100 kyr cycles, the rounded rectangles suggest zones of increased spectral power during 405 kyr maxima, caused by amplitude modulation of the 100 kyr cycles by 405 kyr eccentricity. Based on the filter outputs, alternating orange and white horizontal bands delineate the 405 kyr eccentricity cycles. Based on this figure, the Givetian contains 10.75 such cycles, that is, 4.35 Myr.

sections are dominated by shallow-water facies. Nevertheless, they permit correlation with the Givetian conodont Standard zonation (Bultynck 1987; Gouwy & Bultynck 2003). *Polygnathus hemiansatus*, the index species for the base of the Givetian, occurs near the top of the lower part of the Hanonet Fm in the 'La Couvinoise' section (Bultynck & Hollevoet 1999). Also *Icriodus oblquimarginatus* first occurs at this level, 35 m above the base of the 'La Couvinoise' section. The uncertainty on this position of the Eifelian–Givetian boundary is rather confined, as conodont samples were collected at *c.* 2 m intervals in this part of the section (Bultynck & Hollevoet 1999). Therefore, in the present study, we put the Eifelian–Givetian boundary at 35 ± 2 m for the 'La Couvinoise' section. The base of the Frasnian Stage is defined by the first occurrence of the conodont *Ancyrodella rotundiloba*. Bultynck *et al.* (1988) observed the first appearance of this species *c.* 1.5 m above the base of the Nismes Fm in multiple sections in the Dinant Synclinorium. Recently, however, the Givetian–Frasnian boundary in the study area was displaced to a slightly lower stratigraphic position, based on concomitant changes in ostracod assemblages and microfacies (Casier & Préat 2009; De Vleeschouwer *et al.* 2010). The consistent position of the Givetian–Frasnian boundary, just above the base of the Nismes Fm, in numerous studied sections within the Dinant Synclinorium, allows us to place the Givetian–Frasnian boundary at this specific stratigraphic level in the La Thure section (Coen-Aubert & Boulvain 2006). We put the Givetian–Frasnian boundary in the 'La Thure' section 1 m above the base of the Nismes Fm. Given the extensive biostratigraphic documentation and rich conodont faunas of the Nismes Fm, the uncertainty on the stratigraphic position of the Givetian–Frasnian boundary in the 'La Thure' section is conservatively put at 155 ± 2 m.

Methodology

The cyclostratigraphy presented in this study is based on the MS values of 2134 samples, from four different sections, over 1076 m of stratigraphic section. For each sample, three MS measurements were performed on a KLY-3 kappabridge device at the University of Liège (Belgium). The presented MS value is the average of the three measurements, and has been divided by the sample mass (0.01 g precision) to obtain the mass-specific MS.

The MS signal in marine sedimentary rocks is considered a proxy for the supply rate of the magnetic susceptible lithogenic or detrital fraction to the marine system (Ellwood *et al.* 2000). Therefore, MS is often used as a climatic and environmental proxy. However, diagenesis, remagnetization and low-grade metamorphism can potentially obscure the original, depositional MS signal, especially in Palaeozoic rocks. Da Silva *et al.* (2013) and Mabille & Boulvain (2007) demonstrated that, in most Devonian sections in Belgium, a good relationship exists between MS trends and facies evolution and between MS and geochemical proxies for detrital inputs, despite a remagnetization event described for the Devonian of Belgium (Zegers *et al.* 2003). This relation was observed, among others, for the 'La Couvinoise' and 'Monts de Baileux' sections, which are considered in this study. In other words, despite a diagenetic impact and remagnetization, primary palaeoenvironmental information is still contained by the magnetic susceptibility signal. Hence, this study can with confidence rely on MS as a proxy for climatic and environmental change and assess the potential imprint of the astronomical cycles.

The potential imprint of the astronomical cycles into the MS signals is evaluated using the continuous wavelet transform (CWT). The CWT is used to decompose a one-dimensional magnetic susceptibility time-series into its two-dimensional time-frequency representation. This method reveals the persistency of (astronomical) periodicities along the studied sections and provides a tool to detect variations in accumulation rate through associated changes in cycle thickness. Wavelet software was provided by Torrence & Compo (1998), using the Morlet wavelet function with wave number 6, zero-padding to the next higher power of 2, spacing between discrete scales $(\Delta j) = 0.25$, smallest scale $(S_0) = 2\Delta t$, and number of scales $= (\log_2(N\Delta t/S_0)/\Delta j) + 1$.

Multitaper method (MTM) spectral analysis is used to assess the frequency composition of MS, whereas we use the Redfit method to carry out spectral analysis on the digitized microfacies curve. Spectral analysis of the MS records is carried out after detrending and interpolating the records to equally spaced intervals. The MS datasets are analysed using the MTM (Thomson 1982) as implemented in the SSA-MTM Toolkit (Ghil *et al.* 2002). The MTM is performed using three discrete prolate spheroidal sequences as data tapers to compromise between spectral resolution and sidelobe reduction. Small variations in accumulation rate behave like phase modulations, and introduce multiple spurious spectral peaks (Muller & MacDonald 2000). We choose the MTM because it averages these sidelobes into the main peak and thereby gives a superior estimate of the true spectral power. To assess whether or not the strongest spectral peaks are statistically different from the red noise spectrum, the 95% confidence level (CL) is calculated (robust AR(1) estimation, median smoothing window width = $(10\Delta t)^{-1}$, log fit, $f_{\mathrm{Nyquist}} = 2/\Delta t$). To carry out spectral analysis of microfacies variations, each microfacies is assigned a different code and a quantified microfacies curve is obtained. The microfacies curve of the 'La Thure' section was digitized by assigning a value 0 to microfacies attributed to a drowned carbonate platform. Microfacies that correspond to a distal-ramp palaeoenvironment receive value 1, and microfacies that were deposited on a mid-ramp receive value 2. Microfacies that were deposited on a carbonate platform are attributed values between 3 and 17, where a higher numerical value displays a more proximal setting. For the spectral analysis of the 'La Thure' microfacies curve, we choose to use the Redfit method rather than the MTM, because the first method is specifically designed to estimate red noise spectra from unevenly spaced data series. Hence, we avoid interpolation over stratigraphic intervals where microfacies data are scarce. Frequency-selective filters or Gaussian band-pass filters isolate and extract the components of signals associated with a specific range of frequencies. We employ band-pass filters to assess the behaviour of a specific range of frequencies in a studied signal using the Analyseries software (Paillard *et al.* 1996).

Results and discussion

Continuous wavelet transform

The MS signal of the 'La Couvinoise' section has been investigated for a possible astronomical imprint in a previous paper (De Vleeschouwer *et al.* 2012*a*). Therein, we recognized the strong influence of precession on the monsoonal dynamics at the palaeogeographic position of Belgium, on the eastern side of the tropical Euramerican continent. The short 100 kyr eccentricity cycle was recognized in the amplitude-envelope of the precessional signal in MS and microfacies. According to figure 6 in De Vleeschouwer *et al.* (2012*a*), 6.5 short eccentricity cycles can be counted in the 85 m-thick 'La Couvinoise' section. These 100 kyr cycles are represented by the blue curve, shown on top of the MS signal in Figure 2. The 100 kyr cycles were obtained by band-pass filtering the MS signal between 6.9 and 9.13 m in the lower part of the section, deposited in an open-marine environment, and between 15.95 and 19.58 m in the upper part of the section, deposited in a fore-reef environment. The widths of the band-pass filters were determined by multiplying the periodicity of the precession cycles (values in De Vleeschouwer *et al.* 2012*a*) by 5.5, following the ratio between 100 kyr eccentricity and *c.* 18 kyr precession (Berger *et al.* 1992). On the CWT (Fig. 2), the 100 kyr cycles are represented by a slightly elevated spectral power for a *c.* 8 m periodicity in the open marine part of the section, and a strongly elevated spectral power for a *c.* 16 m periodicity in the fore-reef environment. Moreover, in the fore-reef environment, the CWT indicates elevated spectral power for a *c.* 3.2 m period that was interpreted as the result of precessional forcing in De Vleeschouwer *et al.* (2012*a*).

The 'Monts de Baileux' section covers a much longer stratigraphic interval than the 'La Couvinoise' section. As a consequence, the CWT provides better insight into the behaviour of 10^5 yr scale cycles, which is essential for the astrochronological purposes of this paper. The CWT displays a very strong, stable and uninterrupted band of high spectral power in the low-frequency part of its time–frequency space: in the lower 150 m of the section, the periodicity of this zone of high spectral power is *c.* 45 m, while in the upper part its periodicity is *c.* 60 m. Also, for a periodicity around 16 m, increased spectral power can be observed throughout almost the entire section. This band of increased spectral power is, in contrast to the low-frequency spectral peak, frequently interrupted and displays a bifurcation (spliting and braiding) pattern. These *c.* 16 m-thick cycles in the 'Monts de Baileux' section are the equivalent of the 100 kyr cycles in the 'La Couvinoise' section, where these cycles have a similar thickness in the upper part of the section. From this interpretation it follows that the low-frequency cycles are the result of 405 kyr-long eccentricity forcing. This interpretation is supported by the discussed characteristics of the CWT's time–frequency space, as the short eccentricity cycle is expected to display bifurcations because of amplitude modulation by the long eccentricity cycle. Bifurcations are not expected for the 405 kyr cycle, which is extremely phase-coherent and stable. The 405 kyr cycles are filtered from the MS signal by applying a broad band-pass between 33.33 and 100 m, and plotted in olive on top of the MS signal (Fig. 2). A band-pass filter between 9.09 and 20 m, plotted in blue, shows the 100 kyr cycles in the MS signal of the 'Mont de Baileux' section. The amplitude envelope of these 100 kyr cycles is plotted by a light-blue dashed line, which shows amplitude modulation at the rhythm of the 405 kyr eccentricity. From astronomical theory, high-amplitude 100 kyr cycles are expected when the 405 kyr eccentricity cycle is at a maximum. In this way, the phase relationship between the low-frequency filter output and the 405 kyr eccentricity cycle is uncovered: eccentricity is high when the low-frequency filter is at a maximum.

The 'Fromelennes–Flohimont' section comprises more than 450 m of stratigraphy, including four different formations. In the Trois-Fontaines and Terres d'Haures Fms, the MS signal of the

'Fromelennes–Flohimont' section is very similar to that of the 'Monts de Baileux' section, allowing for an accurate and detailed correlation. The MS signal of the 'Fromelennes–Flohimont' section is characterized by some significant sampling breaks, where the section is covered by vegetation (Fig. 2). We divided the MS signal into four different parts accordingly, and we carried out CWT on the four different parts of the 'Fromelennes–Flohimont' MS signal separately. In the lower part of the section, between 90 and 185 m, the observed distribution of spectral power is similar to that observed in the upper part of the 'Monts de Baileux' section. This does not come as a surprise, given the similar patterns in MS in the overlapping part of both sections. Hence, the interpretation of the cyclicity is identical for both sections: a *c.* 60 m periodicity is ascribed to 405 kyr eccentricity forcing, while a *c.* 16 m periodicity is associated with 100 kyr eccentricity. The three upper intervals of the 'Fromelennes–Flohimont' section are too short to unambiguously distinguish the imprint of the 405 kyr cycle. The corresponding CWTs show a bifurcation pattern around periodicity 16 m, interpreted as the result of 100 kyr forcing. The same band-pass filters have been applied as for the 'Monts de Baileux' section, showing the 405 kyr cycles in olive and the 100 kyr cycles in blue (Fig. 2). In the lower part of the section, the 100 kyr cycles are clearly amplitude modulated by 405 kyr eccentricity: this is a strong indication that the astronomical interpretation is correct.

The 'La Thure' section covers the entire Mont d'Haurs and Fromelennes Fms, and stretches into the Nismes Fm. From lithostratigraphy, one can immediately deduce that the accumulation rate in this section is significantly lower than in the 'Fromelennes–Flohimont' section. For example, the Mont d'Haurs Fm in 'La Thure' covers only *c.* 80 m; the same formation in 'Fromelennes–Flohimont' spans *c.* 180 m. The CWT demonstrates a very strong and stable zone of high spectral power for a *c.* 30 m period, especially in the upper part of the section, which would correspond to the 405 kyr eccentricity cycle, given the above-mentioned ratio in accumulation rate. Around periodicity 8 m, the splitting and braiding pattern is remarkably explicit, and a strong indication for the imprint of 100 kyr eccentricity. Band-pass filtering was carried out between 23.53 and 30.77 m to display the 405 kyr cycles in green and between 5 and 10 m for the 100 kyr cycles. Despite the obvious bifurcation pattern in the CWT, the amplitude modulation of the 100 kyr cycles in this section is not in phase with the 405 kyr cycles, as would be expected from astronomical theory. However, this phase-lagged amplitude modulation does not undermine the astronomical interpretation, as phase and amplitude distortions can be induced by the non-linear translation of sea-level change to offshore sediment flux (Laurin *et al.* 2005).

Givetian astrochronology

The 405 kyr eccentricity cycle is very stable from an astronomical point of view (Laskar *et al.* 2011). Therefore, even in the Palaeozoic, the stable periodicity of the 405 kyr cycle can be used as a geochronometer (e.g. Hinnov *et al.* 2013; Wu *et al.* 2013). Indeed, a cyclostratigraphy that is based on this astronomical-forcing component reliably estimates the duration of events and stratigraphic intervals. Therefore, in first instance, we use the 405 kyr cycle for estimating the duration of the Givetian. Subsequently, this estimate is refined based on higher-frequency cycles. In 'La Couvinoise', the Eifelian–Givetian boundary is put at 35 m above the base of the section. From Figure 2, it can be inferred that this stage boundary occurs during a maximum of the 405 kyr eccentricity cycle. When zooming in, this stratigraphic position corresponds to the maximum of the second 100 kyr eccentricity cycle that is contained within this 405 kyr cycle. In other words, the earliest Givetian covers the last 250 kyr of this first 405 kyr cycle. The overlying ten 405 kyr cycles all fall entirely within the Givetian Stage. The Givetian–Frasnian boundary is put at 155 m above the base of the section, which coincides with the onset of a 405 kyr cycle. More accurately, it corresponds to the first 100 kyr eccentricity maximum of this 405 kyr cycle. Consequently, the latest Givetian comprises the first 50 kyr of this long-eccentricity cycle. The summary of the above results is a total duration of the Givetian of 4.35 Myr (Table 1). Obviously, some uncertainties apply when making such an estimate. First of all, there is stratigraphic uncertainty on the position of the stage boundaries. For the Eifelian–Givetian boundary, stratigraphic uncertainty is ± 2 m, and for stratigraphic position of the Givetian–Frasnian boundary the same amount of uncertainty is considered. Using the accumulation rates that result from our astronomical interpretation (16 cm/kyr in 'La Couvinoise' and 7 cm/kyr in 'La Thure') , the stratigraphic uncertainties translate into chronologic uncertainties of ± 0.015 and 0.03 Myr, respectively. We also take a 'counting error' of ± 0.405 Myr into consideration, as the possibility exists that a 405 kyr cycle is either overlooked or counted twice, leading to a total uncertainty of ± 0.45 Myr. To conclude, this study estimates the duration of the Givetian at 4.35 ± 0.45 Myr. This result suggests that the most recent International Chronostratigraphic Chart (GTS2012) slightly overestimates the duration of the Givetian (5 Myr in Becker *et al.* 2012). Our estimate, however, is in

Table 1. *Astrochronologic estimation of the duration of the Givetian Stage*

Interval	Givetian contains			Uncertainty	
	Number of cycles	Cycle duration (Myr)	Duration (Myr)	Stratigraphic uncertainty	Chronologic uncertainty (Myr)
Eifelian–Givetian	2.5	0.1	0.25	±2 m	±0.015
Givetian	10	0.405	4.05	±1 cycle	±0.405
Givetian–Frasnian	0.5	0.1	0.05	±2 m	±0.030
Total duration			**4.35**		**±0.45**

The Givetian Stage holds 10 complete 405 kyr cycles and three 100 kyr cycles, accounting for 4.35 Myr. The stratigraphic uncertainty added to a counting error of one 405 kyr cycle results in a total uncertainty of ±0.45 Myr on the duration of the Givetian.

perfect agreement with the Devonian chronology of Kaufmann (2006), in which the Givetian is assigned a duration of 4.4 Myr.

The environmental response to astronomical forcing. Figure 3a shows the complete stratigraphic interval of the studied part of the 'La Thure' section. In this photograph, the 405 kyr cycles are not immediately apparent from the lithology. For this reason, the eccentricity cycles are highlighted by alternating orange and transparent bands. However, when the composition and appearance of the carbonate rocks of 'La Thure' are studied in more detail, by looking at the microfacies, the imprint of astronomical climate forcing becomes apparent. In Figure 3b, the 'La Thure' microfacies curve is

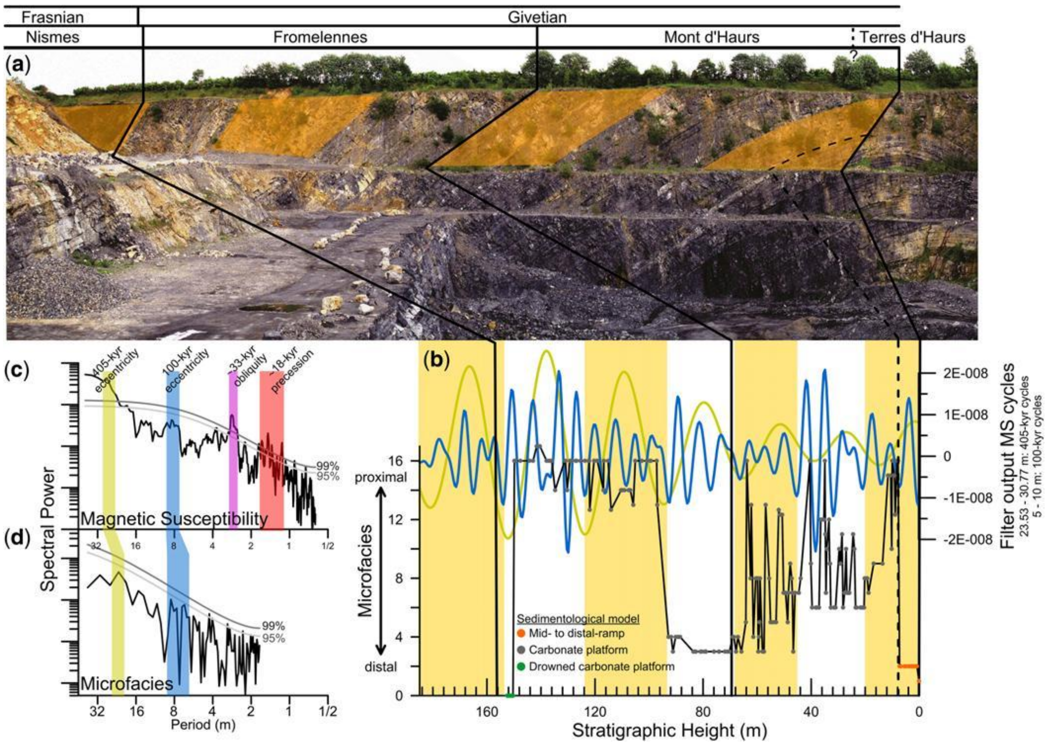

Fig. 3. (**a**) Photograph of the studied part of the La Thure section. The alternating orange and transparent surfaces correspond to the horizontal bands that delineate the 405 kyr cycles in Figure 2. (**b**) The microfacies curve of the La Thure section (black), compared with the 100 kyr (blue) and 405 kyr (green) band-pass filter output extracted from the magnetic susceptibility signal, also exhibits a strong imprint of 100 kyr eccentricity forcing. (**c**) The spectral plot of the MS signal of La Thure and (**d**) the spectral plot of the microfacies curve of La Thure demonstrate spectral peaks that can be related to the different astronomical parameters.

compared with the 100 and 405 kyr eccentricity cycles, extracted from the MS signal of that section. This comparison shows that the 100 kyr cycles observed in the MS signal of 'La Thure' are remarkably similar to variations in microfacies, especially in the Mont d'Haurs Fm. Higher MS values seem to occur in sediments that have been deposited in more proximal palaeoenvironments. This observation is in line with expectations, as Da Silva *et al.* (2009) found that, on carbonate platforms, average magnetic susceptibility generally increases towards the top of shallowing-upward sequences. When relative sea-level is low, the source of magnetic susceptible minerals (fluvial or aeolian input) is nearer. When relative sea-level is high, magnetic minerals are more dispersed and diluted by increased carbonate accumulation (Hinnov *et al.* 2013). The astronomical signature in the spectral plot of the 'La Thure' MS signal is clearly dominated by obliquity and precession (Fig. 3c). The astronomical signature in the spectral plot of the microfacies series is less clear (Fig. 3d). However, the microfacies variability in the Mont d'Haurs Fm related to 100 kyr eccentricity results in a spectral peak exceeding the 95% CL at periodicity 7.64 m (Fig. 3d). At higher frequencies (lower periods) multiple spectral peaks reach the 95% CL (Fig. 3d), for which an astronomical interpretation is not as obvious as for the spectral plot of the MS series (Fig. 3c). These results indicate that the studied MS signal bears the imprint of both changes in water depth (i.e. relative sea-level) as variations in detrital inputs to the marine system. Both sources of variability are at least partially under the influence of astronomical climate forcing. Through its insolation forcing, precession has an immediate impact on monsoonal dynamics (De Vleeschouwer *et al.* 2012*a*). Therefore, the fluvial and aeolian flux of magnetic minerals towards the studied Givetian carbonate platform was driven by astronomical forcing. Relative sea-level change is determined by variability in continental ice volume and ocean water temperature, among other factors. Since the microfacies cyclicity is characterized by a relatively strong eccentricity component, we infer that Givetian sea-level fluctuations were influenced by eccentricity-modulated precession.

Implications for palaeoclimate. During the Middle Devonian, the Dinant Synclinorium was situated on the eastern rim of the Euramerican continent, which stretched across the tropical latitudes of the southern hemisphere. The palaeolatitude of the studied sections is estimated around 22°S (Torsvik *et al.* 2012; Scotese 2013). At this latitude, Milankovitch variations in incoming solar radiation are dominated by precession, with just a minor influence of obliquity during periods of low eccentricity. Eccentricity plays a negligible role as a direct driver of variations in incoming solar radiation, but it is a significant astronomical parameter as the amplitude modulator of climatic precession. Therefore, the recognition of eccentricity cycles in the studied Givetian marine sedimentary archive shows that the Mid-Devonian palaeoclimate was receptive for astronomical climate forcing, dominated by precession. Indeed, De Vleeschouwer *et al.* (2012*a*) concluded that precession was the dominant astronomical parameter in the 'La Couvinoise' section. In this paper, the same inference is made for the 'Monts de Baileux', 'Fromelennes–Flohimont' and 'La Thure' sections, as increased spectral

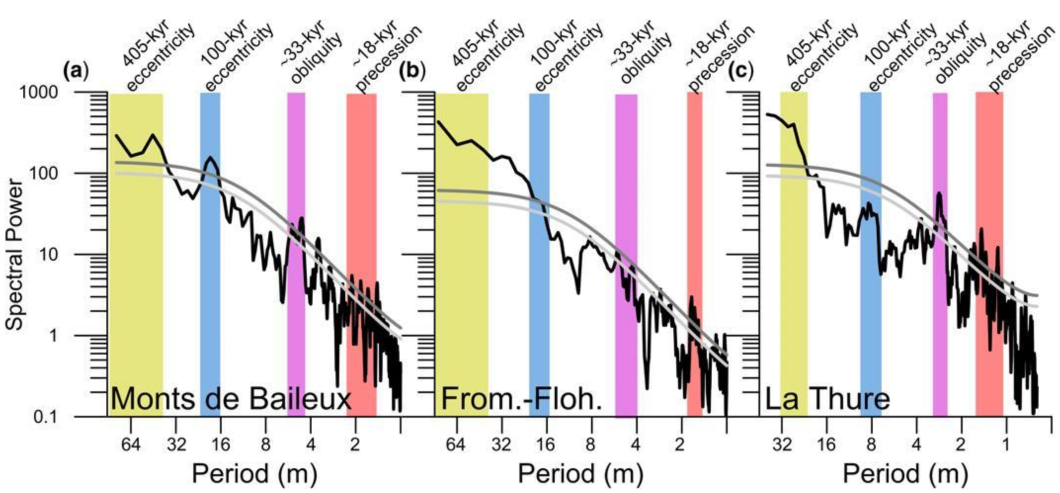

Fig. 4. Spectral plots of the magnetic susceptibility signals of (**a**) 'Monts de Baileux', (**b**) 'Fromelennes–Flohimont' and (**c**) 'La Thure'.

power is observed in the frequency domain where precession is expected (Fig. 4). Remarkably, all three of these spectral plots also show increased spectral power at the frequency of obliquity. This is rather unexpected, as no strong obliquity influence was observed in the 'La Couvinoise' section (De Vleeschouwer *et al.* 2012*a*). Also, as pointed out above, obliquity only has a very limited influence in the variations of incoming solar radiation at tropical latitudes. Hence, the observation of an obliquity imprint at the tropical palaeolatitude of the study area suggests some sort of climatic teleconnection. A climatic teleconnection implies that climate variations at a certain place are related to climatic changes at large distances (typically thousands of kilometres). Continental ice sheets are an excellent example of an important agent in climatic teleconnections: as ice sheets occur at high latitudes, they are under the strong influence of obliquity. The extent of high-latitude ice sheets has an important influence on global and low-latitude climate. Therefore, for the Middle Devonian, we infer that continental ice sheets most probably existed at the high latitudes of Gondwana. However, except for the Famennian, the Devonian is considered an ice-free period. Recently though, some papers challenged previous assumptions of ice-free greenhouse climates for the early Eocene, mid-Cretaceous (Miller *et al.* 2005) and Middle Devonian (Elrick *et al.* 2009), based on stratigraphic and oxygen isotope evidence. Also oxygen isotopes in apatite (Joachimski *et al.* 2009) demonstrate intermediate tropical temperatures (23–25 °C) for the Middle Devonian, contradicting the traditional view that the extensive Middle Devonian mega-reefs reflect an extremely warm global climate. In other words, the observation of an obliquity imprint in the studied Middle Devonian tropical environmental archives of southern Belgium supports the claim of Elrick *et al.* (2009) that significant continental ice sheets grew and melted on 10^5–10^6 year timescales during the Middle Devonian.

Conclusion

Time-series analysis on magnetic susceptibility variations in four different Givetian sections from the Dinant Synclinorium (southern Belgium) reveals the imprint of the different astronomical parameters (eccentricity, obliquity, precession). This disclosure has implications both for the understanding of the palaeoclimate of the Givetian and for the chronology of this stage. First, the imprint of obliquity in the studied sedimentary archives from a tropical palaeolocation suggests that, during the Givetian, a teleconnection existed between the high and the low latitudes, which is an indirect indication of the presence of continental ice. Thus, most probably, the Givetian did not experience such an extremely hot ice-free greenhouse climate, as was long thought in the traditional view. Second, the recognition of a clear signature of eccentricity forcing in the studied sedimentary archive demonstrates that – in the near future – it will be possible to extend the astronomical timescale into the Palaeozoic Era. Without doubt, the next generation of Devonian timescales will incorporate astrochronological information, set in a framework of high-precision U–Pb dates (De Vleeschouwer & Parnell 2014). In this light, the results of the present work provide time-scale builders with an revised estimate of the duration of the Givetian Stage: 4.35 $\pm$ 0.45 Myr. This estimate differs significantly from previous cyclostratigraphic assessments of the duration of the Givetian (Ellwood *et al.* 2011*b*; House 1995). Despite the remarks that can be made on the latter works (see the Introduction), it is crucial that cyclostratigraphic analyses yield similar results to be useful for timescale construction. Therefore, it is important to conduct more cyclostratigraphic studies on Givetian sections worldwide, in order to confront the different results and attain a consensus on how these results relate to each other.

D. D. V. wrote the paper and carried out cyclostratigraphic analyses. A. C. D. S., F. B., D. P. and C. L. carried out field and laboratory work. D. P. created the microfacies curve. P. C. provided feedback and revised the paper. This work is supported by a PhD fellowship awarded by the Research Foundation – Flanders assigned to D. D. V. This paper is part of the UNESCO International Geoscience Program (IGCP-580), entitled 'Application of magnetic susceptibility as a palaeoclimatic proxy on Palaeozoic sedimentary rocks and characterization of the magnetic signal' and IGCP-596. P. C. acknowledges support from the Hercules Foundation, Research Foundation – Flanders (grant G009113), VUB strategic Research Program. This contribution is in part funded by the Interuniversity Attraction Poles Program 'Planet Topers' initiated by the Belgian Science Policy Office. The authors thank Dr S. Gouwy for discussions on conodont biostratigraphy.

References

Bai, S. L. 1995. Milankovitch cyclicity and time scale of the middle and upper Devonian. *International Geology Review*, **37**, 1109–1114.

Becker, R. T., Gradstein, F. M. & Hammer, O. 2012. The Devonian period. *In*: Gradstein, F. M., Ogg, J. G. & Smith, A. G. (eds) *The Geologic Time Scale 2012*. Elsevier, Amsterdam, 559–601.

Berger, A., Loutre, M. F. & Laskar, J. 1992. Stability of the astronomical frequencies over the earth's history for Paleoclimate Studies. *Science*, **255**, 560–565.

Boulvain, F., Mabille, C., Poulain, G. & Da Silva, A. C. 2009. Towards a Palaeogeographical and

Sequential framework for the Givetian of Belgium. *Geologica Belgica*, **12**, 161–178.

Boulvain, F., Da Silva, A. C., Mabille, C., Hladil, J., Gersl, M., Koptikova, L. & Schnabl, P. 2010*a*. Magnetic Susceptibility correlation of km-thick Eifelian–Frasnian sections (Ardennes and Moravia). *Geologica Belgica*, **13**, 301–310.

Boulvain, F., Mabille, C., Poulain, G. & Da Silva, A. C. 2010*b*. A magnetic susceptibility curve for the Devonian limestone from Belgium. *Geologica Belgica*, **13**, 113–117.

Bultynck, P. 1987. Pelagic and neritic conodont successions from the Givetian of pre-Sahara Morocco and the Ardennes. *Bulletin-Institut royal des sciences naturelles de Belgique. Sciences de la terre*, **57**, 149–181.

Bultynck, P. & Hollevoet, C. 1999. The Eifelian–Givetian boundary and Struve's Middle Devonian Great Gap in the Couvin area (Ardennes, southern Belgium). *Senckenbergiana lethaea*, **79**, 3–11.

Bultynck, P., Casier, J.-G. *et al.* 1988. Pre-Congress excursion to the Devonian stratotypes in Belgium. *Bulletin de la Société belge de Géologie*, **96**, 249–288.

Casier, J.-G. & Préat, A. 2009. Late Givetian to Middle Frasnian ostracods from Nismes (Dinant Synclinorium, Belgium) and their lithological context. *Bulletin de l'Institut royal des Sciences naturelles de Belgique, Sciences de la Terre*, **79**, 87–115.

Chen, D. Z. & Tucker, M. E. 2003. The Frasnian–Famennian mass extinction: insights from high-resolution sequence stratigraphy and cyclostratigraphy in South China. *Palaeogeography Palaeoclimatology Palaeoecology*, **193**, 87–111, http://dx.doi.org/10.1016/S0031-0182(02)00716-2

Chlupáč, I. 2000. Cyclicity and duration of Lower Devonian stages: observations from the Barrandian area, Czech Republic. *Neues Jahrbuch Fur Geologie Und Palaontologie-Abhandlungen*, **215**, 97–124.

Clack, J. A. 2007. Devonian climate change, breathing, and the origin of the tetrapod stem group. *Integrative and Comparative Biology*, **47**, 510–523.

Clack, J. A. 2009. The fin to limb transition: new data, interpretations, and hypotheses from paleontology and developmental biology. *Annual Review of Earth and Planetary Sciences*, **37**, 163–179, http://dx.doi.org/10.1146/annurev.earth.36.031207.124146

Coen-Aubert, M. & Boulvain, F. 2006. Frasnian. *Geologica Belgica*, **9**, 19–25.

Da Silva, A. C. & Boulvain, F. 2006. Upper Devonian carbonate platform correlations and sea level variations recorded in magnetic susceptibility. *Paleogeography, Paleoclimatology, Palaeoecology*, **240**, 373–388, http://dx.doi.org/10.1016/j.palaeo.2006.02.012

Da Silva, A.-C., Mabille, C. & Boulvain, F. 2009. Influence of sedimentary setting on the use of magnetic susceptibility: examples from the Devonian of Belgium. *Sedimentology*, **56**, 1292–1306.

Da Silva, A. C., De Vleeschouwer, D. *et al.* 2013. Magnetic susceptibility as a high-resolution correlation tool and as a climatic proxy in Paleozoic rocks – merits and pitfalls: examples from the Devonian in Belgium. *Marine and Petroleum Geology*, **46**, 173–189, http://dx.doi.org/10.1016/j.marpetgeo.2013.06.012

De Vleeschouwer, D. & Parnell, A. C. 2014. Reducing time-scale uncertainty for the Devonian by integrating astrochronology and Bayesian statistics. *Geology*, **42**, 491–494.

De Vleeschouwer, X., Petitclerc, E., Spassov, S. & Preat, A. 2010. The Givetian–Frasnian boundary at Nismes parastratotype (Belgium): the magnetic susceptibility signal controlled by ferromagnetic minerals. *Geologica Belgica*, **13**, 351–366.

De Vleeschouwer, D., Da Silva, A. C., Boulvain, F., Crucifix, M. & Claeys, P. 2012*a*. Precessional and half-precessional climate forcing of Mid-Devonian monsoon-like dynamics. *Climate of the Past*, **8**, 337–351, http://dx.doi.org/10.5194/cp-8-337-2012

De Vleeschouwer, D., Whalen, M. T., Day, J. E. & Claeys, P. 2012*b*. Cyclostratigraphic calibration of the Frasnian (Late Devonian) time scale (western Alberta, Canada). *Geological Society of America Bulletin*, **124**, 928–942, http://dx.doi.org/10.1130/B30547.1

De Vleeschouwer, D., Rakociński, M., Racki, G., Bond, D. P. G., Sobień, K. & Claeys, P. 2013. The astronomical rhythm of Late-Devonian climate change (Kowala section, Holy Cross Mountains, Poland). *Earth and Planetary Science Letters*, **365**, 25–37.

Ellwood, B. B., Crick, R. E., El Hassani, A., Benoist, S. L. & Young, R. H. 2000. Magnetosusceptibility event and cyclostratigraphy (MSEC) in marine rocks and the question of detrital input v. carbonate productivity. *Geology*, **28**, 1135–1138.

Ellwood, B. B., Algeo, T. J., El Hassani, A., Tomkin, J. H. & Rowe, H. D. 2011*a*. Defining the timing and duration of the Kacak Interval within the Eifelian/Givetian boundary GSSP, Mech Irdane, Morocco, using geochemical and magnetic susceptibility patterns. *Palaeogeography Palaeoclimatology Palaeoecology*, **304**, 74–84, http://dx.doi.org/10.1016/j.palaeo.2010.10.012

Ellwood, B. B., Tomkin, J. H. *et al.* 2011*b*. A climate-driven model and development of a floating point time scale for the entire Middle Devonian Givetian Stage: a test using magnetostratigraphic susceptibility as a climate proxy. *Palaeogeography Palaeoclimatology Palaeoecology*, **304**, 85–95, http://dx.doi.org/10.1016/j.palaeo.2010.10.014

Elrick, M., Berkyova, S., Klapper, G., Sharp, Z., Joachimski, M. & Fryda, J. 2009. Stratigraphic and oxygen isotope evidence for My-scale glaciation driving eustasy in the Early-Middle Devonian greenhouse world. *Palaeogeography Palaeoclimatology Palaeoecology*, **276**, 170–181, http://dx.doi.org/10.1016/j.palaeo.2009.03.008

Garcia-Alcalde, J. L., Ellwood, B. B., Soto, F., Truyols-Massoni, M. & Tomkin, J. H. 2012. Precise timing of the Upper Taghanic Biocrisis, Geneseo Bioevent, in the Middle-Upper Givetian (Middle Devonian) boundary in Northern Spain using biostratigraphic and magnetic susceptibility data sets. *Palaeogeography Palaeoclimatology Palaeoecology*, **313**, 26–40, http://dx.doi.org/10.1016/j.palaeo.2011.10.006

Ghil, M., Allen, M. R. *et al.* 2002. Advanced spectral methods for climatic time series. *Reviews of Geophysics*, **40**, 1–41, http://dx.doi.org/10.1029/2000RG000092

Gouwy, S. & Bultynck, P. 2003. Conodont based graphic correlation of the Middle Devonian

Formations of the Ardenne (Belgium): implications for stratigraphy and construction of a regional composite. *Revista española de micropaleontología*, **35**, 315–344.

Gradstein, F. M., Ogg, J. G. & Smith, A. G. 2004. *A Geological Time Scale 2004*. Cambridge University Press, Cambridge.

Gradstein, F. M., Ogg, J. G., Schmitz, M. & Ogg, G. 2012. *The Geologic Time Scale 2012 2-Volume Set*. Elsevier, Oxford.

Hinnov, L. A., Kodama, K. P., Anastasio, D. J., Elrick, M. & Latta, D. K. 2013. Global Milankovitch cycles recorded in rock magnetism of the shallow marine lower Cretaceous Cupido Formation, northeastern Mexico. *In*: Jovane, J., Herrero-Bervera, E., Hinnov, L. A. & Housen, B. A. (eds) *Magnetic Methods and the Timing of Geological Processes*. Geological Society, London, Special Publications, **373**, 325–340, http://dx.doi.org/10.1144/sp373.20

House, M. R. 1995. Devonian precessional and other signatures for establishing a Givetian timescale. *In*: House, M. R. & Gale, A. S. (eds) *Orbital forcing timescales and cyclostratigraphy*. Geological Society, London, Special Publications, **85**, 37–49.

Joachimski, M. M., Breisig, S. *et al.* 2009. Devonian climate and reef evolution: insights from oxygen isotopes in apatite. *Earth and Planetary Science Letters*, **284**, 599–609, http://dx.doi.org/10.1016/j.epsl.2009.05.028

Kaufmann, B. 2006. Calibrating the Devonian Time Scale – a synthesis of U–Pb ID-TIMS ages and relative, time-linear conodont stratigraphy. *Earth-Science Reviews*, **76**, 175–190, http://dx.doi.org/10.1016/j.earscirev.2006.01.001

Klapper, G. 1971. Sequence within the conodont genus Polygnathus in the New York lower Middle Devonian. *Geologica et Palaeontologica*, **5**, 59–79.

Laskar, J., Fienga, A., Gastineau, M. & Manche, H. 2011. La2010: a new orbital solution for the long-term motion of the Earth. *Astronomy & Astrophysics*, **532**, http://dx.doi.org/10.1051/0004-6361/201116836.

Laurin, J., Meyers, S. R., Sageman, B. B. & Waltham, D. 2005. Phase-lagged amplitude modulation of hemipelagic cycles: a potential tool for recognition and analysis of sea-level change. *Geology*, **33**, 569–572, http://dx.doi.org/10.1130/G21350.1

Long, J. A., Trinajstic, K., Young, G. C. & Senden, T. 2008. Live birth in the Devonian period. *Nature*, **453**, 650–652.

Long, J. A., Trinajstic, K. & Johanson, Z. 2009. Devonian arthrodire embryos and the origin of internal fertilization in vertebrates. *Nature*, **457**, 1124–1127.

Lourens, L., Hilgen, F., Shackleton, N., Laskar, J. & Wilson, D. 2004. The Neogene Period. *In*: Gradstein, F., Ogg, J. G. & Smith, A. G. (eds) *A Geologic Time Scale 2004*. Cambridge University Press, Cambridge, 610.

Mabille, C. & Boulvain, F. 2007. Sedimentology and magnetic susceptibility of the Upper Eifelian – Lower Givetian (Middle Devonian) in southwestern Belgium: insights into carbonate platform initiation. *In*: Alvaro, J. J., Aretz, M. *et al.* (eds) *Palaeozoic Reefs and Bioaccumulations: Climatic and Evolutionary Controls*. Geological Society, London, Special Publications, **275**, 109–124.

Mabille, C. & Boulvain, F. 2008. Les Monts De Baileux Section: detailed Sedimentology and Magnetic Susceptibility of Hanonet, Trois-Fontaines and Terres D'haurs Formations (Eifelian/Givetian Boundary and Lower Givetian, Sw Belgium). *Geologica Belgica*, **11**, 93–121.

Meyers, S. R. 2008. Resolving Milankovitchian controversies: the Triassic Latemar Limestone and the Eocene Green River Formation. *Geology*, **36**, 319–322, http://dx.doi.org/10.1130/G24423a.1

Meyers, S. R., Siewert, S. E. *et al.* 2012. Intercalibration of radioisotopic and astrochronologic time scales for the Cenomanian-Turonian boundary interval, Western Interior Basin, USA. *Geology*, **40**, 7–10, http://dx.doi.org/10.1130/G32261.1

Miller, K. G., Wright, J. D. & Browning, J. V. 2005. Visions of ice sheets in a greenhouse world. *Marine Geology*, **217**, 215–231.

Mintz, J. S., Driese, S. G. & White, J. D. 2010. Environmental and Ecological Variability of Middle Devonian (Givetian) Forests in Appalachian Basin Paleosols, New York, United States. *Palaios*, **25**, 85–96, http://dx.doi.org/10.2110/palo.2009.p09-086r

Muller, R. A. & MacDonald, G. J. 2000. *Ice Ages and Astronomical Causes. Data, Spectral AnalysisSpectral Analysis and MechanismsMechanisms*. Springer, Chichester.

Paillard, D., Labeyrie, L. & Yiou, P. 1996. Macintosh program performs time-series analysis. *Eos Transactions AGU*, **77**, 379.

Preat, A., Bultynck, P. & Brice, D. 2006. Givetian. *Geologica Belgica*, **9**, 9–18.

Roden, M. K., Parrish, R. R. & Miller, D. S. 1990. The Absolute Age of the Eifelian Tioga Ash Bed, Pennsylvania. *Journal of Geology*, **98**, 282–285.

Rotondo, K. & Over, D. 2000. Biostratigraphic age of the Belpre Ash (Frasnian), Chattanooga and Rhinestreet shales in the Appalachian Basin. *Geological Society of America Abstracts with Programs*, **32**, 1–70.

Scotese, C. 2013. Devonian paleogeographic maps by CR Scotese. www.scotese.com [accessed 30 May 2013].

Stein, W. E., Mannolini, F., Hernick, L. V., Landing, E. & Berry, C. M. 2007. Giant cladoxylopsid trees resolve the enigma of the Earth's earliest forest stumps at Gilboa. *Nature*, **446**, 904–907, http://dx.doi.org/10.1038/Nature05705

Stein, W. E., Berry, C. M., Hernick, L. V. & Mannolini, F. 2012. Surprisingly complex community discovered in the mid-Devonian fossil forest at Gilboa. *Nature*, **483**, 78–81, http://dx.doi.org/10.1038/Nature10819

Thomson, D. J. 1982. Spectrum estimation and harmonic-analysis. *Proceedings of the IEEE*, **70**, 1055–1096.

Torrence, C. & Compo, G. P. 1998. A practical guide to wavelet analysis. *Bulletin of the American Meteorological Society*, **79**, 61–78, http://dx.doi.org/10.1175/1520-0477(1998)079<0061:Apgtwa>2.s0.Co;2

Torsvik, T. H., Van der Voo, R. *et al.* 2012. Phanerozoic polar wander, palaeogeography and dynamics. *Earth-Science Reviews*, **114**, 325–368, http://dx.doi.org/10.1016/j.earscirev.2012.06.007

TUCKER, R. D., BRADLEY, D. C., STRAETEN, C. A. V., HARRIS, A. G., EBERT, J. R. & MCCUTCHEON, S. R. 1998. New U–Pb zircon ages and the duration and division of Devonian time. *Earth and Planetary Science Letters*, **158**, 175–186.

WU, H., ZHANG, S., HINNOV, L. A., JIANG, G., FENG, Q., LI, H. & YANG, T. 2013. Time-calibrated Milankovitch cycles for the late Permian. *Nature Communications*, **4**, 1–8, http://dx.doi.org/10.1038/ncomms3452

ZEGERS, T. E., DEKKERS, M. J. & BAILY, S. 2003. Late Carboniferous to Permian remagnetization of Devonian limestones in the Ardennes: role of temperature, fluids, and deformation. *Journal of Geophysical Research*, **108**, 5/1–5/19.